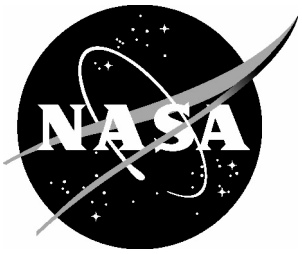
NASA/TM-20250001360



Experimental Investigation of Woven Thermal Protection System Material Roughness Effects on Transition Onset and Turbulent Heating Augmentation at Mach 6

Brian R. Hollis
Langley Research Center, Hampton, Virginia

Kevin E. Hollingsworth
Jacobs Technology, Inc., Hampton, Virginia

February 2025

NASA STI Program Report Series

Since its founding, NASA has been dedicated to the advancement of aeronautics and space science. The NASA scientific and technical information (STI) program plays a key part in helping NASA maintain this important role.

The NASA STI program operates under the auspices of the Agency Chief Information Officer. It collects, organizes, provides for archiving, and disseminates NASA's STI. The NASA STI program provides access to the NTRS Registered and its public interface, the NASA Technical Reports Server, thus providing one of the largest collections of aeronautical and space science STI in the world. Results are published in both non-NASA channels and by NASA in the NASA STI Report Series, which includes the following report types:

- TECHNICAL PUBLICATION. Reports of completed research or a major significant phase of research that present the results of NASA Programs and include extensive data or theoretical analysis. Includes compilations of significant scientific and technical data and information deemed to be of continuing reference value. NASA counterpart of peer-reviewed formal professional papers but has less stringent limitations on manuscript length and extent of graphic presentations.

- TECHNICAL MEMORANDUM. Scientific and technical findings that are preliminary or of specialized interest, e.g., quick release reports, working papers, and bibliographies that contain minimal annotation. Does not contain extensive analysis.

- CONTRACTOR REPORT. Scientific and technical findings by NASA-sponsored contractors and grantees.

- CONFERENCE PUBLICATION. Collected papers from scientific and technical conferences, symposia, seminars, or other meetings sponsored or co-sponsored by NASA.

- SPECIAL PUBLICATION. Scientific, technical, or historical information from NASA programs, projects, and missions, often concerned with subjects having substantial public interest.

- TECHNICAL TRANSLATION. English-language translations of foreign scientific and technical material pertinent to NASA's mission.

Specialized services also include organizing and publishing research results, distributing specialized research announcements and feeds, providing information desk and personal search support, and enabling data exchange services.

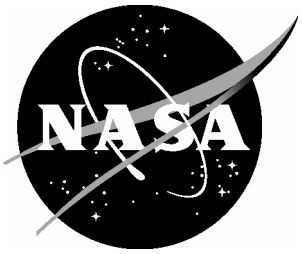
For more information about the NASA STI program, see the following:

- Access the NASA STI program home page at http://www.sti.nasa.gov

- Help desk contact information:

https://www.sti.nasa.gov/sti-contact-form/ and select the "General" help request type.

NASA/TM-20250001360



Experimental Investigation of Woven Thermal Protection System Material Roughness Effects on Transition Onset and Turbulent Heating Augmentation at Mach 6

Brian R. Hollis
Langley Research Center, Hampton, Virginia

Kevin E. Hollingsworth
Jacobs Technology, Inc., Hampton, Virginia

National Aeronautics and
Space Administration

Langley Research Center
Hampton, Virginia 23681-2199

February 2025

National Aeronautics and
Space Administration

Langley Research Center
Hampton, Virginia 23681-2199

February 2025

The use of trademarks or names of manufacturers in this report is for accurate reporting and does not constitute an official endorsement, either expressed or implied, of such products or manufacturers by the National Aeronautics and Space Administration.

Available from:

NASA STI Program / Mail Stop 148
NASA Langley Research Center
Hampton, VA 23681-2199
Fax: 757-864-6500

Table of Contents

Table of Contents i
List of Tables ii
Abstract 9
Nomenclature 10
  Symbols 10
  Subscripts and Superscripts 11
  Acronyms 11
Introduction 11
Background 11
Experimental Tools and Methods 12
  Wind Tunnel Models 12
    Model Geometries 12
    Woven TPS Patterns 12
    Model Fabrication 13
  Wind Tunnel Test Facility 13
    Facility Description 13
    Facility Operating Conditions and Test Matrices 13
  Experimental Data 14
    Data Acquisition and Reduction 14
    Data Mapping and Presentation 15
    Phosphor Thermography Data Quality 16
    Heat Transfer Data Uncertainty 16
    Calibration Correction for Heat Transfer Data 16
Computational Tools and Methods 18
Experimental Data Analysis 19
  Transition Onset Location Definition 19
  Reynolds Number Effects on Heating and Transition 20
  Roughness Height Effects on Heating and Transition 20
  General Reynolds Number and Roughness Height Trends 21
  Roughness Heating Augmentation 21
  Transition Onset Data and Correlation 21
Summary 23
Acknowledgements 23
References 23
Appendix A. Sphere-Cone Geometry Global Heating Images 149
Appendix B. Spherical-Cap Geometry Global Heating Images 195

List of Tables

Table 1. Model geometry parameters. 25
Table 2. Model weave parameters. 25
Table 3. Nominal 20-Inch Mach 6 Air Tunnel Freestream Conditions for Tests 7070 and 7074. 26
Table 4. Nominal 20-Inch Mach 6 Air Tunnel Reservoir Conditions for Tests 7070 and 7074. 26
Table 5. 20-Inch Mach 6 Air Tunnel Test 7070 run matrix for smooth sphere-cone model. 27
Table 6. 20-Inch Mach 6 Air Tunnel Test 7070 run matrix for smooth spherical-cap model. 27
Table 7. 20-Inch Mach 6 Air Tunnel Test 7070 run matrix for sphere-cone models with weave and seams. 28
Table 8. 20-Inch Mach 6 Air Tunnel Test 7070 run matrix for spherical-cap models with weave and seams. 29
Table 9. 20-Inch Mach 6 Air Tunnel Test 7074 run matrix for sphere-cone models with weave only 30
Table 10. 20-Inch Mach 6 Air Tunnel Test 7074 run matrix for spherical-cap models with weave only 31
Table 11. Transition locations for Test 7074 spherical-cap 5-weave model without seams. 32
Table 12. Transition locations for Test 7074 spherical-cap 10-weave model without seams 33
Table 13. Transition locations for Test 7074 spherical-cap 15-weave model without seams 34
Table 14. Transition locations for Test 7074 spherical-cap 20-weave model without seams. 35
Table 15. Transition locations for Test 7074 sphere-cone 5-weave model without seams. 36
Table 16. Transition locations for Test 7074 sphere-cone 10-weave model without seams. 37
Table 17. Transition locations for Test 7074 sphere-cone 15-weave model without seams. 39
Table 18. Transition locations for Test 7074 sphere-cone 20-weave model without seams. 41
Table 19. Transition locations for Test 7070 spherical-cap 5-weave model with seams. 42
Table 20. Transition locations for Test 7070 spherical-cap 15-weave model with seams. 43
Table 21. Transition locations for Test 7070 spherical-cap 20-weave model with seams. 44
Table 22. Transition locations for Test 7070 sphere-cone 5-weave model with seams. 45
Table 23. Transition locations for Test 7070 sphere-cone 10-weave model with seams. 46
Table 24. Transition locations for Test 7070 sphere-cone 15-weave model with seams. 48
Table 25. Transition locations for Test 7070 sphere-cone 20-weave model with seams 50

List of Figures

Figure 1. Discrete surface roughness types.....52
Figure 2. Distributed surface roughness types.....52
Figure 3. Sphere-cone geometry.....53
Figure 4. Spherical-cap geometry.....53
Figure 5. Weave details – two-dimensional representation.....54
Figure 6. Surface scan of 20-mil sphere-cone model with seams.....55
Figure 7. Surface scan of 20-mil weave sphere-cone model without seams.....55
Figure 8. Sample Model Photographs –20-mil weave sphere-cone model with seams.....56
Figure 9. Sample Model Photographs – 15-mil spherical-cap model without seams.....57
Figure 10. Schematic of Langley Research Center 20-Inch Mach 6 Air Tunnel.....58
Figure 11. Langley Research Center 20-Inch Mach 6 Air Tunnel test section.....58
Figure 12. Modified operating points for the 20-Inch Mach 6 Air Tunnel.....59
Figure 13. Sample phosphor thermography 2-D image data.....60
Figure 14. Sample 3-D mapping of phosphor thermography data.....60
Figure 15. Streamlines for data extraction on sphere-cone geometry.....61
Figure 16. Streamlines for data extraction on spherical-cap geometry.....61
Figure 17. Illustration of camera field-of-view for hemisphere model in 20-Inch Mach 6 Air Tunnel.....62
Figure 18. CFD predictions for hemisphere heating at wind tunnel conditions.....63
Figure 19. Measured hemisphere stagnation point heating from pretest calibration.....63
Figure 20. Calibration correction example for sphere-cone model.....64
Figure 21. Calibration correction example for spherical-cap model.....64
Figure 22. Centerline profiles of roughness effects on k/δ, sphere-cone geometry.....65
Figure 23. Centerline profiles of roughness effects on k/δ, spherical-cap geometry.....66
Figure 24. Centerline profiles of roughness effects on Re_{k+}, sphere-cone geometry.....67
Figure 25. Centerline profiles of roughness effects on Re_{k+}, spherical-cap geometry.....68
Figure 26. Tangent-slope-intercept method for determination of effect transition onset location.....69
Figure 27. Comparison of irregular transition wedges vs. mean transition front.....69
Figure 28. Reynolds Number effects: sphere-cone geometry, smooth model images.....70
Figure 29. Reynolds number effects: sphere-cone geometry, smooth model plots.....71
Figure 30. Reynolds Number effects: sphere-cone geometry, 5-mil weave without seams model images.....72
Figure 31. Reynolds Number effects: sphere-cone geometry, 5-mil weave without seams model plots.....73
Figure 32. Reynolds Number effects: sphere-cone geometry, 5-mil weave with seams model images.....74
Figure 33. Reynolds Number effects: sphere-cone geometry, 5-mil weave with seams model plots.....75
Figure 34. Reynolds Number effects: sphere-cone geometry, 10-mil weave without seams model images.....76
Figure 35. Reynolds Number effects: sphere-cone geometry, 10-mil weave without seams model plots.....77
Figure 36. Reynolds Number effects: sphere-cone geometry, 10-mil weave with seams model images.....78
Figure 37. Reynolds Number effects: sphere-cone geometry, 10-mil weave with seams model plots.....79
Figure 38. Reynolds Number effects: sphere-cone geometry, 15-mil weave without seams model images.....80
Figure 39. Reynolds Number effects: sphere-cone geometry, 15-mil weave without seams model plots.....81
Figure 40. Reynolds Number effects: sphere-cone geometry, 15-mil weave with seams model images.....82
Figure 41. Reynolds Number effects: sphere-cone geometry, 15-mil weave with seams model plots.....83
Figure 42. Reynolds Number effects: sphere-cone geometry, 20-mil weave without seams model images.....84
Figure 43. Reynolds number effects: sphere-cone geometry, 20-mil weave without seams plots.....85
Figure 44. Reynolds Number effects: sphere-cone geometry, 20-mil weave with seams model images.....86
Figure 45. Reynolds Number effects: sphere-cone geometry, 20-mil weave with seams model plots.....87
Figure 46. Reynolds Number effects: spherical-cap geometry, smooth model images.....88
Figure 47. Reynolds number effects: spherical-cap geometry, smooth model plots.....89
Figure 48. Reynolds Number effects: spherical-cap geometry, 5-mil weave without seams model images.....90
Figure 49. Reynolds number effects: spherical-cap geometry, 5-mil weave without seams plots.....91
Figure 50. Reynolds Number effects: spherical-cap geometry, 5-mil weave with seams model images.....92
Figure 51. Reynolds number effects: spherical-cap geometry, 5-mil weave with seams plots.....93
Figure 52. Reynolds Number effects: spherical-cap geometry, 10-mil weave without seams model images.....94
Figure 53. Reynolds number effects: spherical-cap geometry, 10-mil weave without seams plots.....95

Figure 54. Reynolds Number effects: spherical-cap geometry, 10-mil weave with seams model images.....96
Figure 55. Reynolds number effects: spherical-cap geometry, 10-mil weave with seams plots.....97
Figure 56. Reynolds Number effects: spherical-cap geometry, 15-mil weave without seams model images. 98
Figure 57. Reynolds number effects: spherical-cap geometry, 15-mil weave without seams plots.....99
Figure 58. Reynolds Number effects: spherical-cap geometry, 15-mil weave with seams model images.....100
Figure 59. Reynolds number effects: spherical-cap geometry, 15-mil weave with seams plots.....101
Figure 60. Reynolds Number effects: spherical-cap geometry, 20-mil weave without seams model images. 102
Figure 61. Reynolds number effects: spherical-cap geometry, 20-mil weave without seams plots.....103
Figure 62. Reynolds Number effects: spherical-cap geometry, 20-mil weave with seams model images.....104
Figure 63. Reynolds number effects: spherical-cap geometry, 20-mil weave with seams plots.....105
Figure 64. Weave-height effects: sphere-cone geometry, $Re_\infty = 1.0\times10^6$/ft images. 106
Figure 65. Weave-height effects: sphere-cone geometry, $Re_\infty = 1.0\times10^6$/ft plots.....107
Figure 66. Weave-height effects: sphere-cone geometry, $Re_\infty = 2.0\times10^6$/ft images. 108
Figure 67. Weave-height effects: sphere-cone geometry, $Re_\infty = 2.0\times10^6$/ft plots.....109
Figure 68. Weave-height effects: sphere-cone geometry, $Re_\infty = 3.0\times10^6$/ft images. 110
Figure 69. Weave-height effects: sphere-cone geometry, $Re_\infty = 3.0\times10^6$/ft plots.....111
Figure 70. Weave-height effects: sphere-cone geometry, $Re_\infty = 5.0\times10^6$/ft images. 112
Figure 71. Weave-height effects: sphere-cone geometry, $Re_\infty = 5.0\times10^6$/ft plots.....113
Figure 72. Weave-height effects: sphere-cone geometry, $Re_\infty = 5.2\times10^6$/ft images. 114
Figure 73. Weave-height effects: sphere-cone geometry, $Re_\infty = 5.2\times10^6$/ft plots.....115
Figure 74. Weave-height effects: sphere-cone geometry, $Re_\infty = 6.5\times10^6$/ft images. 116
Figure 75. Weave-height effects: sphere-cone geometry, $Re_\infty = 6.5\times10^6$/ft plots.....117
Figure 76. Weave-height effects: sphere-cone geometry, $Re_\infty = 6.8\times10^6$/ft images. 118
Figure 77. Weave-height effects: sphere-cone geometry, $Re_\infty = 6.8\times10^6$/ft plots.....119
Figure 78. Weave-height effects: sphere-cone geometry, $Re_\infty = 7.3\times10^6$/ft images. 120
Figure 79. Weave-height effects: sphere-cone geometry, $Re_\infty = 7.3\times10^6$/ft plots.....121
Figure 80. Weave-height effects: sphere-cone geometry, $Re_\infty = 7.7\times10^6$/ft images. 122
Figure 81. Weave-height effects: sphere-cone geometry, $Re_\infty = 7.7\times10^6$/ft plots.....123
Figure 82. Weave-height effects: sphere-cone geometry, $Re_\infty = 8.2\times10^6$/ft images. 124
Figure 83. Weave-height effects: sphere-cone geometry, $Re_\infty = 8.2\times10^6$/ft plots.....125
Figure 84. Weave-height effects: spherical-cap geometry, $Re_\infty = 1.0\times10^6$/ft images. 126
Figure 85. Weave-height effects: spherical-cap geometry, $Re_\infty = 1.0\times10^6$/ft plots.....127
Figure 86. Weave-height effects: spherical-cap geometry, $Re_\infty = 2.0\times10^6$/ft images. 128
Figure 87. Weave-height effects: spherical-cap geometry, $Re_\infty = 2.0\times10^6$/ft plots.....129
Figure 88. Weave-height effects: spherical-cap geometry, $Re_\infty = 3.0\times10^6$/ft images. 130
Figure 89. Weave-height effects: spherical-cap geometry, $Re_\infty = 3.0\times10^6$/ft plots.....131
Figure 90. Weave-height effects: spherical-cap geometry, $Re_\infty = 5.0\times10^6$/ft images. 132
Figure 91. Weave-height effects: spherical-cap geometry, $Re_\infty = 5.0\times10^6$/ft plots.....133
Figure 92. Weave-height effects: spherical-cap geometry, $Re_\infty = 5.3\times10^6$/ft images. 134
Figure 93. Weave-height effects: spherical-cap geometry, $Re_\infty = 5.3\times10^6$/ft plots.....135
Figure 94. Weave-height effects: spherical-cap geometry, $Re_\infty = 6.3\times10^6$/ft images. 136
Figure 95. Weave-height effects: spherical-cap geometry, $Re_\infty = 6.3\times10^6$/ft plots.....137
Figure 96. Weave-height effects: spherical-cap geometry, $Re_\infty = 6.8\times10^6$/ft images. 138
Figure 97. Weave-height effects: spherical-cap geometry, $Re_\infty = 6.8\times10^6$/ft plots.....139
Figure 98. Weave-height effects: spherical-cap geometry, $Re_\infty = 7.3\times10^6$/ft images. 140
Figure 99. Weave-height effects: spherical-cap geometry, $Re_\infty = 7.3\times10^6$/ft plots.....141
Figure 100. Weave-height effects: spherical-cap geometry, $Re_\infty = 7.6\times10^6$/ft images. 142
Figure 101. Weave-height effects: spherical-cap geometry, $Re_\infty = 7.6\times10^6$/ft plots.....143
Figure 102. Weave-height effects: spherical-cap geometry, $Re_\infty = 8.2\times10^6$/ft images. 144
Figure 103. Weave-height effects: spherical-cap geometry, $Re_\infty = 8.2\times10^6$/ft plots.....145
Figure 104. Roughness transition correlation applied to prior datasets.....146
Figure 105. Roughness transition correlation applied to woven roughness. 147
Figure 106. Trend line comparison for different roughness types.....148
Figure 107. Test 7070, Run 14: $Re_\infty = 1.0\times10^6$/ft, sphere-cone, smooth OML.....150
Figure 108. Test 7070, Run 11: $Re_\infty = 2.0\times10^6$/ft, sphere-cone, smooth OML.....150
Figure 109. Test 7070, Run 12: $Re_\infty = 3.0\times10^6$/ft, sphere-cone, smooth OML.....151

Figure 110. Test 7070, Run 13: $Re_\infty = 5.0\times10^6$/ft, sphere-cone, smooth OML. 151
Figure 111. Test 7070, Run 95: $Re_\infty = 5.3\times10^6$/ft, sphere-cone, smooth OML. 152
Figure 112. Test 7070, Run 15: $Re_\infty = 6.5\times10^6$/ft, sphere-cone, smooth OML. 152
Figure 113. Test 7070, Run 94: $Re_\infty = 6.8\times10^6$/ft, sphere-cone, smooth OML. 153
Figure 114. Test 7070, Run 16: $Re_\infty = 7.3\times10^6$/ft, sphere-cone, smooth OML. 153
Figure 115. Test 7070, Run 93: $Re_\infty = 7.7\times10^6$/ft, sphere-cone, smooth OML. 154
Figure 116. Test 7070, Run 17: $Re_\infty = 8.2\times10^6$/ft, sphere-cone, smooth OML. 154
Figure 117. Test 7074, Run 20: $Re_\infty = 1.0\times10^6$/ft, sphere-cone, 5-mil weave. 155
Figure 118. Test 7074, Run 11: $Re_\infty = 2.0\times10^6$/ft, sphere-cone, 5-mil weave. 155
Figure 119. Test 7074, Run 16: $Re_\infty = 3.0\times10^6$/ft, sphere-cone, 5-mil weave. 156
Figure 120. Test 7074, Run 15: $Re_\infty = 5.0\times10^6$/ft, sphere-cone, 5-mil weave. 156
Figure 121. Test 7074, Run 19: $Re_\infty = 5.3\times10^6$/ft, sphere-cone, 5-mil weave. 157
Figure 122. Test 7074, Run 14: $Re_\infty = 6.5\times10^6$/ft, sphere-cone, 5-mil weave. 157
Figure 123. Test 7074, Run 18: $Re_\infty = 6.8\times10^6$/ft, sphere-cone, 5-mil weave. 158
Figure 124. Test 7074, Run 13: $Re_\infty = 7.2\times10^6$/ft, sphere-cone, 5-mil weave. 158
Figure 125. Test 7074, Run 17: $Re_\infty = 7.7\times10^6$/ft, sphere-cone, 5-mil weave. 159
Figure 126. Test 7074, Run 12: $Re_\infty = 8.2\times10^6$/ft, sphere-cone, 5-mil weave. 159
Figure 127. Test 7074, Run 06: $Re_\infty = 1.0\times10^6$/ft, sphere-cone, 10-mil weave. 160
Figure 128. Test 7074, Run 01: $Re_\infty = 2.0\times10^6$/ft, sphere-cone, 10-mil weave. 160
Figure 129. Test 7074, Run 02: $Re_\infty = 3.0\times10^6$/ft, sphere-cone, 10-mil weave. 161
Figure 130. Test 7074, Run 03: $Re_\infty = 5.0\times10^6$/ft, sphere-cone, 10-mil weave. 161
Figure 131. Test 7074, Run 08: $Re_\infty = 5.3\times10^6$/ft, sphere-cone, 10-mil weave. 162
Figure 132. Test 7074, Run 04: $Re_\infty = 6.5\times10^6$/ft, sphere-cone, 10-mil weave. 162
Figure 133. Test 7074, Run 09: $Re_\infty = 6.8\times10^6$/ft, sphere-cone, 10-mil weave. 163
Figure 134. Test 7074, Run 05: $Re_\infty = 7.3\times10^6$/ft, sphere-cone, 10-mil weave. 163
Figure 135. Test 7074, Run 10: $Re_\infty = 7.8\times10^6$/ft, sphere-cone, 10-mil weave. 164
Figure 136. Test 7074, Run 07: $Re_\infty = 8.2\times10^6$/ft, sphere-cone, 10-mil weave. 164
Figure 137. Test 7074, Run 27: $Re_\infty = 1.0\times10^6$/ft, sphere-cone, 15-mil weave. 165
Figure 138. Test 7074, Run 26: $Re_\infty = 2.0\times10^6$/ft, sphere-cone, 15-mil weave. 165
Figure 139. Test 7074, Run 25: $Re_\infty = 3.0\times10^6$/ft, sphere-cone, 15-mil weave. 166
Figure 140. Test 7074, Run 21: $Re_\infty = 5.0\times10^6$/ft, sphere-cone, 15-mil weave. 166
Figure 141. Test 7074, Run 28: $Re_\infty = 5.3\times10^6$/ft, sphere-cone, 15-mil weave. 167
Figure 142. Test 7074, Run 22: $Re_\infty = 6.5\times10^6$/ft, sphere-cone, 15-mil weave. 167
Figure 143. Test 7074, Run 29: $Re_\infty = 6.8\times10^6$/ft, sphere-cone, 15-mil weave. 168
Figure 144. Test 7074, Run 23: $Re_\infty = 7.3\times10^6$/ft, sphere-cone, 15-mil weave. 168
Figure 145. Test 7074, Run 31: $Re_\infty = 7.7\times10^6$/ft, sphere-cone, 15-mil weave. 169
Figure 146. Test 7074, Run 24: $Re_\infty = 8.2\times10^6$/ft, sphere-cone, 15-mil weave. 169
Figure 147. Test 7074, Run 34: $Re_\infty = 1.0\times10^6$/ft, sphere-cone, 20-mil weave. 170
Figure 148. Test 7074, Run 35: $Re_\infty = 2.0\times10^6$/ft, sphere-cone, 20-mil weave. 170
Figure 149. Test 7074, Run 36: $Re_\infty = 3.0\times10^6$/ft, sphere-cone, 20-mil weave. 171
Figure 150. Test 7074, Run XX: $Re_\infty = 5.0\times10^6$/ft, sphere-cone, 20-mil weave. 171
Figure 151. Test 7074, Run 32: $Re_\infty = 5.3\times10^6$/ft, sphere-cone, 20-mil weave. 172
Figure 152. Test 7074, Run XX: $Re_\infty = 6.5\times10^6$/ft, sphere-cone, 20-mil weave. 172
Figure 153. Test 7074, Run 33: $Re_\infty = 6.8\times10^6$/ft, sphere-cone, 20-mil weave. 173
Figure 154. Test 7074, Run XX: $Re_\infty = 7.3\times10^6$/ft, sphere-cone, 20-mil weave. 173
Figure 155. Test 7074, Run 37: $Re_\infty = 7.6\times10^6$/ft, sphere-cone, 20-mil weave. 174
Figure 156. Test 7074, Run 38: $Re_\infty = 8.2\times10^6$/ft, sphere-cone, 20-mil weave. 174
Figure 157. Test 7070, Run 39: $Re_\infty = 1.0\times10^6$/ft, sphere-cone, 5-mil weave with seam. 175
Figure 158. Test 7070, Run 40: $Re_\infty = 2.0\times10^6$/ft, sphere-cone, 5-mil weave with seam. 175
Figure 159. Test 7070, Run 41: $Re_\infty = 3.0\times10^6$/ft, sphere-cone, 5-mil weave with seam. 176
Figure 160. Test 7070, Run 42: $Re_\infty = 5.0\times10^6$/ft, sphere-cone, 5-mil weave with seam. 176
Figure 161. Test 7070, Run XX: $Re_\infty = 5.3\times10^6$/ft, sphere-cone, 5-mil weave with seam. 177
Figure 162. Test 7070, Run 43: $Re_\infty = 6.5\times10^6$/ft, sphere-cone, 5-mil weave with seam. 177
Figure 163. Test 7070, Run XX: $Re_\infty = 6.8\times10^6$/ft, sphere-cone, 5-mil weave with seam. 178
Figure 164. Test 7070, Run 44: $Re_\infty = 7.2\times10^6$/ft, sphere-cone, 5-mil weave with seam. 178
Figure 165. Test 7070, Run 66: $Re_\infty = 7.7\times10^6$/ft, sphere-cone, 5-mil weave with seam. 179

Figure 166. Test 7070, Run 45: $Re_\infty = 8.2\times10^6$/ft, sphere-cone, 5-mil weave with seam. 179
Figure 167. Test 7070, Run 49: $Re_\infty = 1.0\times10^6$/ft, sphere-cone, 10-mil weave with seam. 180
Figure 168. Test 7070, Run 50: $Re_\infty = 2.0\times10^6$/ft, sphere-cone, 10-mil weave with seam. 180
Figure 169. Test 7070, Run 51: $Re_\infty = 3.0\times10^6$/ft, sphere-cone, 10-mil weave with seam. 181
Figure 170. Test 7070, Run 52: $Re_\infty = 5.0\times10^6$/ft, sphere-cone, 10-mil weave with seam. 181
Figure 171. Test 7070, Run XX: $Re_\infty = 5.3\times10^6$/ft, sphere-cone, 10-mil weave with seam. 182
Figure 172. Test 7070, Run 48: $Re_\infty = 6.5\times10^6$/ft, sphere-cone, 10-mil weave with seam. 182
Figure 173. Test 7070, Run 63: $Re_\infty = 6.8\times10^6$/ft, sphere-cone, 10-mil weave with seam. 183
Figure 174. Test 7070, Run 47: $Re_\infty = 7.3\times10^6$/ft, sphere-cone, 10-mil weave with seam. 183
Figure 175. Test 7070, Run 62: $Re_\infty = 7.8\times10^6$/ft, sphere-cone, 10-mil weave with seam. 184
Figure 176. Test 7070, Run 46: $Re_\infty = 8.2\times10^6$/ft, sphere-cone, 10-mil weave with seam. 184
Figure 177. Test 7070, Run 55: $Re_\infty = 1.0\times10^6$/ft, sphere-cone, 15-mil weave with seam. 185
Figure 178. Test 7070, Run 61: $Re_\infty = 2.0\times10^6$/ft, sphere-cone, 15-mil weave with seam. 185
Figure 179. Test 7070, Run 60: $Re_\infty = 3.0\times10^6$/ft, sphere-cone, 15-mil weave with seam. 186
Figure 180. Test 7070, Run 57: $Re_\infty = 5.0\times10^6$/ft, sphere-cone, 15-mil weave with seam. 186
Figure 181. Test 7070, Run XX: $Re_\infty = 5.3\times10^6$/ft, sphere-cone, 15-mil weave with seam. 187
Figure 182. Test 7070, Run 56: $Re_\infty = 6.5\times10^6$/ft, sphere-cone, 15-mil weave with seam. 187
Figure 183. Test 7070, Run 59: $Re_\infty = 6.8\times10^6$/ft, sphere-cone, 15-mil weave with seam. 188
Figure 184. Test 7070, Run 54: $Re_\infty = 7.3\times10^6$/ft, sphere-cone, 15-mil weave with seam. 188
Figure 185. Test 7070, Run 58: $Re_\infty = 7.7\times10^6$/ft, sphere-cone, 15-mil weave with seam. 189
Figure 186. Test 7070, Run 53: $Re_\infty = 8.2\times10^6$/ft, sphere-cone, 15-mil weave with seam. 189
Figure 187. Test 7070, Run 80: $Re_\infty = 1.0\times10^6$/ft, sphere-cone, 20-mil weave with seam. 190
Figure 188. Test 7070, Run 81: $Re_\infty = 2.0\times10^6$/ft, sphere-cone, 20-mil weave with seam. 190
Figure 189. Test 7070, Run 79: $Re_\infty = 3.0\times10^6$/ft, sphere-cone, 20-mil weave with seam. 191
Figure 190. Test 7070, Run 78: $Re_\infty = 5.0\times10^6$/ft, sphere-cone, 20-mil weave with seam. 191
Figure 191. Test 7070, Run XX: $Re_\infty = 5.3\times10^6$/ft, sphere-cone, 20-mil weave with seam. 192
Figure 192. Test 7070, Run XX: $Re_\infty = 6.5\times10^6$/ft, sphere-cone, 20-mil weave with seam. 192
Figure 193. Test 7070, Run 77: $Re_\infty = 6.8\times10^6$/ft, sphere-cone, 20-mil weave with seam. 193
Figure 194. Test 7070, Run XX: $Re_\infty = 7.3\times10^6$/ft, sphere-cone, 20-mil weave with seam. 193
Figure 195. Test 7070, Run 75: $Re_\infty = 7.6\times10^6$/ft, sphere-cone, 20-mil weave with seam. 194
Figure 196. Test 7070, Run 76: $Re_\infty = 8.2\times10^6$/ft, sphere-cone, 20-mil weave with seam. 194
Figure 197. Test 7070, Run 25: $Re_\infty = 1.0\times10^6$/ft, spherical-cap, smooth OML. 196
Figure 198. Test 7070, Run 26: $Re_\infty = 2.0\times10^6$/ft, spherical-cap, smooth OML. 196
Figure 199. Test 7070, Run 27: $Re_\infty = 3.0\times10^6$/ft, spherical-cap, smooth OML. 197
Figure 200. Test 7070, Run 28: $Re_\infty = 5.0\times10^6$/ft, spherical-cap, smooth OML. 197
Figure 201. Test 7070, Run XX: $Re_\infty = 5.3\times10^6$/ft, spherical-cap, smooth OML. 198
Figure 202. Test 7070, Run 29: $Re_\infty = 6.5\times10^6$/ft, spherical-cap, smooth OML. 198
Figure 203. Test 7070, Run 91: $Re_\infty = 6.8\times10^6$/ft, spherical-cap, smooth OML. 199
Figure 204. Test 7070, Run 30: $Re_\infty = 7.3\times10^6$/ft, spherical-cap, smooth OML. 199
Figure 205. Test 7070, Run 96: $Re_\infty = 7.7\times10^6$/ft, spherical-cap, smooth OML. 200
Figure 206. Test 7070, Run 31: $Re_\infty = 8.2\times10^6$/ft, spherical-cap, smooth OML. 200
Figure 207. Test 7074, Run 68: $Re_\infty = 1.0\times10^6$/ft, spherical-cap, 5-mil weave. 201
Figure 208. Test 7074, Run 69: $Re_\infty = 2.0\times10^6$/ft, spherical-cap, 5-mil weave. 201
Figure 209. Test 7074, Run 70: $Re_\infty = 3.0\times10^6$/ft, spherical-cap, 5-mil weave. 202
Figure 210. Test 7074, Run XX: $Re_\infty = 5.0\times10^6$/ft, spherical-cap, 5-mil weave. 202
Figure 211. Test 7074, Run 66: $Re_\infty = 5.3\times10^6$/ft, spherical-cap, 5-mil weave. 203
Figure 212. Test 7074, Run XX: $Re_\infty = 6.5\times10^6$/ft, spherical-cap, 5-mil weave. 203
Figure 213. Test 7074, Run 67: $Re_\infty = 6.8\times10^6$/ft, spherical-cap, 5-mil weave. 204
Figure 214. Test 7074, Run XX: $Re_\infty = 7.2\times10^6$/ft, spherical-cap, 5-mil weave. 204
Figure 215. Test 7074, Run 71: $Re_\infty = 7.7\times10^6$/ft, spherical-cap, 5-mil weave. 205
Figure 216. Test 7074, Run 72: $Re_\infty = 8.2\times10^6$/ft, spherical-cap, 5-mil weave. 205
Figure 217. Test 7074, Run XX: $Re_\infty = 1.0\times10^6$/ft, spherical-cap, 10-mil weave. 206
Figure 218. Test 7074, Run 55: $Re_\infty = 2.0\times10^6$/ft, spherical-cap, 10-mil weave. 206
Figure 219. Test 7074, Run 50: $Re_\infty = 3.0\times10^6$/ft, spherical-cap, 10-mil weave. 207
Figure 220. Test 7074, Run XX: $Re_\infty = 5.0\times10^6$/ft, spherical-cap, 10-mil weave. 207
Figure 221. Test 7074, Run 51: $Re_\infty = 5.3\times10^6$/ft, spherical-cap, 10-mil weave. 208

Figure 222. Test 7074, Run XX: $Re_\infty = 6.5\times10^6$/ft, spherical-cap, 10-mil weave. 208
Figure 223. Test 7074, Run 52: $Re_\infty = 6.8\times10^6$/ft, spherical-cap, 10-mil weave. 209
Figure 224. Test 7074, Run XX: $Re_\infty = 7.3\times10^6$/ft, spherical-cap, 10-mil weave. 209
Figure 225. Test 7074, Run 53: $Re_\infty = 7.8\times10^6$/ft, spherical-cap, 10-mil weave. 210
Figure 226. Test 7074, Run 54: $Re_\infty = 8.2\times10^6$/ft, spherical-cap, 10-mil weave. 210
Figure 227. Test 7074, Run 78: $Re_\infty = 1.0\times10^6$/ft, spherical-cap, 15-mil weave. 211
Figure 228. Test 7074, Run 79: $Re_\infty = 2.0\times10^6$/ft, spherical-cap, 15-mil weave. 211
Figure 229. Test 7074, Run 77: $Re_\infty = 3.0\times10^6$/ft, spherical-cap, 15-mil weave. 212
Figure 230. Test 7074, Run XX: $Re_\infty = 5.0\times10^6$/ft, spherical-cap, 15-mil weave. 212
Figure 231. Test 7074, Run 73: $Re_\infty = 5.3\times10^6$/ft, spherical-cap, 15-mil weave. 213
Figure 232. Test 7074, Run XX: $Re_\infty = 6.5\times10^6$/ft, spherical-cap, 15-mil weave. 213
Figure 233. Test 7074, Run 74: $Re_\infty = 6.8\times10^6$/ft, spherical-cap, 15-mil weave. 214
Figure 234. Test 7074, Run XX: $Re_\infty = 7.3\times10^6$/ft, spherical-cap, 15-mil weave. 214
Figure 235. Test 7074, Run 75: $Re_\infty = 7.7\times10^6$/ft, spherical-cap, 15-mil weave. 215
Figure 236. Test 7074, Run 76: $Re_\infty = 8.2\times10^6$/ft, spherical-cap, 15-mil weave. 215
Figure 237. Test 7074, Run 42: $Re_\infty = 1.0\times10^6$/ft, spherical-cap, 20-mil weave. 216
Figure 238. Test 7074, Run 41: $Re_\infty = 2.0\times10^6$/ft, spherical-cap, 20-mil weave. 216
Figure 239. Test 7074, Run 40: $Re_\infty = 3.0\times10^6$/ft, spherical-cap, 20-mil weave. 217
Figure 240. Test 7074, Run XX: $Re_\infty = 5.0\times10^6$/ft, spherical-cap, 20-mil weave. 217
Figure 241. Test 7074, Run 39: $Re_\infty = 5.3\times10^6$/ft, spherical-cap, 20-mil weave. 218
Figure 242. Test 7074, Run XX: $Re_\infty = 6.5\times10^6$/ft, spherical-cap, 20-mil weave. 218
Figure 243. Test 7074, Run 43: $Re_\infty = 6.8\times10^6$/ft, spherical-cap, 20-mil weave. 219
Figure 244. Test 7074, Run XX: $Re_\infty = 7.3\times10^6$/ft, spherical-cap, 20-mil weave. 219
Figure 245. Test 7074, Run 45: $Re_\infty = 7.6\times10^6$/ft, spherical-cap, 20-mil weave. 220
Figure 246. Test 7074, Run 46: $Re_\infty = 8.2\times10^6$/ft, spherical-cap, 20-mil weave. 220
Figure 247. Test 7070, Run 38: $Re_\infty = 1.0\times10^6$/ft, spherical-cap, 5-mil weave with seam. 221
Figure 248. Test 7070, Run 37: $Re_\infty = 2.0\times10^6$/ft, spherical-cap, 5-mil weave with seam. 221
Figure 249. Test 7070, Run 36: $Re_\infty = 3.0\times10^6$/ft, spherical-cap, 5-mil weave with seam. 222
Figure 250. Test 7070, Run 32: $Re_\infty = 5.0\times10^6$/ft, spherical-cap, 5-mil weave with seam. 222
Figure 251. Test 7070, Run XX: $Re_\infty = 5.3\times10^6$/ft, spherical-cap, 5-mil weave with seam. 223
Figure 252. Test 7070, Run 33: $Re_\infty = 6.5\times10^6$/ft, spherical-cap, 5-mil weave with seam. 223
Figure 253. Test 7070, Run 67: $Re_\infty = 6.8\times10^6$/ft, spherical-cap, 5-mil weave with seam. 224
Figure 254. Test 7070, Run 34: $Re_\infty = 7.2\times10^6$/ft, spherical-cap, 5-mil weave with seam. 224
Figure 255. Test 7070, Run 66: $Re_\infty = 7.7\times10^6$/ft, spherical-cap, 5-mil weave with seam. 225
Figure 256. Test 7070, Run 35: $Re_\infty = 8.2\times10^6$/ft, spherical-cap, 5-mil weave with seam. 225
Figure 257. Test 7070, Run XX: $Re_\infty = 1.0\times10^6$/ft, spherical-cap, 10-mil weave with seam. 226
Figure 258. Test 7070, Run XX: $Re_\infty = 2.0\times10^6$/ft, spherical-cap, 10-mil weave with seam. 226
Figure 259. Test 7070, Run XX: $Re_\infty = 3.0\times10^6$/ft, spherical-cap, 10-mil weave with seam. 227
Figure 260. Test 7070, Run XX: $Re_\infty = 5.0\times10^6$/ft, spherical-cap, 10-mil weave with seam. 227
Figure 261. Test 7070, Run XX: $Re_\infty = 5.3\times10^6$/ft, spherical-cap, 10-mil weave with seam. 228
Figure 262. Test 7070, Run XX: $Re_\infty = 6.5\times10^6$/ft, spherical-cap, 10-mil weave with seam. 228
Figure 263. Test 7070, Run XX: $Re_\infty = 6.8\times10^6$/ft, spherical-cap, 10-mil weave with seam. 229
Figure 264. Test 7070, Run XX: $Re_\infty = 7.3\times10^6$/ft, spherical-cap, 10-mil weave with seam. 229
Figure 265. Test 7070, Run XX: $Re_\infty = 7.8\times10^6$/ft, spherical-cap, 10-mil weave with seam. 230
Figure 266. Test 7070, Run XX: $Re_\infty = 8.2\times10^6$/ft, spherical-cap, 10-mil weave with seam. 230
Figure 267. Test 7070, Run 82: $Re_\infty = 1.0\times10^6$/ft, spherical-cap, 15-mil weave with seam. 231
Figure 268. Test 7070, Run 83: $Re_\infty = 2.0\times10^6$/ft, spherical-cap, 15-mil weave with seam. 231
Figure 269. Test 7070, Run 84: $Re_\infty = 3.0\times10^6$/ft, spherical-cap, 15-mil weave with seam. 232
Figure 270. Test 7070, Run 85: $Re_\infty = 5.0\times10^6$/ft, spherical-cap, 15-mil weave with seam. 232
Figure 271. Test 7070, Run XX: $Re_\infty = 5.3\times10^6$/ft, spherical-cap, 15-mil weave with seam. 233
Figure 272. Test 7070, Run XX: $Re_\infty = 6.5\times10^6$/ft, spherical-cap, 15-mil weave with seam. 233
Figure 273. Test 7070, Run 86: $Re_\infty = 6.8\times10^6$/ft, spherical-cap, 15-mil weave with seam. 234
Figure 274. Test 7070, Run XX: $Re_\infty = 7.3\times10^6$/ft, spherical-cap, 15-mil weave with seam. 234
Figure 275. Test 7070, Run 87: $Re_\infty = 7.7\times10^6$/ft, spherical-cap, 15-mil weave with seam. 235
Figure 276. Test 7070, Run 88: $Re_\infty = 8.2\times10^6$/ft, spherical-cap, 15-mil weave with seam. 235
Figure 277. Test 7070, Run 71: $Re_\infty = 1.0\times10^6$/ft, spherical-cap, 20-mil weave with seam. 236

Figure 278. Test 7070, Run 72: $Re_\infty = 2.0\times10^6$/ft, spherical-cap, 20-mil weave with seam. 236
Figure 279. Test 7070, Run 68: $Re_\infty = 3.0\times10^6$/ft, spherical-cap, 20-mil weave with seam. 237
Figure 280. Test 7070, Run 69: $Re_\infty = 5.0\times10^6$/ft, spherical-cap, 20-mil weave with seam. 237
Figure 281. Test 7070, Run XX: $Re_\infty = 5.3\times10^6$/ft, spherical-cap, 20-mil weave with seam. 238
Figure 282. Test 7070, Run XX: $Re_\infty = 6.5\times10^6$/ft, spherical-cap, 20-mil weave with seam. 238
Figure 283. Test 7070, Run 70: $Re_\infty = 6.8\times10^6$/ft, spherical-cap, 20-mil weave with seam. 239
Figure 284. Test 7070, Run XX: $Re_\infty = 7.3\times10^6$/ft, spherical-cap, 20-mil weave with seam. 239
Figure 285. Test 7070, Run 73: $Re_\infty = 7.6\times10^6$/ft, spherical-cap, 20-mil weave with seam. 240
Figure 286. Test 7070, Run 74: $Re_\infty = 8.2\times10^6$/ft, spherical-cap, 20-mil weave with seam. 240

Abstract

An experimental investigation of woven thermal protection system material surface roughness effects on boundary-layer transition and turbulent heating has been performed at hypersonic test conditions. Two representative entry vehicle geometries, a sphere-cone aeroshell and a spherical-cap aeroshell, were considered. Cast ceramic models of each geometry were fabricated with surface textures that simulated a woven thermal protection material and aeroheating and boundary-layer transition onset data were obtained on these models using global phosphor thermography. Wind tunnel testing was performed at Mach 6 over a range of Reynolds numbers sufficient to produce laminar, transitional, and turbulent flow. The experimental heating and boundary-layer transition data are presented herein, as are comparisons to laminar and turbulent smooth-wall heat transfer distributions from computational flow field simulations. The boundary-layer transition data were found to correlate with a functional representation developed in prior roughness studies. However, a shift in the correlation curve indicates the need for a comprehensive analysis of roughness-height definitions for the current woven roughness data, as well as the sand-grain and hexcomb roughness datasets from which the correlation was developed.

Nomenclature

Symbols

D_T	thread diameter
H_0	tunnel total (reservoir) enthalpy
H_{300K}	wall enthalpy at 300 K
H_{AW}	adiabatic wall enthalpy
H_k	roughness height enthalpy
H_W	wall enthalpy
h	measured heat-transfer film coefficient
h_{FR}	Fay-Riddell theory heat-transfer film coefficient
h_T	thread peak height
k	roughness height correlation parameter
L_{PP}	thread peak-to-peak distance
M_e	boundary-layer edge Mach number
M_∞	free stream Mach number
q	heat transfer rate
R	model radius
R_N	model nose radius
R_C	model corner radius
R_T	thread radius
Re_{k+}	roughness height Reynolds number
Re_θ	boundary-layer momentum thickness Reynolds number
Re_∞	free stream unit Reynolds number
r_{stag}	approximate radius of edge Mach stagnation cutoff region
S_T	thread spacing
s	surface running length to edge Mach cutoff
s_0	surface running length from stagnation point
T_e	boundary-layer edge temperature
$T_{w,AVG}$	average wall temperature
T_∞	free stream temperature
U_e	boundary-layer velocity
U_τ	smooth-wall friction velocity
U_∞	free stream velocity
x, y, z	Cartesian coordinates
X_{TR}	transition correlation disturbance parameter
Y_{TR}	transition correlation flow field parameter
β_N	model spherical nose included angle
β_{POHL}	modified Pohlhausen parameter
δ	boundary layer thickness
ϕ	streamline angular coordinate identifier
ϕ_{corr}	heating calibration corrector factor
λ_{POHL}	Pohlhausen parameter
ν_e	boundary-layer edge kinematic viscosity
μ_w	wall viscosity
ρ_e	boundary-layer edge density

ρ_∞	free stream density
θ	boundary-layer momentum thickness

Subscripts and Superscripts

∞	wind tunnel free stream condition
0	wind tunnel stagnation or reservoir condition
e	boundary layer edge condition
k	roughness height condition
TR	transition location
w	model wall condition

Acronyms

CFD	Computational Fluid Dynamics
HEEET	Heatshield for Extreme Entry Environments Technology
IHEAT	Imaging for Hypersonic Experimental Aerothermodynamic Testing
LAL	Langley Aerothermodynamic Laboratories
LAURA	Langley Aerothermodynamic Upwind Relaxation Algorithm
OML	Outer Mold Line
3DMCP	Three-Dimensional Mid-Density Carbon Phenolic
TPS	Thermal Protection System

Introduction

This report serves to document an experimental dataset of woven material roughness effects on boundary-layer transition and heating augmentation. The data were obtained through hypersonic wind tunnel testing of two representative entry vehicle aeroshell geometries with roughness patterns that simulated a woven material thermal protection system (TPS). This report represents a reference document that can be used as the basis for future detailed analysis of the heat transfer distributions and boundary-layer transition onset locations measured in the test program.

This study is a direct follow-on to previous studies of ablated TPS with distributed sand-grain pattern roughness effects (Refs. [1-2]), hexcomb pattern roughness effects (Ref. [3]), and blocked TPS roughness effects (Refs. [4]). The same aeroshell geometries and test conditions used in those studies were also employed in this work to develop a consistent database of roughness effects on different types of thermal protection systems relevant to past, current, and future NASA missions.

Background

"Roughness" is a generic term in aerospace literature that encompasses many types of surface features that deviate from that of a smooth outer mold line (OML) surface. Roughness can be divided into two general types: discrete and distributed. Discrete roughness (Figure 1) includes surface features such as: a) protruding compression pads or recessed cavities at mechanical attachment points; b) steps or gaps between heat shield tiles or blocks resulting from differential ablation of the TPS and the filler material between them; and c) physical damage to a TPS. Distributed roughness (Figure 2) includes features such as: a) regular patterns resulting from ablation of hexcomb-structure TPS; b) deflections of a flexible TPS over its support structure when subjected to aerodynamic loading; c) random "sand-grain" features resulting from

ablation of a monolithic TPS; or d) the texture of overlapping fibers on a woven TPS.

Data on the effects of surface roughness are valuable because the roughness of an entry vehicle's TPS can promote earlier boundary-layer transition and produce higher turbulent heating (and shear) levels than would be expected based on an idealized, smooth-surface analysis. However, due to the complexities of roughness effects, a vehicle's TPS is typically designed using analytical, computational, and/or experimental techniques based on the assumption of a smooth surface. The effects of roughness on the aerothermodynamic environment are then included through approximate engineering correlations and methods.

The purpose of this test program was to obtain aerothermodynamic performance data on an entry system with a woven TPS material. An example of such material is the Three-Dimensional Mid-Density Carbon Phenolic (3DMCP) material [5] developed under the Heatshield for Extreme Entry Environments Technology (HEEET) program [6] that has been proposed for the Earth Entry System of a Mars Sample Return Mission. The data obtained in this test program are intended for use in the development and/or validation of engineering correlations for woven roughness transition and heating augmentation. These data can also serve as the basis for development and/or validation of higher-fidelity, numerical flow-field simulation models for roughness effects.

Experimental Tools and Methods

Wind Tunnel Models

Model Geometries

Roughness effects data were obtained on two representative entry vehicle geometries: a sphere-cone geometry (Figure 3) and a spherical-cap geometry (Figure 4). The sphere-cone geometry is representative of the Mars Viking – Mars Pathfinder – Mars Exploration Rover – Mars Phoenix – Mars Science Laboratory – Mars 2020 family of entry vehicles used in NASA's robotic Mars exploration missions. The spherical-cap geometry is representative of the Mercury – Gemini – Apollo – Orion family of entry vehicles employed in NASA's crewed space program. Geometric parameters for both model configurations are listed in Table 1. Multiple wind tunnel models of each configuration were fabricated with a woven TPS patterns of various heights, as detailed below. The geometries are identical to those of the previous studies [2-4] except for the surface roughness type used in this program.

Woven TPS Patterns

Surface textures representative of a woven TPS (such as 3DMCP) were applied to the surfaces of the two geometries. The woven TPS was represented as a mesh of intersecting "threads" as illustrated by the two-dimensional representation in Figure 5. Each thread is represented as a circular cross-section extruding along a sinusoidal trace, with the thread surfaces merging at the intersections. The pertinent parameters of the weave patterns, including spacing, peak-to-value periodicity and maximum texture height above waterline (the underlying outer mold line), are all represented in terms of the thread radius. Four nominal thread radii patterns were designed with peak heights of 0.020, 0.015, 0.010 and 0.005 inches (20, 15, 10, 5 mil) and the parameters for these patterns are listed in Table 2.

To define weave patterns on the actual three-dimensional wind tunnel model geometries, the two-dimensional textures were conformally projected onto the model surface. To prevent excessive deformation of the weave dimensions, the weave was split into eight "petals" arranged around a circular nose segment.

Surface were generated both with and without a "seam" that represented the stitching between petals of an actual TPS material layout. The seams had an elliptical cross section with major and minor axes dimensions of 0.030 inches and 0.010 inches (3 mil and 10 mil), respectively. Examples of surface scans of wind tunnel models with and without seams between the petals are shown in Figure 6 for a sphere-cone with 20-mil weave with seams and Figure 7 for a sphere-cone with 20-mil weave without seams.

Model Fabrication

Ceramic wind models for use with global phosphor thermography were fabricated both geometries with each of the four weave heights both with and without seams between the petals. The fabrication process for ceramic models is discussed in detail in Ref. [7]. The first step in fabrication of a smooth-surface model is the production of a rapid-prototype pattern of the geometry using a 3D wax printing machine. Investment casting is then used to make a mold from the pattern. A thin-shell silica ceramic model is then slip-cast from the mold, dried and sintered. The shell is then backfilled with a hydraulically setting magnesia ceramic for strength and support and mounted on a stainless-steel support sting. Finally, the model is coated with a mixture of phosphors that luminesce under ultraviolet lighting and fiducial marks are placed at specified locations on the surface for image registration.

Sample photographs of cast ceramic sphere-cone and spherical-cap roughness models are shown in Figure 8 and Figure 9, respectively. Large weave-height photographs are provided here because the photographic image contrast and resolution were generally not sufficient to display the smaller height weave patterns. However, all the weave heights did produce measurable effects on boundary-layer transition and surface heating

Wind Tunnel Test Facility

Facility Description

Hypersonic wind tunnel testing of the woven sur models was performed in the NASA Langley Aerothermodynamics Laboratory (LAL) 20-Inch Mach 6 Air Tunnel. This wind tunnel is described in brief below and more detailed information on the LAL facilities can be found in Refs. [8–9].

The 20-Inch Mach 6 Air Tunnel (Figure 10 – Figure 11) is a blow-down facility in which heated, dried, and filtered air is used as the test gas. The tunnel has a two-dimensional contoured nozzle that opens into a 20.5 in. × 20.0 in. test section. The tunnel is equipped with a bottom-mounted injection system with a -5-deg to +55-deg pitch range and ±5-deg yaw range that can transfer a model from a sheltered model box to the tunnel centerline in less than 0.5 sec. Run times of up to 15 minutes are possible in this facility, although for the current aeroheating study, run times of only a few seconds were required. The nominal reservoir conditions of this facility produce perfect-gas free stream flows with Mach numbers between 5.8 and 6.1 and unit Reynolds numbers of 0.5×10^6/ft to 8.3×10^6/ft. With its wide Reynolds number operating range capable of producing laminar, transitional, or turbulent flow on most geometries, this tunnel is primarily used for heat-transfer and boundary-layer transition studies.

Facility Operating Conditions and Test Matrices

Data were obtained in Tests 7070 and 7074 in the 20-Inch Mach 6 Air Tunnel at multiple unit-Reynolds number test conditions ranging from $Re_\infty = 1.0\times10^6$/ft to 8.2×10^6/ft with nominal free stream conditions listed in Table 3. The initial test plan called for repeating the same model angles of attack (α = 16 deg for

the sphere-cone and α = 28 deg for the spherical-cap) and the same Reynolds number points as in the previous [3-4] roughness studies. However, as will be detailed later, for Reynolds number points above 5×10^6/ft, temperatures on the woven surface roughness models began to exceed the operational limits of the global phosphor thermography system, leading to data loss. Therefore, new conditions for the higher Reynolds number points were employed that would prevent this data loss by reducing the reservoir stagnation temperature while maintaining the reservoir stagnation pressure to produce approximately the same freestream Reynolds number. These new and old operating points are shown in Figure 12 and are tabulated in Table 3 and Table 4 with the new conditions identified by the '-alt' suffix.

A total of 179 runs were conducted in these test programs. Run matrices for each model geometry (sphere-cone and spherical-cap) and roughness type (smooth, weave with seams and weave without seams) are given in Table 5 through Table 10. Entries in these tables are sorted first by weave height, then by free stream unit Reynolds number. Free stream velocity (U_∞), density (ρ_∞), temperature (T_∞), unit Reynolds number (Re_∞), and Mach number (M_∞) are provided in these tables. Additionally, an average model surface temperature (T_w), enthalpy difference (ΔH_{tot}), and reference heat transfer film-coefficient value (h_{FR}) are provided. The temperature is the average over the model surface when the thermographic phosphor image was obtained and is provided because boundary-layer transition is known to be sensitive to wall temperature. The enthalpy term is defined as the difference $H_0 - H_{300K}$ between the free stream total enthalpy and the wall enthalpy at cold wall (300 K) conditions. The film coefficient is the value from the Fay-Riddell theory (Ref. [10]) at cold wall conditions, where the radius is the nose radius of the model geometry.

Experimental Data

Data Acquisition and Reduction

Aeroheating data were obtained using the two-color, relative-intensity, global phosphor thermography method (Ref. [11]) and reduced using the IHEAT (Imaging for Hypersonic Experimental Aerothermodynamic Testing) code (Refs. [12–13]). In this method, a model is illuminated by ultraviolet light sources that induce temperature-dependent fluorescence of the phosphor coating. Fluorescent intensity images of a model are taken in the tunnel before and during a run using a three-color, charge-coupled device camera and the images are processed to determine heat-transfer distributions. The intensity data are then converted to temperatures using pretest calibrations of the data acquisition system.

Heat-transfer film coefficients are determined by assuming a step function in the film coefficient from the prerun temperature to the run temperature, which corresponds to a parabolic temperature-time history. The heating data are reported in terms of the ratio h/h_{FR} where the heat-transfer film coefficient, h, is defined in terms of enthalpy as:

$$\boldsymbol{h = q/\Delta H_{TOT} = q/(H_{AW} - H_w) = q/(H_0 - H_w)} \quad (1)$$

In the calculation of the heat-transfer film coefficient, it is assumed that for a blunt-body, the adiabatic wall enthalpy H_{AW} is equal to the free stream total enthalpy of the tunnel, H_0, and the wall enthalpy H_W is the determined from the surface temperature at each image pixel. This heat transfer coefficient definition provides a theoretically near-constant value over the course of a run since the decrease in time of the heat transfer rate in the numerator as the model surface becomes hotter is balanced by the decrease of the enthalpy-difference term in the denominator.

Data Mapping and Presentation

The two-dimensional (2-D) image data output from IHEAT (Figure 13) for each run were transformed to account for optical perspective effects and mapped to a three-dimensional (3-D) CAD surface of the wind tunnel model (Figure 14). To accomplish this mapping, perspective, translational, and rotational transformations were first performed on the 3-D CAD surface until its 2-D projection matched that of the 2-D image data. The image data were then assigned transformed (x, y, z) coordinates based on interpolation between the image and projected surface geometry. Finally, the transformation was inverted to obtain an orthographic, 3-D heating distribution map of the experimental data.

An additional data manipulation was performed to extract the streamline-based heating distributions from the mapped wind tunnel data set. These streamline-based data sets are used in boundary-layer transition analyses and for comparisons of Reynolds number and roughness effects. For each run, streamlines were defined based on the boundary-layer edge velocity vectors from the computed flow fields (to be discussed in the next section). Thirty-six streamline termini were established at locations spaced in 10-deg increments around the circumference of the geometry and the streamlines were then traced backward from each terminus toward the flow field stagnation point. Each streamline is identified by the angular location, ϕ, of its terminus. The resulting streamlines are shown in Figure 15 for the sphere-cone geometry and in Figure 16 for the spherical-cap geometry. The geometric (x, y, z) coordinates along each streamline were then interpolated onto the 3-D mapped image and h/h_{FR} heating data were extracted along each streamline in terms of s_0/R, which is the normalized streamline distance from the stagnation point. Additionally, the predicted flow field quantities (boundary-layer height, momentum-thickness Reynolds number, etc.) were also extracted along these streamlines and combined with the wind tunnel data set to enable transition onset analyses.

One additional complication needs to be noted with respect to extraction of data along streamlines. The extraction algorithm tended to fail near the stagnation point where the velocity vectors approached zero; essentially, the physical location became indeterminate, resulting in unreliable path-lengths through the stagnation region. This problem was resolved by stopping the reverse tracing of the streamlines from the outer edge of the model toward that stagnation point at the location where the edge Mach number, M_e, dropped below 0.025. The "true" streamline length value, s_0 was determined from an estimate of the physical length from the M_e cutoff to the stagnation region as a function of the streamline terminus angular location ϕ and the approximate radius of the stagnation region, r_{stag}:

$$\boldsymbol{s_0 = s + \Delta s} \tag{2}$$

$$\boldsymbol{\Delta s = cos(2\phi) \times r_{stag}/3 + r_{stag}} \text{ , where } \boldsymbol{r_{stag} \cong 0.003\ m} \tag{3}$$

In the body of this report, plotted data will be shown in terms of s/R, as that is the quantity in which the data were extracted along streamlines. The estimated actual distance, s_0/R, can be determined using Eqs. (2) and (3).

The mapped data from all runs are collected in the Appendices and presented therein as large, high-resolution images. These images are ordered by model geometry, roughness height, and Reynolds numbers. Smaller images will be shown in the body of the report along with streamline-based heating distributions.

Phosphor Thermography Data Quality

An important factor that influences the quality of phosphor thermography data quality is the local surface inclination at a given point on the model with respect to both the camera and the UV lights. Phosphor thermography provides the best results when the surface to be imaged is normal to the camera, which reduces perspective distortion and image smearing, and when the surface is well illuminated, which induces the best temperature response of the phosphor coating. Because of the three-dimensional nature of a wind tunnel model, the entire surface of a model cannot be optimally imaged, or in some cases cannot even be viewed. For blunt bodies such as those in this test, the windward centerline region of the model – the 'bottom' of the model with respect to the view orientation - is the area where the data quality is most affected. This situation is illustrated for a simple hemispherical model in Figure 17. Because of this limitation, windward region data are only regarded as qualitative, not quantitative. Although image data from this region will be shown, quantitative plotted data and transition location data will not be provided for the streamlines originating from the ϕ = 160-deg through 200-deg termini.

Heat Transfer Data Uncertainty

The experimental uncertainty for convective heat transfer measurements on a *smooth, blunt body geometry* model in the 20-Inch Mach 6 Air Tunnel is quantified as a function of net uncertainties resulting from: the data acquisition method (±10%); flow quality and test-condition repeatability (±5%); and the accuracy of the 3D mapping process (±10%), which results in an overall root-sum-squared value of ±15%. Experience with this technique indicates that these values are usually conservative and agreement between laminar, smooth-wall measured and predicted heating levels is generally well within this range.

Calibration Correction for Heat Transfer Data

A central premise in the analysis of wind tunnel heating data is that for a given Mach number, the normalized heat transfer film coefficient, h/h_{FR}, at any point on a geometry remains constant with varying Reynolds number at perfect gas conditions for attached flow over a blunt body. This behavior is demonstrated through CFD simulations for a 2-inch diameter hemisphere over the current range of test conditions. As shown in Figure 18, laminar simulations using the LAURA code (see section below on Computational Tools and Methods) predict a constant value of h/h_{FR} = 1.06 at the hemisphere stagnation point for all test condition Reynolds numbers. The fact that the ratio is not exactly 1 is due to the differences between a modern CFD prediction for the film coefficient at perfect-gas wind tunnel conditions and the semiempirical Fay-Riddell correlation for the film coefficient based on approximate boundary-layer solutions for reacting-gas flight conditions. That the two predictions are so close is a testament to the utility of the original Fay-Riddell method that was developed in the 1950s.

While the CFD predictions do indeed demonstrate a constant value of h/h_{FR} for the wind tunnel conditions, the same behavior is generally not observed during in the experimental data; instead, a dependency on free stream Reynolds number is frequently observed. This dependency is illustrated in Figure 19 by stagnation point heating data from pretest checkout and calibration runs on a phosphor-coated, 2 inch radius hemisphere. Instead of a constant value for h/h_{FR}, the measured values were observed to be at or below the predicted values, depending on Reynolds number. A second-order polynomial fit to the measured heating values that reflect this variation is also shown on the plot.

There are several potential sources of uncertainty which could be producing this dependency including: variations in the bulk materials used to cast the ceramic wind tunnel models; the consistency of the thermographic phosphor mixture used to coat the models; the fidelity of the phosphor intensity/temperature

calibrations; degradation of the UV lighting or imaging camera; and/or the flow quality of the wind tunnel. It was beyond the scope of this study to resolve whether any, or all, of these factors influenced the experimental data; rather a post-test calibration correction to the test data was generated using the results of the hemisphere checkout runs.

Because the differences in predicted and measured stagnation point film-coefficient ratios fell within the estimated uncertainty of ±15% range cited in the previous section, these results could be considered "acceptable" from an experimental perspective. However, because the differences can be represented by a Reynolds number dependent bias function, as opposed to a random dispersion, an additional data processing step was conducted to calibrate the heating data based on the hemisphere data. The original data were modified using the polynomial curve fits as per Eqs. (4) through (6). This procedure is now commonly employed to provide an *in-situ* calibration of thermographic phosphor data.

However, while this calibration has been employed successfully to remove the Reynolds number dependency in previous studies, the results were unsatisfactory for many of the models used in the current study. A clear offset was observed between the calibrated sphere-cone and spherical cap model comparisons to laminar predictions as well as with a large volume of data on these geometries from multiple previous test programs. This offset was traced to the time frame in which the models were fabricated: because of delays in the facility schedule (largely due to a backlog resulting from site access restrictions during the COVID pandemic), the spherical-cap wind tunnel models were left in storage for more than six months, whereas the sphere-cone models were fabricated within approximately a month of the test program. Phosphor coatings are known to degrade over time and the use of such old models is contra-indicated. Unfortunately, the procurement budget for this test program did not permit the fabrication of a new set of spherical-cap models, so the existing old models were employed "as-is". Through comparisons with archival data and laminar predictions, a correction factor (β_{age}) was determined to account for the degradation of the spherical-cap model phosphor coatings and applied as per Eq. (7). Sample plots showing the difference between uncalibrated and calibrated data are provided in Figure 20 for the sphere-cone geometry and Figure 21 for the spherical cap geometry. All data and results presented herein reflect these calibration corrections.

$$(\boldsymbol{h/h_{FR}})_{exp,corr} = (\boldsymbol{h/h_{FR}})_{exp} \times (\boldsymbol{h_{CFD}/h_{FR}})_{hemi-stag} \times \emptyset_{corr} \tag{4}$$

$$(\boldsymbol{h_{CFD}/h_{FR}})_{hemi-stag} = \mathbf{1.06} \tag{5}$$

$$\emptyset_{corr} = \mathbf{1}/(\boldsymbol{A} + \boldsymbol{Bx} + \boldsymbol{Cx^2}), \text{ and } \boldsymbol{x} = \boldsymbol{Re_\infty}/\mathbf{1,000,000}, \text{ where:}$$
$$\boldsymbol{A} = \mathbf{0.8016}$$
$$\boldsymbol{B} = \mathbf{0.0849} \tag{6}$$
$$\boldsymbol{C} = -\mathbf{0.0075}$$

$$(\boldsymbol{h/h_{FR}})_{exp,age-corr} = (\boldsymbol{h/h_{FR}})_{exp,corr} \times \boldsymbol{\beta_{age}}, \text{ where}$$
$$\boldsymbol{\beta_{age}} = \begin{Bmatrix} \mathbf{1.00} & \text{"new" sphere-cone models} \\ \mathbf{0.89} & \text{"old" spherical-cap models} \end{Bmatrix} \tag{7}$$

Computational Tools and Methods

Flow field solutions were generated using the LAURA (Langley Aerothermodynamic Upwind Relaxation Algorithm) code. LAURA (Refs. [14–15]) is a three-dimensional, structured-grid, finite-volume solver that includes perfect-gas and nonequilibrium chemistry options, a variety of turbulence models, and ablation and radiative transport capabilities. LAURA solutions were used for comparisons of predicted heating levels with the measured data and to define the streamlines along which to extract the mapped experimental data, as described above.

Solutions were computed on multiblock grids of each geometry with a smooth (no woven roughness) outer mold line. Grid adaption was performed to align the grid outer boundary with the bow shock and to cluster cells near the surface to produce wall cell Reynolds numbers on the order of 1 to 10. Free stream conditions were set to the nominal wind tunnel conditions for each operating point as given in Table 3. For these wind tunnel conditions, the perfect-gas air option was used. Both laminar and turbulent solutions were generated. Turbulent cases were computed using the Cebeci-Smith algebraic model with fully turbulent flow over the entire geometry. Because the computations were performed on a smooth geometry, they are not quantitively applicable to the actual wind tunnel tests performed on rough-surface models with heating augmentation but are still provided for qualitative comparisons.

For the wall temperature boundary condition, a change in the normal practice for wind tunnel simulations of setting this value to a "cold-wall" ambient temperature (because of the small variation in heat-transfer coefficient with temperature) was employed. Literature on roughness effects indicates a dependence of transition onset location on the ratio of boundary-layer edge temperature to wall temperature T_e/T_w. To approximately account for this effect (which was expected to be small, but non-negligible, for these test conditions), the computations were performed using a uniform "hot-wall" wall temperature set to the average of the measured surface temperature on the model. These values varied between ~ 325 K to 410 K, depending on roughness height and Reynolds number.

The flow field solutions also provided boundary-layer parameters that can be used in the correlation of transition and heating augmentation data. Centerline profiles of selected boundary-layer parameters are presented to provide insight into the range of the test data and potential relevance to flight missions.

The ratio of the physical roughness height to that of the boundary-layer, k/δ, has a first-order influence on transition onset. Centerline distributions of k/δ are presented in Figure 22 for the sphere-cone geometry and in Figure 23 for the spherical-cap geometry for the range of roughness heights and free stream Reynolds number conditions. In these figures, k is the weave roughness height and δ is the physical height of the boundary layer. Values of k/δ varied over two orders of magnitude depending on roughness height and Reynolds numbers. The smallest k/δ values are within the boundary layer, while the highest exceed the boundary layer height.

The turbulent roughness height Reynolds number, Re_{k+} as per Eq. (8), can be used as a correlation parameter for turbulent roughness heating augmentation. Centerline distributions of Re_{k+} are presented in Figure 24 and Figure 25 for the sphere-cone geometry and spherical-cap geometries, respectively, for the range of roughness heights and free stream Reynolds number conditions. Values of Re_{k+} also vary over two orders of magnitude, indicative of laminar flow at the lowest levels and roughness-augmented turbulent flow at the highest levels.

$$Re_{k+} = \rho_w U_\tau k_{PV50}/\mu_w, \text{ where } U_\tau = \sqrt{\tau_w/\rho_w} \quad (8)$$

Experimental Data Analysis

Transition Onset Location Definition

From a flow physics standpoint, transition onset is defined as the point where smooth, laminar flow in the boundary layer begins to break down into small eddies. This location can, in theory, be determined through flow field imaging and/or diagnostic techniques (e.g., high-frequency pressure measurements, laser velocimetry) to determine when fluctuations in a quantity of interest, such as the mean velocity, exceeded a specified criterion. However, in this study, the only measurements are of the surface temperature and (through data reduction) the surface heating. For such measurements, the differences in temperature or heating levels between laminar flow and transitional flow can be too subtle at some conditions to permit precise definition of the onset location. This measurement is more difficult when the local roughness height is small, in which case, the change from laminar to transitional/turbulent flow is gradual, but easier when the local roughness height is large, and the transition length is very short.

In lieu of a precise measurement of the transition location, transition onset is defined herein through a common approach in which an "effective" or "apparent" onset point is determined through the "tangent-slope-intercept" method. As shown in Figure 26, using sample data for a hemisphere from [1] , the effective transition onset location is identified as the point where a line drawn tangent to the slope of the heat-transfer distribution curve through the transition region intercepts the nominal, laminar level. While this method does not necessarily identify the precise location at which fluctuations in the boundary-layer flow begin, it is consistent with common practice for determining the roughness-induced transition location via surface-based measurement techniques. This method also permits a more consistent means of identifying a relevant transition parameter, since identification of the small rise in heating levels at the actual transition onset location would be highly susceptible to error through surface measurement techniques alone. If the data herein are compared to other datasets, then it will be necessary to ensure that the same definition of transition onset is applied to ensure consistency.

While this effective transition onset location is easy to define in principle, in practice, there can still be considerable uncertainty in determining the effects of roughness on transition location because of the difficulty in precisely defining the relevant roughness height. Consider again the distributed roughness hemisphere example, where now the heating data are shown in image form (Figure 27) rather than a plotted distribution. In the ideal case, where the surface roughness was invariant over the entire model surface, the transition onset location would be at a constant streamline length around the circumference of the model since the flow field is axisymmetric. However, as shown in Figure 27, there are clearly circumferential variations in the transition onset location. These variations occur because the local roughness height at any given location can vary from the nominal value for many reasons, including: the fidelity of the model fabrication process; the uniformity in application of the phosphor coating; and damage to the coating due to handling of the model or particle impacts during testing.

For an axisymmetric flow such as that over the example hemisphere, it was possible to reduce the uncertainty in the transition onset location by averaging multiple onset locations around the body to determine a mean value. This approach was followed for the hemispheres considered in [1]. However, for the three-dimensional flow fields produced by the geometries considered herein, that was not possible.

Thus, transition correlations drawn from this dataset can be expected to have greater scatter than those that were derived for axisymmetric geometries.

Reynolds Number Effects on Heating and Transition

The effects of Reynolds number on the heating levels and boundary-layer transition onset locations are illustrated for each woven roughness height pattern in Figure 28 through Figure 45 for the sphere-cone geometry and Figure 46 through Figure 63 for the spherical-cap geometry. Two figures are provided for each case: in the first figure, global heating images are shown for each Reynolds number, ordered left-to-right, top-to-bottom in terms of increasing Reynolds number; in the second figure, line plots of h/h_{FR} vs. s/R are shown, ordered left-to-right, top-to-bottom in terms of streamline angular coordinate. To maintain consistent formatting, blank images with "Run XX" titles are included even for test point combinations (Reynolds number, weave height, model geometry) which were not actually run due either to schedule limitations or to substation of the new "alternate" conditions in place of standard conditions.

For brevity and clarity, all the streamlines are not plotted in these figures. Instead, streamlines are shown at 30 deg increments from 0 deg to 150 deg. As noted earlier, the data for streamlines between 160 deg and 200 deg are considered qualitative, not quantitative, and were thus omitted. Data for streamlines from 210 deg to 360 deg are nominally symmetric with the data from 0 deg to 150 deg, although in practice, model surface irregularities can cause asymmetric behavior. Such local asymmetries can be observed in the images that accompany the line plots.

In these line-plots, the CFD predictions for smooth-wall, laminar and turbulent heating levels are also shown. Because the laminar heat-transfer film coefficient ratio, h/h_{FR}, remains nearly constant with Reynolds number, only the lowest Reynolds number laminar prediction is shown for each case. However, since this invariance does not hold for turbulent flow, turbulent predictions are shown for each Reynolds number. As noted previously, simulations for these cases were treated as fully turbulent flow over the entire geometry. These turbulent predictions are shown for qualitative comparisons only, since the actual transition occurred at different locations for each test condition / model geometry and since the turbulent heating levels were augmented above smooth-wall levels by the surface roughness.

Roughness Height Effects on Heating and Transition

The same data are shown in the next group of figures, but they are reordered to show the effects of the woven surface roughness height on transition and heating at each Reynolds number. The sphere-cone data are shown in Figure 64 through Figure 83 and the spherical-cap data are shown in Figure 84 through Figure 103. Again, two figures are provided for each case: in the first figure, global heating images are shown for each Reynolds number, ordered left-to-right, top-to-bottom in terms of increasing roughness height; in the second figure, line plots of h/h_{FR} vs. s/R are shown, ordered left-to-right, top-to-bottom in terms of streamline angular coordinate and blank figures titled "Run XX" for cases that were not run are included to maintain consistent page formatting. As with the Reynold number effects figure set, both laminar and turbulent CFD heating predictions are shown in each line plot. It is assumed that facility noise effects on transition are minimal in these data because the woven surface roughness promotes a "bypass transition" mode [16] that is separate from the small disturbance growth modes of conventional stability theory analyses.

General Reynolds Number and Roughness Height Trends

In these line plots for Reynolds number and roughness height effects, the laminar CFD predictions allow for baseline assessment of the computational accuracy through comparisons with the low Reynolds number, small roughness height cases for which transition did not occur. In general, good agreement between data and predictions was observed for all laminar cases. However, the turbulent predictions are shown only for illustrative purposes since the fully-turbulent, smooth-wall computations do not account for roughness effects on the transition location or heating augmentation above smooth-surface levels.

Reynolds-number and roughness-height effects on transition and heating follow expected trends. As Reynolds number is increased, the transition onset location moves upstream toward the stagnation point of the model. The transition onset location also moves upstream as roughness height is increased and the measured rough-wall turbulent heating levels grow increasingly higher than the predicted smooth-wall turbulent heating levels. The effects of the seams on transition were indeterminate. For the smallest weave height cases (5 mil), the fidelity of the ceramic casting was on the order of the weave size and thus the boundary-layer transition fronts were irregular for most cases with or without seams. For the large weave cases, the seam and the weave dimensions were of the same order and thus no additional effect of the weave was expected nor clearly identifiable in the data.

Roughness Heating Augmentation

In this report, analysis of the heating augmentation due to the roughness patterns is limited to the expected observation that heating levels increase with weave roughness height. This limitation is due to the complexities of the problem and the goal of quickly releasing this data set as a basis for further analysis. For any given roughness height / Reynolds number / body-point location, the heating augmentation with respect to smooth-wall laminar or turbulent predictions can be determined through reference to the data and figures presented herein. However, the development of engineering correlations or numerical models for simulation of these data depend on not just modeling the effects of roughness on heating, but also modeling the effects of roughness on transition onset; that is, it is not possible to accurately predict heating levels without being able to first predict the transition onset location. Implementation of a transition model into a CFD code and generation of transitional flow field solutions will be deferred to future in-depth analyses.

Transition Onset Data and Correlation

As per discussion above, transition locations (or lack thereof) were determined along each of 36 different streamlines for every run using the tangent-slope-intercept method. Discounting the windward streamline data from the ϕ = 160-deg through 200-deg rays with poor viewing angles and lighting, 4278 data points (138 runs × 31 rays/model) on the state of the boundary layer were obtained. Tabulations of these transition onset data for each streamline are given in Table 11 through Table 25. Tabular entries are only provided for the 2467 streamlines along which transition was noted. For reference, the boundary-layer momentum thickness, Re_θ, value at transition is also listed. This quantity, along with the roughness height, is a first-order factor in the correlation of roughness transition data.

A correlation for the effects of roughness on boundary-layer transition was developed originally [1] based on a survey of transition data on hemispherical geometries with distributed sand-grain roughness as per Eq. (9) through Eq. (12). The roughness height parameter, k, in this formulation depends on the roughness type as per Eq. (12); for the new woven roughness data in this work, the thread radius was assumed to be the relevant dimension as the starting point for correlating this dataset.

$$Y_{TR} = \mathbf{165} \times (X_{TR})^{-0.5} \tag{9}$$

where:

$$Y_{TR} = (Re_{\theta})_{TR} \tag{10}$$

$$X_{TR} = \left[\left(\frac{kT_e}{\theta T_w}\right)\left(\frac{H_e}{H_k}\right)^{-1}(M_e)^{-0.5}\right]_{TR} \tag{11}$$

$$k = \begin{cases} k_{PV50} & \text{sand-grain roughness} \\ h_{hex} & \text{hexcomb pattern depth} \\ R_T & \text{thread radius} \quad \text{(assumed)} \end{cases} \tag{12}$$

This original correlation was subsequently modified account for the effects of varying pressure gradient in the non-axisymmetric flows over the current sphere-cone and spherical-cap geometries with patterned hexcomb roughness [3] and also applied to distributed roughness on these geometries [2] as per Eqs. (13) through (18). In this modified correlation, the pressure gradient effects are included through a modified Pohlhausen parameter, β_{POHL}, which is derived from the original Pohlhausen parameter, λ_{POHL}.

$$Y_{TR} = \mathbf{171.4} \times (X_{TR})^{-0.6299} \tag{13}$$

where:

$$Y_{TR} = (Re_{\theta})_{TR} \tag{14}$$

$$X_{TR} = \left[\left(\frac{kT_e}{\theta T_w}\right)^{0.45}\left(\frac{H_e}{H_k}\right)^{-1.8}(M_e)^{-0.6}(\beta_{POHL})^{-0.5}\right]_{TR} \tag{15}$$

$$log(1/\beta_{POHL}) = \overline{\lambda}_{POHL} \tag{16}$$

$$\overline{\lambda}_{POHL} = min[10, max(-10, \lambda_{POHL})] \tag{17}$$

$$\lambda_{POHL} = \frac{dU_e}{ds}\frac{\delta^2}{v_e} \tag{18}$$

In the Pohlhausen parameter, the pressure gradient is related to the velocity through the Bernoulli equation, which is approximately valid for the low Mach number boundary-layer conditions of a blunt body. The boundary-layer height, δ, and dynamic viscosity, ν_e, terms provide a consistent nondimensionalization

of the velocity gradient over a wide range of conditions. However, to be used in the power-law form of this correlation, the pressure gradient term must have a positive value, and must also be limited to prevent computational overflow or underflow at the aeroshell shoulder or stagnation point. Thus, the original Pohlhausen parameter is modified by *min* and *max* limiters and redefined through the *log* function to ensure a positive value.

The utility of this correlation is demonstrated for both the sand-grain and hexcomb roughness data sets in Figure 104. The hexcomb transition data points fell with ±20% of the correlation, while the sand grain data set – for which sand-grain heights exhibited a gaussian scatter – fell with ±50% of the correlation. The new woven roughness data transition data points are plotted in terms of the correlation variable in Figure 105. Both sphere-cone and spherical-cap data sets follow the correlation trend and exhibit scatter of the same magnitude as the prior data sets. However, as shown in Figure 106, the woven roughness trend line is shifted "rightward" from the sand-grain and hexcomb data. This is not surprising as these data sets are based on three very different types of roughness and for this initial analysis, the thread radius, R_T, was used in the correlation only to evaluate its efficacy.

Clearly, a reassessment of roughness height definitions is warranted now that three large datasets are available which account for sand-grain, hexcomb and woven roughness types. These three datasets should be reconcilable with a "shape parameter" inclusion in the correlation as per previous studies, e.g. [17]. However, a synthesis of these different roughness types and definition of appropriate shape-factors is beyond the scope of this limited test report and will be deferred to a future analysis.

Summary

The effects of pattern surface roughness patterns simulating that of a heat shield with a woven TPS on hypersonic boundary-layer transition and turbulent heating have been investigated through wind tunnel testing of two representative entry vehicle geometries. Heating and transition onset data were obtained at Mach 6 over a range of roughness heights and free stream Reynolds numbers sufficient to produce laminar, transitional, and turbulent flow. Boundary-layer transition onset locations were tabulated, and heating distributions were provided in both line plot and image forms. Measured heating levels were found to increase with both Reynolds number and roughness height. The transition onset location trend was found to follow the form of the previous sand-grain and hexcomb data sets, but with a shift in the correlation curve. A more targeted analysis of roughness height definitions and shape-factor corrections to the definitions is warranted.

Acknowledgements

This work was supported by the NASA Entry Systems Modeling Project within the Game Changing Development Program of the Space Technology Mission Directorate.

References

1. Hollis, B. R., "Experimental Investigation of Roughness Effects on Transition Onset and Turbulent Heating Augmentation on a Hemisphere at Mach 6 and Mach 10," NASA/M-2017-219613, May 2017.
2. Hollis, B. R. and Hollingsworth, K. E., "Experimental Investigation of Distributed Sand-Grain Roughness Effects on Transition Onset and Turbulent Heating Augmentation at Mach 6," NASA/TM-2022-0005643/Revision 1, February 2023.

3. Hollis, B. R., “Experimental Investigation of Hexcomb-Pattern Roughness Effects on Transition Onset and Turbulent Heating Augmentation at Mach 6,” NASA/TM-2019-220424, November 2019.

4. Hollis, B. R. and Hollingsworth, K. E., “Experimental Investigation of Block-TPS Fence/Gap Roughness Effects on Transition Onset and Turbulent Heating Augmentation at Mach 6,” NASA/TM-2023-0001707, February 2023.

5. Shrestha, P., Schroeder, O., Bellas Chatzigeorgis, G., Schulz, J. A., Palmer, G., Johnston, C. and Stern, E. C., “Coupled Simulations of Shoulder Ablation of an Aeroshell,” AIAA Paper 2024-1684, AIAA SciTech 2024 Forum, January 8-12, 2004, Orlando, FL.

6. Milos, F. S., Chen, Y.-K., and Mazhari, M., “Arcjet Tests and Thermal Response Analysis for Dual-Layer Woven Carbon Phenolic,” *Journal of Spacecraft and Rockets*, Vol. 55, No. 3, May-June 2018, pp. 712-722.

7. Buck, G. M., “Rapid Model Fabrication and Testing for Aerospace Vehicles,” AIAA Paper 2000-0826, 38th AIAA Aerospace Sciences Meeting and Exhibit, Reno, NV, January 10-13, 2000.

8. Berger, K., Rufer, S., Hollingsworth, K. and Wright, S., “NASA Langley Aerothermodynamic Laboratory: Hypersonic Testing Capabilities,” AIAA Paper 2015-1337, 53rd AIAA Aerospace Sciences Meeting, Kissimmee, FL, January 5-9, 2015.

9. Hollis, B. R., Berger, K. T., Berry, S. A., Brauckmann, G. J., et al, “Entry, Descent, and Landing Aerothermodynamics: NASA Langley Experimental Capabilities and Contributions,” AIAA Paper 2014-1154, AIAA 52nd Aerospace Science Meeting, National Harbor, MD, January 13-17, 2014.

10. Fay, J. A., and Riddell, F. R., “Theory of Stagnation Point Heat Transfer in Dissociated Air,” *Journal of Aeronautical Sciences*, Vol. 25, No. 2., February 1958, pp. 73-85.

11. Buck, G. M., “Surface Temperature/Heat Transfer Measurement Using a Quantitative Phosphor Thermography System,” AIAA Paper 91-0064, 29th Aerospace Sciences Meeting, Reno, NV, January 7-10, 1991.

12. Merski, N. R., “Global Aeroheating Wind-Tunnel Measurements Using Improved Two-Color Phosphor Thermography Methods,” *Journal of Spacecraft and Rockets*, Vol. 36, No. 2, March-April 1999, pp. 160-170.

13. Mason, M. L and Rufer, S. J., “Features of the Upgraded Imaging for Hypersonic Experimental Aeroheating Testing (IHEAT) Software,” AIAA Paper 2016-4322, AIAA Aviation Forum, Washington, DC, June 13-17, 2016.

14. Gnoffo, P. A., “An Upwind-Biased, Point-Implicit Algorithm for Viscous, Compressible Perfect-Gas Flows,” NASA TP-2953, February 1990.

15. Thompson, K. B. Hollis, B. R., Johnston, C. O., Kleb, B. L, Lessard, V. R. and Mazaheri, A., "LAURA User's Manual: 5.6," NASA TM-2020-220566, February 2020.

16. Morkovin,M.V.,“CriticalEvaluationofTransitionfromLaminartoTurbulentShearLayerswith Emphasis on Hypersonically Travelling Blunt Bodies”, Air Force Flight Dynamics Laboratory, AFFDL-TR-68-1949, March 1969.

17. Van Rij, J. A., Belnap, B. J., and Ligrani, P. M., “Analysis and Experiments on Three-Dimensional, Irregular Surface Roughness,”, *Journal of Fluids and Engineering*, Vol. 124, September 2002, pp. 671-677.

Table 1. Model geometry parameters.

Model geometry	Model radius, R		Nose radius, R_N		Corner radius, R_C		Nose included angle, β	R_N/R	R_C/R
	in.	m	in.	m	in.	m	deg.		
Sphere-cone	3.000	0.0762	1.500	0.0371	0.1500	0.00381	20.00	0.5	0.050
Spherical-cap	3.000	0.0762	7.200	0.1829	0.3000	0.00762	23.04	2.4	0.100

Table 2. Model weave parameters.

Pattern ID	Thread Radius, R_T		Thread Spacing, S_T		Peak-to-Peak Distance L_{PP}		Peak Height, h_P	
	mil	mm	mil	mm	mil	mm	mil	mm
5-mil	5	0.1270	12.5	0.3175	25	0.6350	5	0.1270
10-mil	10	0.2540	25.0	0.6350	50	1.2700	10	0.2540
15-mil	15	0.3810	37.5	0.9525	75	1.9050	15	0.3810
20-mil	20	0.5080	50	1.2700	100	2.5400	20	0.5080

Table 3. Nominal 20-Inch Mach 6 Air Tunnel Freestream Conditions for Tests 7070 and 7074.

Condition	Re_∞ (1/ft)	Re_∞ (1/m)	M_∞	T_∞ (K)	ρ_∞ (kg/m^3)	U_∞ (m/s)	ΔH (J/kg)	h_{FR} (kg/m^2-s) sphere-cone	h_{FR} (kg/m^2-s) spherical-cap
1	1.04E+06	3.41E+06	5.90	61.78	1.63E-	929.63	1.93E+05	1.75E-01	8.01E-02
2	2.04E+06	6.71E+06	5.97	62.31	3.17E-	944.57	2.08E+05	2.50E-01	1.14E-01
3	3.04E+06	9.97E+06	6.00	62.58	4.71E-	950.64	2.14E+05	3.07E-01	1.40E-01
4	5.04E+06	1.65E+07	6.03	63.20	7.82E-	959.31	2.23E+05	4.00E-01	1.82E-01
4-alt	5.26E+06	1.73E+07	6.03	61.63	8.07E-	946.01	2.08E+05	3.99E-01	1.82E-01
5	6.55E+06	2.15E+07	6.05	63.20	1.01E-	960.62	2.24E+05	4.56E-01	2.08E-01
5-alt	6.77E+06	2.22E+07	6.04	61.94	1.04E-	949.72	2.12E+05	4.55E-01	2.08E-01
6	7.28E+06	2.39E+07	6.05	63.12	1.13E-	960.35	2.24E+05	4.80E-01	2.19E-01
6-alt	7.61E+06	2.50E+07	6.05	61.52	1.16E-	946.45	2.09E+05	4.80E-01	2.19E-01
7	8.21E+06	2.69E+07	6.04	58.97	1.23E-	923.45	1.84E+05	4.78E-01	2.18E-01

Table 4. Nominal 20-Inch Mach 6 Air Tunnel Reservoir Conditions for Tests 7070 and 7074.

Condition	P_0 (Pa)	P_0 (psi)	T_0 (K)	T_0 (F)
1	4.082E+05	59.2	491	423
2	8.626E+05	125.1	505	449
3	1.321E+06	191.5	511	460
4	2.270E+06	329.2	520	476
4-alt	2.266E+06	328.7	506	451
5	2.966E+06	430.2	521	478
5-alt	2.957E+06	428.8	510	458
6	3.296E+06	478.0	521	478
6-alt	3.293E+06	477.7	507	452
7	3.291E+06	477.3	484	410

Table 5. 20-Inch Mach 6 Air Tunnel Test 7070 run matrix for smooth sphere-cone model.

Cond.	Run	Geom.	Weave (mil)	Seam	α (deg)	Re_∞ (1/ft)	M_∞	T_∞ (K)	ρ_∞ (kg/m^3)	U_∞ (m/s)	ΔH (J/kg)	h_{FR} (kg/m^2-s)	$T_{w,avg}$ (K)
1	14	sphere-cone	N/A	N/A	16	1.03E+06	5.90	62.0	1.62E-02	931.0	1.95E+05	1.75E-01	314
2	11	sphere-cone	N/A	N/A	16	2.05E+06	5.97	62.3	3.18E-02	944.7	2.08E+05	2.50E-01	325
3	12	sphere-cone	N/A	N/A	16	3.05E+06	6.00	62.6	4.73E-02	950.7	2.14E+05	3.07E-01	336
4	13	sphere-cone	N/A	N/A	16	5.04E+06	6.03	63.2	7.81E-02	959.2	2.22E+05	3.99E-01	350
4-alt	95	sphere-cone	N/A	N/A	16	5.25E+06	6.03	61.5	8.04E-02	944.8	2.07E+05	3.98E-01	340
5	15	sphere-cone	N/A	N/A	16	6.53E+06	6.05	63.3	1.01E-01	961.5	2.25E+05	4.56E-01	364
5-alt	94	sphere-cone	N/A	N/A	16	6.79E+06	6.04	61.8	1.04E-01	948.2	2.11E+05	4.54E-01	349
6	16	sphere-cone	N/A	N/A	16	7.20E+06	6.05	63.5	1.12E-01	963.5	2.27E+05	4.80E-01	371
6-alt	93	sphere-cone	N/A	N/A	16	7.66E+06	6.05	61.3	1.17E-01	944.6	2.07E+05	4.79E-01	355
7	17	sphere-cone	N/A	N/A	16	8.17E+06	6.04	59.2	1.23E-01	925.2	1.86E+05	4.79E-01	361

Table 6. 20-Inch Mach 6 Air Tunnel Test 7070 run matrix for smooth spherical-cap model.

Cond.	Run	Geom.	Weave (mil)	Seam	α (deg)	Re_∞ (1/ft)	M_∞	T_∞ (K)	ρ_∞ (kg/m^3)	U_∞ (m/s)	ΔH (J/kg)	h_{FR} (kg/m^2-s)	$T_{w,avg}$ (K)
1	25	spherical-cap	N/A	N/A	28	1.03E+06	5.90	61.9	1.61E-02	930.2	1.94E+05	7.96E-02	310
2	26	spherical-cap	N/A	N/A	28	2.03E+06	5.97	62.3	3.16E-02	944.6	2.08E+05	1.14E-01	322
3	27	spherical-cap	N/A	N/A	28	3.05E+06	6.00	62.6	4.73E-02	950.7	2.14E+05	1.40E-01	330
4	28	spherical-cap	N/A	N/A	28	5.00E+06	6.03	63.3	7.76E-02	960.4	2.24E+05	1.82E-01	346
4-alt						Condition 4-alt not run							
5	29	spherical-cap	N/A	N/A	28	6.59E+06	6.05	63.0	1.02E-01	958.8	2.22E+05	2.08E-01	352
5-alt	91	spherical-cap	N/A	N/A	28	6.88E+06	6.04	61.4	1.05E-01	945.3	2.07E+05	2.08E-01	345
6	30	spherical-cap	N/A	N/A	28	7.32E+06	6.05	63.0	1.13E-01	959.3	2.22E+05	2.19E-01	361
6-alt	96	spherical-cap	N/A	N/A	28	7.64E+06	6.05	61.4	1.17E-01	944.9	2.07E+05	2.19E-01	349
7	31	spherical-cap	N/A	N/A	28	8.25E+06	6.04	58.9	1.24E-01	922.5	1.83E+05	2.19E-01	348

Table 7. 20-Inch Mach 6 Air Tunnel Test 7070 run matrix for sphere-cone models with weave and seams.

Cond.	Run	Geom.	Weave (mil)	Seam	α (deg)	Re_∞ (1/ft)	M_∞	T_∞ (K)	ρ_∞ (kg/m^3)	U_∞ (m/s)	ΔH (J/kg)	h_{FR} (kg/m^2-s)	$T_{w,avg}$ (K)
1	39	sphere-cone	5	Y	16	1.04E+06	5.90	61.9	1.63E-02	930.3	1.94E+05	1.76E-01	313
2	40	sphere-cone	5	Y	16	2.02E+06	5.97	62.4	3.15E-02	945.6	2.09E+05	2.49E-01	325
3	41	sphere-cone	5	Y	16	3.04E+06	6.00	62.8	4.72E-02	952.9	2.16E+05	3.08E-01	335
4	42	sphere-cone	5	Y	16	5.05E+06	6.03	63.4	7.85E-02	960.8	2.24E+05	4.01E-01	352
4-alt	Condition 4-alt not run												
5	43	sphere-cone	5	Y	16	6.57E+06	6.05	63.1	1.02E-01	959.7	2.23E+05	4.56E-01	375
5-alt	Condition 5-alt not run												
6	44	sphere-cone	5	Y	16	7.32E+06	6.05	63.0	1.13E-01	959.0	2.22E+05	4.81E-01	388
6-alt	Condition 6-alt not run												
7	45	sphere-cone	5	Y	16	8.26E+06	6.04	58.8	1.24E-01	922.1	1.83E+05	4.79E-01	373
1	49	sphere-cone	10	Y	16	1.05E+06	5.90	61.9	1.64E-02	930.4	1.94E+05	1.76E-01	315
2	50	sphere-cone	10	Y	16	2.04E+06	5.97	62.3	3.17E-02	944.8	2.08E+05	2.50E-01	328
3	51	sphere-cone	10	Y	16	3.08E+06	6.00	62.1	4.75E-02	946.7	2.09E+05	3.06E-01	342
4	52	sphere-cone	10	Y	16	5.10E+06	6.03	63.1	7.91E-02	958.5	2.22E+05	4.01E-01	387
4-alt	Condition 4-alt not run												
5	48	sphere-cone	10	Y	16	6.56E+06	6.05	63.1	1.02E-01	960.1	2.23E+05	4.56E-01	402
5-alt	63	sphere-cone	10	Y	16	6.75E+06	6.04	62.0	1.04E-01	950.6	2.13E+05	4.55E-01	397
6	47	sphere-cone	10	Y	16	7.30E+06	6.05	63.1	1.13E-01	960.3	2.23E+05	4.81E-01	407
6-alt	62	sphere-cone	10	Y	16	7.69E+06	6.05	61.3	1.17E-01	944.1	2.06E+05	4.80E-01	398
7	46	sphere-cone	10	Y	16	8.25E+06	6.04	58.9	1.24E-01	923.1	1.84E+05	4.79E-01	388
1	55	sphere-cone	15	Y	16	1.06E+06	5.90	61.6	1.65E-02	928.5	1.92E+05	1.76E-01	317
2	61	sphere-cone	15	Y	16	2.03E+06	5.97	62.3	3.15E-02	944.4	2.08E+05	2.49E-01	346
3	60	sphere-cone	15	Y	16	3.02E+06	6.00	62.8	4.69E-02	952.1	2.15E+05	3.07E-01	369
4	57	sphere-cone	15	Y	16	5.06E+06	6.03	63.1	7.85E-02	958.7	2.22E+05	4.00E-01	400
4-alt	Condition 4-alt not run												
5	56	sphere-cone	15	Y	16	6.56E+06	6.05	63.1	1.02E-01	960.0	2.23E+05	4.56E-01	405
5-alt	59	sphere-cone	15	Y	16	6.84E+06	6.04	61.7	1.05E-01	947.4	2.10E+05	4.56E-01	405
6	54	sphere-cone	15	Y	16	7.25E+06	6.05	63.3	1.12E-01	962.1	2.25E+05	4.81E-01	380
6-alt	58	sphere-cone	15	Y	16	7.74E+06	6.05	61.1	1.18E-01	943.0	2.05E+05	4.80E-01	405
7	53	sphere-cone	15	Y	16	8.22E+06	6.04	59.1	1.23E-01	924.3	1.85E+05	4.79E-01	395
1	80	sphere-cone	20	Y	16	1.05E+06	5.90	61.9	1.64E-02	930.5	1.94E+05	1.77E-01	316
2	81	sphere-cone	20	Y	16	2.04E+06	5.97	62.3	3.16E-02	944.8	2.08E+05	2.49E-01	346
3	79	sphere-cone	20	Y	16	3.05E+06	6.00	62.5	4.72E-02	950.2	2.13E+05	3.07E-01	370
4	78	sphere-cone	20	Y	16	5.06E+06	6.03	63.1	7.84E-02	958.3	2.22E+05	4.00E-01	401
4-alt	Condition 4-alt not run												
5	Condition 5 not run												
5-alt	77	sphere-cone	20	Y	16	6.86E+06	6.04	61.6	1.05E-01	946.9	2.09E+05	4.56E-01	406
6	Condition 6 not run												
6-alt	75	sphere-cone	20	Y	16	7.64E+06	6.05	61.5	1.17E-01	946.3	2.08E+05	4.80E-01	407
7	76	sphere-cone	20	Y	16	8.26E+06	6.04	58.8	1.24E-01	922.4	1.83E+05	4.79E-01	398

Table 8. 20-Inch Mach 6 Air Tunnel Test 7070 run matrix for spherical-cap models with weave and seams.

Cond.	Run	Geom.	Weave (mil)	Seam	α (deg)	Re_∞ (1/ft)	M_∞	T_∞ (K)	ρ_∞ (kg/m^3)	U_∞ (m/s)	ΔH (J/kg)	h_{FR} (kg/m^2-s)	$T_{w,avg}$ (K)
1	38	spherical-cap	5	Y	28	1.05E+06	5.90	61.8	1.64E-02	929.9	1.93E+05	8.04E-02	314
2	37	spherical-cap	5	Y	28	2.04E+06	5.97	62.4	3.17E-02	945.5	2.09E+05	1.14E-01	327
3	36	spherical-cap	5	Y	28	3.03E+06	6.00	62.7	4.71E-02	951.9	2.15E+05	1.40E-01	335
4	32	spherical-cap	5	Y	28	5.06E+06	6.03	63.1	7.84E-02	958.5	2.22E+05	1.82E-01	347
4-alt	33	spherical-cap	5	Y	28	6.55E+06	6.05	63.2	1.02E-01	960.6	2.24E+05	2.08E-01	379
5	67	spherical-cap	5	Y	28	6.86E+06	6.04	61.6	1.05E-01	946.5	2.09E+05	2.08E-01	373
5-alt	34	spherical-cap	5	Y	28	7.31E+06	6.05	63.1	1.13E-01	960.1	2.23E+05	2.20E-01	391
6	66	spherical-cap	5	Y	28	7.68E+06	6.05	61.2	1.17E-01	944.0	2.06E+05	2.19E-01	382
6-alt	35	spherical-cap	5	Y	28	8.27E+06	6.04	58.8	1.24E-01	922.3	1.83E+05	2.19E-01	376
7	38	spherical-cap	5	Y	28	1.05E+06	5.90	61.8	1.64E-02	929.9	1.93E+05	8.04E-02	314
1	Condition 1 not run, model not available												
2	Condition 2 not run, model not available												
3	Condition 3 not run, model not available												
4	Condition 4 not run, model not available												
4-alt	Condition 4-alt not run, model not available												
5	Condition 5 not run, model not available												
5-alt	Condition 5-alt not run, model not available												
6	Condition 6 not run, model not available												
6-alt	Condition 6-alt not run, model not available												
7	Condition 7 not run, model not available												
1	82	spherical-cap	15	Y	28	1.05E+06	5.90	61.8	1.64E-02	930.1	1.94E+05	8.04E-02	311
2	83	spherical-cap	15	Y	28	2.06E+06	5.97	62.3	3.19E-02	944.2	2.07E+05	1.14E-01	323
3	84	spherical-cap	15	Y	28	3.03E+06	6.00	62.6	4.70E-02	950.9	2.14E+05	1.40E-01	347
4	85	spherical-cap	15	Y	28	5.06E+06	6.03	63.2	7.85E-02	959.0	2.22E+05	1.83E-01	385
4-alt	Condition 4-alt not run												
5	Condition 5 not run												
5-alt	86	spherical-cap	15	Y	28	6.88E+06	6.04	61.5	1.05E-01	946.2	2.08E+05	2.08E-01	395
6	Condition 6 not run												
6-alt	87	spherical-cap	15	Y	28	7.53E+06	6.05	61.9	1.16E-01	950.0	2.12E+05	2.19E-01	401
7	88	spherical-cap	15	Y	28	8.28E+06	6.04	58.8	1.24E-01	922.2	1.83E+05	2.19E-01	389
1	71	spherical-cap	20	Y	28	1.07E+06	5.90	61.5	1.67E-02	928.3	1.92E+05	8.09E-02	315
2	72	spherical-cap	20	Y	28	2.05E+06	5.97	62.3	3.18E-02	944.3	2.07E+05	1.14E-01	340
3	68	spherical-cap	20	Y	28	3.04E+06	6.00	62.7	4.72E-02	951.3	2.14E+05	1.40E-01	360
4	69	spherical-cap	20	Y	28	5.04E+06	6.03	63.2	7.83E-02	959.3	2.23E+05	1.82E-01	391
4-alt	Condition 4-alt not run												
5	Condition 5 not run												
5-alt	70	spherical-cap	20	Y	28	6.72E+06	6.04	62.2	1.03E-01	951.9	2.15E+05	2.08E-01	398
6	Condition 6 not run												
6-alt	73	spherical-cap	20	Y	28	7.65E+06	6.05	61.3	1.17E-01	944.8	2.07E+05	2.19E-01	399
7	74	spherical-cap	20	Y	28	8.17E+06	6.04	59.2	1.23E-01	925.5	1.86E+05	2.19E-01	392

Table 9. 20-Inch Mach 6 Air Tunnel Test 7074 run matrix for sphere-cone models with weave only.

Cond.	Run	Geom.	Weave (mil)	Seam	α (deg)	Re_∞ (1/ft)	M_∞	T_∞ (K)	ρ_∞ (kg/m^3)	U_∞ (m/s)	ΔH (J/kg)	h_{FR} (kg/m^2-s)	$T_{w,avg}$ (K)
1	20	sphere-cone	5	N	16	1.04E+06	5.90	61.9	1.62E-02	930.7	1.94E+05	1.75E-01	309
2	11	sphere-cone	5	N	16	2.05E+06	5.97	62.2	3.19E-02	943.9	2.07E+05	2.50E-01	322
3	16	sphere-cone	5	N	16	3.06E+06	6.00	62.5	4.74E-02	950.0	2.13E+05	3.08E-01	332
4	15	sphere-cone	5	N	16	5.04E+06	6.03	63.3	7.82E-02	960.0	2.23E+05	4.00E-01	349
4-alt	19	sphere-cone	5	N	16	5.25E+06	6.03	61.6	8.04E-02	946.0	2.08E+05	3.98E-01	346
5	14	sphere-cone	5	N	16	6.54E+06	6.05	63.0	1.01E-01	958.8	2.22E+05	4.54E-01	375
5-alt	18	sphere-cone	5	N	16	6.84E+06	6.04	61.4	1.05E-01	945.1	2.07E+05	4.54E-01	374
6	13	sphere-cone	5	N	16	7.22E+06	6.05	63.1	1.12E-01	960.4	2.24E+05	4.78E-01	389
6-alt	17	sphere-cone	5	N	16	7.55E+06	6.05	61.9	1.16E-01	949.8	2.12E+05	4.80E-01	387
7	12	sphere-cone	5	N	16	8.23E+06	6.04	58.9	1.23E-01	922.6	1.84E+05	4.78E-01	375
1	6	sphere-cone	10	N	16	1.06E+06	5.90	61.8	1.66E-02	930.4	1.94E+05	1.77E-01	312
2	1	sphere-cone	10	N	16	2.05E+06	5.97	62.3	3.18E-02	944.6	2.08E+05	2.50E-01	318
3	2	sphere-cone	10	N	16	3.07E+06	6.00	62.5	4.76E-02	950.0	2.13E+05	3.08E-01	335
4	3	sphere-cone	10	N	16	5.12E+06	6.03	62.8	7.92E-02	955.6	2.19E+05	4.00E-01	380
4-alt	8	sphere-cone	10	N	16	5.30E+06	6.03	61.4	8.11E-02	944.4	2.07E+05	3.99E-01	377
5	4	sphere-cone	10	N	16	6.48E+06	6.05	63.5	1.01E-01	963.0	2.26E+05	4.55E-01	401
5-alt	9	sphere-cone	10	N	16	6.73E+06	6.04	62.0	1.03E-01	950.4	2.13E+05	4.54E-01	396
6	5	sphere-cone	10	N	16	7.28E+06	6.05	63.0	1.13E-01	959.7	2.23E+05	4.80E-01	406
6-alt	10	sphere-cone	10	N	16	7.60E+06	6.05	61.7	1.16E-01	947.6	2.10E+05	4.80E-01	402
7	7	sphere-cone	10	N	16	8.22E+06	6.04	59.0	1.23E-01	923.5	1.84E+05	4.79E-01	387
1	27	sphere-cone	15	N	16	1.06E+06	5.90	61.8	1.66E-02	930.1	1.94E+05	1.77E-01	317
2	26	sphere-cone	15	N	16	2.04E+06	5.97	62.4	3.17E-02	944.9	2.08E+05	2.50E-01	352
3	25	sphere-cone	15	N	16	3.02E+06	6.00	62.6	4.68E-02	950.6	2.14E+05	3.06E-01	373
4	21	sphere-cone	15	N	16	5.01E+06	6.03	63.3	7.78E-02	960.2	2.24E+05	3.99E-01	402
4-alt	28	sphere-cone	15	N	16	5.20E+06	6.03	61.9	7.99E-02	948.0	2.11E+05	3.98E-01	396
5	22	sphere-cone	15	N	16	6.60E+06	6.05	62.9	1.02E-01	958.4	2.21E+05	4.56E-01	416
5-alt	29	sphere-cone	15	N	16	6.87E+06	6.04	61.4	1.05E-01	945.3	2.07E+05	4.55E-01	407
6	23	sphere-cone	15	N	16	7.29E+06	6.05	63.1	1.13E-01	960.1	2.23E+05	4.80E-01	437
6-alt	31	sphere-cone	15	N	16	7.66E+06	6.05	61.4	1.17E-01	945.0	2.07E+05	4.80E-01	404
7	24	sphere-cone	15	N	16	8.23E+06	6.04	59.0	1.23E-01	923.7	1.85E+05	4.79E-01	401
1	34	sphere-cone	20	N	16	1.09E+06	5.91	60.6	1.68E-02	921.6	1.85E+05	1.77E-01	318
2	35	sphere-cone	20	N	16	2.04E+06	5.97	62.3	3.17E-02	944.1	2.07E+05	2.50E-01	349
3	36	sphere-cone	20	N	16	3.06E+06	6.00	62.5	4.74E-02	950.2	2.13E+05	3.07E-01	371
4	Condition 4 not run												
4-alt	32	sphere-cone	20	N	16	5.29E+06	6.03	61.6	8.10E-02	945.4	2.08E+05	3.99E-01	393
5	Condition 5 not run												
5-alt	33	sphere-cone	20	N	16	6.83E+06	6.04	61.8	1.05E-01	948.4	2.11E+05	4.56E-01	402
6	Condition 6 not run												
6-alt	37	sphere-cone	20	N	16	7.62E+06	6.05	61.6	1.17E-01	947.2	2.09E+05	4.80E-01	391
7	38	sphere-cone	20	N	16	8.15E+06	6.04	59.2	1.22E-01	925.6	1.87E+05	4.78E-01	399

Table 10. 20-Inch Mach 6 Air Tunnel Test 7074 run matrix for spherical-cap models with weave only.

Cond.	Run	Geom.	Weave (mil)	Seam	α (deg)	Re_∞ (1/ft)	M_∞	T_∞ (K)	ρ_∞ (kg/m^3)	U_∞ (m/s)	ΔH (J/kg)	h_{FR} (kg/m^2-s)	$T_{w,avg}$ (K)
1	68	spherical-cap	5	N	28	9.71E+05	5.89	62.0	1.52E-02	929.6	1.93E+05	7.75E-02	303
2	69	spherical-cap	5	N	28	2.10E+06	5.98	62.2	3.26E-02	943.9	2.07E+05	1.15E-01	316
3	70	spherical-cap	5	N	28	3.03E+06	6.00	62.6	4.70E-02	950.7	2.14E+05	1.40E-01	322
4						Condition 4 not run							
4-alt	66	spherical-cap	5	N	28	5.28E+06	6.03	61.6	8.09E-02	945.4	2.08E+05	1.82E-01	337
5						Condition 5 not run							
5-alt	67	spherical-cap	5	N	28	6.78E+06	6.04	61.7	1.04E-01	947.4	2.10E+05	2.07E-01	364
6						Condition 6 not run							
6-alt	71	spherical-cap	5	N	28	7.50E+06	6.05	61.8	1.15E-01	948.9	2.11E+05	2.18E-01	378
7	72	spherical-cap	5	N	28	8.17E+06	6.04	58.9	1.22E-01	922.6	1.83E+05	2.18E-01	368
1						Condition 1 data acquisition problem							
2	55	spherical-cap	10	N	28	2.06E+06	5.97	62.3	3.19E-02	944.6	2.08E+05	1.14E-01	310
3	50	spherical-cap	10	N	28	3.03E+06	6.00	62.5	4.70E-02	950.1	2.13E+05	1.40E-01	328
4						Condition 4 not run							
4-alt	51	spherical-cap	10	N	28	5.23E+06	6.03	61.7	8.02E-02	947.0	2.09E+05	1.82E-01	371
5						Condition 5 not run							
5-alt	52	spherical-cap	10	N	28	6.89E+06	6.04	61.3	1.05E-01	944.1	2.06E+05	2.07E-01	387
6						Condition 6 not run							
6-alt	53	spherical-cap	10	N	28	7.56E+06	6.05	61.6	1.16E-01	947.1	2.09E+05	2.18E-01	391
7	54	spherical-cap	10	N	28	8.18E+06	6.04	59.0	1.23E-01	923.6	1.85E+05	2.18E-01	378
1	78	spherical-cap	15	N	28	1.11E+06	5.91	61.8	1.74E-02	931.4	1.95E+05	8.30E-02	301
2	79	spherical-cap	15	N	28	2.03E+06	5.97	62.2	3.15E-02	943.8	2.07E+05	1.14E-01	322
3	77	spherical-cap	15	N	28	3.02E+06	6.00	62.6	4.68E-02	950.6	2.14E+05	1.39E-01	349
4						Condition 4 not run							
4-alt	73	spherical-cap	15	N	28	5.28E+06	6.03	61.6	8.09E-02	945.6	2.08E+05	1.82E-01	370
5						Condition 5 not run							
5-alt	74	spherical-cap	15	N	28	6.76E+06	6.04	61.9	1.04E-01	949.0	2.11E+05	2.07E-01	389
6						Condition 6 not run							
6-alt	75	spherical-cap	15	N	28	7.53E+06	6.05	61.7	1.15E-01	947.6	2.10E+05	2.18E-01	395
7	76	spherical-cap	15	N	28	8.25E+06	6.04	58.7	1.24E-01	921.1	1.82E+05	2.18E-01	381
1	42	spherical-cap	20	N	28	1.06E+06	5.90	61.8	1.66E-02	930.1	1.94E+05	8.09E-02	314
2	41	spherical-cap	20	N	28	2.04E+06	5.97	62.3	3.17E-02	944.7	2.08E+05	1.14E-01	331
3	40	spherical-cap	20	N	28	3.05E+06	6.00	62.5	4.72E-02	950.2	2.13E+05	1.40E-01	354
4						Condition 4 not run							
4-alt	39	spherical-cap	20	N	28	5.29E+06	6.03	61.6	8.10E-02	946.2	2.09E+05	1.83E-01	379
5						Condition 5 not run							
5-alt	43	spherical-cap	20	N	28	6.79E+06	6.04	61.8	1.04E-01	948.4	2.11E+05	2.08E-01	395
6						Condition 6 not run							
6-alt	45	spherical-cap	20	N	28	7.69E+06	6.05	61.2	1.17E-01	943.9	2.06E+05	2.19E-01	399
7	46	spherical-cap	20	N	28	8.19E+06	6.04	59.0	1.23E-01	923.7	1.85E+05	2.18E-01	390

Table 11. Transition locations for Test 7074 spherical-cap 5-weave model without seams.

Run	Ray	s_0/R	Re_θ	Run	Ray	s_0/R	Re_θ	Run	Ray	s_0/R	Re_θ
66	0	0.956	173.9	67	340	0.768	161.6	71	350	0.548	127.5
66	10	1.234	211.6	67	350	0.727	154.7	72	0	0.586	134.3
66	20	0.808	150.1	71	0	0.622	141.6	72	10	0.671	151.9
66	30	1.208	203.6	71	10	0.680	152.9	72	20	0.681	153.3
66	50	1.138	191.9	71	20	0.689	155.0	72	30	0.673	149.3
66	330	1.323	217.3	71	30	0.678	149.9	72	40	0.598	134.5
66	340	1.157	201.4	71	40	0.604	136.0	72	50	0.655	143.0
66	350	0.885	162.8	71	50	0.662	144.4	72	60	0.585	128.0
67	0	0.766	161.0	71	60	0.594	129.0	72	70	0.708	147.3
67	10	0.733	156.3	71	70	0.719	148.7	72	80	0.751	150.6
67	20	0.758	160.3	71	80	0.765	154.2	72	90	0.755	147.5
67	30	0.739	154.8	71	90	0.762	148.7	72	100	0.772	146.9
67	40	0.731	152.8	71	100	0.783	147.1	72	110	0.755	139.8
67	50	0.749	153.1	71	110	0.771	141.4	72	120	0.631	116.1
67	60	0.857	168.3	71	120	0.661	122.2	72	130	0.658	115.7
67	70	0.839	162.6	71	130	0.688	119.5	72	140	0.566	99.7
67	80	0.843	159.8	71	140	0.602	103.5	72	230	0.722	122.1
67	90	0.815	152.0	71	230	0.742	121.9	72	240	0.694	125.3
67	100	1.034	169.2	71	240	0.728	132.0	72	250	0.687	128.5
67	240	0.841	136.7	71	250	0.718	134.2	72	260	0.759	144.0
67	250	0.949	153.7	71	260	0.796	149.4	72	270	0.706	140.3
67	260	0.970	165.9	71	270	0.740	144.7	72	280	0.756	150.8
67	270	0.824	152.7	71	280	0.806	160.8	72	290	0.746	153.4
67	280	0.880	165.1	71	290	0.762	156.5	72	300	0.645	137.6
67	290	0.868	166.7	71	300	0.678	143.0	72	310	0.629	137.5
67	300	0.884	171.7	71	310	0.662	143.5	72	320	0.611	137.0
67	310	0.768	156.6	71	320	0.645	143.4	72	330	0.574	130.5
67	320	0.744	154.8	71	330	0.590	133.6	72	340	0.506	119.2
67	330	0.684	145.1	71	340	0.520	122.5	72	350	0.515	121.2

Table 12. Transition locations for Test 7074 spherical-cap 10-weave model without seams

Run	Ray	s_0/R	Re_θ	Run	Ray	s_0/R	Re_θ	Run	Ray	s_0/R	Re_θ
50	0	0.536	83.1	51	330	0.368	73.7	53	130	0.269	53.2
50	10	0.606	93.2	51	340	0.376	76.2	53	140	0.277	54.5
50	20	0.863	124.1	51	350	0.368	75.7	53	220	0.297	58.0
50	30	1.047	143.1	52	0	0.203	50.9	53	230	0.304	59.6
50	40	1.012	137.4	52	10	0.230	55.0	53	240	0.284	56.3
50	50	1.122	148.0	52	20	0.254	60.1	53	250	0.255	52.8
50	80	0.764	102.9	52	30	0.276	62.6	53	260	0.258	54.5
50	90	0.774	101.6	52	40	0.280	63.0	53	270	0.241	51.6
50	100	0.847	105.9	52	50	0.254	56.3	53	280	0.206	45.3
50	260	0.812	102.6	52	60	0.205	45.7	53	290	0.178	40.9
50	270	0.825	106.7	52	70	0.168	37.5	53	300	0.218	50.9
50	280	0.742	100.2	52	80	0.197	41.3	53	310	0.242	58.0
50	290	1.038	134.1	52	90	0.201	41.0	53	320	0.229	56.6
50	300	0.677	95.6	52	100	0.261	51.6	53	330	0.214	53.8
50	310	0.795	111.6	52	110	0.284	54.4	53	340	0.203	51.6
50	320	0.858	119.5	52	120	0.278	53.0	53	350	0.238	61.0
50	330	0.852	120.7	52	130	0.281	52.2	54	0	0.194	51.8
50	340	0.868	124.6	52	140	0.282	51.8	54	10	0.220	58.8
50	350	0.810	118.2	52	220	0.301	55.2	54	20	0.246	64.8
51	0	0.329	69.5	52	230	0.308	56.3	54	30	0.263	65.8
51	10	0.373	78.0	52	240	0.298	56.7	54	40	0.265	66.2
51	20	0.384	78.4	52	250	0.266	50.5	54	50	0.224	56.2
51	30	0.385	77.3	52	260	0.268	52.2	54	60	0.191	46.5
51	40	0.395	77.4	52	270	0.253	51.1	54	70	0.150	36.2
51	50	0.477	90.6	52	280	0.218	46.2	54	80	0.179	41.0
51	60	0.479	89.3	52	290	0.186	39.8	54	90	0.184	42.4
51	70	0.526	95.7	52	300	0.227	49.0	54	100	0.245	52.8
51	80	0.396	72.9	52	310	0.252	56.0	54	110	0.275	58.3
51	90	0.464	81.6	52	320	0.235	53.7	54	120	0.264	54.0
51	100	0.476	82.3	52	330	0.226	52.1	54	130	0.263	52.5
51	110	0.494	82.3	52	340	0.208	49.4	54	140	0.259	51.7
51	120	0.466	76.6	52	350	0.246	58.3	54	220	0.287	56.5
51	130	0.474	76.0	53	0	0.200	52.6	54	230	0.291	59.2
51	140	0.420	66.1	53	10	0.222	58.1	54	240	0.271	56.8
51	220	0.414	65.9	53	20	0.250	63.6	54	250	0.233	49.7
51	230	0.435	69.4	53	30	0.266	64.6	54	260	0.248	53.4
51	240	0.442	73.1	53	40	0.271	65.5	54	270	0.235	52.6
51	250	0.477	79.7	53	50	0.240	57.7	54	280	0.193	44.6
51	260	0.447	76.7	53	60	0.195	46.8	54	290	0.165	39.1
51	270	0.395	70.4	53	70	0.157	36.7	54	300	0.213	51.0
51	280	0.333	61.7	53	80	0.186	42.4	54	310	0.236	57.4
51	290	0.434	79.8	53	90	0.194	42.0	54	320	0.221	55.3
51	300	0.379	72.4	53	100	0.250	53.2	54	330	0.208	53.5
51	310	0.420	81.3	53	110	0.284	57.7	54	340	0.199	51.8
51	320	0.373	73.6	53	120	0.269	54.3	54	350	0.231	60.4

Table 13. Transition locations for Test 7074 spherical-cap 15-weave model without seams

Run	Ray	s_0/R	Re_θ	Run	Ray	s_0/R	Re_θ	Run	Ray	s_0/R	Re_θ
79	0	0.469	61.3	73	80	0.166	32.3	75	40	0.151	36.4
79	10	0.493	64.3	73	90	0.196	35.7	75	50	0.102	25.8
79	20	0.573	72.3	73	100	0.224	40.2	75	60	0.110	26.4
79	30	0.750	90.2	73	110	0.233	41.3	75	70	0.100	23.6
79	40	0.823	96.3	73	120	0.237	40.5	75	80	0.134	31.2
79	50	0.761	89.1	73	130	0.278	47.1	75	90	0.143	31.8
79	60	0.955	104.9	73	140	0.270	44.4	75	100	0.154	34.0
79	80	0.892	96.4	73	220	0.357	58.3	75	110	0.161	34.4
79	90	0.735	80.2	73	230	0.345	58.0	75	120	0.161	33.5
79	100	0.775	82.3	73	240	0.313	53.2	75	130	0.151	32.2
79	260	0.814	84.7	73	250	0.311	53.6	75	140	0.161	32.7
79	270	0.703	77.7	73	260	0.235	42.5	75	220	0.273	53.1
79	280	0.856	92.8	73	270	0.234	43.5	75	230	0.276	54.9
79	320	0.973	109.3	73	280	0.202	37.6	75	240	0.202	42.1
79	330	0.763	91.4	73	290	0.175	34.5	75	250	0.177	37.7
79	340	0.688	84.8	73	300	0.195	38.4	75	260	0.188	40.0
79	350	0.536	68.4	73	310	0.229	46.3	75	270	0.174	37.1
77	0	0.290	48.4	73	320	0.227	47.0	75	280	0.147	33.0
77	10	0.365	58.5	73	330	0.230	48.2	75	290	0.134	30.3
77	20	0.452	70.7	73	340	0.221	47.2	75	300	0.125	30.3
77	30	0.420	65.7	73	350	0.272	58.2	75	310	0.099	24.7
77	40	0.442	66.9	74	0	0.158	40.6	75	320	0.136	33.6
77	50	0.418	62.8	74	10	0.178	44.9	75	330	0.185	45.9
77	60	0.486	70.7	74	20	0.140	34.7	75	340	0.162	42.1
77	70	0.498	71.5	74	30	0.143	35.0	75	350	0.149	39.2
77	80	0.450	63.3	74	40	0.183	42.0	76	0	0.141	39.7
77	90	0.399	55.4	74	50	0.118	27.5	76	10	0.151	41.0
77	100	0.467	62.6	74	60	0.111	25.4	76	20	0.104	29.8
77	110	0.517	66.8	74	70	0.113	26.4	76	30	0.120	31.6
77	120	0.420	54.7	74	80	0.143	31.3	76	40	0.142	36.8
77	130	0.412	51.9	74	90	0.148	30.7	76	50	0.095	25.5
77	140	0.481	58.1	74	100	0.159	33.2	76	60	0.101	25.8
77	220	0.492	59.3	74	110	0.189	37.2	76	70	0.091	23.0
77	230	0.511	63.0	74	120	0.188	36.4	76	80	0.130	30.3
77	240	0.643	78.7	74	130	0.163	31.5	76	90	0.136	31.8
77	250	0.653	82.6	74	140	0.221	41.6	76	100	0.147	32.0
77	260	0.687	88.0	74	220	0.301	55.9	76	110	0.157	34.8
77	270	0.652	85.8	74	230	0.252	48.3	76	120	0.152	33.6
77	280	0.682	91.2	74	240	0.213	40.8	76	130	0.144	30.2
77	290	0.690	94.3	74	250	0.194	37.7	76	140	0.154	33.2
77	300	0.523	75.3	74	260	0.190	38.3	76	220	0.263	51.8
77	310	0.489	72.5	74	270	0.180	37.1	76	230	0.262	52.4
77	320	0.290	45.4	74	280	0.158	33.1	76	240	0.198	42.8
77	330	0.401	62.7	74	290	0.139	30.4	76	250	0.175	38.8
77	340	0.378	60.3	74	300	0.133	30.0	76	260	0.175	38.9
77	350	0.414	65.7	74	310	0.106	25.7	76	270	0.163	37.1
73	0	0.214	46.8	74	320	0.157	36.7	76	280	0.134	32.0
73	10	0.232	50.5	74	330	0.189	44.2	76	290	0.124	29.7
73	20	0.220	48.1	74	340	0.168	41.7	76	300	0.113	26.8
73	30	0.211	44.3	74	350	0.155	37.8	76	310	0.091	21.9
73	40	0.199	42.5	75	0	0.148	39.8	76	320	0.130	33.4
73	50	0.215	44.5	75	10	0.160	43.0	76	330	0.179	46.4
73	60	0.142	29.5	75	20	0.113	29.9	76	340	0.155	41.1
73	70	0.121	24.4	75	30	0.123	31.7	76	350	0.142	39.5

Table 14. Transition locations for Test 7074 spherical-cap 20-weave model without seams.

Run	Ray	s_0/R	Re_θ	Run	Ray	s_0/R	Re_θ	Run	Ray	s_0/R	Re_θ
41	0	1.433	148.9	39	80	0.266	49.5	45	40	0.123	31.9
41	10	1.307	139.2	39	90	0.266	48.0	45	50	0.128	32.1
41	90	0.835	89.0	39	100	0.377	64.7	45	60	0.135	32.6
41	100	1.030	97.7	39	110	0.379	63.3	45	70	0.123	28.4
41	110	0.844	84.0	39	120	0.382	62.2	45	80	0.101	23.8
41	130	0.661	64.2	39	130	0.338	54.6	45	90	0.119	26.6
41	140	0.549	53.8	39	140	0.360	57.8	45	100	0.213	45.1
41	240	0.764	74.7	39	220	0.342	54.4	45	110	0.206	43.3
41	250	0.837	83.2	39	230	0.395	64.5	45	120	0.260	51.4
41	270	0.855	89.7	39	240	0.383	62.8	45	130	0.204	41.6
41	280	1.255	117.9	39	250	0.389	66.2	45	140	0.240	46.1
41	290	1.074	111.9	39	260	0.432	74.2	45	220	0.141	28.3
41	300	0.768	86.8	39	270	0.391	69.2	45	230	0.161	32.9
41	310	0.748	86.7	39	280	0.385	68.9	45	240	0.168	33.7
41	320	0.736	86.9	39	290	0.384	70.7	45	250	0.153	32.9
41	330	0.885	102.0	39	300	0.381	72.1	45	260	0.147	31.1
41	340	1.021	115.4	39	310	0.399	76.6	45	270	0.143	31.2
41	350	1.581	157.8	39	320	0.381	75.2	45	280	0.156	34.3
40	0	0.431	68.1	39	330	0.396	78.2	45	290	0.162	36.3
40	10	0.430	67.5	39	340	0.356	72.5	45	300	0.160	38.4
40	20	0.465	72.3	39	350	0.305	64.1	45	310	0.154	36.0
40	30	0.428	65.7	43	0	0.210	51.3	45	320	0.212	50.2
40	40	0.409	62.1	43	10	0.273	65.0	45	330	0.172	42.7
40	50	0.388	58.9	43	20	0.249	60.0	45	340	0.168	42.8
40	60	0.390	58.3	43	30	0.235	55.2	45	350	0.158	40.4
40	70	0.402	58.7	43	40	0.255	58.8	46	0	0.144	39.5
40	80	0.611	83.3	43	50	0.240	54.1	46	10	0.137	37.4
40	90	0.590	78.4	43	60	0.267	58.0	46	20	0.151	39.5
40	100	0.824	101.9	43	70	0.262	55.2	46	30	0.120	31.3
40	110	0.744	90.5	43	80	0.241	50.7	46	40	0.136	34.7
40	120	0.659	79.2	43	90	0.249	49.9	46	50	0.121	31.0
40	130	0.510	62.7	43	100	0.290	56.5	46	60	0.134	32.8
40	140	0.527	62.9	43	110	0.271	52.3	46	70	0.121	28.9
40	230	0.620	73.7	43	120	0.320	60.3	46	80	0.094	22.6
40	240	0.698	83.4	43	130	0.291	52.9	46	90	0.112	26.3
40	250	0.748	91.6	43	140	0.302	55.2	46	100	0.197	42.3
40	260	0.709	90.1	43	220	0.157	31.0	46	110	0.196	41.9
40	270	0.648	85.2	43	230	0.182	35.6	46	120	0.233	47.9
40	280	0.685	91.7	43	240	0.172	34.7	46	130	0.185	38.0
40	290	0.662	90.7	43	250	0.162	32.5	46	140	0.222	45.0
40	300	0.693	95.6	43	260	0.151	31.8	46	220	0.128	28.1
40	310	0.665	94.6	43	270	0.193	39.7	46	230	0.149	32.1
40	320	0.560	82.7	43	280	0.213	45.5	46	240	0.149	31.6
40	330	0.517	78.0	43	290	0.193	41.9	46	250	0.134	29.7
40	340	0.488	75.2	43	300	0.201	43.7	46	260	0.132	30.1
40	350	0.439	68.7	43	310	0.315	69.2	46	270	0.125	27.5
39	0	0.288	60.6	43	320	0.324	71.8	46	280	0.140	32.5
39	10	0.308	64.2	43	330	0.292	66.9	46	290	0.145	34.2
39	20	0.280	58.8	43	340	0.222	52.8	46	300	0.148	35.4
39	30	0.323	64.8	43	350	0.264	61.7	46	310	0.152	36.6
39	40	0.322	64.6	45	0	0.150	39.4	46	320	0.198	47.9
39	50	0.307	60.6	45	10	0.147	39.2	46	330	0.162	41.1
39	60	0.293	56.9	45	20	0.154	40.1	46	340	0.158	41.2
39	70	0.326	61.3	45	30	0.120	30.6	46	350	0.153	40.2

Table 15. Transition locations for Test 7074 sphere-cone 5-weave model without seams.

Run	Ray	s_0/R	Re_θ	Run	Ray	s_0/R	Re_θ	Run	Ray	s_0/R	Re_θ
15	0	0.932	221.4	18	0	0.779	228.4	17	0	0.725	228.7
15	10	1.105	230.6	18	10	0.740	211.5	17	10	0.718	215.8
15	20	1.251	224.0	18	20	0.808	206.6	17	20	0.713	195.8
15	30	1.081	208.5	18	30	0.778	191.3	17	30	0.672	176.2
15	40	1.084	201.5	18	40	0.651	161.9	17	40	0.585	152.8
15	50	1.018	187.2	18	50	0.615	147.2	17	50	0.525	134.5
15	60	0.961	174.3	18	60	0.558	133.8	17	60	0.499	126.5
15	70	0.940	164.3	18	70	0.607	138.0	17	70	0.513	125.8
15	280	0.937	154.8	18	80	0.544	121.2	17	80	0.512	121.1
15	290	0.855	155.6	18	90	0.592	124.8	17	90	0.529	119.1
15	300	0.828	160.0	18	100	0.511	106.9	17	100	0.475	105.6
15	310	0.855	168.8	18	110	0.550	108.6	17	110	0.466	100.3
15	320	0.890	182.4	18	120	0.581	108.9	17	120	0.463	95.8
15	330	0.896	187.7	18	130	0.603	106.7	17	130	0.468	92.2
15	340	0.975	207.7	18	140	0.615	104.2	17	140	0.513	96.1
15	350	1.012	223.0	18	220	0.685	109.0	17	220	0.651	112.0
19	0	0.939	224.4	18	230	0.724	118.1	17	230	0.613	112.3
19	10	1.101	231.8	18	240	0.811	129.7	17	240	0.586	114.5
19	20	1.236	227.2	18	250	0.583	113.6	17	250	0.549	112.6
19	30	1.071	208.7	18	260	0.551	114.3	17	260	0.494	109.3
19	40	1.064	202.0	18	270	0.744	147.6	17	270	0.643	138.5
19	50	0.985	185.7	18	280	0.595	129.8	17	280	0.536	125.8
19	60	0.941	174.9	18	290	0.595	135.9	17	290	0.554	133.9
19	70	0.924	163.0	18	300	0.560	134.9	17	300	0.519	131.2
19	280	0.926	156.1	18	310	0.572	137.7	17	310	0.477	121.5
19	290	0.843	155.5	18	320	0.550	138.5	17	320	0.517	135.5
19	300	0.829	162.6	18	330	0.589	149.2	17	330	0.512	134.0
19	310	0.838	168.3	18	340	0.725	190.5	17	340	0.652	181.1
19	320	0.871	180.5	18	350	0.764	216.5	17	350	0.705	214.0
19	330	0.868	184.6	13	0	0.735	227.6	12	0	0.715	232.0
19	340	0.953	206.5	13	10	0.727	215.5	12	10	0.685	213.4
19	350	0.992	223.2	13	20	0.734	198.8	12	20	0.678	192.1
14	0	0.788	228.0	13	30	0.716	184.3	12	30	0.638	172.3
14	10	0.785	218.2	13	40	0.603	155.9	12	40	0.572	153.6
14	20	0.817	207.1	13	50	0.550	137.9	12	50	0.500	131.4
14	30	0.795	194.1	13	60	0.522	130.7	12	60	0.491	127.8
14	40	0.686	169.2	13	70	0.539	130.3	12	70	0.485	122.1
14	50	0.646	153.1	13	80	0.527	122.6	12	80	0.493	120.7
14	60	0.600	141.8	13	90	0.546	121.9	12	90	0.503	117.8
14	70	0.643	143.6	13	100	0.496	108.7	12	100	0.460	104.9
14	80	0.566	124.0	13	110	0.483	101.2	12	110	0.449	98.4
14	90	0.618	127.9	13	120	0.492	98.3	12	120	0.435	93.4
14	100	0.603	120.4	13	130	0.474	92.5	12	130	0.447	92.1
14	110	0.575	112.1	13	140	0.525	97.0	12	140	0.485	93.6
14	120	0.633	114.9	13	220	0.662	112.2	12	220	0.633	112.6
14	130	0.621	108.3	13	230	0.625	113.9	12	230	0.588	112.9
14	140	0.636	105.7	13	240	0.615	115.8	12	240	0.553	112.1
14	250	0.638	120.3	13	250	0.556	112.7	12	250	0.538	114.4
14	260	0.580	117.2	13	260	0.515	110.8	12	260	0.478	108.3
14	270	0.744	146.5	13	270	0.675	142.3	12	270	0.611	137.6
14	280	0.618	133.0	13	280	0.572	129.8	12	280	0.518	125.2
14	290	0.618	139.1	13	290	0.566	135.1	12	290	0.539	134.0
14	300	0.595	139.6	13	300	0.529	131.7	12	300	0.488	127.8
14	310	0.639	151.8	13	310	0.497	125.8	12	310	0.452	119.1
14	320	0.571	143.2	13	320	0.524	135.9	12	320	0.512	136.8
14	330	0.638	160.9	13	330	0.540	140.7	12	330	0.498	132.4
14	340	0.759	196.7	13	340	0.662	181.2	12	340	0.632	180.4
14	350	0.775	216.3	13	350	0.725	214.7	12	350	0.663	208.7

Table 16. Transition locations for Test 7074 sphere-cone 10-weave model without seams.

Run	Ray	s_0/R	Re_θ	Run	Ray	s_0/R	Re_θ	Run	Ray	s_0/R	Re_θ
2	0	0.801	159.9	8	70	0.195	43.3	9	70	0.133	33.9
2	30	0.919	148.5	8	80	0.175	39.9	9	80	0.130	33.0
2	40	0.780	130.0	8	90	0.219	47.1	9	90	0.149	36.7
2	50	0.609	102.8	8	100	0.207	42.2	9	100	0.141	34.2
2	60	0.522	87.5	8	110	0.179	36.1	9	110	0.142	32.6
2	70	0.644	100.9	8	120	0.189	37.7	9	120	0.161	36.0
2	80	0.798	111.6	8	130	0.292	53.1	9	130	0.210	44.5
2	90	0.631	91.8	8	140	0.374	63.3	9	140	0.240	47.4
2	100	0.736	97.7	8	150	0.289	47.1	9	220	0.321	60.9
2	110	0.837	98.3	8	220	0.471	76.2	9	230	0.218	46.3
2	120	0.575	75.3	8	230	0.397	69.5	9	240	0.244	52.4
2	130	0.819	53.2	8	240	0.347	63.6	9	250	0.170	39.2
2	240	0.722	87.4	8	250	0.247	48.4	9	260	0.158	37.8
2	250	0.841	98.6	8	260	0.406	77.2	9	270	0.152	37.3
2	270	0.912	113.9	8	270	0.322	65.8	9	280	0.190	46.6
2	280	0.929	121.5	8	280	0.324	69.3	9	290	0.189	47.1
2	290	0.579	92.3	8	290	0.266	58.2	9	300	0.224	55.5
2	300	0.564	93.7	8	300	0.310	68.2	9	310	0.239	57.4
2	310	0.590	99.2	8	310	0.330	70.5	9	320	0.274	64.3
2	320	0.562	98.2	8	320	0.343	71.4	9	330	0.300	65.4
2	330	0.744	127.7	8	330	0.386	77.9	9	340	0.233	43.2
2	340	0.556	100.9	8	340	0.379	70.5	9	350	0.256	44.7
2	350	0.711	142.3	8	350	0.371	65.5	5	0	0.218	36.4
3	0	0.326	53.4	4	0	0.250	41.6	5	10	0.208	36.1
3	10	0.331	55.8	4	10	0.240	40.1	5	20	0.210	39.3
3	20	0.271	44.7	4	20	0.237	42.9	5	30	0.241	50.9
3	30	0.360	70.6	4	30	0.276	57.7	5	40	0.184	41.4
3	40	0.275	55.8	4	40	0.224	50.1	5	50	0.168	41.3
3	50	0.303	64.5	4	50	0.220	51.5	5	60	0.144	36.9
3	60	0.233	50.8	4	60	0.167	41.2	5	70	0.131	34.4
3	70	0.199	44.0	4	70	0.142	35.5	5	80	0.128	34.4
3	80	0.183	40.1	4	80	0.137	34.7	5	90	0.130	34.2
3	90	0.233	49.3	4	90	0.156	37.7	5	100	0.113	28.6
3	100	0.218	45.0	4	100	0.143	34.5	5	110	0.114	29.1
3	110	0.184	37.3	4	110	0.141	32.5	5	120	0.148	35.2
3	120	0.196	38.2	4	120	0.169	37.5	5	130	0.192	42.5
3	130	0.297	52.1	4	130	0.226	46.4	5	140	0.229	47.1
3	140	0.376	62.2	4	140	0.267	52.2	5	220	0.277	55.8
3	220	0.507	79.5	4	220	0.338	64.0	5	230	0.197	43.4
3	230	0.445	74.5	4	230	0.300	60.2	5	240	0.226	50.7
3	240	0.386	68.5	4	240	0.273	57.0	5	250	0.164	39.3
3	250	0.266	51.4	4	250	0.198	44.6	5	260	0.151	37.6
3	260	0.422	79.4	4	260	0.187	43.0	5	270	0.128	33.4
3	270	0.338	68.3	4	270	0.165	40.5	5	280	0.167	42.7
3	280	0.326	68.6	4	280	0.220	53.3	5	290	0.159	41.4
3	290	0.289	62.4	4	290	0.203	49.7	5	300	0.214	54.7
3	300	0.316	69.1	4	300	0.242	59.3	5	310	0.210	50.8
3	310	0.338	71.9	4	310	0.248	57.6	5	320	0.250	58.6
3	320	0.361	75.7	4	320	0.289	65.2	5	330	0.285	62.2
3	330	0.401	82.2	4	330	0.313	66.7	5	340	0.208	39.1
3	340	0.396	74.6	4	340	0.252	46.0	5	350	0.240	41.6
3	350	0.376	66.4	4	350	0.281	50.1	10	0	0.204	35.4
8	0	0.320	51.7	9	0	0.229	38.1	10	10	0.202	36.3
8	10	0.323	53.8	9	10	0.222	37.6	10	20	0.183	34.9
8	20	0.270	44.5	9	20	0.220	40.5	10	30	0.234	50.6
8	30	0.349	68.5	9	30	0.250	52.6	10	40	0.180	41.4
8	40	0.258	51.9	9	40	0.195	44.0	10	50	0.160	38.8
8	50	0.292	61.1	9	50	0.189	44.3	10	60	0.132	35.2
8	60	0.222	48.9	9	60	0.161	40.1				

Table 16 (cont.)

Run	Ray	s_0/R	Re_θ	Run	Ray	s_0/R	Re_θ	Run	Ray	s_0/R	Re_θ
10	70	0.120	31.8	10	310	0.193	47.8	7	120	0.137	33.8
10	80	0.137	36.6	10	320	0.232	54.4	7	130	0.174	39.9
10	90	0.128	33.4	10	330	0.268	59.5	7	140	0.224	49.0
10	100	0.103	27.5	10	340	0.180	35.2	7	220	0.253	54.1
10	110	0.108	27.9	10	350	0.228	40.1	7	230	0.159	36.3
10	120	0.135	32.7	7	0	0.194	34.7	7	240	0.196	46.4
10	130	0.183	40.7	7	10	0.188	35.0	7	250	0.130	34.1
10	140	0.235	49.0	7	20	0.179	34.9	7	260	0.137	35.8
10	220	0.271	55.8	7	30	0.221	48.0	7	270	0.105	28.8
10	230	0.177	39.4	7	40	0.173	40.8	7	280	0.138	36.5
10	240	0.216	50.0	7	50	0.147	36.1	7	290	0.136	36.4
10	250	0.151	37.8	7	60	0.133	36.3	7	300	0.181	47.3
10	260	0.144	36.7	7	70	0.119	32.4	7	310	0.186	46.9
10	270	0.123	32.3	7	80	0.132	36.3	7	320	0.221	52.3
10	280	0.157	40.5	7	90	0.124	33.1	7	330	0.256	57.2
10	290	0.143	37.9	7	100	0.093	25.2	7	340	0.168	32.8
10	300	0.199	51.0	7	110	0.094	25.6	7	350	0.223	40.0

Table 17. Transition locations for Test 7074 sphere-cone 15-weave model without seams.

Run	Ray	s_0/R	Re_θ	Run	Ray	s_0/R	Re_θ	Run	Ray	s_0/R	Re_θ
26	0	0.608	99.1	21	10	0.319	52.9	22	20	0.155	27.1
26	10	0.579	92.8	21	20	0.224	36.1	22	30	0.106	20.7
26	20	0.462	61.7	21	30	0.184	32.1	22	40	0.099	21.2
26	30	0.307	38.0	21	40	0.177	34.0	22	50	0.143	32.7
26	40	0.354	48.8	21	50	0.197	40.1	22	60	0.098	23.6
26	50	0.346	47.7	21	60	0.110	25.1	22	70	0.096	24.3
26	60	0.395	55.7	21	70	0.132	28.9	22	80	0.079	21.5
26	70	0.379	51.9	21	80	0.123	26.0	22	90	0.118	29.4
26	80	0.449	58.2	21	90	0.140	29.7	22	100	0.117	28.2
26	90	0.478	59.7	21	100	0.135	28.6	22	110	0.125	29.4
26	100	0.528	62.4	21	110	0.152	31.3	22	120	0.144	32.7
26	110	0.672	70.9	21	120	0.146	29.1	22	130	0.171	36.0
26	120	0.318	38.2	21	130	0.167	31.9	22	140	0.130	26.4
26	130	0.484	51.9	21	140	0.177	31.5	22	220	0.098	20.9
26	140	0.479	49.4	21	220	0.152	28.0	22	230	0.142	30.6
26	220	0.584	57.5	21	230	0.169	32.1	22	240	0.140	31.5
26	230	0.515	53.8	21	240	0.162	32.1	22	250	0.136	31.6
26	240	0.369	43.5	21	250	0.156	31.4	22	260	0.137	32.7
26	250	0.468	54.6	21	260	0.154	32.0	22	270	0.127	30.8
26	260	0.499	59.7	21	270	0.145	31.1	22	280	0.123	29.9
26	270	0.503	62.0	21	280	0.149	32.0	22	290	0.116	28.8
26	280	0.506	64.9	21	290	0.172	37.4	22	300	0.144	34.9
26	290	0.494	65.8	21	300	0.179	37.5	22	310	0.176	39.5
26	300	0.386	54.2	21	310	0.212	43.2	22	320	0.176	37.4
26	310	0.428	59.3	21	320	0.234	45.4	22	330	0.196	37.5
26	320	0.421	58.3	21	330	0.276	51.0	22	340	0.180	31.5
26	330	0.526	74.2	21	340	0.259	42.2	22	350	0.200	32.9
26	340	0.535	78.0	21	350	0.374	65.8	29	0	0.151	25.9
26	350	0.539	77.1	28	0	0.206	30.5	29	10	0.193	32.6
25	0	0.406	56.5	28	10	0.297	48.5	29	20	0.139	25.4
25	10	0.512	81.8	28	20	0.205	33.5	29	30	0.090	18.3
25	20	0.352	49.5	28	30	0.167	27.4	29	40	0.168	36.2
25	30	0.291	42.5	28	40	0.122	22.1	29	50	0.131	29.5
25	40	0.300	48.4	28	50	0.164	33.6	29	60	0.089	23.1
25	50	0.295	48.1	28	60	0.094	21.0	29	70	0.093	24.6
25	60	0.301	51.3	28	70	0.125	27.9	29	80	0.075	19.3
25	70	0.294	48.8	28	80	0.105	23.7	29	90	0.106	26.2
25	80	0.305	50.4	28	90	0.126	27.1	29	100	0.107	26.5
25	90	0.194	32.4	28	100	0.124	26.8	29	110	0.111	26.7
25	100	0.187	30.2	28	110	0.128	26.8	29	120	0.118	26.8
25	110	0.169	27.5	28	120	0.160	32.0	29	130	0.159	33.8
25	120	0.255	37.3	28	130	0.203	37.5	29	140	0.122	25.9
25	130	0.351	46.9	28	140	0.167	30.9	29	220	0.083	19.1
25	140	0.285	37.6	28	220	0.146	27.7	29	230	0.139	31.5
25	220	0.361	46.1	28	230	0.165	32.2	29	240	0.137	30.3
25	230	0.352	47.0	28	240	0.154	30.2	29	250	0.130	30.2
25	240	0.293	42.4	28	250	0.153	31.3	29	260	0.126	30.6
25	250	0.233	36.4	28	260	0.139	29.7	29	270	0.124	30.0
25	260	0.242	38.2	28	270	0.136	29.8	29	280	0.109	27.5
25	270	0.310	49.8	28	280	0.153	33.2	29	290	0.119	29.6
25	280	0.356	57.2	28	290	0.178	38.9	29	300	0.143	34.5
25	290	0.373	61.2	28	300	0.180	38.3	29	310	0.175	39.6
25	300	0.341	57.4	28	310	0.206	41.3	29	320	0.172	36.9
25	310	0.358	59.4	28	320	0.233	44.7	29	330	0.189	37.0
25	320	0.317	50.4	28	330	0.276	50.1	29	340	0.176	31.8
25	330	0.413	66.2	28	340	0.252	39.7	29	350	0.196	33.0
25	340	0.467	75.8	28	350	0.368	63.9	23	0	0.139	24.3
25	350	0.511	81.8	22	0	0.159	26.6	23	10	0.153	26.8
21	0	0.216	31.1	22	10	0.203	33.5				

Table 17 (cont.)

Run	Ray	s_0/R	Re_θ	Run	Ray	s_0/R	Re_θ	Run	Ray	s_0/R	Re_θ
23	20	0.129	23.7	31	10	0.141	26.3	24	0	0.110	20.6
23	30	0.074	16.2	31	20	0.128	25.1	24	10	0.138	25.2
23	40	0.157	33.8	31	30	0.146	30.0	24	20	0.124	23.6
23	50	0.118	26.3	31	40	0.143	32.7	24	40	0.129	28.5
23	60	0.089	23.4	31	50	0.107	25.5	24	50	0.087	22.0
23	70	0.079	21.5	31	60	0.084	22.9	24	70	0.082	23.0
23	80	0.067	18.4	31	70	0.074	21.2	24	80	0.067	20.1
23	90	0.104	26.4	31	80	0.065	18.6	24	90	0.059	16.9
23	100	0.107	26.8	31	90	0.087	23.9	24	100	0.086	23.9
23	110	0.109	26.2	31	100	0.096	24.6	24	110	0.106	27.2
23	120	0.118	27.0	31	110	0.107	26.7	24	120	0.106	26.9
23	130	0.146	32.3	31	120	0.109	27.1	24	130	0.133	30.6
23	140	0.113	25.3	31	130	0.136	31.6	24	140	0.101	23.2
23	220	0.083	21.0	31	140	0.104	23.1	24	220	0.069	17.1
23	230	0.136	30.9	31	220	0.068	17.7	24	230	0.125	30.0
23	240	0.134	30.5	31	230	0.134	31.4	24	240	0.116	28.7
23	250	0.130	30.5	31	240	0.128	31.1	24	250	0.122	30.4
23	260	0.126	31.0	31	250	0.122	29.7	24	260	0.114	29.3
23	270	0.120	30.1	31	260	0.123	31.5	24	270	0.107	28.4
23	280	0.107	27.3	31	270	0.109	28.2	24	280	0.100	27.4
23	290	0.114	29.1	31	280	0.099	27.4	24	290	0.101	28.0
23	300	0.143	35.0	31	290	0.102	27.6	24	300	0.142	36.6
23	310	0.165	37.4	31	300	0.139	36.0	24	310	0.155	37.4
23	320	0.172	37.1	31	310	0.163	39.4	24	320	0.160	35.2
23	330	0.179	35.3	31	320	0.173	39.6	24	330	0.172	34.6
23	340	0.183	33.3	31	330	0.177	37.0	24	340	0.160	30.0
23	350	0.196	33.2	31	340	0.168	32.6	24	350	0.179	31.8
31	0	0.137	25.4	31	350	0.188	34.0				

Table 18. Transition locations for Test 7074 sphere-cone 20-weave model without seams.

Run	Ray	s_0/R	Re_θ	Run	Ray	s_0/R	Re_θ	Run	Ray	s_0/R	Re_θ
34	30	1.205	99.9	36	300	0.401	67.1	33	330	0.173	34.5
34	40	0.987	89.4	36	310	0.398	67.2	33	340	0.209	38.7
34	70	0.642	59.9	36	320	0.393	65.6	33	350	0.218	37.0
34	120	0.546	43.4	36	330	0.369	57.9	37	0	0.181	33.3
34	130	0.652	47.4	36	340	0.344	48.8	37	10	0.179	33.2
34	140	0.563	41.5	36	350	0.378	53.7	37	20	0.201	39.6
34	230	0.709	49.6	32	0	0.262	39.3	37	30	0.201	43.6
34	240	0.608	46.5	32	10	0.232	34.3	37	40	0.111	26.5
34	250	0.720	54.0	32	20	0.264	42.9	37	50	0.126	30.8
34	260	0.805	61.1	32	30	0.275	50.6	37	60	0.091	25.9
35	0	0.392	45.1	32	40	0.222	43.4	37	70	0.094	25.6
35	10	0.545	79.2	32	50	0.243	49.8	37	80	0.086	23.8
35	20	0.508	73.0	32	60	0.158	35.6	37	90	0.098	27.4
35	30	0.470	65.6	32	70	0.143	32.1	37	100	0.120	31.9
35	40	0.521	74.1	32	80	0.125	28.5	37	110	0.137	34.5
35	50	0.425	59.1	32	90	0.125	26.9	37	120	0.143	35.8
35	60	0.492	67.9	32	100	0.149	30.9	37	130	0.157	36.2
35	70	0.577	74.5	32	110	0.167	34.2	37	140	0.108	25.3
35	80	0.482	62.9	32	120	0.180	34.3	37	220	0.084	21.5
35	90	0.605	72.3	32	130	0.236	42.3	37	230	0.117	28.3
35	100	0.616	70.5	32	140	0.232	40.9	37	240	0.149	36.4
35	110	0.703	73.4	32	220	0.262	46.3	37	250	0.101	26.1
35	120	0.494	54.4	32	230	0.197	37.2	37	260	0.118	31.0
35	130	0.602	60.6	32	240	0.226	42.7	37	270	0.129	34.9
35	140	0.513	52.3	32	250	0.202	39.4	37	280	0.106	28.1
35	230	0.699	66.7	32	260	0.178	37.3	37	290	0.098	27.2
35	240	0.646	66.6	32	270	0.175	36.8	37	300	0.112	29.1
35	250	0.595	65.5	32	280	0.188	39.9	37	310	0.115	28.5
35	260	0.601	68.5	32	290	0.185	40.5	37	320	0.130	29.5
35	270	0.571	69.3	32	300	0.160	35.5	37	330	0.131	27.7
35	280	0.819	92.3	32	310	0.180	36.2	37	340	0.192	38.2
35	290	0.634	80.6	32	320	0.197	36.9	37	350	0.194	35.8
35	300	0.519	71.1	32	330	0.265	48.4	38	0	0.175	31.9
35	310	0.566	77.6	32	340	0.243	38.9	38	10	0.173	31.7
35	320	0.550	77.8	32	350	0.242	35.7	38	20	0.188	36.4
35	330	0.450	62.3	33	0	0.226	36.7	38	30	0.194	41.2
35	340	0.532	77.6	33	10	0.204	34.7	38	40	0.108	25.4
35	350	0.540	77.5	33	20	0.228	41.7	38	50	0.126	30.6
36	0	0.324	42.1	33	30	0.228	47.1	38	60	0.088	25.3
36	10	0.332	44.6	33	40	0.184	41.1	38	70	0.083	23.4
36	20	0.319	44.3	33	50	0.166	38.5	38	80	0.076	20.7
36	30	0.340	52.4	33	60	0.122	30.5	38	90	0.096	26.8
36	40	0.335	55.3	33	70	0.115	29.7	38	100	0.120	31.7
36	50	0.369	61.9	33	80	0.098	25.5	38	110	0.124	31.1
36	60	0.400	67.8	33	90	0.108	26.9	38	120	0.139	34.1
36	70	0.445	71.8	33	100	0.140	33.9	38	130	0.153	35.1
36	80	0.386	61.6	33	110	0.141	32.5	38	140	0.102	23.7
36	90	0.385	59.7	33	120	0.149	34.0	38	220	0.081	20.7
36	100	0.378	56.4	33	130	0.199	41.6	38	230	0.125	30.1
36	110	0.209	32.7	33	140	0.171	35.2	38	240	0.148	36.2
36	120	0.283	40.8	33	220	0.146	31.3	38	250	0.098	25.6
36	130	0.432	56.5	33	230	0.165	36.4	38	260	0.103	27.4
36	140	0.346	45.1	33	240	0.177	38.9	38	270	0.125	32.8
36	220	0.427	54.2	33	250	0.129	30.1	38	280	0.101	27.4
36	230	0.414	54.5	33	260	0.131	31.1	38	290	0.098	27.1
36	240	0.390	53.8	33	270	0.142	34.2	38	300	0.104	27.2
36	250	0.318	46.9	33	280	0.129	32.8	38	310	0.115	27.9
36	260	0.257	40.7	33	290	0.124	31.7	38	320	0.130	28.8
36	270	0.218	36.2	33	300	0.128	31.9	38	330	0.129	26.5
36	280	0.278	45.6	33	310	0.140	32.0	38	340	0.174	33.8
36	290	0.467	74.8	33	320	0.162	35.1	38	350	0.192	35.0

Table 19. Transition locations for Test 7070 spherical-cap 5-weave model with seams.

Run	Ray	s_0/R	Re_θ	Run	Ray	s_0/R	Re_θ	Run	Ray	s_0/R	Re_θ
32	0	1.119	193.1	67	100	0.785	140.7	66	60	0.639	136.4
32	10	1.113	192.5	67	110	0.869	146.9	66	70	0.675	140.6
32	20	1.045	183.1	67	120	0.801	133.6	66	80	0.687	139.9
32	30	1.085	185.6	67	130	0.748	117.1	66	90	0.745	146.5
32	40	1.140	190.5	67	250	0.916	150.4	66	100	0.751	142.8
32	50	1.107	185.2	67	260	0.978	165.0	66	110	0.793	143.8
32	60	1.103	180.7	67	270	0.835	152.8	66	120	0.748	132.9
32	70	1.056	172.4	67	280	0.809	153.4	66	130	0.716	121.7
32	80	1.212	180.9	67	290	0.733	143.4	66	250	0.860	150.9
32	310	1.246	202.4	67	300	0.730	145.4	66	260	0.866	157.9
32	320	1.094	184.2	67	310	0.645	133.8	66	270	0.776	150.3
32	330	0.907	161.3	67	320	0.574	123.9	66	280	0.756	150.6
32	340	1.033	181.0	67	330	0.546	118.5	66	290	0.637	133.3
32	350	1.092	189.3	67	340	0.523	116.3	66	300	0.581	125.4
33	0	0.549	119.7	67	350	0.546	120.6	66	310	0.531	118.3
33	10	0.667	142.4	34	0	0.514	118.2	66	320	0.495	113.7
33	20	0.643	136.7	34	10	0.593	134.0	66	330	0.470	109.1
33	30	0.636	134.3	34	20	0.562	127.0	66	340	0.464	109.4
33	40	0.677	140.0	34	30	0.587	130.8	66	350	0.477	113.3
33	50	0.726	145.7	34	40	0.583	128.0	35	0	0.498	119.5
33	60	0.733	144.1	34	50	0.651	138.6	35	10	0.554	132.1
33	70	0.746	144.5	34	60	0.633	133.3	35	20	0.524	124.2
33	80	0.770	145.0	34	70	0.670	137.3	35	30	0.520	122.4
33	90	0.798	145.7	34	80	0.680	135.6	35	40	0.545	125.0
33	100	0.830	145.8	34	90	0.746	143.7	35	50	0.583	130.6
33	110	0.871	144.6	34	100	0.734	137.1	35	60	0.586	129.4
33	120	0.768	128.6	34	110	0.802	142.1	35	70	0.622	133.6
33	270	0.938	164.2	34	120	0.748	130.7	35	80	0.617	129.1
33	280	0.852	157.9	34	130	0.719	119.5	35	90	0.756	149.8
33	290	0.805	153.0	34	250	0.878	151.3	35	100	0.700	138.0
33	300	0.785	151.8	34	260	1.255	119.0	35	110	0.717	135.2
33	310	0.693	140.5	34	270	0.777	147.9	35	120	0.688	126.0
33	320	0.614	129.1	34	280	0.780	151.8	35	130	0.655	117.5
33	330	0.632	133.4	34	290	0.638	131.0	35	230	0.695	121.2
33	340	0.616	132.0	34	300	0.596	125.9	35	240	0.847	142.6
33	350	0.607	131.0	34	310	0.557	121.2	35	250	0.838	152.0
67	0	0.558	124.1	34	320	0.515	115.3	35	260	0.833	157.5
67	10	0.649	140.0	34	330	0.520	117.5	35	270	0.736	146.4
67	20	0.607	132.1	34	340	0.524	119.8	35	280	0.729	149.2
67	30	0.625	133.4	34	350	0.527	120.7	35	290	0.582	125.1
67	40	0.638	135.5	66	0	0.523	123.1	35	300	0.574	126.3
67	50	0.710	145.3	66	10	0.614	141.7	35	310	0.502	114.7
67	60	0.701	140.7	66	20	0.569	131.1	35	320	0.484	112.0
67	70	0.734	143.5	66	30	0.578	130.3	35	330	0.473	111.6
67	80	0.760	145.6	66	40	0.579	130.1	35	340	0.503	120.3
67	90	0.790	147.4	66	50	0.650	141.3	35	350	0.483	115.7

Table 20. Transition locations for Test 7070 spherical-cap 15-weave model with seams.

Run	Ray	s_0/R	Re_θ	Run	Ray	s_0/R	Re_θ	Run	Ray	s_0/R	Re_θ
84	0	0.513	79.2	85	310	0.250	49.4	87	120	0.254	51.1
84	10	0.526	81.1	85	320	0.308	60.6	87	130	0.257	50.3
84	20	0.500	77.3	85	330	0.317	63.2	87	140	0.265	50.0
84	30	0.523	79.3	85	340	0.243	50.8	87	150	0.260	50.1
84	40	0.349	54.7	85	350	0.271	56.9	87	220	0.183	36.8
84	50	0.762	106.5	86	0	0.219	54.3	87	230	0.197	40.4
84	60	0.585	82.9	86	10	0.194	47.6	87	240	0.206	42.3
84	70	0.763	103.1	86	20	0.249	59.0	87	250	0.191	39.0
84	80	0.860	110.9	86	30	0.223	52.0	87	260	0.186	39.7
84	90	0.779	100.0	86	40	0.219	49.6	87	270	0.184	41.0
84	100	0.860	105.6	86	50	0.234	52.5	87	280	0.192	43.2
84	250	0.833	99.4	86	60	0.198	43.8	87	290	0.178	41.1
84	260	0.815	101.2	86	70	0.216	46.4	87	300	0.155	36.8
84	270	0.809	103.8	86	80	0.218	46.7	87	310	0.160	37.5
84	280	0.790	104.0	86	90	0.246	49.8	87	320	0.173	41.6
84	290	0.826	109.6	86	100	0.246	49.3	87	330	0.177	43.0
84	300	0.813	110.0	86	110	0.249	49.6	87	340	0.178	44.5
84	310	0.791	110.2	86	120	0.265	50.3	87	350	0.198	51.3
84	320	0.766	108.6	86	130	0.267	49.8	88	0	0.156	43.7
84	330	0.762	108.9	86	140	0.272	50.4	88	10	0.150	40.7
84	340	0.822	117.3	86	220	0.205	39.1	88	20	0.179	46.5
84	350	0.731	107.2	86	230	0.211	39.8	88	30	0.202	51.6
85	0	0.245	51.3	86	240	0.220	41.4	88	40	0.187	46.4
85	10	0.241	51.3	86	250	0.205	40.9	88	50	0.197	48.4
85	20	0.312	64.2	86	260	0.203	41.1	88	60	0.167	39.9
85	30	0.273	55.6	86	270	0.192	39.5	88	70	0.197	46.0
85	40	0.264	53.3	86	280	0.209	43.8	88	80	0.188	43.1
85	50	0.277	53.7	86	290	0.186	40.1	88	90	0.211	47.3
85	60	0.240	46.5	86	300	0.162	36.9	88	100	0.223	47.8
85	70	0.271	50.8	86	310	0.176	40.3	88	110	0.223	47.4
85	80	0.268	49.0	86	320	0.211	47.8	88	120	0.250	52.2
85	90	0.299	52.7	86	330	0.255	59.7	88	130	0.250	51.7
85	100	0.267	46.2	86	340	0.200	48.0	88	220	0.148	32.0
85	110	0.270	46.4	86	350	0.217	51.8	88	230	0.160	33.8
85	120	0.285	47.2	87	0	0.192	49.8	88	240	0.175	38.5
85	130	0.301	49.9	87	10	0.174	45.9	88	250	0.169	36.5
85	140	0.304	49.5	87	20	0.198	49.4	88	260	0.161	35.7
85	220	0.263	42.2	87	30	0.185	45.9	88	270	0.163	37.0
85	230	0.298	48.9	87	40	0.196	47.0	88	280	0.165	38.8
85	240	0.282	46.9	87	50	0.202	48.5	88	290	0.157	37.4
85	250	0.283	47.9	87	60	0.183	43.4	88	300	0.136	33.1
85	260	0.265	45.7	87	70	0.201	45.5	88	310	0.146	36.7
85	270	0.301	53.5	87	80	0.204	43.9	88	320	0.133	33.6
85	280	0.281	51.1	87	90	0.230	49.1	88	330	0.141	35.6
85	290	0.317	59.1	87	100	0.236	49.3	88	340	0.155	41.3
85	300	0.204	40.5	87	110	0.240	48.4	88	350	0.185	48.5

Table 21. Transition locations for Test 7070 spherical-cap 20-weave model with seams.

Run	Ray	s_0/R	Re_θ	Run	Ray	s_0/R	Re_θ	Run	Ray	s_0/R	Re_θ
72	0	0.595	74.0	68	270	0.316	44.1	70	100	0.166	33.6
72	10	0.576	72.2	68	280	0.287	42.2	70	110	0.173	34.9
72	20	0.805	94.0	68	290	0.316	46.1	70	120	0.175	35.7
72	30	0.683	81.8	68	300	0.377	56.0	70	130	0.201	39.6
72	40	0.715	84.1	68	310	0.343	52.5	70	140	0.174	34.7
72	50	0.728	84.1	68	320	0.368	56.6	70	220	0.213	39.5
72	60	0.696	80.1	68	330	0.395	61.1	70	230	0.225	43.5
72	70	0.732	82.0	68	340	0.380	60.4	70	240	0.204	40.3
72	80	0.631	71.0	68	350	0.328	52.8	70	250	0.199	40.1
72	90	0.667	72.7	69	0	0.143	32.1	70	260	0.187	37.9
72	100	0.738	77.4	69	10	0.159	35.2	70	270	0.188	39.4
72	110	0.899	86.0	69	20	0.148	31.7	70	280	0.148	31.8
72	130	0.510	52.1	69	30	0.270	54.6	70	290	0.145	32.2
72	220	0.579	55.3	69	40	0.251	49.3	70	300	0.119	27.4
72	240	0.813	76.1	69	50	0.231	44.9	70	310	0.128	30.3
72	250	0.876	85.2	69	60	0.196	37.3	70	320	0.154	36.4
72	260	0.801	83.1	69	70	0.154	29.2	70	330	0.165	39.9
72	270	0.633	69.8	69	80	0.140	26.2	70	340	0.153	38.1
72	280	0.728	80.3	69	90	0.181	32.2	73	90	0.109	25.5
72	290	0.826	90.7	69	100	0.255	44.3	73	100	0.127	28.6
72	300	0.737	83.5	69	110	0.216	36.6	73	110	0.148	32.3
72	310	0.756	87.1	69	120	0.192	31.9	73	120	0.155	33.2
72	320	0.702	82.9	69	130	0.259	42.3	73	130	0.162	33.1
72	330	0.826	95.5	69	140	0.265	42.0	73	140	0.124	27.4
72	340	0.678	82.4	69	220	0.261	42.0	73	220	0.184	36.9
72	350	0.595	74.2	69	230	0.264	42.8	73	230	0.186	37.3
68	0	0.314	51.2	69	240	0.244	41.1	73	240	0.175	37.3
68	10	0.321	52.3	69	250	0.257	43.9	73	250	0.168	34.9
68	20	0.472	72.6	69	260	0.238	41.4	73	260	0.156	34.5
68	30	0.421	64.9	69	270	0.250	44.7	73	270	0.163	36.1
68	40	0.476	71.2	69	280	0.213	40.4	73	280	0.119	27.7
68	50	0.409	60.7	69	290	0.198	37.7	73	290	0.116	27.5
68	60	0.397	58.0	69	300	0.182	36.3	74	90	0.089	20.9
68	70	0.376	53.8	69	310	0.181	36.9	74	100	0.108	25.0
68	80	0.319	45.6	69	320	0.224	45.2	74	110	0.138	29.6
68	90	0.367	50.5	69	330	0.233	47.2	74	120	0.148	31.6
68	100	0.424	56.3	69	340	0.217	46.4	74	130	0.144	30.1
68	110	0.466	60.4	69	350	0.244	51.3	74	140	0.102	23.5
68	120	0.482	60.2	70	20	0.166	40.7	74	220	0.167	33.4
68	130	0.480	59.5	70	30	0.173	40.8	74	230	0.165	33.4
68	140	0.491	58.6	70	40	0.182	42.6	74	240	0.166	34.0
68	220	0.451	54.7	70	50	0.163	37.0	74	250	0.151	33.0
68	230	0.412	51.6	70	60	0.131	29.4	74	260	0.139	30.8
68	240	0.487	62.3	70	70	0.129	28.3	74	270	0.144	32.3
68	250	0.484	63.2	70	80	0.103	22.0	74	280	0.100	22.8
68	260	0.438	59.0	70	90	0.133	28.7	74	290	0.098	23.5

Table 22. Transition locations for Test 7070 sphere-cone 5-weave model with seams.

Run	Ray	s_0/R	Re_θ	Run	Ray	s_0/R	Re_θ	Run	Ray	s_0/R	Re_θ
42	0	0.627	167.1	43	300	0.643	148.6	44	340	0.541	145.8
42	10	0.572	145.2	43	310	0.673	158.0	44	350	0.563	164.0
42	20	0.891	196.2	43	320	0.691	168.9	45	0	0.604	193.2
42	30	0.996	200.0	43	330	0.708	175.2	45	10	0.567	173.9
42	40	1.000	194.2	43	340	0.634	166.2	45	20	0.508	139.0
42	50	1.014	186.5	43	350	0.592	169.7	45	30	0.558	151.3
42	60	1.066	181.5	44	0	0.596	178.9	45	40	0.479	128.9
42	70	1.048	170.5	44	10	0.574	170.8	45	50	0.481	127.1
42	300	1.019	178.5	44	20	0.546	147.3	45	60	0.438	115.3
42	310	0.906	175.5	44	30	0.568	149.1	45	70	0.471	119.6
42	320	1.021	195.9	44	40	0.513	134.0	45	80	0.507	124.0
42	330	1.117	209.6	44	50	0.506	128.4	45	90	0.571	131.6
42	340	0.927	201.3	44	60	0.445	113.6	45	100	0.551	122.6
42	350	0.753	190.3	44	70	0.493	119.8	45	110	0.604	125.8
43	0	0.609	177.3	44	80	0.552	128.0	45	120	0.583	116.5
43	10	0.581	165.8	44	90	0.576	127.2	45	240	0.573	115.0
43	20	0.694	181.0	44	100	0.567	119.6	45	250	0.550	115.9
43	30	0.595	149.1	44	110	0.627	123.1	45	260	0.634	134.8
43	40	0.685	167.5	44	120	0.606	115.3	45	270	0.622	139.4
43	50	0.680	158.1	44	240	0.595	114.7	45	280	0.585	139.0
43	60	0.740	165.5	44	250	0.586	117.3	45	290	0.582	141.8
43	70	0.639	143.3	44	260	0.669	135.1	45	300	0.530	136.6
43	80	0.666	140.2	44	270	0.643	137.4	45	310	0.555	144.3
43	90	0.643	131.9	44	280	0.607	137.0	45	320	0.563	152.1
43	100	0.748	139.8	44	290	0.604	142.3	45	330	0.542	146.7
43	260	0.883	150.4	44	300	0.546	135.7	45	340	0.522	143.7
43	270	0.778	150.5	44	310	0.575	143.2	45	350	0.546	155.5
43	280	0.751	151.9	44	320	0.585	151.8				
43	290	0.702	153.1	44	330	0.562	146.5				

Table 23. Transition locations for Test 7070 sphere-cone 10-weave model with seams.

Run	Ray	s_0/R	Re_θ	Run	Ray	s_0/R	Re_θ	Run	Ray	s_0/R	Re_θ
51	0	0.585	112.1	48	270	0.255	59.7	47	280	0.210	52.9
51	10	0.555	104.2	48	280	0.268	63.7	47	290	0.237	60.8
51	20	0.647	119.5	48	290	0.265	63.5	47	300	0.231	60.1
51	30	0.721	124.1	48	300	0.283	69.6	47	310	0.274	67.3
51	50	0.984	143.3	48	310	0.292	69.0	47	320	0.256	60.6
51	290	0.696	106.3	48	320	0.306	70.6	47	330	0.249	53.4
51	300	0.686	109.5	48	330	0.333	71.8	47	340	0.165	31.1
51	310	0.895	136.2	48	340	0.246	44.1	47	350	0.193	34.3
51	320	1.010	152.3	48	350	0.242	40.2	62	0	0.183	33.1
51	330	0.855	141.3	63	0	0.229	37.9	62	10	0.188	34.4
51	340	0.874	151.6	63	10	0.183	32.1	62	20	0.216	42.2
51	350	0.551	102.0	63	20	0.236	43.4	62	30	0.317	71.9
52	0	0.281	43.1	63	30	0.333	73.4	62	40	0.265	63.3
52	10	0.250	36.6	63	40	0.331	77.9	62	50	0.339	85.6
52	20	0.277	45.2	63	50	0.357	85.6	62	60	0.361	93.0
52	30	0.352	68.4	63	60	0.406	98.2	62	70	0.297	75.4
52	40	0.359	74.5	63	70	0.347	83.8	62	80	0.339	84.5
52	50	0.399	84.9	63	80	0.401	92.4	62	90	0.386	91.3
52	60	0.419	88.9	63	90	0.435	96.1	62	100	0.411	93.4
52	70	0.443	91.4	63	100	0.475	99.1	62	110	0.197	47.4
52	80	0.513	100.4	63	110	0.234	52.9	62	120	0.187	44.3
52	90	0.602	109.6	63	120	0.244	52.3	62	130	0.226	49.6
52	100	0.625	108.0	63	130	0.438	82.6	62	140	0.273	56.1
52	110	0.697	111.1	63	140	0.360	66.9	62	220	0.283	57.0
52	120	0.656	101.6	63	220	0.303	58.4	62	230	0.240	52.5
52	220	0.452	71.0	63	230	0.279	56.7	62	240	0.222	50.3
52	230	0.416	69.7	63	240	0.245	52.2	62	250	0.164	39.4
52	240	0.357	63.3	63	250	0.198	45.0	62	260	0.150	38.1
52	250	0.356	66.7	63	260	0.169	40.1	62	270	0.163	43.1
52	260	0.400	75.3	63	270	0.224	52.8	62	280	0.192	49.8
52	270	0.449	86.4	63	280	0.250	59.3	62	290	0.222	58.0
52	280	0.380	78.3	63	290	0.255	63.4	62	300	0.192	49.4
52	290	0.466	95.8	63	300	0.295	71.8	62	310	0.250	63.4
52	300	0.422	89.9	63	310	0.280	66.8	62	320	0.248	60.1
52	310	0.403	86.1	63	320	0.300	71.4	62	330	0.224	48.8
52	320	0.378	79.4	63	330	0.317	69.6	62	340	0.165	32.0
52	330	0.411	85.3	63	340	0.213	39.5	62	350	0.180	33.1
52	340	0.301	52.2	63	350	0.238	40.3	46	0	0.169	31.4
52	350	0.274	43.8	47	0	0.179	31.2	46	10	0.188	34.5
48	0	0.193	32.1	47	10	0.172	30.5	46	20	0.222	43.1
48	10	0.195	33.1	47	20	0.226	42.7	46	30	0.317	72.2
48	20	0.252	45.6	47	30	0.328	74.0	46	40	0.251	59.9
48	30	0.340	73.7	47	40	0.266	63.7	46	50	0.306	77.9
48	40	0.338	78.9	47	50	0.339	84.6	46	60	0.318	83.2
48	50	0.357	85.2	47	60	0.368	93.6	46	70	0.283	74.5
48	60	0.380	90.9	47	70	0.308	77.3	46	80	0.313	79.7
48	70	0.369	87.5	47	80	0.349	84.1	46	90	0.326	80.5
48	80	0.377	86.5	47	90	0.427	97.4	46	100	0.358	83.9
48	90	0.435	94.1	47	100	0.415	92.6	46	110	0.188	45.5
48	100	0.525	106.5	47	110	0.276	63.1	46	120	0.178	41.8
48	110	0.396	80.6	47	120	0.194	44.7	46	130	0.219	50.1
48	120	0.251	52.2	47	130	0.236	49.8	46	140	0.220	47.7
48	130	0.442	82.9	47	140	0.279	56.2	46	220	0.277	57.7
48	140	0.414	75.4	47	220	0.285	56.1	46	230	0.253	56.0
48	220	0.326	60.3	47	230	0.247	52.8	46	240	0.211	50.0
48	230	0.301	58.9	47	240	0.220	49.4	46	250	0.160	39.2
48	240	0.257	53.7	47	250	0.173	41.8	46	260	0.155	39.4
48	250	0.215	48.3	47	260	0.145	36.4	46	270	0.151	40.4
48	260	0.182	42.5	47	270	0.169	43.1	46	280	0.161	43.7

Table 23 (cont.)

Run	Ray	s_0/R	Re_θ	Run	Ray	s_0/R	Re_θ	Run	Ray	s_0/R	Re_θ
46	290	0.208	57.0	46	320	0.230	54.7	46	350	0.185	34.2
46	300	0.179	46.7	46	330	0.223	48.7				
46	310	0.238	60.5	46	340	0.161	31.6				

Table 24. Transition locations for Test 7070 sphere-cone 15-weave model with seams.

Run	Ray	s_0/R	Re_θ	Run	Ray	s_0/R	Re_θ	Run	Ray	s_0/R	Re_θ
61	0	0.585	90.1	57	50	0.275	57.5	59	60	0.151	36.6
61	10	0.555	83.4	57	60	0.261	54.9	59	70	0.183	45.5
61	20	0.672	100.7	57	70	0.260	55.6	59	80	0.229	55.2
61	30	0.572	81.6	57	80	0.265	55.9	59	90	0.215	51.1
61	40	0.529	74.9	57	90	0.263	53.1	59	100	0.158	38.1
61	50	0.574	78.1	57	100	0.258	51.2	59	110	0.162	37.0
61	60	0.624	82.6	57	110	0.279	53.6	59	120	0.089	21.3
61	70	0.707	87.9	57	120	0.209	39.8	59	130	0.106	23.5
61	80	0.342	46.5	57	130	0.156	28.9	59	140	0.089	20.1
61	90	0.407	52.0	57	140	0.160	29.0	59	220	0.116	25.5
61	100	0.643	72.0	57	220	0.169	30.6	59	230	0.065	16.2
61	110	0.748	76.4	57	230	0.118	23.5	59	240	0.064	16.5
61	220	0.363	39.5	57	240	0.169	33.0	59	250	0.051	13.2
61	240	0.702	70.2	57	250	0.305	57.9	59	260	0.167	39.1
61	250	0.470	55.0	57	260	0.246	48.8	59	270	0.171	41.1
61	260	0.629	71.5	57	270	0.232	48.2	59	280	0.187	45.2
61	270	0.405	51.9	57	280	0.252	52.5	59	290	0.072	19.2
61	280	0.806	91.3	57	290	0.224	48.3	59	300	0.100	24.1
61	290	0.727	89.3	57	300	0.209	45.0	59	310	0.116	27.2
61	300	0.712	91.9	57	310	0.187	37.7	59	320	0.107	23.9
61	310	0.575	78.7	57	320	0.238	47.1	59	330	0.091	19.0
61	320	0.530	75.5	57	330	0.198	34.5	59	340	0.093	18.6
61	330	0.462	63.9	57	340	0.167	26.4	59	350	0.113	21.4
61	340	0.451	58.8	57	350	0.206	30.5	54	0	0.160	29.7
61	350	0.564	86.7	56	0	0.165	28.6	54	10	0.163	30.4
60	0	0.538	87.0	56	10	0.199	33.9	54	20	0.152	29.9
60	10	0.511	81.5	56	20	0.252	46.5	54	30	0.146	30.5
60	20	0.297	38.9	56	30	0.170	33.4	54	40	0.147	32.6
60	30	0.419	67.8	56	40	0.171	36.1	54	50	0.161	39.6
60	40	0.346	56.2	56	50	0.183	41.8	54	60	0.140	38.7
60	50	0.322	53.1	56	60	0.194	46.7	54	70	0.149	39.8
60	60	0.292	49.7	56	70	0.197	48.0	54	80	0.206	54.6
60	70	0.281	48.2	56	80	0.230	55.5	54	90	0.186	48.2
60	80	0.297	48.6	56	90	0.223	52.1	54	100	0.139	36.3
60	90	0.345	53.5	56	100	0.182	42.4	54	110	0.134	34.6
60	100	0.377	55.9	56	110	0.182	40.5	54	120	0.088	22.8
60	110	0.426	59.8	56	120	0.100	24.3	54	130	0.081	20.2
60	120	0.465	62.5	56	130	0.133	28.4	54	140	0.083	20.6
60	130	0.568	70.4	56	140	0.137	28.6	54	220	0.064	16.5
60	140	0.249	33.7	56	220	0.090	20.4	54	230	0.063	15.7
60	220	0.219	29.9	56	230	0.105	23.3	54	240	0.058	15.1
60	230	0.478	61.4	56	240	0.101	23.4	54	250	0.056	16.5
60	240	0.520	67.9	56	250	0.080	19.9	54	260	0.151	38.9
60	250	0.456	63.5	56	260	0.175	41.8	54	270	0.156	40.8
60	260	0.406	60.3	56	270	0.173	41.1	54	280	0.099	27.1
60	270	0.373	58.6	56	280	0.231	54.4	54	290	0.092	25.5
60	280	0.331	53.7	56	290	0.114	29.1	54	300	0.116	32.3
60	290	0.268	46.3	56	300	0.124	30.0	54	310	0.120	29.2
60	300	0.318	54.1	56	310	0.131	30.9	54	320	0.100	23.2
60	310	0.485	80.9	56	320	0.116	25.6	54	330	0.084	18.7
60	320	0.439	73.9	56	330	0.114	23.0	54	340	0.082	17.8
60	330	0.464	76.9	56	340	0.111	21.5	54	350	0.101	20.6
60	340	0.285	37.0	56	350	0.123	22.6	58	0	0.139	25.6
60	350	0.276	33.4	59	0	0.165	28.6	58	10	0.154	28.1
57	0	0.176	26.1	59	10	0.199	34.0	58	20	0.147	28.0
57	10	0.223	32.3	59	20	0.204	37.4	58	30	0.146	29.4
57	20	0.273	44.6	59	30	0.154	30.5	58	40	0.144	31.5
57	30	0.208	36.1	59	40	0.169	36.0	58	50	0.148	35.8
57	40	0.270	53.2	59	50	0.171	39.0				

Table 24 (cont.)

Run	Ray	s_0/R	Re_θ	Run	Ray	s_0/R	Re_θ	Run	Ray	s_0/R	Re_θ
58	60	0.116	31.9	58	330	0.086	18.9	53	120	0.062	17.1
58	70	0.139	36.9	58	340	0.076	16.5	53	130	0.056	15.4
58	80	0.195	50.3	58	350	0.111	21.8	53	140	0.063	16.8
58	90	0.162	41.9	53	0	0.141	25.7	53	220	0.118	27.8
58	100	0.103	27.7	53	10	0.152	28.1	53	230	0.051	14.9
58	110	0.099	25.5	53	20	0.144	27.8	53	240	0.048	14.0
58	120	0.077	19.0	53	30	0.137	27.8	53	270	0.069	20.2
58	130	0.062	15.7	53	40	0.135	29.4	53	300	0.078	21.9
58	140	0.068	17.1	53	50	0.140	33.7	53	310	0.089	21.5
58	220	0.146	32.5	53	60	0.106	27.9	53	320	0.077	18.5
58	230	0.053	15.0	53	70	0.125	34.1	53	330	0.072	16.6
58	240	0.045	13.0	53	80	0.165	44.2	53	340	0.069	15.8
58	300	0.088	25.0	53	90	0.126	33.5	53	350	0.124	23.9
58	310	0.112	26.8	53	100	0.096	25.4				
58	320	0.096	21.9	53	110	0.095	25.8				

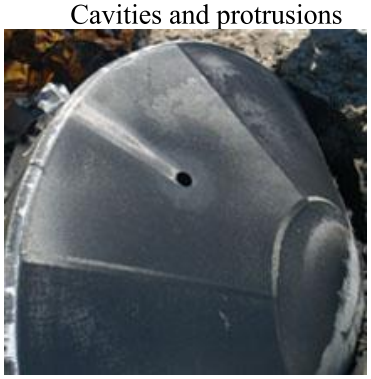
Table 25. Transition locations for Test 7070 sphere-cone 20-weave model with seams

Run	Ray	s_0/R	Re_θ	Run	Ray	s_0/R	Re_θ	Run	Ray	s_0/R	Re_θ
80	70	0.796	69.5	79	350	0.411	58.7	75	0	0.170	30.1
80	290	1.078	80.2	78	0	0.215	30.7	75	10	0.214	37.2
81	0	0.592	93.7	78	10	0.214	31.7	75	20	0.231	43.5
81	10	0.571	91.0	78	20	0.313	53.3	75	30	0.153	30.9
81	20	0.682	102.1	78	30	0.220	38.0	75	40	0.156	34.9
81	30	0.581	82.9	78	40	0.215	40.4	75	50	0.157	36.8
81	40	0.617	86.8	78	50	0.222	44.6	75	60	0.167	43.9
81	50	0.444	62.3	78	60	0.239	51.0	75	70	0.189	49.4
81	60	0.454	63.3	78	70	0.256	55.0	75	80	0.151	39.1
81	70	0.597	77.0	78	80	0.236	50.0	75	90	0.151	38.9
81	80	0.674	81.5	78	90	0.198	40.5	75	100	0.126	32.0
81	90	0.791	86.9	78	100	0.183	37.1	75	110	0.135	33.5
81	100	0.809	83.3	78	110	0.193	38.2	75	120	0.125	30.5
81	110	0.671	71.1	78	120	0.155	30.0	75	130	0.163	37.6
81	120	0.421	47.9	78	130	0.255	45.4	75	140	0.159	34.0
81	130	0.624	62.4	78	140	0.258	44.9	75	220	0.198	42.4
81	140	0.497	50.6	78	220	0.254	43.2	75	230	0.164	38.1
81	220	0.610	59.3	78	230	0.208	37.6	75	240	0.144	35.1
81	230	0.668	64.8	78	240	0.219	41.4	75	250	0.136	33.8
81	240	0.643	66.6	78	250	0.190	37.5	75	260	0.132	32.8
81	250	0.855	80.5	78	260	0.184	37.2	75	270	0.148	38.2
81	260	0.648	72.9	78	270	0.178	36.8	75	280	0.130	34.8
81	270	0.696	79.5	78	280	0.203	43.2	75	290	0.168	42.8
81	280	0.632	77.0	78	290	0.240	52.1	75	300	0.159	41.7
81	290	0.496	66.5	78	300	0.244	51.4	75	310	0.206	50.5
81	300	0.453	63.1	78	310	0.265	55.1	75	320	0.202	46.1
81	310	0.427	59.7	78	320	0.263	51.4	75	330	0.257	55.3
81	320	0.571	81.3	78	330	0.303	56.8	75	340	0.233	44.0
81	330	0.584	83.7	78	340	0.300	50.9	75	350	0.188	33.5
81	340	0.598	89.6	78	350	0.221	32.5	76	0	0.166	29.7
81	350	0.614	100.8	77	0	0.180	29.7	76	10	0.186	33.1
79	0	0.295	36.2	77	10	0.222	36.4	76	20	0.206	39.1
79	10	0.484	74.9	77	20	0.255	45.7	76	30	0.137	27.3
79	20	0.467	76.1	77	30	0.171	33.4	76	40	0.147	32.5
79	30	0.399	63.4	77	40	0.173	36.9	76	50	0.139	33.6
79	40	0.299	47.4	77	50	0.180	40.5	76	60	0.163	42.9
79	50	0.383	64.1	77	60	0.173	42.7	76	70	0.161	43.4
79	60	0.357	61.0	77	70	0.201	49.7	76	80	0.139	37.0
79	70	0.372	61.4	77	80	0.166	40.3	76	90	0.145	37.5
79	80	0.372	60.3	77	90	0.169	40.7	76	100	0.106	27.8
79	90	0.356	55.8	77	100	0.137	32.3	76	110	0.125	30.8
79	100	0.238	38.1	77	110	0.157	35.9	76	120	0.121	29.9
79	110	0.356	52.4	77	120	0.137	30.5	76	130	0.143	34.0
79	120	0.340	48.7	77	130	0.178	37.3	76	140	0.135	30.6
79	130	0.487	62.4	77	140	0.179	36.3	76	220	0.172	38.2
79	140	0.441	54.8	77	220	0.216	41.9	76	230	0.149	34.6
79	220	0.574	68.2	77	230	0.179	37.3	76	240	0.125	31.4
79	230	0.517	64.9	77	240	0.167	37.5	76	250	0.138	34.3
79	240	0.457	61.0	77	250	0.153	35.8	76	260	0.115	29.4
79	250	0.320	46.8	77	260	0.148	34.8	76	270	0.116	31.0
79	260	0.548	77.4	77	270	0.135	33.4	76	280	0.121	32.6
79	270	0.490	73.7	77	280	0.164	40.2	76	290	0.157	42.1
79	280	0.359	58.1	77	290	0.174	43.5	76	300	0.142	38.6
79	290	0.308	51.7	77	300	0.174	42.6	76	310	0.180	44.0
79	300	0.302	51.9	77	310	0.231	53.8	76	320	0.187	42.5
79	310	0.323	53.7	77	320	0.220	48.3	76	330	0.246	52.7
79	320	0.359	59.2	77	330	0.238	47.7	76	340	0.205	39.1
79	330	0.357	54.9	77	340	0.255	45.8	76	350	0.168	30.2
79	340	0.464	75.1	77	350	0.200	33.5	66	0	0.956	173.9

Table 25 (cont).

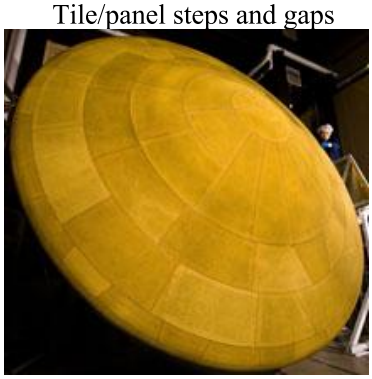
Run	Ray	s_0/R	Re_θ	Run	Ray	s_0/R	Re_θ	Run	Ray	s_0/R	Re_θ
66	10	1.234	211.6	67	340	0.768	161.6	71	350	0.548	127.5
66	20	0.808	150.1	67	350	0.727	154.7	72	0	0.586	134.3
66	30	1.208	203.6	71	0	0.622	141.6	72	10	0.671	151.9
66	50	1.138	191.9	71	10	0.680	152.9	72	20	0.681	153.3
66	330	1.323	217.3	71	20	0.689	155.0	72	30	0.673	149.3
66	340	1.157	201.4	71	30	0.678	149.9	72	40	0.598	134.5
66	350	0.885	162.8	71	40	0.604	136.0	72	50	0.655	143.0
67	0	0.766	161.0	71	50	0.662	144.4	72	60	0.585	128.0
67	10	0.733	156.3	71	60	0.594	129.0	72	70	0.708	147.3
67	20	0.758	160.3	71	70	0.719	148.7	72	80	0.751	150.6
67	30	0.739	154.8	71	80	0.765	154.2	72	90	0.755	147.5
67	40	0.731	152.8	71	90	0.762	148.7	72	100	0.772	146.9
67	50	0.749	153.1	71	100	0.783	147.1	72	110	0.755	139.8
67	60	0.857	168.3	71	110	0.771	141.4	72	120	0.631	116.1
67	70	0.839	162.6	71	120	0.661	122.2	72	130	0.658	115.7
67	80	0.843	159.8	71	130	0.688	119.5	72	140	0.566	99.7
67	90	0.815	152.0	71	140	0.602	103.5	72	230	0.722	122.1
67	100	1.034	169.2	71	230	0.742	121.9	72	240	0.694	125.3
67	240	0.841	136.7	71	240	0.728	132.0	72	250	0.687	128.5
67	250	0.949	153.7	71	250	0.718	134.2	72	260	0.759	144.0
67	260	0.970	165.9	71	260	0.796	149.4	72	270	0.706	140.3
67	270	0.824	152.7	71	270	0.740	144.7	72	280	0.756	150.8
67	280	0.880	165.1	71	280	0.806	160.8	72	290	0.746	153.4
67	290	0.868	166.7	71	290	0.762	156.5	72	300	0.645	137.6
67	300	0.884	171.7	71	300	0.678	143.0	72	310	0.629	137.5
67	310	0.768	156.6	71	310	0.662	143.5	72	320	0.611	137.0
67	320	0.744	154.8	71	320	0.645	143.4	72	330	0.574	130.5
67	330	0.684	145.1	71	330	0.590	133.6	72	340	0.506	119.2
				71	340	0.520	122.5	72	350	0.515	121.2

Cavities and protrusions



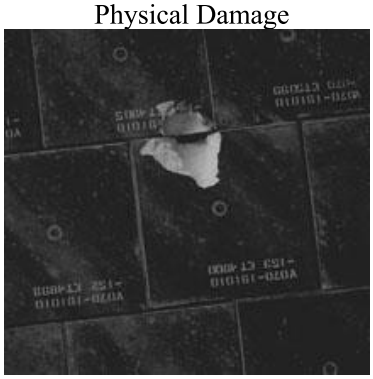
a) Heat shield attachment point cavity on Genesis entry vehicle

Tile/panel steps and gaps



b) TPS block panels on MSL entry vehicle

Physical Damage



c) Damaged TPS tile on Shuttle Orbiter

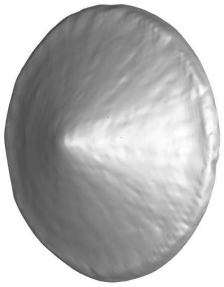
Figure 1. Discrete surface roughness types.

Pattern



a) Hexcomb cavities on Apollo ablated TPS

Flexible TPS



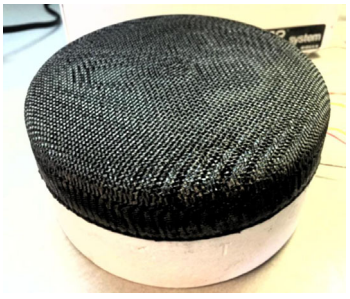
b) Flexible TPS deflection under aerodynamic load

Sand-grain



c) Ablation of monolithic TPS on Stardust capsule

Woven



c) Arc jet test sample of woven TPS

Figure 2. Distributed surface roughness types.

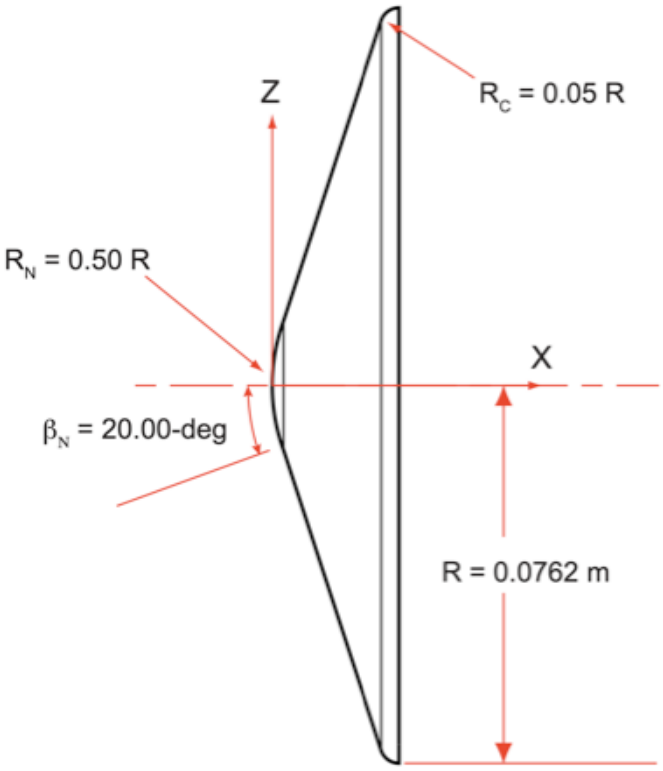


Figure 3. Sphere-cone geometry.

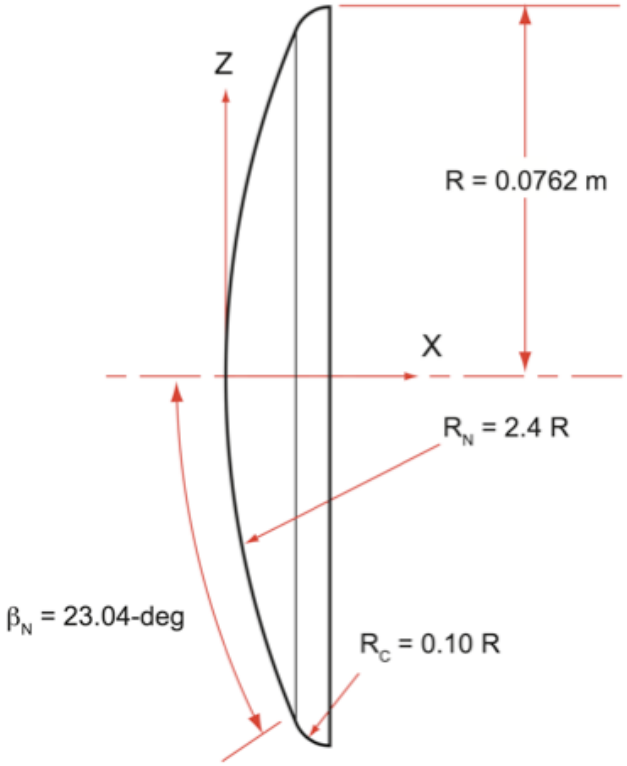


Figure 4. Spherical-cap geometry.

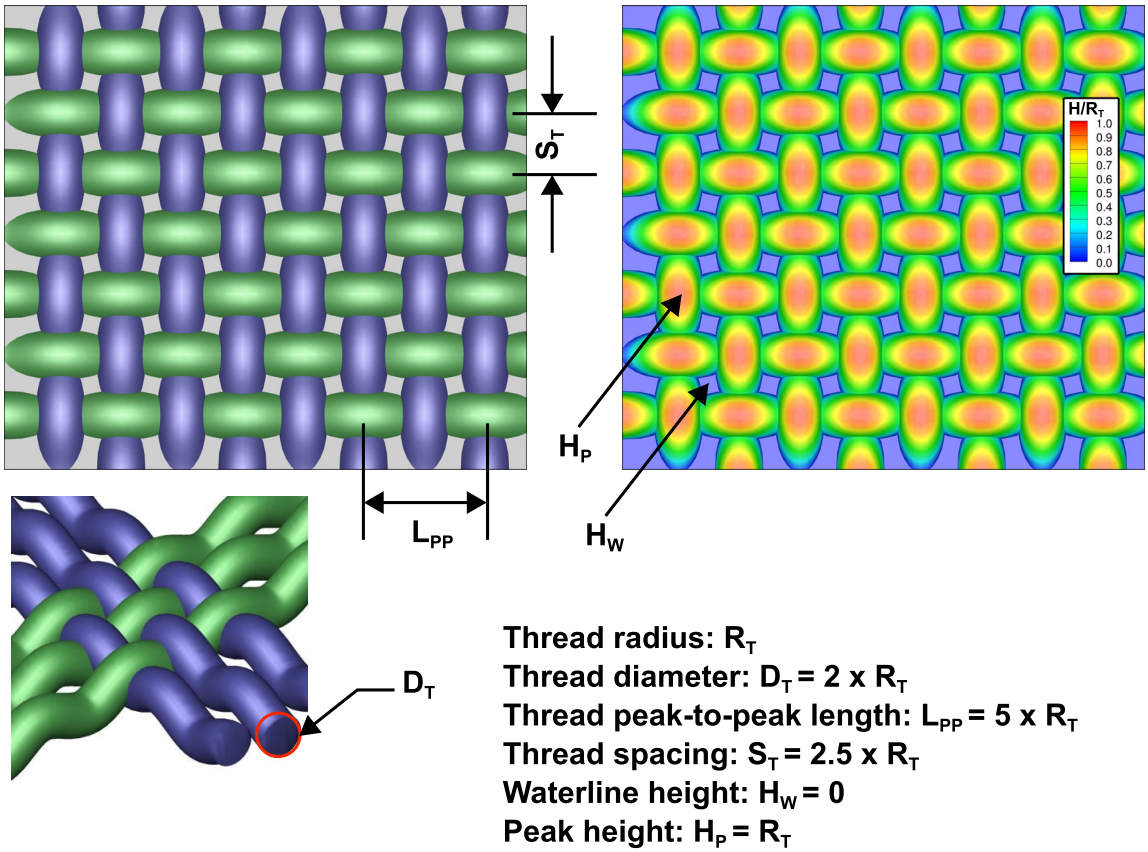
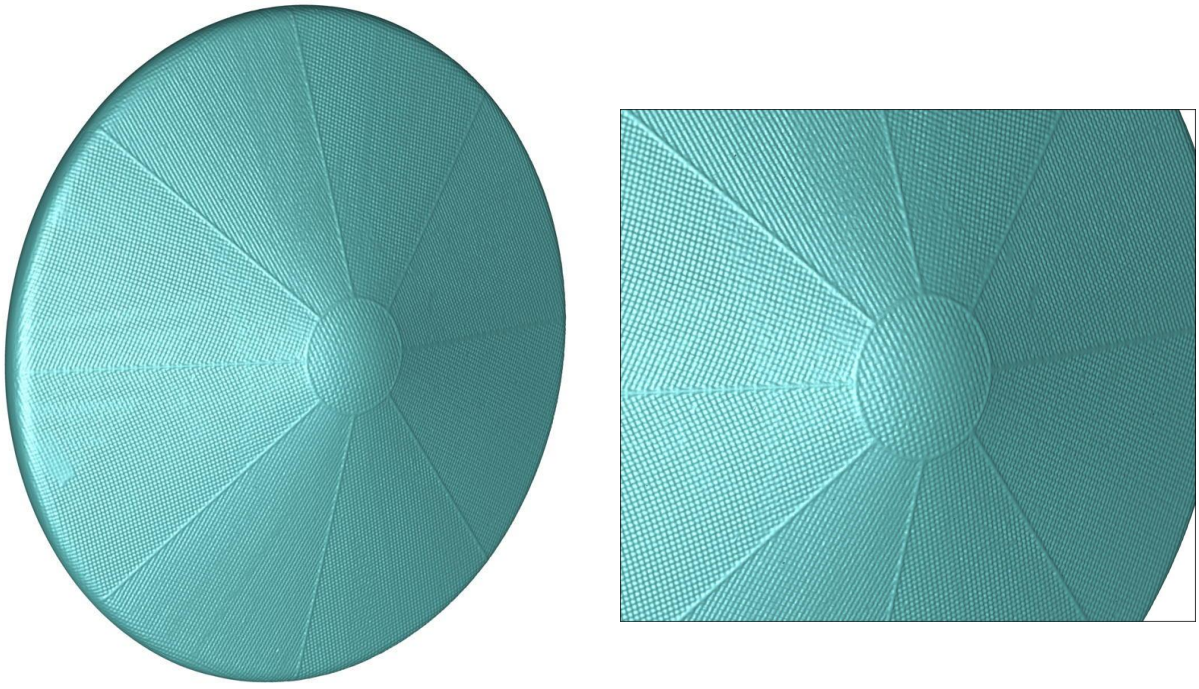
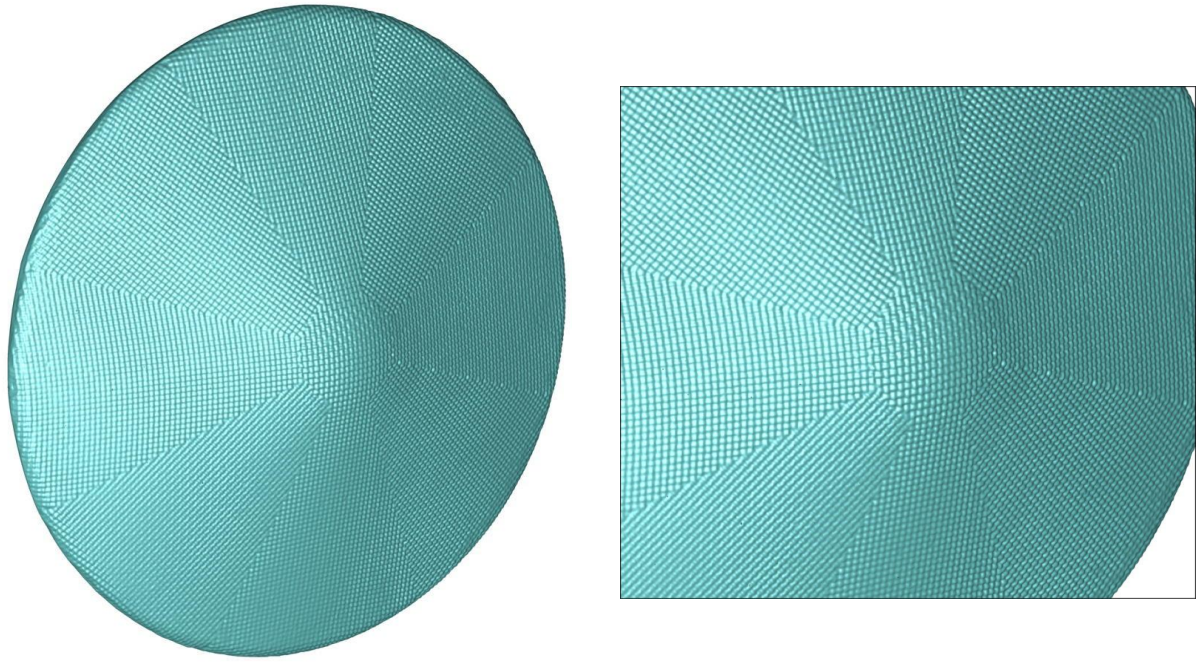


Figure 5. Weave details – two-dimensional representation.



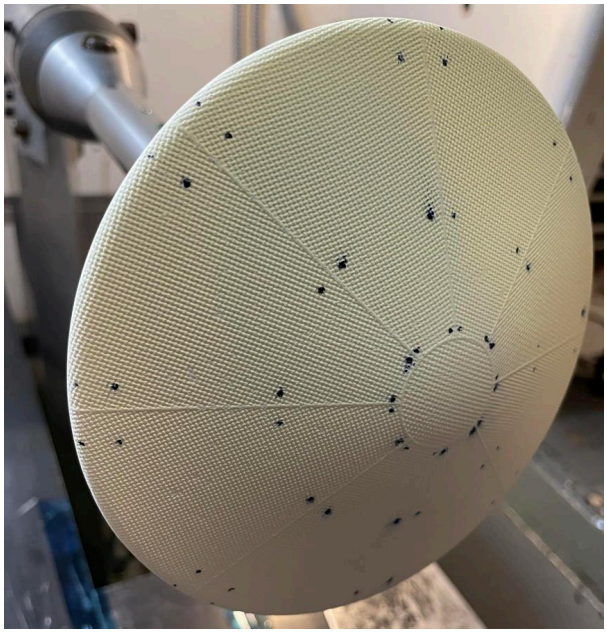
a) Full view b) Close-up view

Figure 6. Surface scan of 20-mil sphere-cone model with seams.

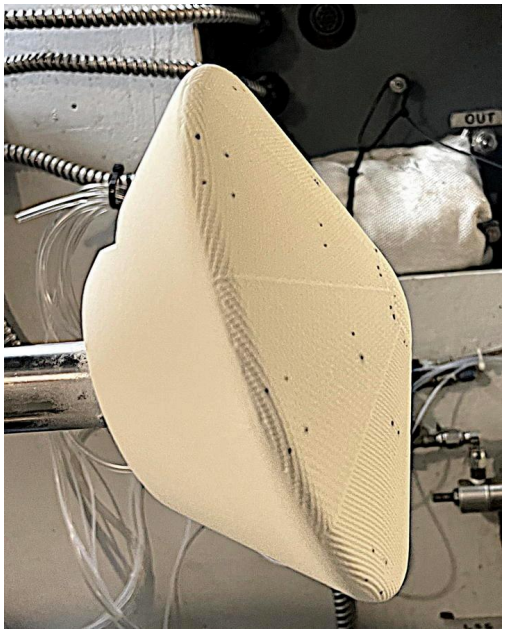


a) Full view b) Close-up view

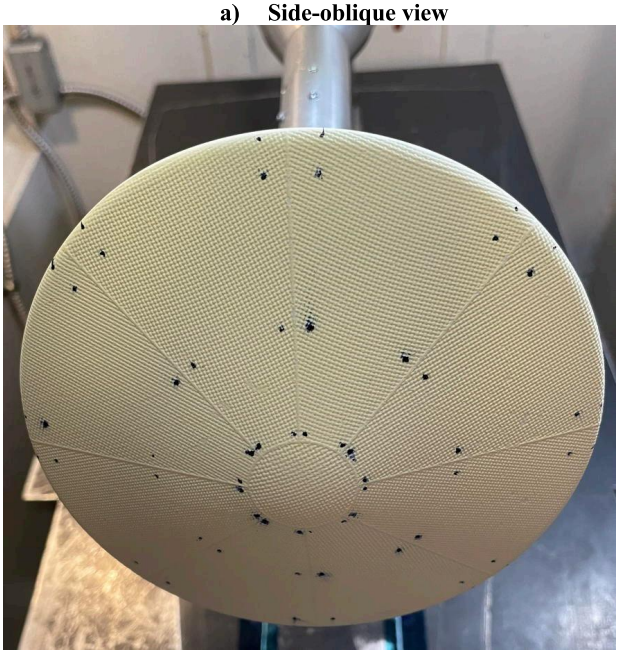
Figure 7. Surface scan of 20-mil weave sphere-cone model without seams.



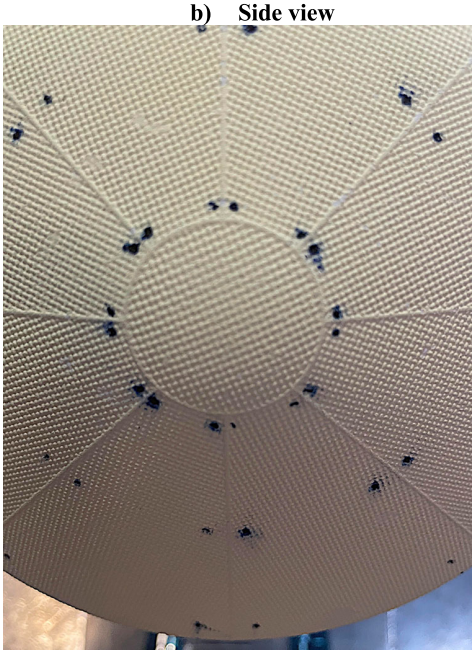
a) Side-oblique view



b) Side view



c) Front view



d) Front close-up view

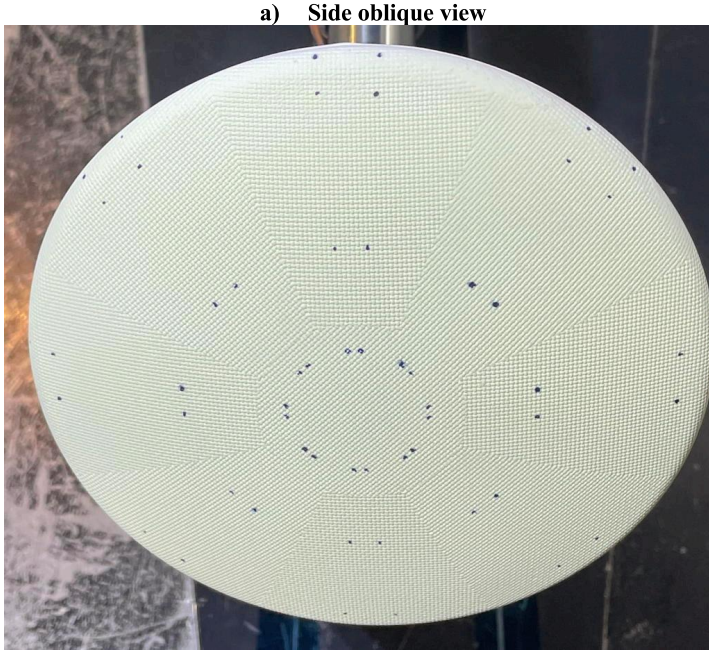
Figure 8. Sample Model Photographs –20-mil weave sphere-cone model with seams



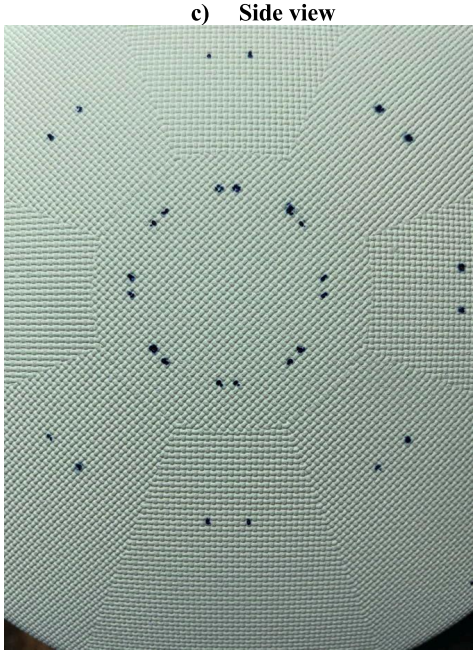
a) Side oblique view



c) Side view



d) Front view



d) Front close-up view

Figure 9. Sample Model Photographs – 15-mil spherical-cap model without seams

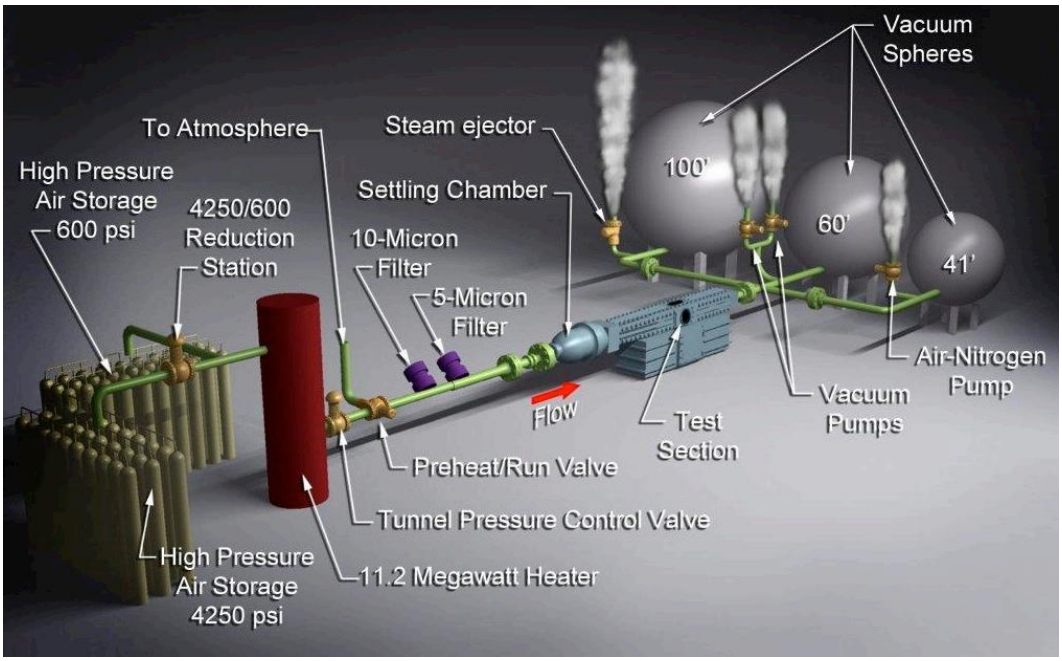


Figure 10. Schematic of Langley Research Center 20-Inch Mach 6 Air Tunnel.



Figure 11. Langley Research Center 20-Inch Mach 6 Air Tunnel test section.

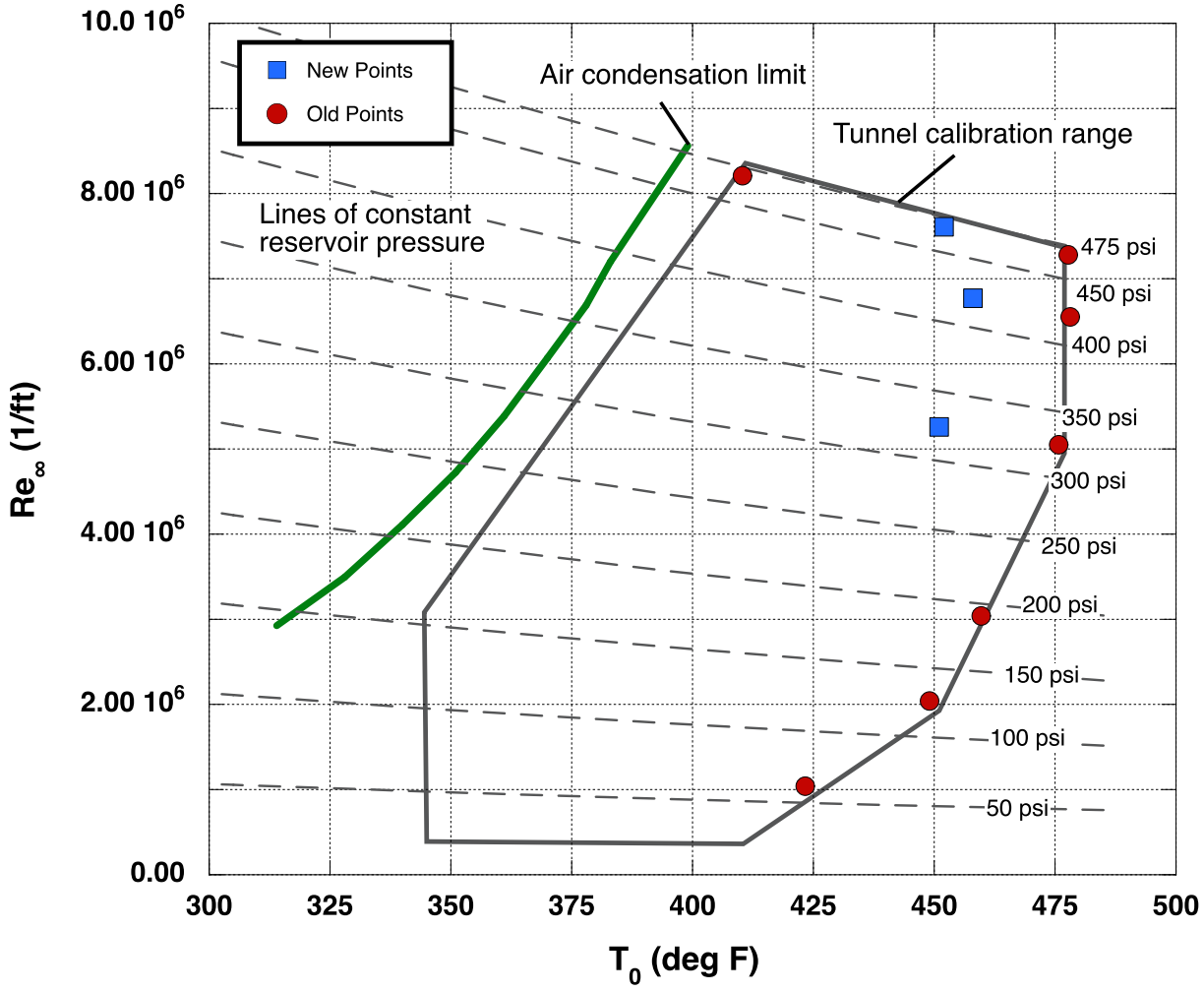


Figure 12. Modified operating points for the 20-Inch Mach 6 Air Tunnel.

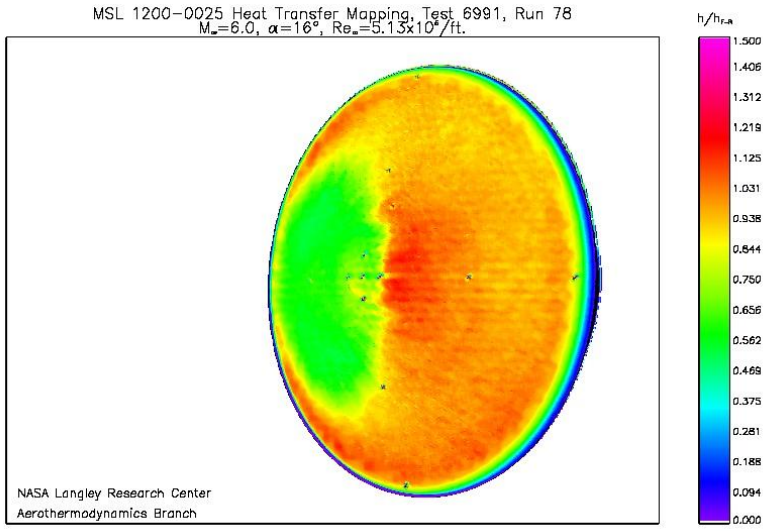


Figure 13. Sample phosphor thermography 2-D image data.

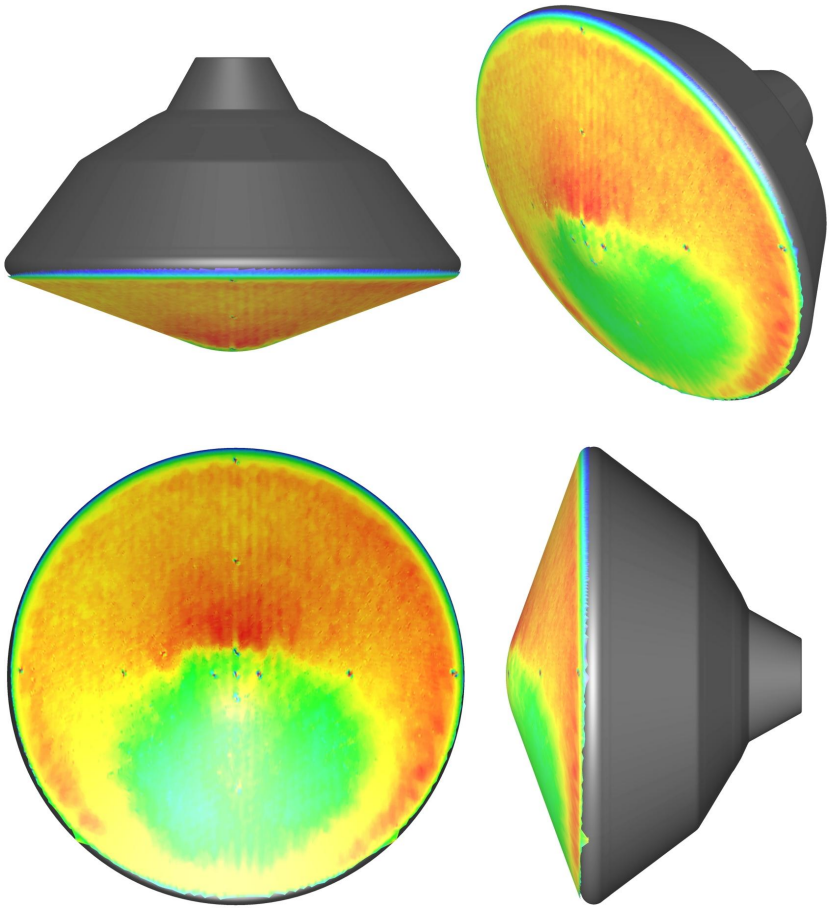


Figure 14. Sample 3-D mapping of phosphor thermography data.

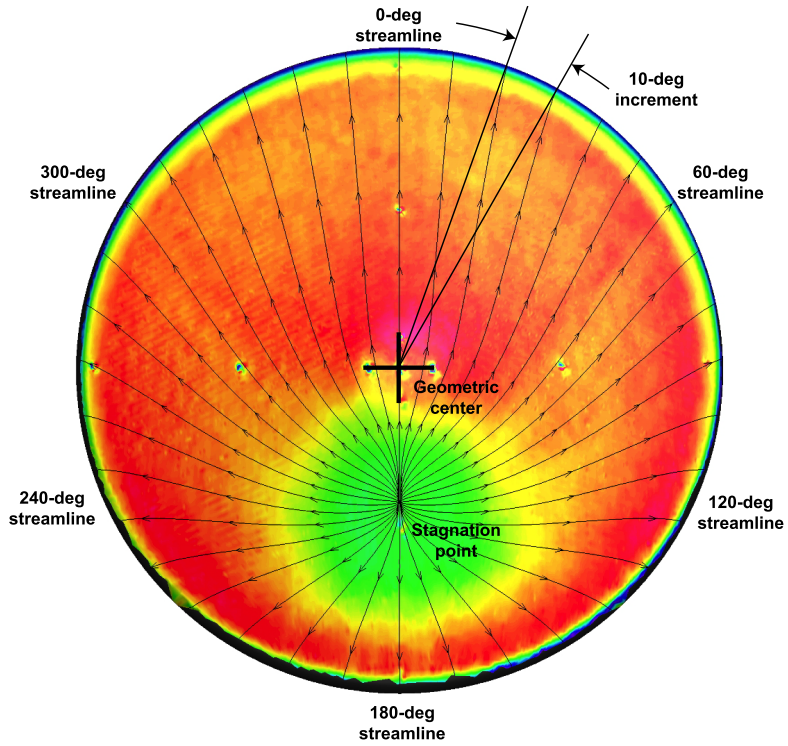


Figure 15. Streamlines for data extraction on sphere-cone geometry.

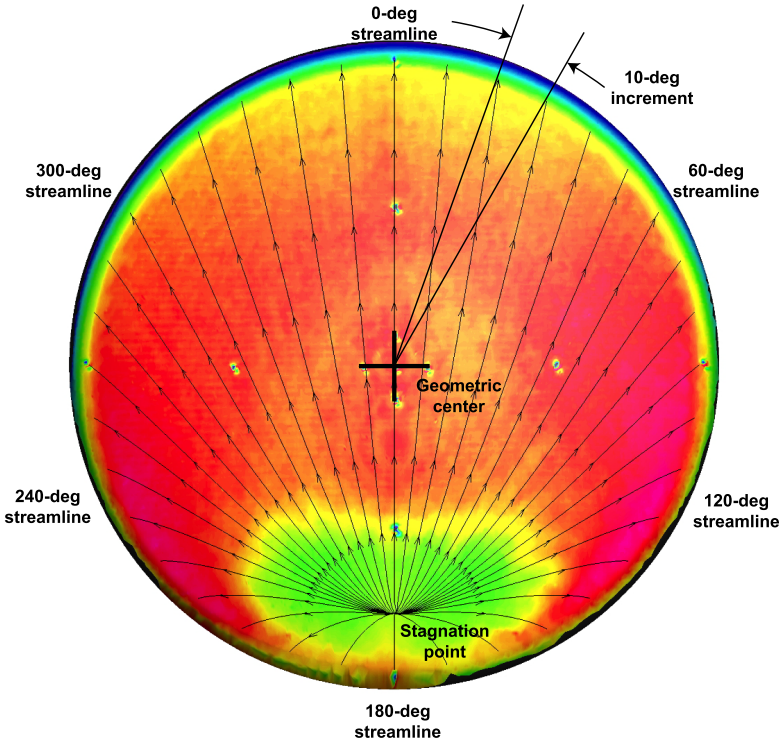


Figure 16. Streamlines for data extraction on spherical-cap geometry.

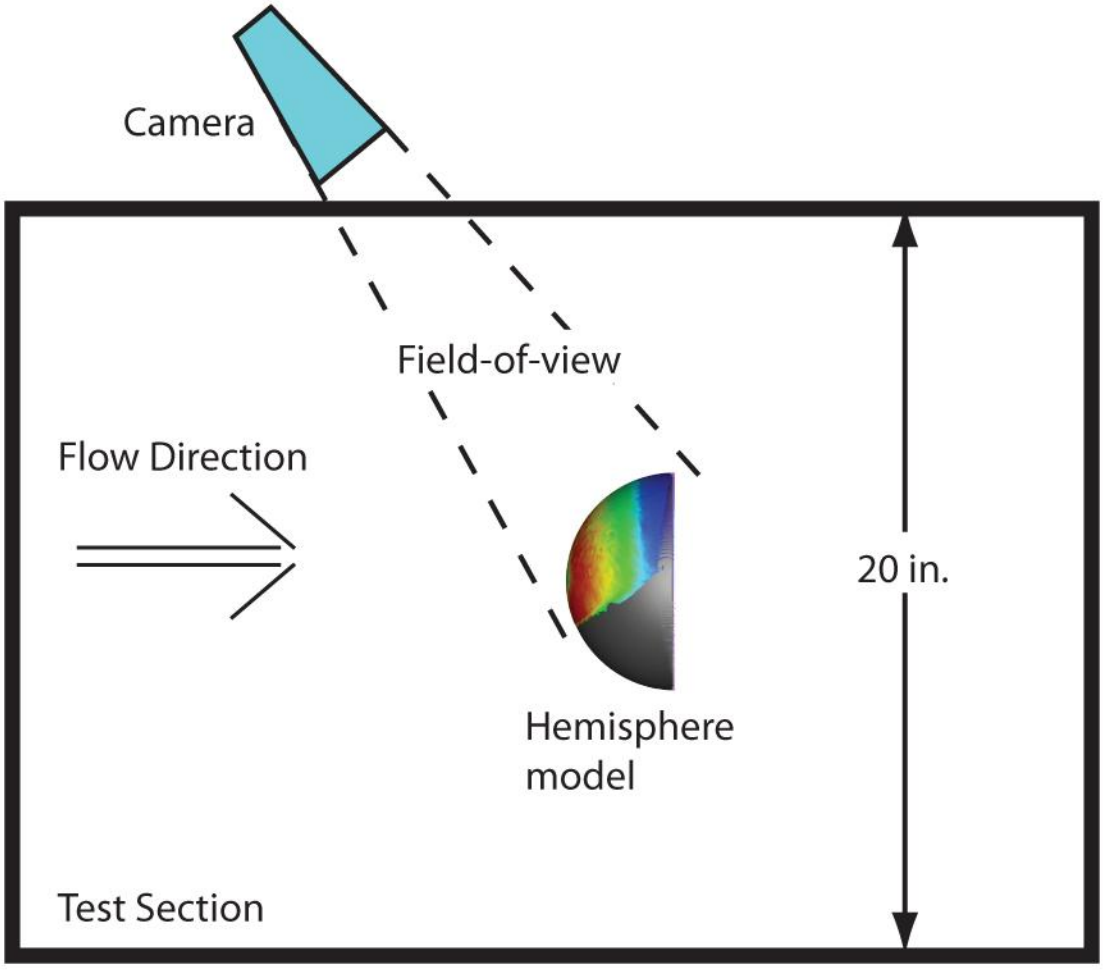


Figure 17. Illustration of camera field-of-view for hemisphere model in 20-Inch Mach 6 Air Tunnel.

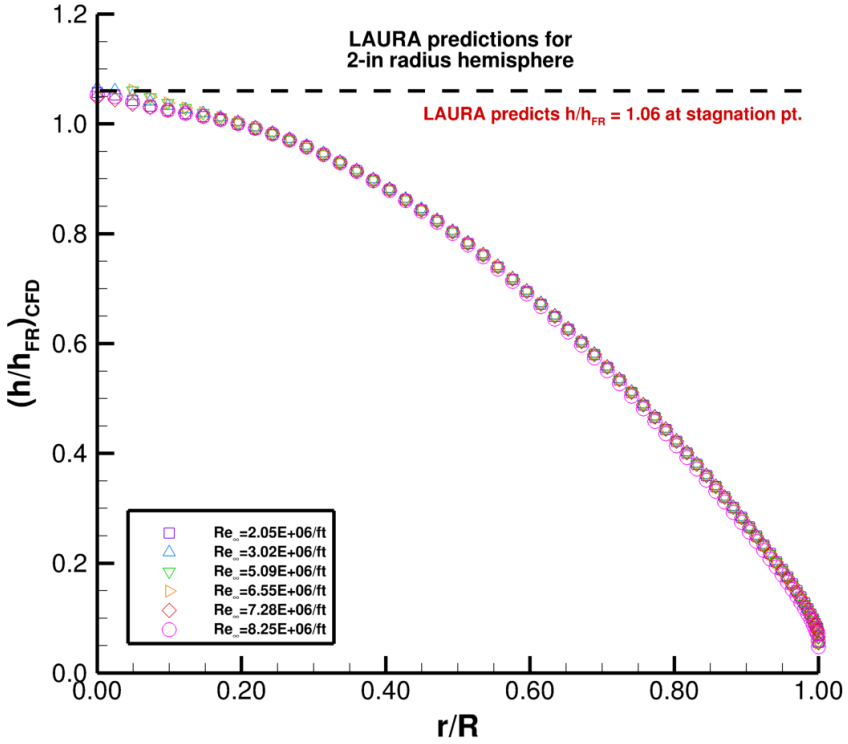


Figure 18. CFD predictions for hemisphere heating at wind tunnel conditions.

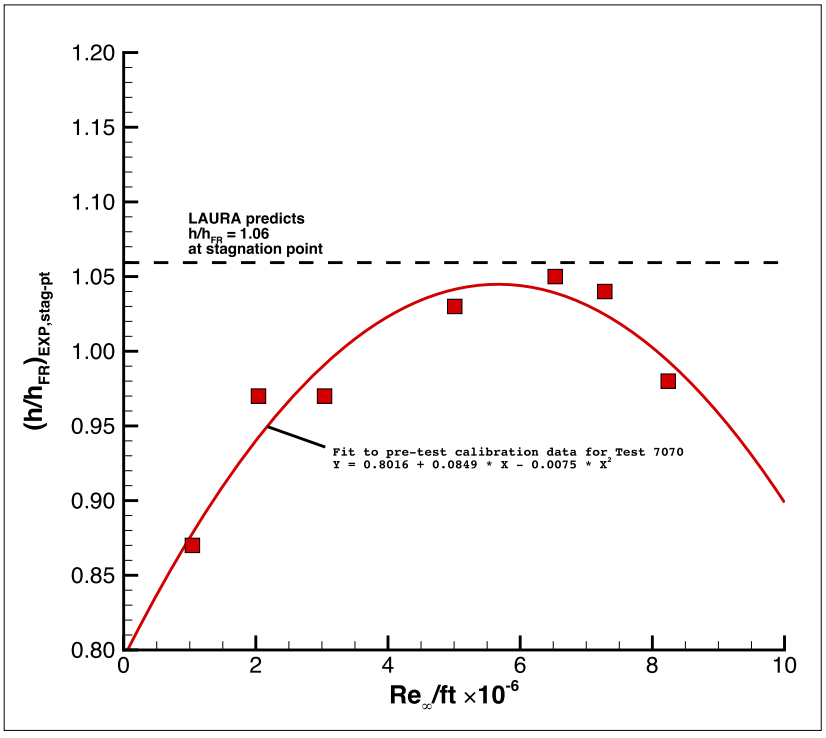
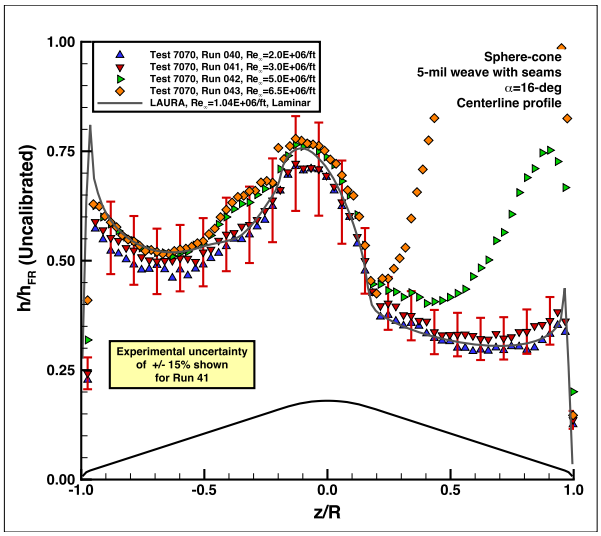
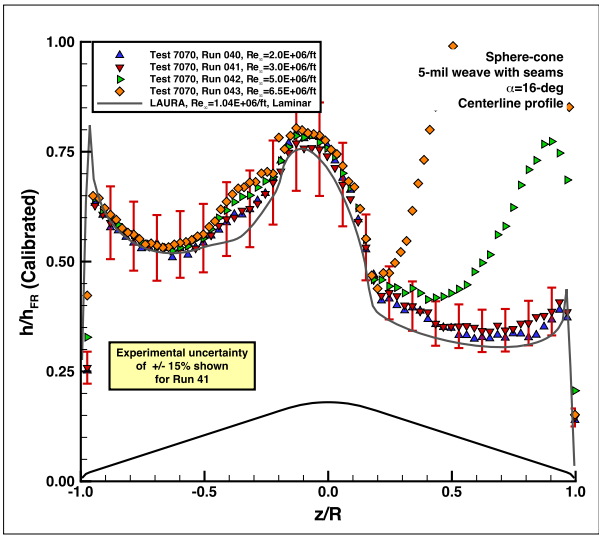


Figure 19. Measured hemisphere stagnation point heating from pretest calibration

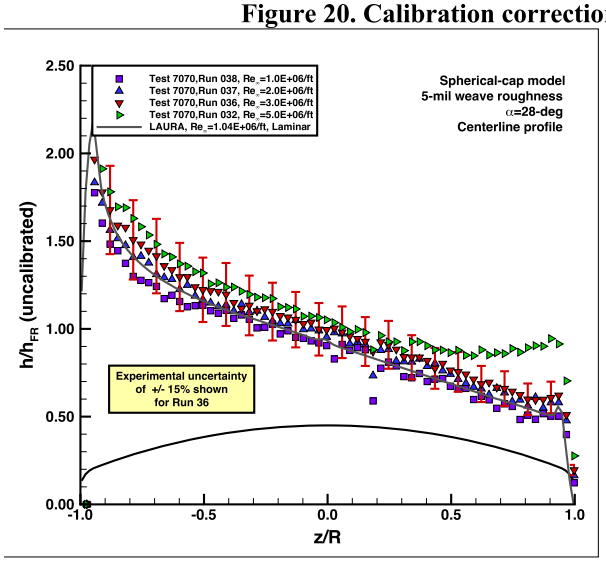


a) Uncalibrated

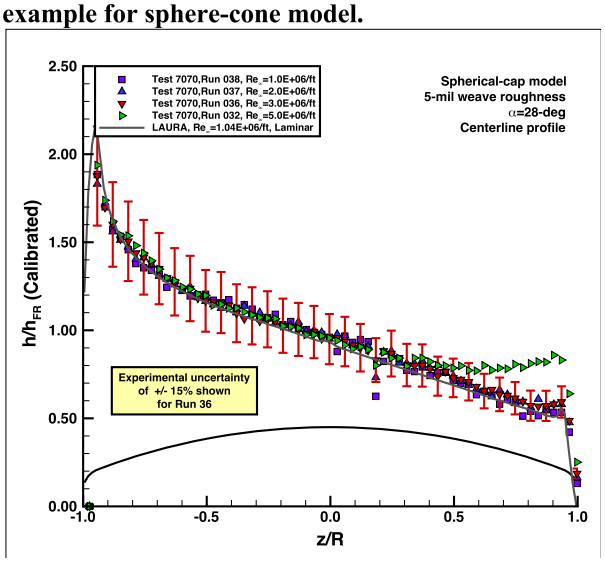


b) Calibrated

Figure 20. Calibration correction example for sphere-cone model.

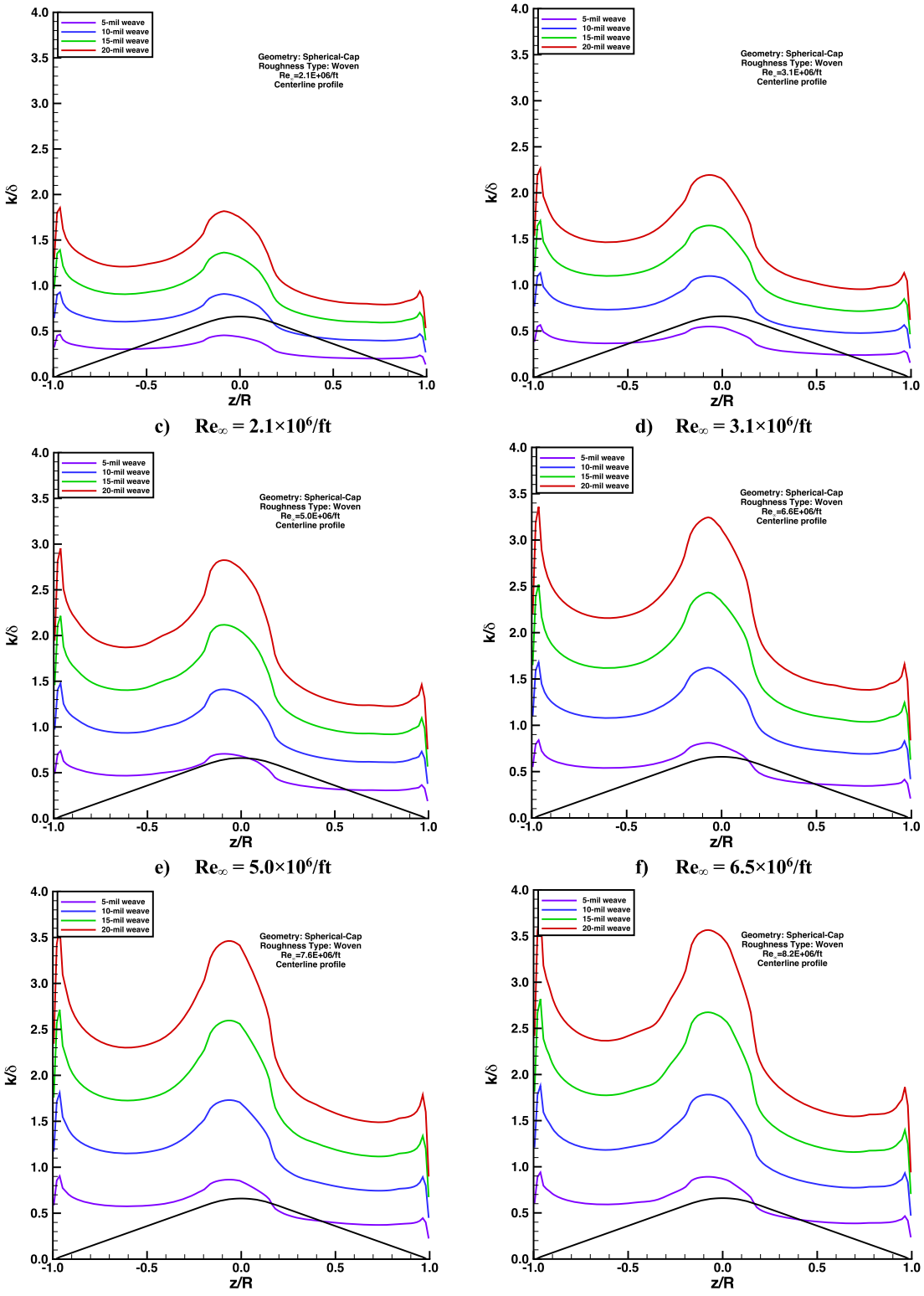


a) Uncalibrated



b) Calibrated

Figure 21. Calibration correction example for spherical-cap model.



c) $Re_\infty = 2.1\times10^6$/ft

d) $Re_\infty = 3.1\times10^6$/ft

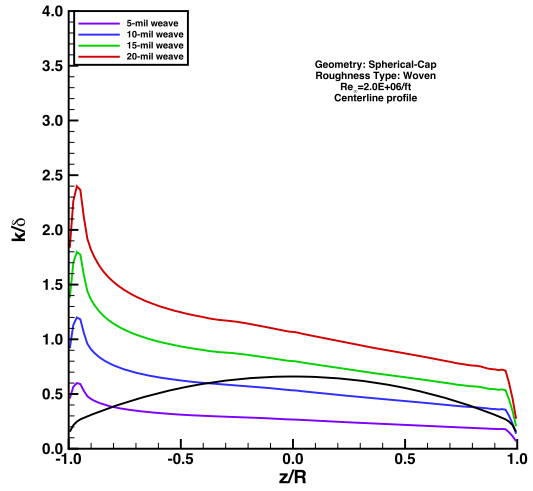
e) $Re_\infty = 5.0\times10^6$/ft

f) $Re_\infty = 6.5\times10^6$/ft

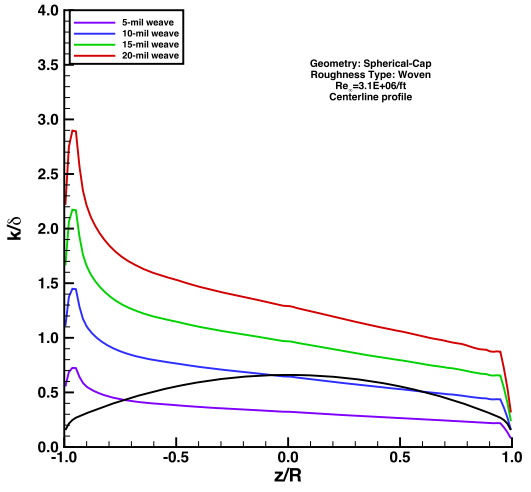
g) $Re_\infty = 7.3\times10^6$/ft

h) $Re_\infty = 8.2\times10^6$/ft

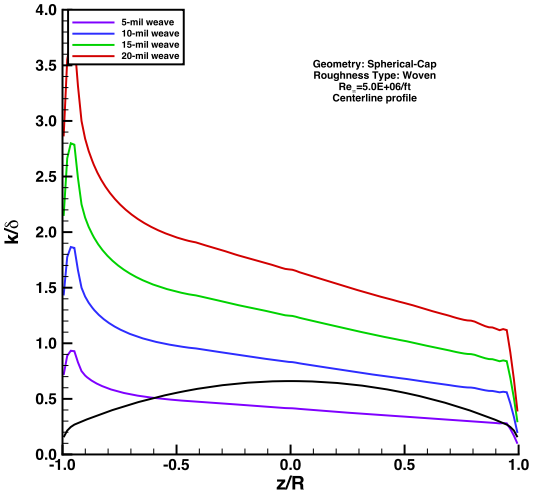
Figure 22. Centerline profiles of roughness effects on k/δ, sphere-cone geometry.



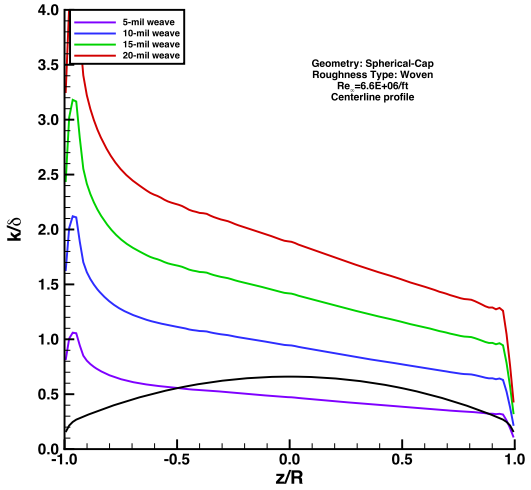
a) $Re_\infty = 2.1\times10^6$/ft



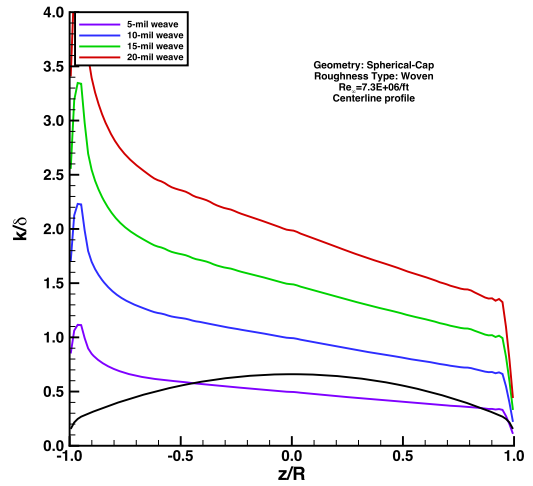
b) $Re_\infty = 3.1\times10^6$/ft



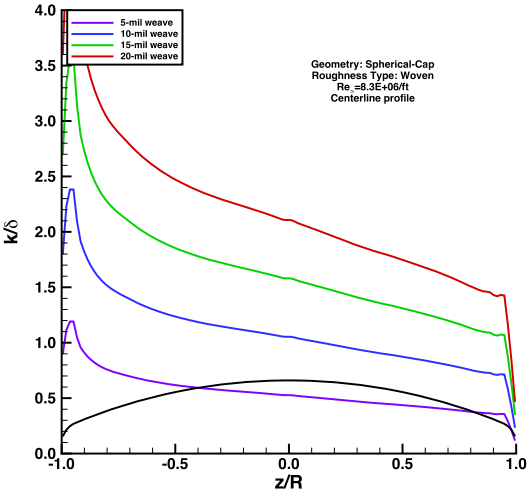
c) $Re_\infty = 5.0\times10^6$/ft



d) $Re_\infty = 6.6\times10^6$/ft



e) $Re_\infty = 7.3\times10^6$/ft



f) $Re_\infty = 8.2\times10^6$/ft

Figure 23. Centerline profiles of roughness effects on k/δ, spherical-cap geometry.

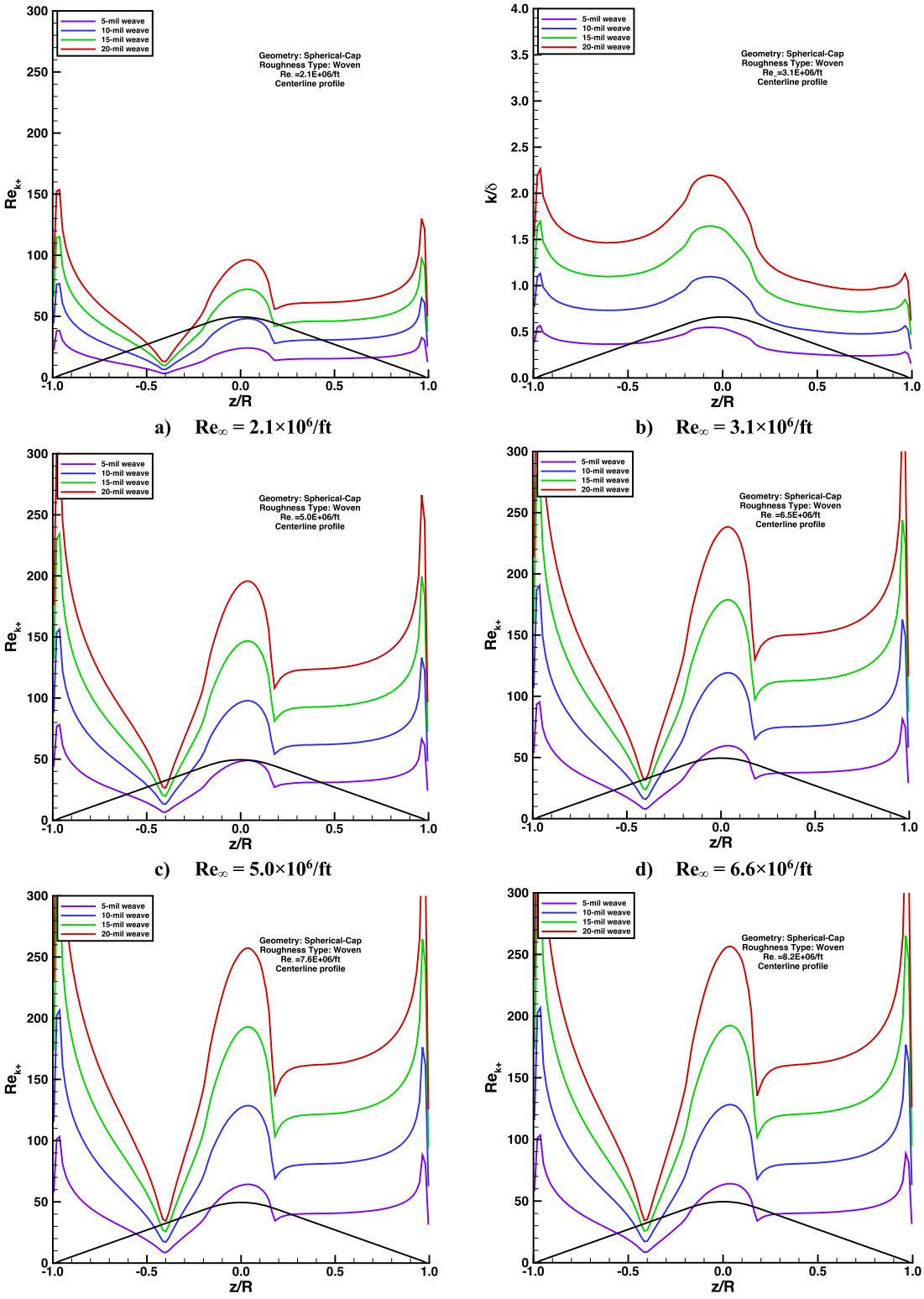
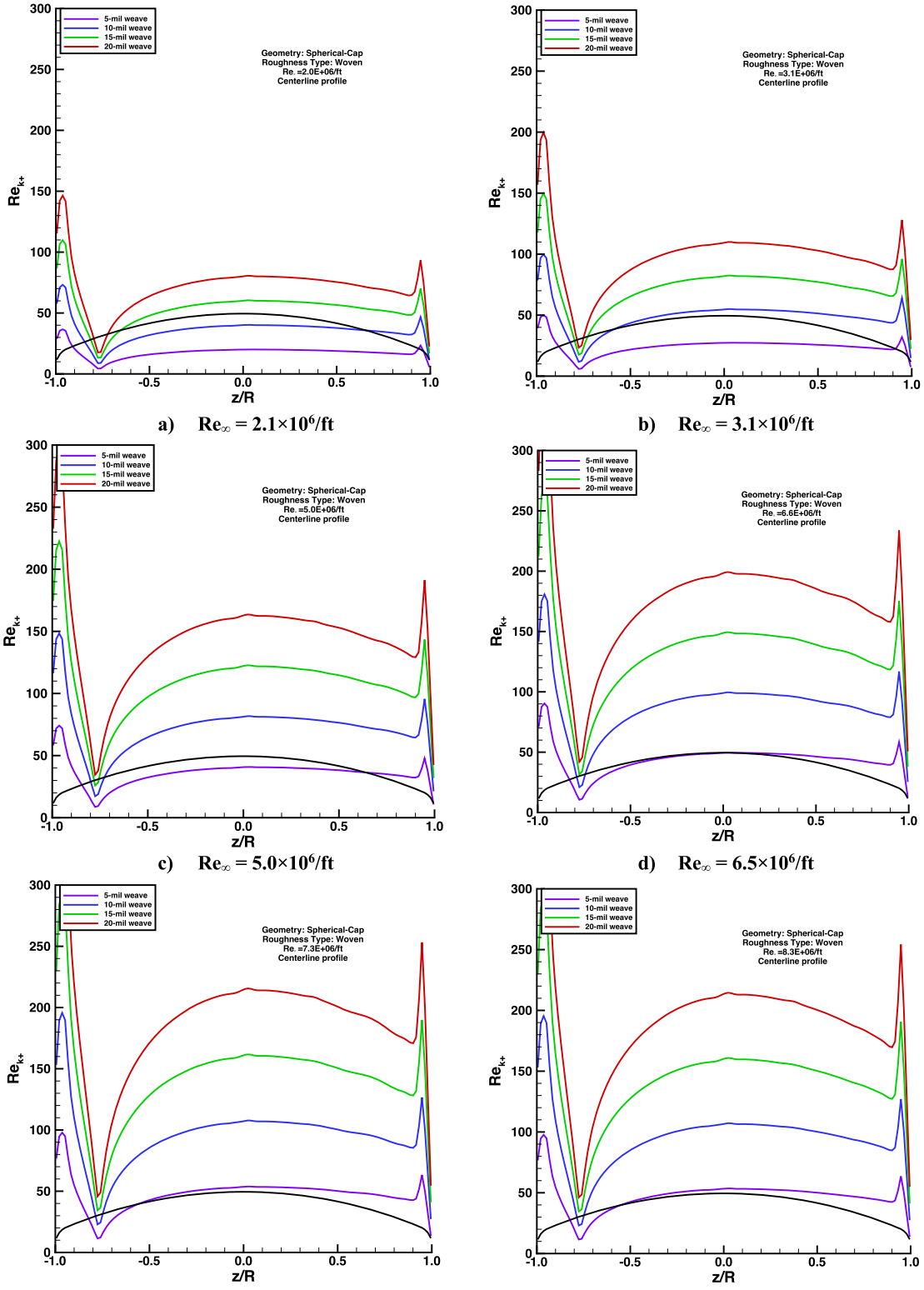


Figure 24. Centerline profiles of roughness effects on Re_{k+}, sphere-cone geometry.



a) $Re_\infty = 2.1\times10^6$/ft

b) $Re_\infty = 3.1\times10^6$/ft

c) $Re_\infty = 5.0\times10^6$/ft

d) $Re_\infty = 6.5\times10^6$/ft

e) $Re_\infty = 7.3\times10^6$/ft

f) $Re_\infty = 8.2\times10^6$/ft

Figure 25. Centerline profiles of roughness effects on Re_{k+}, spherical-cap geometry.

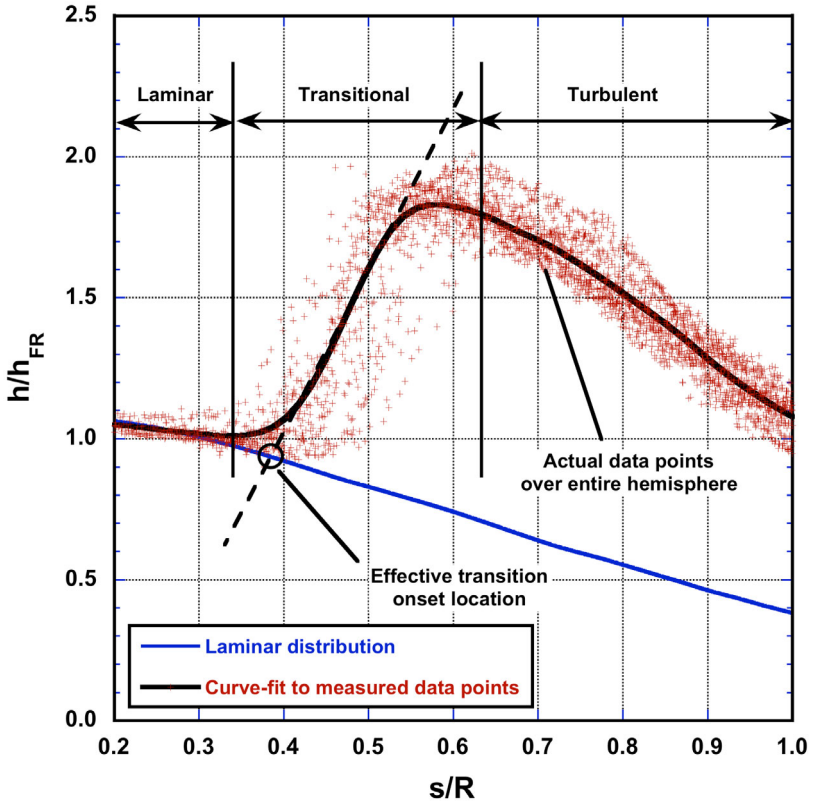


Figure 26. Tangent-slope-intercept method for determination of effect transition onset location.

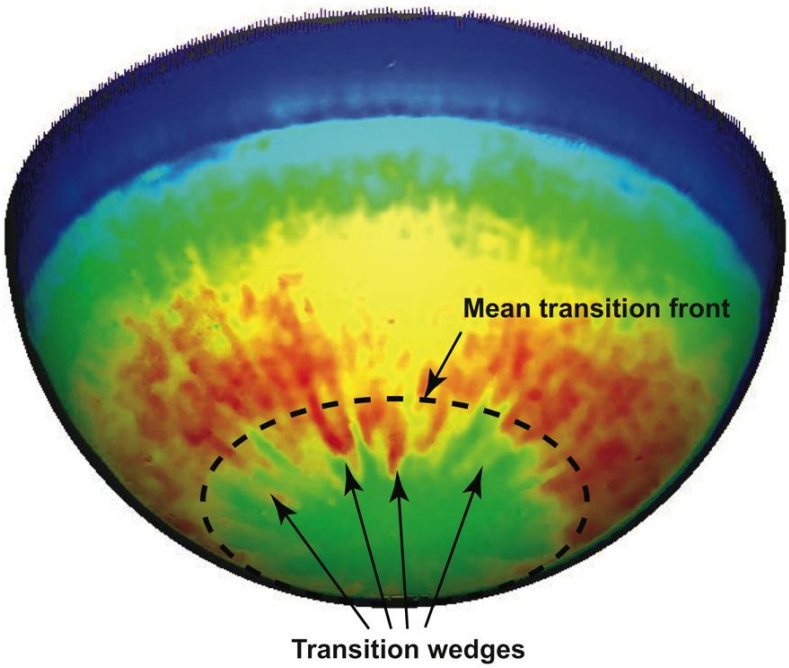
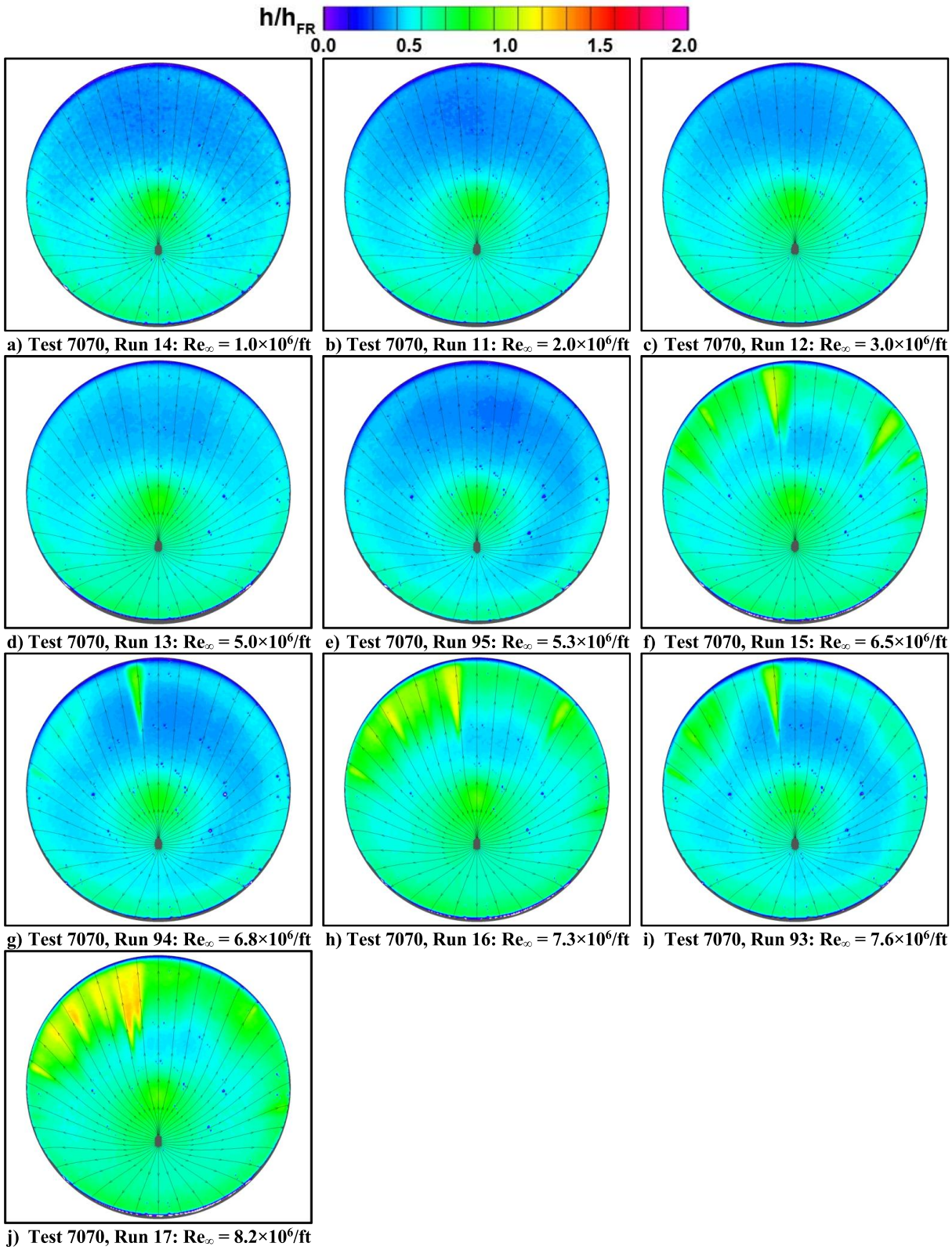


Figure 27. Comparison of irregular transition wedges vs. mean transition front.



a) Test 7070, Run 14: $Re_\infty = 1.0\times10^6$/ft b) Test 7070, Run 11: $Re_\infty = 2.0\times10^6$/ft c) Test 7070, Run 12: $Re_\infty = 3.0\times10^6$/ft

d) Test 7070, Run 13: $Re_\infty = 5.0\times10^6$/ft e) Test 7070, Run 95: $Re_\infty = 5.3\times10^6$/ft f) Test 7070, Run 15: $Re_\infty = 6.5\times10^6$/ft

g) Test 7070, Run 94: $Re_\infty = 6.8\times10^6$/ft h) Test 7070, Run 16: $Re_\infty = 7.3\times10^6$/ft i) Test 7070, Run 93: $Re_\infty = 7.6\times10^6$/ft

j) Test 7070, Run 17: $Re_\infty = 8.2\times10^6$/ft

Figure 28. Reynolds Number effects: sphere-cone geometry, smooth model images.

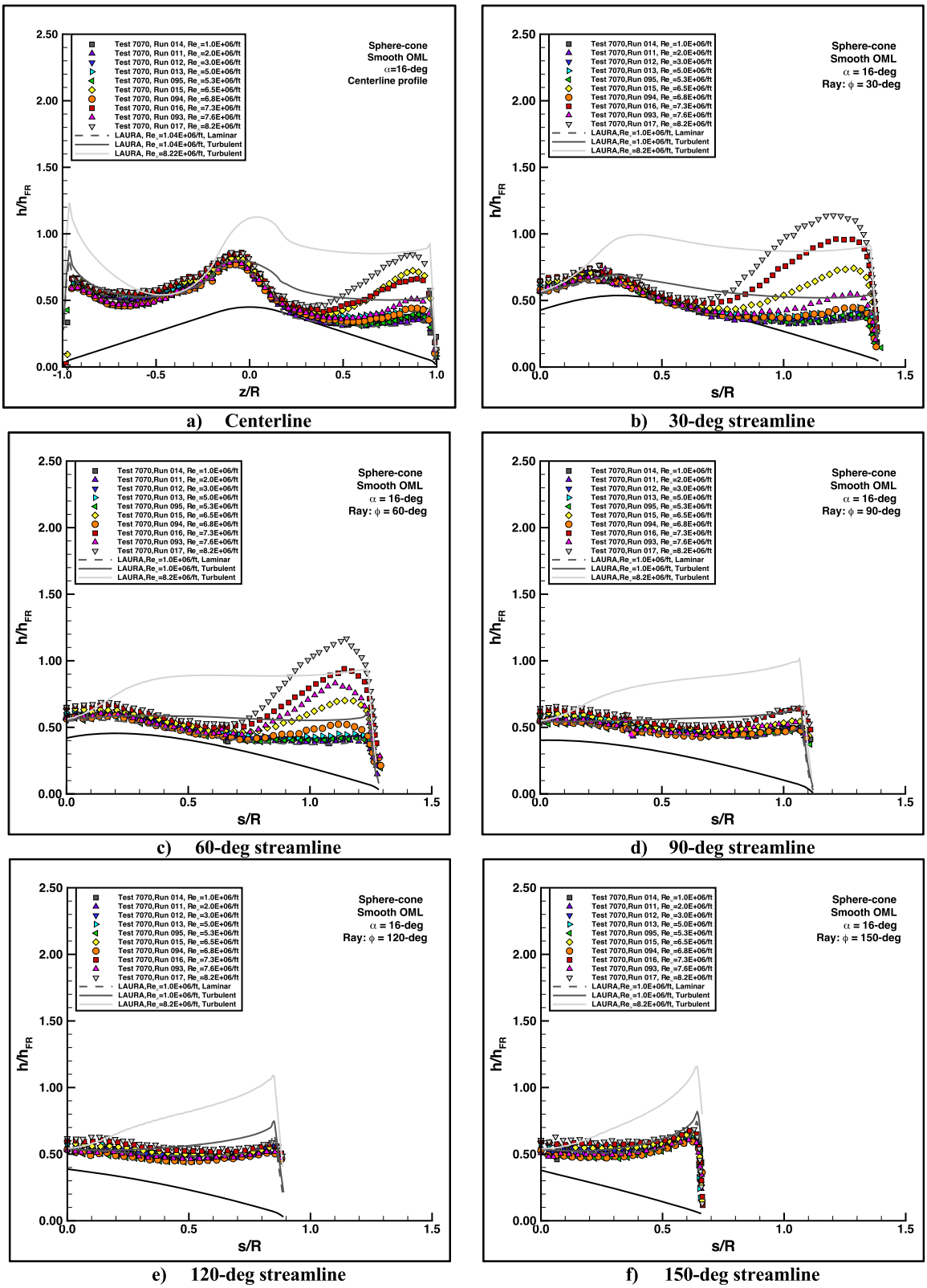
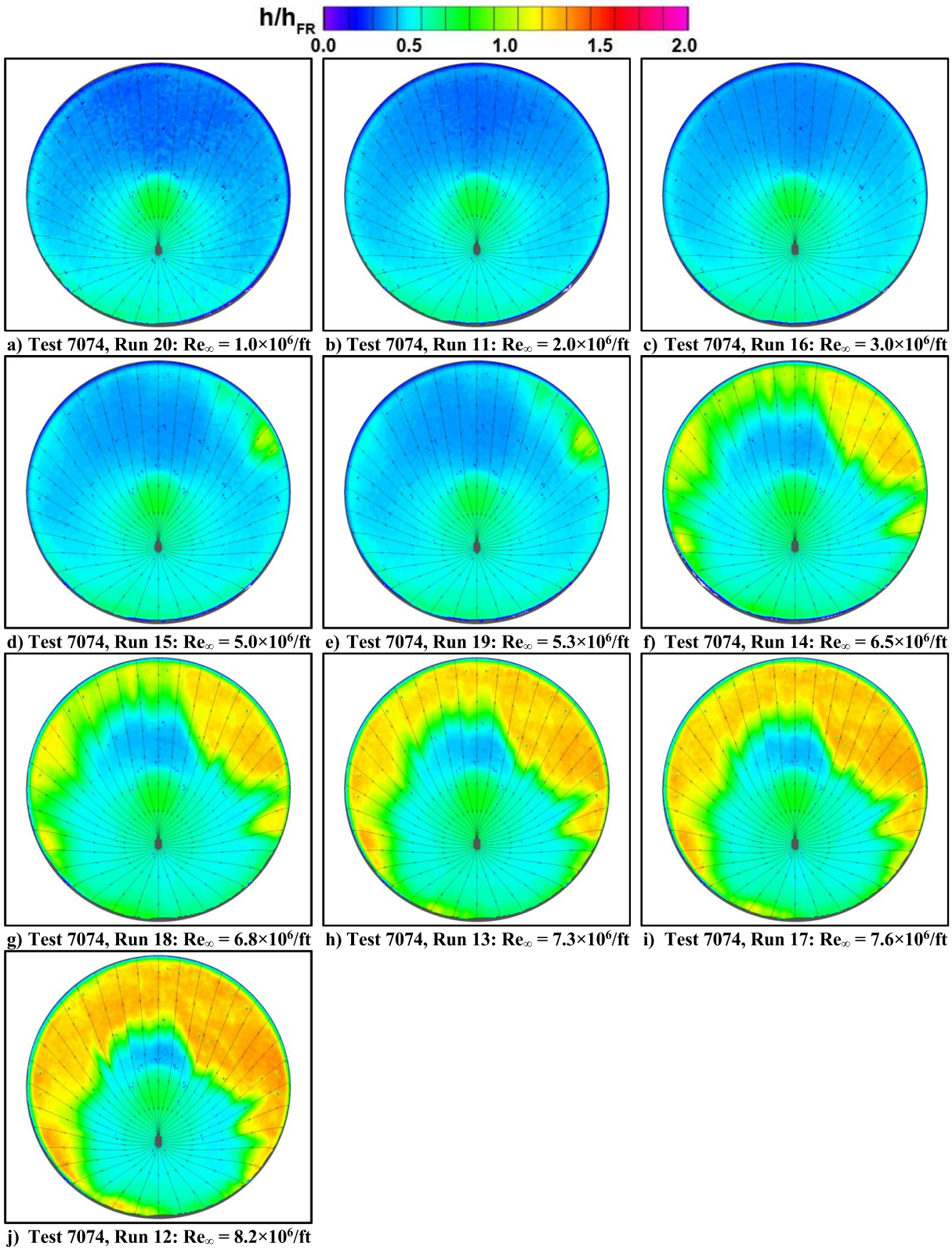


Figure 29. Reynolds number effects: sphere-cone geometry, smooth model plots.



a) Test 7074, Run 20: $Re_\infty = 1.0\times10^6$/ft b) Test 7074, Run 11: $Re_\infty = 2.0\times10^6$/ft c) Test 7074, Run 16: $Re_\infty = 3.0\times10^6$/ft

d) Test 7074, Run 15: $Re_\infty = 5.0\times10^6$/ft e) Test 7074, Run 19: $Re_\infty = 5.3\times10^6$/ft f) Test 7074, Run 14: $Re_\infty = 6.5\times10^6$/ft

g) Test 7074, Run 18: $Re_\infty = 6.8\times10^6$/ft h) Test 7074, Run 13: $Re_\infty = 7.3\times10^6$/ft i) Test 7074, Run 17: $Re_\infty = 7.6\times10^6$/ft

j) Test 7074, Run 12: $Re_\infty = 8.2\times10^6$/ft

Figure 30. Reynolds Number effects: sphere-cone geometry, 5-mil weave without seams model images.

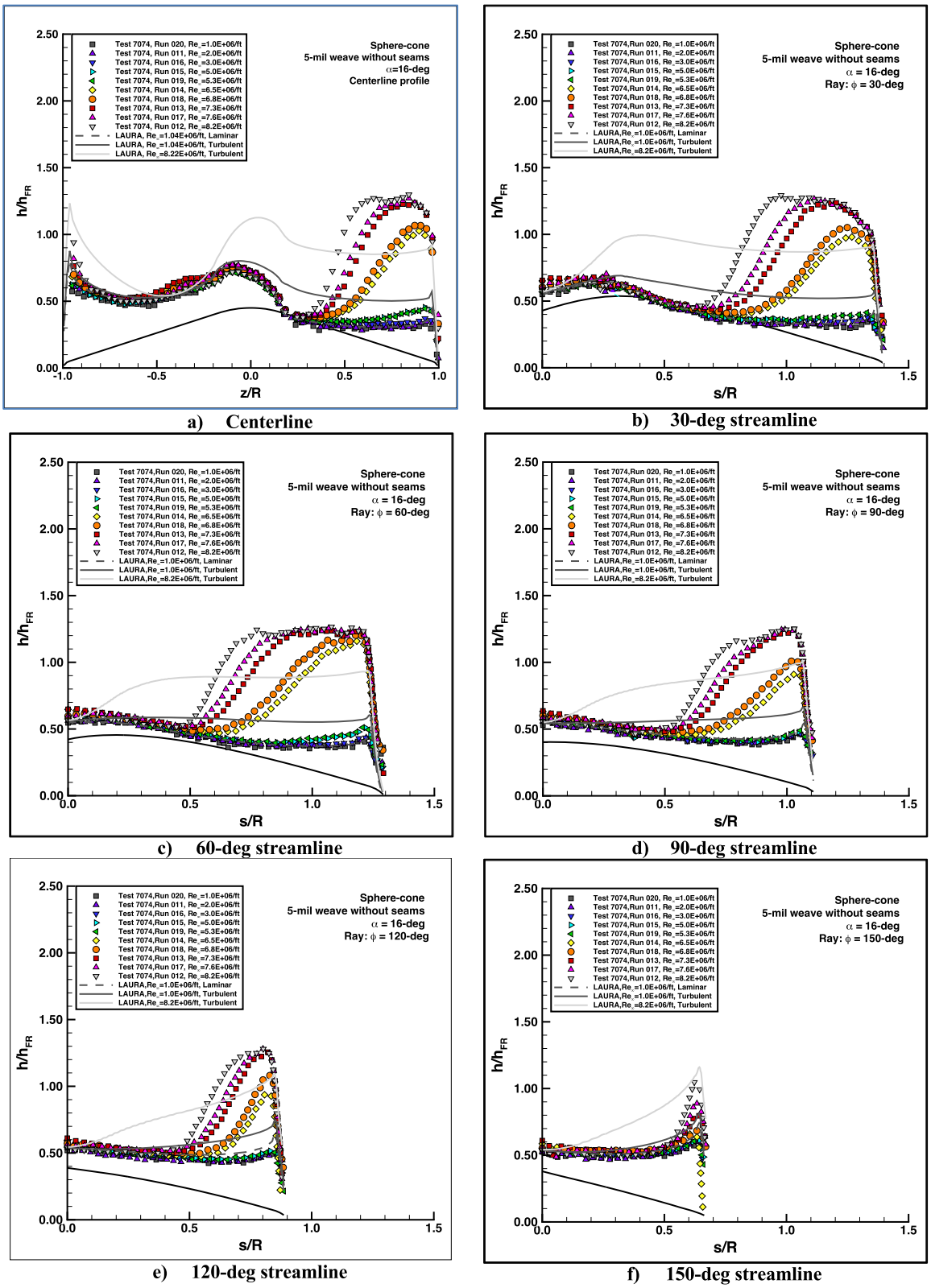
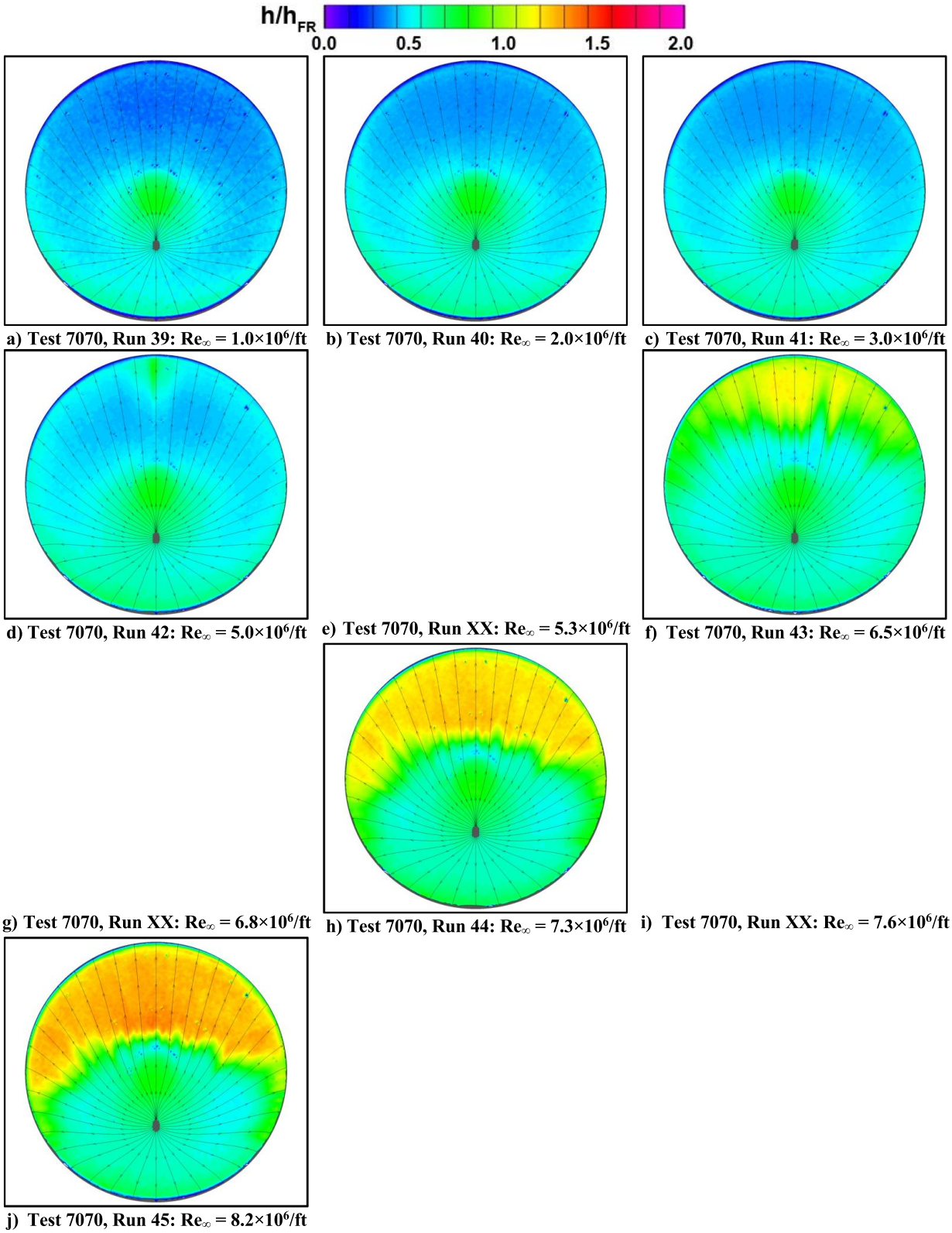


Figure 31. Reynolds Number effects: sphere-cone geometry, 5-mil weave without seams model plots.



a) Test 7070, Run 39: $Re_\infty = 1.0\times10^6$/ft

b) Test 7070, Run 40: $Re_\infty = 2.0\times10^6$/ft

c) Test 7070, Run 41: $Re_\infty = 3.0\times10^6$/ft

d) Test 7070, Run 42: $Re_\infty = 5.0\times10^6$/ft

e) Test 7070, Run XX: $Re_\infty = 5.3\times10^6$/ft

f) Test 7070, Run 43: $Re_\infty = 6.5\times10^6$/ft

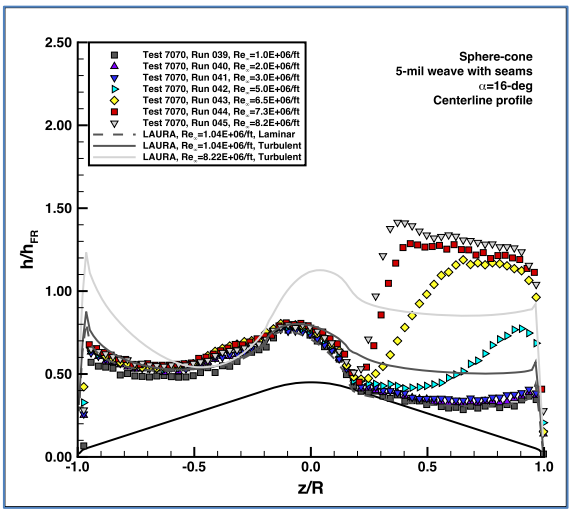
g) Test 7070, Run XX: $Re_\infty = 6.8\times10^6$/ft

h) Test 7070, Run 44: $Re_\infty = 7.3\times10^6$/ft

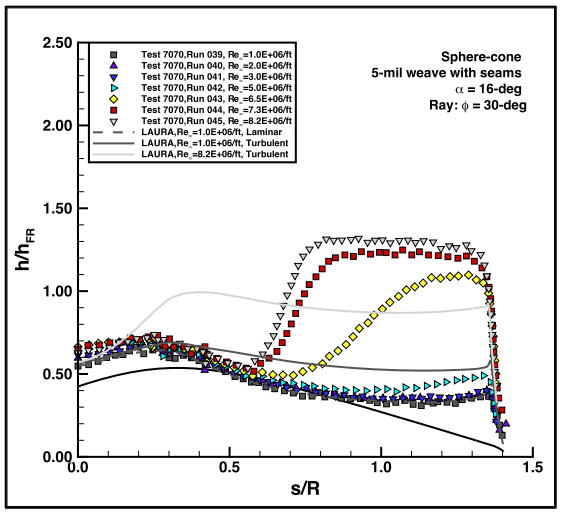
i) Test 7070, Run XX: $Re_\infty = 7.6\times10^6$/ft

j) Test 7070, Run 45: $Re_\infty = 8.2\times10^6$/ft

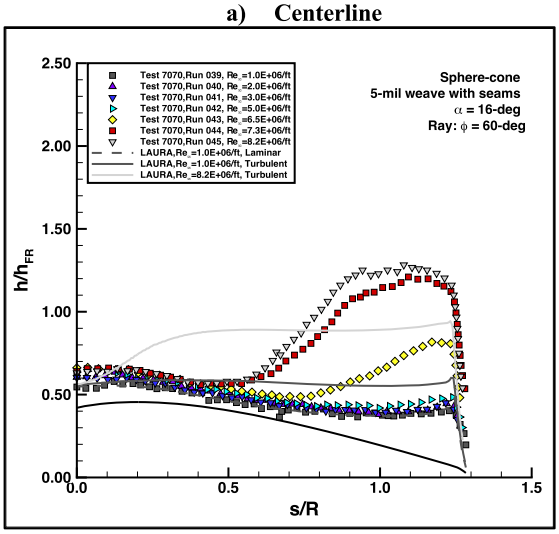
Figure 32. Reynolds Number effects: sphere-cone geometry, 5-mil weave with seams model images.



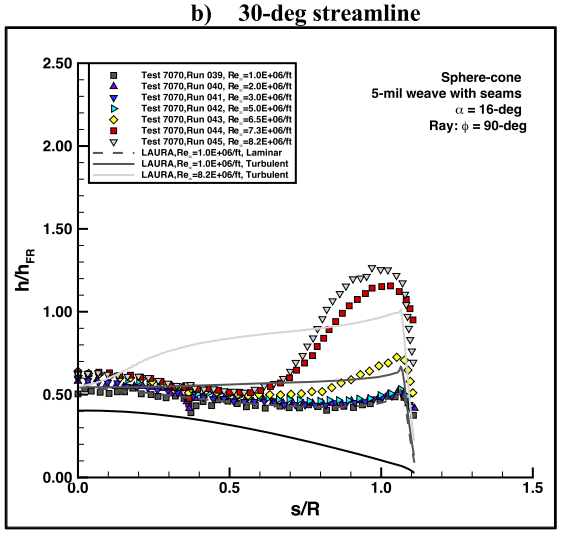
a) Centerline



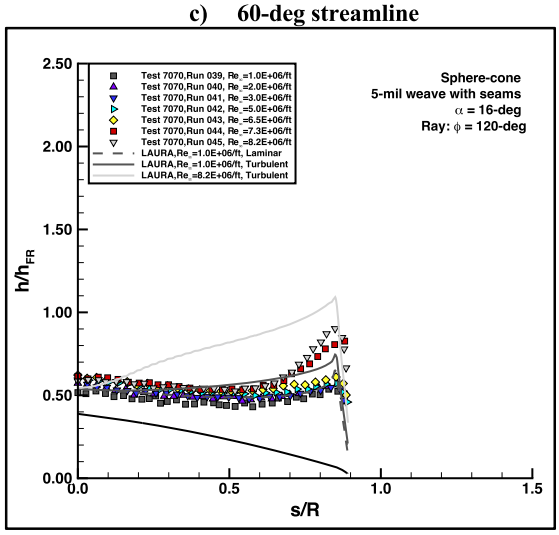
b) 30-deg streamline



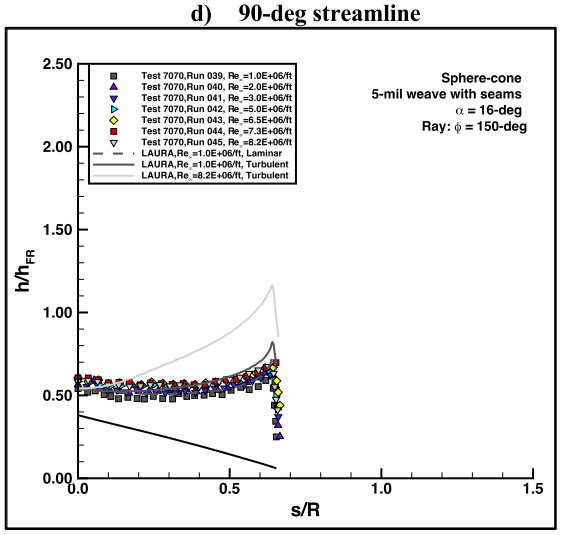
c) 60-deg streamline



d) 90-deg streamline

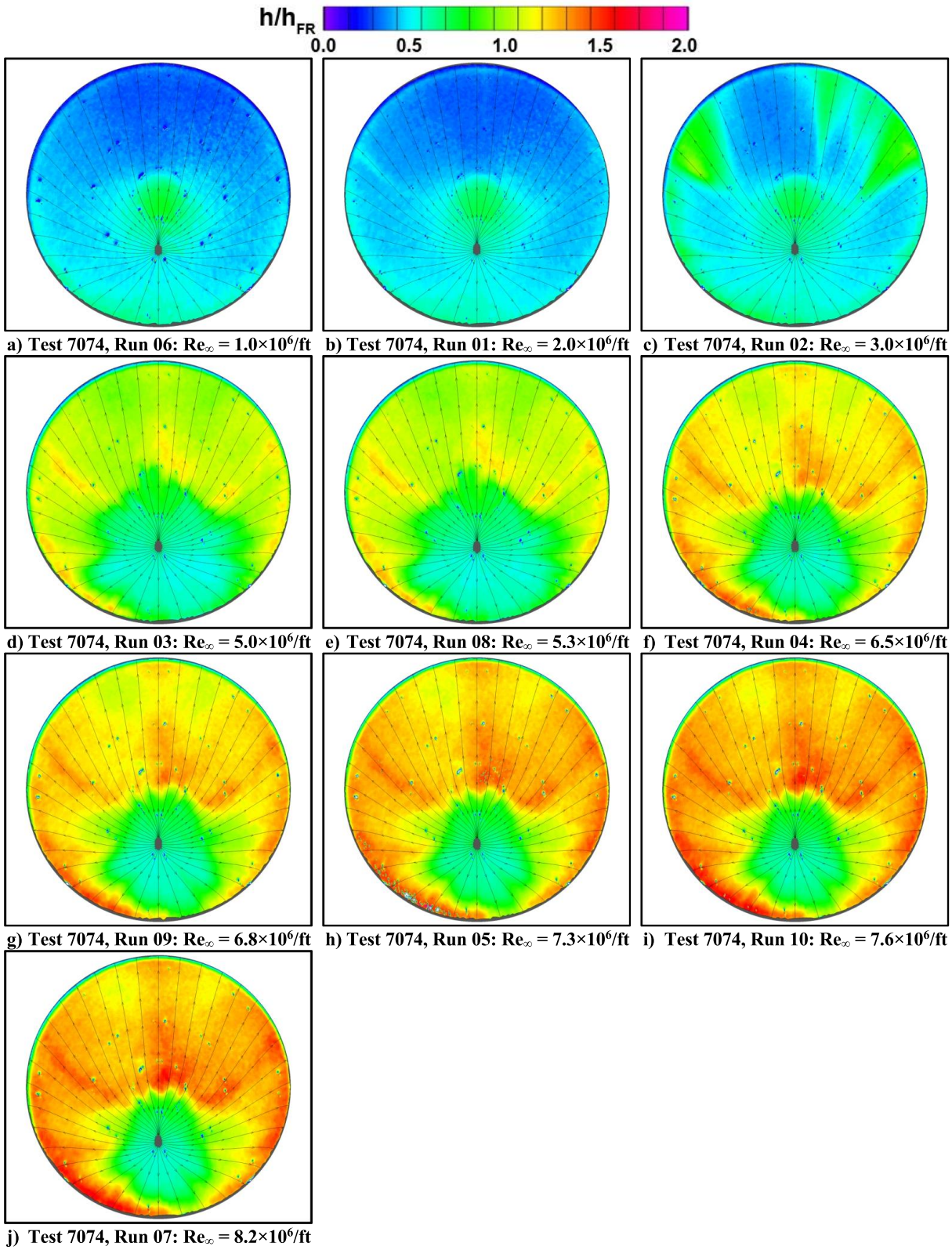


e) 120-deg streamline



f) 150-deg streamline

Figure 33. Reynolds Number effects: sphere-cone geometry, 5-mil weave with seams model plots.



a) Test 7074, Run 06: $Re_\infty = 1.0\times10^6$/ft
b) Test 7074, Run 01: $Re_\infty = 2.0\times10^6$/ft
c) Test 7074, Run 02: $Re_\infty = 3.0\times10^6$/ft
d) Test 7074, Run 03: $Re_\infty = 5.0\times10^6$/ft
e) Test 7074, Run 08: $Re_\infty = 5.3\times10^6$/ft
f) Test 7074, Run 04: $Re_\infty = 6.5\times10^6$/ft
g) Test 7074, Run 09: $Re_\infty = 6.8\times10^6$/ft
h) Test 7074, Run 05: $Re_\infty = 7.3\times10^6$/ft
i) Test 7074, Run 10: $Re_\infty = 7.6\times10^6$/ft
j) Test 7074, Run 07: $Re_\infty = 8.2\times10^6$/ft

Figure 34. Reynolds Number effects: sphere-cone geometry, 10-mil weave without seams model images.

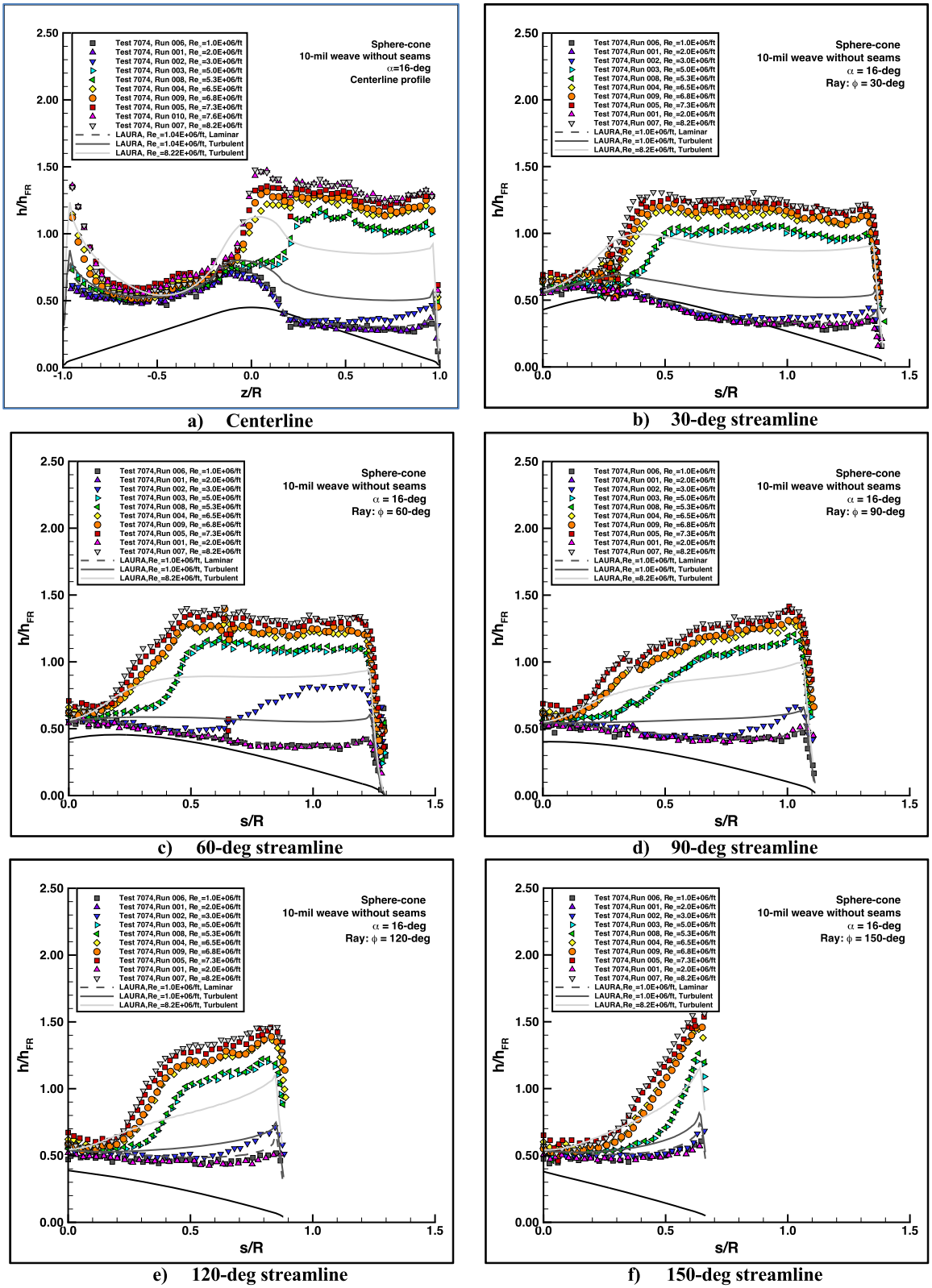
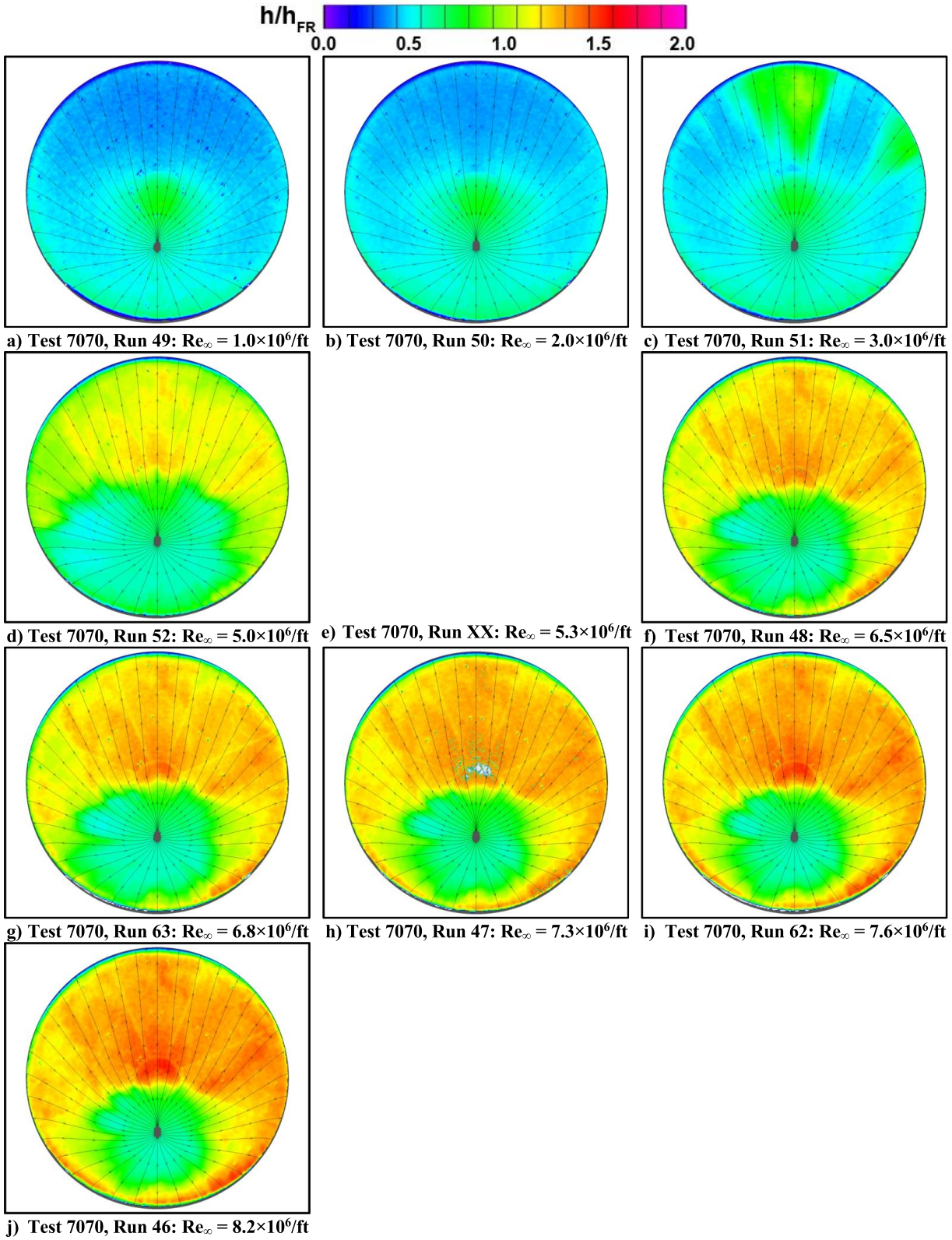


Figure 35. Reynolds Number effects: sphere-cone geometry, 10-mil weave without seams model plots.



a) Test 7070, Run 49: $Re_\infty = 1.0\times10^6$/ft
b) Test 7070, Run 50: $Re_\infty = 2.0\times10^6$/ft
c) Test 7070, Run 51: $Re_\infty = 3.0\times10^6$/ft
d) Test 7070, Run 52: $Re_\infty = 5.0\times10^6$/ft
e) Test 7070, Run XX: $Re_\infty = 5.3\times10^6$/ft
f) Test 7070, Run 48: $Re_\infty = 6.5\times10^6$/ft
g) Test 7070, Run 63: $Re_\infty = 6.8\times10^6$/ft
h) Test 7070, Run 47: $Re_\infty = 7.3\times10^6$/ft
i) Test 7070, Run 62: $Re_\infty = 7.6\times10^6$/ft
j) Test 7070, Run 46: $Re_\infty = 8.2\times10^6$/ft

Figure 36. Reynolds Number effects: sphere-cone geometry, 10-mil weave with seams model images.

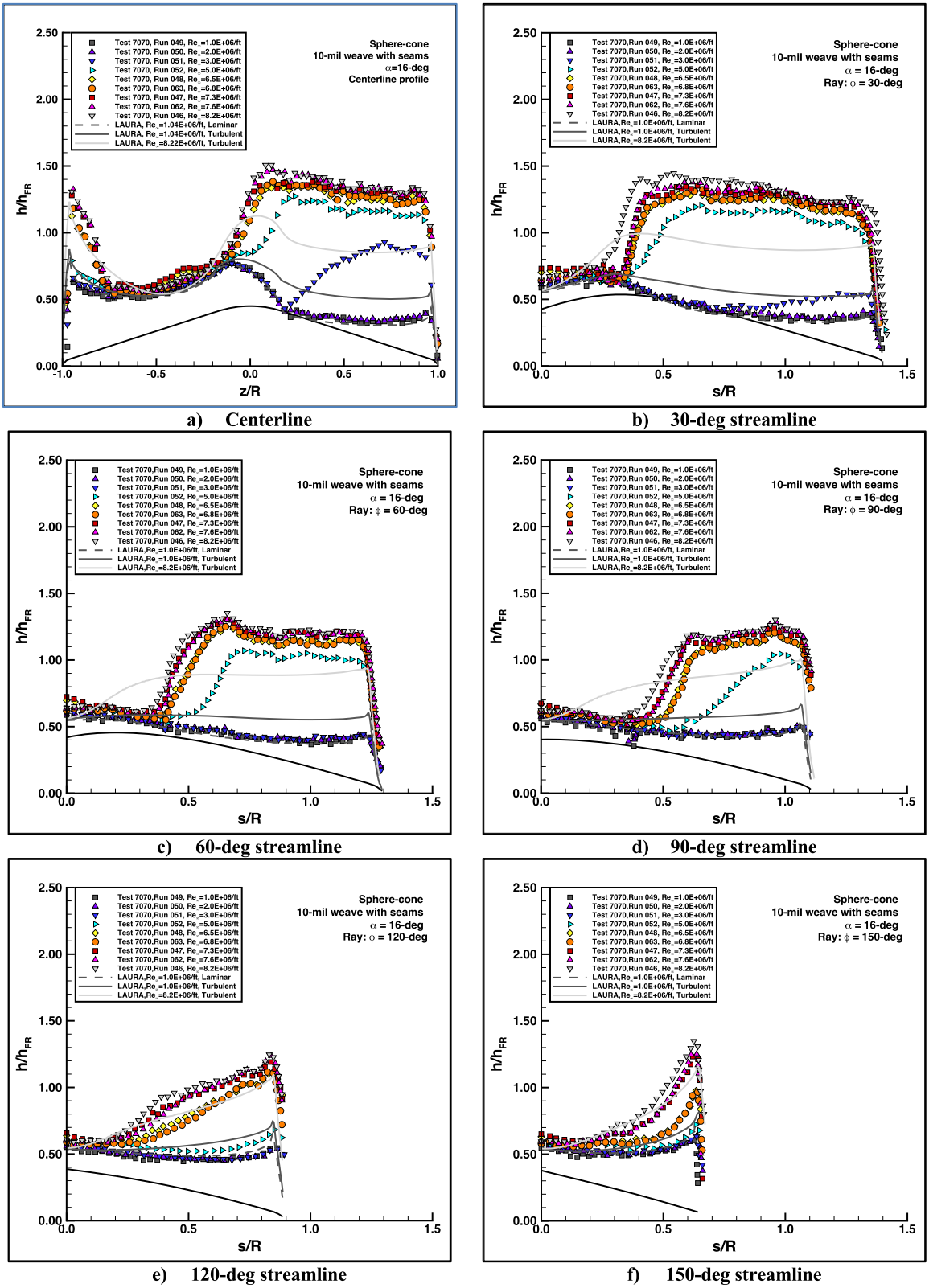
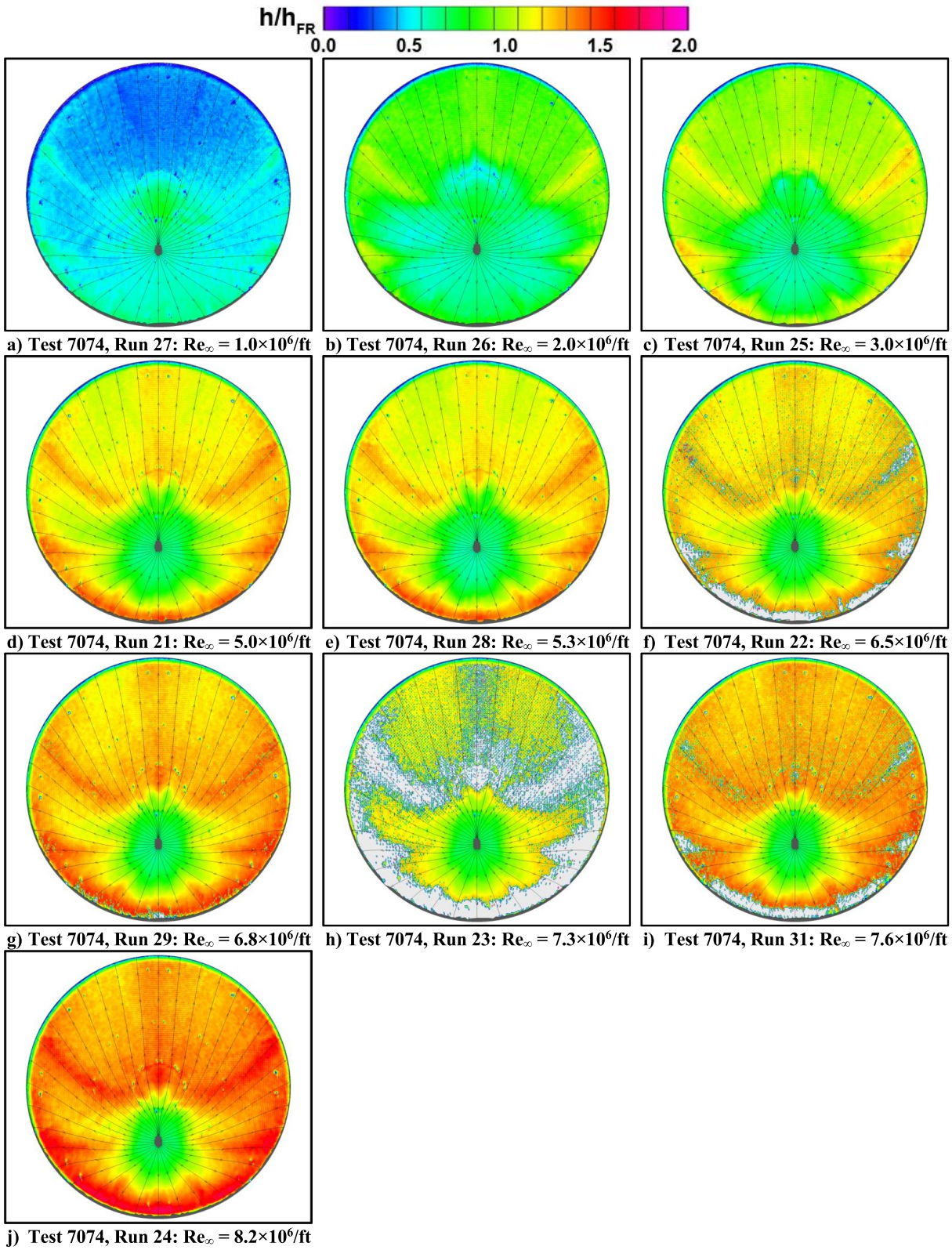


Figure 37. Reynolds Number effects: sphere-cone geometry, 10-mil weave with seams model plots.



a) Test 7074, Run 27: $Re_\infty = 1.0\times10^6$/ft
b) Test 7074, Run 26: $Re_\infty = 2.0\times10^6$/ft
c) Test 7074, Run 25: $Re_\infty = 3.0\times10^6$/ft
d) Test 7074, Run 21: $Re_\infty = 5.0\times10^6$/ft
e) Test 7074, Run 28: $Re_\infty = 5.3\times10^6$/ft
f) Test 7074, Run 22: $Re_\infty = 6.5\times10^6$/ft
g) Test 7074, Run 29: $Re_\infty = 6.8\times10^6$/ft
h) Test 7074, Run 23: $Re_\infty = 7.3\times10^6$/ft
i) Test 7074, Run 31: $Re_\infty = 7.6\times10^6$/ft
j) Test 7074, Run 24: $Re_\infty = 8.2\times10^6$/ft

Figure 38. Reynolds Number effects: sphere-cone geometry, 15-mil weave without seams model images.

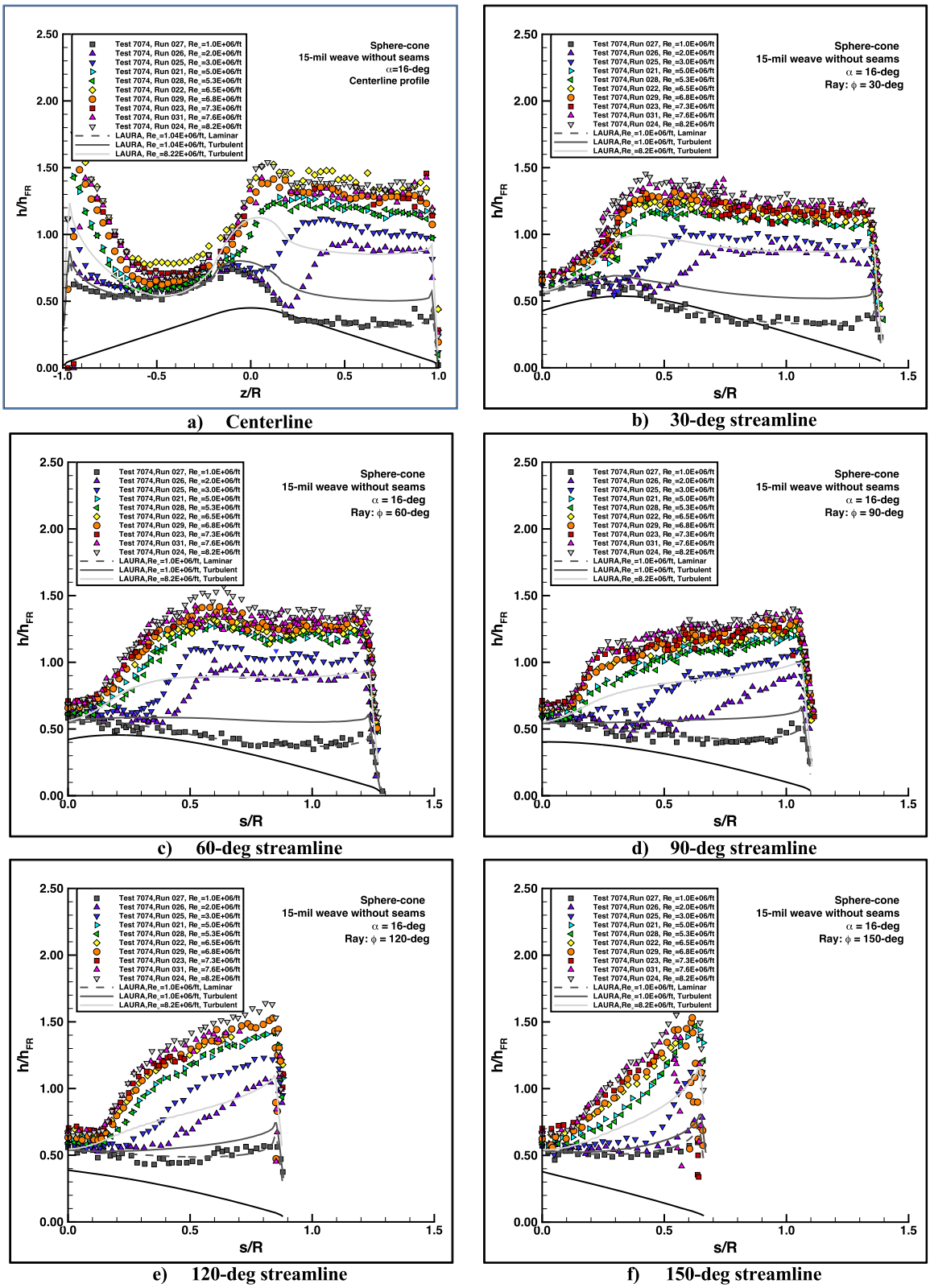
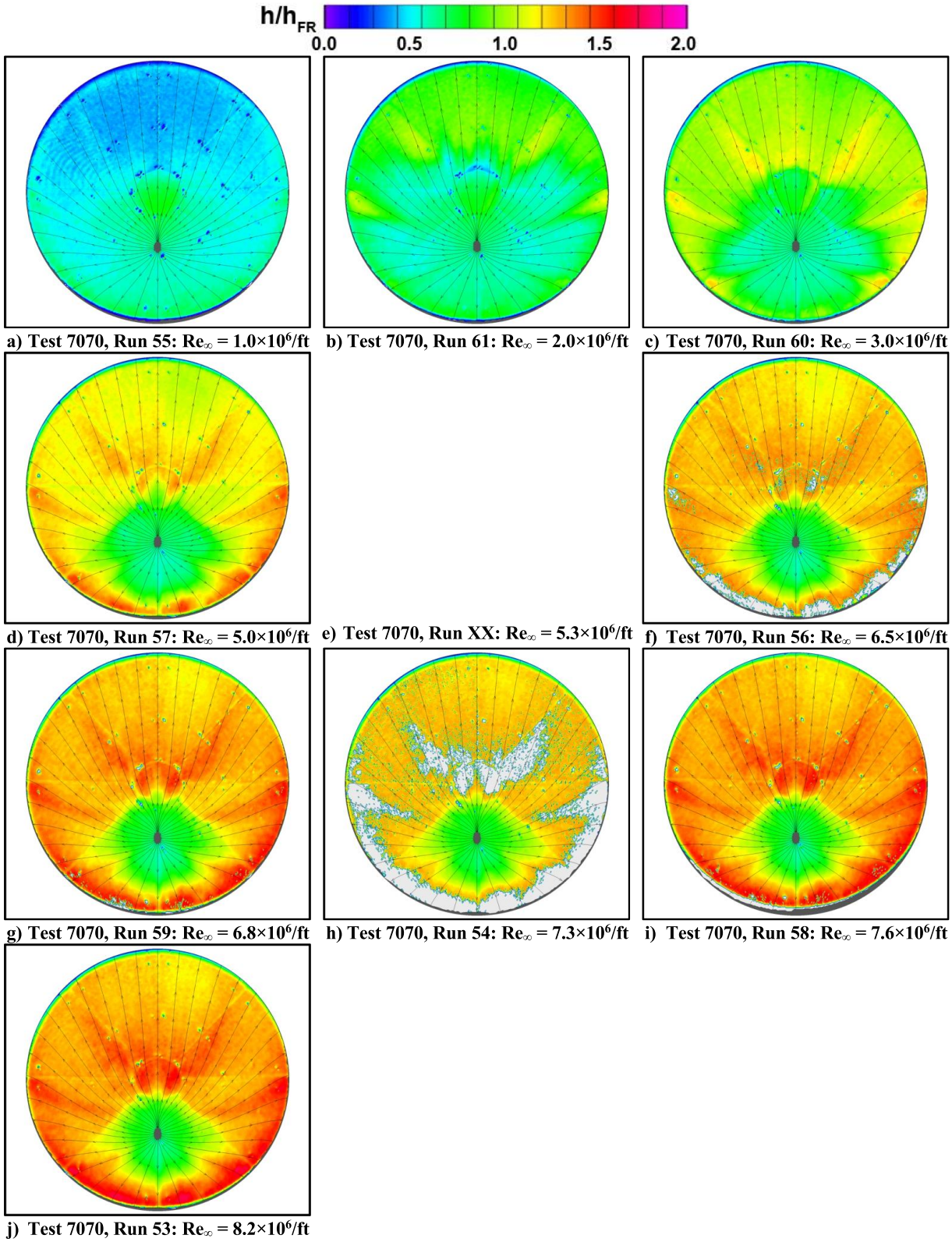


Figure 39. Reynolds Number effects: sphere-cone geometry, 15-mil weave without seams model plots.



a) Test 7070, Run 55: $Re_\infty = 1.0\times10^6$/ft
b) Test 7070, Run 61: $Re_\infty = 2.0\times10^6$/ft
c) Test 7070, Run 60: $Re_\infty = 3.0\times10^6$/ft
d) Test 7070, Run 57: $Re_\infty = 5.0\times10^6$/ft
e) Test 7070, Run XX: $Re_\infty = 5.3\times10^6$/ft
f) Test 7070, Run 56: $Re_\infty = 6.5\times10^6$/ft
g) Test 7070, Run 59: $Re_\infty = 6.8\times10^6$/ft
h) Test 7070, Run 54: $Re_\infty = 7.3\times10^6$/ft
i) Test 7070, Run 58: $Re_\infty = 7.6\times10^6$/ft
j) Test 7070, Run 53: $Re_\infty = 8.2\times10^6$/ft

Figure 40. Reynolds Number effects: sphere-cone geometry, 15-mil weave with seams model images.

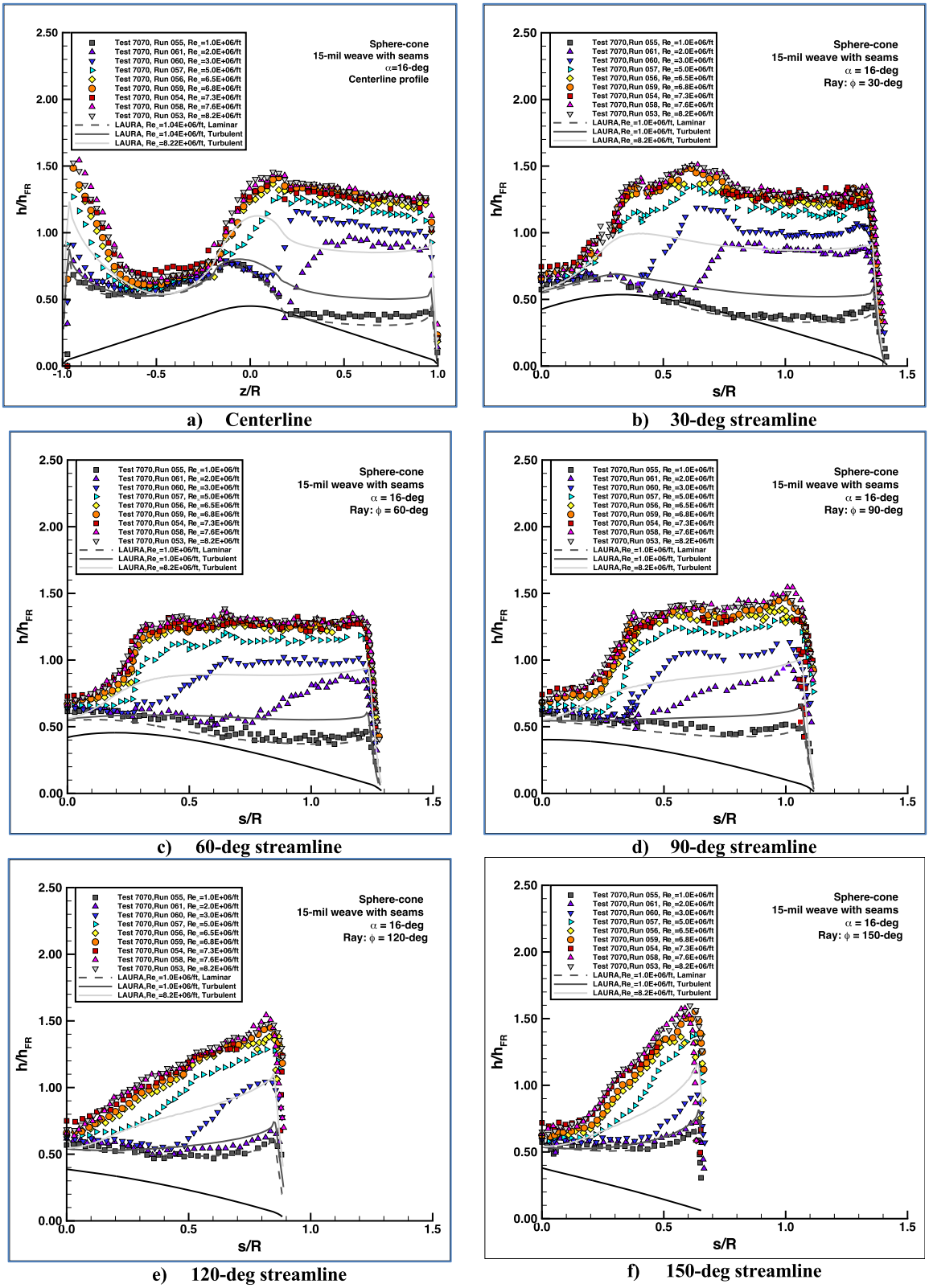
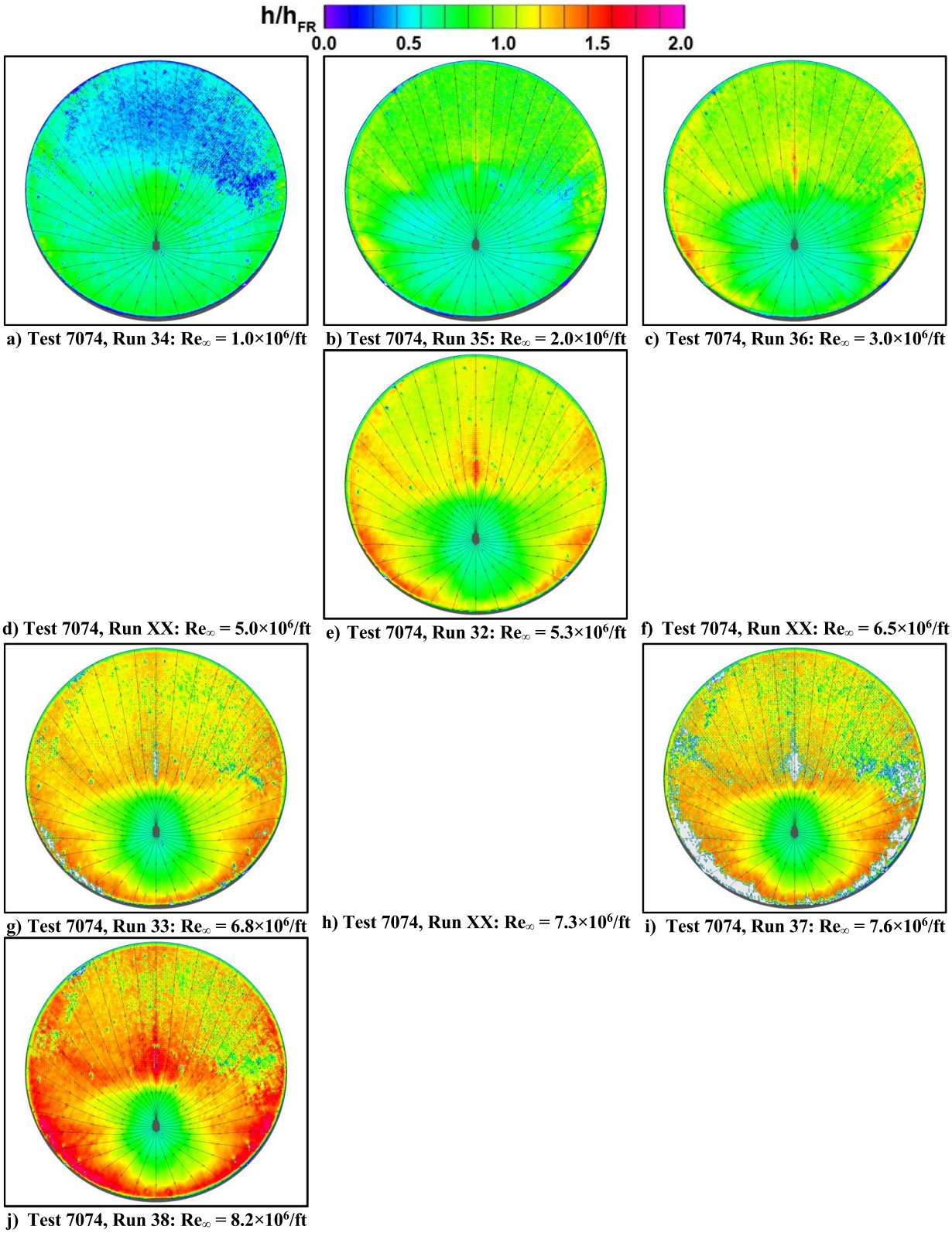


Figure 41. Reynolds Number effects: sphere-cone geometry, 15-mil weave with seams model plots.



a) Test 7074, Run 34: $Re_\infty = 1.0\times10^6$/ft

b) Test 7074, Run 35: $Re_\infty = 2.0\times10^6$/ft

c) Test 7074, Run 36: $Re_\infty = 3.0\times10^6$/ft

d) Test 7074, Run XX: $Re_\infty = 5.0\times10^6$/ft

e) Test 7074, Run 32: $Re_\infty = 5.3\times10^6$/ft

f) Test 7074, Run XX: $Re_\infty = 6.5\times10^6$/ft

g) Test 7074, Run 33: $Re_\infty = 6.8\times10^6$/ft

h) Test 7074, Run XX: $Re_\infty = 7.3\times10^6$/ft

i) Test 7074, Run 37: $Re_\infty = 7.6\times10^6$/ft

j) Test 7074, Run 38: $Re_\infty = 8.2\times10^6$/ft

Figure 42. Reynolds Number effects: sphere-cone geometry, 20-mil weave without seams model images.

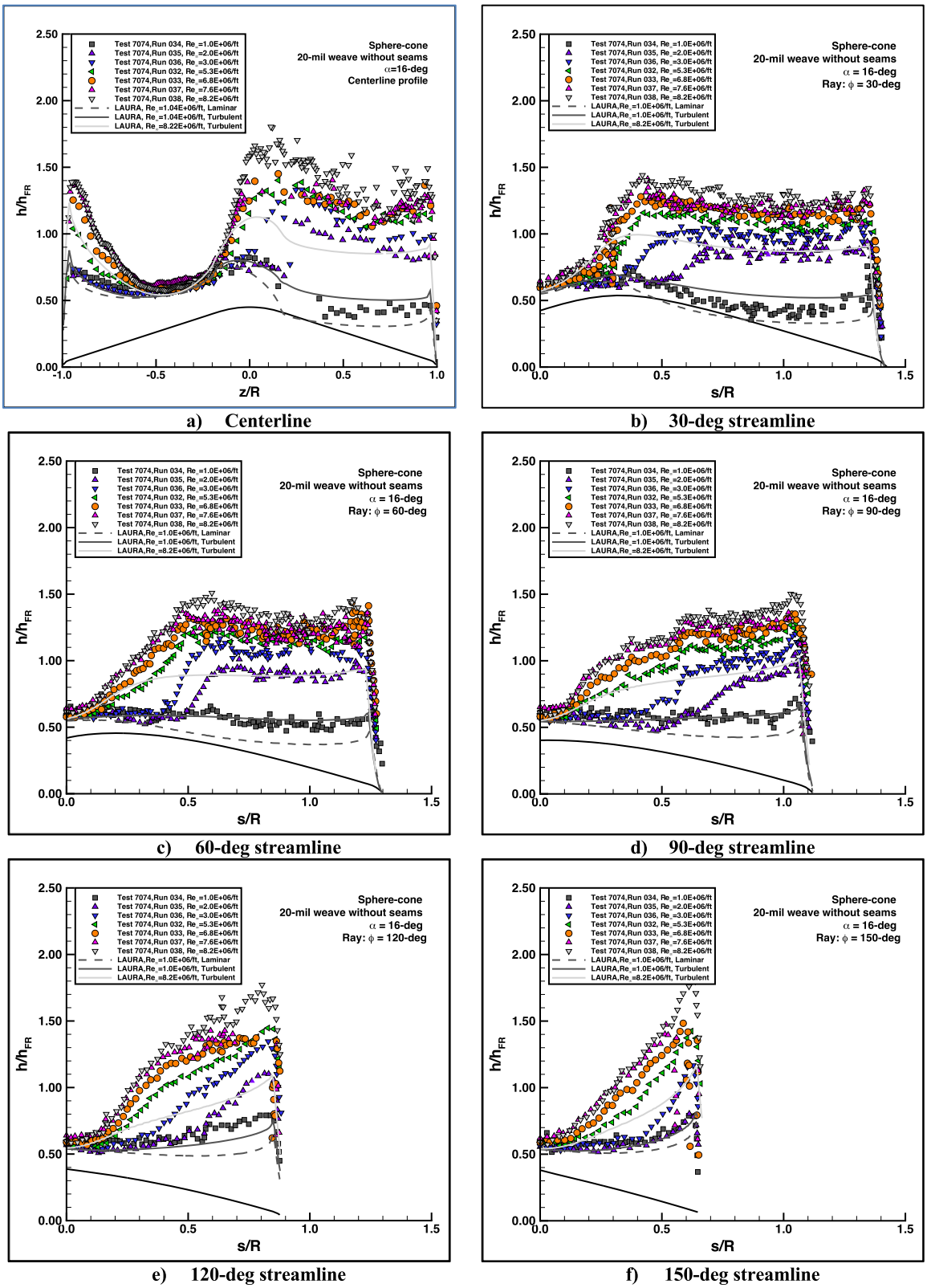
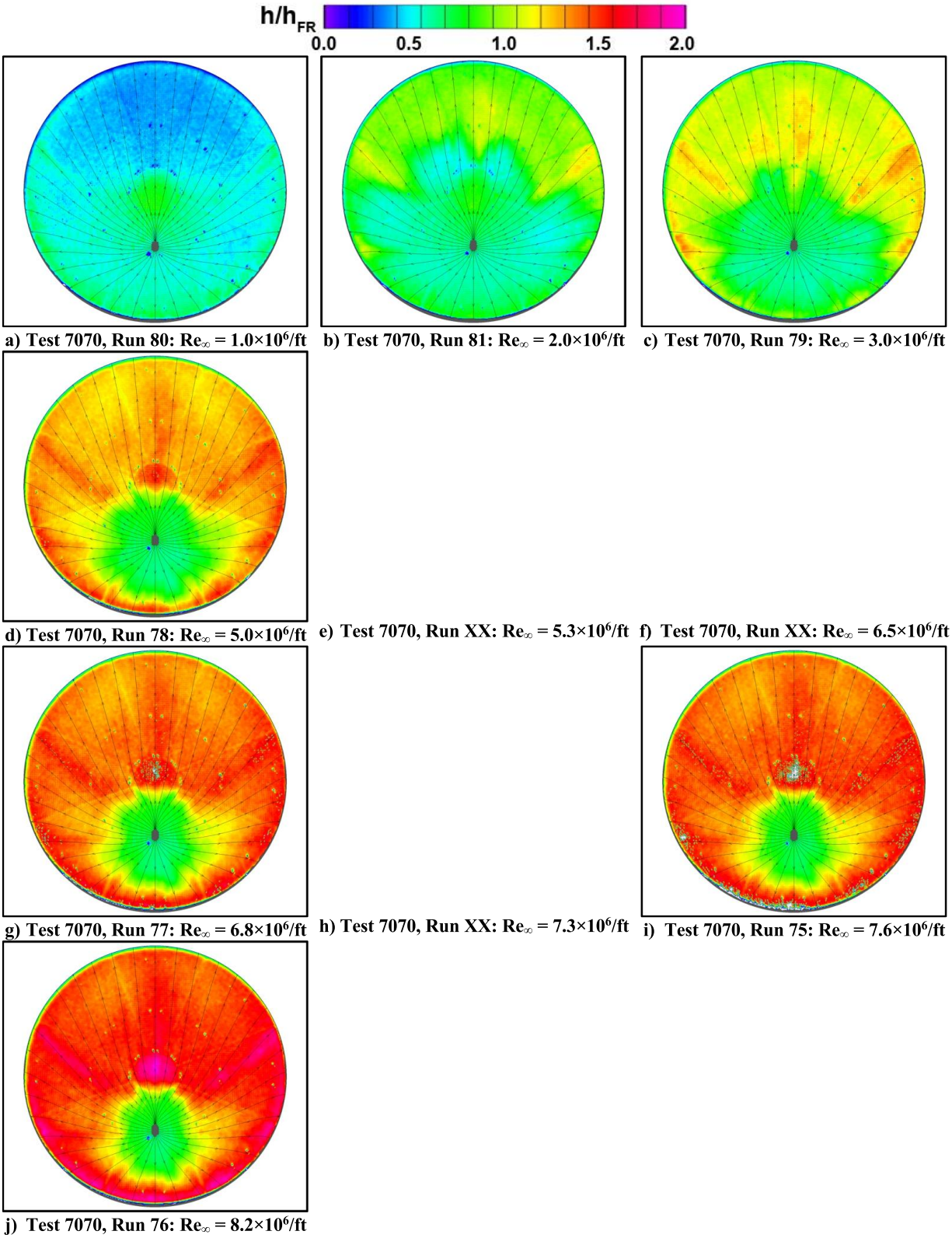


Figure 43. Reynolds number effects: sphere-cone geometry, 20-mil weave without seams plots.



a) Test 7070, Run 80: $Re_\infty = 1.0\times10^6$/ft

b) Test 7070, Run 81: $Re_\infty = 2.0\times10^6$/ft

c) Test 7070, Run 79: $Re_\infty = 3.0\times10^6$/ft

d) Test 7070, Run 78: $Re_\infty = 5.0\times10^6$/ft

e) Test 7070, Run XX: $Re_\infty = 5.3\times10^6$/ft

f) Test 7070, Run XX: $Re_\infty = 6.5\times10^6$/ft

g) Test 7070, Run 77: $Re_\infty = 6.8\times10^6$/ft

h) Test 7070, Run XX: $Re_\infty = 7.3\times10^6$/ft

i) Test 7070, Run 75: $Re_\infty = 7.6\times10^6$/ft

j) Test 7070, Run 76: $Re_\infty = 8.2\times10^6$/ft

Figure 44. Reynolds Number effects: sphere-cone geometry, 20-mil weave with seams model images.

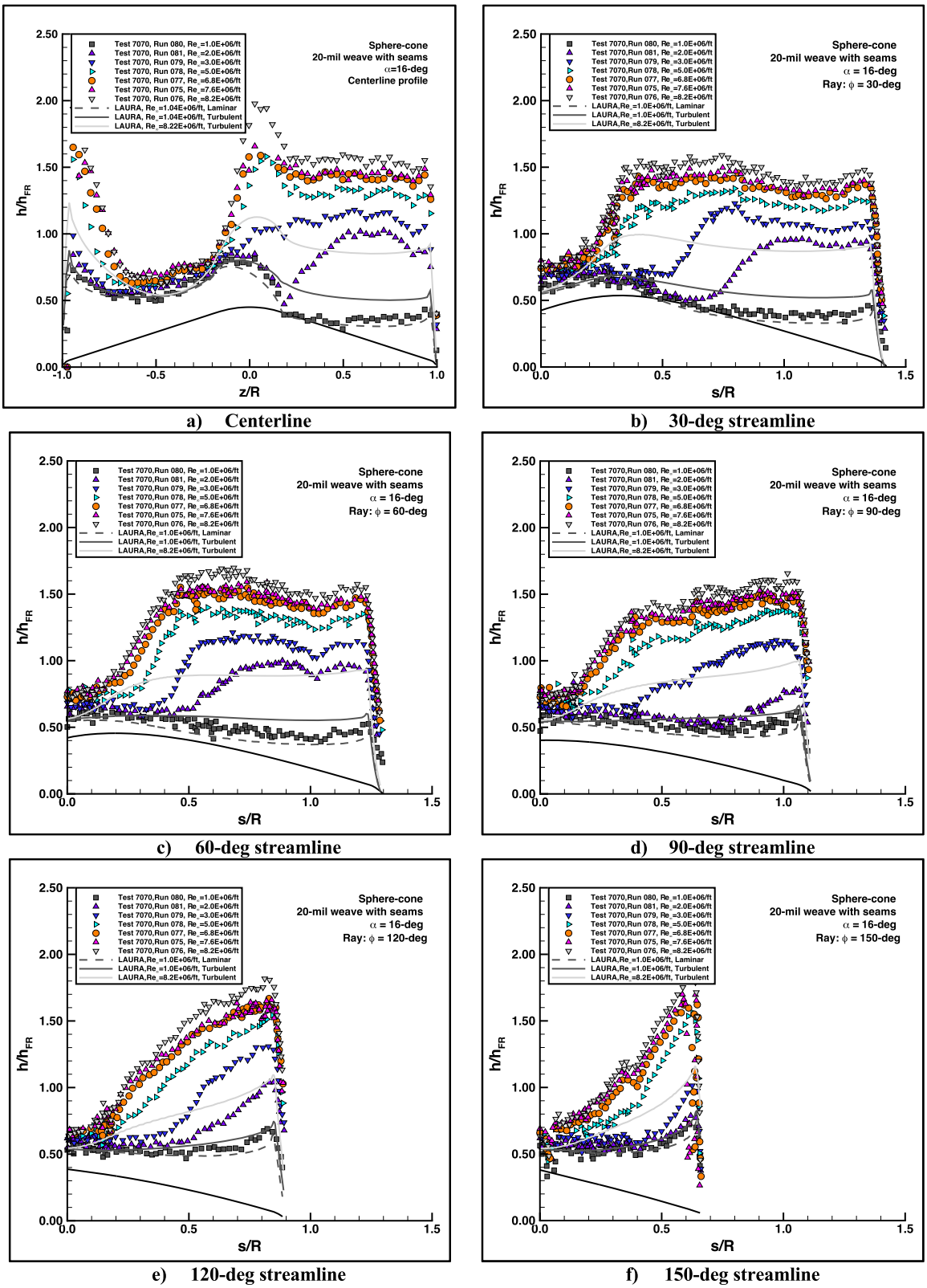
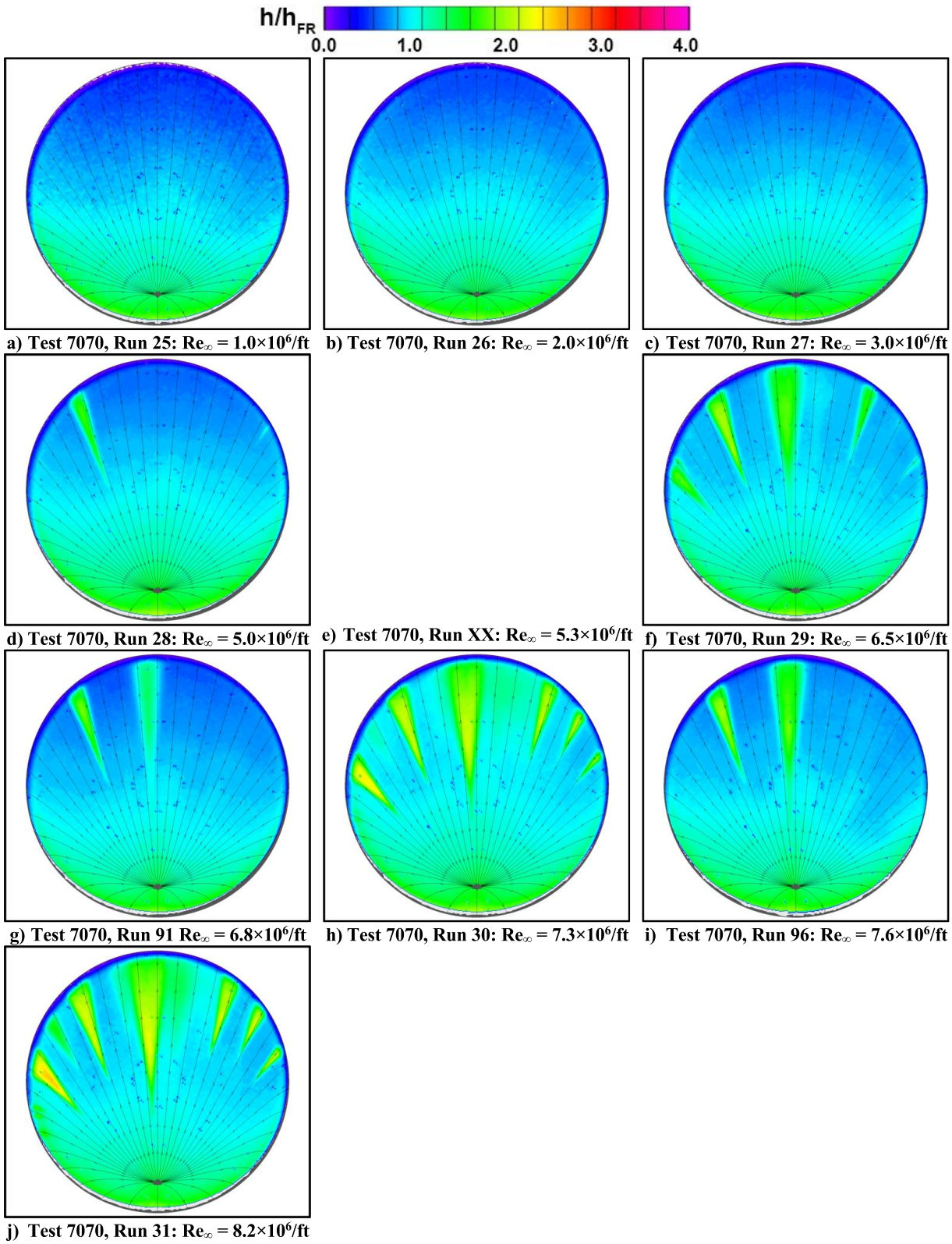


Figure 45. Reynolds Number effects: sphere-cone geometry, 20-mil weave with seams model plots.



a) Test 7070, Run 25: $Re_\infty = 1.0\times10^6$/ft
b) Test 7070, Run 26: $Re_\infty = 2.0\times10^6$/ft
c) Test 7070, Run 27: $Re_\infty = 3.0\times10^6$/ft
d) Test 7070, Run 28: $Re_\infty = 5.0\times10^6$/ft
e) Test 7070, Run XX: $Re_\infty = 5.3\times10^6$/ft
f) Test 7070, Run 29: $Re_\infty = 6.5\times10^6$/ft
g) Test 7070, Run 91 $Re_\infty = 6.8\times10^6$/ft
h) Test 7070, Run 30: $Re_\infty = 7.3\times10^6$/ft
i) Test 7070, Run 96: $Re_\infty = 7.6\times10^6$/ft
j) Test 7070, Run 31: $Re_\infty = 8.2\times10^6$/ft

Figure 46. Reynolds Number effects: spherical-cap geometry, smooth model images.

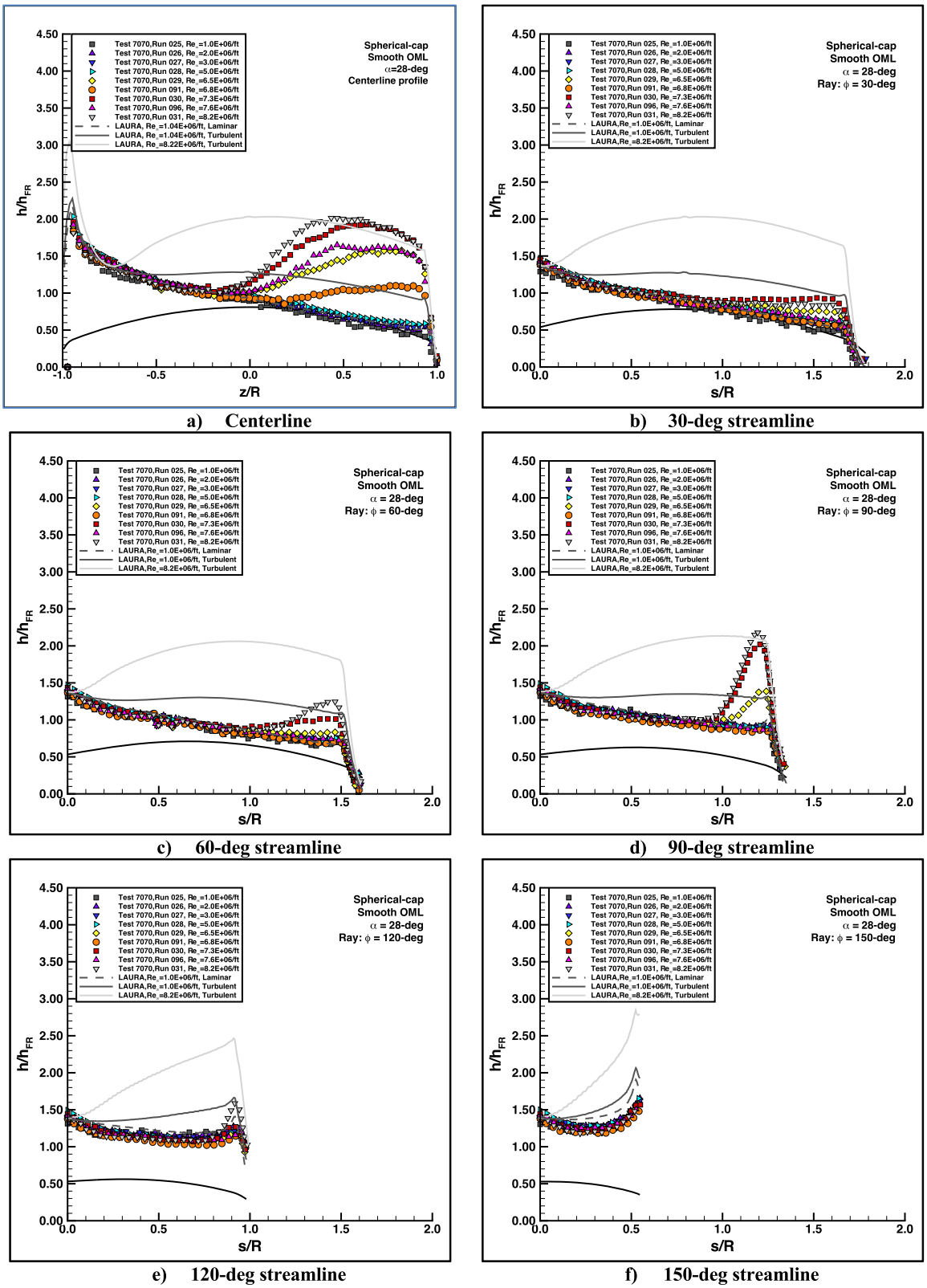
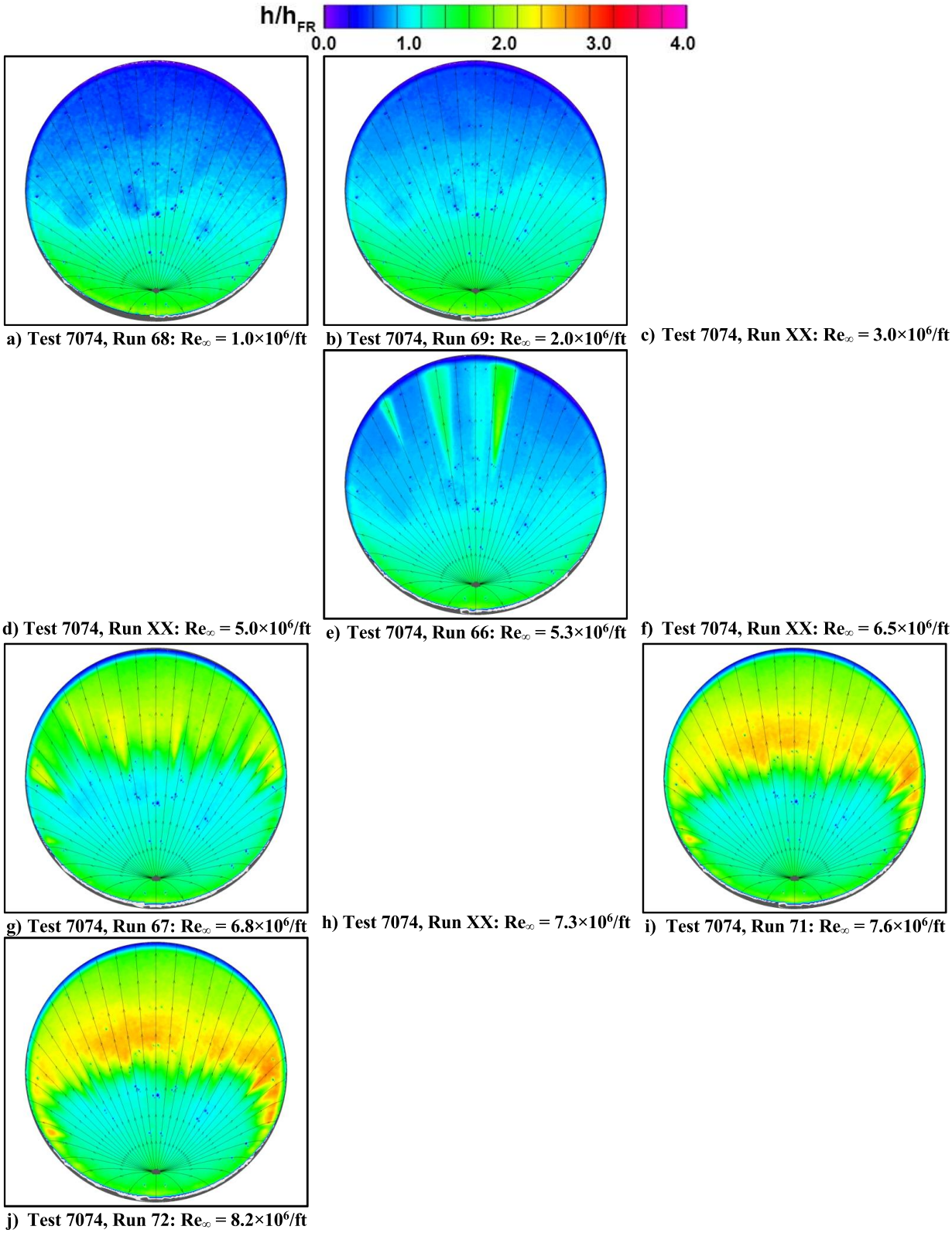


Figure 47. Reynolds number effects: spherical-cap geometry, smooth model plots.



a) Test 7074, Run 68: $Re_\infty = 1.0\times10^6$/ft

b) Test 7074, Run 69: $Re_\infty = 2.0\times10^6$/ft

c) Test 7074, Run XX: $Re_\infty = 3.0\times10^6$/ft

d) Test 7074, Run XX: $Re_\infty = 5.0\times10^6$/ft

e) Test 7074, Run 66: $Re_\infty = 5.3\times10^6$/ft

f) Test 7074, Run XX: $Re_\infty = 6.5\times10^6$/ft

g) Test 7074, Run 67: $Re_\infty = 6.8\times10^6$/ft

h) Test 7074, Run XX: $Re_\infty = 7.3\times10^6$/ft

i) Test 7074, Run 71: $Re_\infty = 7.6\times10^6$/ft

j) Test 7074, Run 72: $Re_\infty = 8.2\times10^6$/ft

Figure 48. Reynolds Number effects: spherical-cap geometry, 5-mil weave without seams model images.

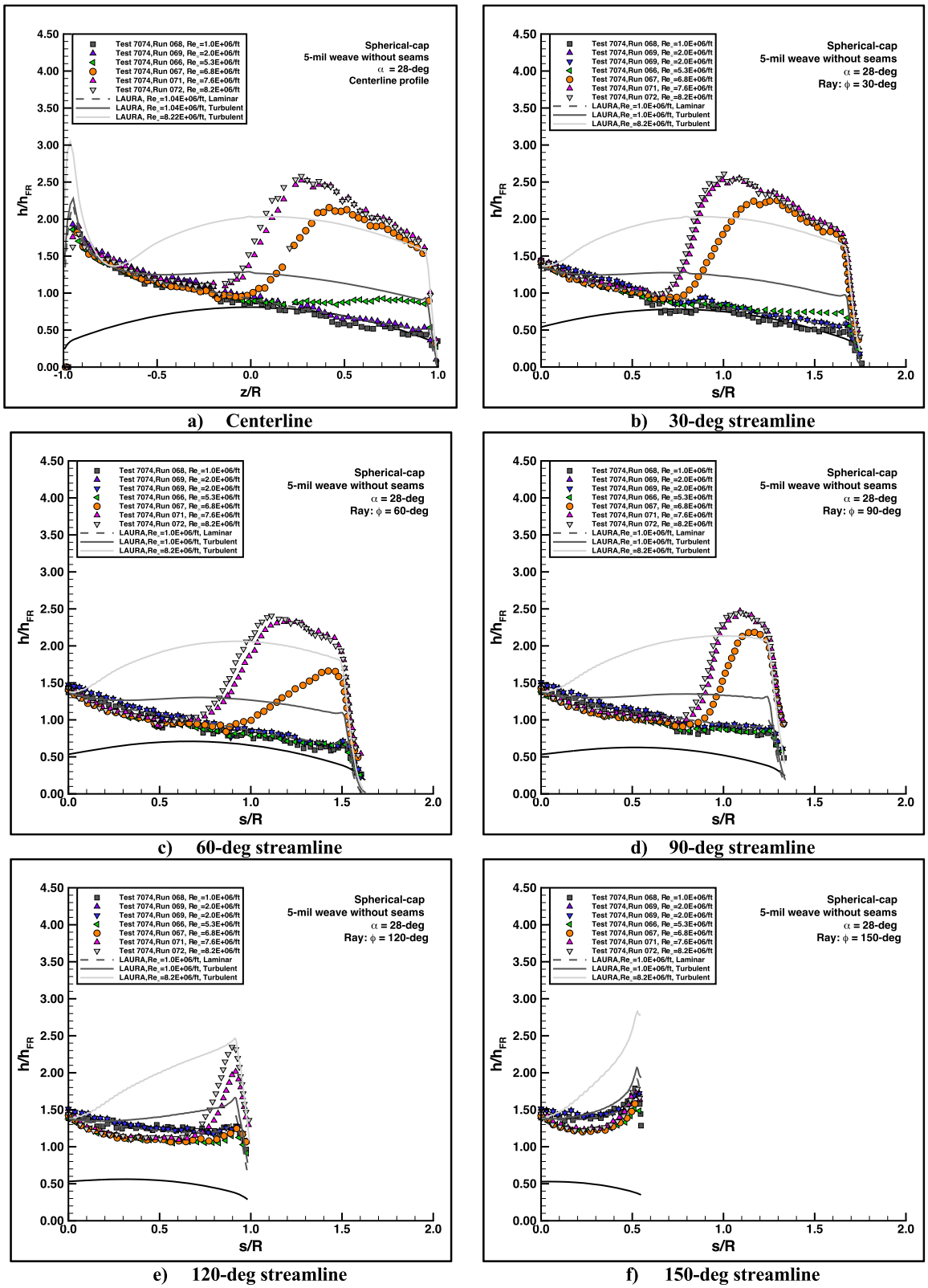
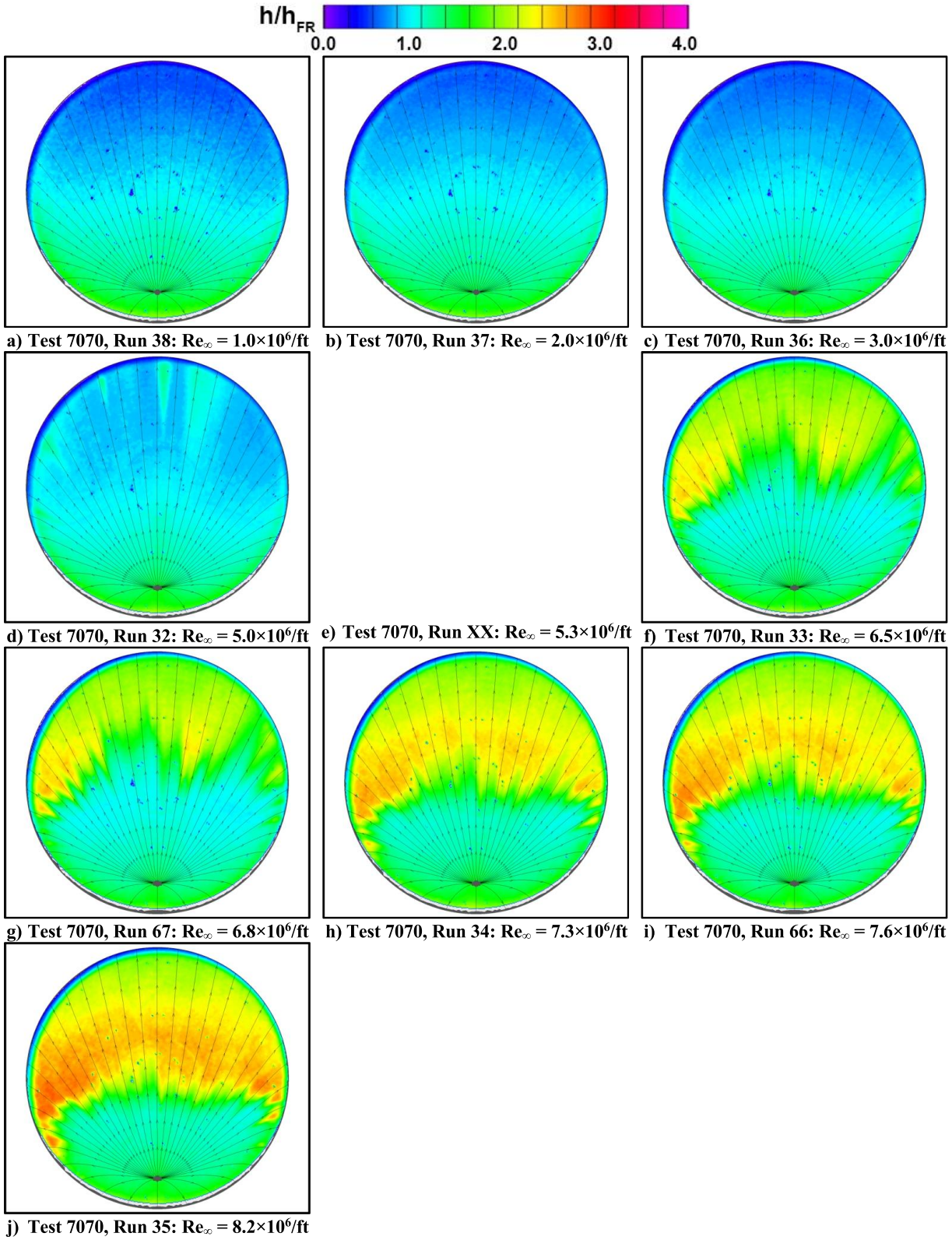


Figure 49. Reynolds number effects: spherical-cap geometry, 5-mil weave without seams plots.



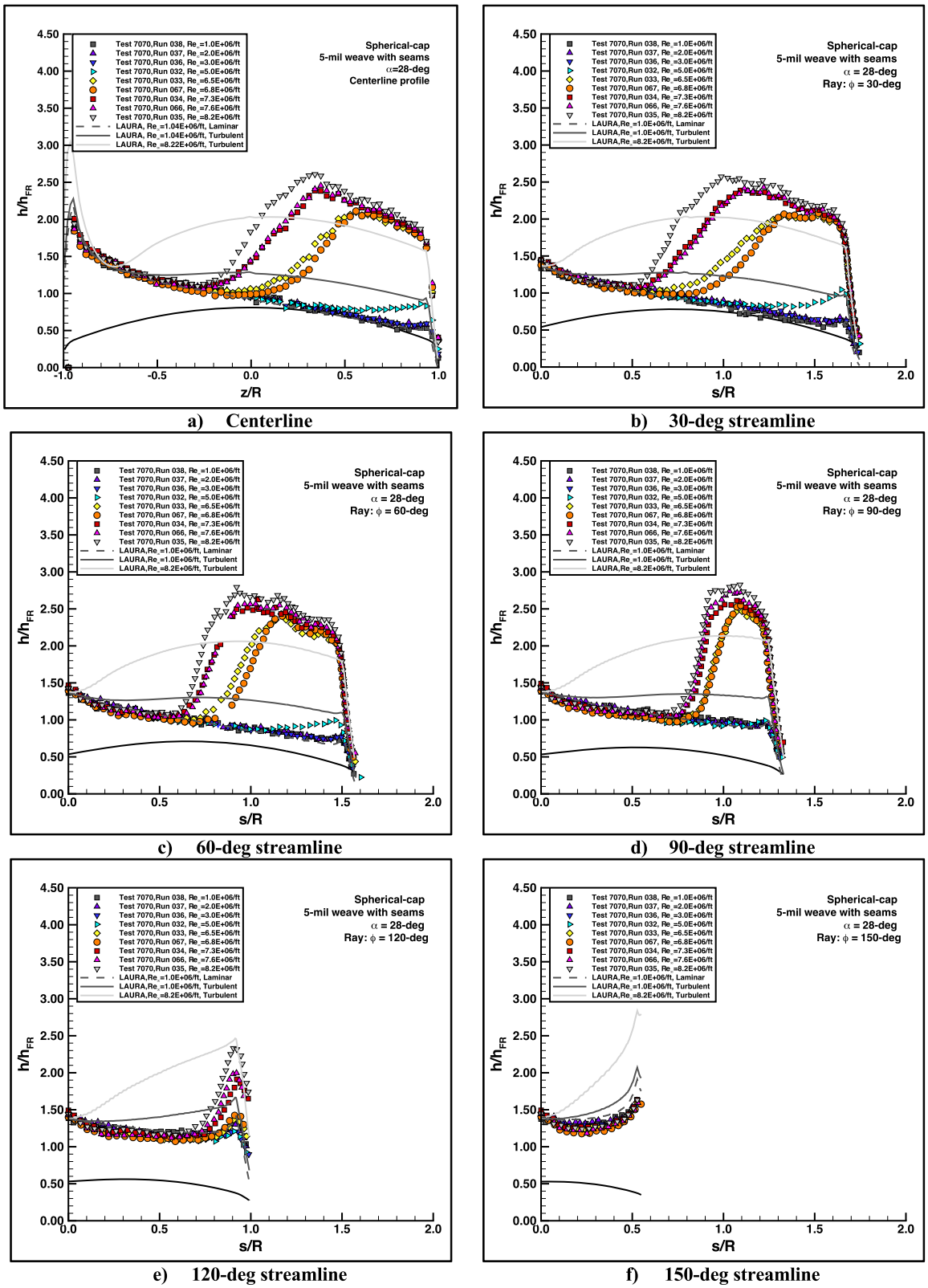
a) Test 7070, Run 38: $Re_\infty = 1.0\times10^6$/ft b) Test 7070, Run 37: $Re_\infty = 2.0\times10^6$/ft c) Test 7070, Run 36: $Re_\infty = 3.0\times10^6$/ft

d) Test 7070, Run 32: $Re_\infty = 5.0\times10^6$/ft e) Test 7070, Run XX: $Re_\infty = 5.3\times10^6$/ft f) Test 7070, Run 33: $Re_\infty = 6.5\times10^6$/ft

g) Test 7070, Run 67: $Re_\infty = 6.8\times10^6$/ft h) Test 7070, Run 34: $Re_\infty = 7.3\times10^6$/ft i) Test 7070, Run 66: $Re_\infty = 7.6\times10^6$/ft

j) Test 7070, Run 35: $Re_\infty = 8.2\times10^6$/ft

Figure 50. Reynolds Number effects: spherical-cap geometry, 5-mil weave with seams model images.

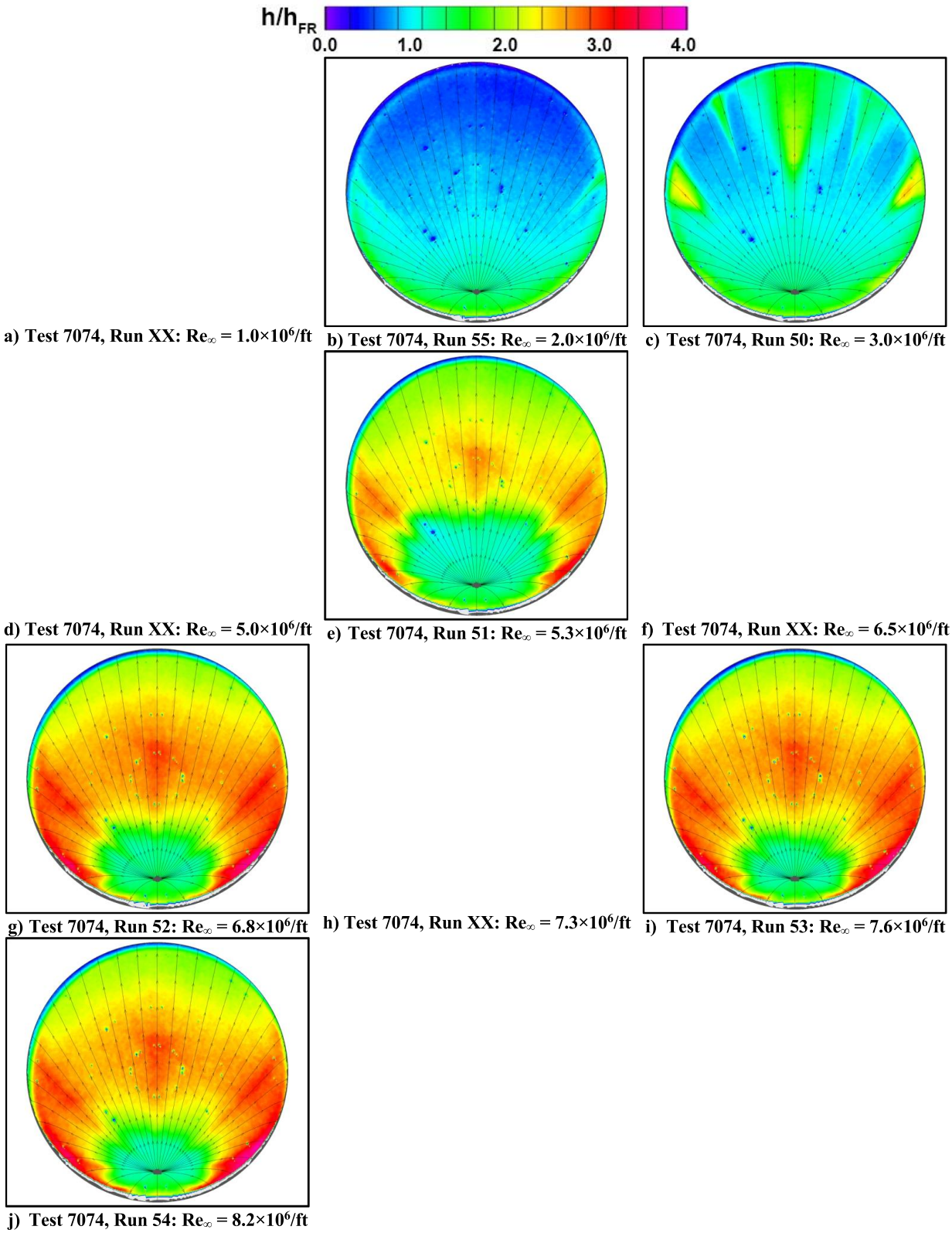


a) Centerline b) 30-deg streamline

c) 60-deg streamline d) 90-deg streamline

e) 120-deg streamline f) 150-deg streamline

Figure 51. Reynolds number effects: spherical-cap geometry, 5-mil weave with seams plots.



a) Test 7074, Run XX: $Re_\infty = 1.0\times10^6$/ft

b) Test 7074, Run 55: $Re_\infty = 2.0\times10^6$/ft

c) Test 7074, Run 50: $Re_\infty = 3.0\times10^6$/ft

d) Test 7074, Run XX: $Re_\infty = 5.0\times10^6$/ft

e) Test 7074, Run 51: $Re_\infty = 5.3\times10^6$/ft

f) Test 7074, Run XX: $Re_\infty = 6.5\times10^6$/ft

g) Test 7074, Run 52: $Re_\infty = 6.8\times10^6$/ft

h) Test 7074, Run XX: $Re_\infty = 7.3\times10^6$/ft

i) Test 7074, Run 53: $Re_\infty = 7.6\times10^6$/ft

j) Test 7074, Run 54: $Re_\infty = 8.2\times10^6$/ft

Figure 52. Reynolds Number effects: spherical-cap geometry, 10-mil weave without seams model images.

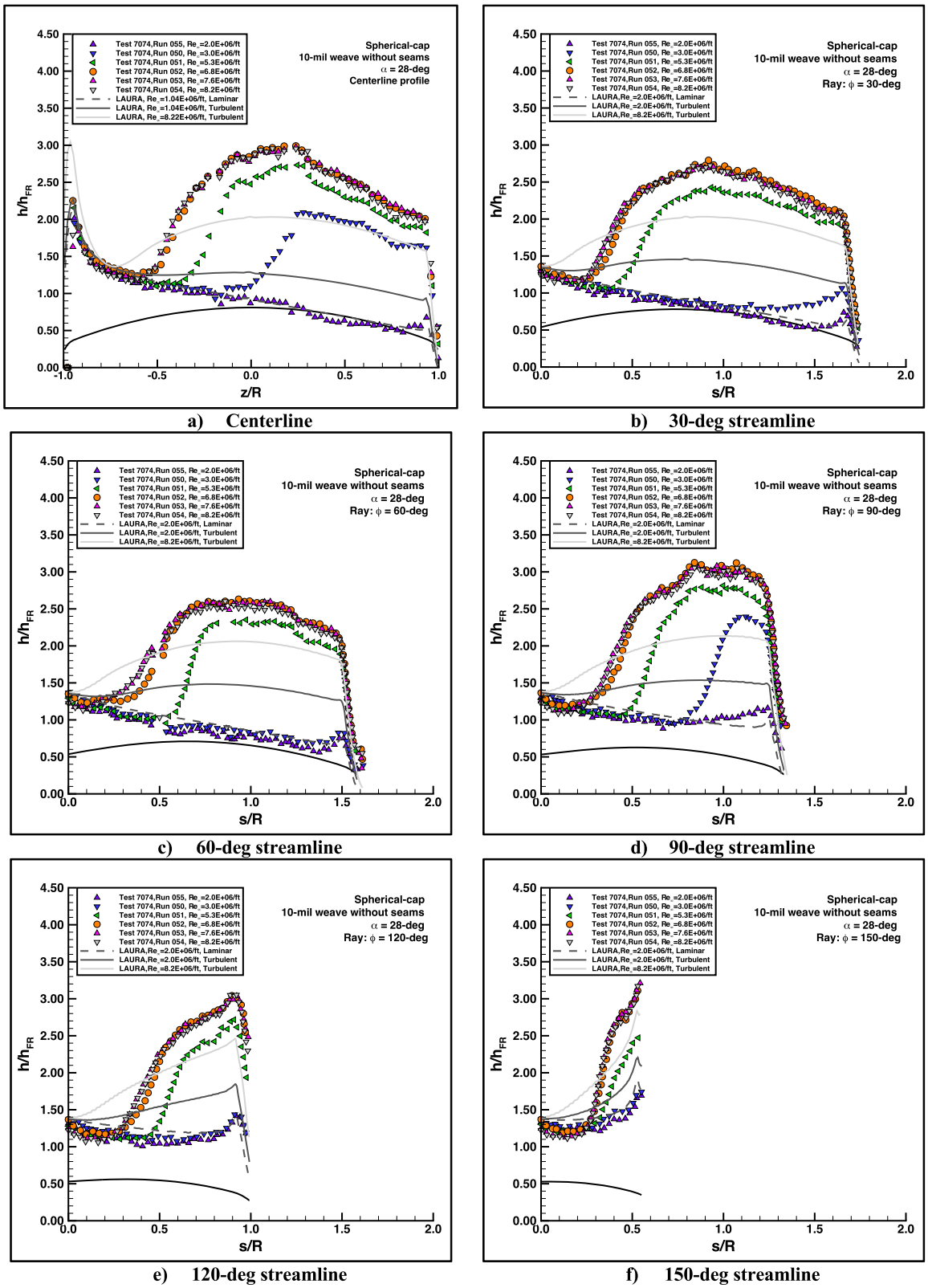
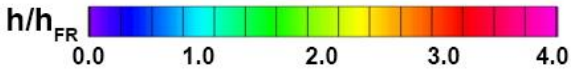


Figure 53. Reynolds number effects: spherical-cap geometry, 10-mil weave without seams plots.



a) Test 7070, Run XX: $Re_\infty = 1.0\times10^6$/ft b) Test 7070, Run XX: $Re_\infty = 2.0\times10^6$/ft c) Test 7070, Run XX: $Re_\infty = 3.0\times10^6$/ft

d) Test 7070, Run XX: $Re_\infty = 5.0\times10^6$/ft e) Test 7070, Run XX: $Re_\infty = 5.3\times10^6$/ft f) Test 7070, Run XX: $Re_\infty = 6.5\times10^6$/ft

g) Test 7070, Run XX: $Re_\infty = 6.8\times10^6$/ft h) Test 7070, Run XX: $Re_\infty = 7.3\times10^6$/ft i) Test 7070, Run XX: $Re_\infty = 7.6\times10^6$/ft

j) Test 7070, Run XX: $Re_\infty = 8.2\times10^6$/ft

Figure 54. Reynolds Number effects: spherical-cap geometry, 10-mil weave with seams model images.

a) Centerline

b) 30-deg streamline

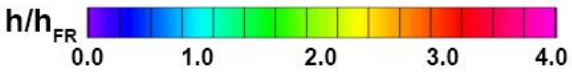
c) 60-deg streamline

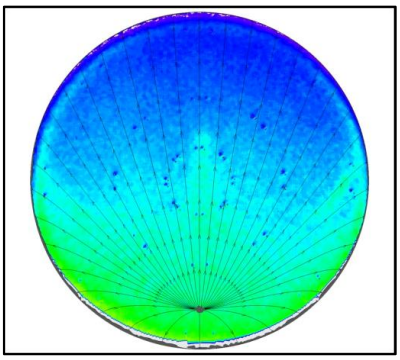
d) 90-deg streamline

e) 120-deg streamline

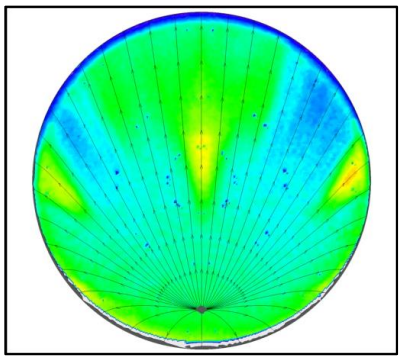
f) 150-deg streamline

Figure 55. Reynolds number effects: spherical-cap geometry, 10-mil weave with seams plots.

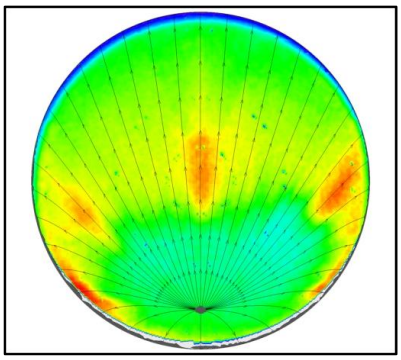




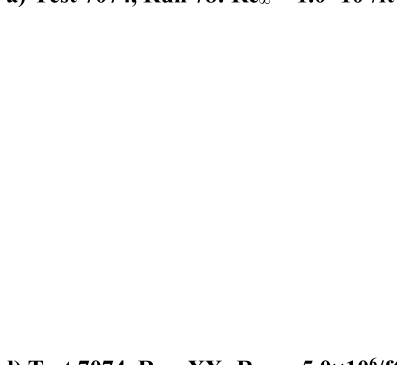
a) Test 7074, Run 78: $Re_\infty = 1.0\times10^6$/ft



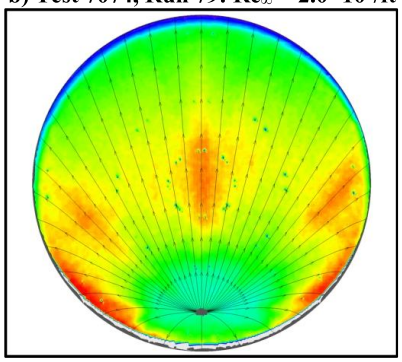
b) Test 7074, Run 79: $Re_\infty = 2.0\times10^6$/ft



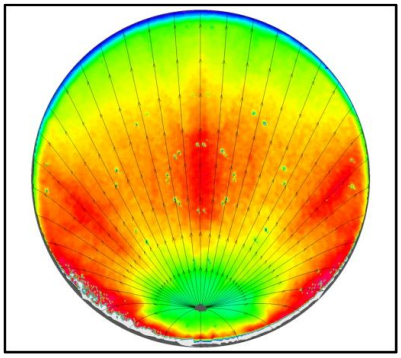
c) Test 7074, Run 77: $Re_\infty = 3.0\times10^6$/ft



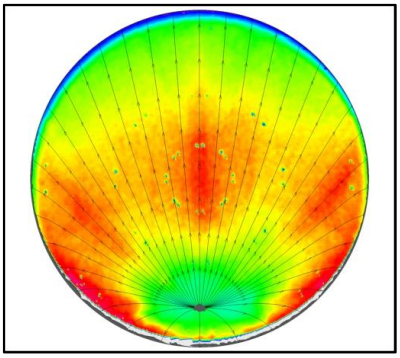
d) Test 7074, Run XX: $Re_\infty = 5.0\times10^6$/ft



e) Test 7074, Run 73: $Re_\infty = 5.3\times10^6$/ft



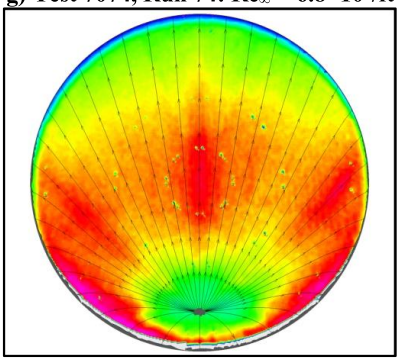
f) Test 7074, Run XX: $Re_\infty = 6.5\times10^6$/ft



g) Test 7074, Run 74: $Re_\infty = 6.8\times10^6$/ft

h) Test 7074, Run XX: $Re_\infty = 7.3\times10^6$/ft

i) Test 7074, Run 75: $Re_\infty = 7.6\times10^6$/ft



j) Test 7074, Run 76: $Re_\infty = 8.2\times10^6$/ft

Figure 56. Reynolds Number effects: spherical-cap geometry, 15-mil weave without seams model images.

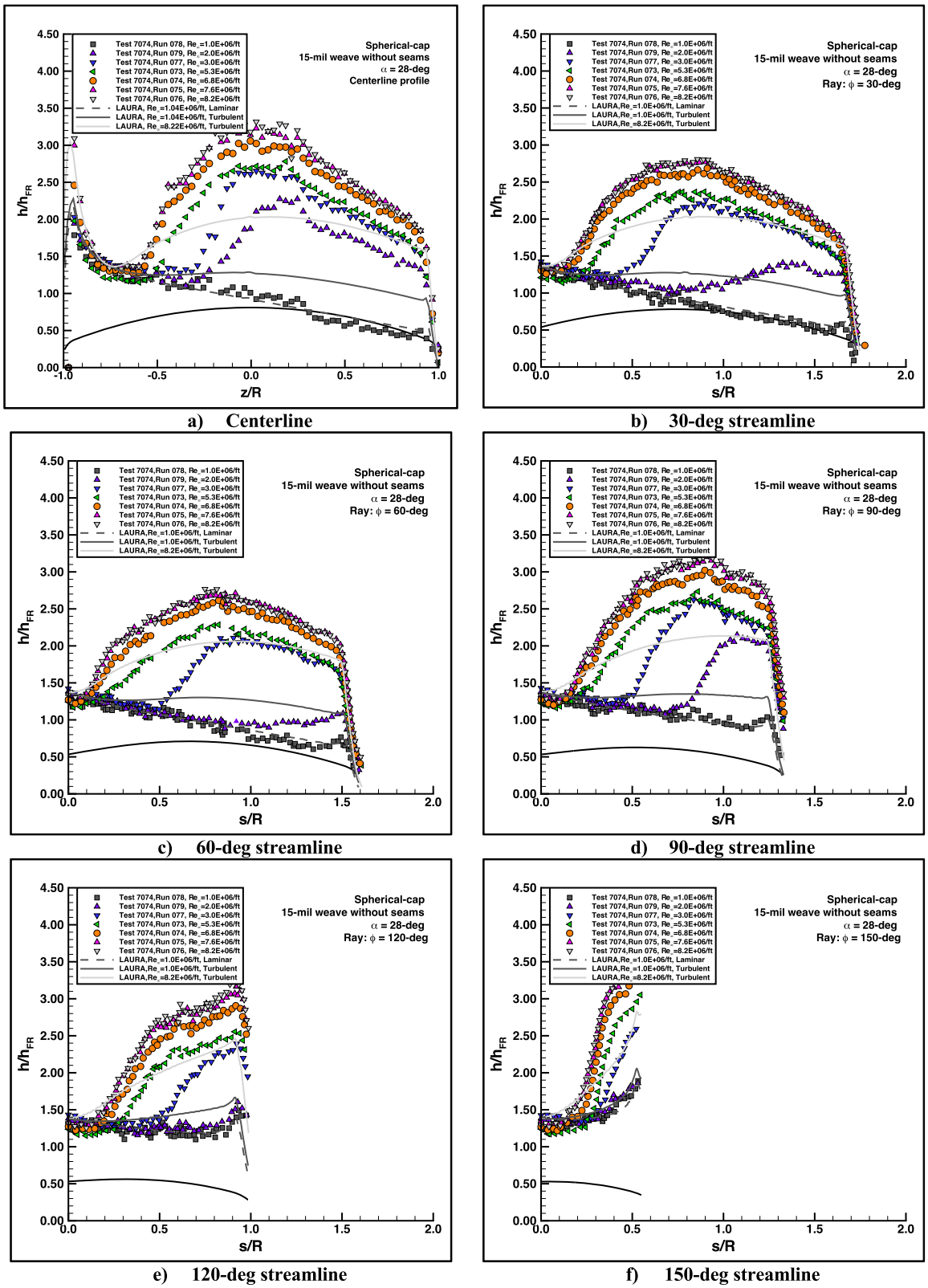
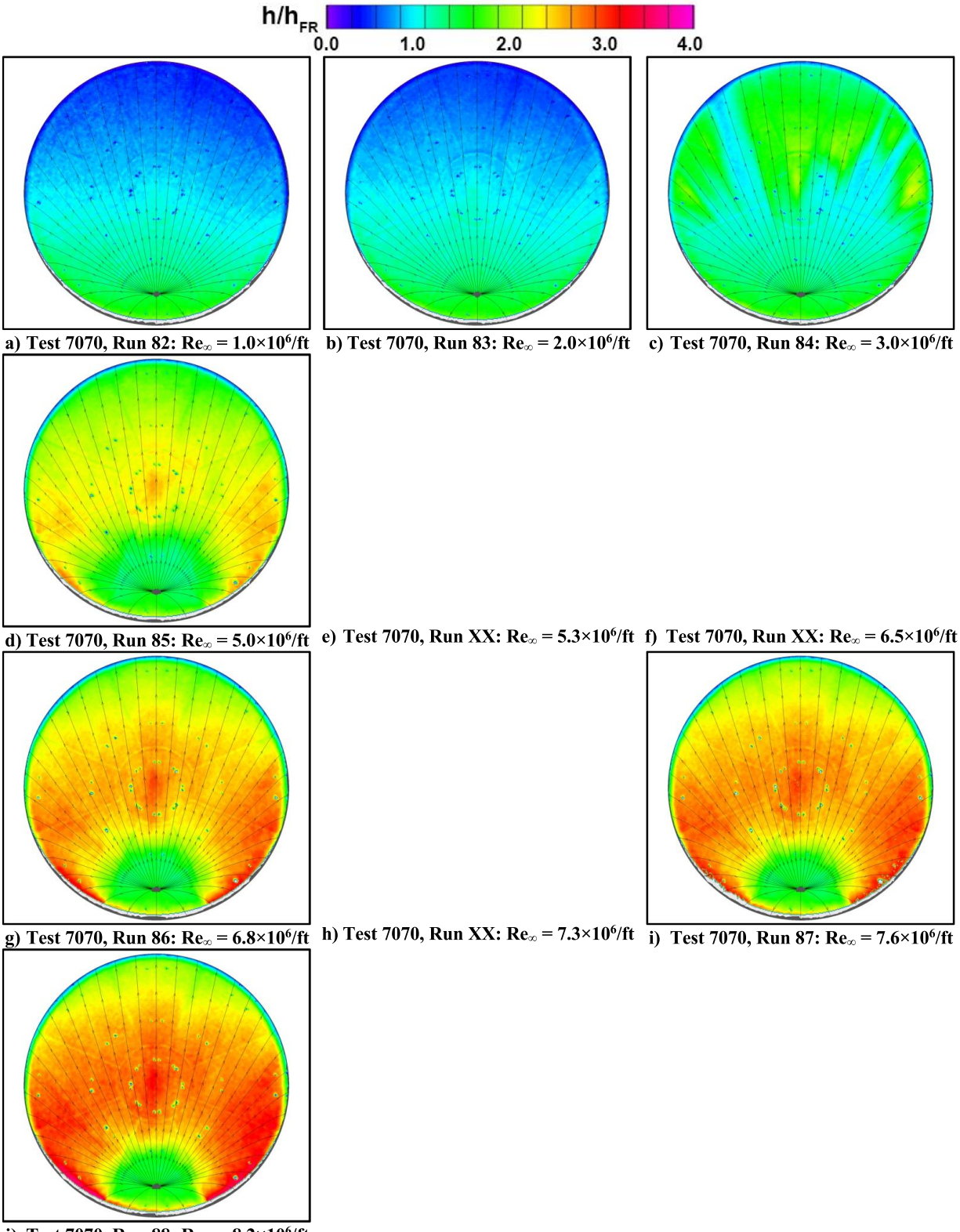


Figure 57. Reynolds number effects: spherical-cap geometry, 15-mil weave without seams plots.



a) Test 7070, Run 82: $Re_\infty = 1.0\times10^6$/ft
b) Test 7070, Run 83: $Re_\infty = 2.0\times10^6$/ft
c) Test 7070, Run 84: $Re_\infty = 3.0\times10^6$/ft
d) Test 7070, Run 85: $Re_\infty = 5.0\times10^6$/ft
e) Test 7070, Run XX: $Re_\infty = 5.3\times10^6$/ft
f) Test 7070, Run XX: $Re_\infty = 6.5\times10^6$/ft
g) Test 7070, Run 86: $Re_\infty = 6.8\times10^6$/ft
h) Test 7070, Run XX: $Re_\infty = 7.3\times10^6$/ft
i) Test 7070, Run 87: $Re_\infty = 7.6\times10^6$/ft
j) Test 7070, Run 88: $Re_\infty = 8.2\times10^6$/ft

Figure 58. Reynolds Number effects: spherical-cap geometry, 15-mil weave with seams model images.

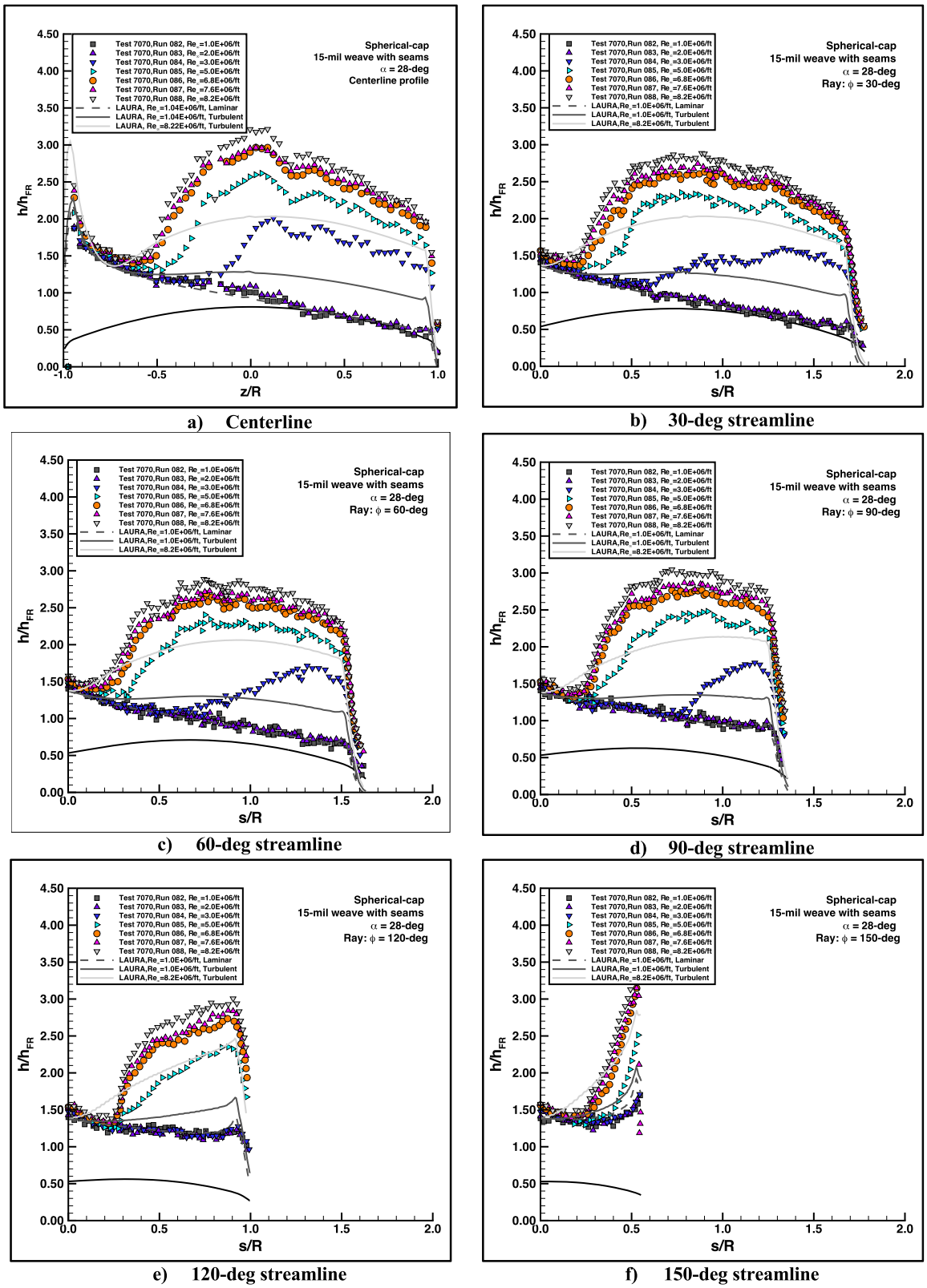
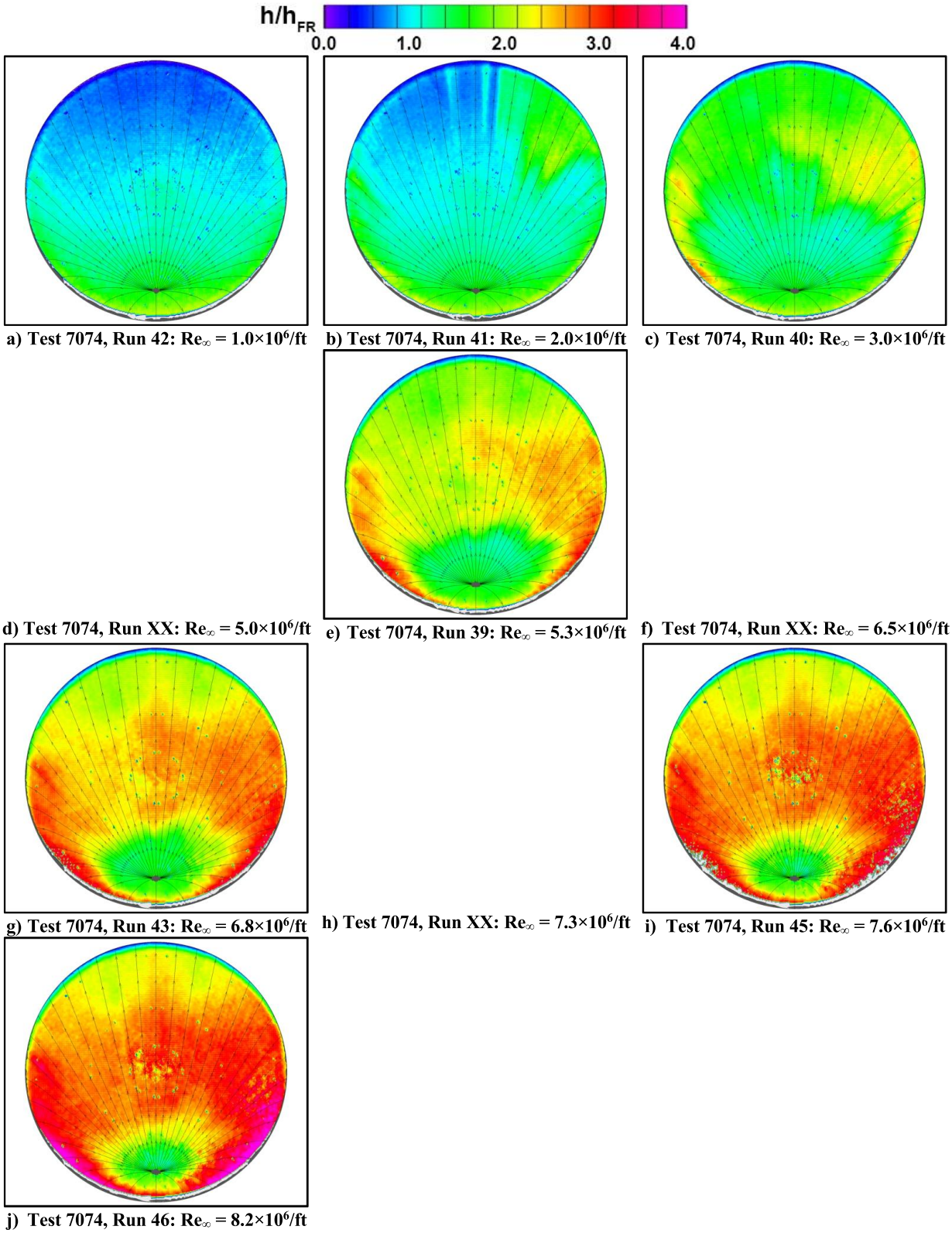


Figure 59. Reynolds number effects: spherical-cap geometry, 15-mil weave with seams plots.



a) Test 7074, Run 42: $Re_\infty = 1.0\times10^6$/ft

b) Test 7074, Run 41: $Re_\infty = 2.0\times10^6$/ft

c) Test 7074, Run 40: $Re_\infty = 3.0\times10^6$/ft

d) Test 7074, Run XX: $Re_\infty = 5.0\times10^6$/ft

e) Test 7074, Run 39: $Re_\infty = 5.3\times10^6$/ft

f) Test 7074, Run XX: $Re_\infty = 6.5\times10^6$/ft

g) Test 7074, Run 43: $Re_\infty = 6.8\times10^6$/ft

h) Test 7074, Run XX: $Re_\infty = 7.3\times10^6$/ft

i) Test 7074, Run 45: $Re_\infty = 7.6\times10^6$/ft

j) Test 7074, Run 46: $Re_\infty = 8.2\times10^6$/ft

Figure 60. Reynolds Number effects: spherical-cap geometry, 20-mil weave without seams model images.

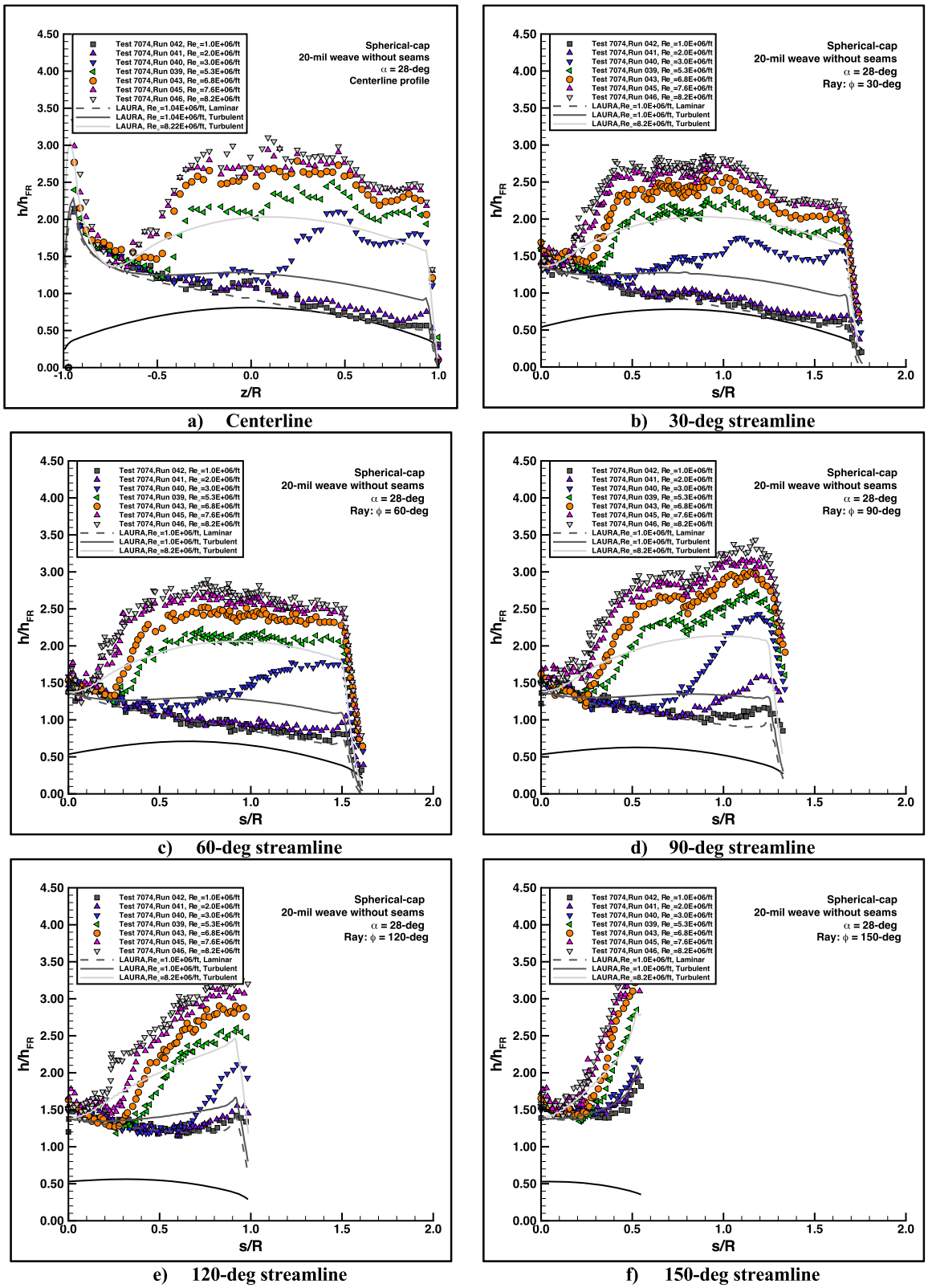
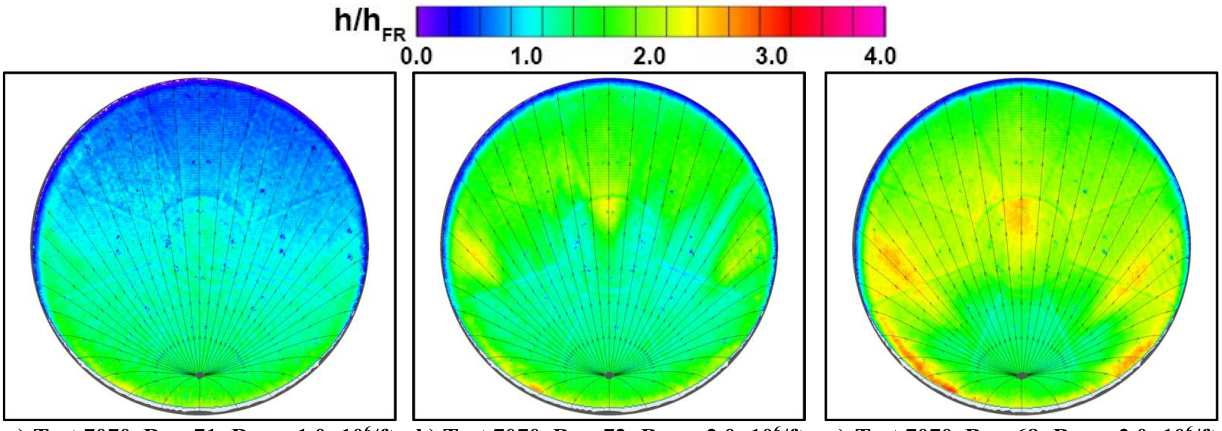


Figure 61. Reynolds number effects: spherical-cap geometry, 20-mil weave without seams plots.



a) Test 7070, Run 71: $Re_\infty = 1.0\times10^6$/ft

b) Test 7070, Run 72: $Re_\infty = 2.0\times10^6$/ft

c) Test 7070, Run 68: $Re_\infty = 3.0\times10^6$/ft

d) Test 7070, Run 69: $Re_\infty = 5.0\times10^6$/ft

e) Test 7070, Run XX: $Re_\infty = 5.3\times10^6$/ft

f) Test 7070, Run XX: $Re_\infty = 6.5\times10^6$/ft

g) Test 7070, Run 70: $Re_\infty = 6.8\times10^6$/ft

h) Test 7070, Run XX: $Re_\infty = 7.3\times10^6$/ft

i) Test 7070, Run 73: $Re_\infty = 7.6\times10^6$/ft

j) Test 7070, Run 74: $Re_\infty = 8.2\times10^6$/ft

Figure 62. Reynolds Number effects: spherical-cap geometry, 20-mil weave with seams model images.

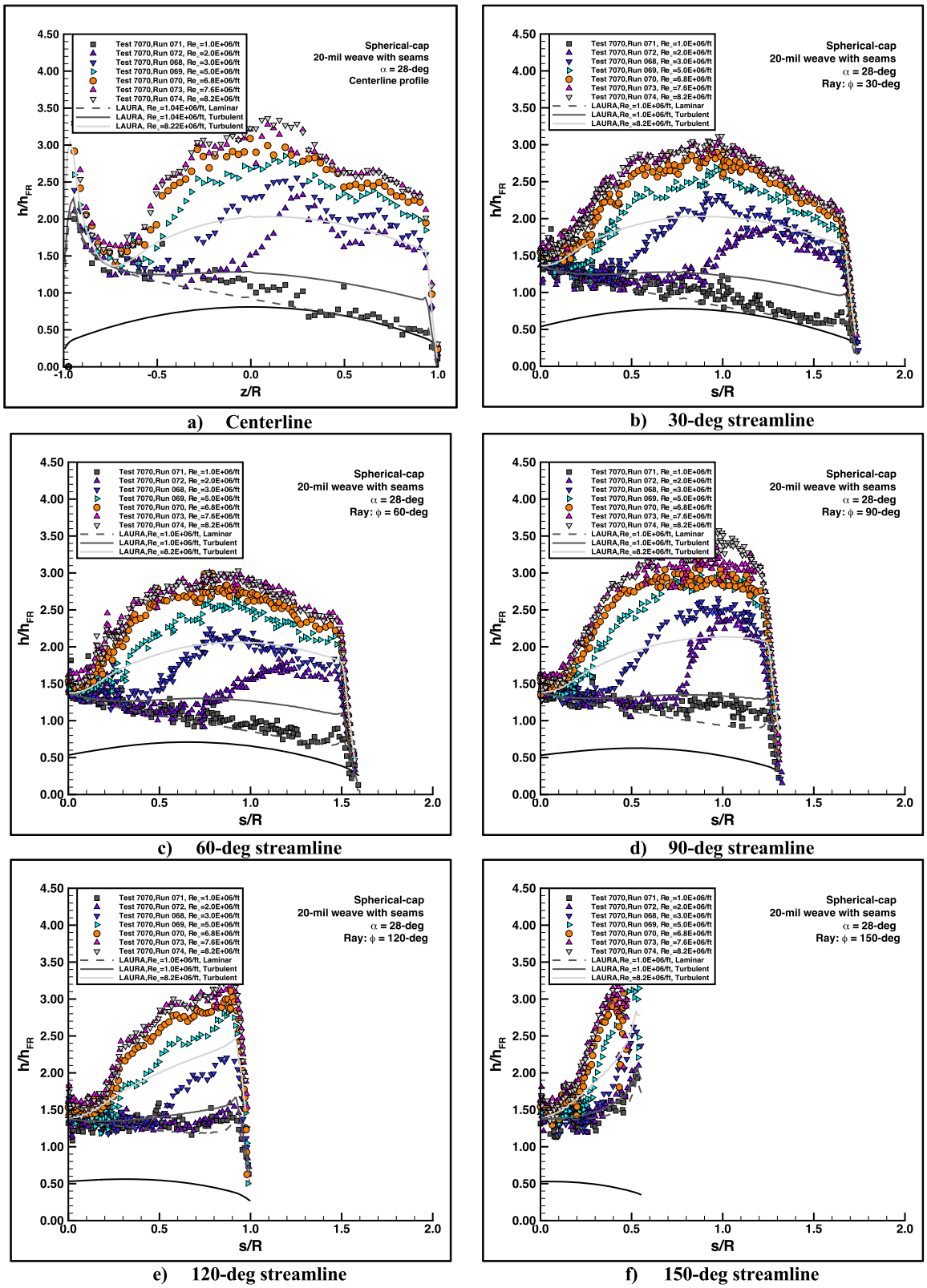
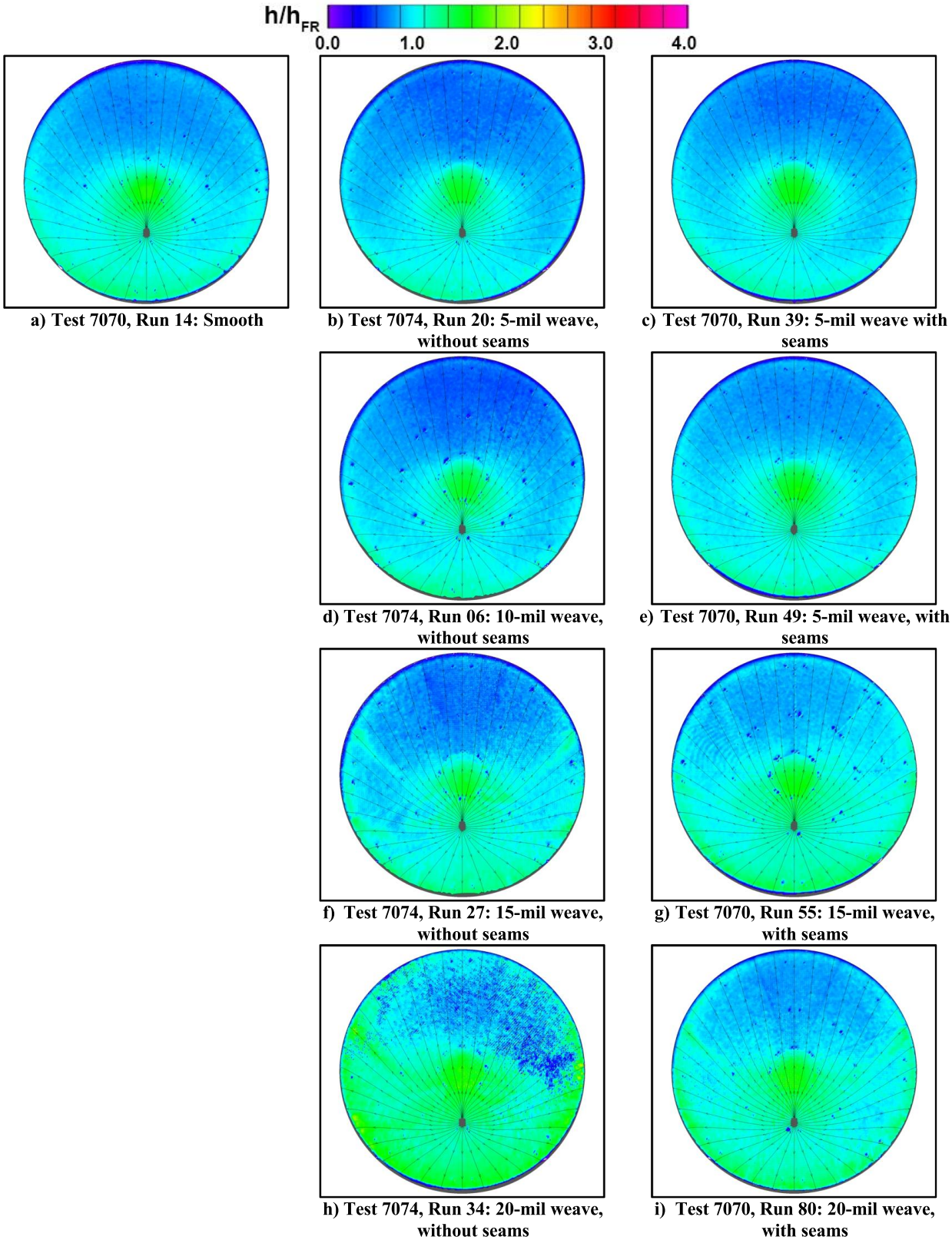


Figure 63. Reynolds number effects: spherical-cap geometry, 20-mil weave with seams plots.



a) Test 7070, Run 14: Smooth

b) Test 7074, Run 20: 5-mil weave, without seams

c) Test 7070, Run 39: 5-mil weave with seams

d) Test 7074, Run 06: 10-mil weave, without seams

e) Test 7070, Run 49: 5-mil weave, with seams

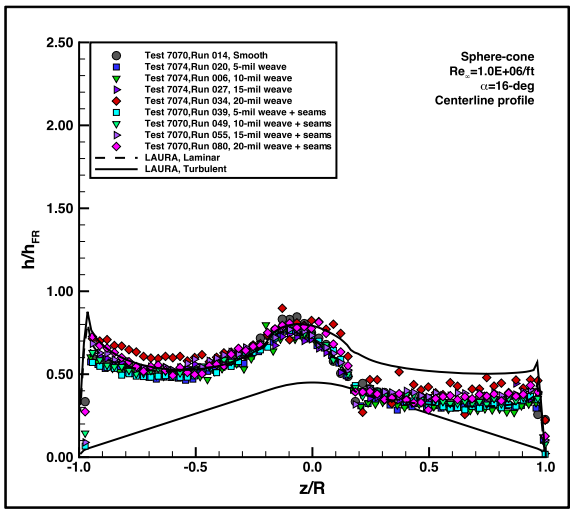
f) Test 7074, Run 27: 15-mil weave, without seams

g) Test 7070, Run 55: 15-mil weave, with seams

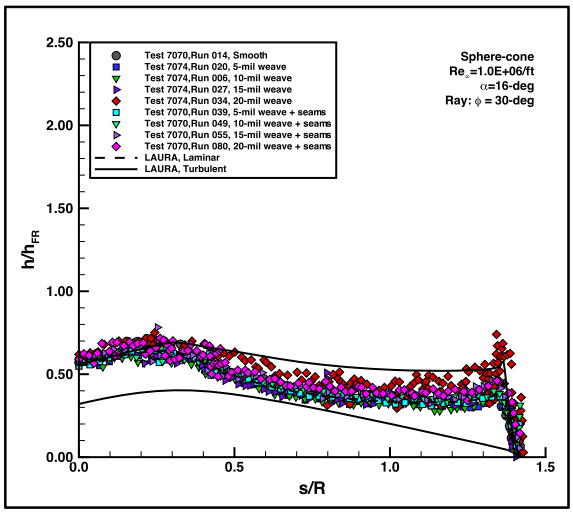
h) Test 7074, Run 34: 20-mil weave, without seams

i) Test 7070, Run 80: 20-mil weave, with seams

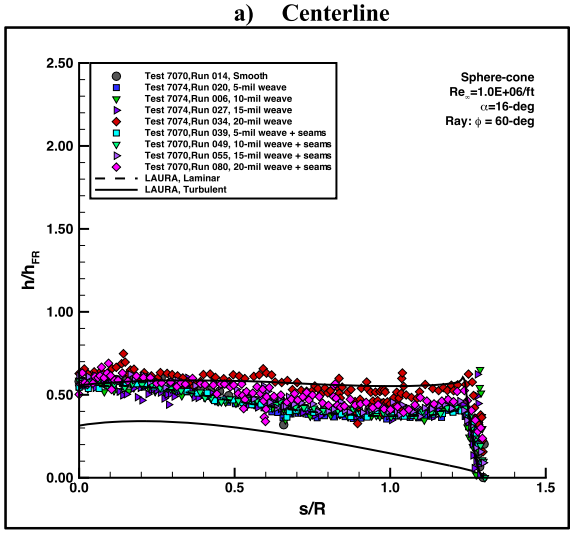
Figure 64. Weave-height effects: sphere-cone geometry, $Re_\infty = 1.0\times10^6$/ft images.



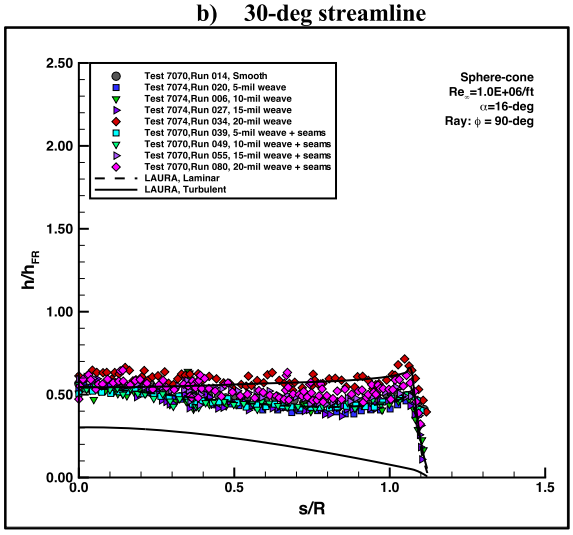
a) Centerline



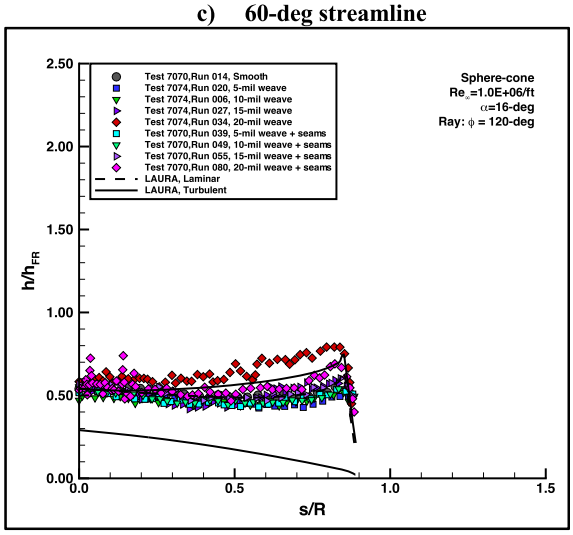
b) 30-deg streamline



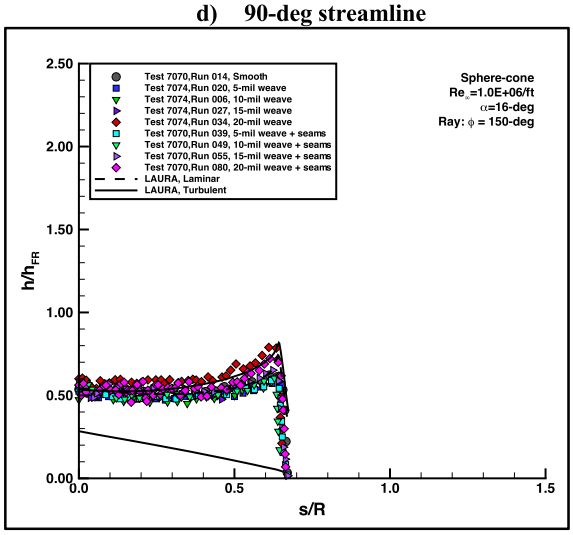
c) 60-deg streamline



d) 90-deg streamline

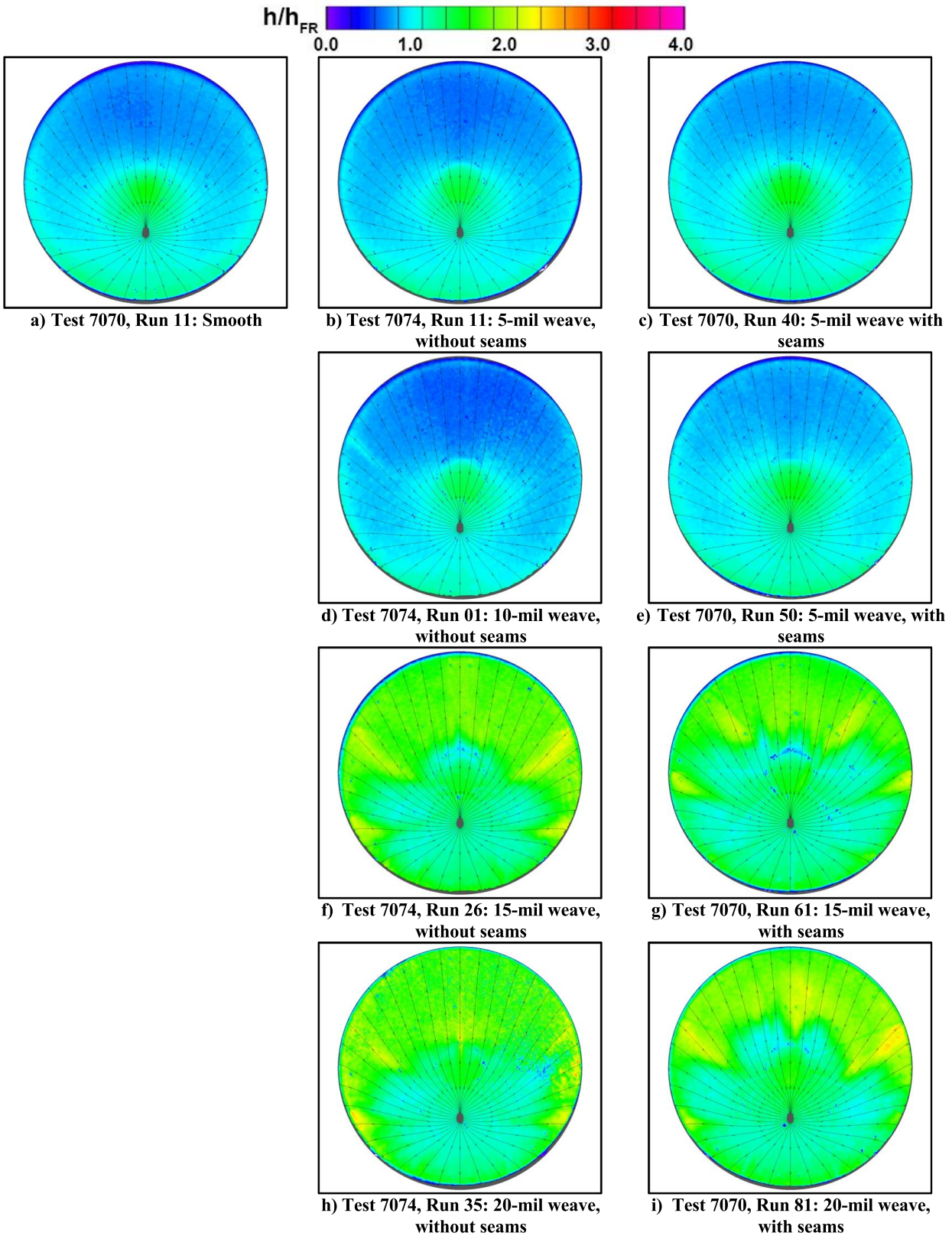


e) 120-deg streamline



f) 150-deg streamline

Figure 65. Weave-height effects: sphere-cone geometry, $Re_\infty = 1.0\times10^6$/ft plots.



a) Test 7070, Run 11: Smooth

b) Test 7074, Run 11: 5-mil weave, without seams

c) Test 7070, Run 40: 5-mil weave with seams

d) Test 7074, Run 01: 10-mil weave, without seams

e) Test 7070, Run 50: 5-mil weave, with seams

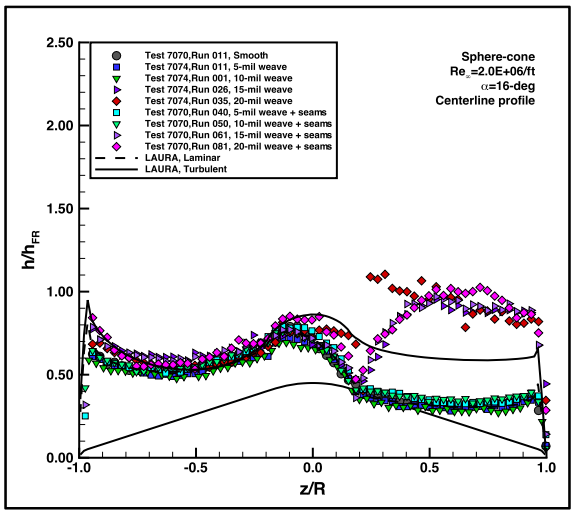
f) Test 7074, Run 26: 15-mil weave, without seams

g) Test 7070, Run 61: 15-mil weave, with seams

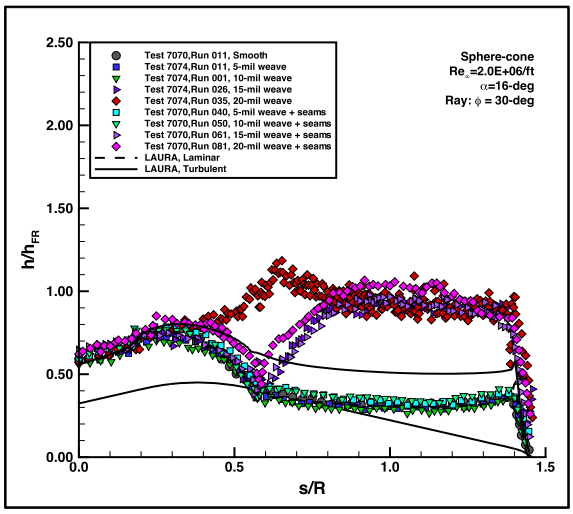
h) Test 7074, Run 35: 20-mil weave, without seams

i) Test 7070, Run 81: 20-mil weave, with seams

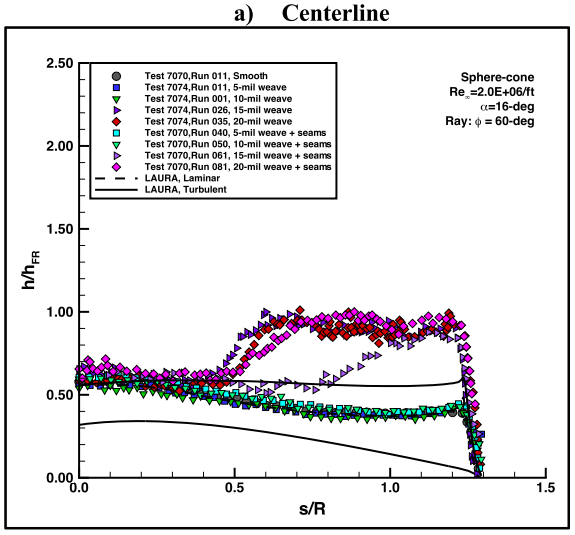
Figure 66. Weave-height effects: sphere-cone geometry, $Re_\infty = 2.0\times10^6$/ft images.



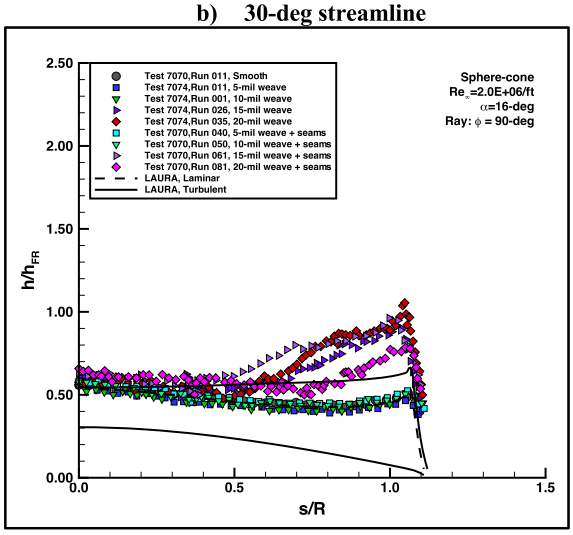
a) Centerline



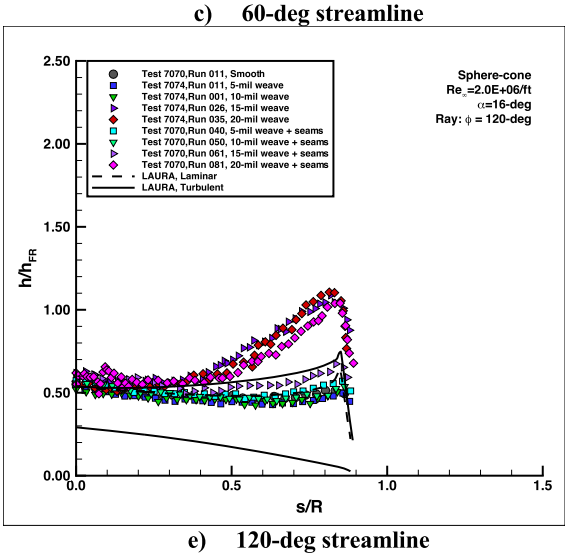
b) 30-deg streamline



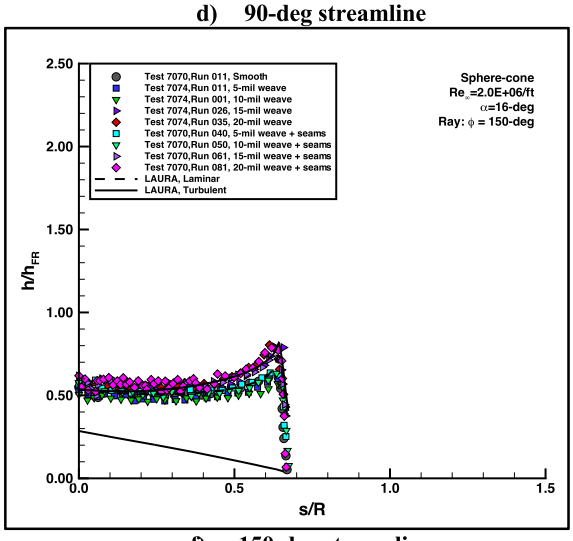
c) 60-deg streamline



d) 90-deg streamline

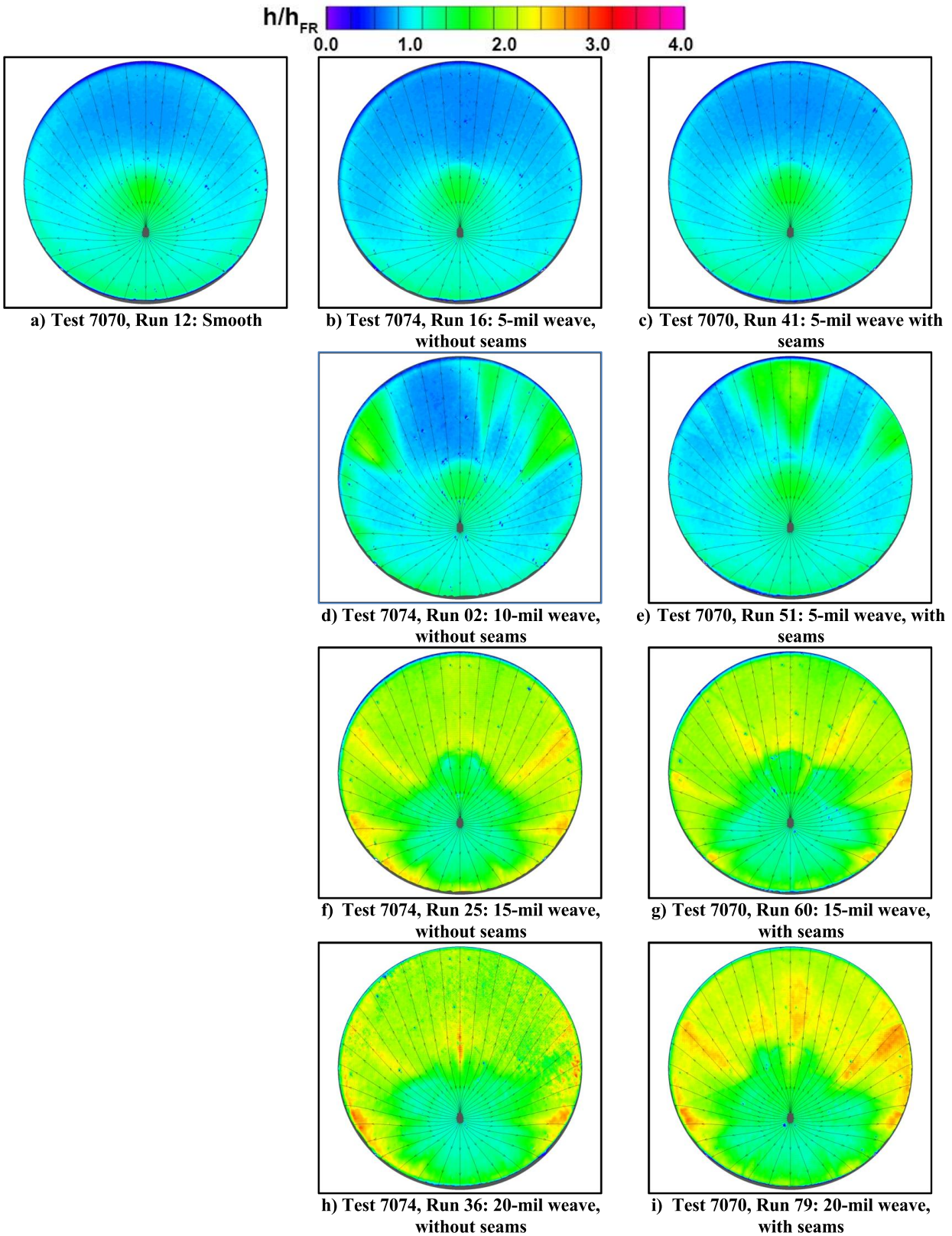


e) 120-deg streamline



f) 150-deg streamline

Figure 67. Weave-height effects: sphere-cone geometry, $Re_\infty = 2.0\times10^6$/ft plots.



a) Test 7070, Run 12: Smooth

b) Test 7074, Run 16: 5-mil weave, without seams

c) Test 7070, Run 41: 5-mil weave with seams

d) Test 7074, Run 02: 10-mil weave, without seams

e) Test 7070, Run 51: 5-mil weave, with seams

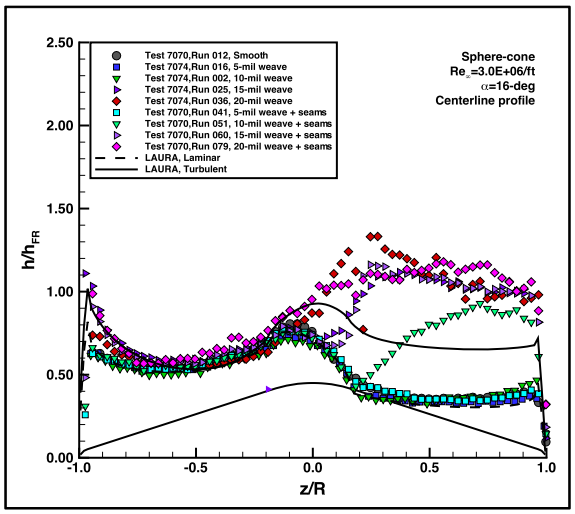
f) Test 7074, Run 25: 15-mil weave, without seams

g) Test 7070, Run 60: 15-mil weave, with seams

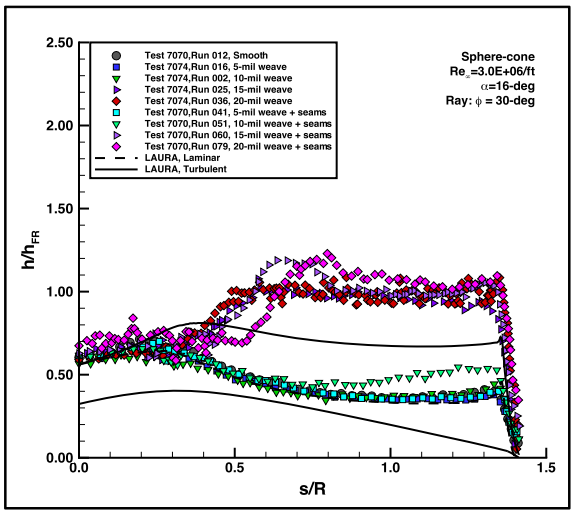
h) Test 7074, Run 36: 20-mil weave, without seams

i) Test 7070, Run 79: 20-mil weave, with seams

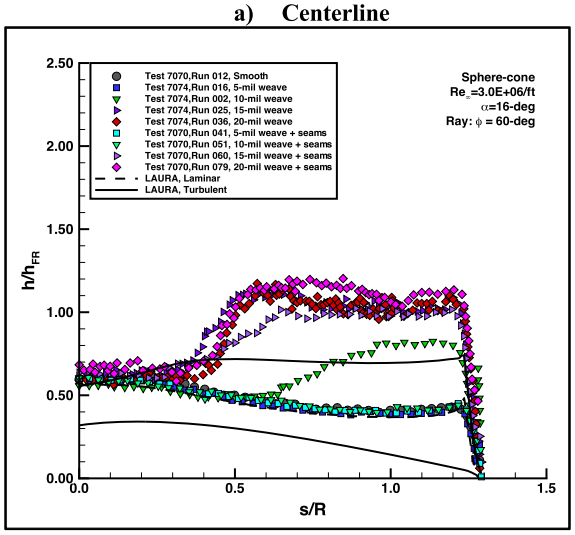
Figure 68. Weave-height effects: sphere-cone geometry, $Re_\infty = 3.0\times10^6$/ft images.



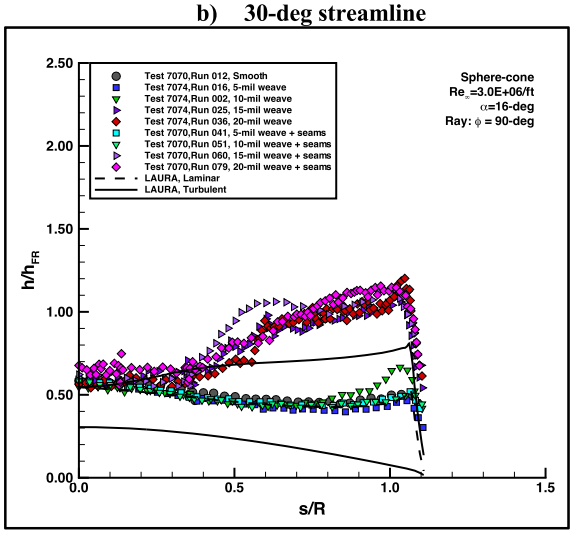
a) Centerline



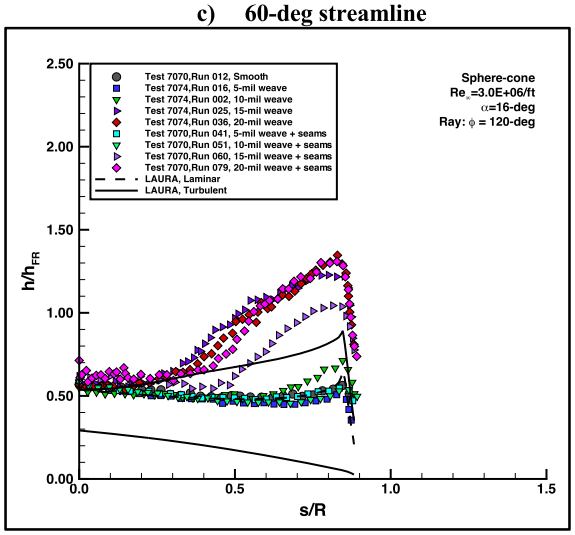
b) 30-deg streamline



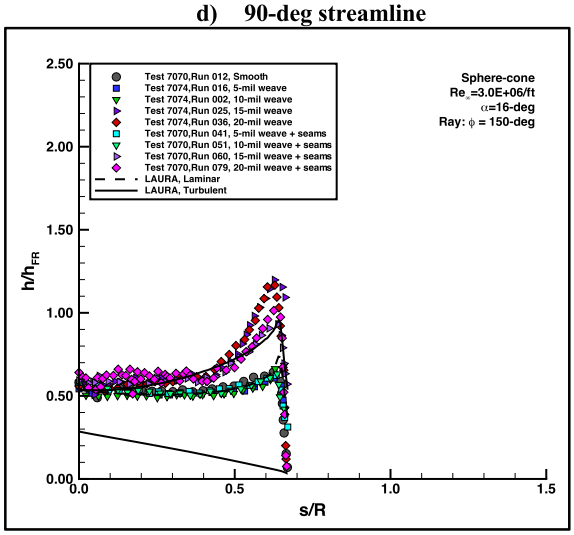
c) 60-deg streamline



d) 90-deg streamline

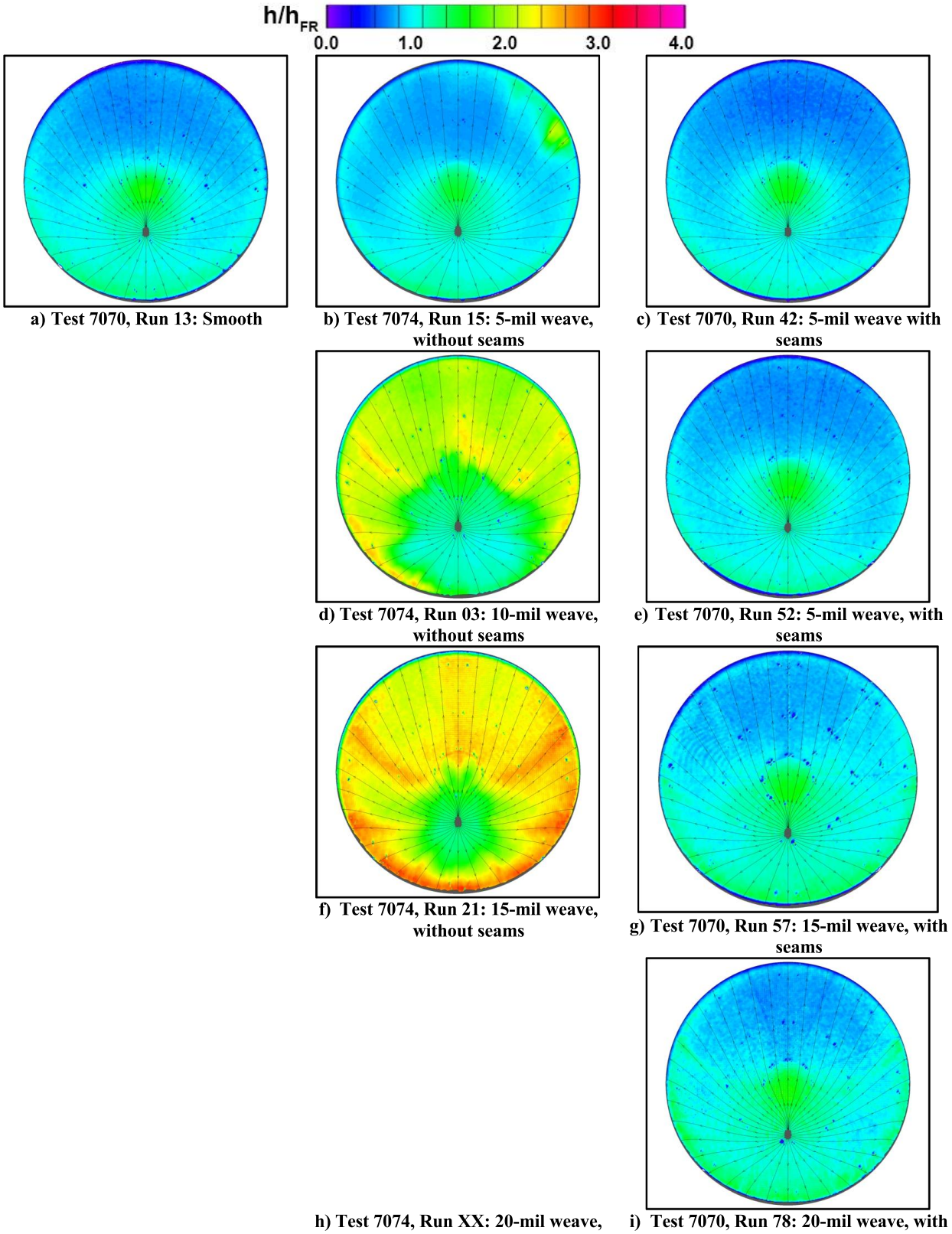


e) 120-deg streamline



f) 150-deg streamline

Figure 69. Weave-height effects: sphere-cone geometry, $Re_\infty = 3.0\times10^6$/ft plots.



a) Test 7070, Run 13: Smooth

b) Test 7074, Run 15: 5-mil weave, without seams

c) Test 7070, Run 42: 5-mil weave with seams

d) Test 7074, Run 03: 10-mil weave, without seams

e) Test 7070, Run 52: 5-mil weave, with seams

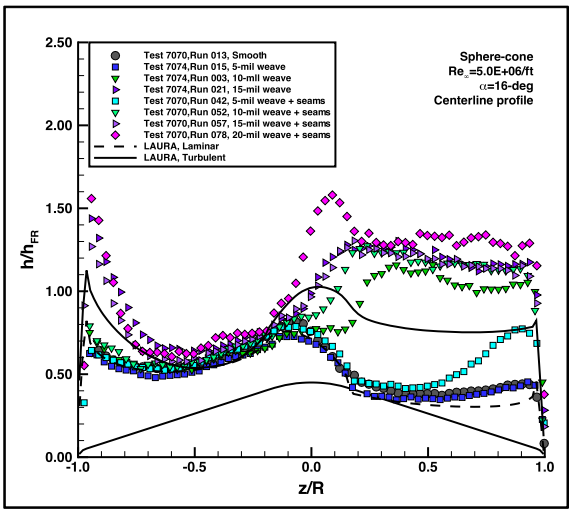
f) Test 7074, Run 21: 15-mil weave, without seams

g) Test 7070, Run 57: 15-mil weave, with seams

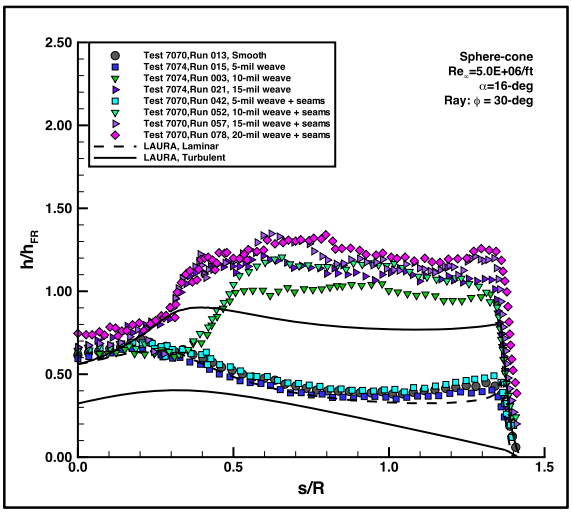
h) Test 7074, Run XX: 20-mil weave, without seams

i) Test 7070, Run 78: 20-mil weave, with seams

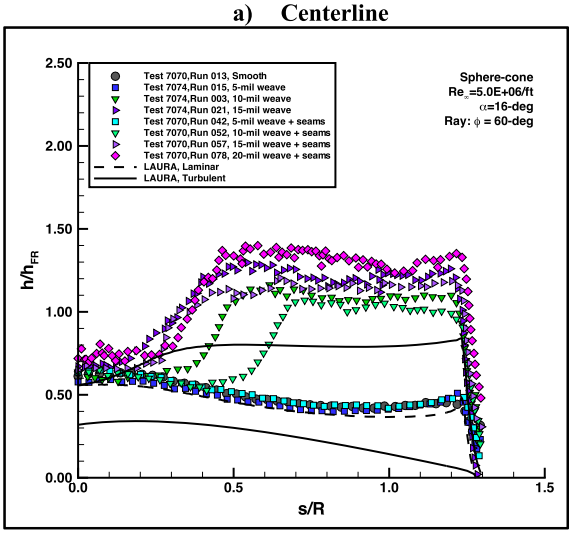
Figure 70. Weave-height effects: sphere-cone geometry, $Re_\infty = 5.0\times10^6$/ft images.



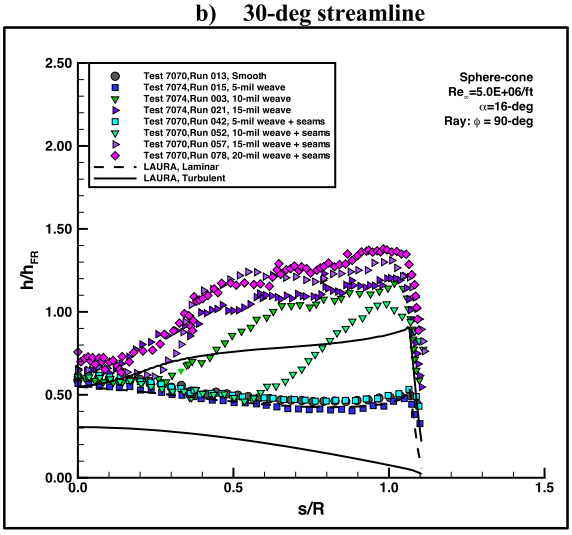
a) Centerline



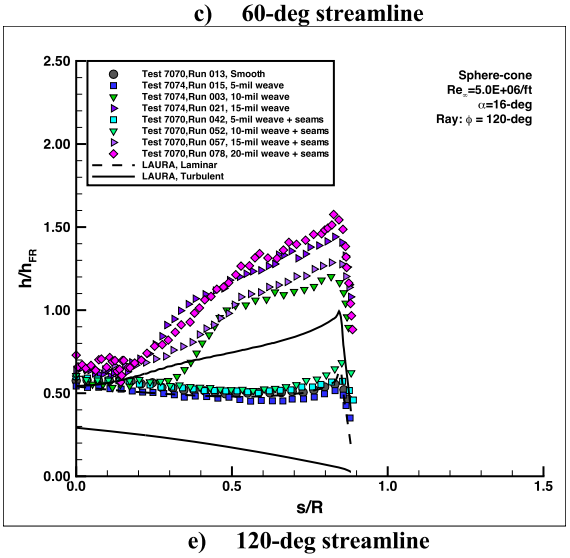
b) 30-deg streamline



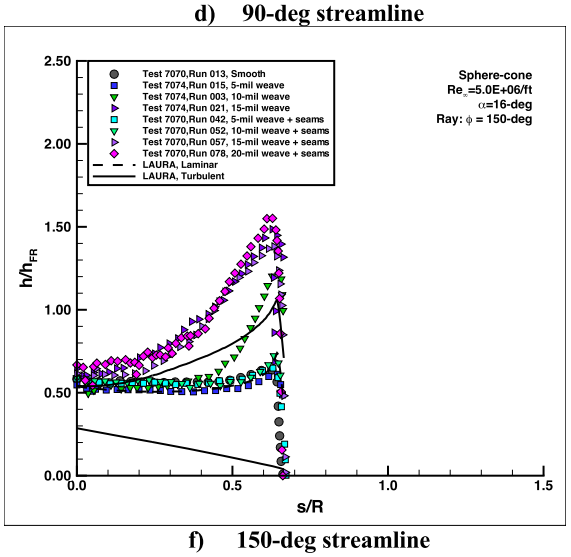
c) 60-deg streamline



d) 90-deg streamline

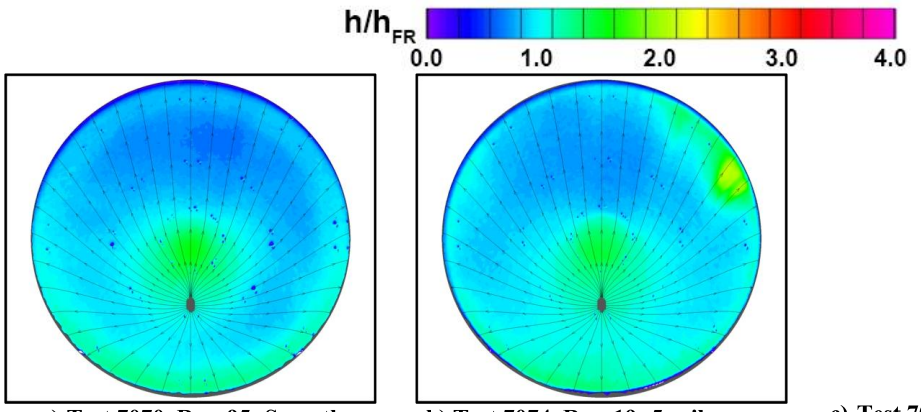


e) 120-deg streamline



f) 150-deg streamline

Figure 71. Weave-height effects: sphere-cone geometry, $Re_\infty = 5.0\times10^6$/ft plots.



a) Test 7070, Run 95: Smooth

b) Test 7074, Run 19: 5-mil weave, without seams

c) Test 7070, Run XX: 5-mil weave with seams

d) Test 7074, Run 08: 10-mil weave, without seams

e) Test 7070, Run XX: 5-mil weave, with seams

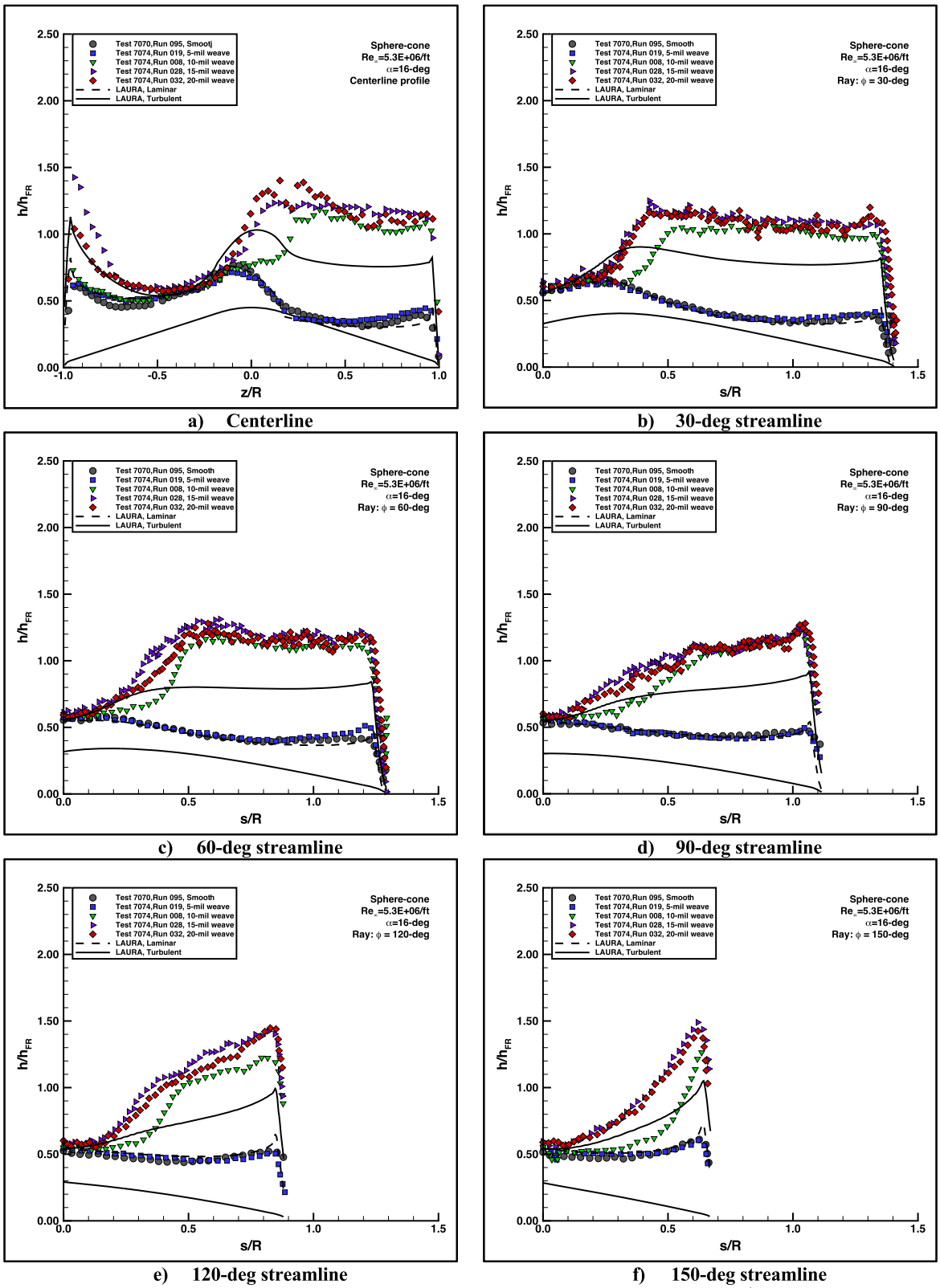
f) Test 7074, Run 28: 15-mil weave, without seams

g) Test 7070, Run XX: 15-mil weave, with seams

h) Test 7074, Run 32: 20-mil weave, without seams

i) Test 7070, Run XX: 20-mil weave, with seams

Figure 72. Weave-height effects: sphere-cone geometry, $Re_\infty = 5.2\times10^6$/ft images.

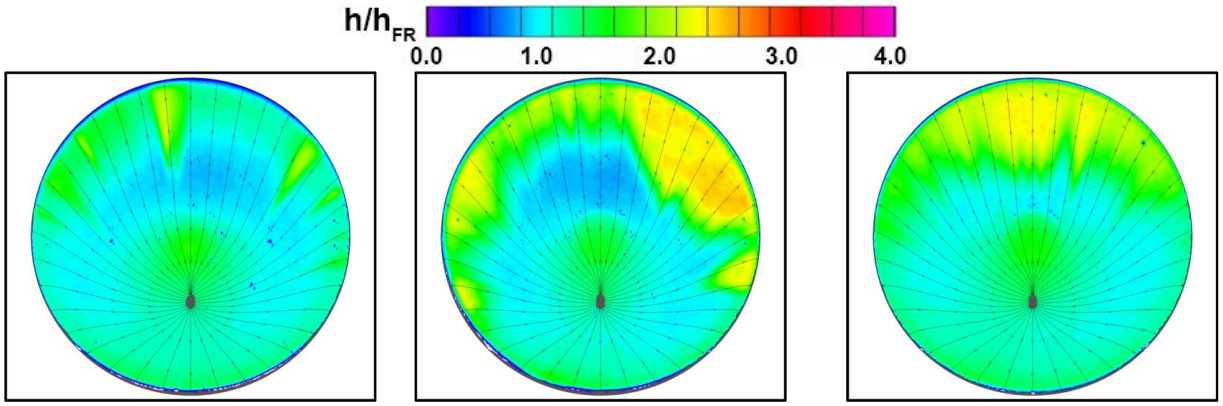


a) Centerline b) 30-deg streamline

c) 60-deg streamline d) 90-deg streamline

e) 120-deg streamline f) 150-deg streamline

Figure 73. Weave-height effects: sphere-cone geometry, $Re_\infty = 5.2\times10^6$/ft plots.



a) Test 7070, Run 15: Smooth

b) Test 7074, Run 14: 5-mil weave, without seams

c) Test 7070, Run 43: 5-mil weave with seams

d) Test 7074, Run 04: 10-mil weave, without seams

e) Test 7070, Run 48: 5-mil weave, with seams

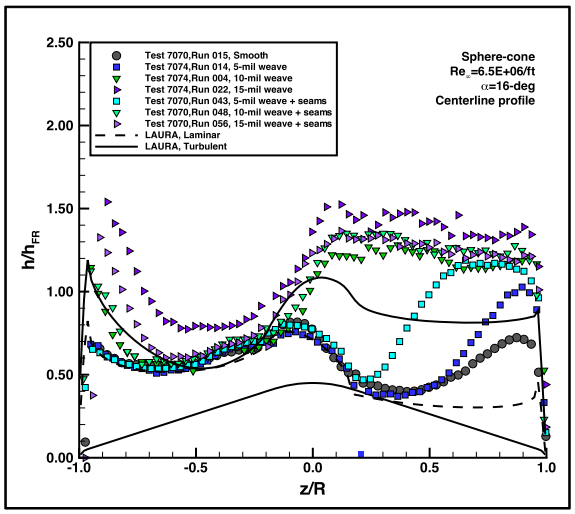
f) Test 7074, Run 22: 15-mil weave, without seams

g) Test 7070, Run 56: 15-mil weave, with seams

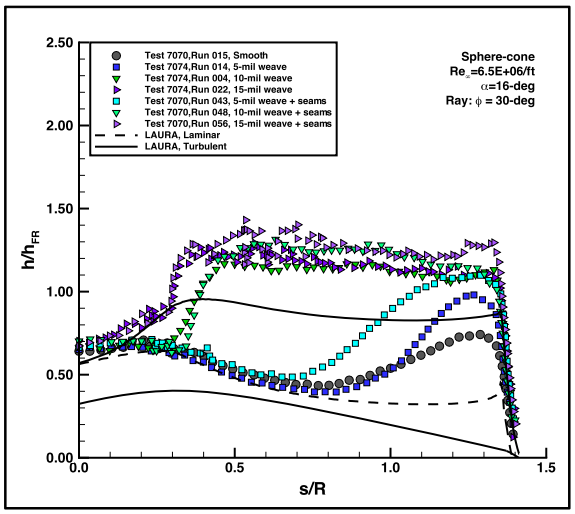
h) Test 7074, Run X: 20-mil weave, without seams

i) Test 7070, Run XX: 20-mil weave, with seams

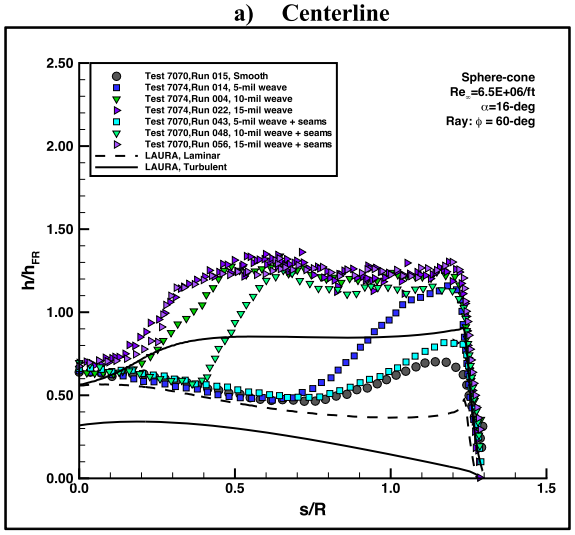
Figure 74. Weave-height effects: sphere-cone geometry, $Re_\infty = 6.5\times10^6$/ft images.



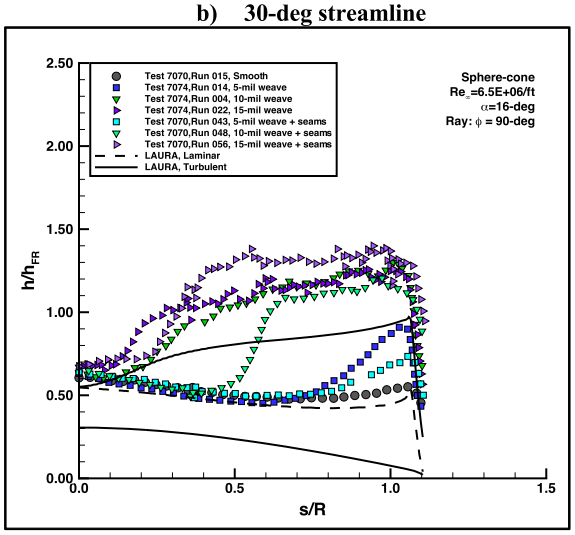
a) Centerline



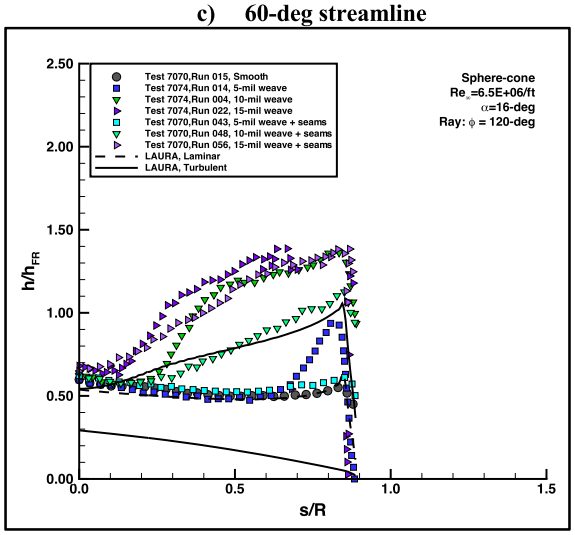
b) 30-deg streamline



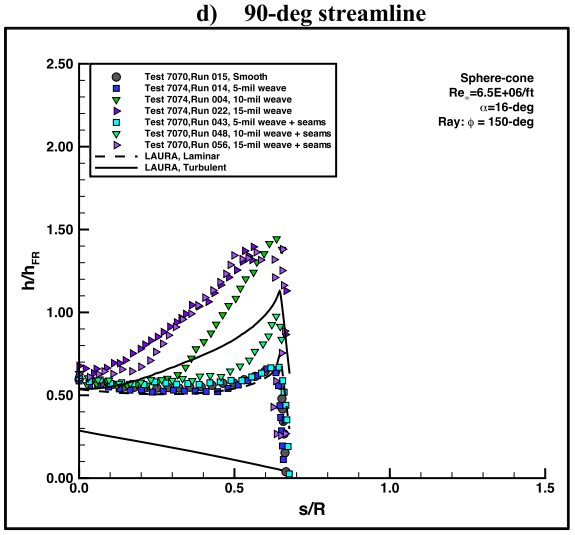
c) 60-deg streamline



d) 90-deg streamline

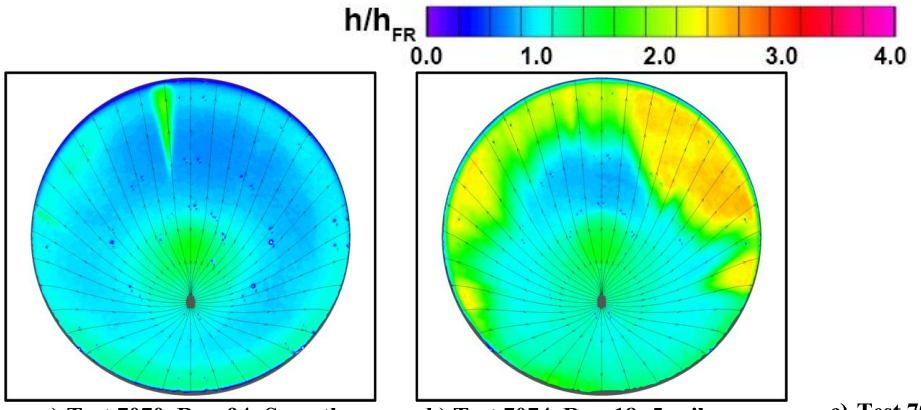


e) 120-deg streamline



f) 150-deg streamline

Figure 75. Weave-height effects: sphere-cone geometry, $Re_\infty = 6.5\times10^6$/ft plots.



a) Test 7070, Run 94: Smooth

b) Test 7074, Run 18: 5-mil weave, without seams

c) Test 7070, Run XX: 5-mil weave with seams

d) Test 7074, Run 09: 10-mil weave, without seams

e) Test 7070, Run 63: 5-mil weave, with seams

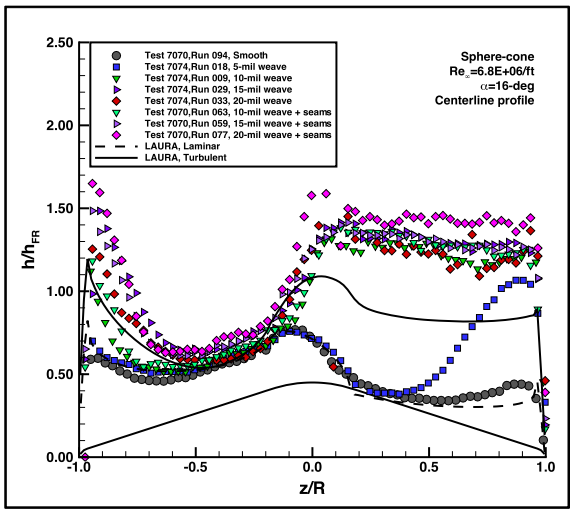
f) Test 7074, Run 29: 15-mil weave, without seams

g) Test 7070, Run 59: 15-mil weave, with seams

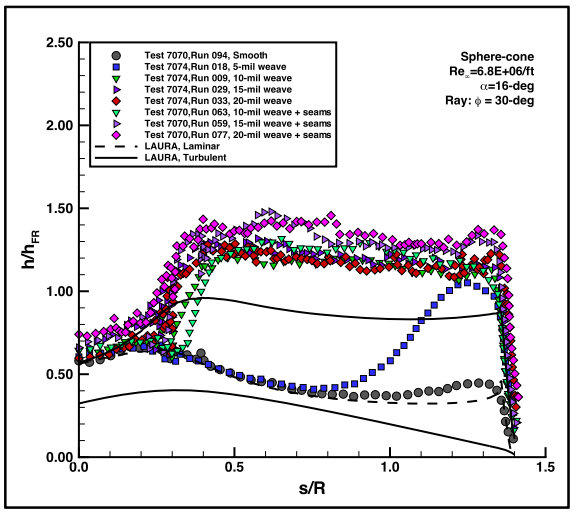
h) Test 7074, Run 33: 20-mil weave, without seams

i) Test 7070, Run 77: 20-mil weave, with seams

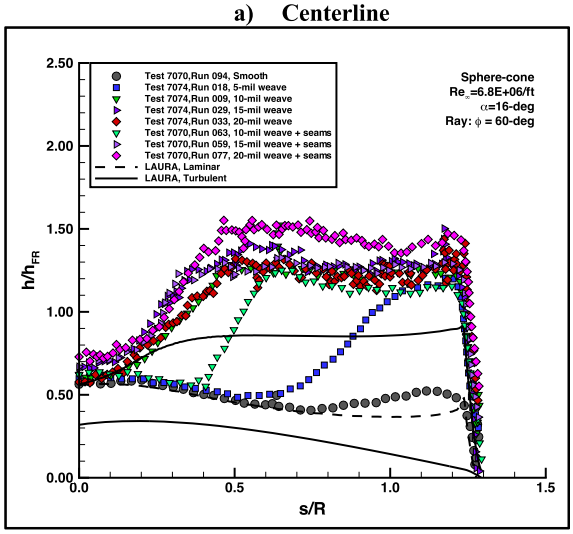
Figure 76. Weave-height effects: sphere-cone geometry, $Re_\infty = 6.8\times10^6$/ft images.



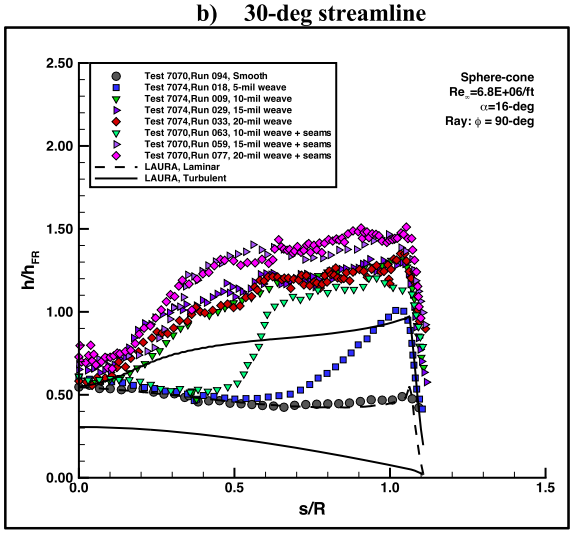
a) Centerline



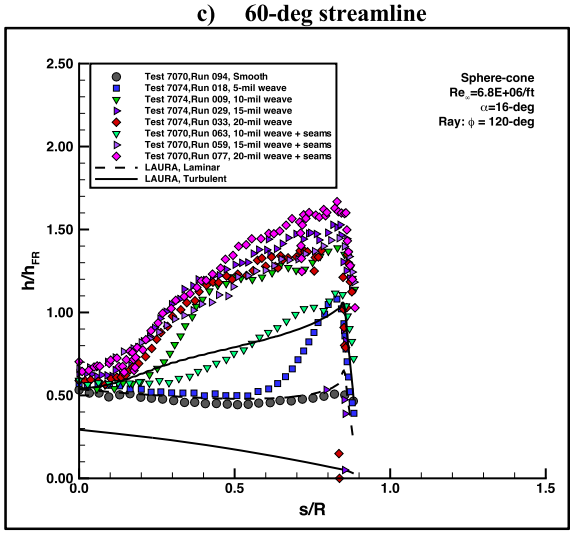
b) 30-deg streamline



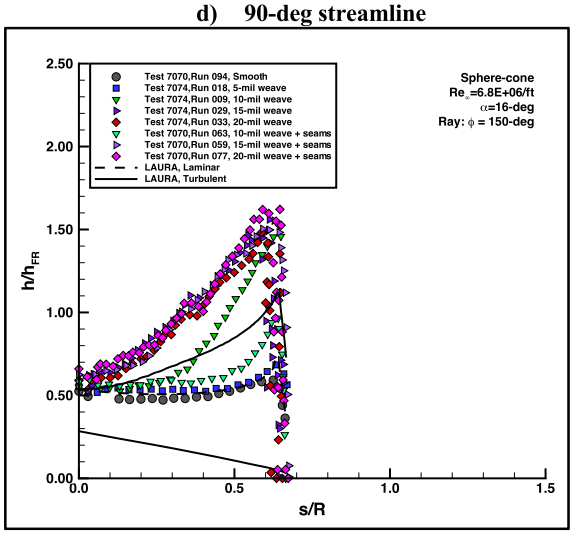
c) 60-deg streamline



d) 90-deg streamline

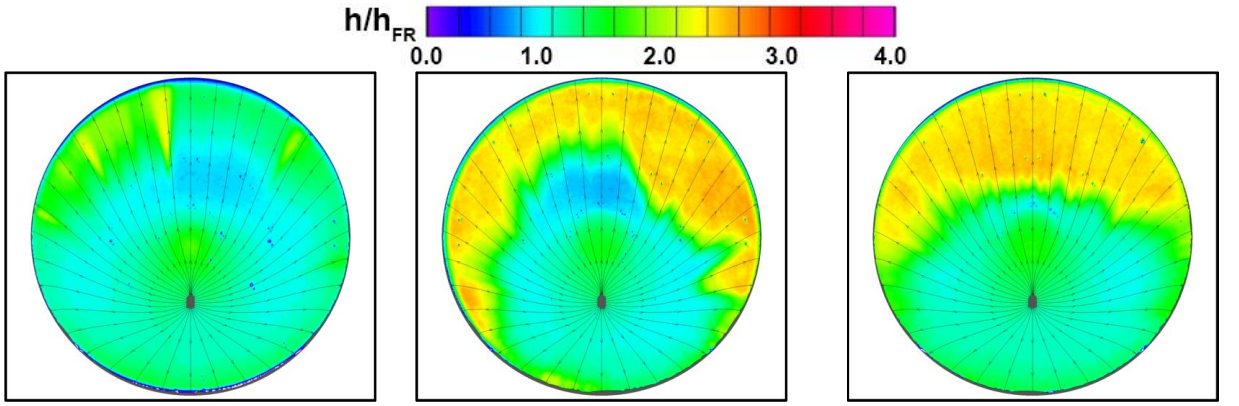


e) 120-deg streamline



f) 150-deg streamline

Figure 77. Weave-height effects: sphere-cone geometry, $Re_\infty = 6.8\times10^6$/ft plots.



a) Test 7070, Run 16: Smooth

b) Test 7074, Run 13: 5-mil weave, without seams

c) Test 7070, Run 44: 5-mil weave with seams

d) Test 7074, Run 05: 10-mil weave, without seams

e) Test 7070, Run 47: 5-mil weave, with seams

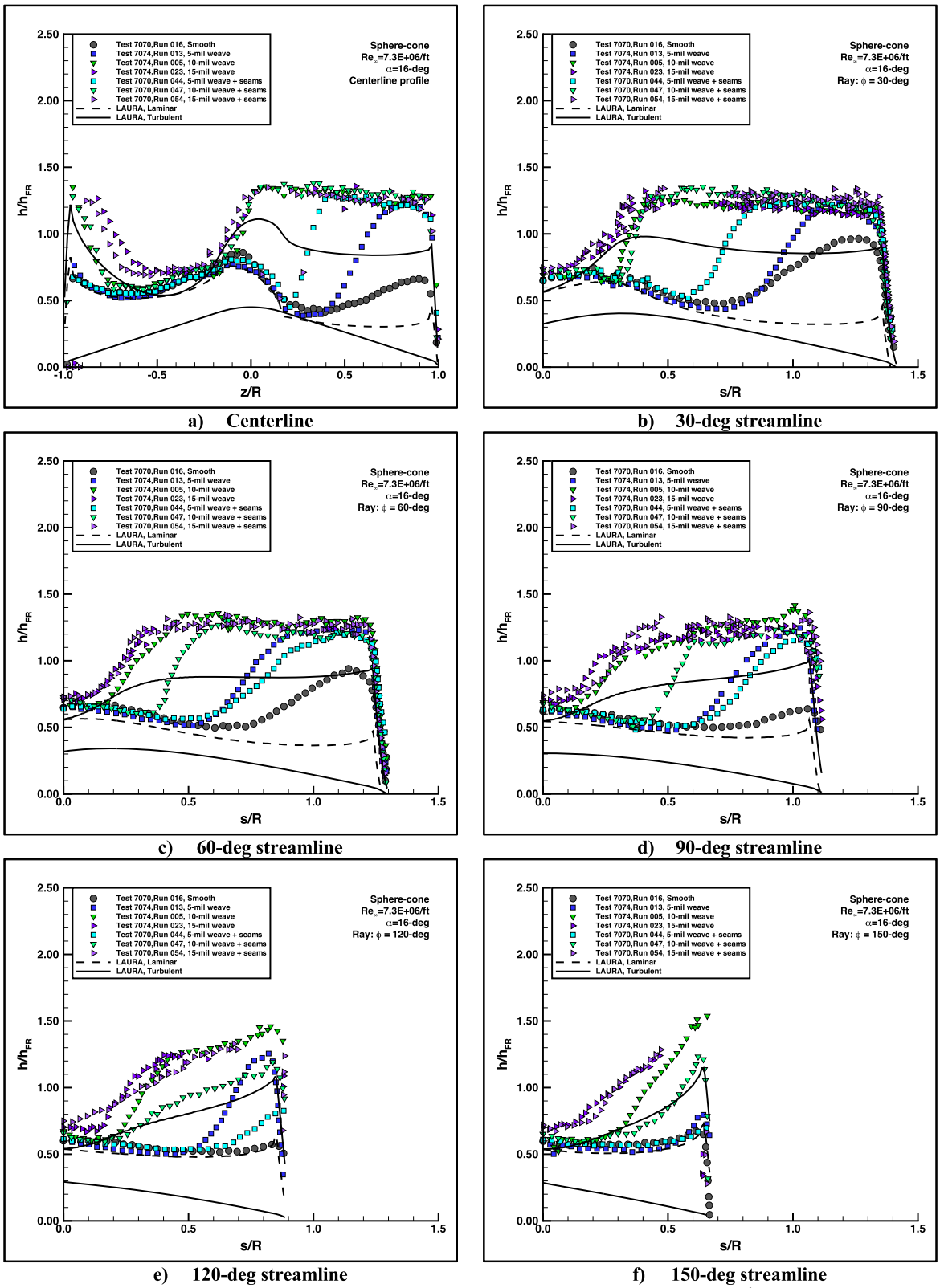
f) Test 7074, Run 23: 15-mil weave, without seams

g) Test 7070, Run 54: 15-mil weave, with seams

h) Test 7074, Run XX: 20-mil weave, without seams

i) Test 7070, Run XX: 20-mil weave, with seams

Figure 78. Weave-height effects: sphere-cone geometry, $Re_\infty = 7.3\times10^6$/ft images.

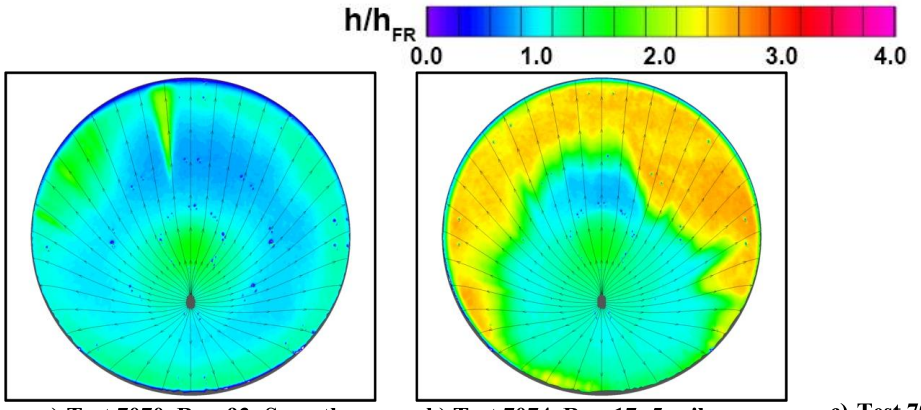


a) Centerline b) 30-deg streamline

c) 60-deg streamline d) 90-deg streamline

e) 120-deg streamline f) 150-deg streamline

Figure 79. Weave-height effects: sphere-cone geometry, $Re_\infty = 7.3\times10^6$/ft plots.



a) Test 7070, Run 93: Smooth

b) Test 7074, Run 17: 5-mil weave, without seams

c) Test 7070, Run XX: 5-mil weave with seams

d) Test 7074, Run 10: 10-mil weave, without seams

e) Test 7070, Run 62: 5-mil weave, with seams

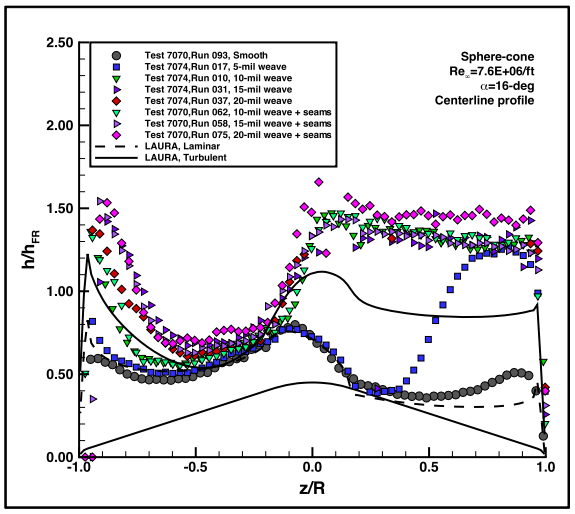
f) Test 7074, Run 31: 15-mil weave, without seams

g) Test 7070, Run 58: 15-mil weave, with seams

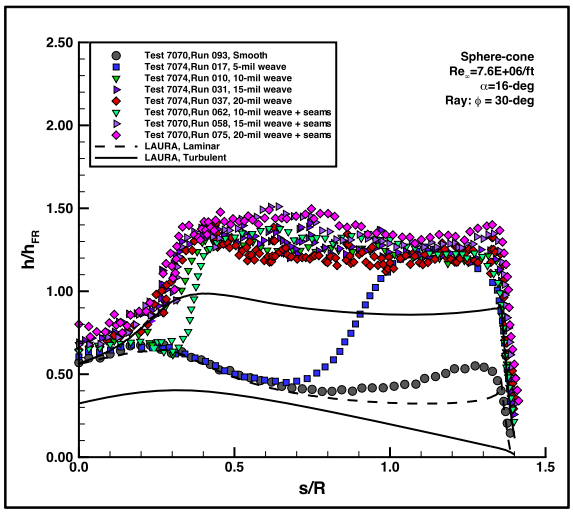
h) Test 7074, Run 37: 20-mil weave, without seams

i) Test 7070, Run 75: 20-mil weave, with seams

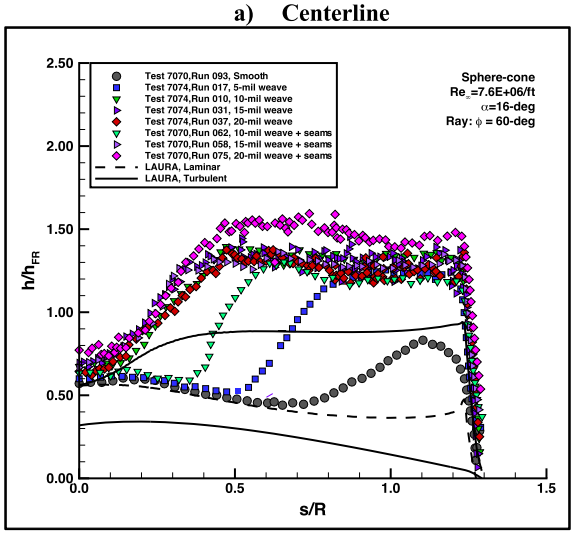
Figure 80. Weave-height effects: sphere-cone geometry, $Re_\infty = 7.7\times10^6$/ft images.



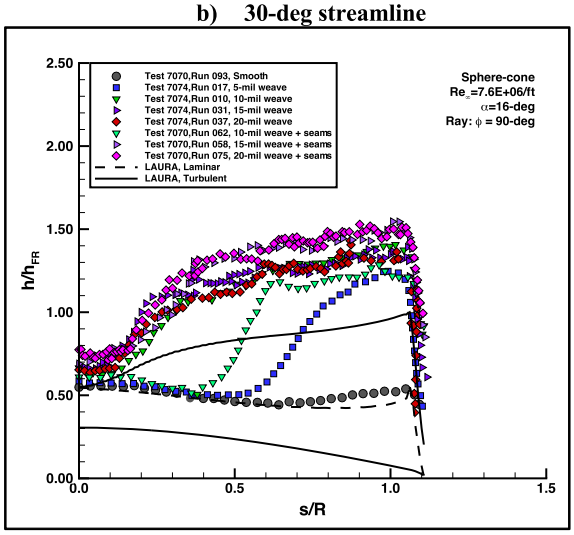
a) Centerline



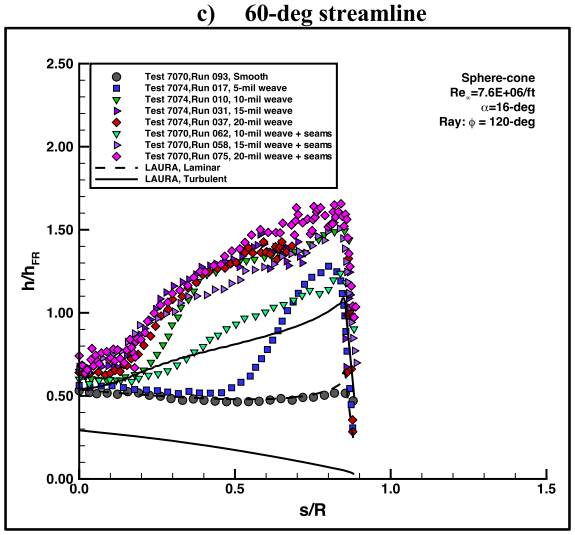
b) 30-deg streamline



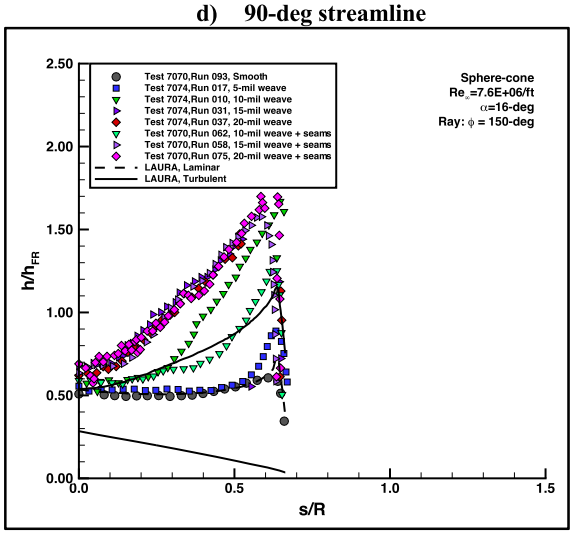
c) 60-deg streamline



d) 90-deg streamline

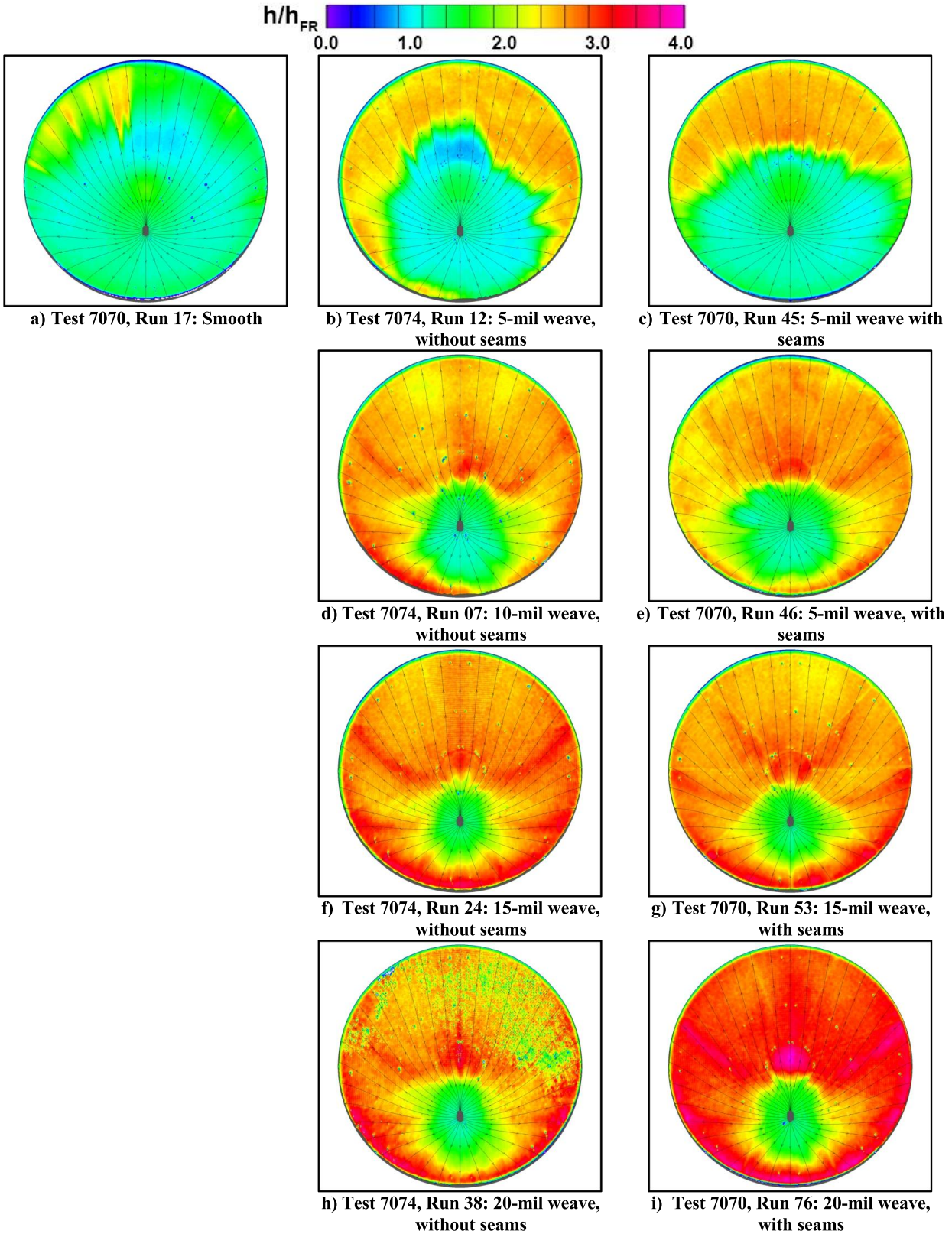


e) 120-deg streamline



f) 150-deg streamline

Figure 81. Weave-height effects: sphere-cone geometry, $Re_\infty = 7.7\times10^6$/ft plots.



a) Test 7070, Run 17: Smooth

b) Test 7074, Run 12: 5-mil weave, without seams

c) Test 7070, Run 45: 5-mil weave with seams

d) Test 7074, Run 07: 10-mil weave, without seams

e) Test 7070, Run 46: 5-mil weave, with seams

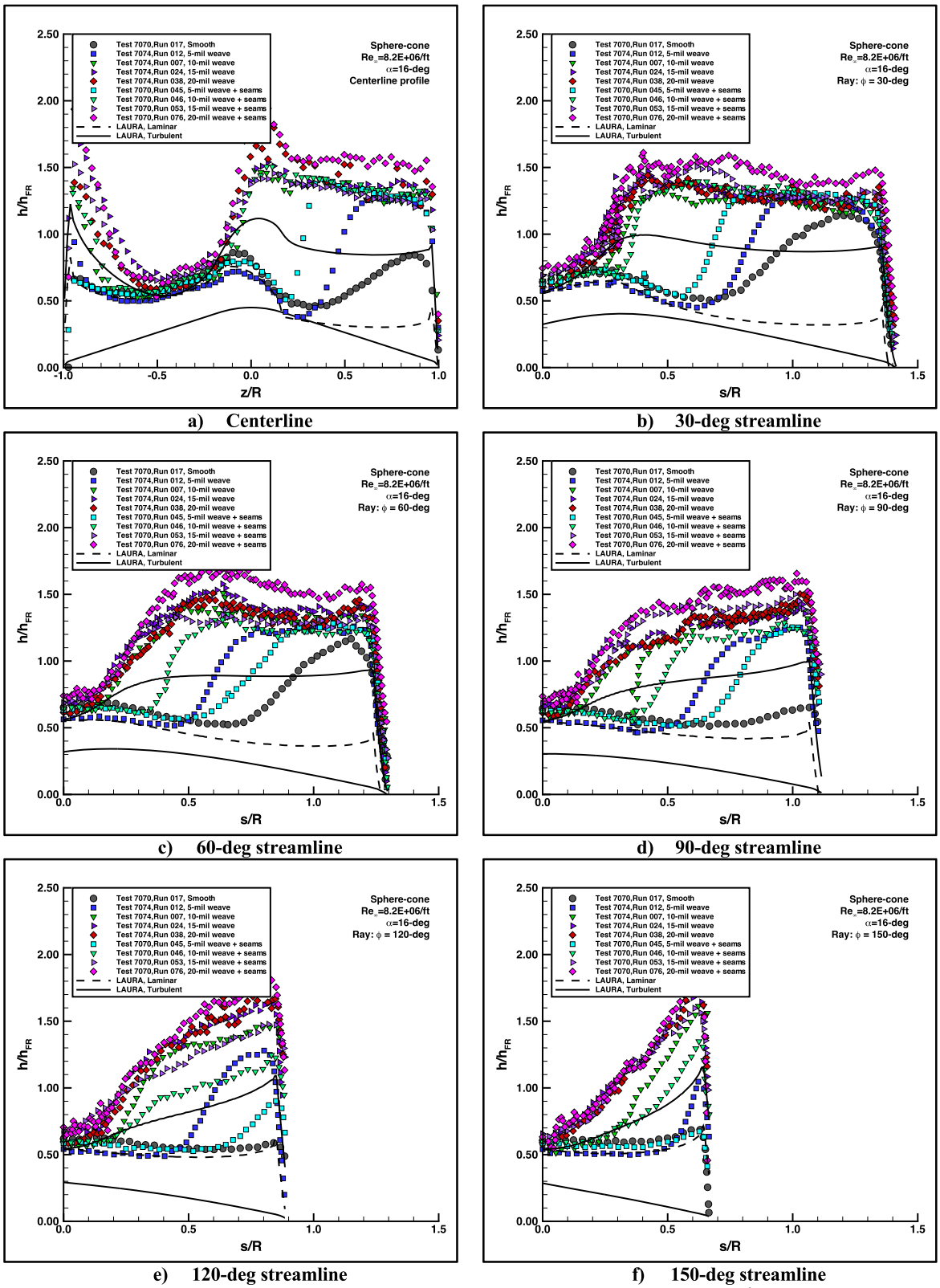
f) Test 7074, Run 24: 15-mil weave, without seams

g) Test 7070, Run 53: 15-mil weave, with seams

h) Test 7074, Run 38: 20-mil weave, without seams

i) Test 7070, Run 76: 20-mil weave, with seams

Figure 82. Weave-height effects: sphere-cone geometry, $Re_\infty = 8.2\times10^6$/ft images.

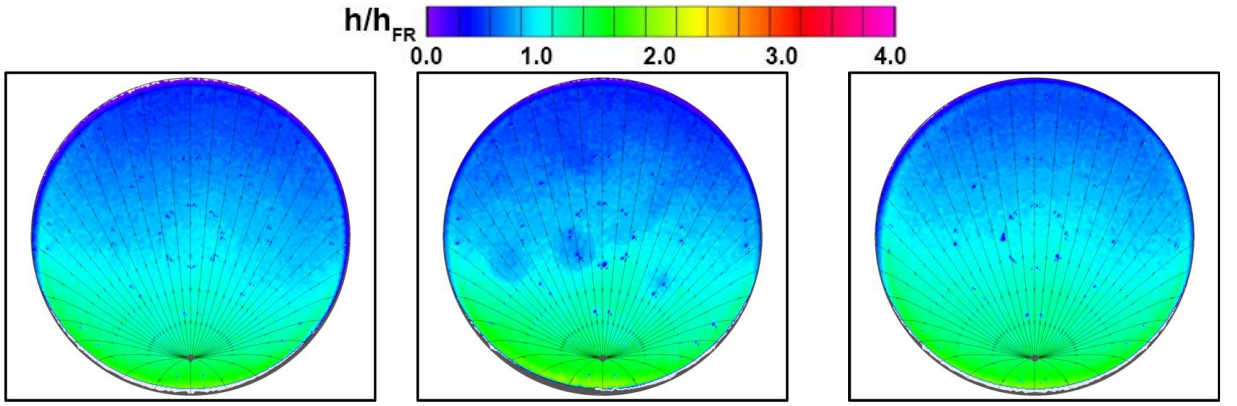


a) Centerline b) 30-deg streamline

c) 60-deg streamline d) 90-deg streamline

e) 120-deg streamline f) 150-deg streamline

Figure 83. Weave-height effects: sphere-cone geometry, $Re_\infty = 8.2\times10^6$/ft plots.



a) Test 7070, Run 25: Smooth

b) Test 7074, Run 68: 5-mil weave, without seams

c) Test 7070, Run 38: 5-mil weave with seams

d) Test 7074, Run XX: 10-mil weave, without seams

e) Test 7070, Run XX: 5-mil weave, with seams

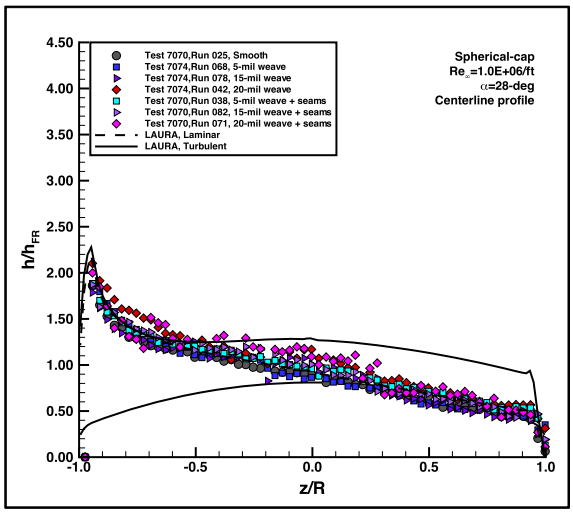
f) Test 7074, Run 78: 15-mil weave, without seams

g) Test 7070, Run 82: 15-mil weave, with seams

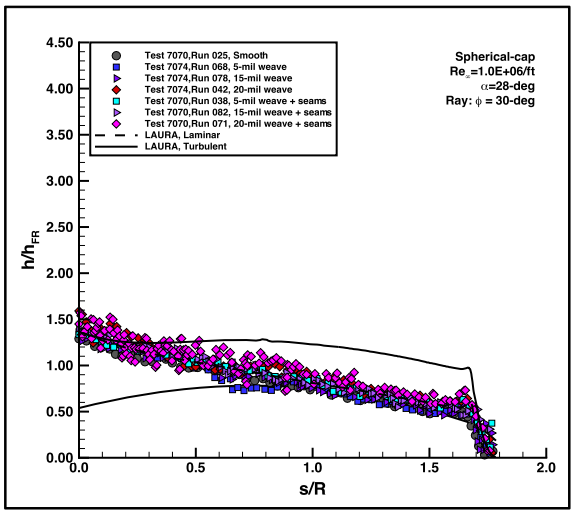
h) Test 7074, Run 42: 20-mil weave, without seams

i) Test 7070, Run 71: 20-mil weave, with seams

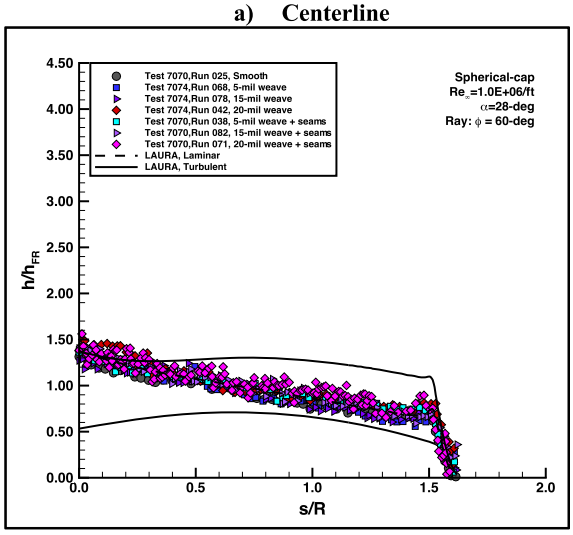
Figure 84. Weave-height effects: spherical-cap geometry, $Re_\infty = 1.0\times10^6$/ft images.



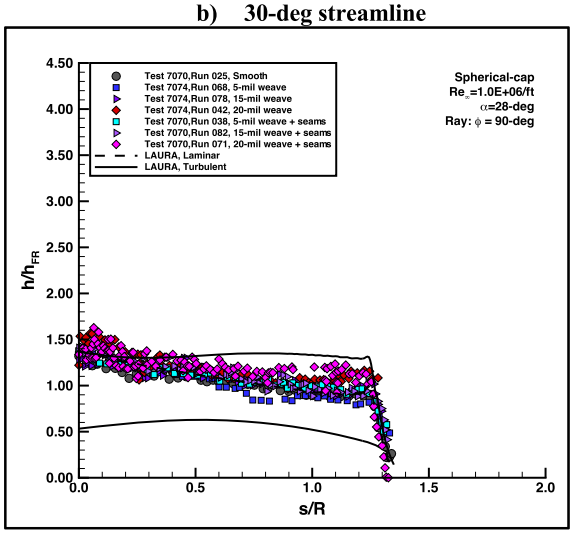
a) Centerline



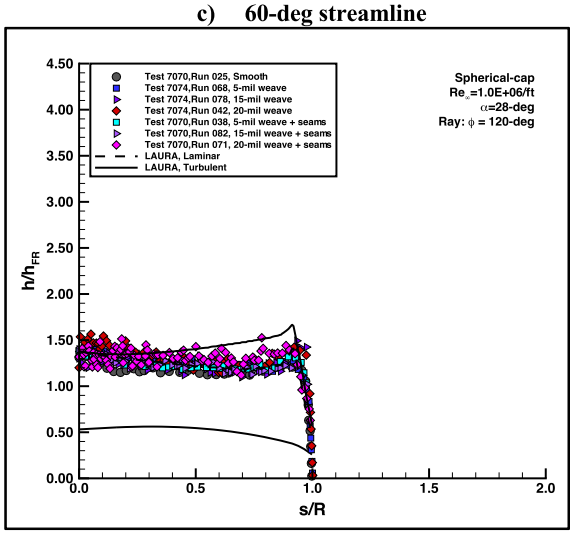
b) 30-deg streamline



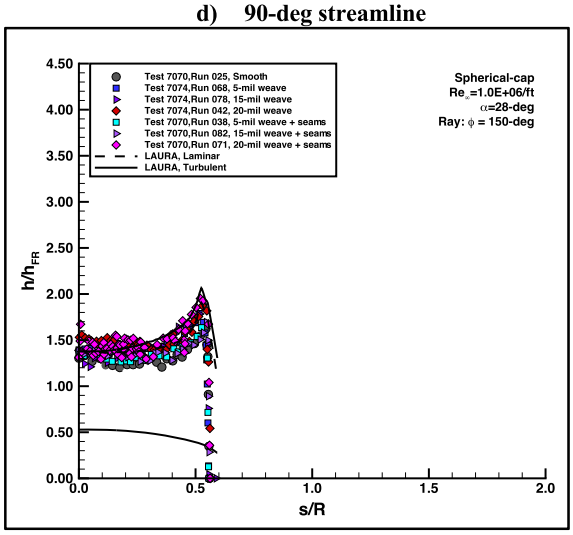
c) 60-deg streamline



d) 90-deg streamline

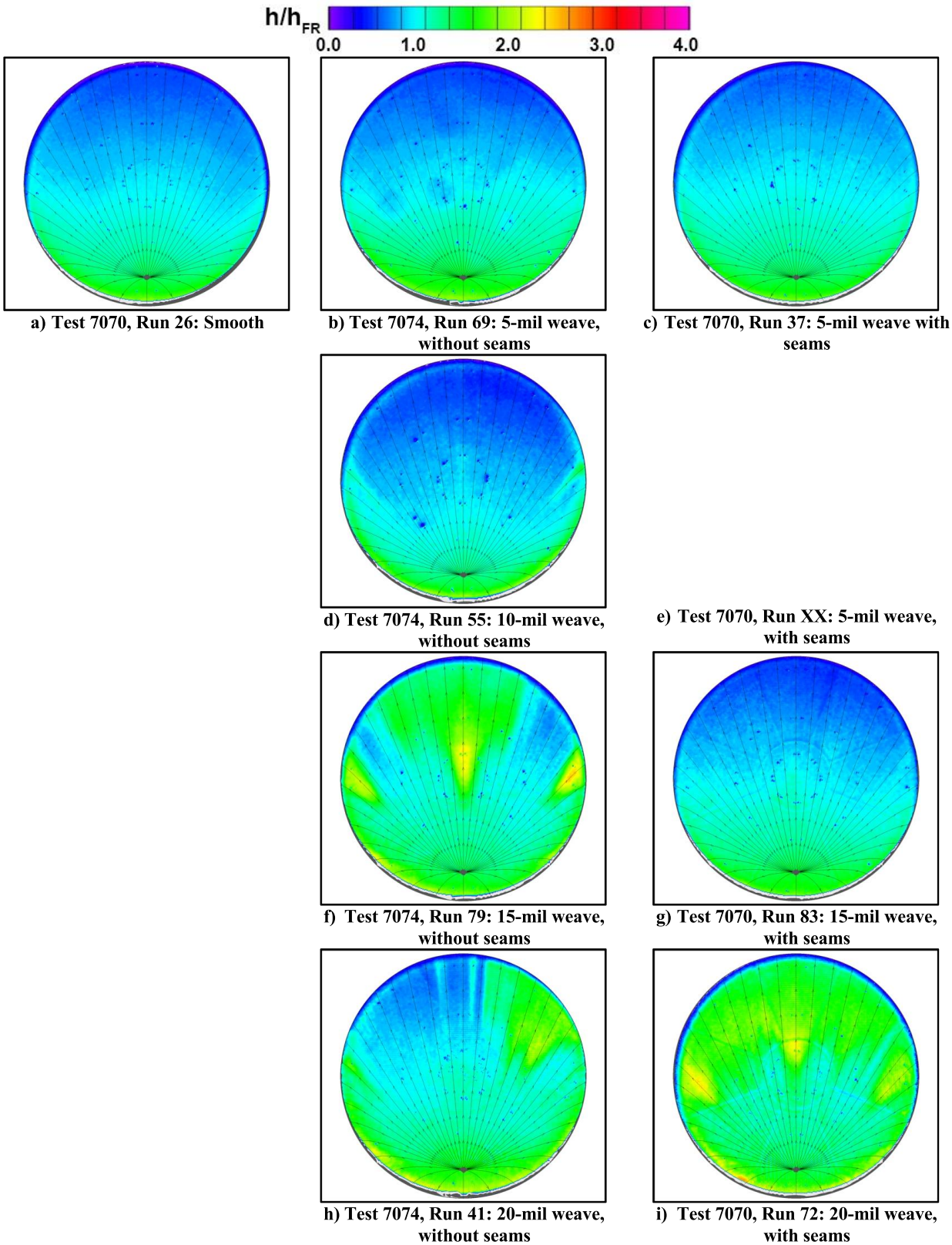


e) 120-deg streamline



f) 150-deg streamline

Figure 85. Weave-height effects: spherical-cap geometry, $Re_\infty = 1.0\times10^6$/ft plots.



a) Test 7070, Run 26: Smooth

b) Test 7074, Run 69: 5-mil weave, without seams

c) Test 7070, Run 37: 5-mil weave with seams

d) Test 7074, Run 55: 10-mil weave, without seams

e) Test 7070, Run XX: 5-mil weave, with seams

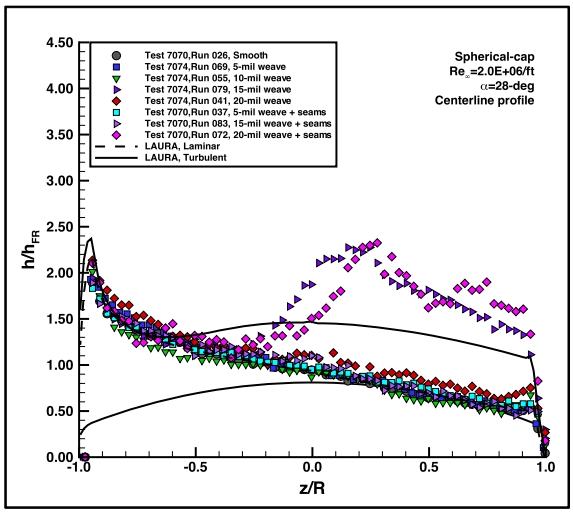
f) Test 7074, Run 79: 15-mil weave, without seams

g) Test 7070, Run 83: 15-mil weave, with seams

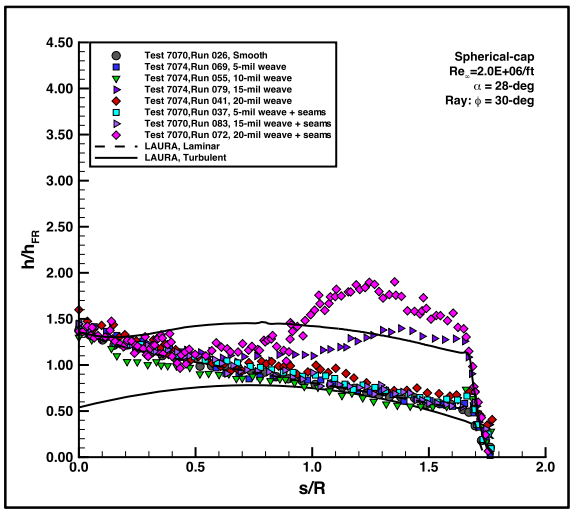
h) Test 7074, Run 41: 20-mil weave, without seams

i) Test 7070, Run 72: 20-mil weave, with seams

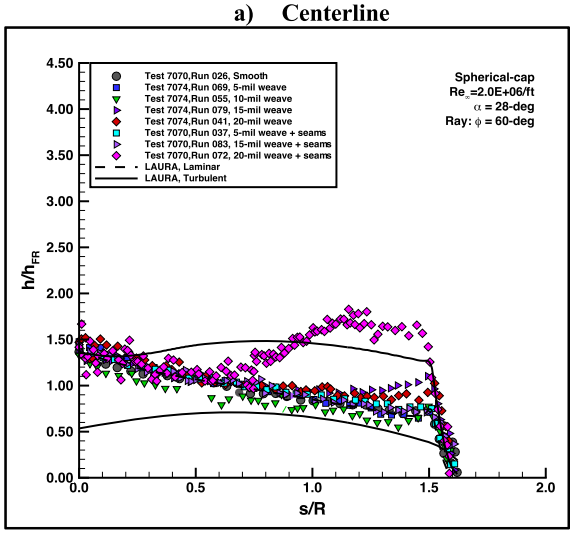
Figure 86. Weave-height effects: spherical-cap geometry, $Re_\infty = 2.0\times10^6$/ft images.



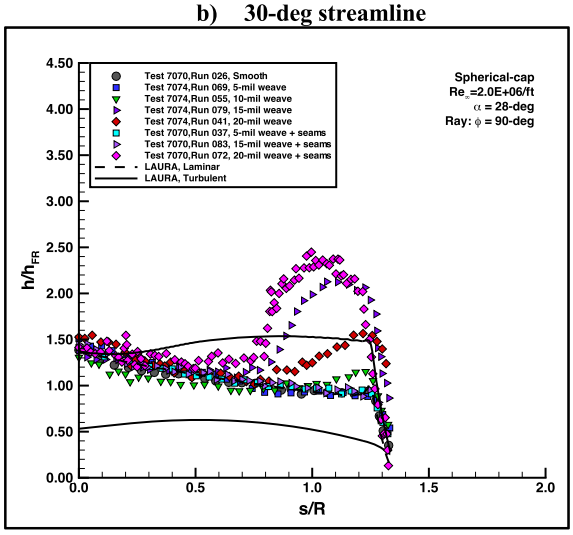
a) Centerline



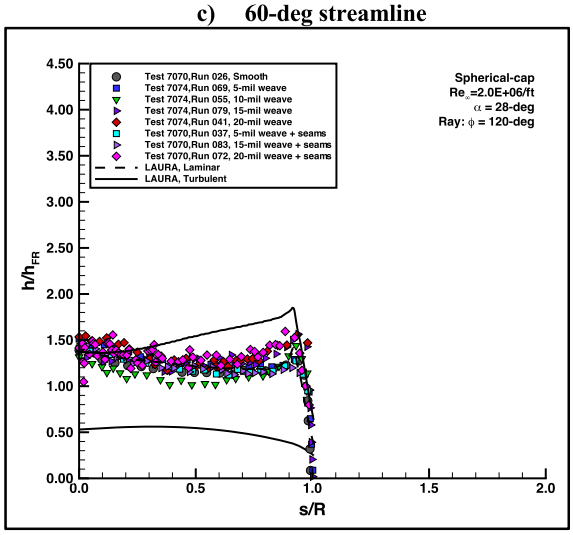
b) 30-deg streamline



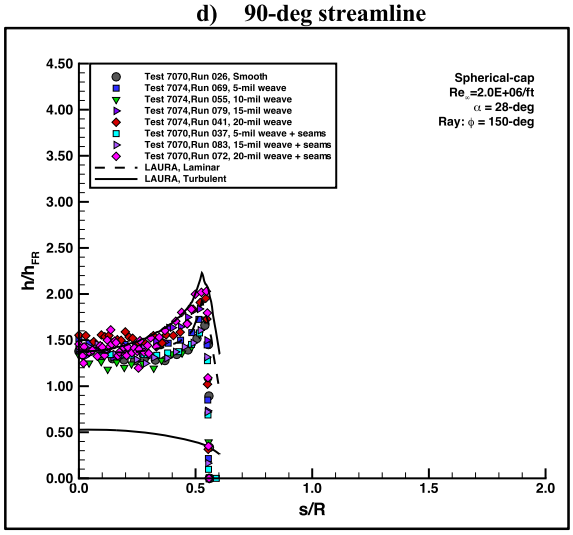
c) 60-deg streamline



d) 90-deg streamline

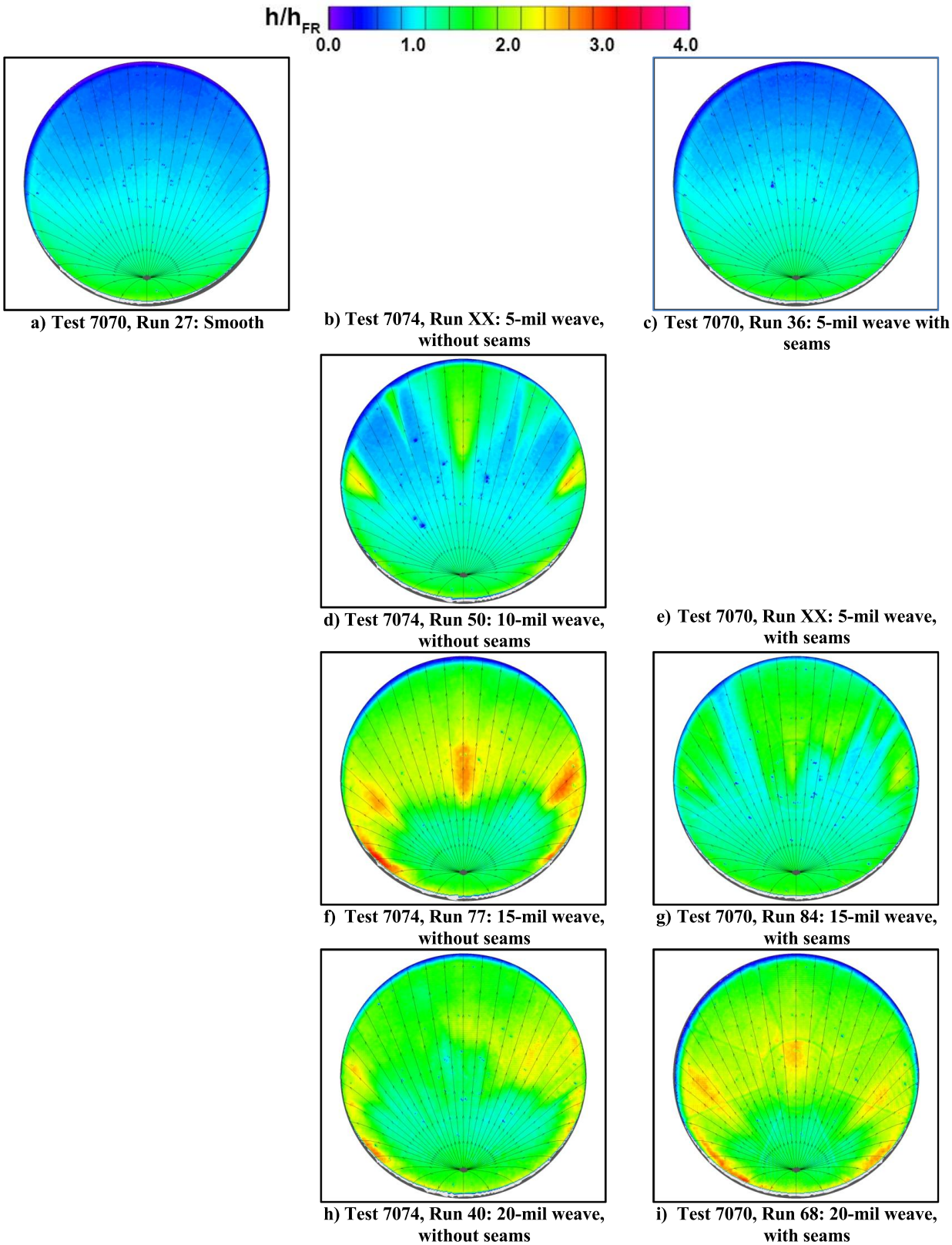


e) 120-deg streamline



f) 150-deg streamline

Figure 87. Weave-height effects: spherical-cap geometry, $Re_\infty = 2.0\times10^6$/ft plots.



a) Test 7070, Run 27: Smooth

b) Test 7074, Run XX: 5-mil weave, without seams

c) Test 7070, Run 36: 5-mil weave with seams

d) Test 7074, Run 50: 10-mil weave, without seams

e) Test 7070, Run XX: 5-mil weave, with seams

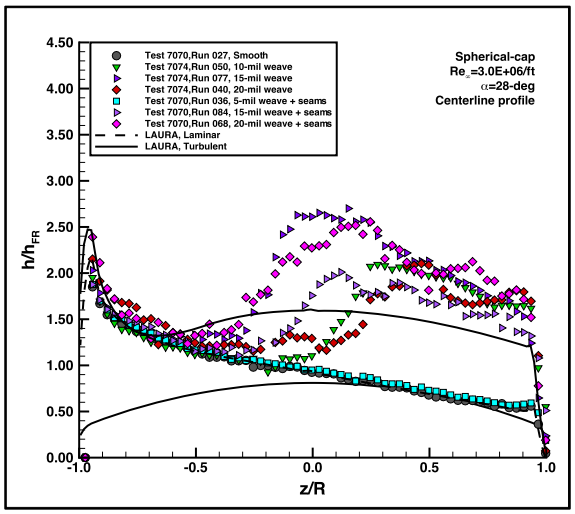
f) Test 7074, Run 77: 15-mil weave, without seams

g) Test 7070, Run 84: 15-mil weave, with seams

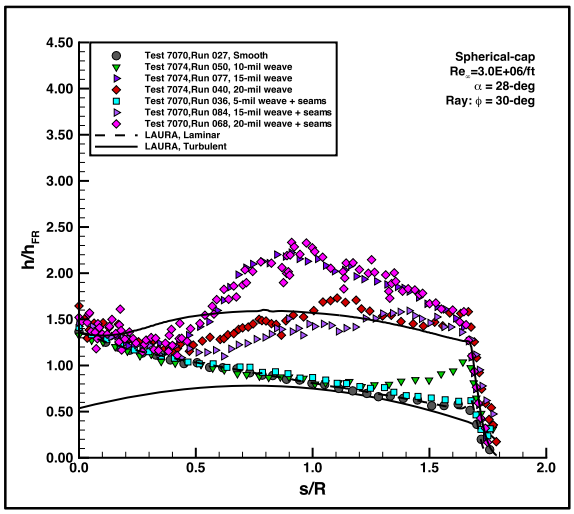
h) Test 7074, Run 40: 20-mil weave, without seams

i) Test 7070, Run 68: 20-mil weave, with seams

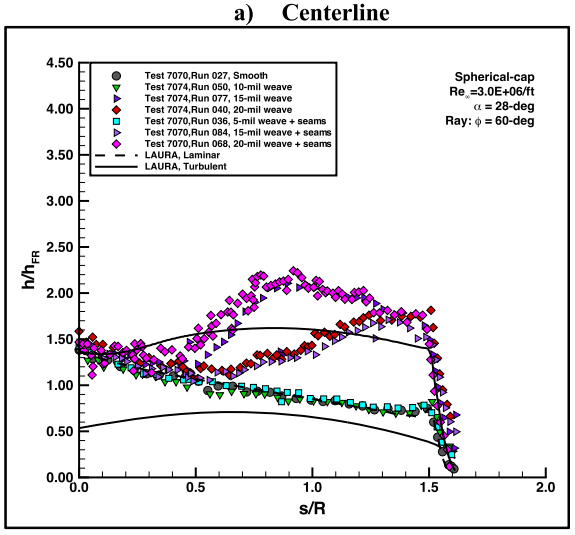
Figure 88. Weave-height effects: spherical-cap geometry, $Re_\infty = 3.0\times10^6$/ft images.



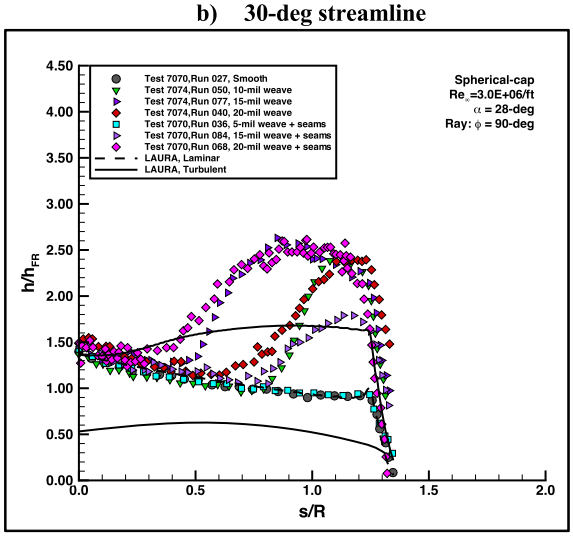
a) Centerline



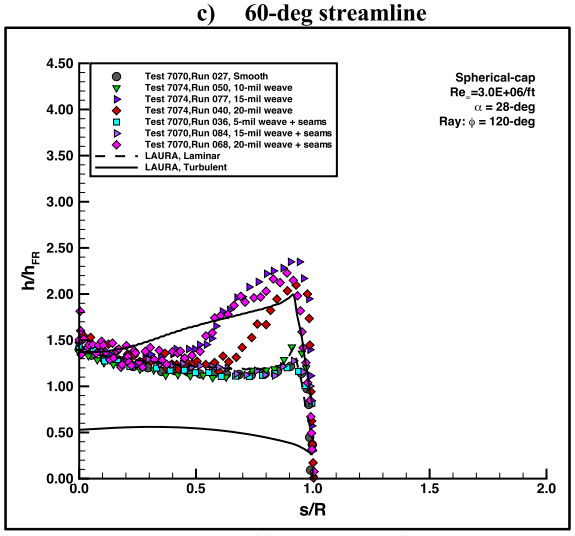
b) 30-deg streamline



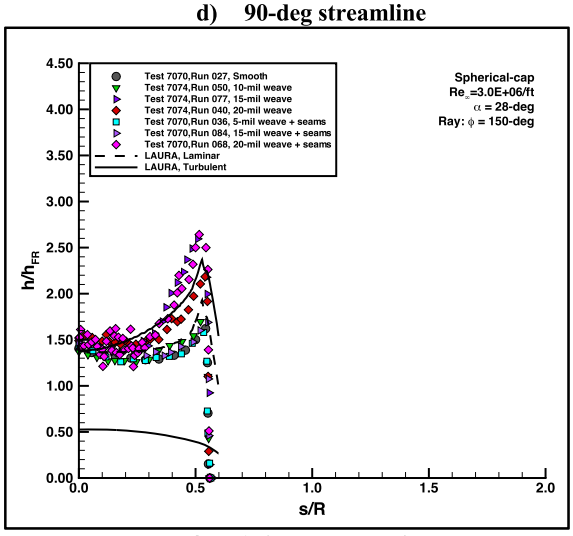
c) 60-deg streamline



d) 90-deg streamline

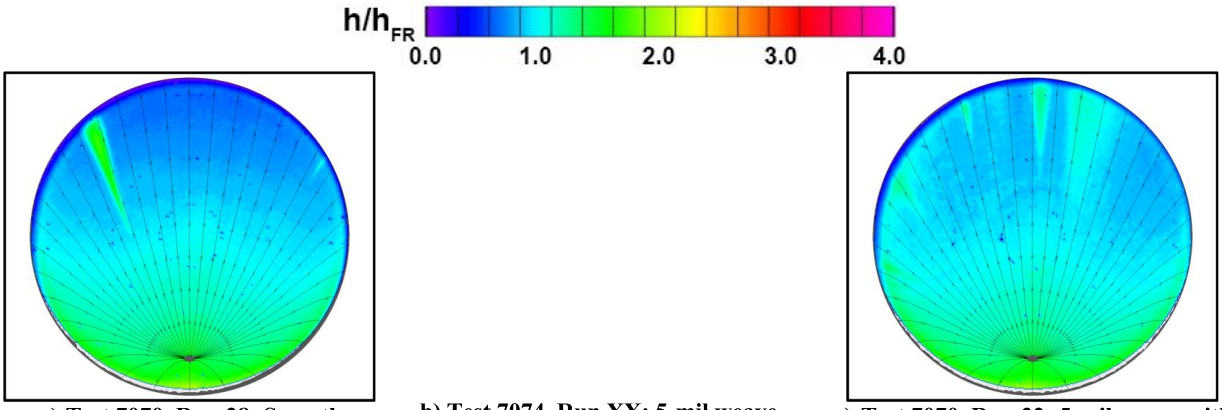


e) 120-deg streamline



f) 150-deg streamline

Figure 89. Weave-height effects: spherical-cap geometry, $Re_\infty = 3.0\times10^6$/ft plots.



a) Test 7070, Run 28: Smooth

b) Test 7074, Run XX: 5-mil weave, without seams

c) Test 7070, Run 32: 5-mil weave with seams

d) Test 7074, Run XX: 10-mil weave, without seams

e) Test 7070, Run XX: 5-mil weave, with seams

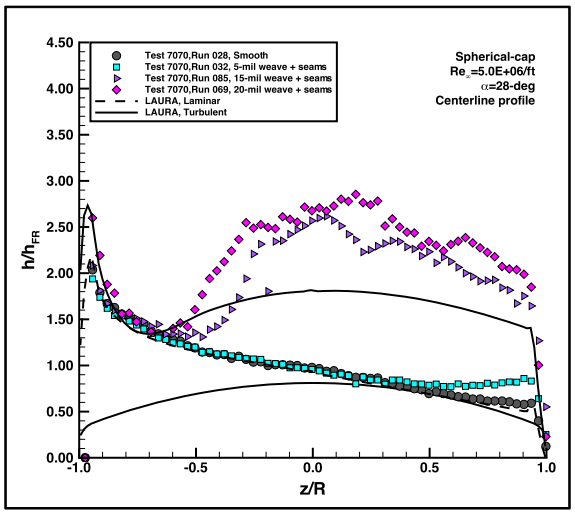
f) Test 7074, Run XX: 15-mil weave, without seams

g) Test 7070, Run 85: 15-mil weave, with seams

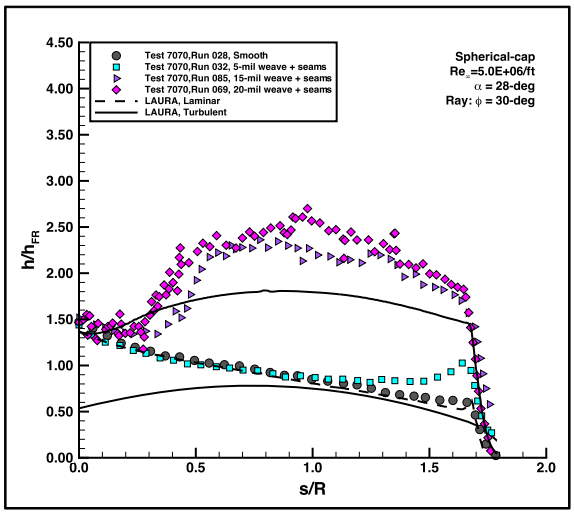
h) Test 7074, Run XX: 20-mil weave, without seams

i) Test 7070, Run 69: 20-mil weave, with seams

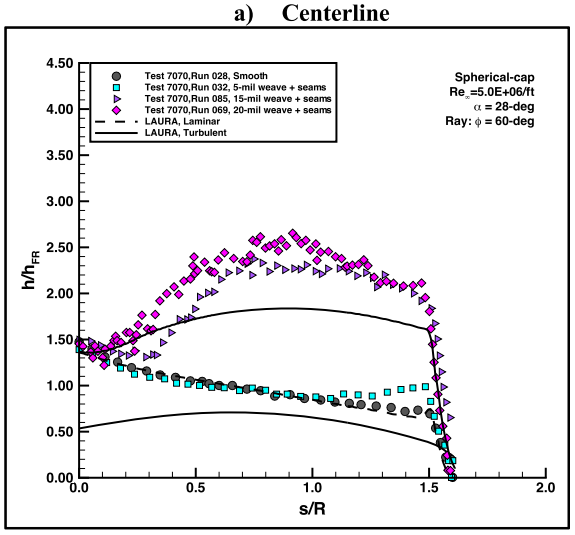
Figure 90. Weave-height effects: spherical-cap geometry, $Re_\infty = 5.0\times10^6$/ft images.



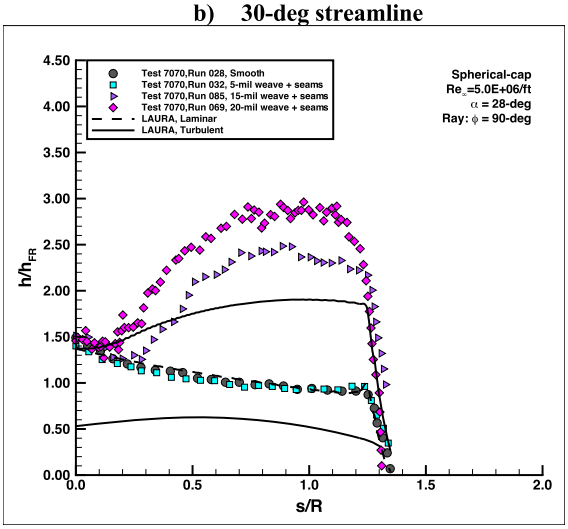
a) Centerline



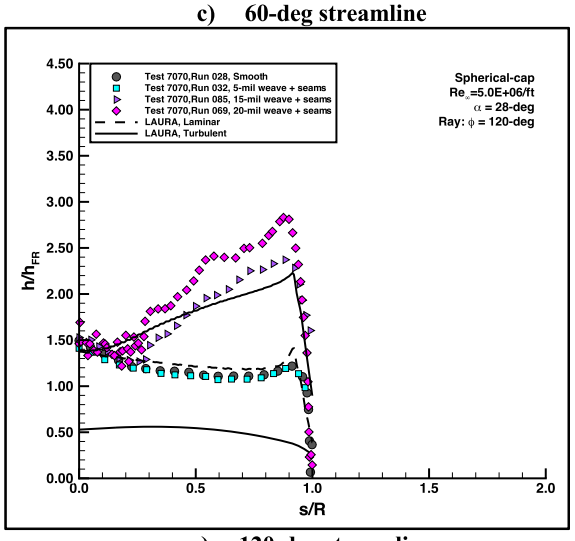
b) 30-deg streamline



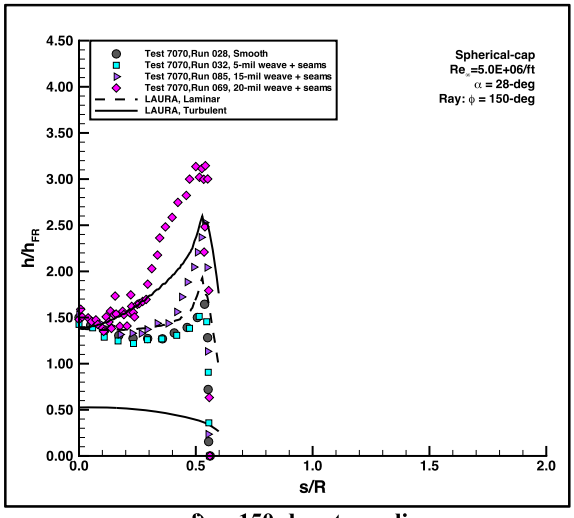
c) 60-deg streamline



d) 90-deg streamline

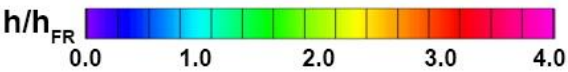


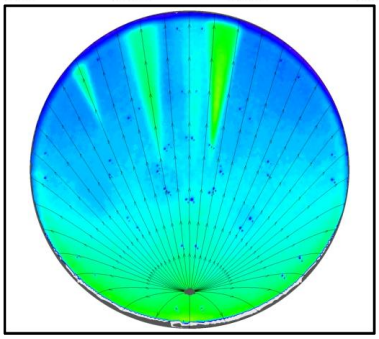
e) 120-deg streamline



f) 150-deg streamline

Figure 91. Weave-height effects: spherical-cap geometry, $Re_\infty = 5.0\times10^6$/ft plots.

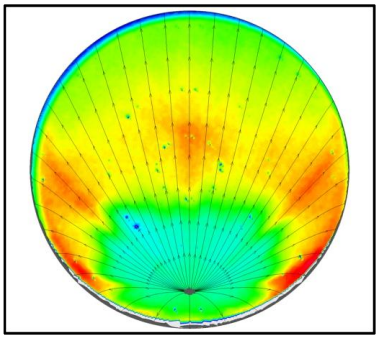




a) Test 7070, Run XX: Smooth

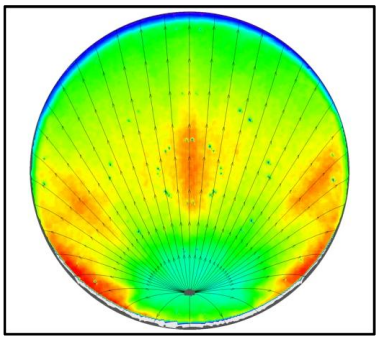
b) Test 7074, Run 66: 5-mil weave, without seams

c) Test 7070, Run XX: 5-mil weave with seams



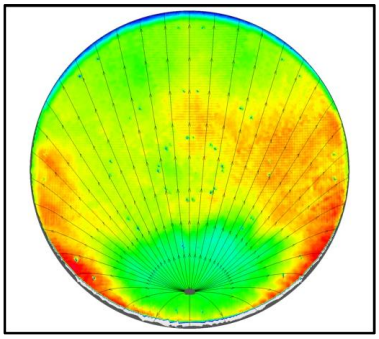
d) Test 7074, Run 51: 10-mil weave, without seams

e) Test 7070, Run XX: 5-mil weave, with seams



f) Test 7074, Run 73: 15-mil weave, without seams

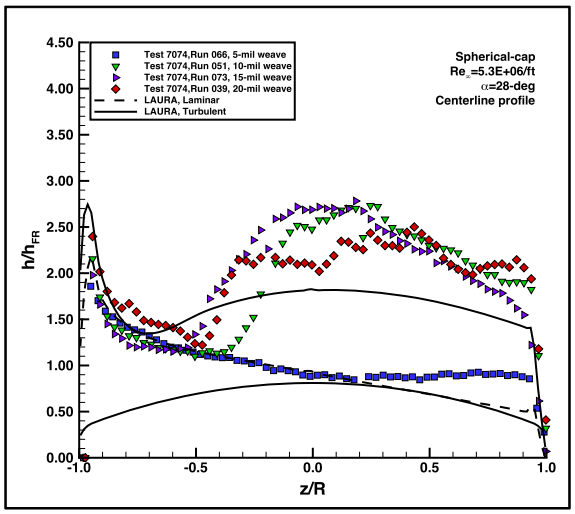
g) Test 7070, Run XX: 15-mil weave, with seams



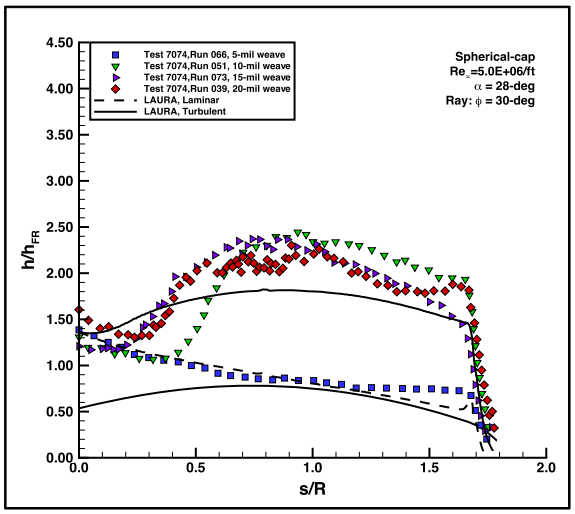
h) Test 7074, Run 39: 20-mil weave, without seams

i) Test 7070, Run XX: 20-mil weave, with seams

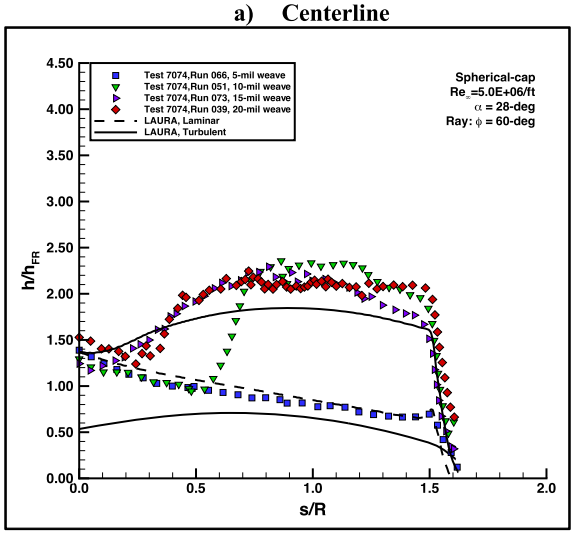
Figure 92. Weave-height effects: spherical-cap geometry, $Re_\infty = 5.3\times10^6$/ft images.



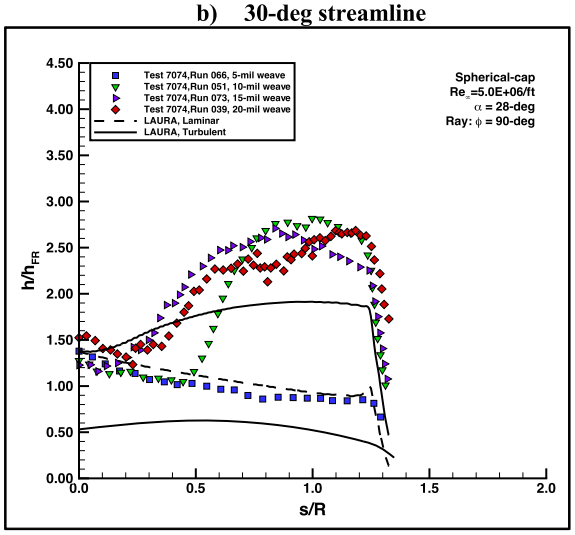
a) Centerline



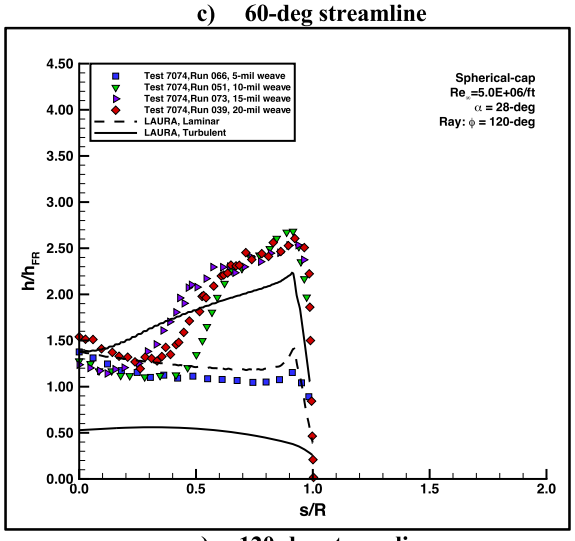
b) 30-deg streamline



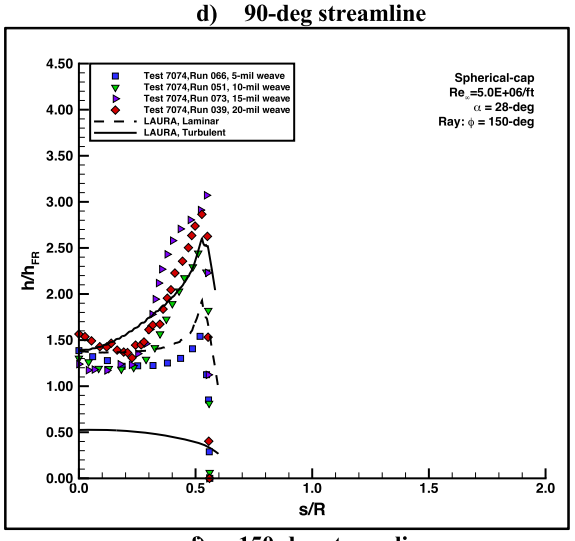
c) 60-deg streamline



d) 90-deg streamline

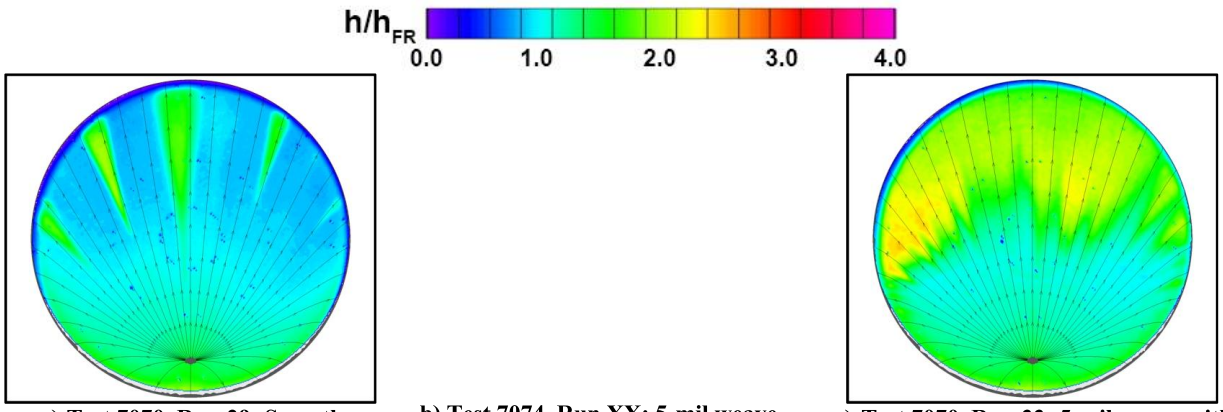


e) 120-deg streamline



f) 150-deg streamline

Figure 93. Weave-height effects: spherical-cap geometry, $Re_\infty = 5.3\times10^6$/ft plots.



a) Test 7070, Run 29: Smooth

b) Test 7074, Run XX: 5-mil weave, without seams

c) Test 7070, Run 33: 5-mil weave with seams

d) Test 7074, Run XX: 10-mil weave, without seams

e) Test 7070, Run XX: 5-mil weave, with seams

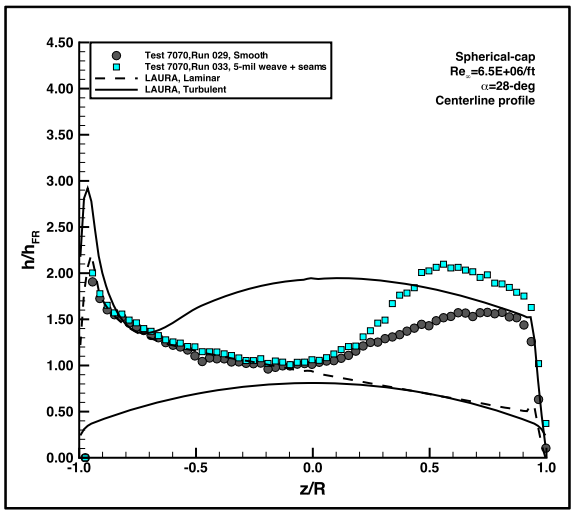
f) Test 7074, Run XX: 15-mil weave, without seams

g) Test 7070, Run XX: 15-mil weave, with seams

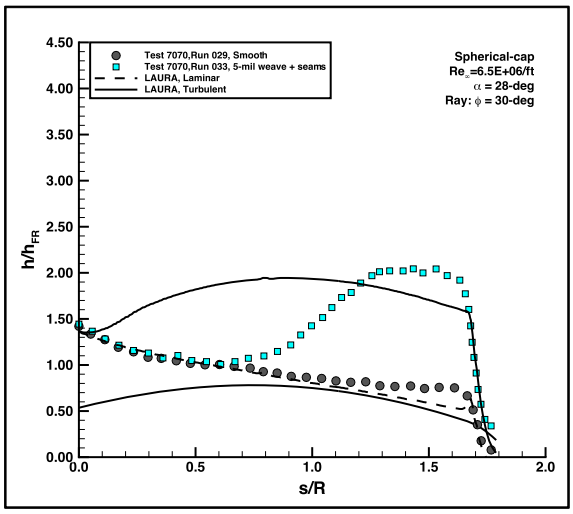
h) Test 7074, Run XX: 20-mil weave, without seams

i) Test 7070, Run XX: 20-mil weave, with seams

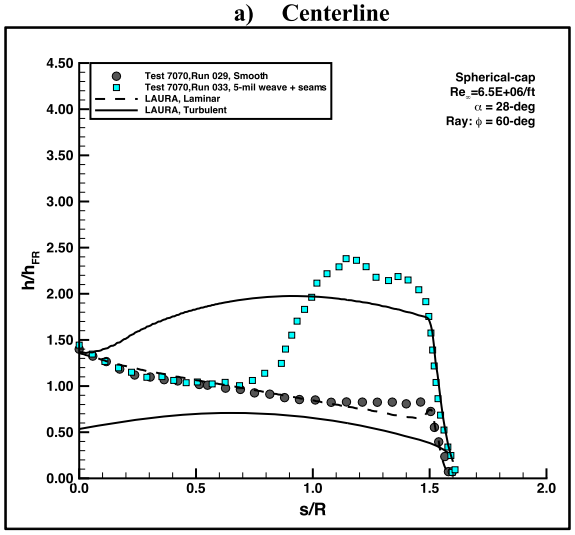
Figure 94. Weave-height effects: spherical-cap geometry, $Re_\infty = 6.3\times10^6$/ft images.



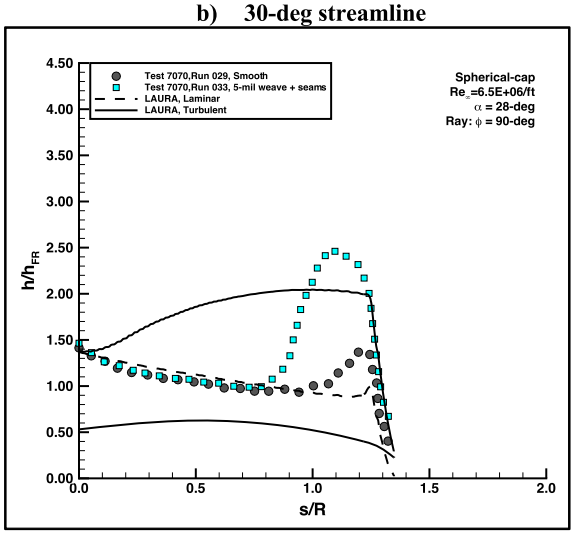
a) Centerline



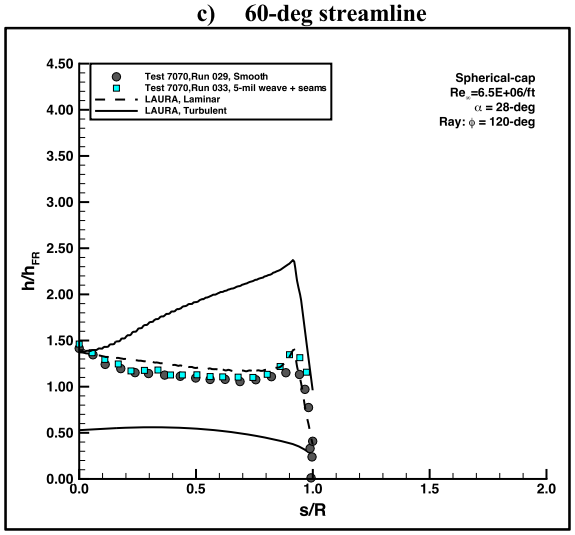
b) 30-deg streamline



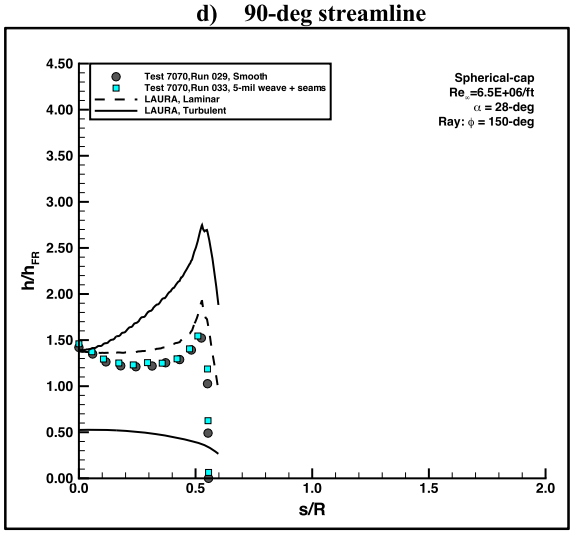
c) 60-deg streamline



d) 90-deg streamline

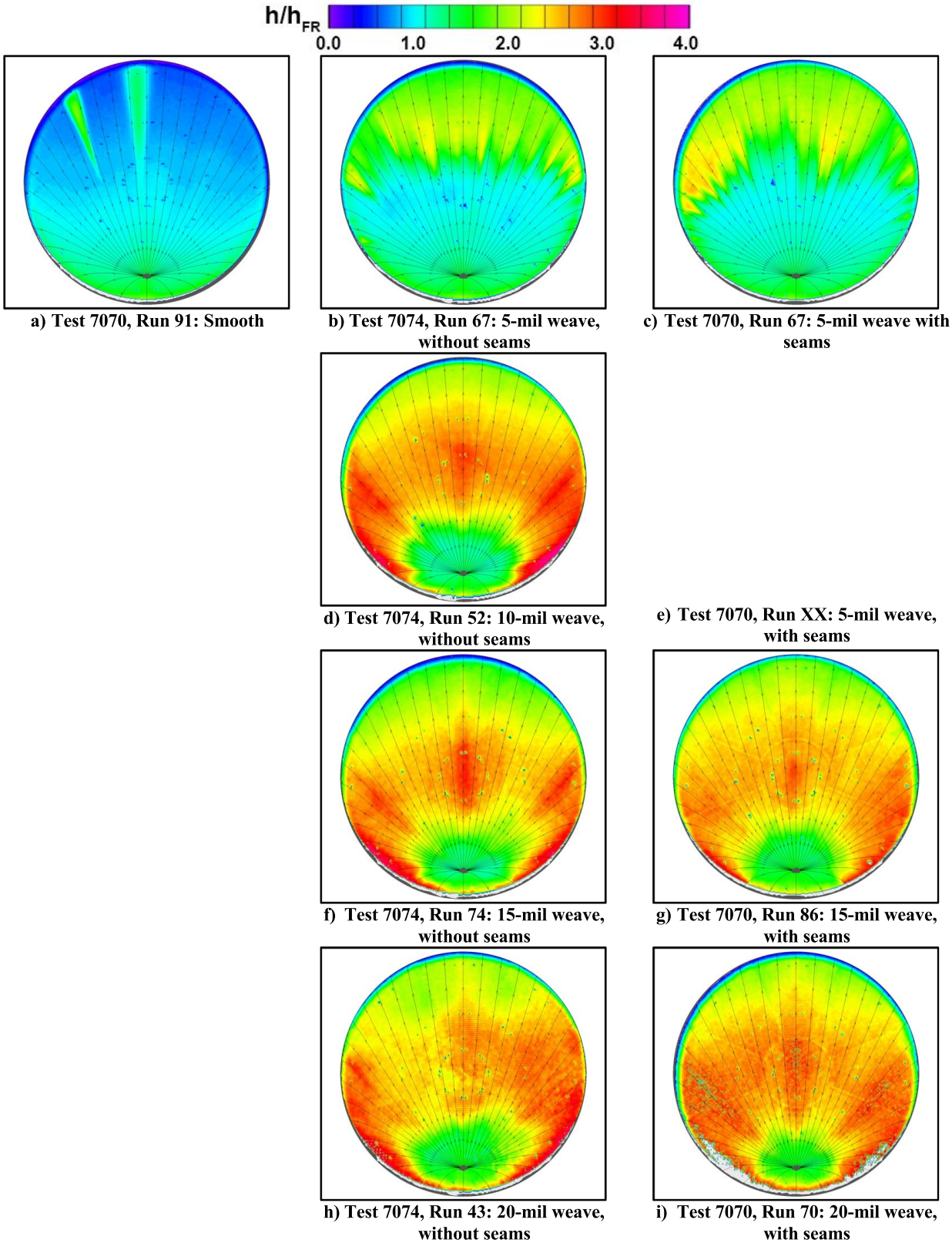


e) 120-deg streamline



f) 150-deg streamline

Figure 95. Weave-height effects: spherical-cap geometry, $Re_\infty = 6.3\times10^6$/ft plots.



a) Test 7070, Run 91: Smooth

b) Test 7074, Run 67: 5-mil weave, without seams

c) Test 7070, Run 67: 5-mil weave with seams

d) Test 7074, Run 52: 10-mil weave, without seams

e) Test 7070, Run XX: 5-mil weave, with seams

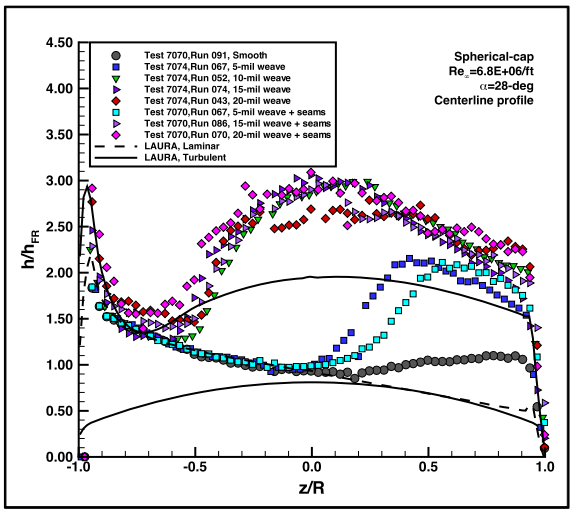
f) Test 7074, Run 74: 15-mil weave, without seams

g) Test 7070, Run 86: 15-mil weave, with seams

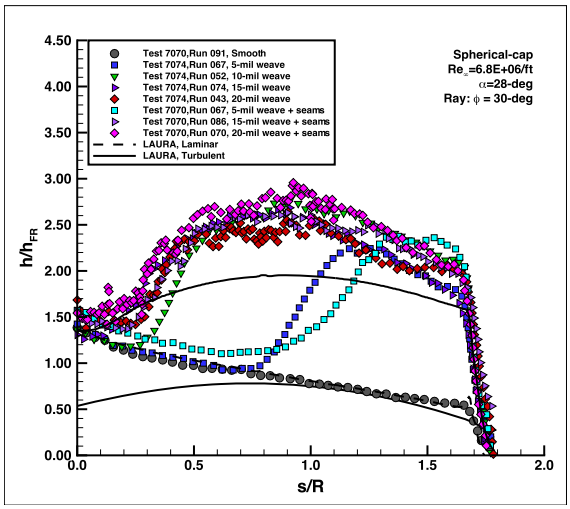
h) Test 7074, Run 43: 20-mil weave, without seams

i) Test 7070, Run 70: 20-mil weave, with seams

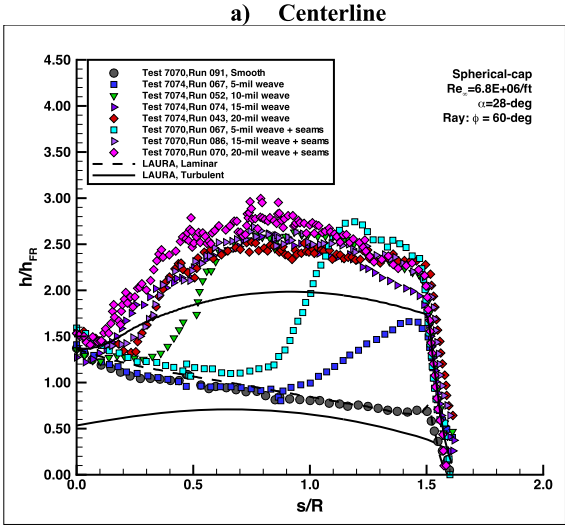
Figure 96. Weave-height effects: spherical-cap geometry, $Re_\infty = 6.8\times10^6$/ft images.



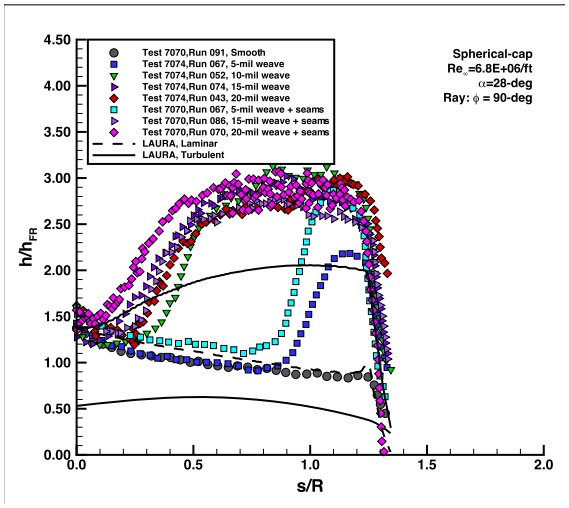
a) Centerline



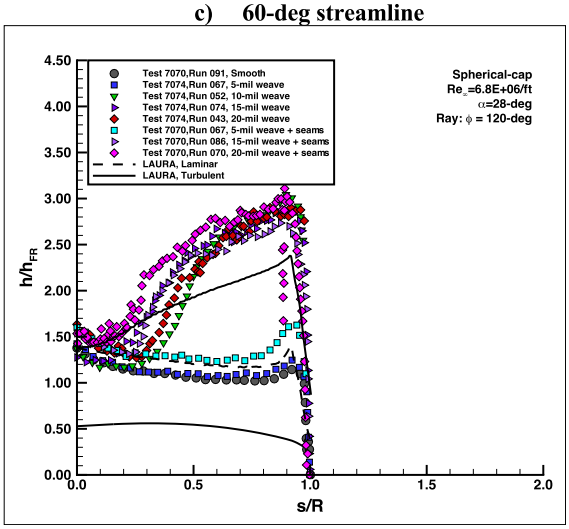
b) 30-deg streamline



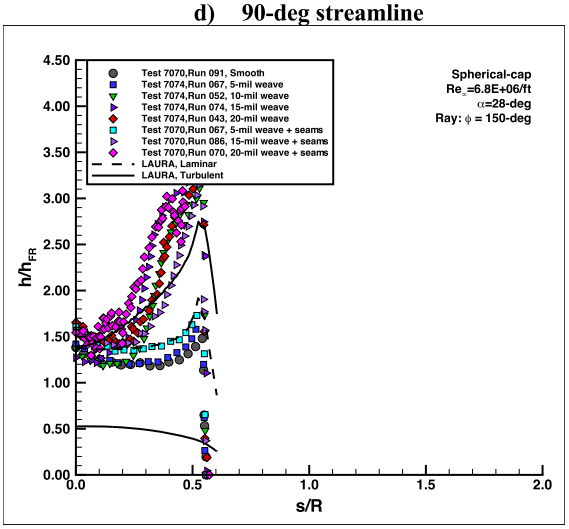
c) 60-deg streamline



d) 90-deg streamline

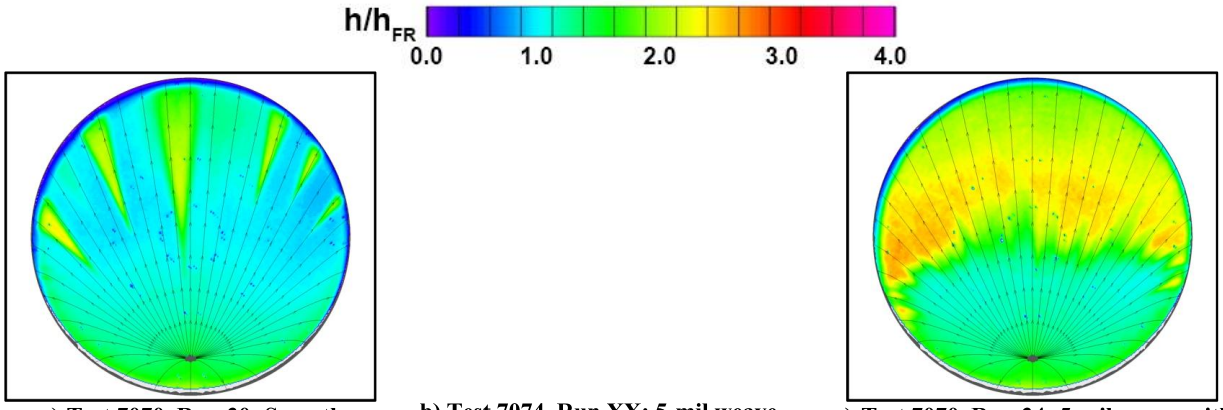


e) 120-deg streamline



f) 150-deg streamline

Figure 97. Weave-height effects: spherical-cap geometry, $Re_\infty = 6.8\times10^6$/ft plots.



a) Test 7070, Run 30: Smooth

b) Test 7074, Run XX: 5-mil weave, without seams

c) Test 7070, Run 34: 5-mil weave with seams

d) Test 7074, Run XX: 10-mil weave, without seams

e) Test 7070, Run XX: 5-mil weave, with seams

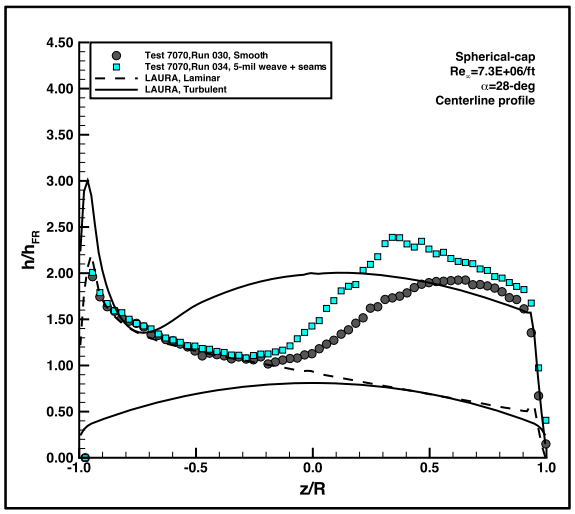
f) Test 7074, Run XX: 15-mil weave, without seams

g) Test 7070, Run XX: 15-mil weave, with seams

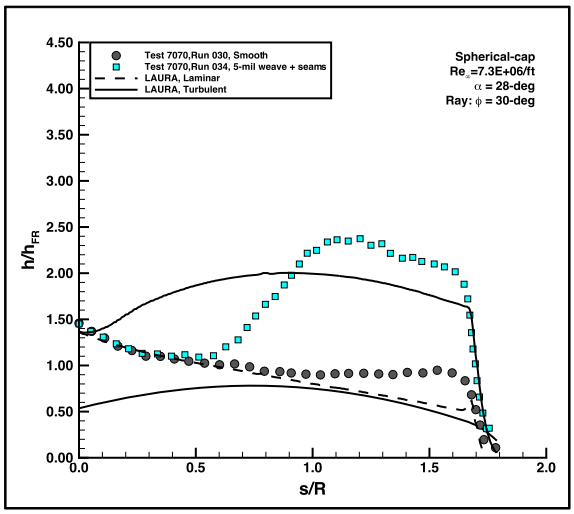
h) Test 7074, Run XX: 20-mil weave, without seams

i) Test 7070, Run XX: 20-mil weave, with seams

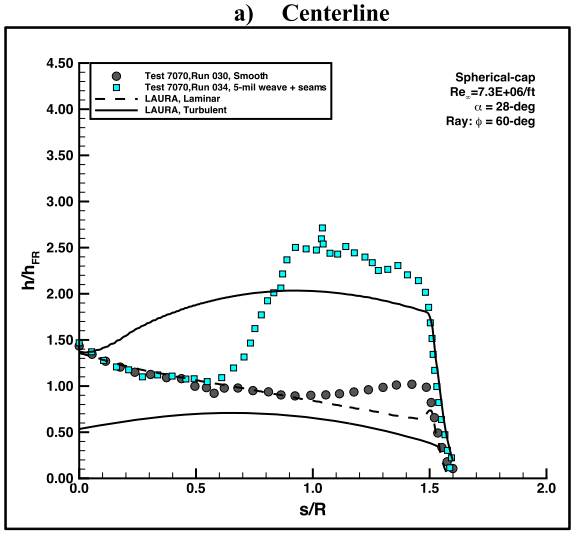
Figure 98. Weave-height effects: spherical-cap geometry, $Re_\infty = 7.3\times10^6$/ft images.



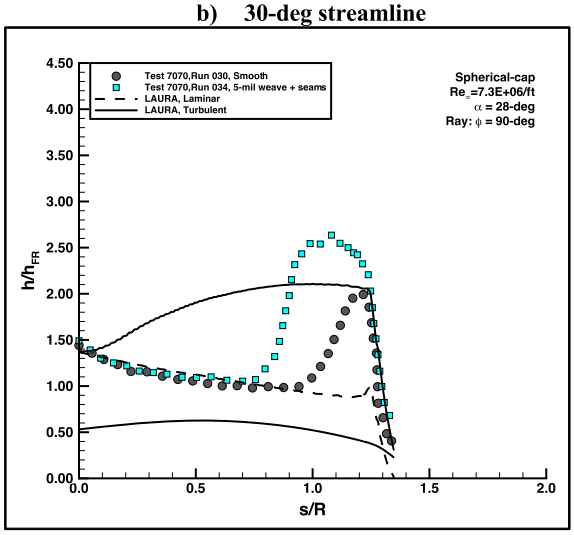
a) Centerline



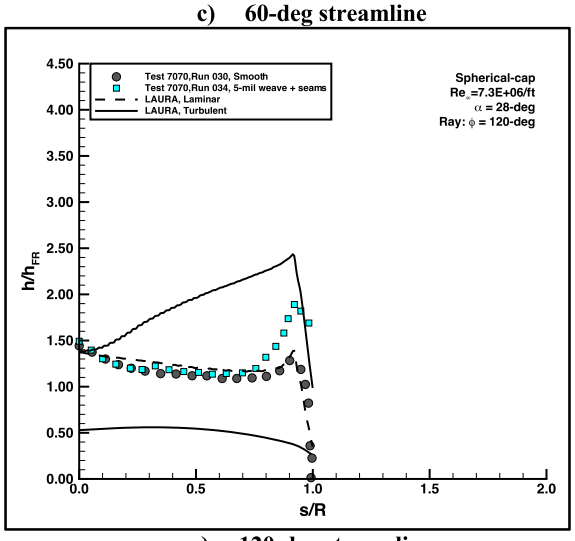
b) 30-deg streamline



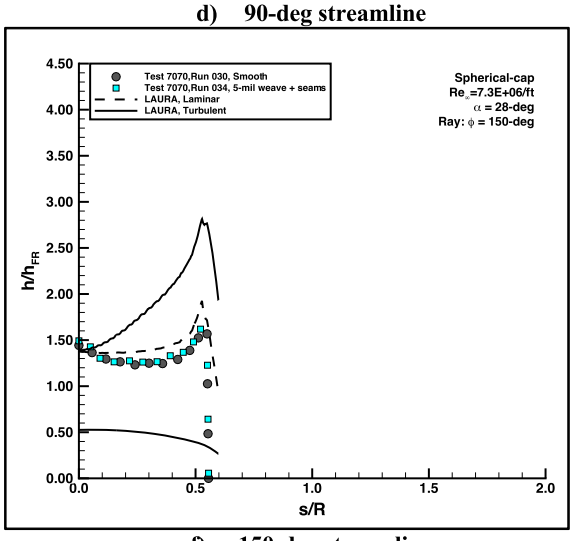
c) 60-deg streamline



d) 90-deg streamline

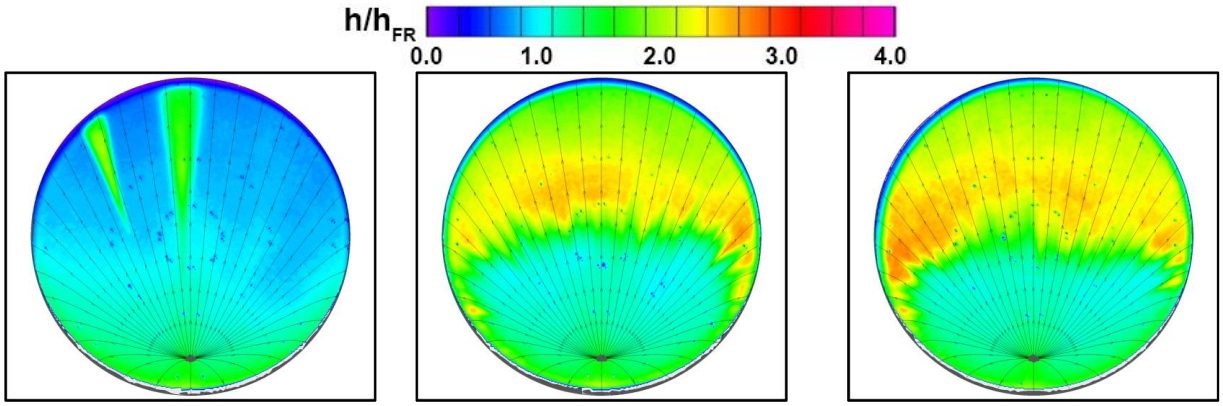


e) 120-deg streamline



f) 150-deg streamline

Figure 99. Weave-height effects: spherical-cap geometry, $Re_\infty = 7.3\times10^6$/ft plots.



a) Test 7070, Run 96: Smooth

b) Test 7074, Run 71: 5-mil weave, without seams

c) Test 7070, Run 66: 5-mil weave with seams

d) Test 7074, Run 53: 10-mil weave, without seams

e) Test 7070, Run XX: 5-mil weave, with seams

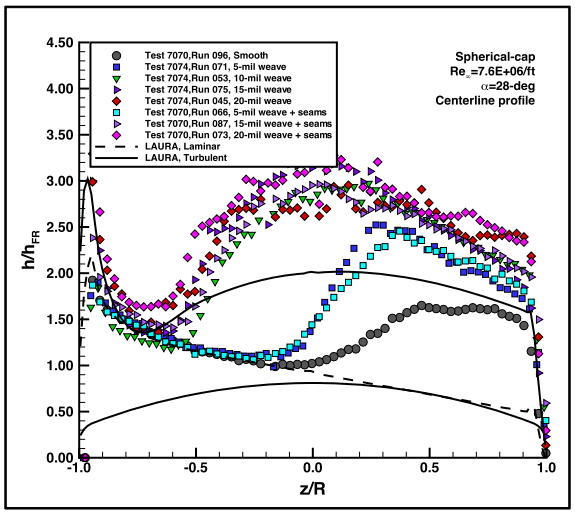
f) Test 7074, Run 75: 15-mil weave, without seams

g) Test 7070, Run 87: 15-mil weave, with seams

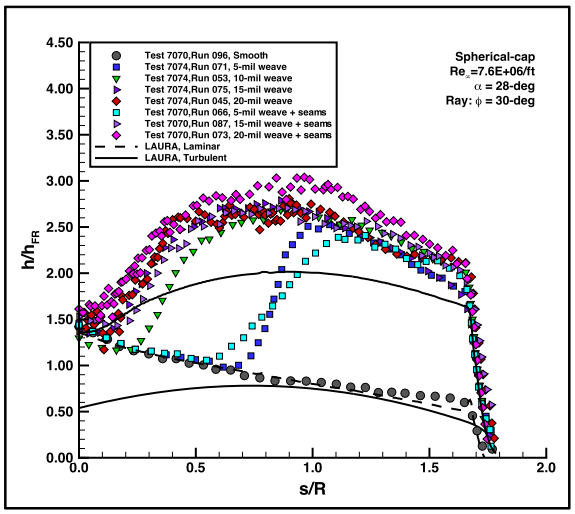
h) Test 7074, Run 45: 20-mil weave, without seams

i) Test 7070, Run 73: 20-mil weave, with seams

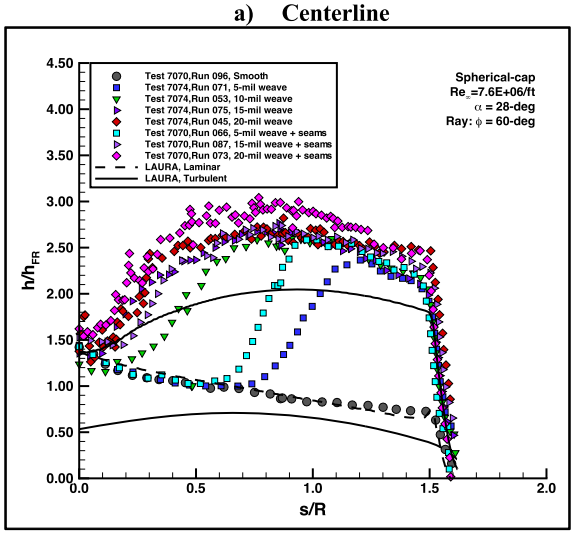
Figure 100. Weave-height effects: spherical-cap geometry, $Re_\infty = 7.6\times10^6$/ft images.



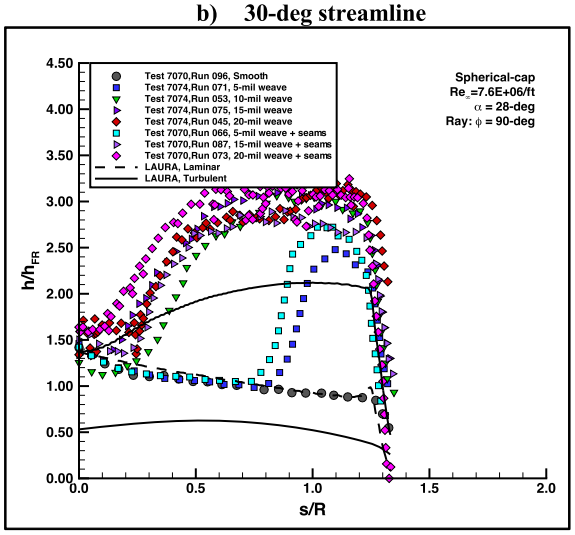
a) Centerline



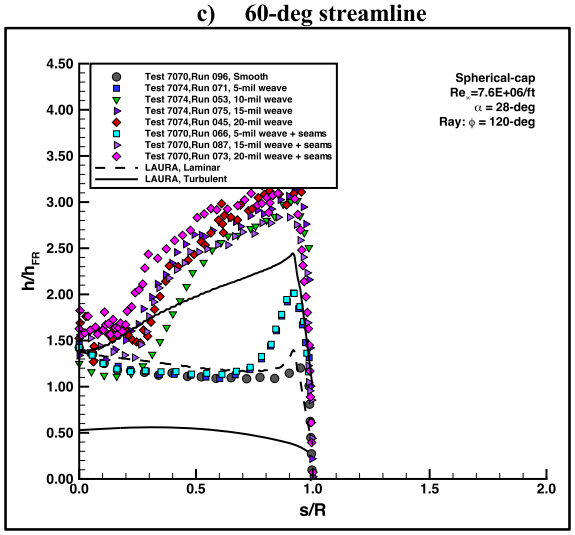
b) 30-deg streamline



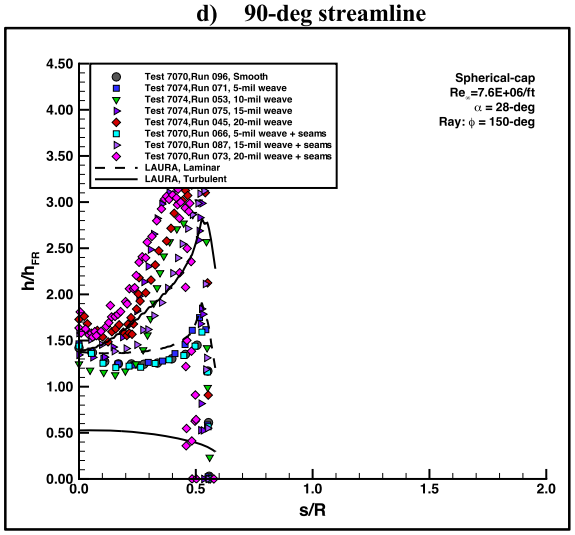
c) 60-deg streamline



d) 90-deg streamline

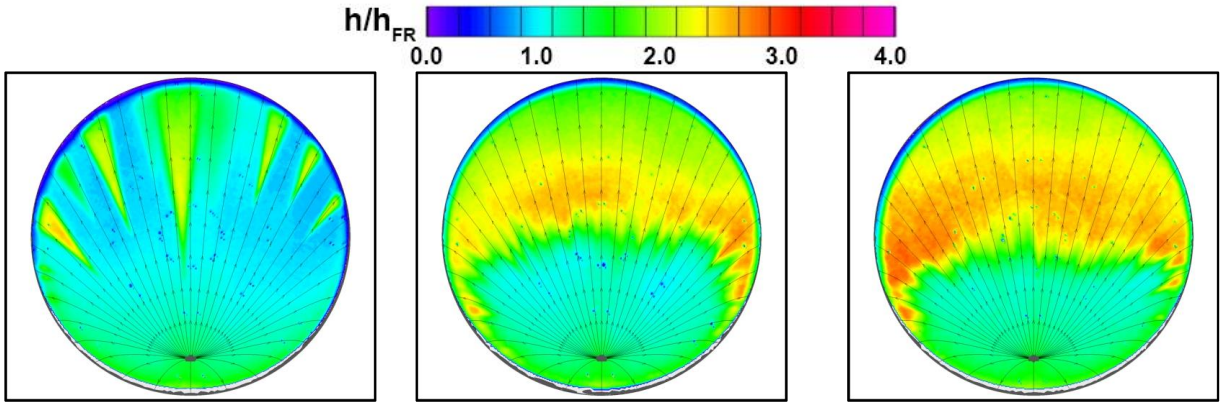


e) 120-deg streamline



f) 150-deg streamline

Figure 101. Weave-height effects: spherical-cap geometry, $Re_\infty = 7.6\times10^6$/ft plots.



a) Test 7070, Run 31: Smooth

b) Test 7074, Run 72: 5-mil weave, without seams

c) Test 7070, Run 35: 5-mil weave with seams

d) Test 7074, Run 54: 10-mil weave, without seams

e) Test 7070, Run XX: 5-mil weave, with seams

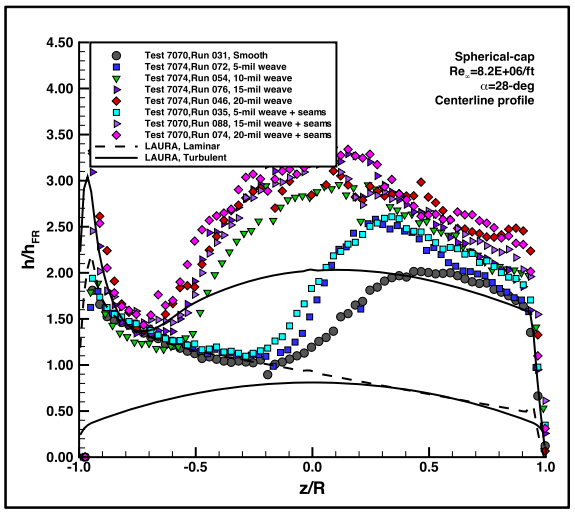
f) Test 7074, Run 76: 15-mil weave, without seams

g) Test 7070, Run 88: 15-mil weave, with seams

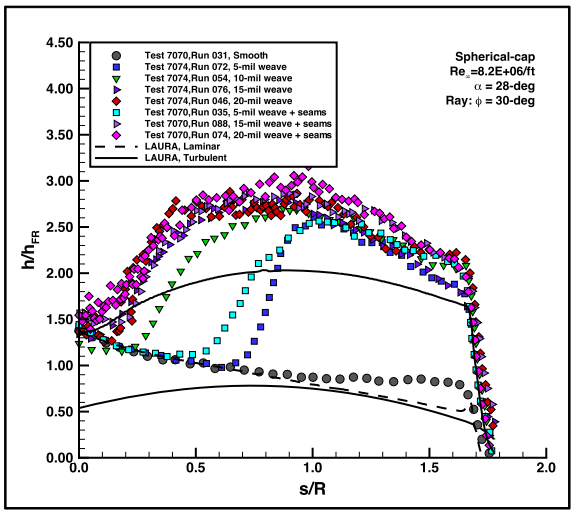
h) Test 7074, Run 46: 20-mil weave, without seams

i) Test 7070, Run 74: 20-mil weave, with seams

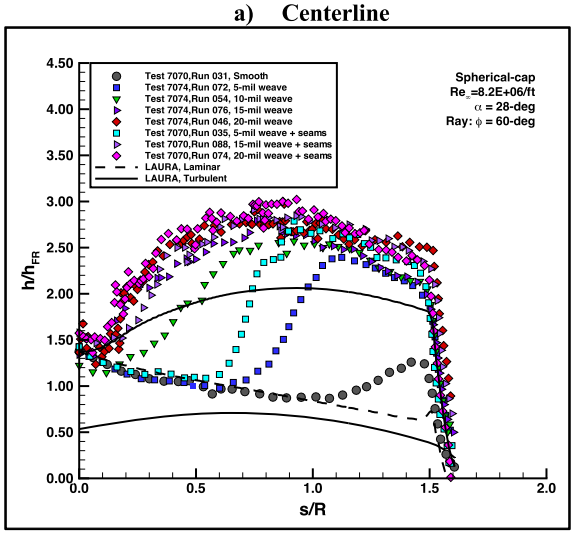
Figure 102. Weave-height effects: spherical-cap geometry, $Re_\infty = 8.2\times10^6$/ft images.



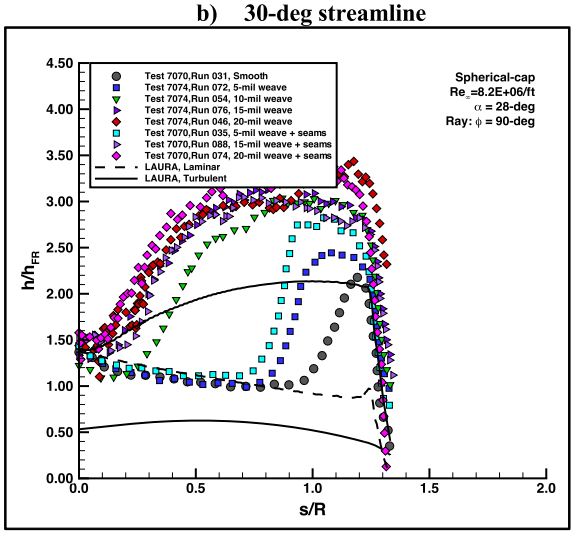
a) Centerline



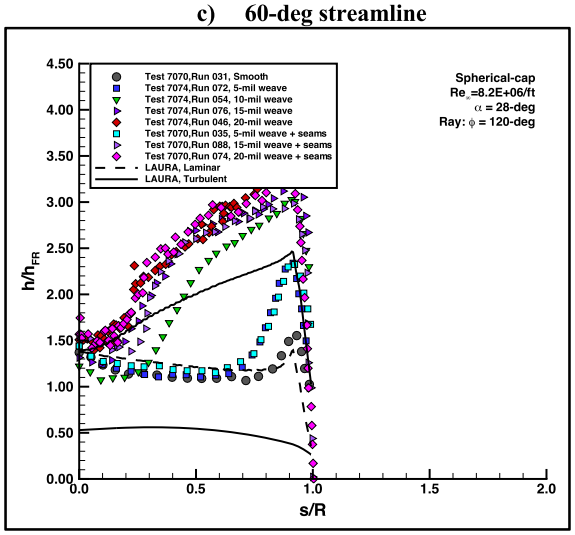
b) 30-deg streamline



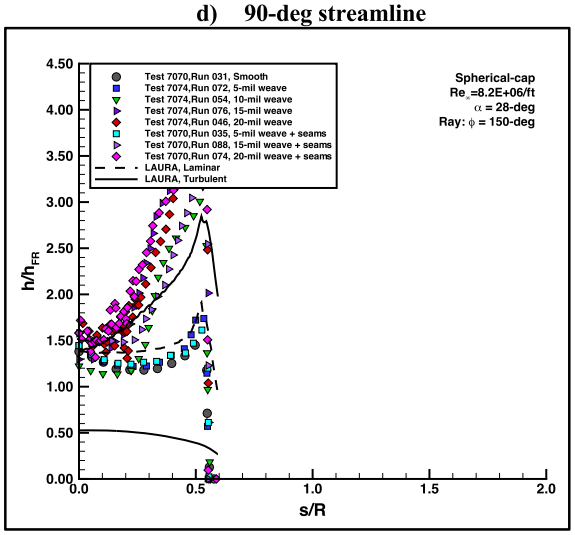
c) 60-deg streamline



d) 90-deg streamline

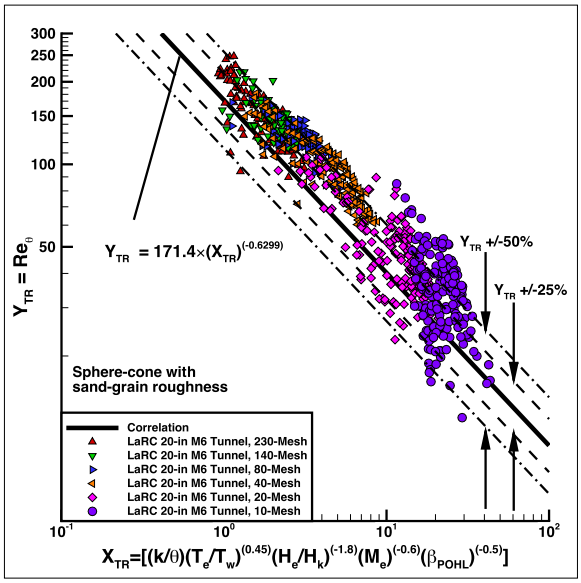


e) 120-deg streamline

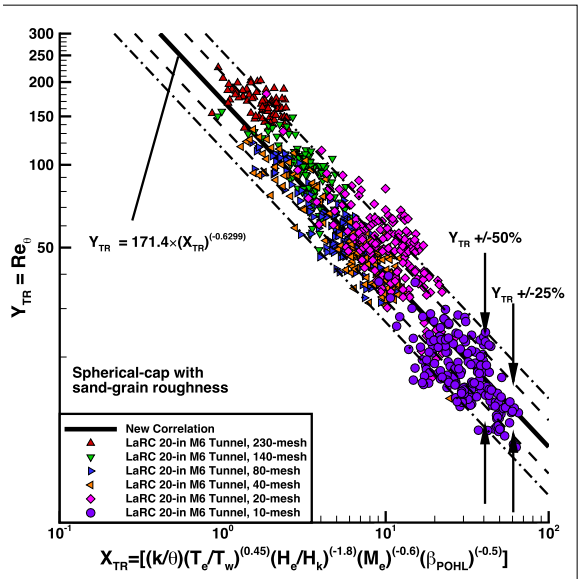


f) 150-deg streamline

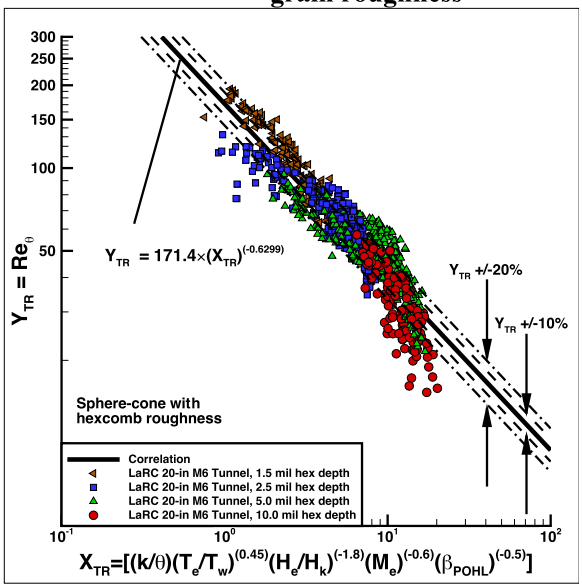
Figure 103. Weave-height effects: spherical-cap geometry, $Re_\infty = 8.2\times10^6$/ft plots.



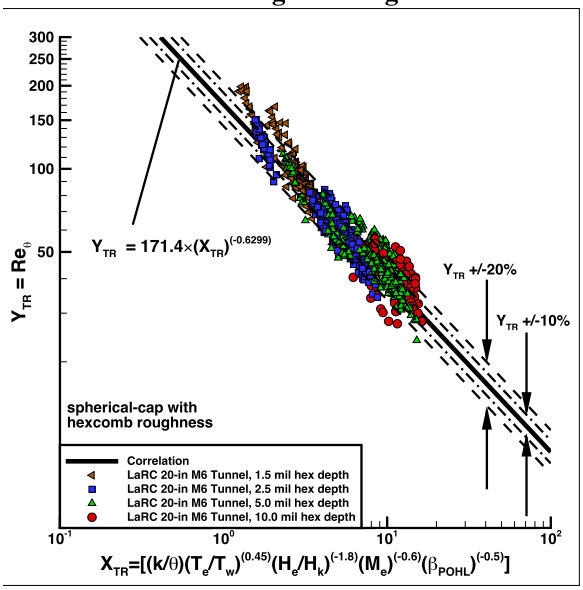
a) sphere-cone geometry with sand-grain roughness



b) spherical-gap geometry with sand-grain roughness

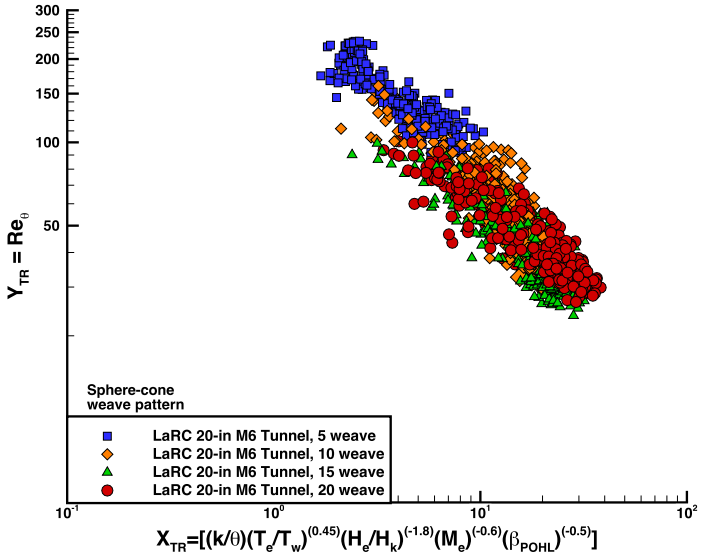


c) sphere-cone geometry with hexcomb roughness

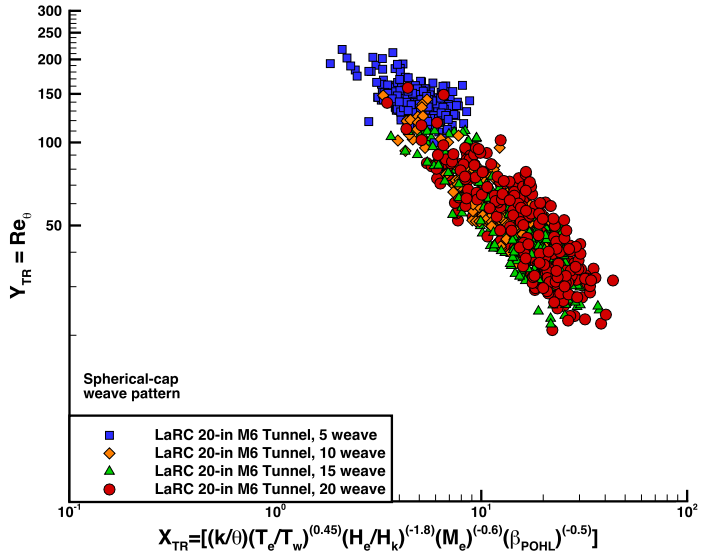


d) spherical-cap geometry with hexcomb roughness

Figure 104. Roughness transition correlation applied to prior datasets.



a) sphere-cone geometry with woven roughness



b) Spherical-cap geometry with woven roughness

Figure 105. Roughness transition correlation applied to woven roughness.

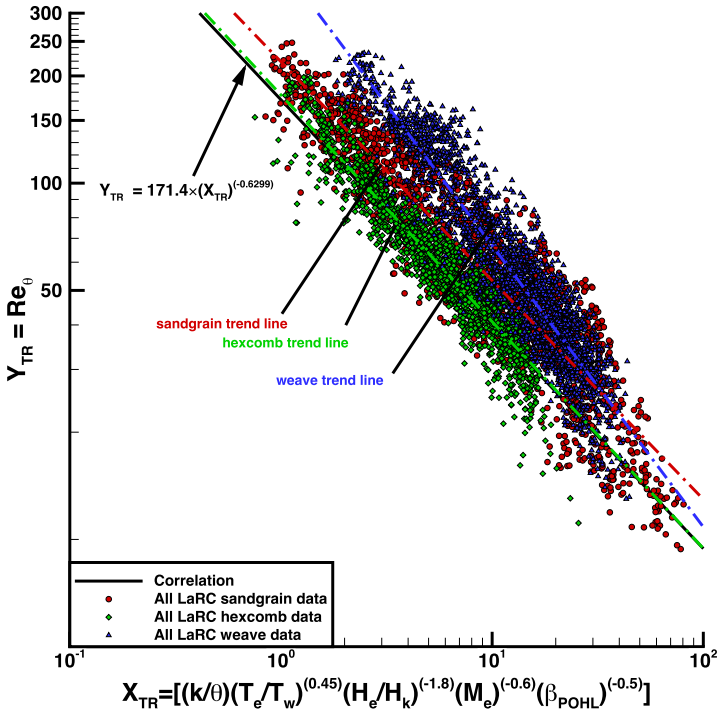


Figure 106. Trend line comparison for different roughness types.

Appendix A. Sphere-Cone Geometry Global Heating Images

Global heating images for the sphere-cone geometry from Test 7070 and 7074 in the LAL 20-Inch Mach 6 Air Tunnel are presented in this Appendix. Smooth OML data are shown in Figure 107 through Figure 116. Woven TPS surface data without seams between the panels are show in Figure 117 through Figure 156. Woven TPS surface data with seams between the panels are show in Figure 157 through Figure 196.

At higher Reynolds numbers and/or larger roughness heights, white patches on the images indicate areas where the measured surface temperatures exceed the calibrated range of the phosphor thermography system and thus no valid data were obtained. Boundary-layer edge streamlines determined from laminar, smooth-surface LAURA simulations have been superimposed on the images to illustrate the nature of the flow field.

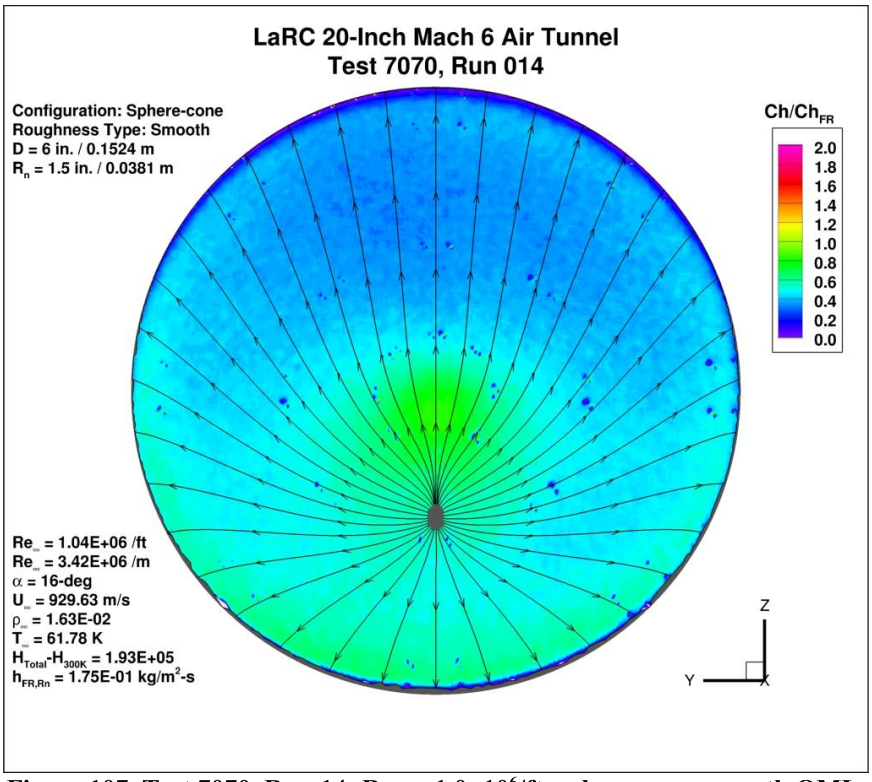


Figure 107. Test 7070, Run 14: $Re_\infty = 1.0\times10^6$/ft, sphere-cone, smooth OML.

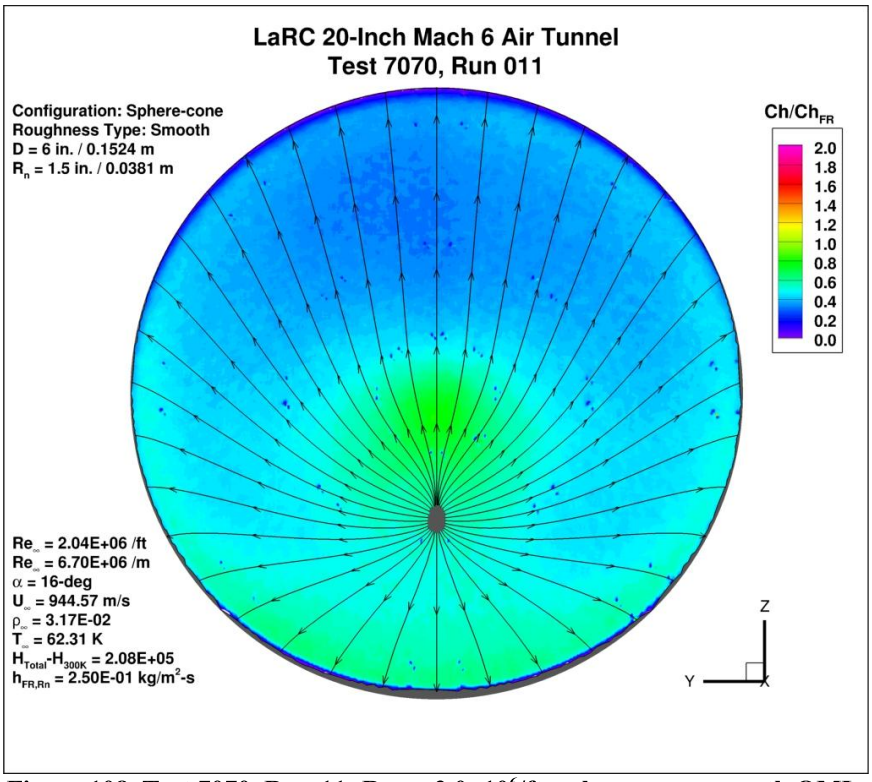


Figure 108. Test 7070, Run 11: $Re_\infty = 2.0\times10^6$/ft, sphere-cone, smooth OML.

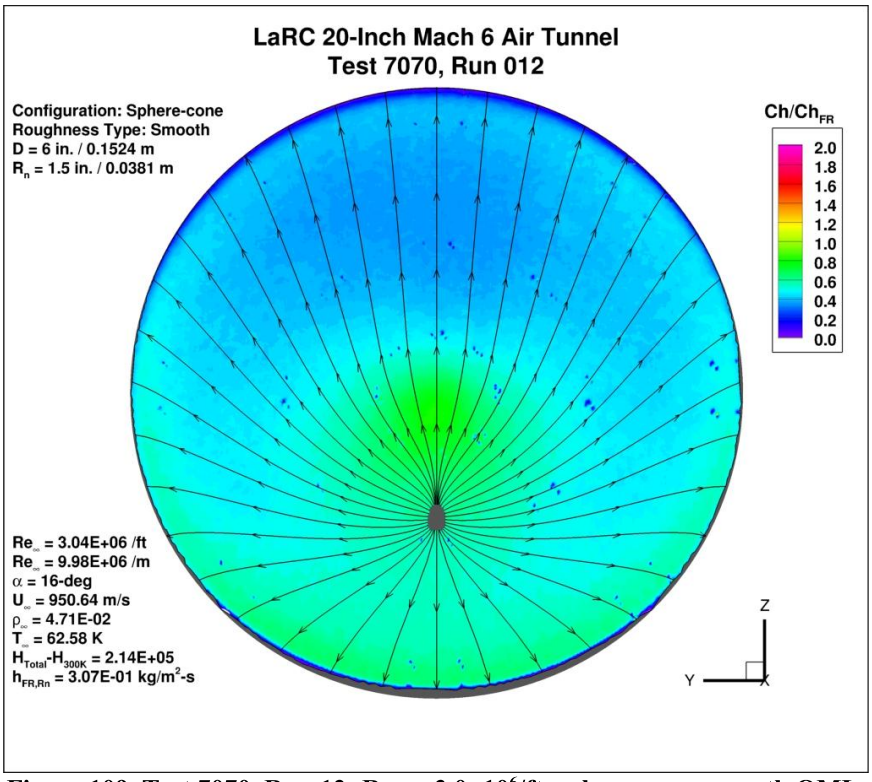


Figure 109. Test 7070, Run 12: $Re_\infty = 3.0\times10^6$/ft, sphere-cone, smooth OML.

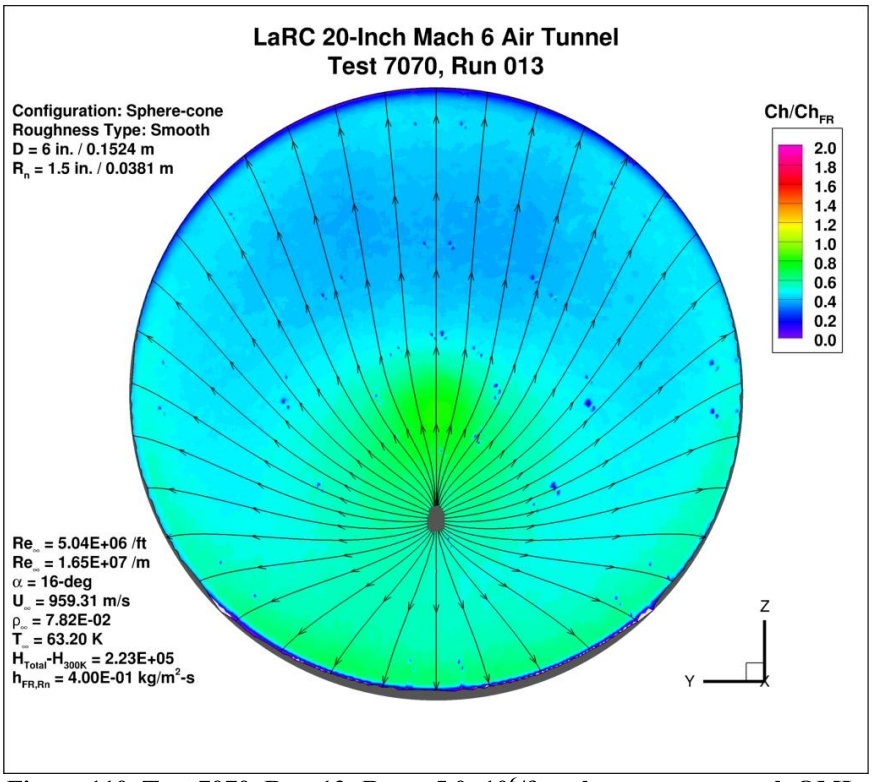


Figure 110. Test 7070, Run 13: $Re_\infty = 5.0\times10^6$/ft, sphere-cone, smooth OML.

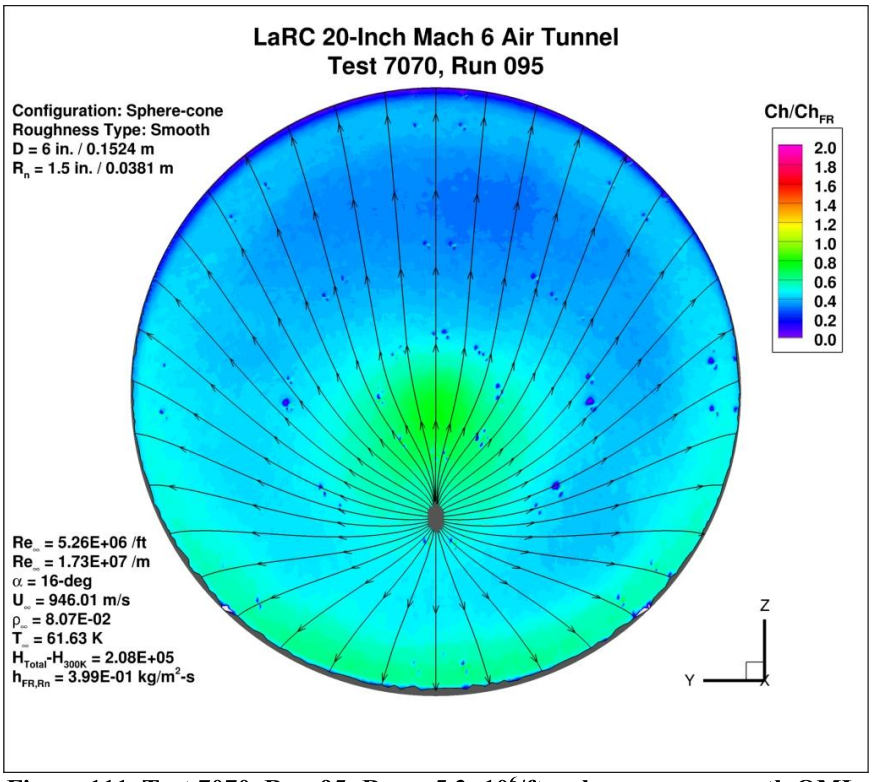


Figure 111. Test 7070, Run 95: $Re_\infty = 5.3\times10^6$/ft, sphere-cone, smooth OML.

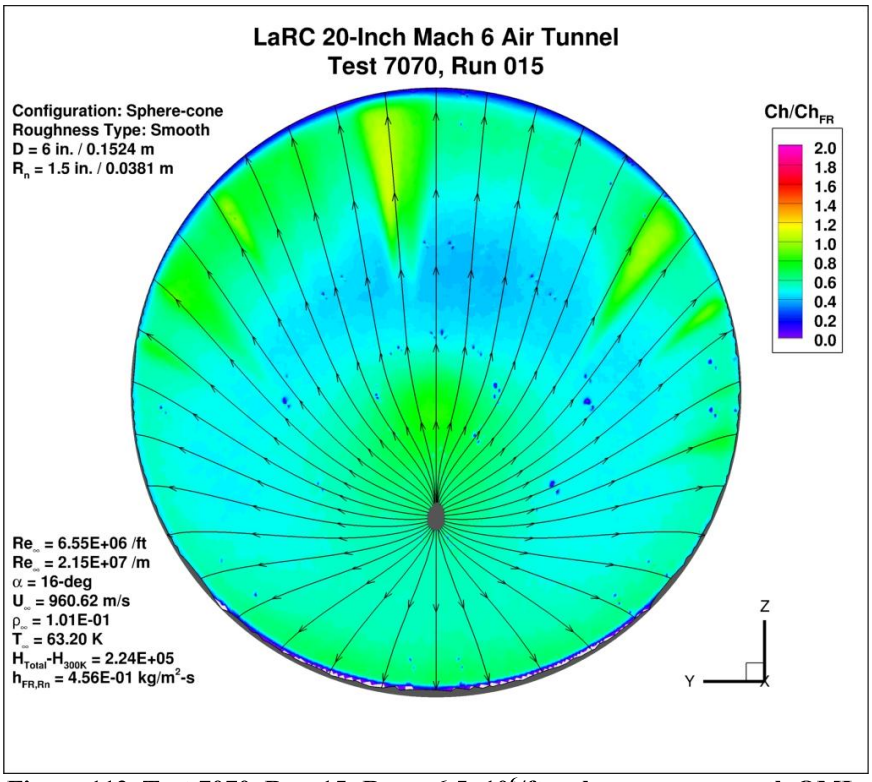


Figure 112. Test 7070, Run 15: $Re_\infty = 6.5\times10^6$/ft, sphere-cone, smooth OML.

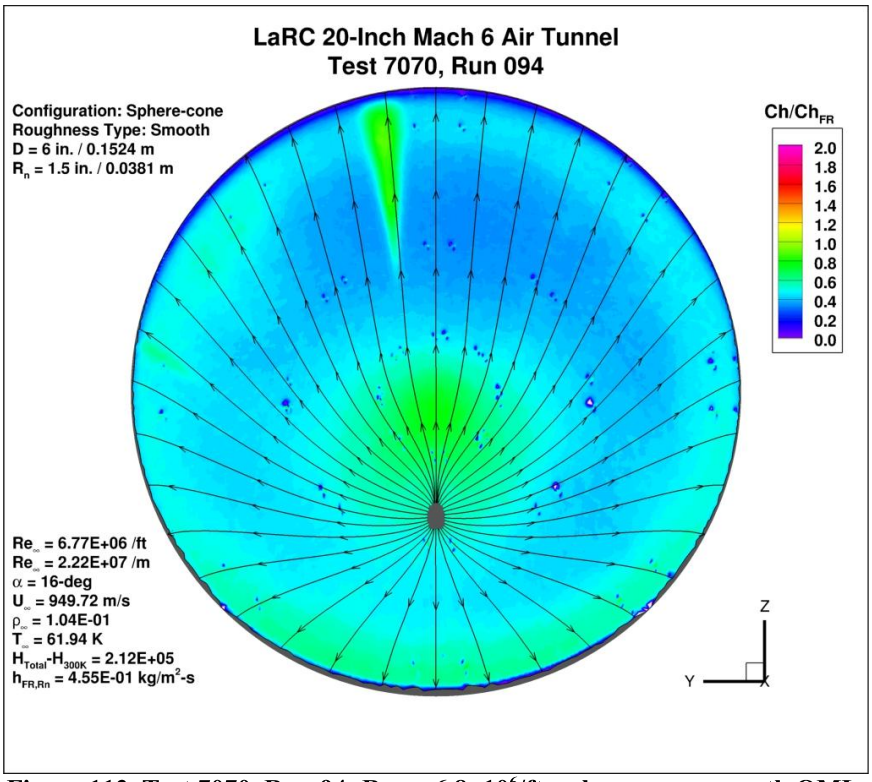


Figure 113. Test 7070, Run 94: $Re_\infty = 6.8\times10^6$/ft, sphere-cone, smooth OML.

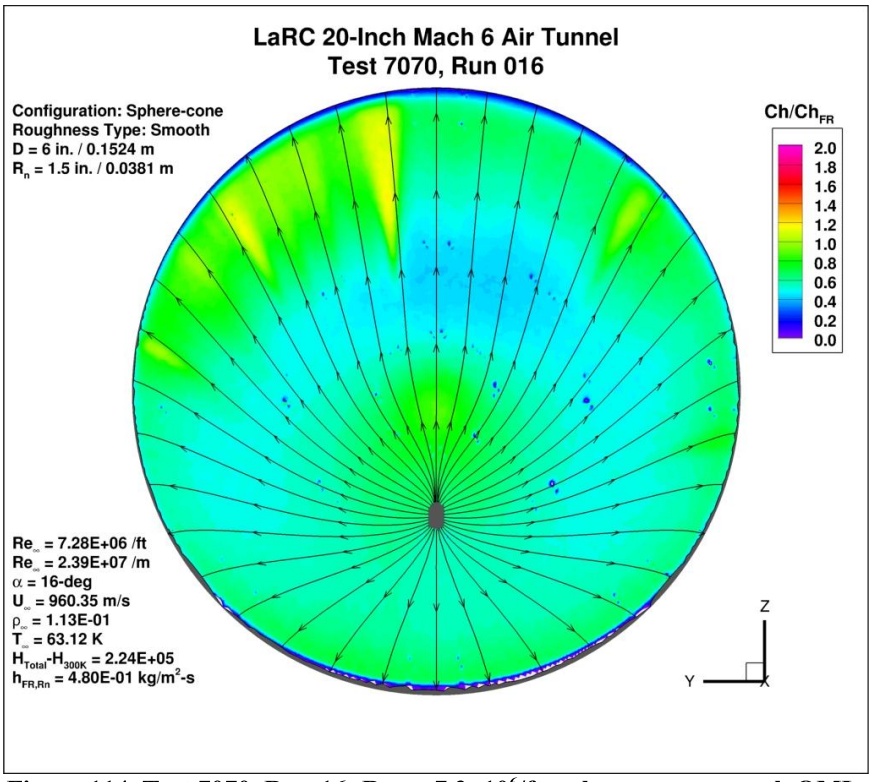


Figure 114. Test 7070, Run 16: $Re_\infty = 7.3\times10^6$/ft, sphere-cone, smooth OML.

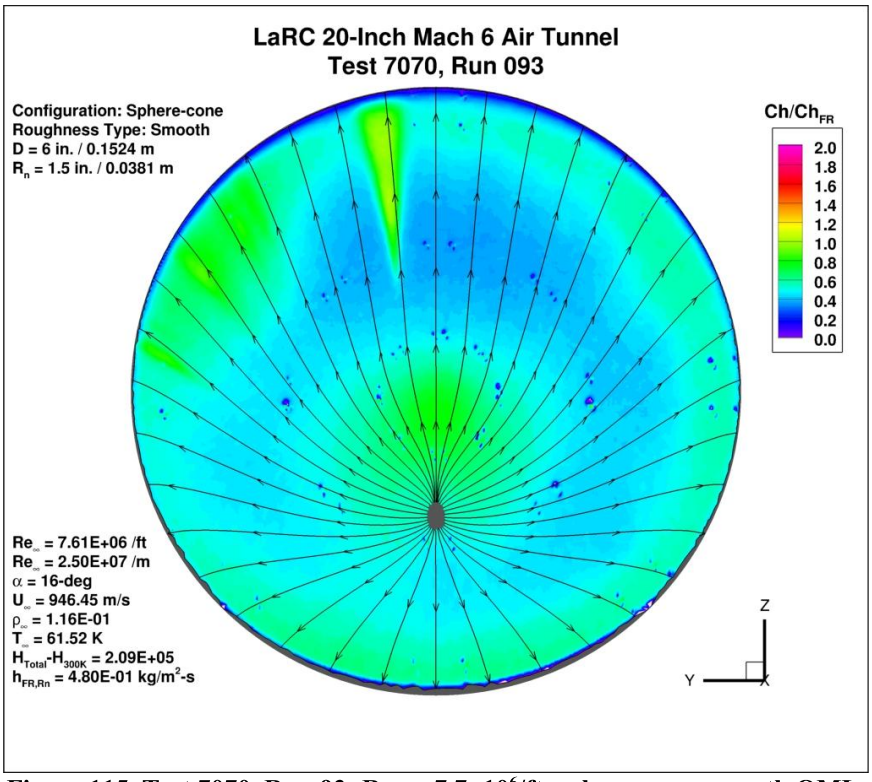


Figure 115. Test 7070, Run 93: $Re_\infty = 7.7\times10^6$/ft, sphere-cone, smooth OML.

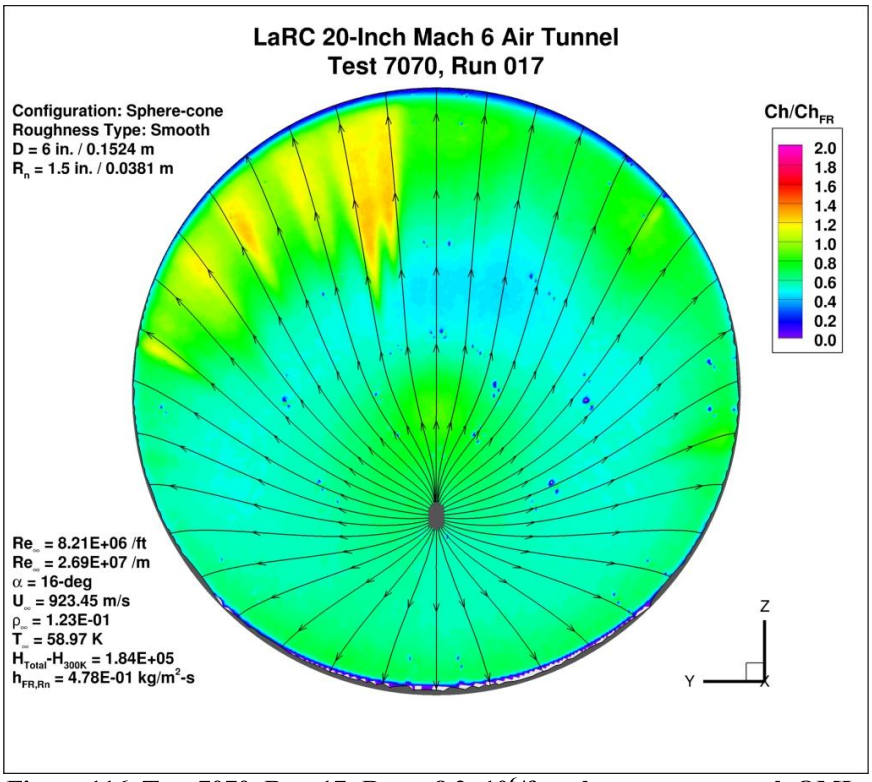


Figure 116. Test 7070, Run 17: $Re_\infty = 8.2\times10^6$/ft, sphere-cone, smooth OML.

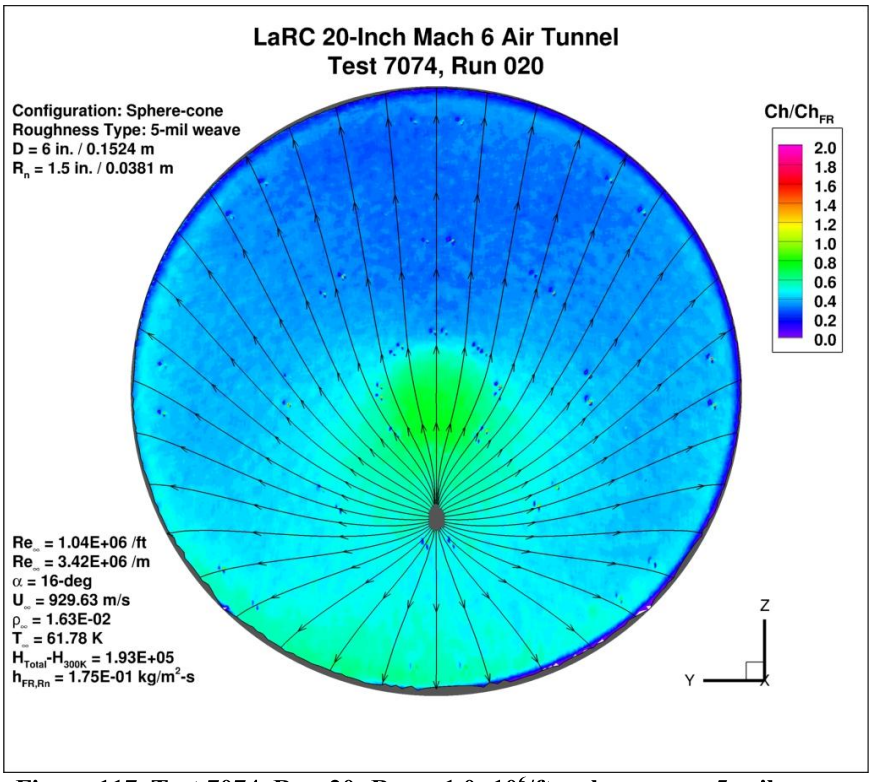


Figure 117. Test 7074, Run 20: $Re_\infty = 1.0\times10^6$/ft, sphere-cone, 5-mil weave.

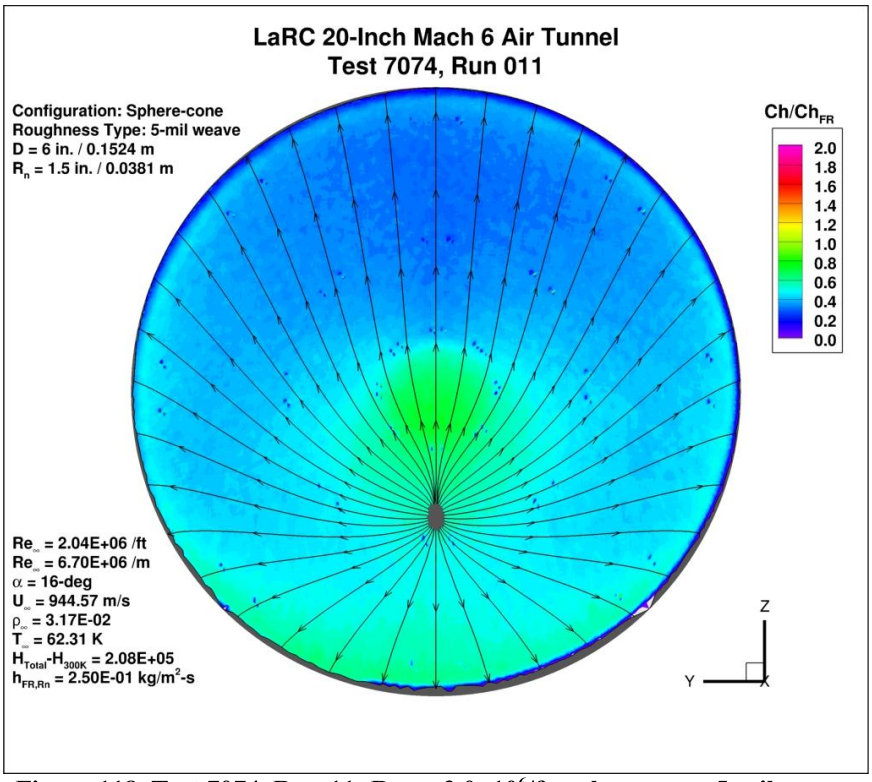


Figure 118. Test 7074, Run 11: $Re_\infty = 2.0\times10^6$/ft, sphere-cone, 5-mil weave.

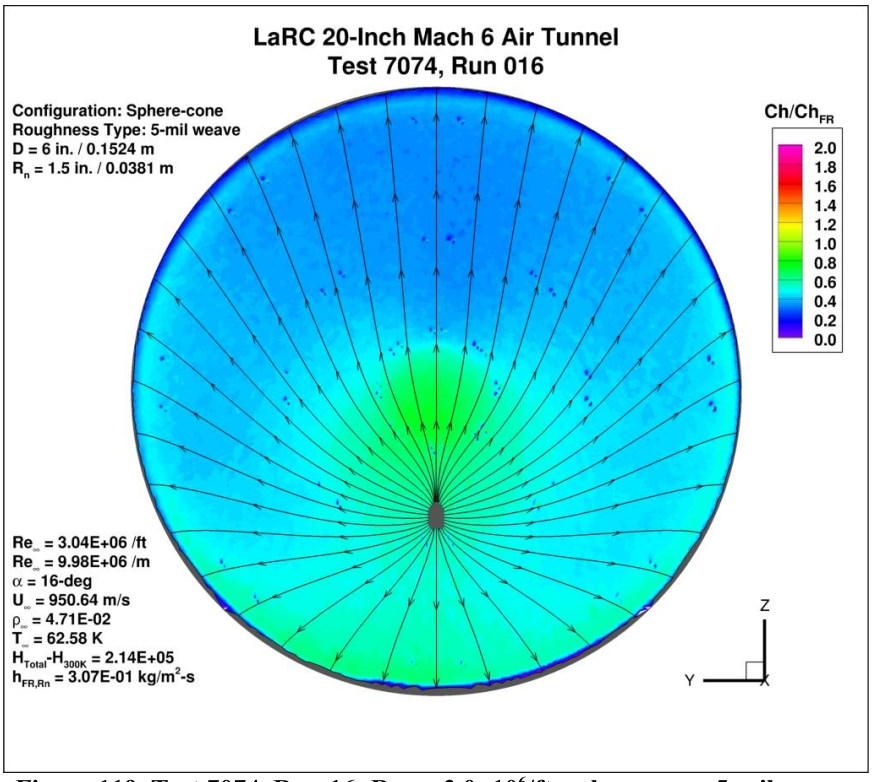


Figure 119. Test 7074, Run 16: $Re_\infty = 3.0\times10^6$/ft, sphere-cone, 5-mil weave.

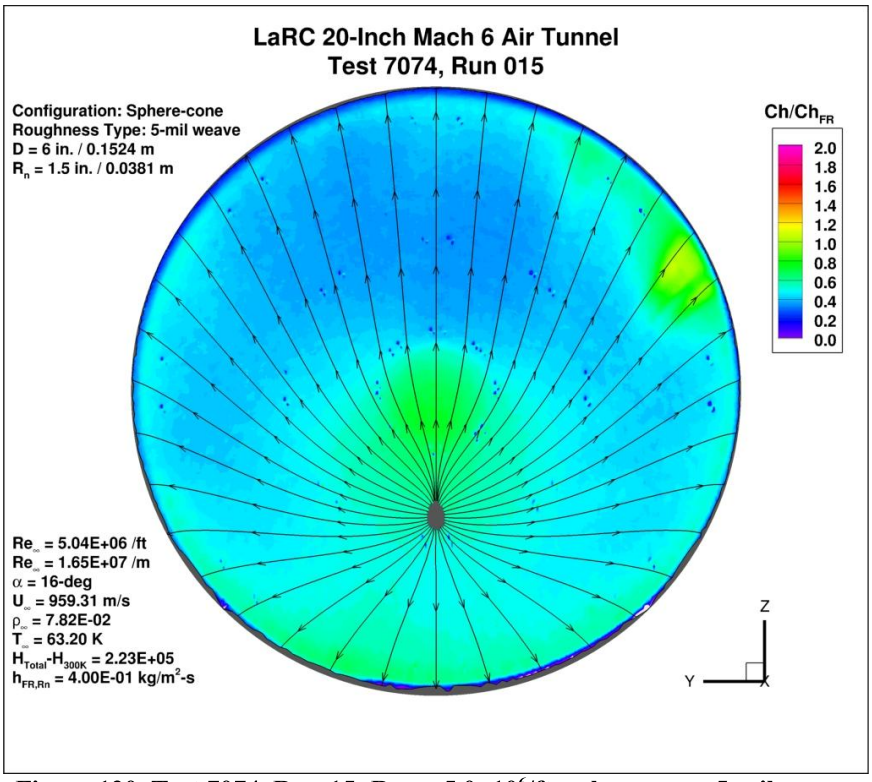


Figure 120. Test 7074, Run 15: $Re_\infty = 5.0\times10^6$/ft, sphere-cone, 5-mil weave.

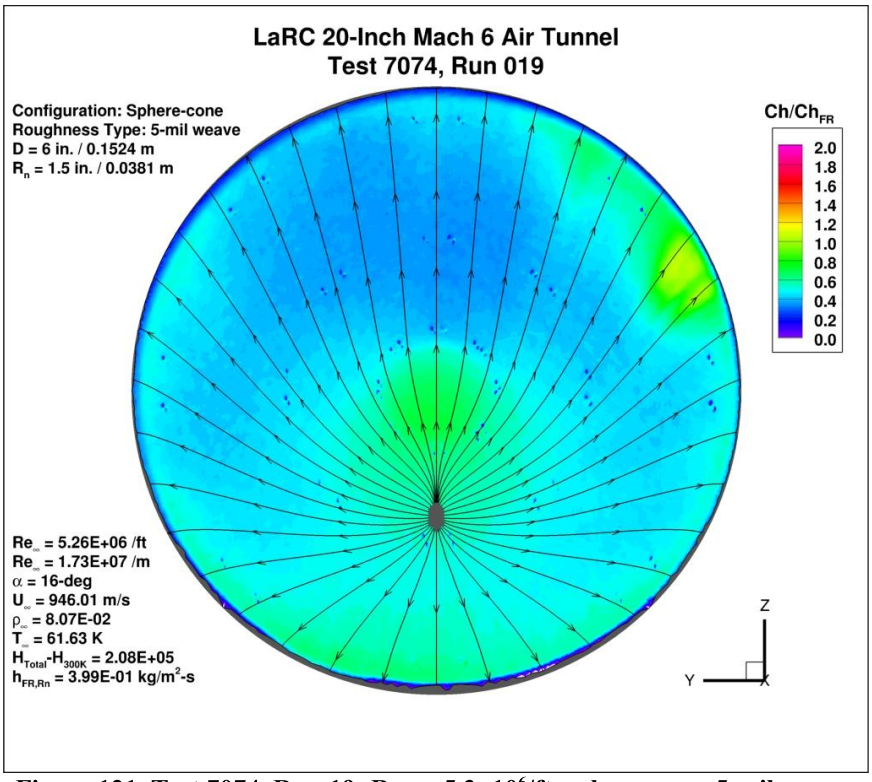


Figure 121. Test 7074, Run 19: $Re_\infty = 5.3\times10^6$/ft, sphere-cone, 5-mil weave.

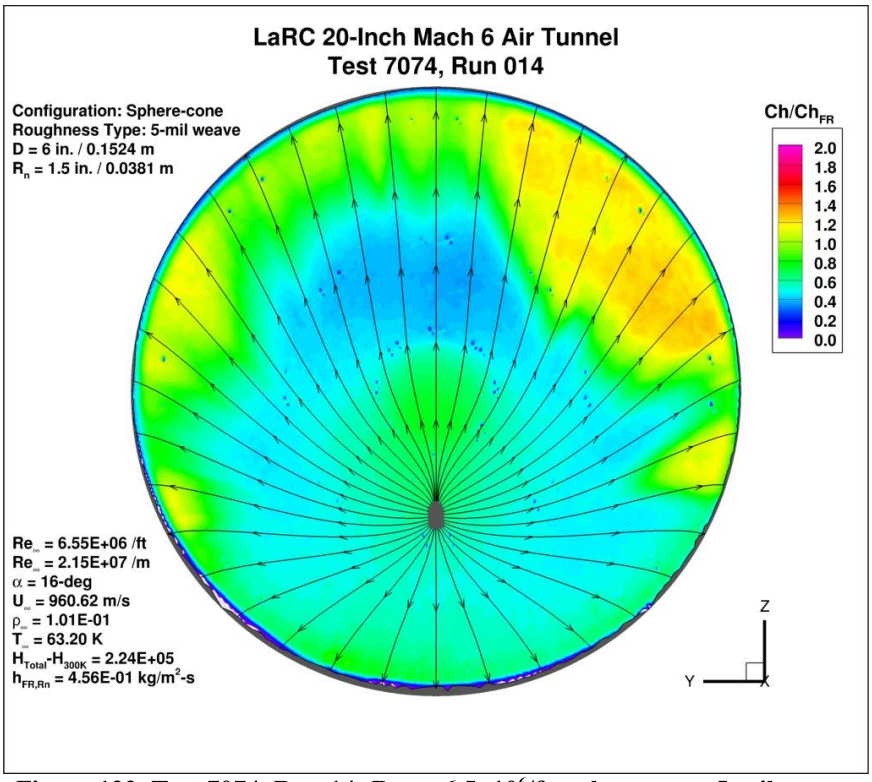


Figure 122. Test 7074, Run 14: $Re_\infty = 6.5\times10^6$/ft, sphere-cone, 5-mil weave.

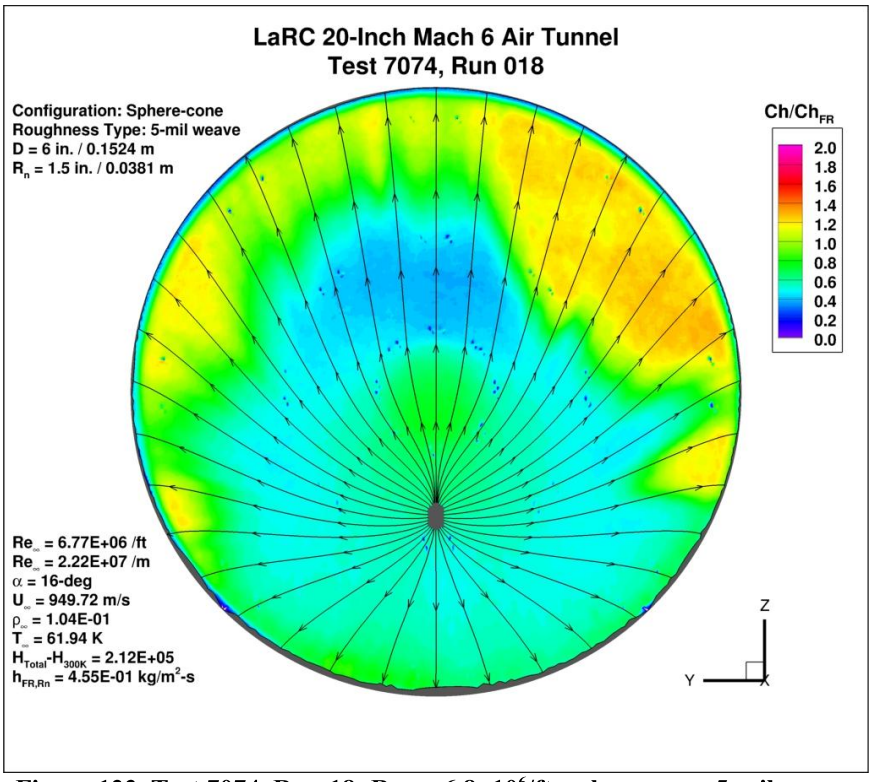


Figure 123. Test 7074, Run 18: $Re_\infty = 6.8\times10^6$/ft, sphere-cone, 5-mil weave.

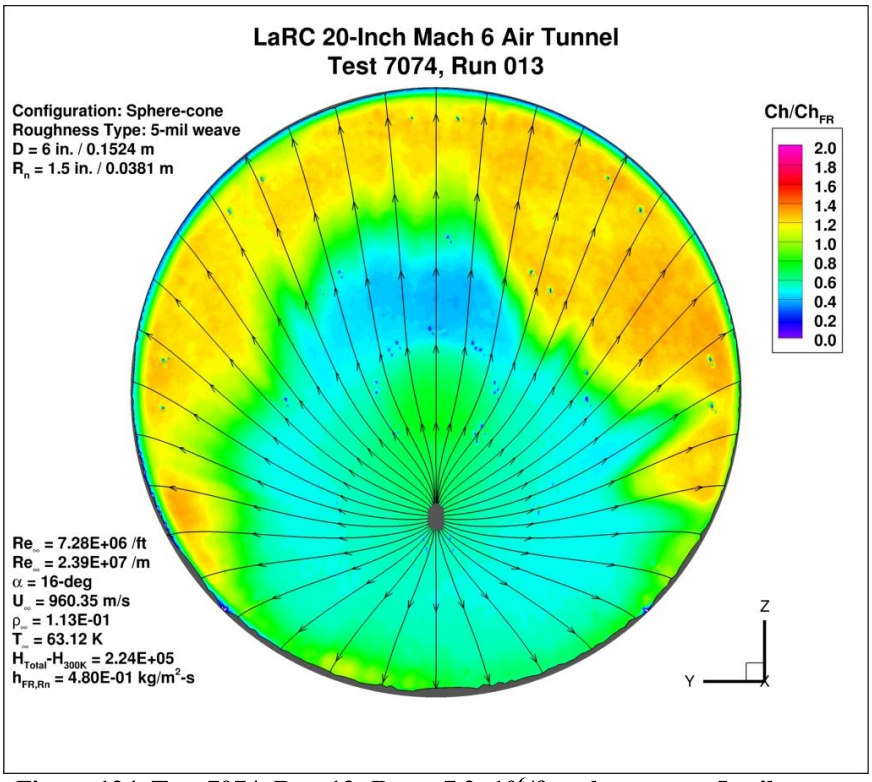


Figure 124. Test 7074, Run 13: $Re_\infty = 7.2\times10^6$/ft, sphere-cone, 5-mil weave.

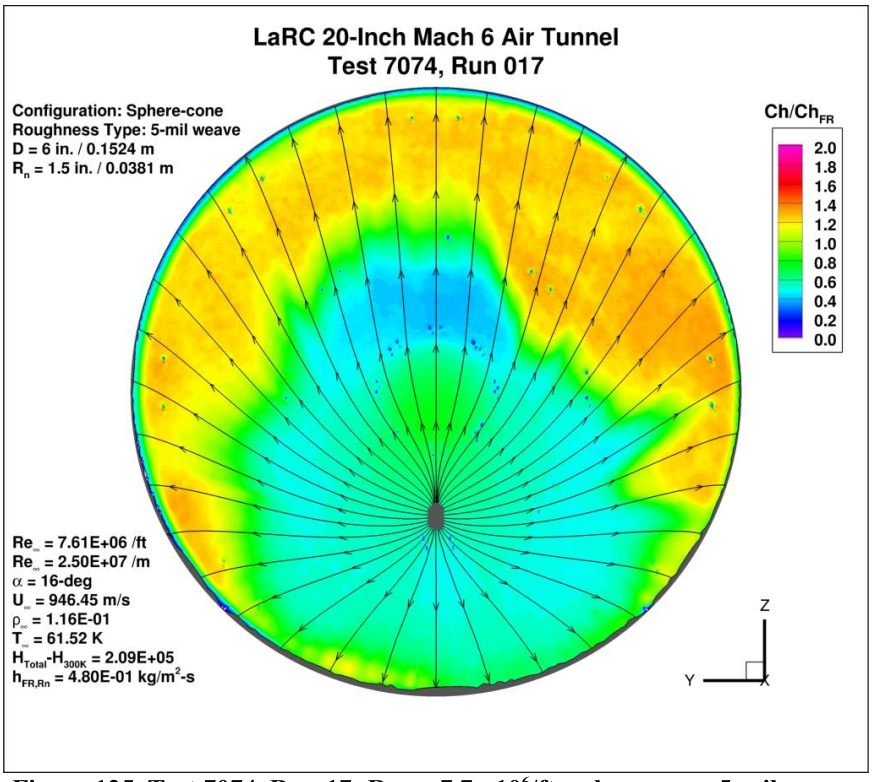


Figure 125. Test 7074, Run 17: Re_∞ = 7.7 ×10^6/ft, sphere-cone, 5-mil weave.

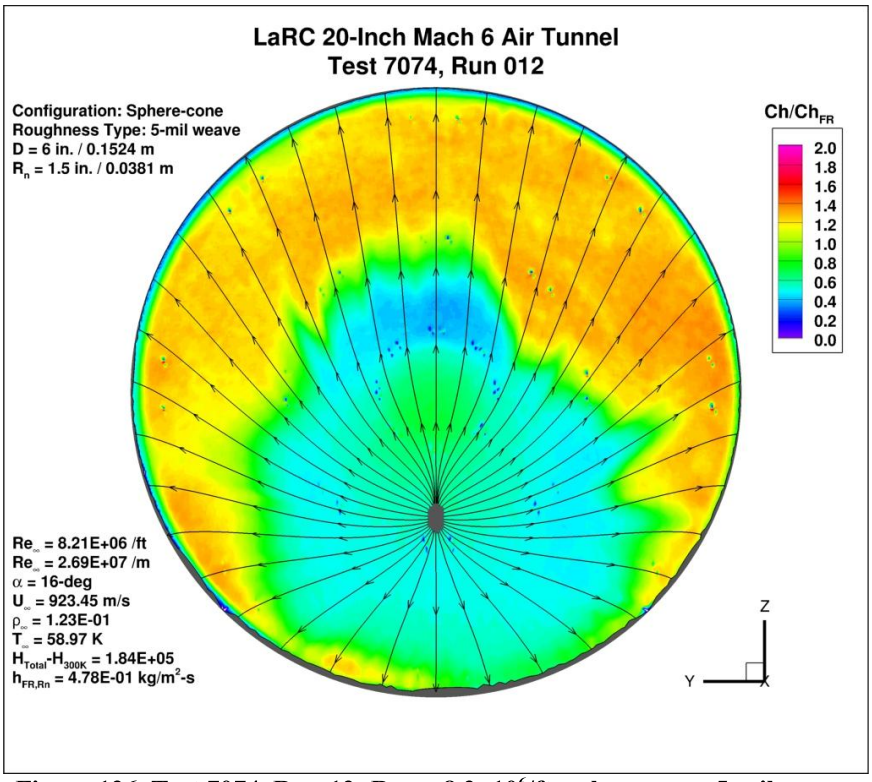


Figure 126. Test 7074, Run 12: Re_∞ = 8.2×10^6/ft, sphere-cone, 5-mil weave.

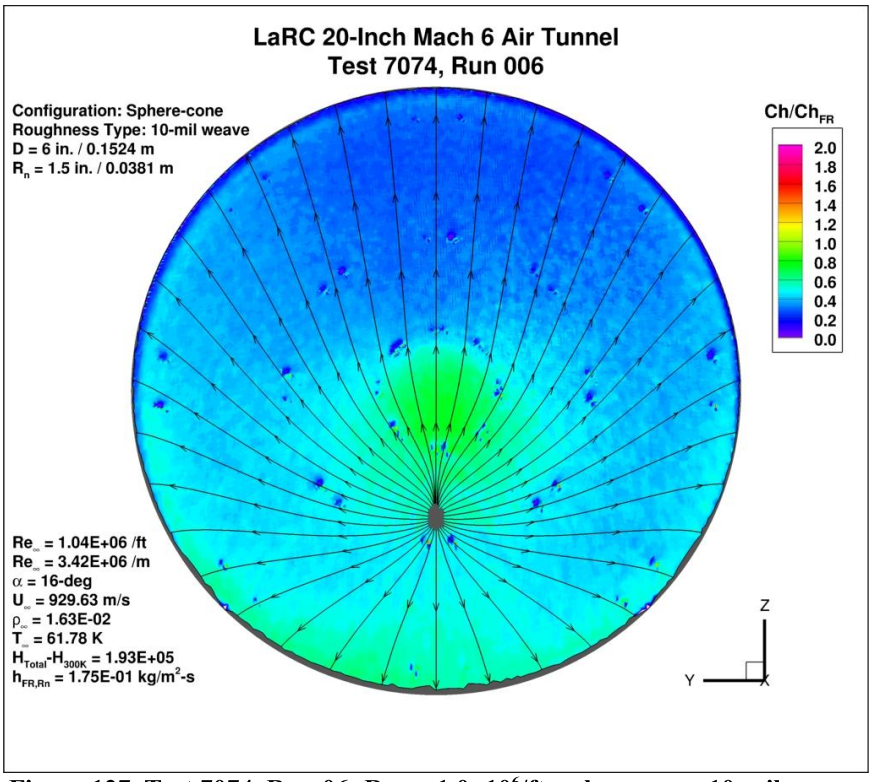


Figure 127. Test 7074, Run 06: $Re_\infty = 1.0\times10^6$/ft, sphere-cone, 10-mil weave.

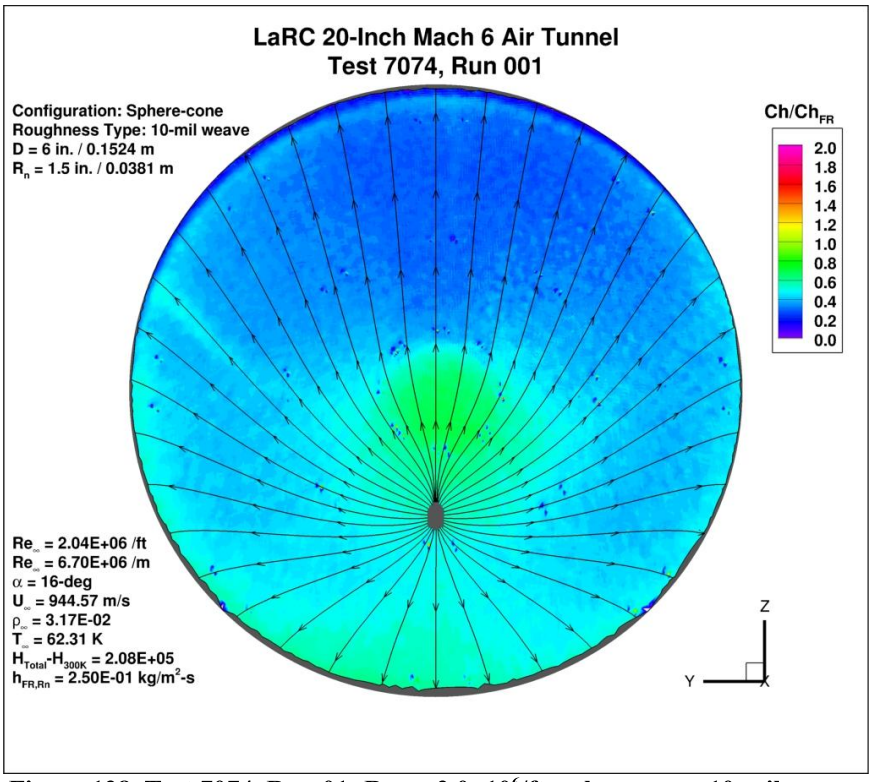


Figure 128. Test 7074, Run 01: $Re_\infty = 2.0\times10^6$/ft, sphere-cone, 10-mil weave.

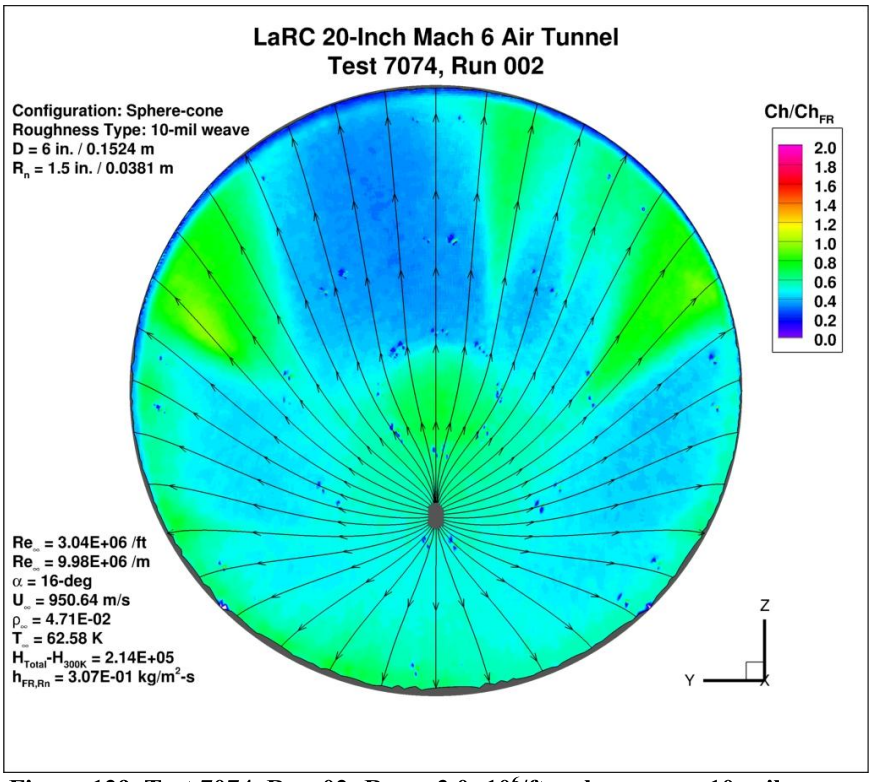


Figure 129. Test 7074, Run 02: $Re_\infty = 3.0\times10^6$/ft, sphere-cone, 10-mil weave.

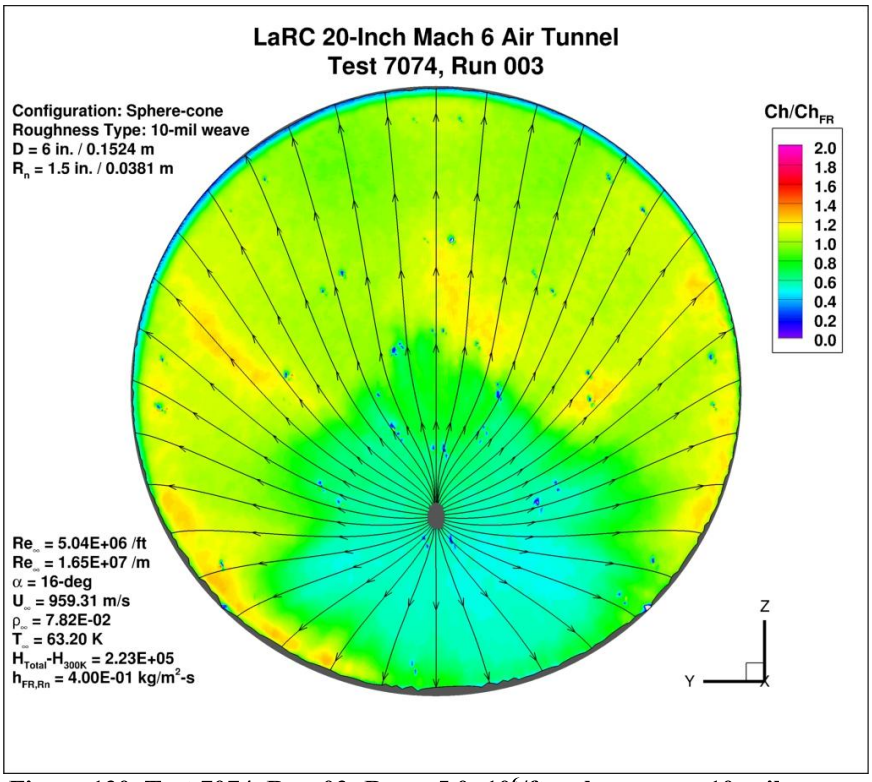


Figure 130. Test 7074, Run 03: $Re_\infty = 5.0\times10^6$/ft, sphere-cone, 10-mil weave.

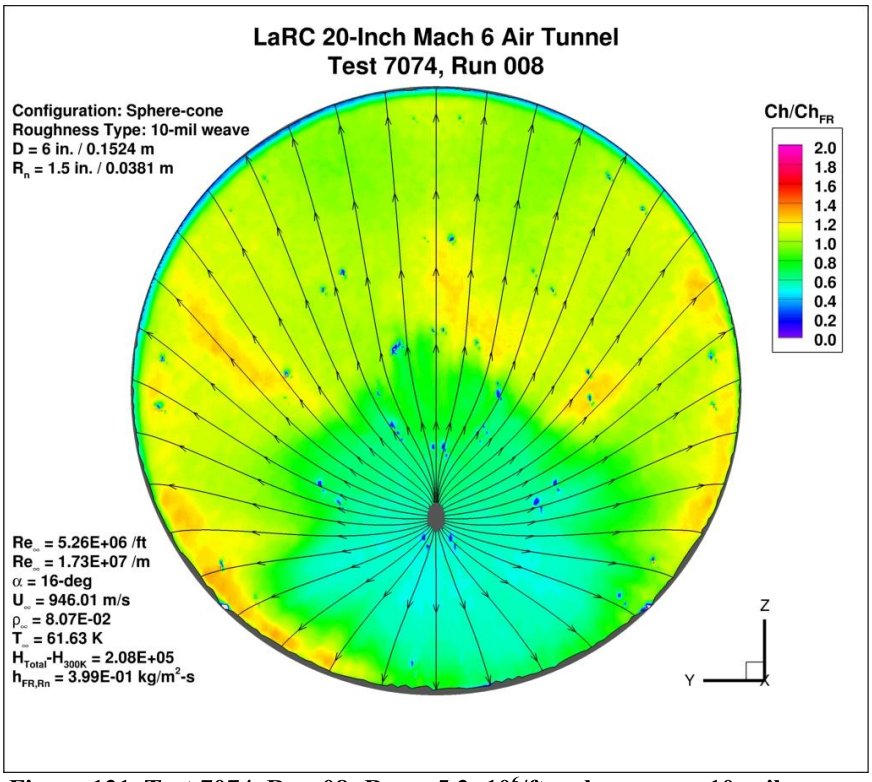


Figure 131. Test 7074, Run 08: $Re_\infty = 5.3\times10^6$/ft, sphere-cone, 10-mil weave.

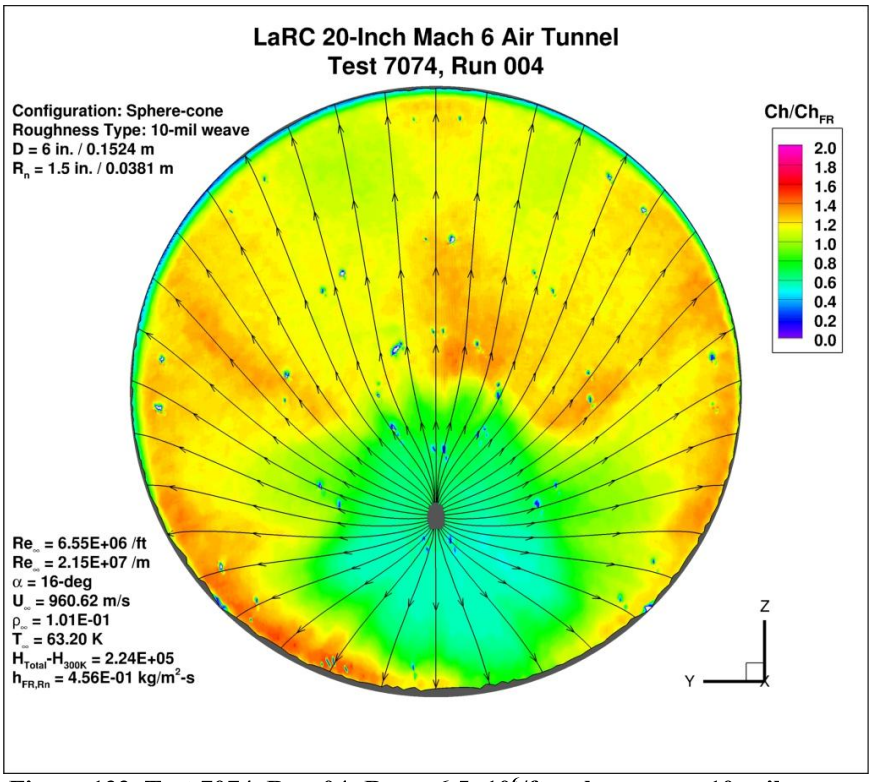


Figure 132. Test 7074, Run 04: $Re_\infty = 6.5\times10^6$/ft, sphere-cone, 10-mil weave.

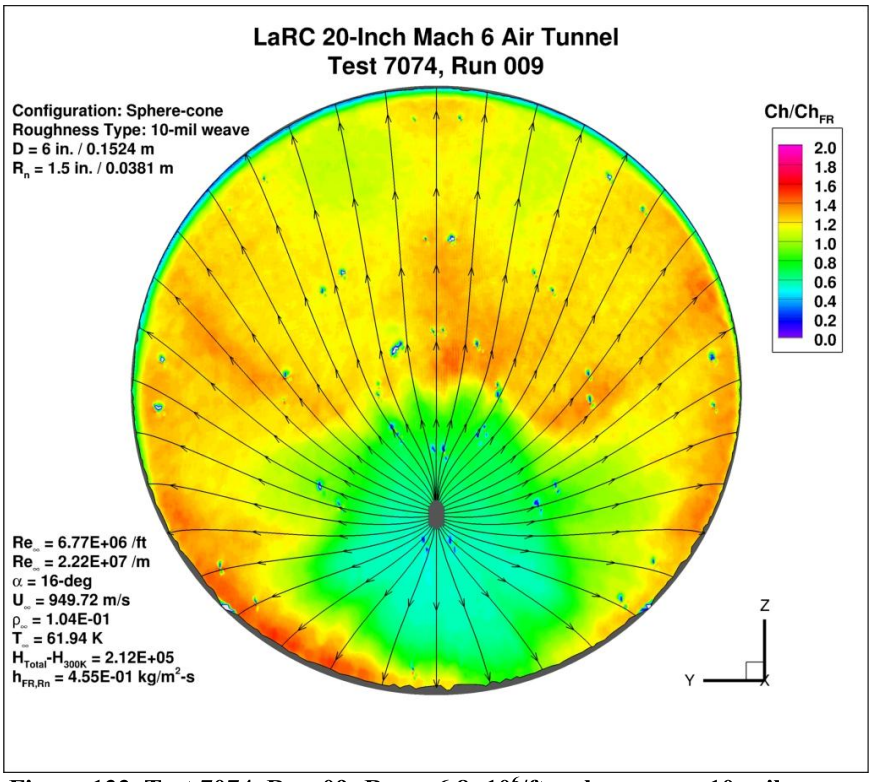


Figure 133. Test 7074, Run 09: $Re_\infty = 6.8\times10^6$/ft, sphere-cone, 10-mil weave.

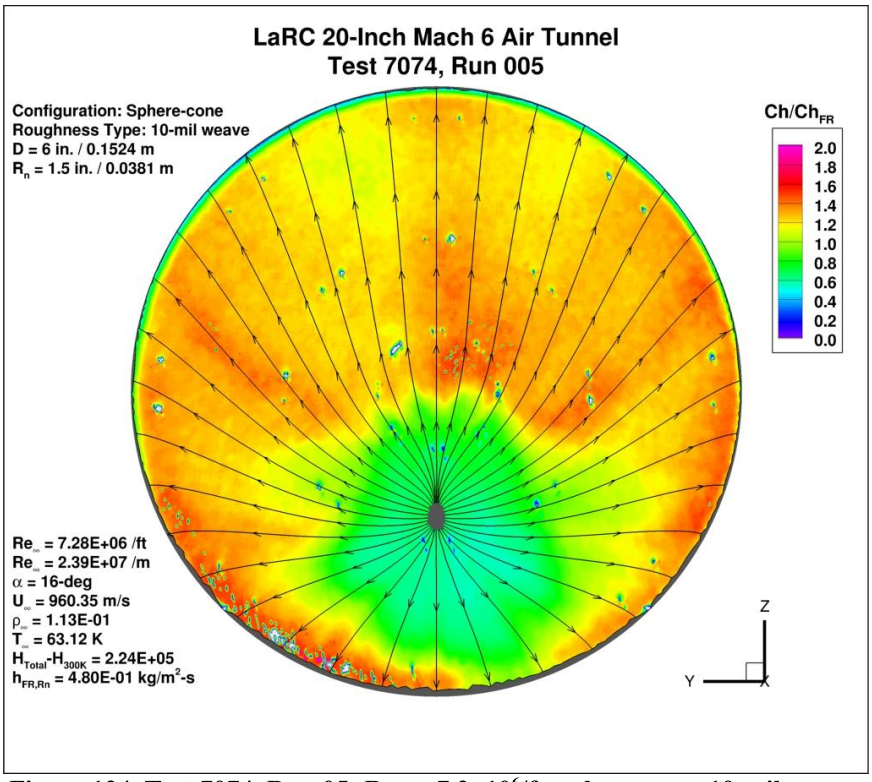


Figure 134. Test 7074, Run 05: $Re_\infty = 7.3\times10^6$/ft, sphere-cone, 10-mil weave.

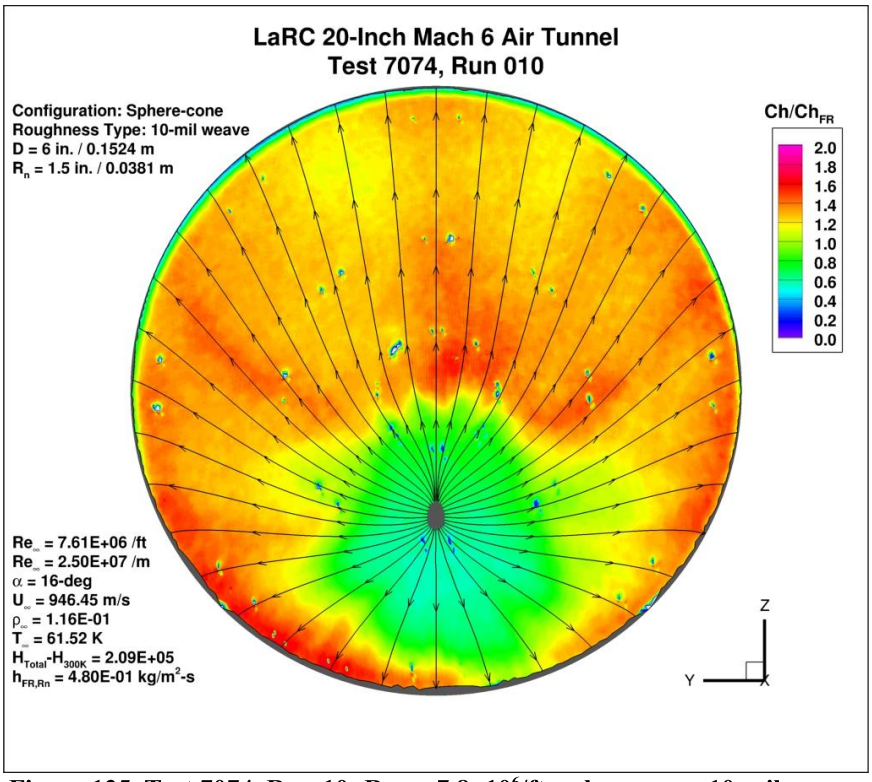


Figure 135. Test 7074, Run 10: $Re_\infty = 7.8\times10^6$/ft, sphere-cone, 10-mil weave.

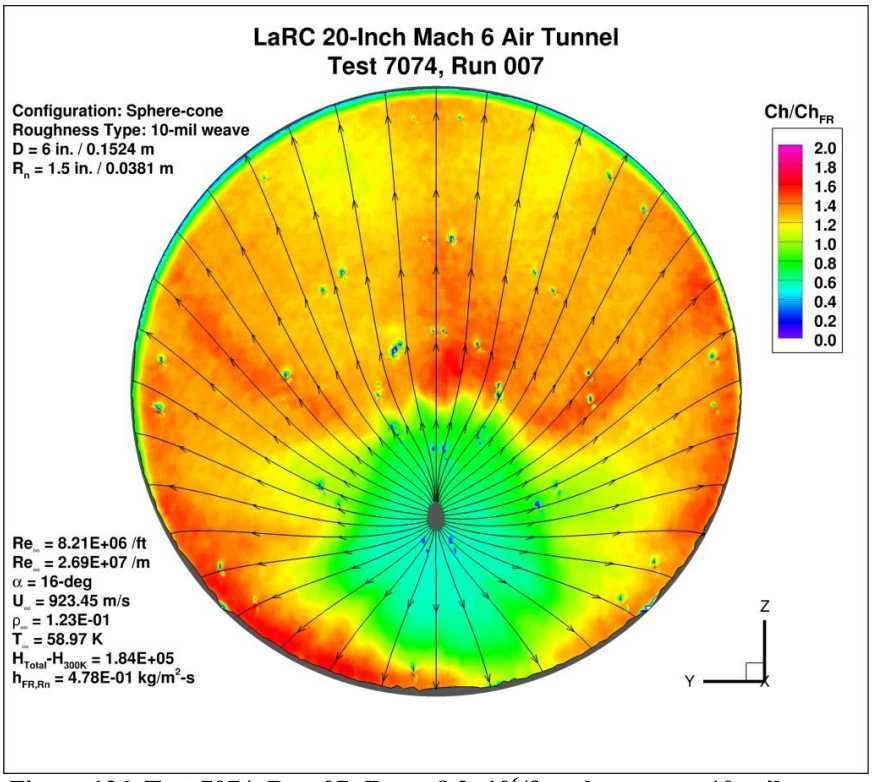


Figure 136. Test 7074, Run 07: $Re_\infty = 8.2\times10^6$/ft, sphere-cone, 10-mil weave.

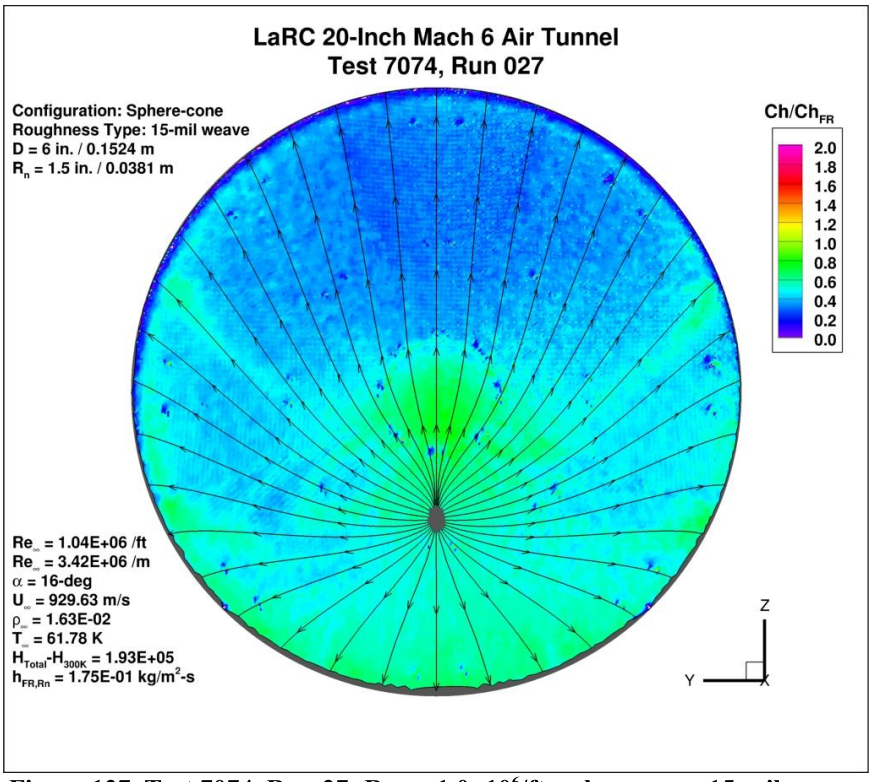


Figure 137. Test 7074, Run 27: $Re_\infty = 1.0\times10^6$/ft, sphere-cone, 15-mil weave.

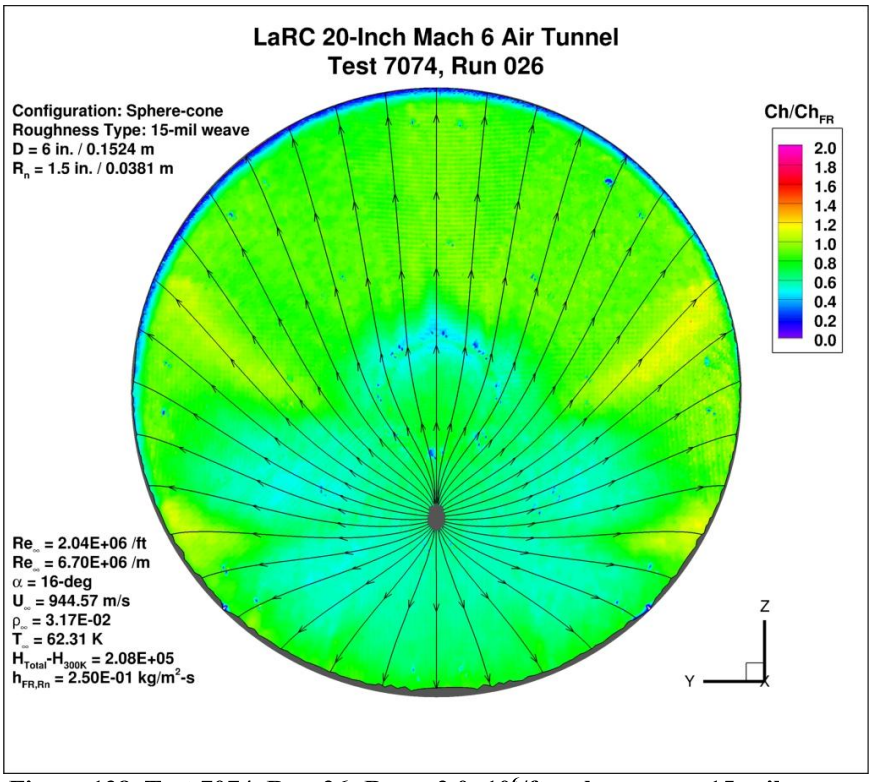


Figure 138. Test 7074, Run 26: $Re_\infty = 2.0\times10^6$/ft, sphere-cone, 15-mil weave.

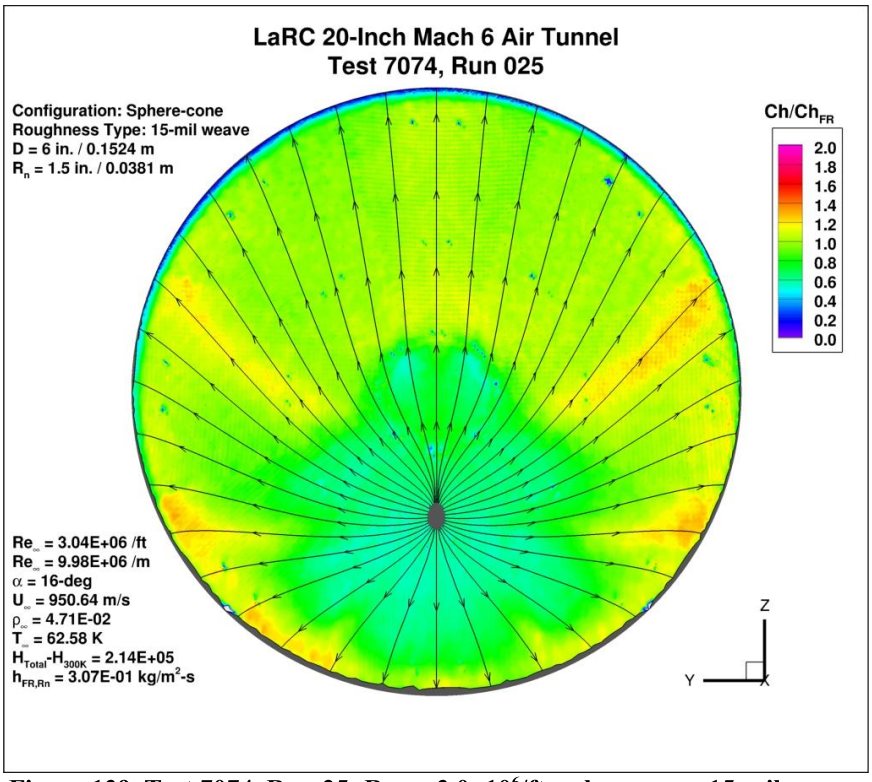


Figure 139. Test 7074, Run 25: $Re_\infty = 3.0\times10^6$/ft, sphere-cone, 15-mil weave.

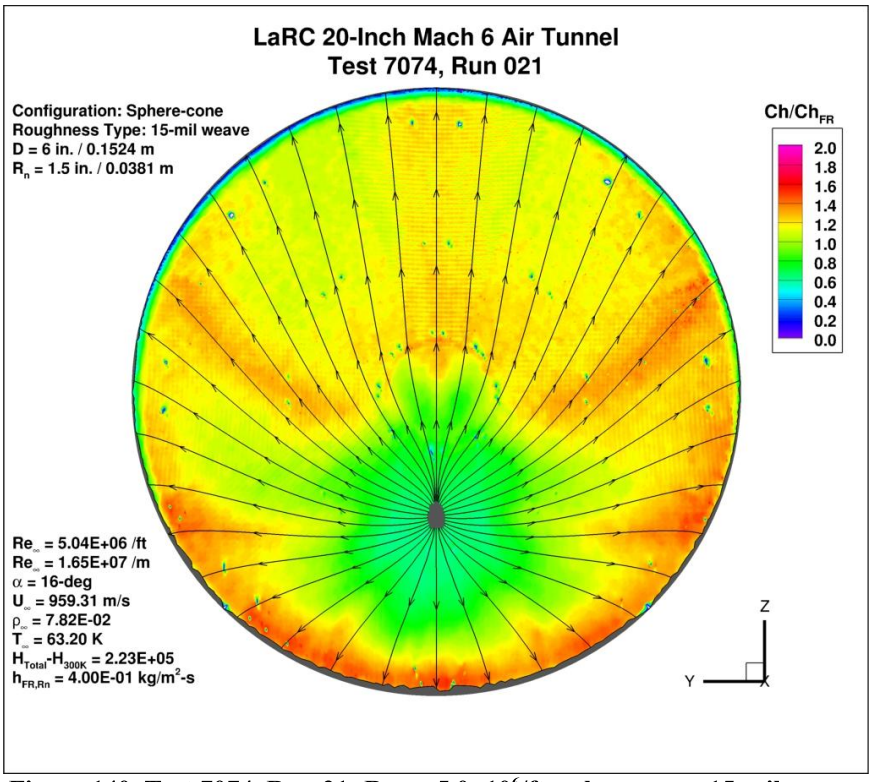


Figure 140. Test 7074, Run 21: $Re_\infty = 5.0\times10^6$/ft, sphere-cone, 15-mil weave.

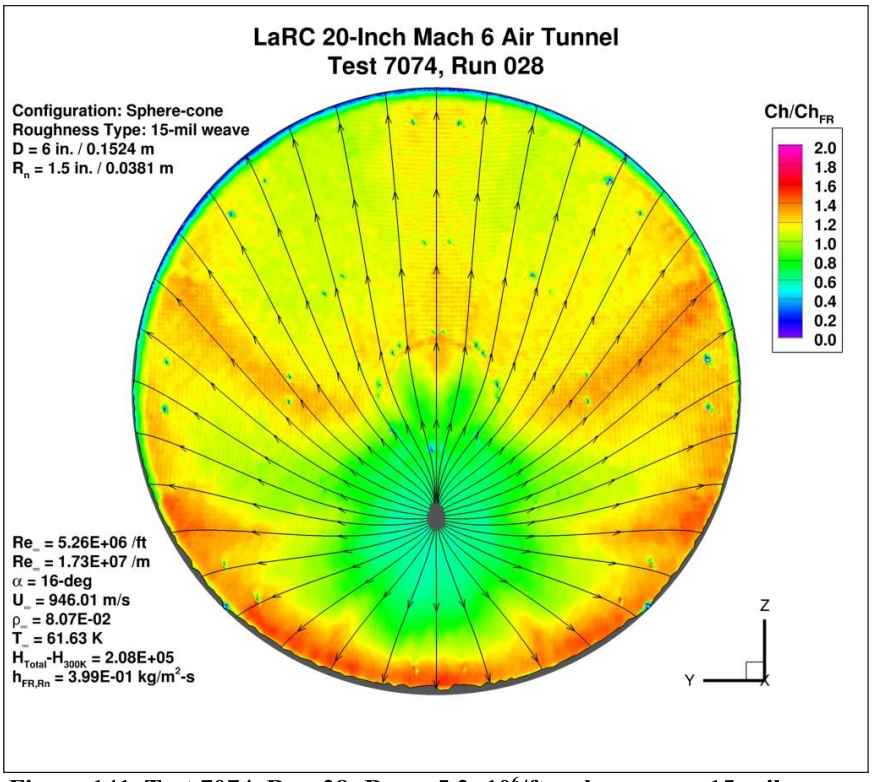


Figure 141. Test 7074, Run 28: $Re_\infty = 5.3\times10^6$/ft, sphere-cone, 15-mil weave.

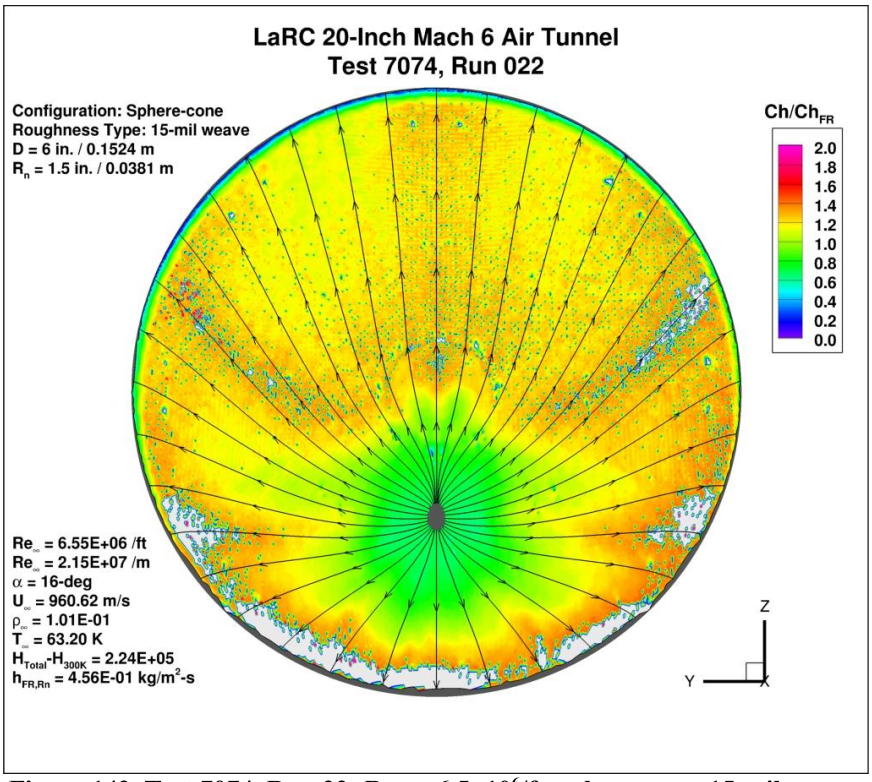


Figure 142. Test 7074, Run 22: $Re_\infty = 6.5\times10^6$/ft, sphere-cone, 15-mil weave.

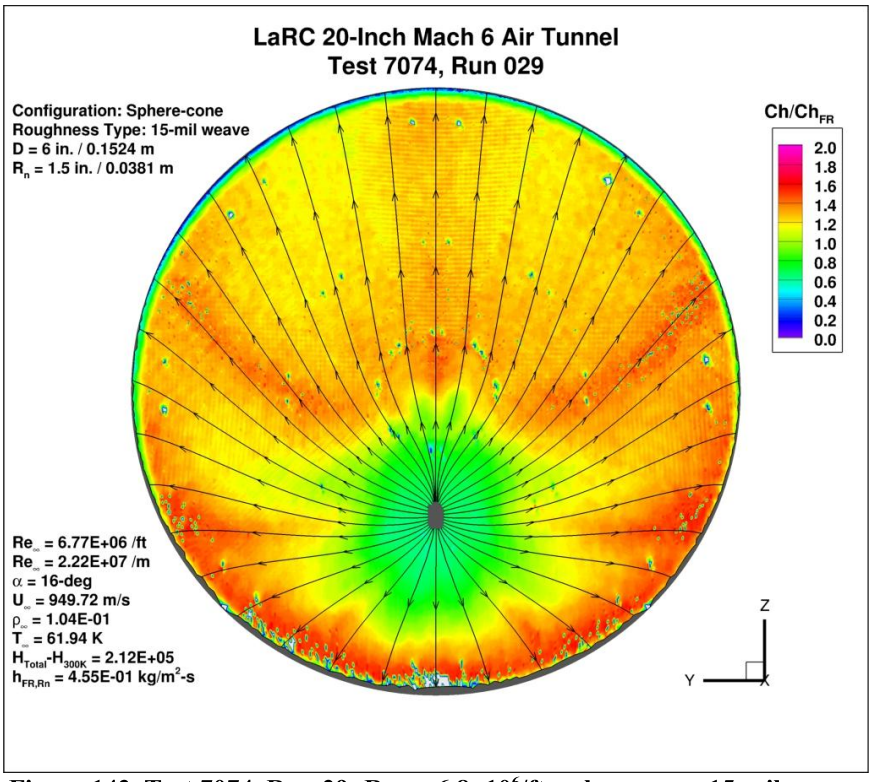


Figure 143. Test 7074, Run 29: $Re_\infty = 6.8\times10^6$/ft, sphere-cone, 15-mil weave.

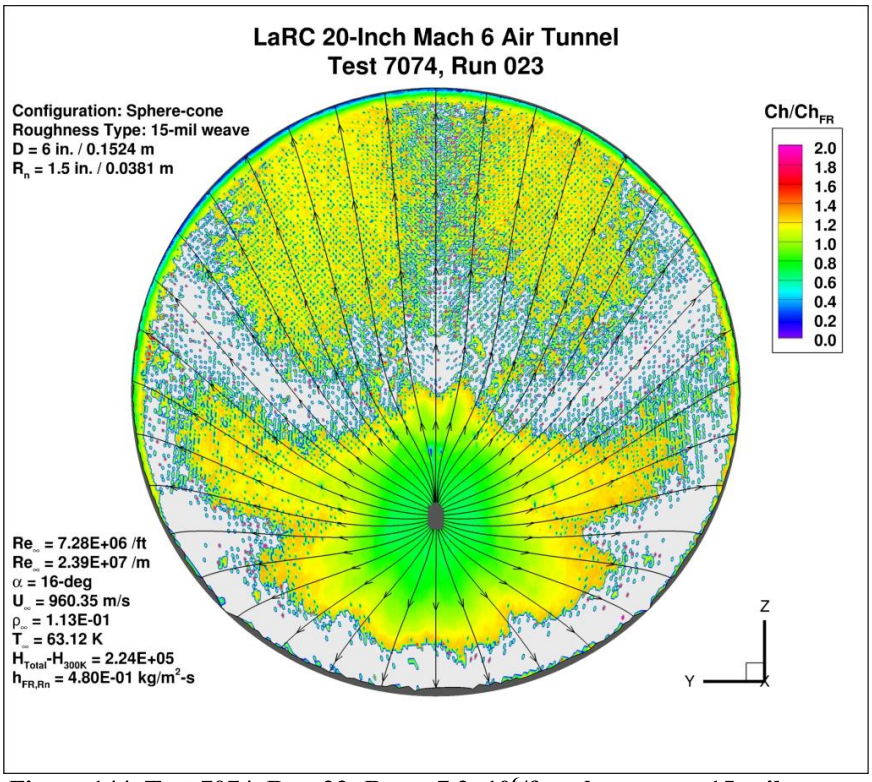


Figure 144. Test 7074, Run 23: $Re_\infty = 7.3\times10^6$/ft, sphere-cone, 15-mil weave.

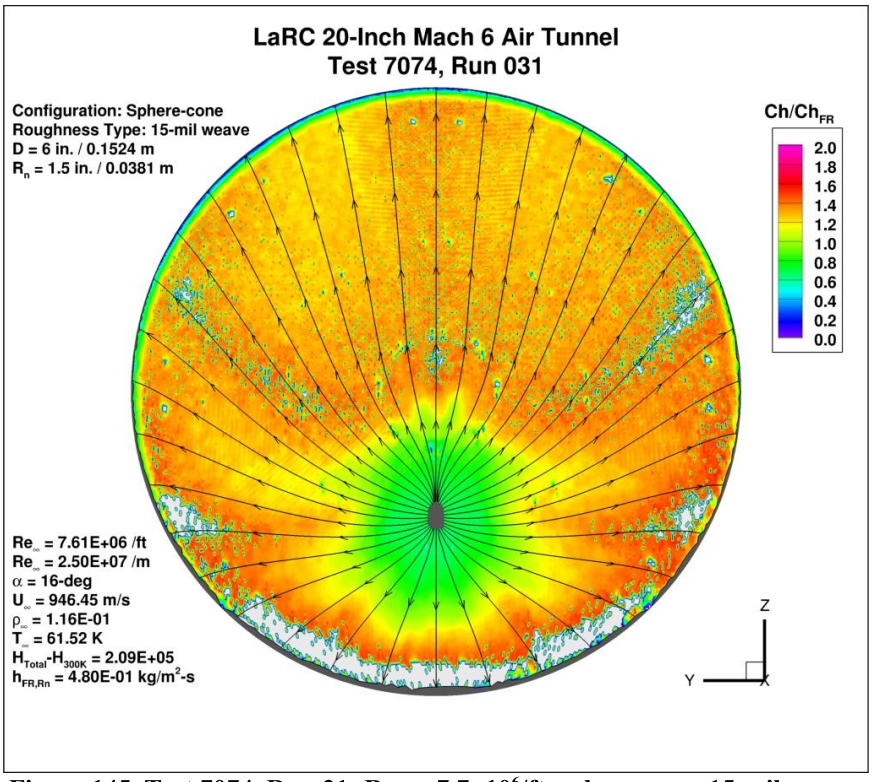


Figure 145. Test 7074, Run 31: $Re_\infty = 7.7\times10^6$/ft, sphere-cone, 15-mil weave.

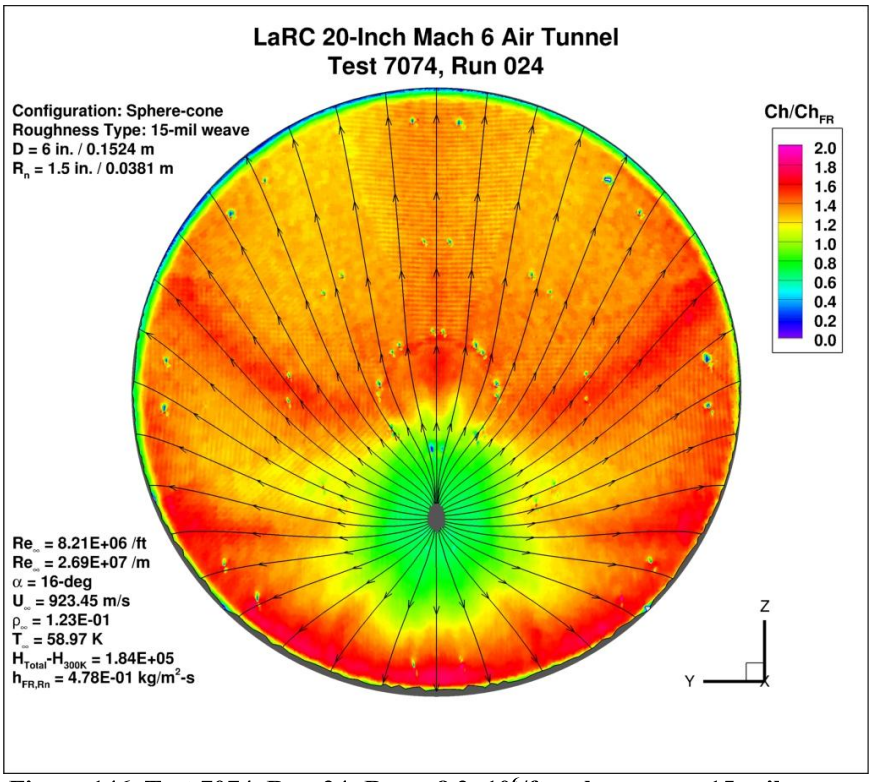


Figure 146. Test 7074, Run 24: $Re_\infty = 8.2\times10^6$/ft, sphere-cone, 15-mil weave.

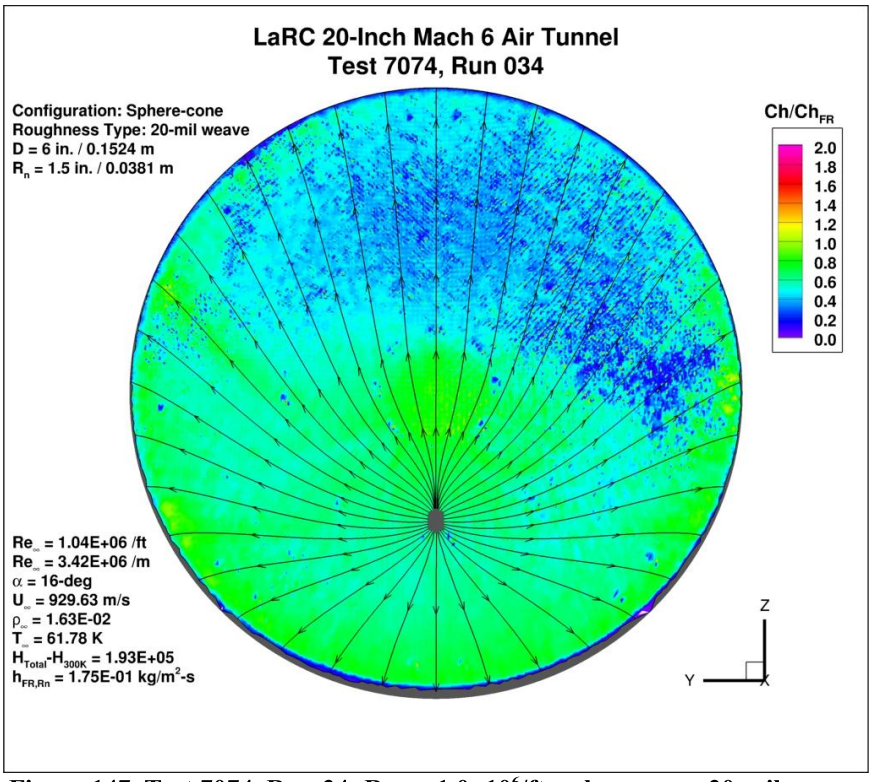


Figure 147. Test 7074, Run 34: $Re_\infty = 1.0\times10^6$/ft, sphere-cone, 20-mil weave.

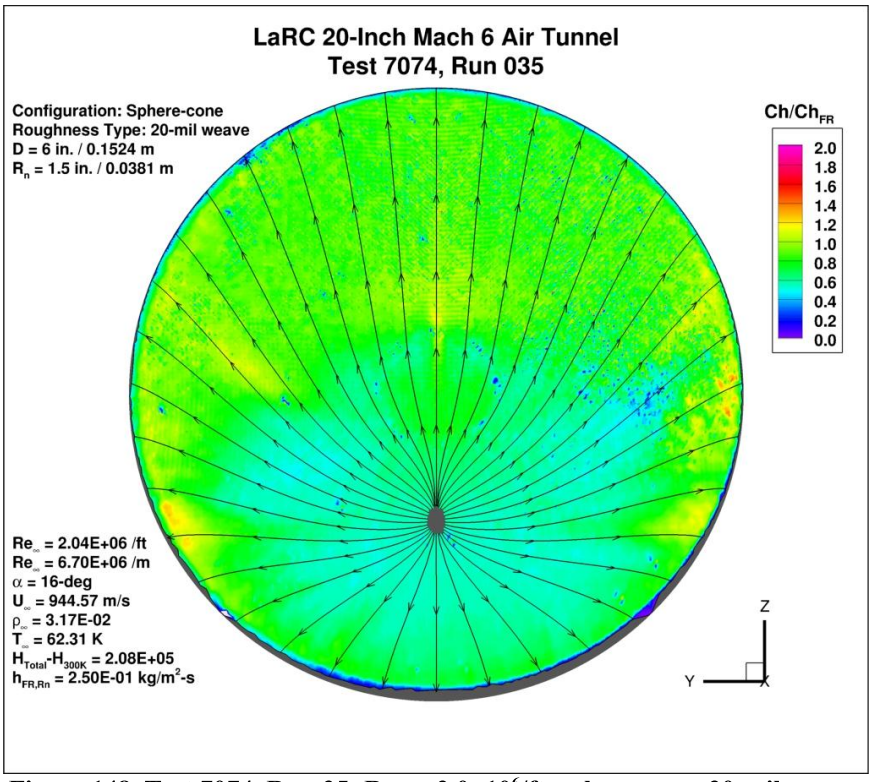


Figure 148. Test 7074, Run 35: $Re_\infty = 2.0\times10^6$/ft, sphere-cone, 20-mil weave.

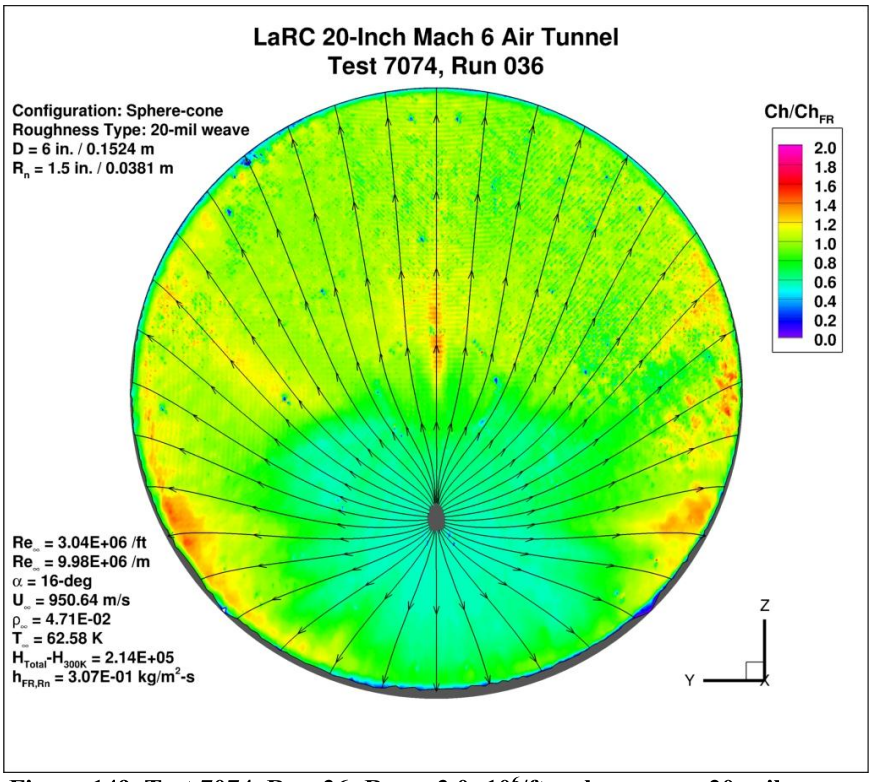


Figure 149. Test 7074, Run 36: $Re_\infty = 3.0\times10^6$/ft, sphere-cone, 20-mil weave.

(Condition was not run)

Figure 150. Test 7074, Run XX: $Re_\infty = 5.0\times10^6$/ft, sphere-cone, 20-mil weave.

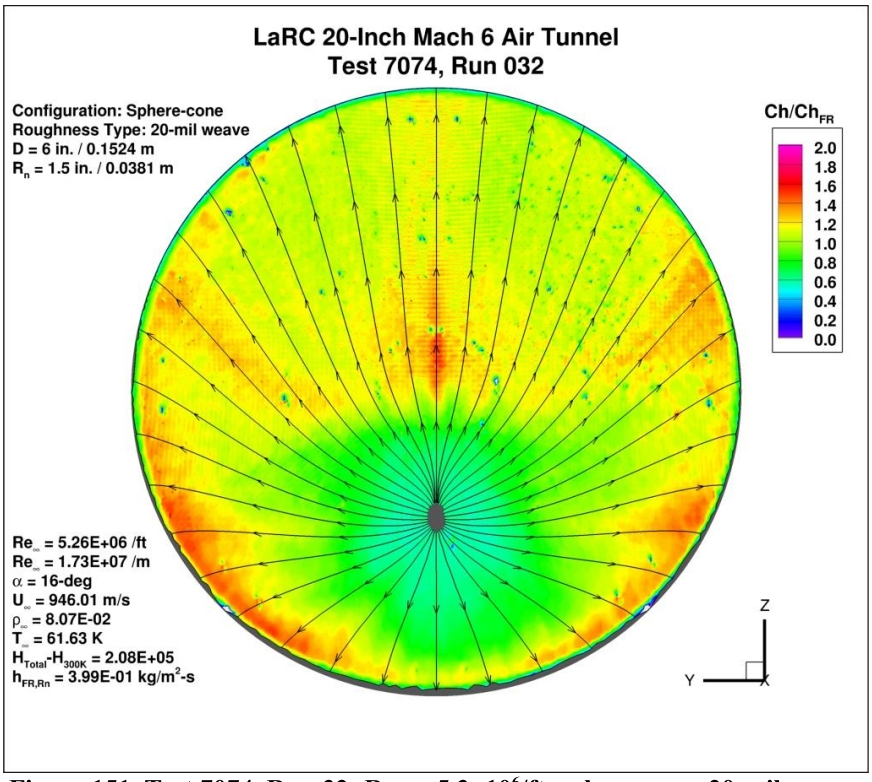
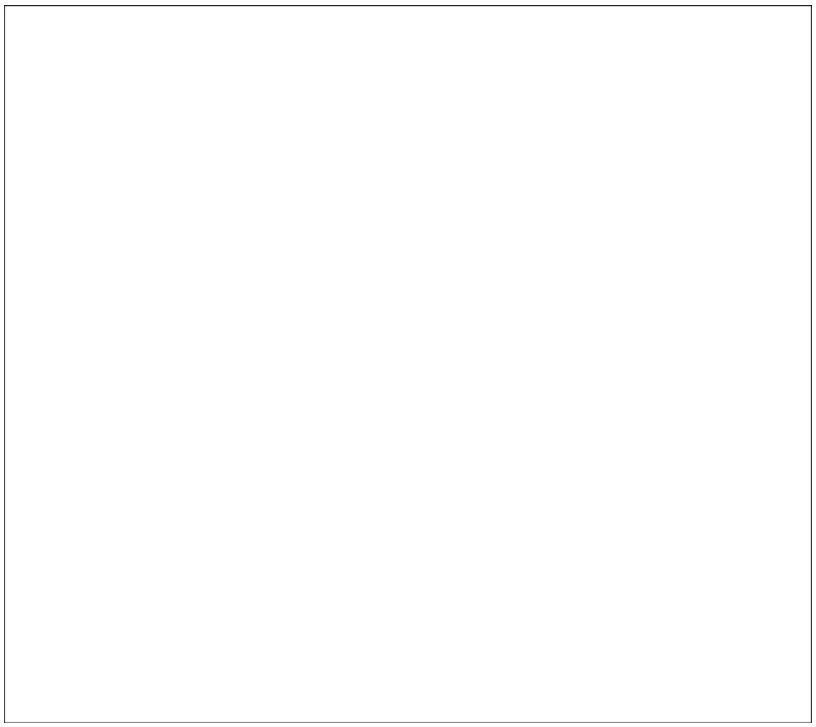


Figure 151. Test 7074, Run 32: $Re_\infty = 5.3\times10^6$/ft, sphere-cone, 20-mil weave.



(Condition was not run)

Figure 152. Test 7074, Run XX: $Re_\infty = 6.5\times10^6$/ft, sphere-cone, 20-mil weave.

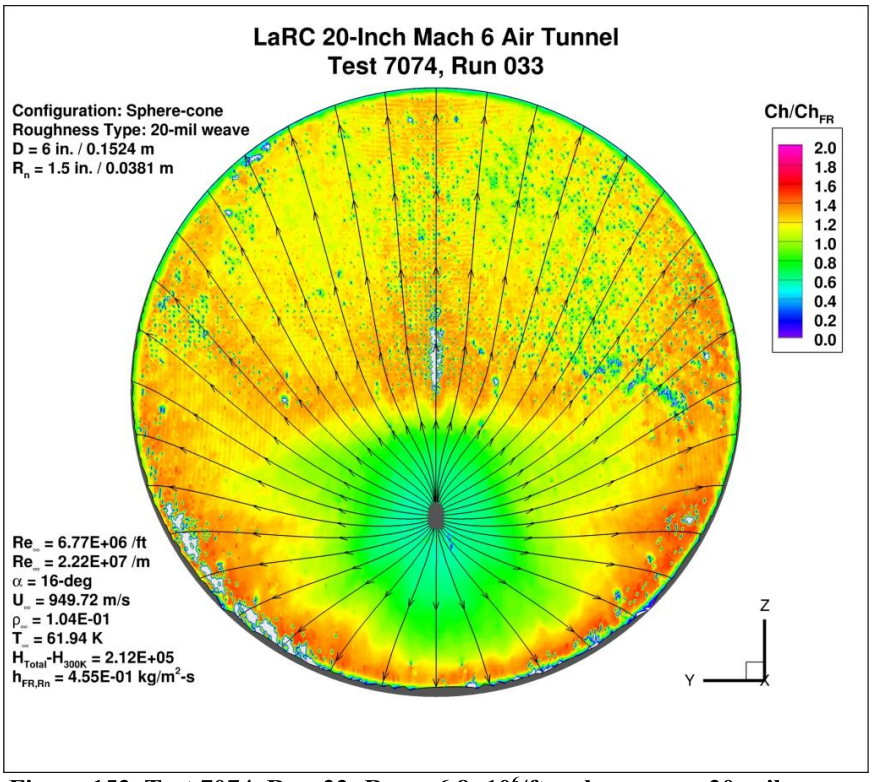


Figure 153. Test 7074, Run 33: $Re_\infty = 6.8\times10^6$/ft, sphere-cone, 20-mil weave.

(Condition was not run)

Figure 154. Test 7074, Run XX: $Re_\infty = 7.3\times10^6$/ft, sphere-cone, 20-mil weave.

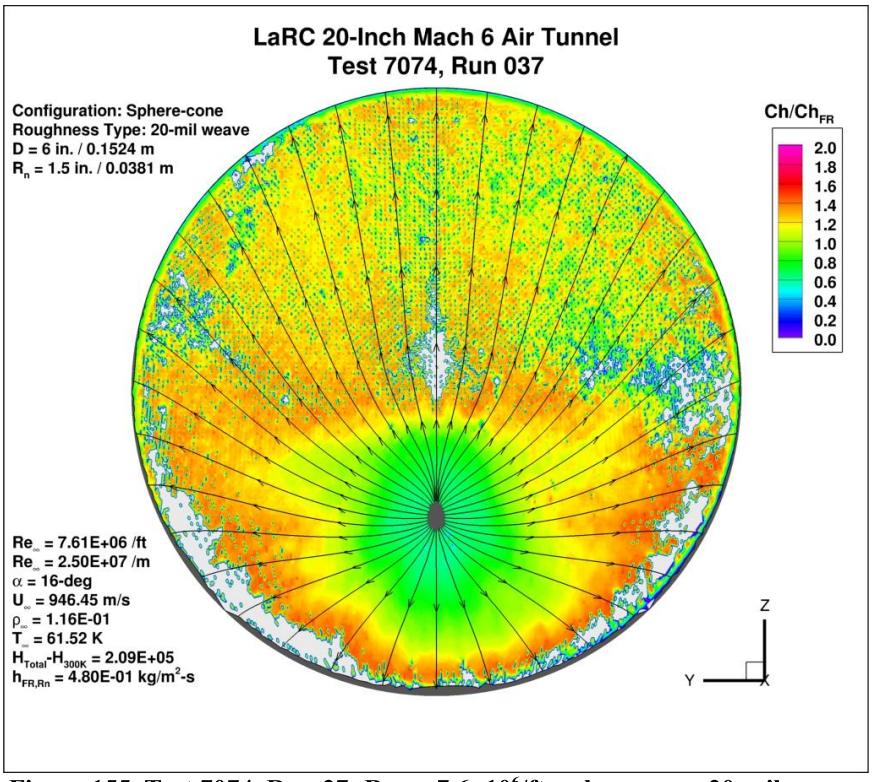


Figure 155. Test 7074, Run 37: $Re_\infty = 7.6\times10^6$/ft, sphere-cone, 20-mil weave.

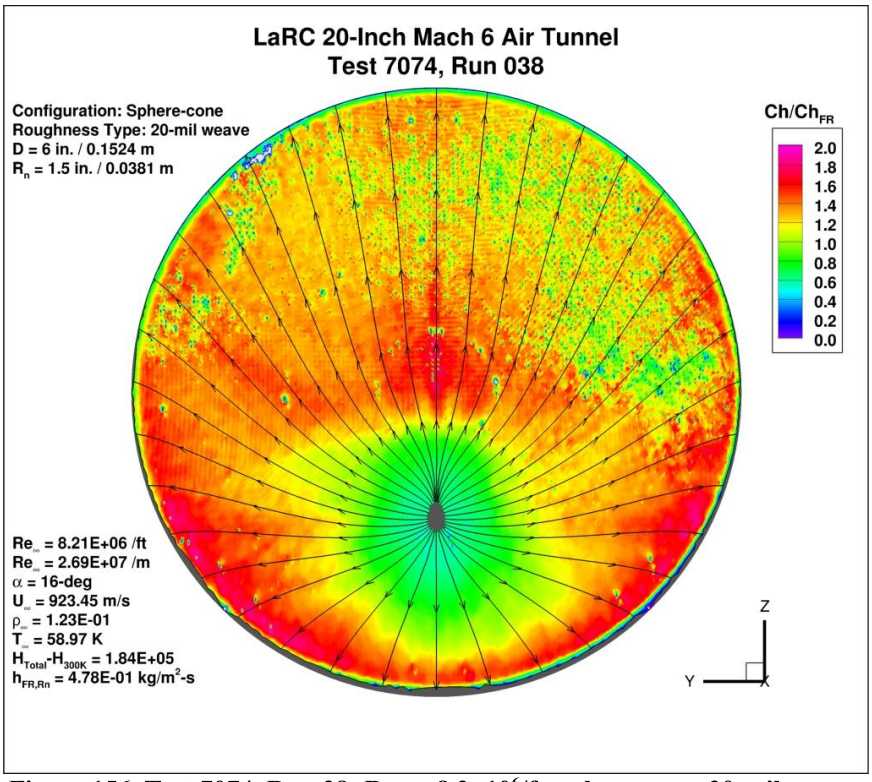


Figure 156. Test 7074, Run 38: $Re_\infty = 8.2\times10^6$/ft, sphere-cone, 20-mil weave.

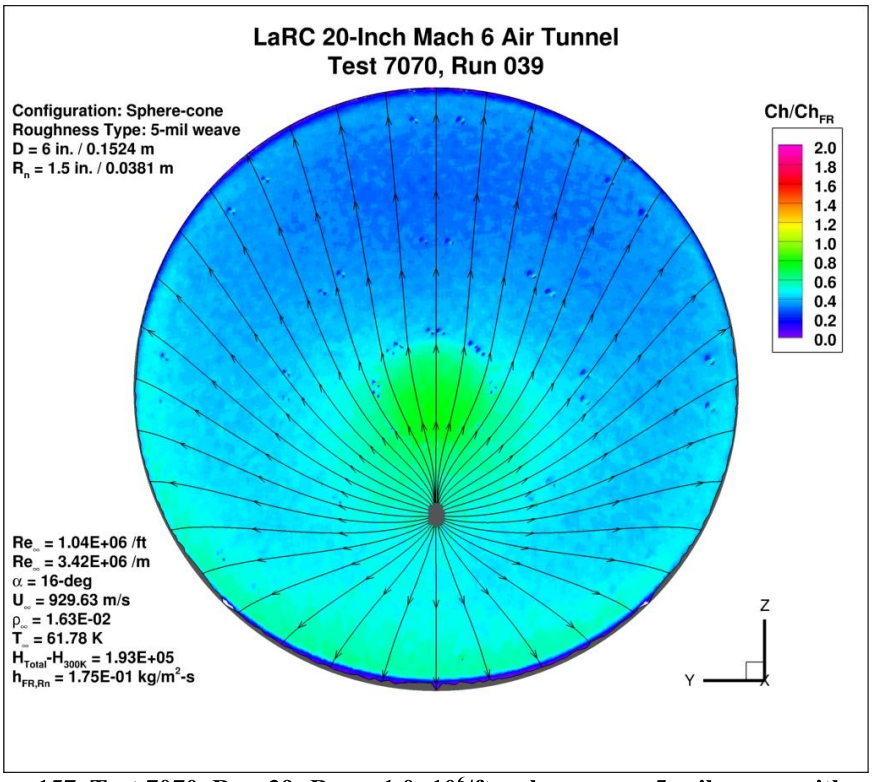


Figure 157. Test 7070, Run 39: $Re_\infty = 1.0\times10^6$/ft, sphere-cone, 5-mil weave with seam.

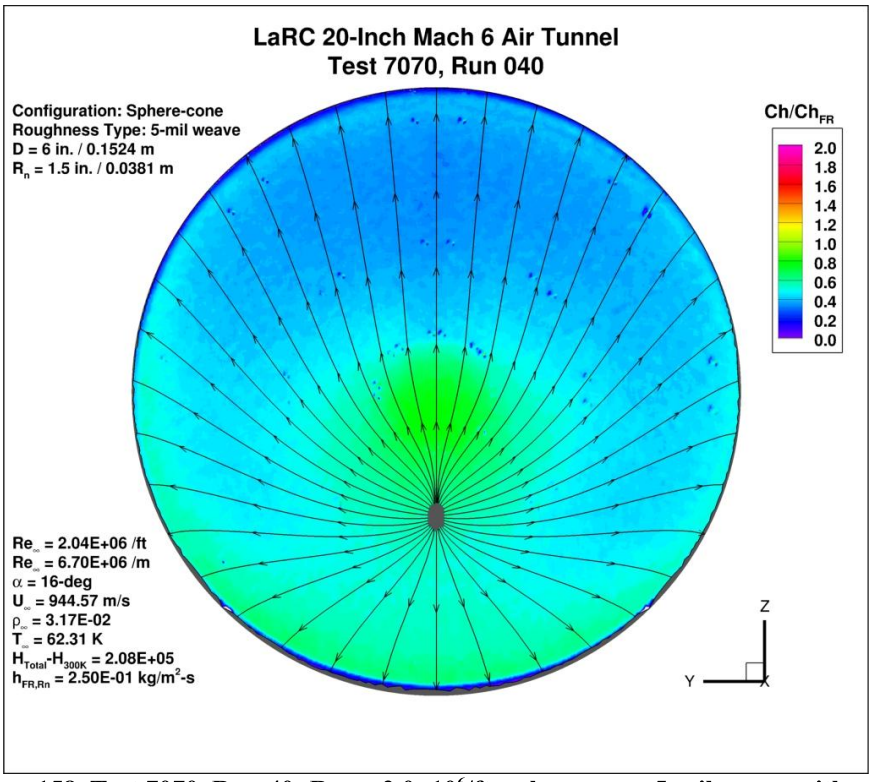


Figure 158. Test 7070, Run 40: $Re_\infty = 2.0\times10^6$/ft, sphere-cone, 5-mil weave with seam.

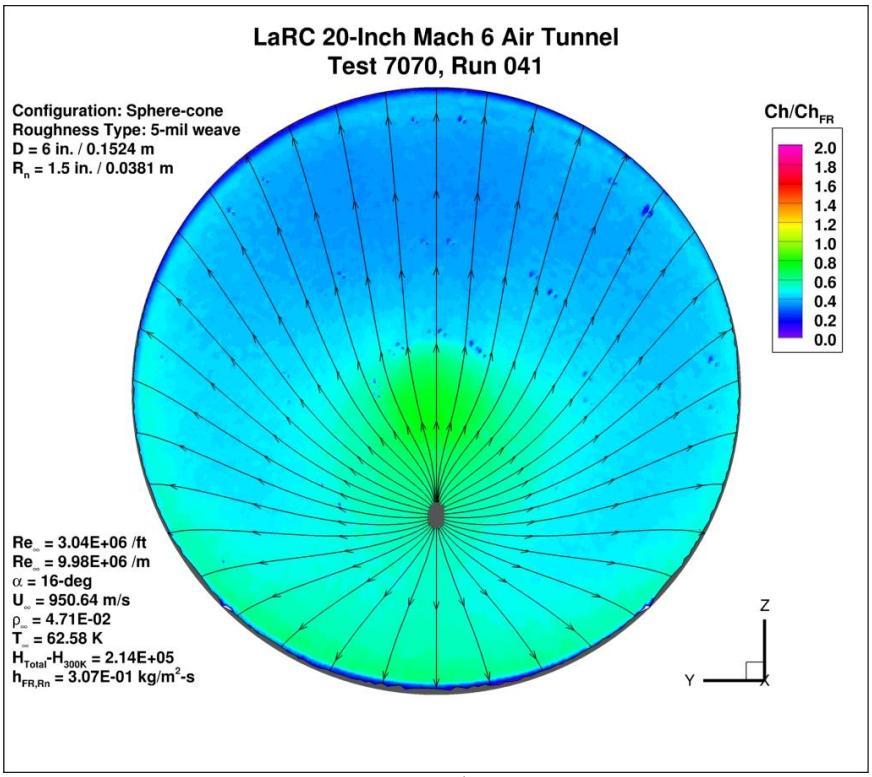


Figure 159. Test 7070, Run 41: $Re_\infty = 3.0\times10^6$/ft, sphere-cone, 5-mil weave with seam.

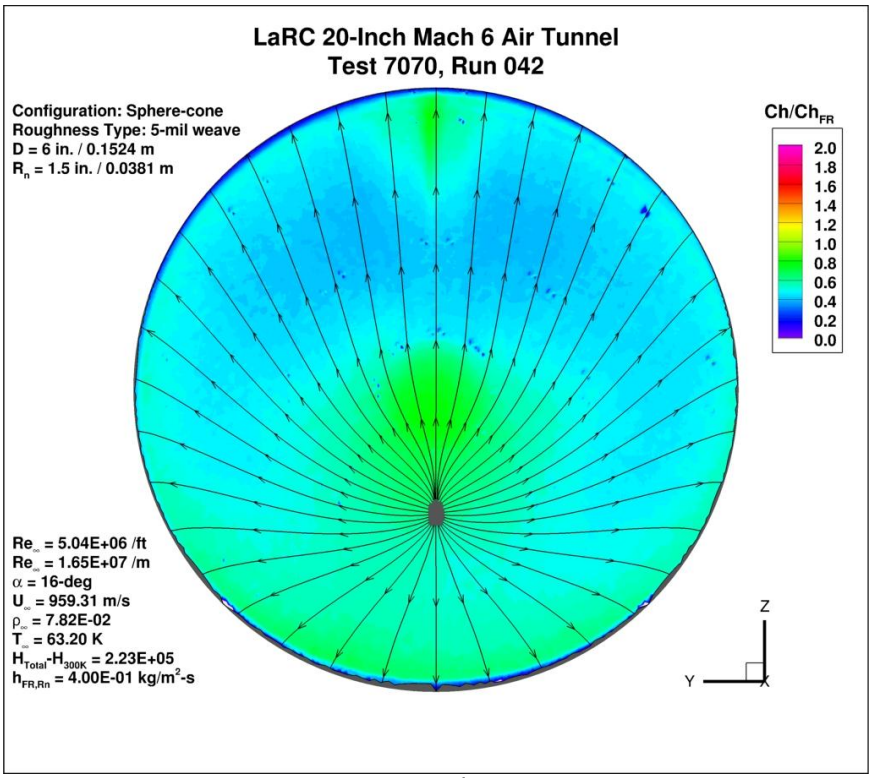
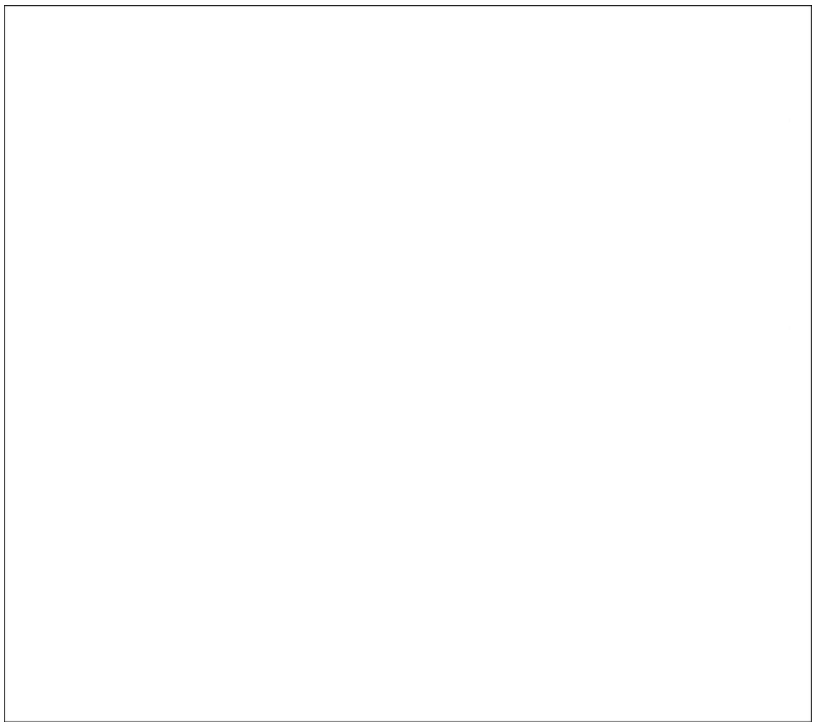


Figure 160. Test 7070, Run 42: $Re_\infty = 5.0\times10^6$/ft, sphere-cone, 5-mil weave with seam.



(Condition was not run)

Figure 161. Test 7070, Run XX: $Re_\infty = 5.3\times10^6$/ft, sphere-cone, 5-mil weave with seam.

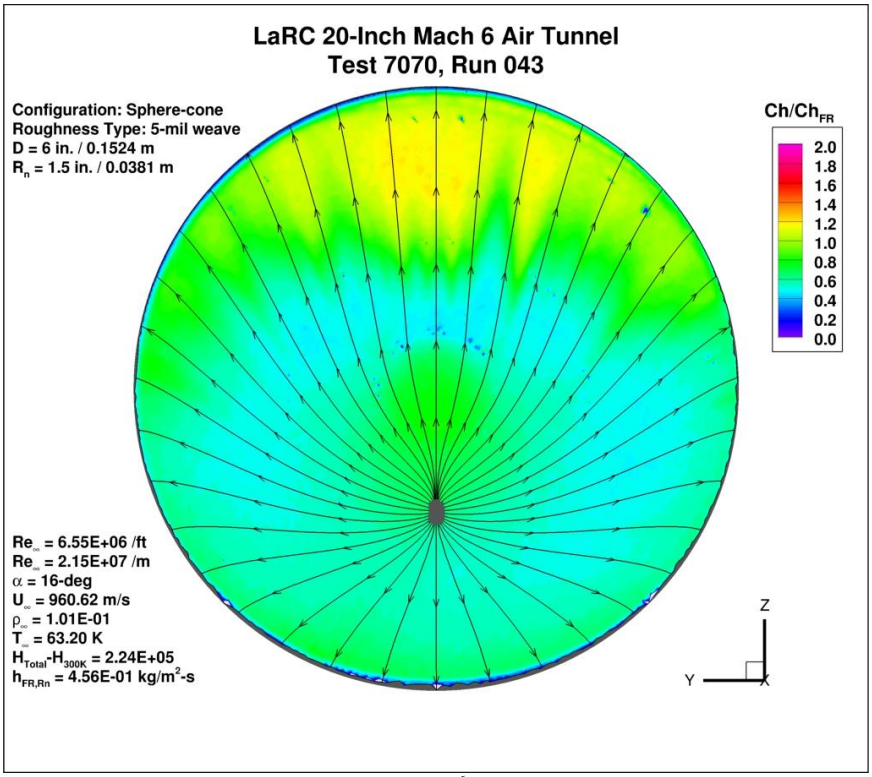
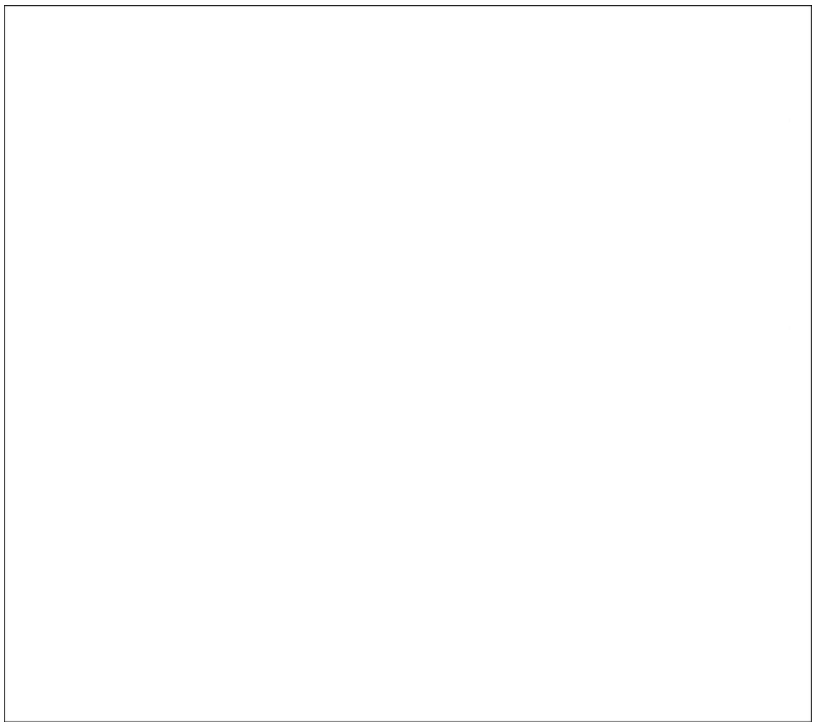


Figure 162. Test 7070, Run 43: $Re_\infty = 6.5\times10^6$/ft, sphere-cone, 5-mil weave with seam.



(Condition was not run)

Figure 163. Test 7070, Run XX: $Re_\infty = 6.8\times10^6$/ft, sphere-cone, 5-mil weave with seam.

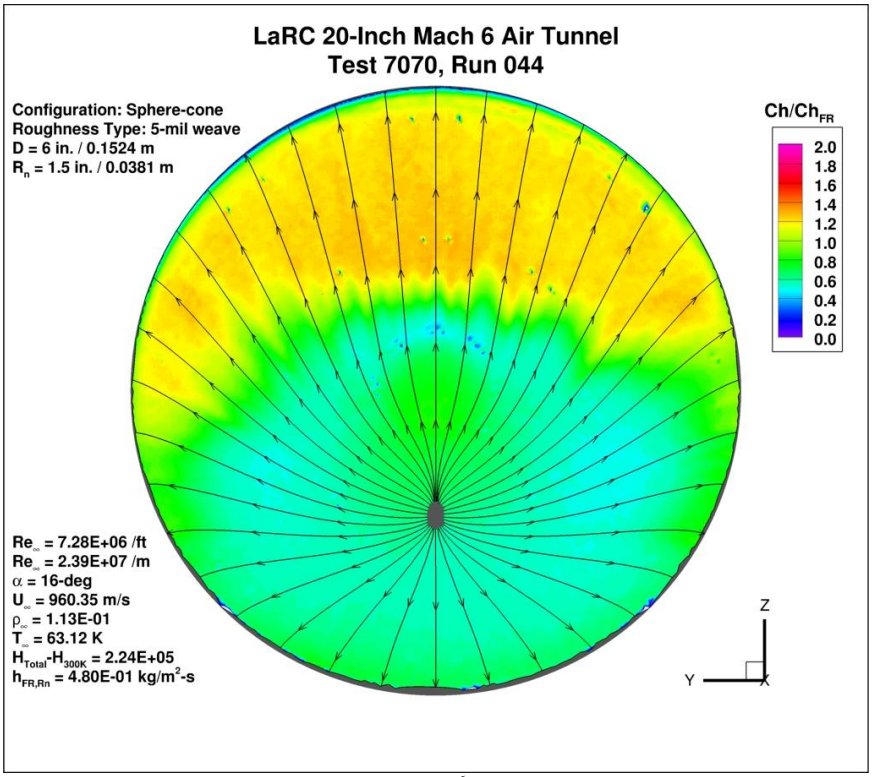


Figure 164. Test 7070, Run 44: $Re_\infty = 7.2\times10^6$/ft, sphere-cone, 5-mil weave with seam.

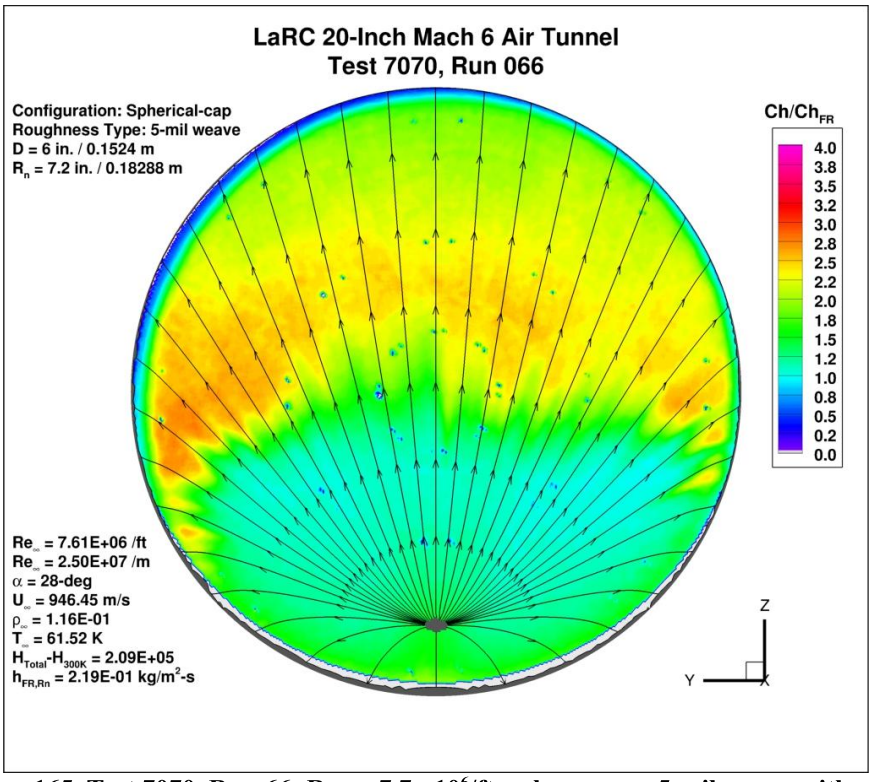


Figure 165. Test 7070, Run 66: $Re_\infty = 7.7 \times 10^6$/ft, sphere-cone, 5-mil weave with seam.

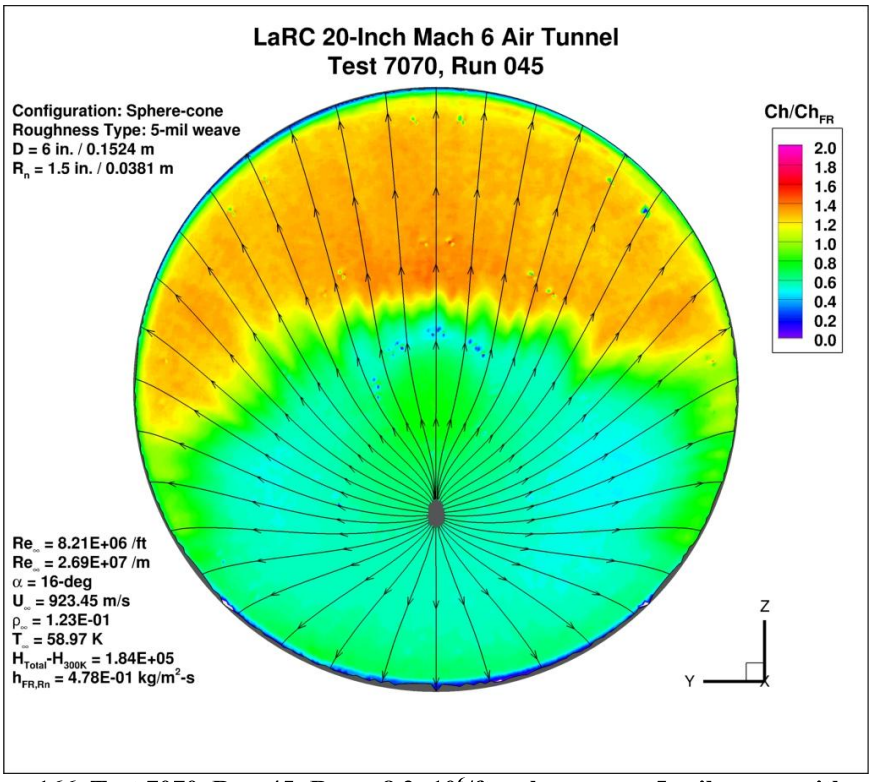


Figure 166. Test 7070, Run 45: $Re_\infty = 8.2 \times 10^6$/ft, sphere-cone, 5-mil weave with seam.

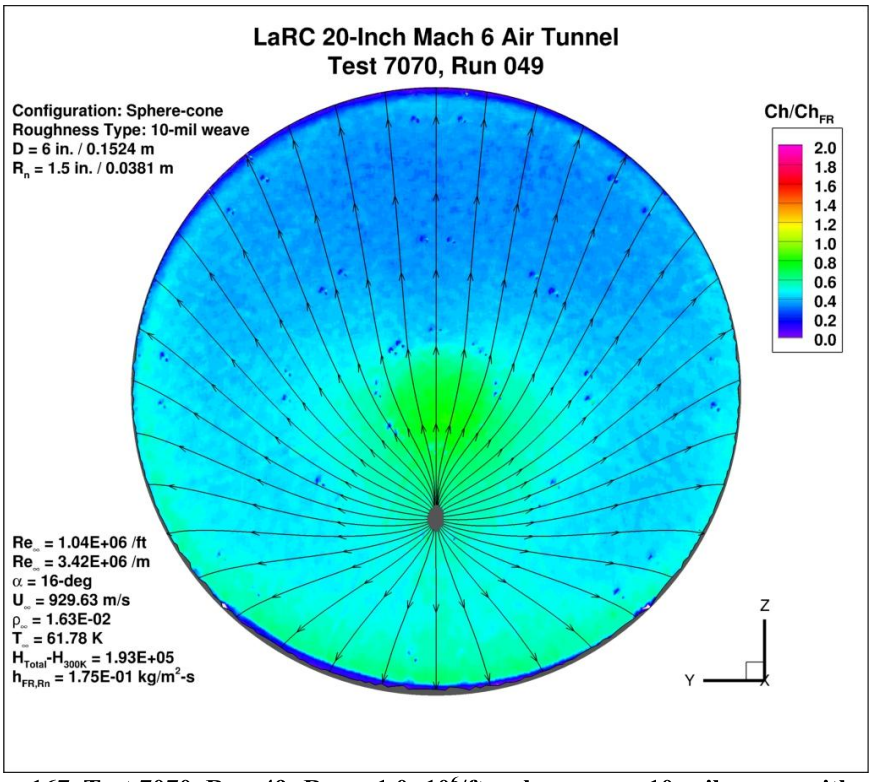


Figure 167. Test 7070, Run 49: $Re_\infty = 1.0\times10^6$/ft, sphere-cone, 10-mil weave with seam.

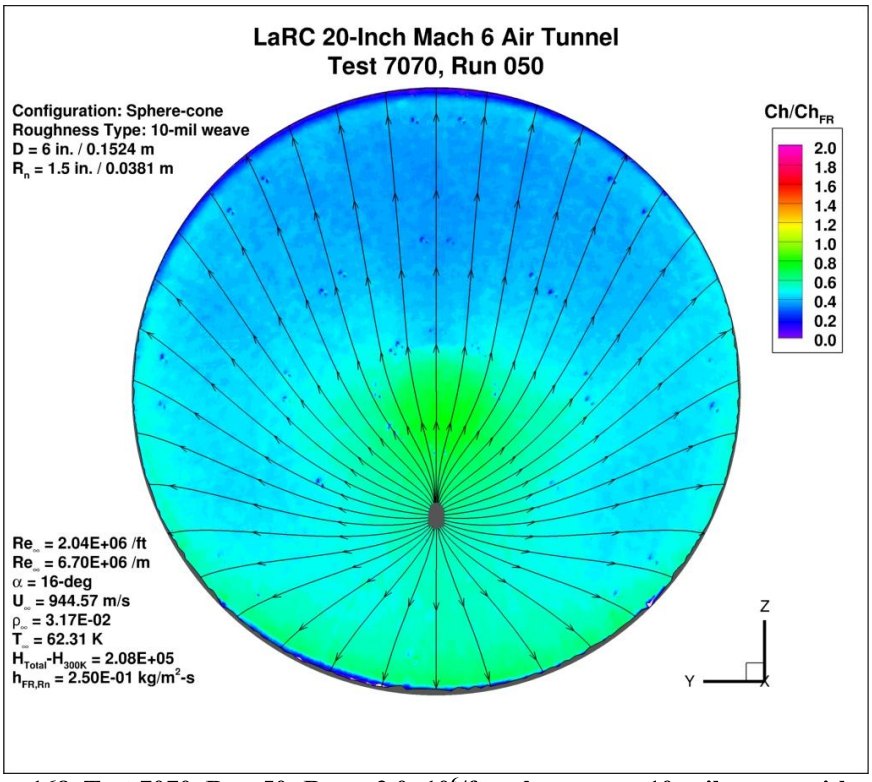


Figure 168. Test 7070, Run 50: $Re_\infty = 2.0\times10^6$/ft, sphere-cone, 10-mil weave with seam.

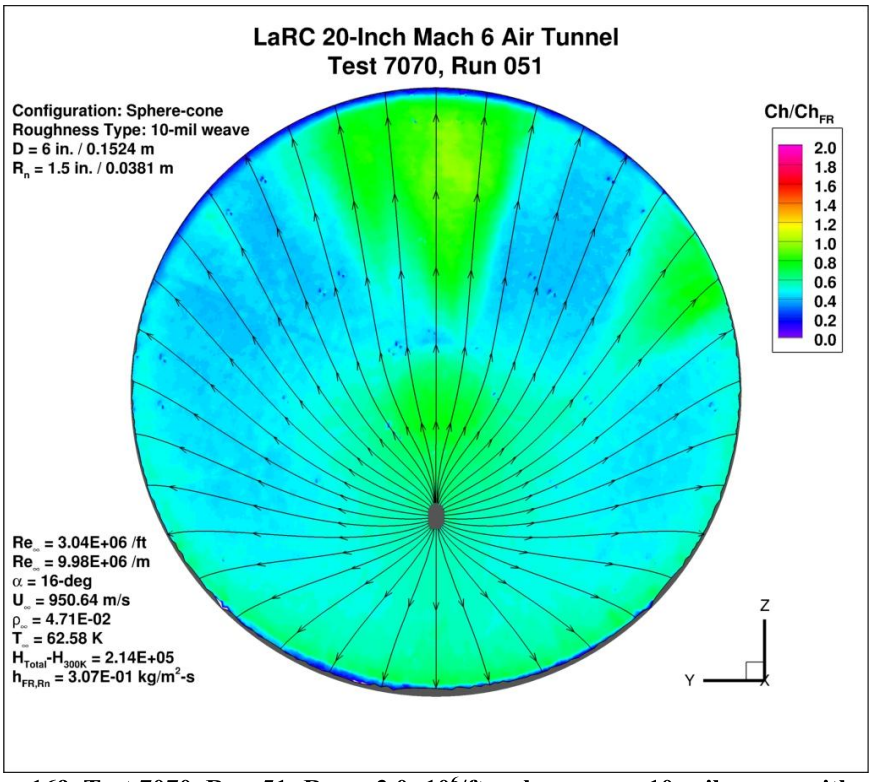


Figure 169. Test 7070, Run 51: $Re_\infty = 3.0\times10^6$/ft, sphere-cone, 10-mil weave with seam.

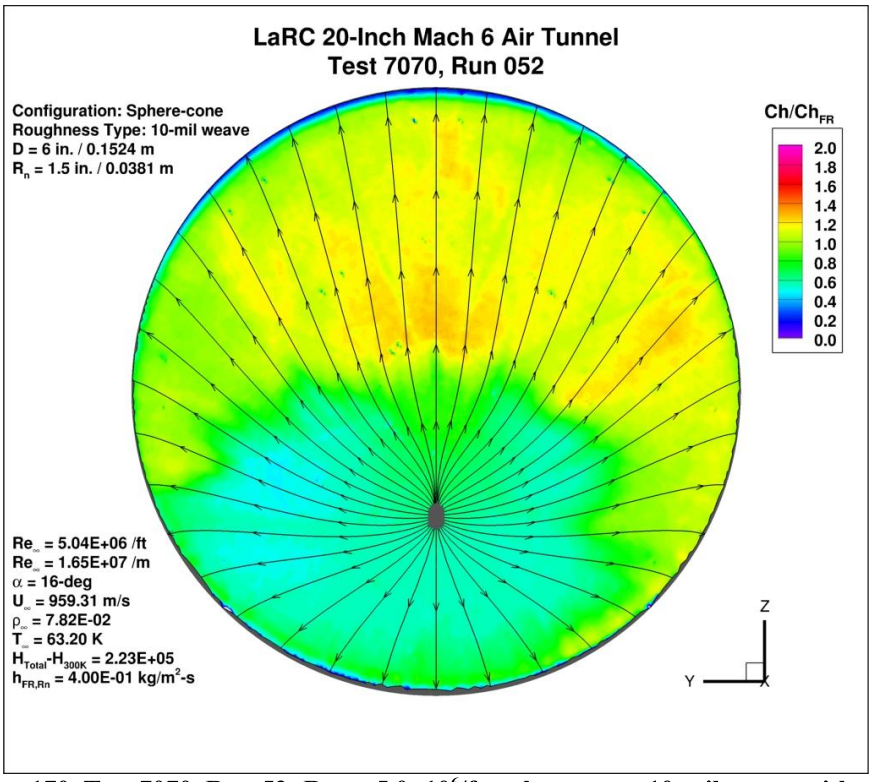
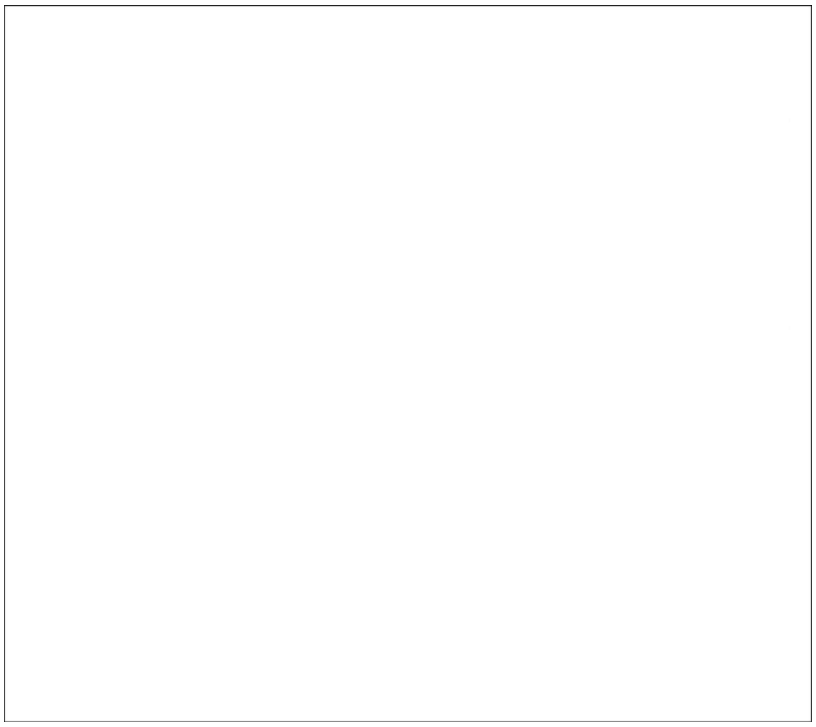


Figure 170. Test 7070, Run 52: $Re_\infty = 5.0\times10^6$/ft, sphere-cone, 10-mil weave with seam.



(Condition was not run)

Figure 171. Test 7070, Run XX: Re_∞ = 5.3×10^6/ft, sphere-cone, 10-mil weave with seam.

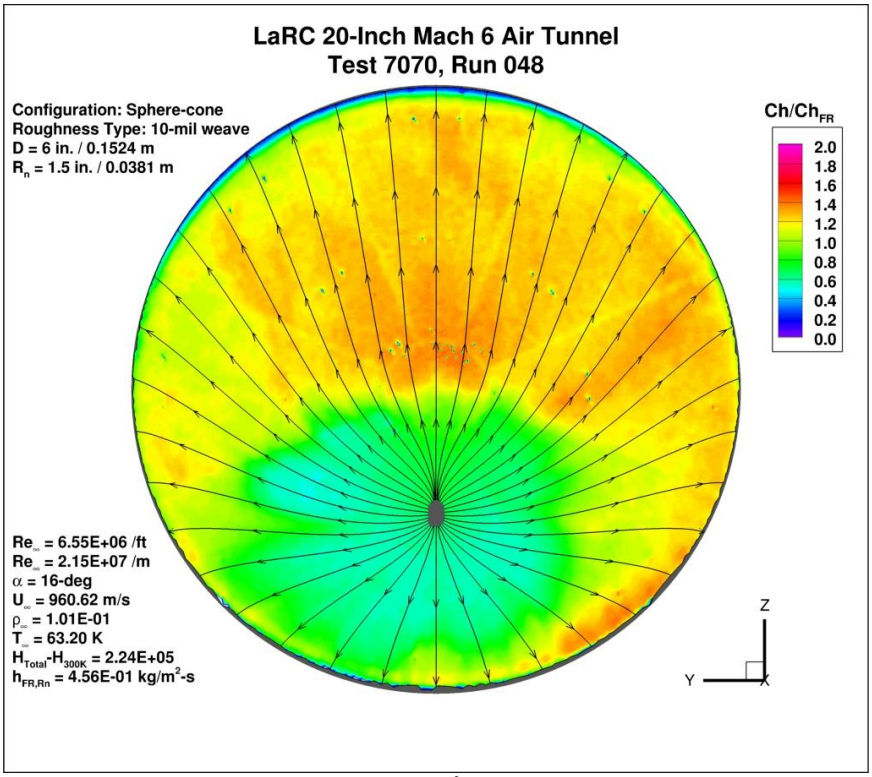


Figure 172. Test 7070, Run 48: Re_∞ = 6.5×10^6/ft, sphere-cone, 10-mil weave with seam.

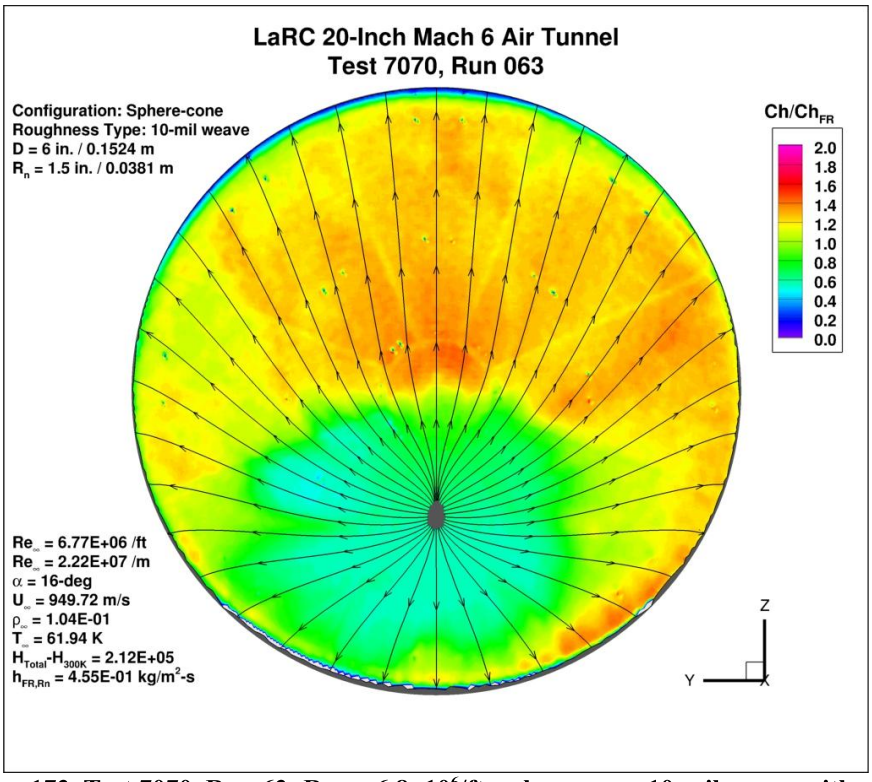


Figure 173. Test 7070, Run 63: $Re_\infty = 6.8\times10^6$/ft, sphere-cone, 10-mil weave with seam.

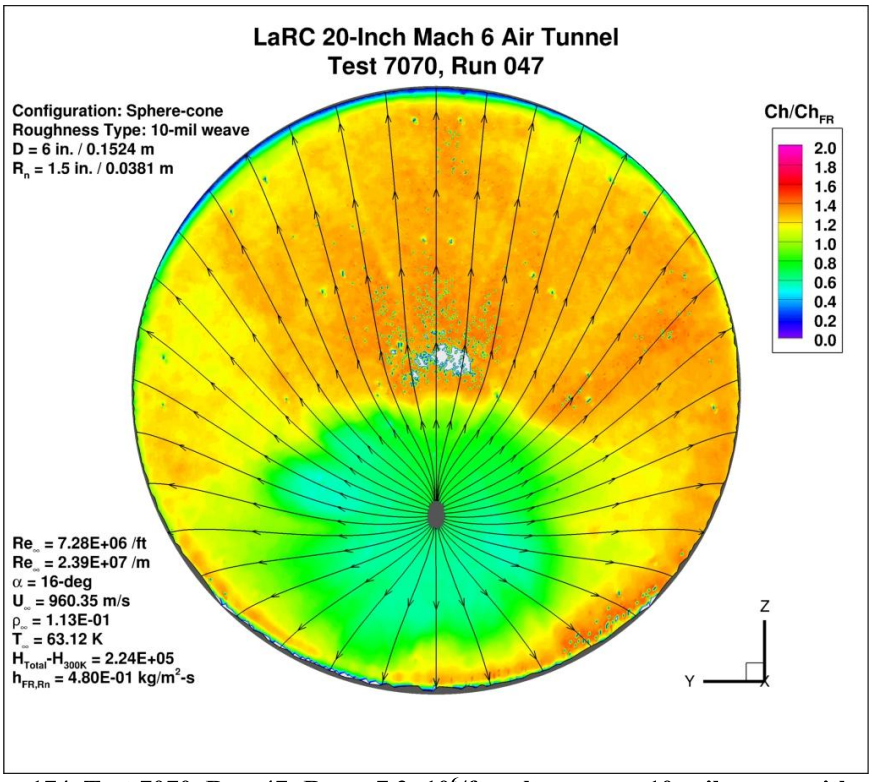


Figure 174. Test 7070, Run 47: $Re_\infty = 7.3\times10^6$/ft, sphere-cone, 10-mil weave with seam.

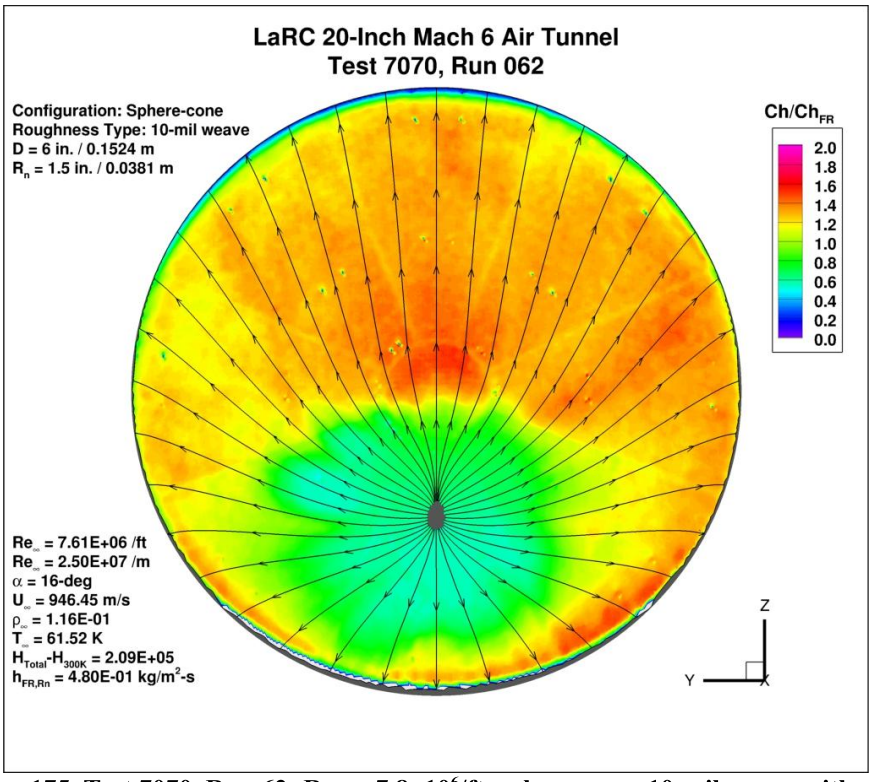


Figure 175. Test 7070, Run 62: $Re_\infty = 7.8\times10^6$/ft, sphere-cone, 10-mil weave with seam.

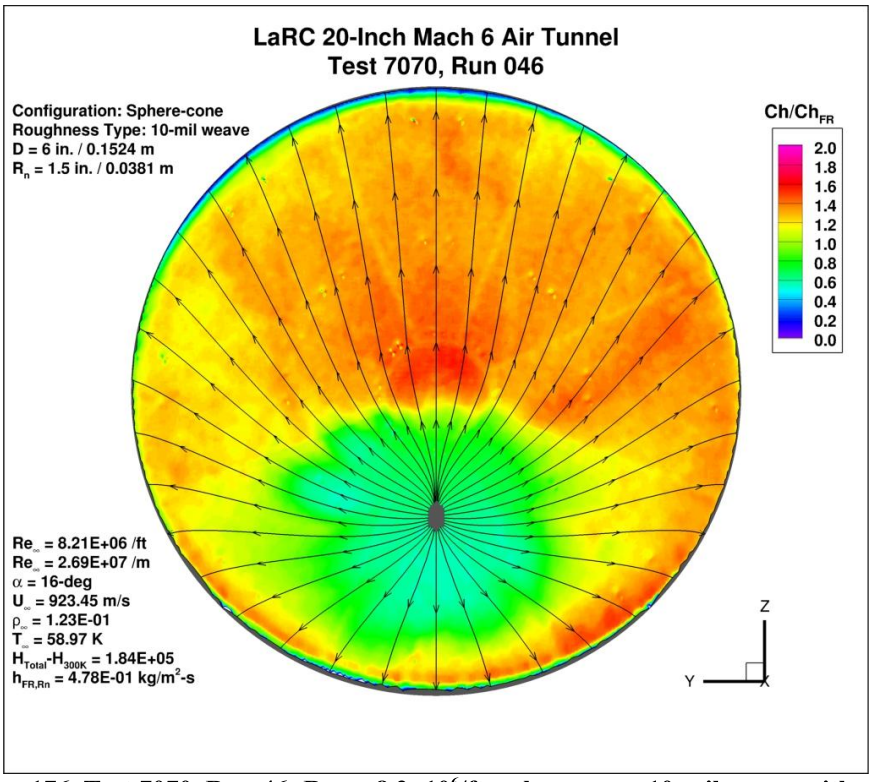


Figure 176. Test 7070, Run 46: $Re_\infty = 8.2\times10^6$/ft, sphere-cone, 10-mil weave with seam.

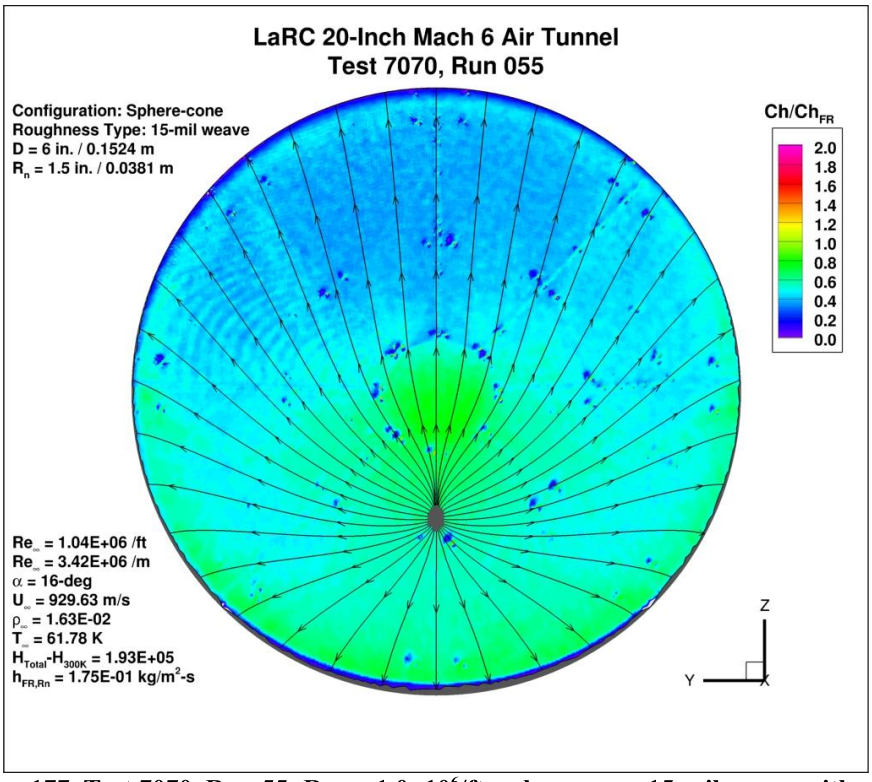


Figure 177. Test 7070, Run 55: $Re_\infty = 1.0\times10^6$/ft, sphere-cone, 15-mil weave with seam.

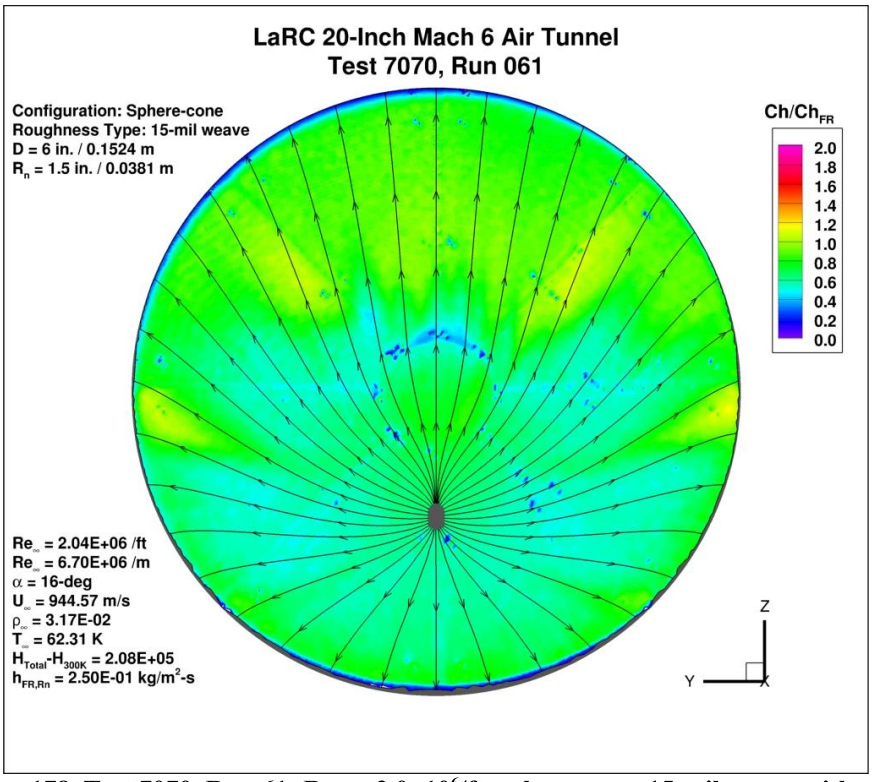


Figure 178. Test 7070, Run 61: $Re_\infty = 2.0\times10^6$/ft, sphere-cone, 15-mil weave with seam.

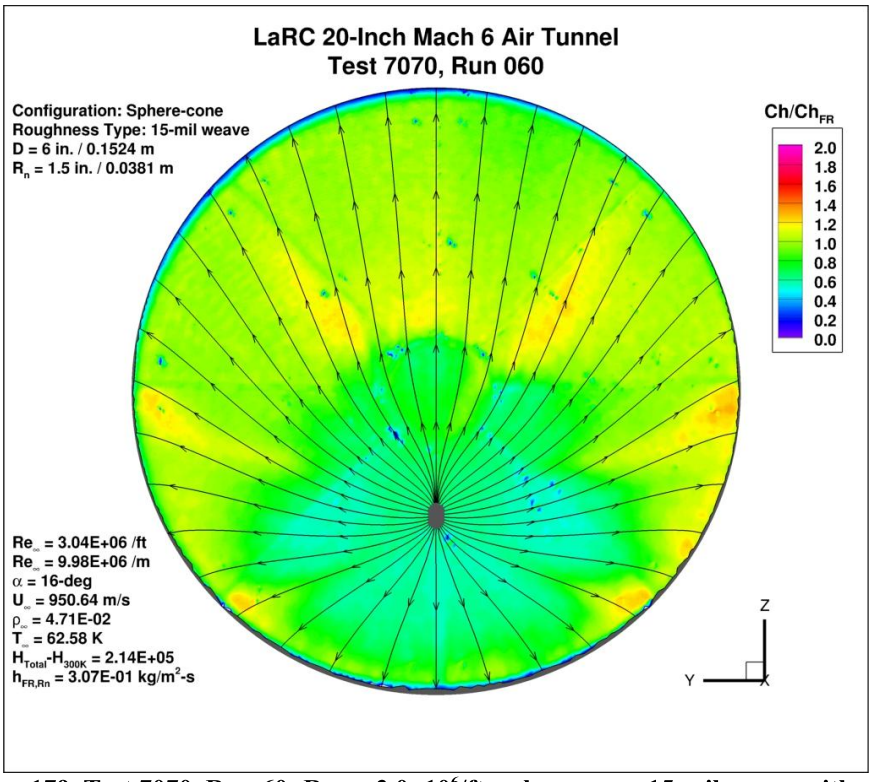


Figure 179. Test 7070, Run 60: $Re_\infty = 3.0\times10^6$/ft, sphere-cone, 15-mil weave with seam.

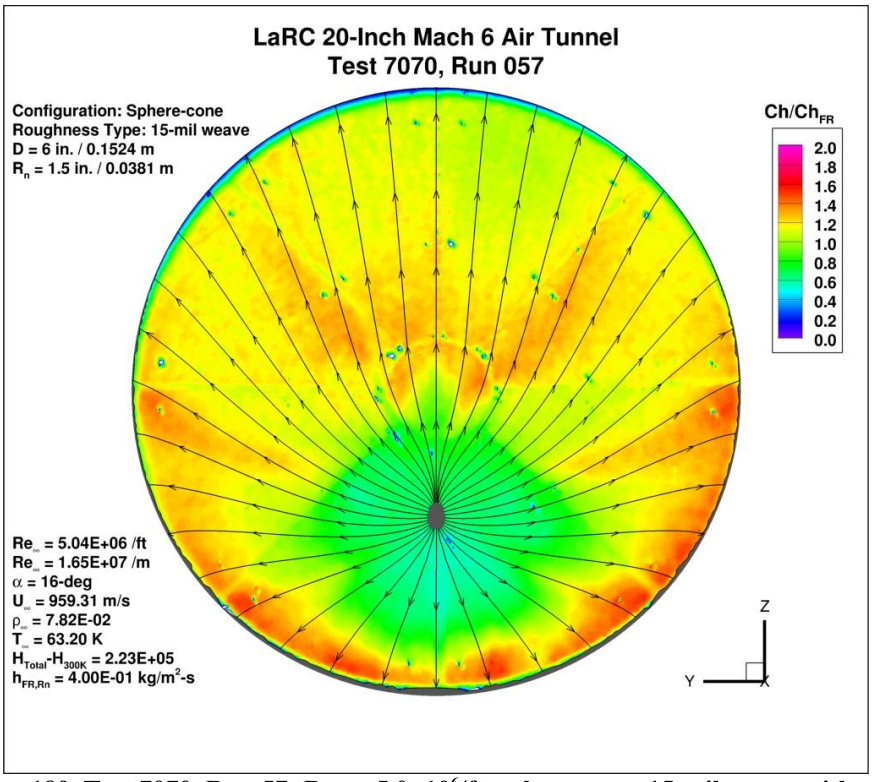
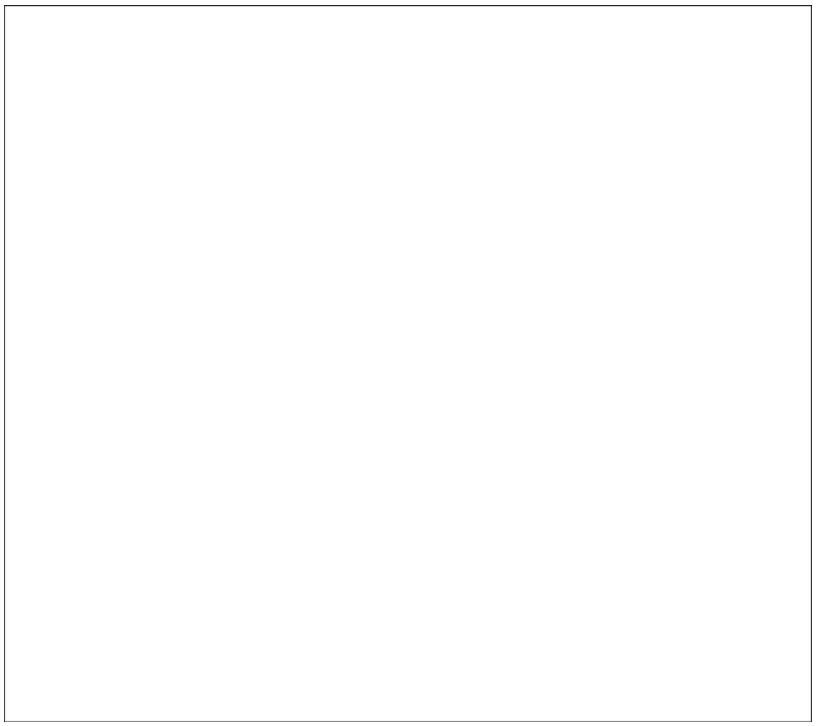


Figure 180. Test 7070, Run 57: $Re_\infty = 5.0\times10^6$/ft, sphere-cone, 15-mil weave with seam.



(Condition was not run)

Figure 181. Test 7070, Run XX: Re_∞ = 5.3×10^6/ft, sphere-cone, 15-mil weave with seam.

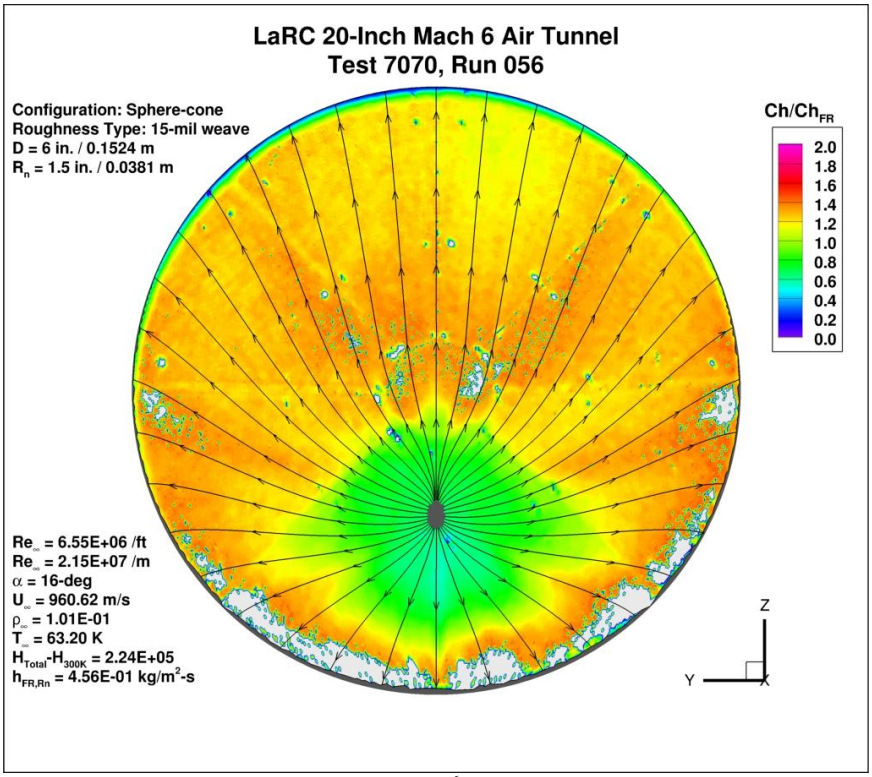


Figure 182. Test 7070, Run 56: Re_∞ = 6.5×10^6/ft, sphere-cone, 15-mil weave with seam.

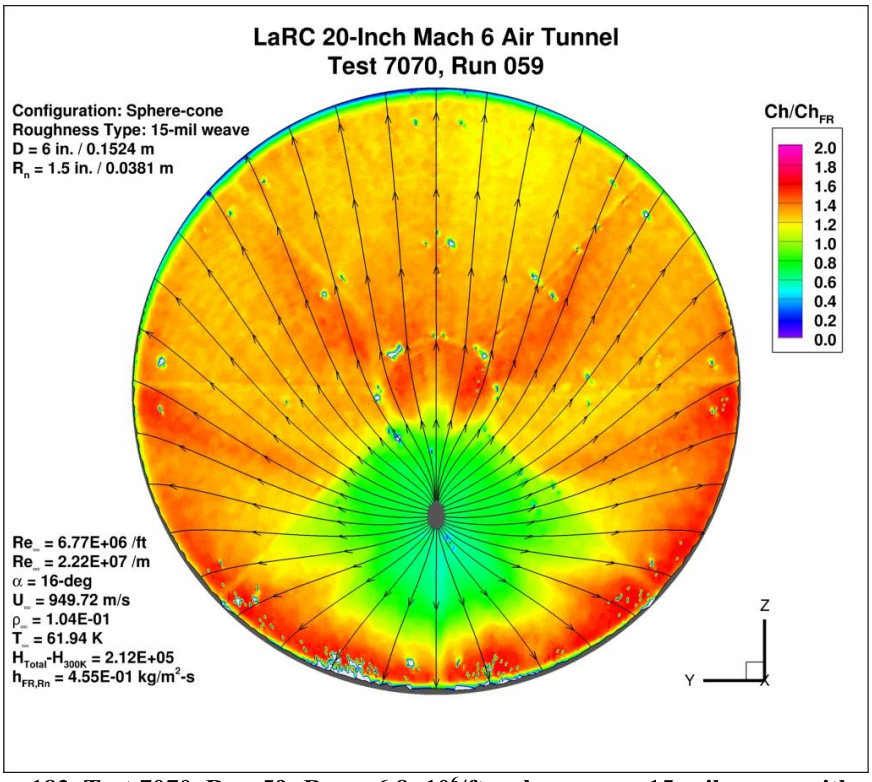


Figure 183. Test 7070, Run 59: $Re_\infty = 6.8\times10^6$/ft, sphere-cone, 15-mil weave with seam.

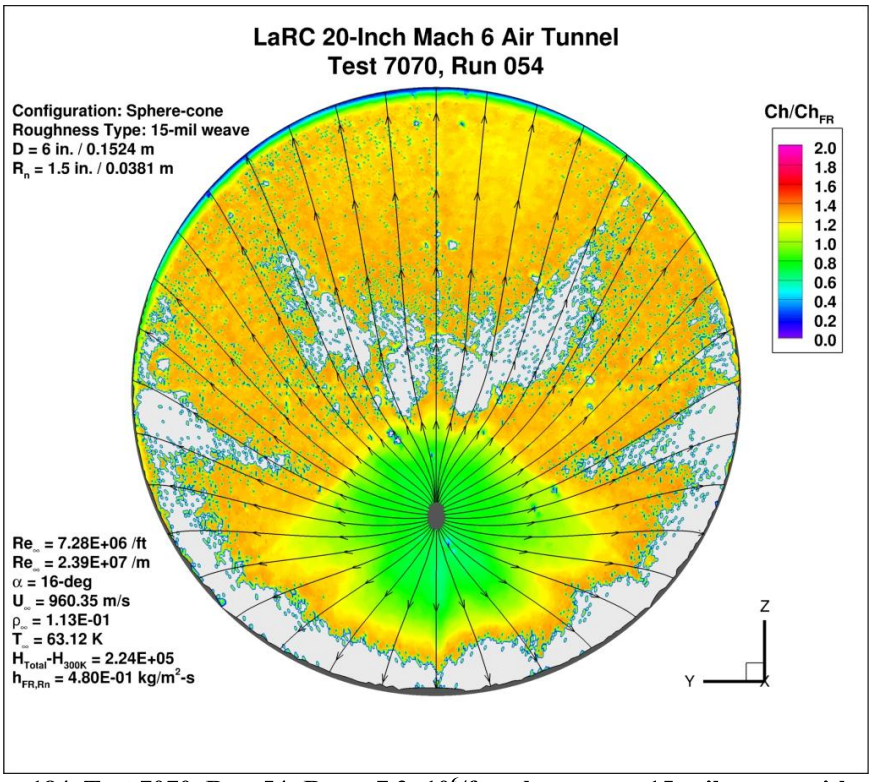


Figure 184. Test 7070, Run 54: $Re_\infty = 7.3\times10^6$/ft, sphere-cone, 15-mil weave with seam.

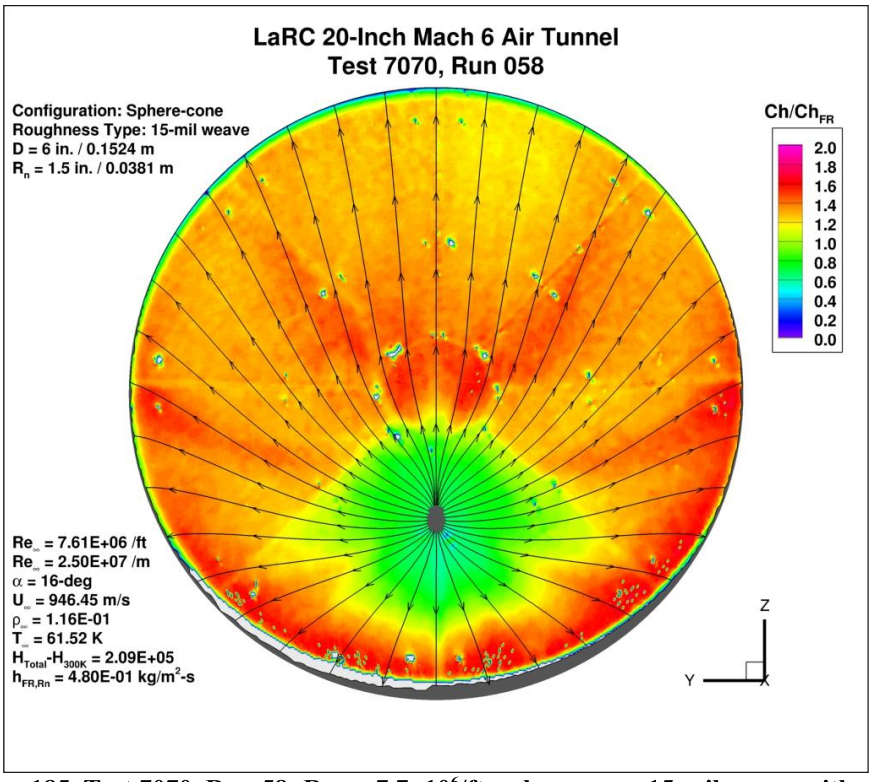


Figure 185. Test 7070, Run 58: $Re_\infty = 7.7\times10^6$/ft, sphere-cone, 15-mil weave with seam.

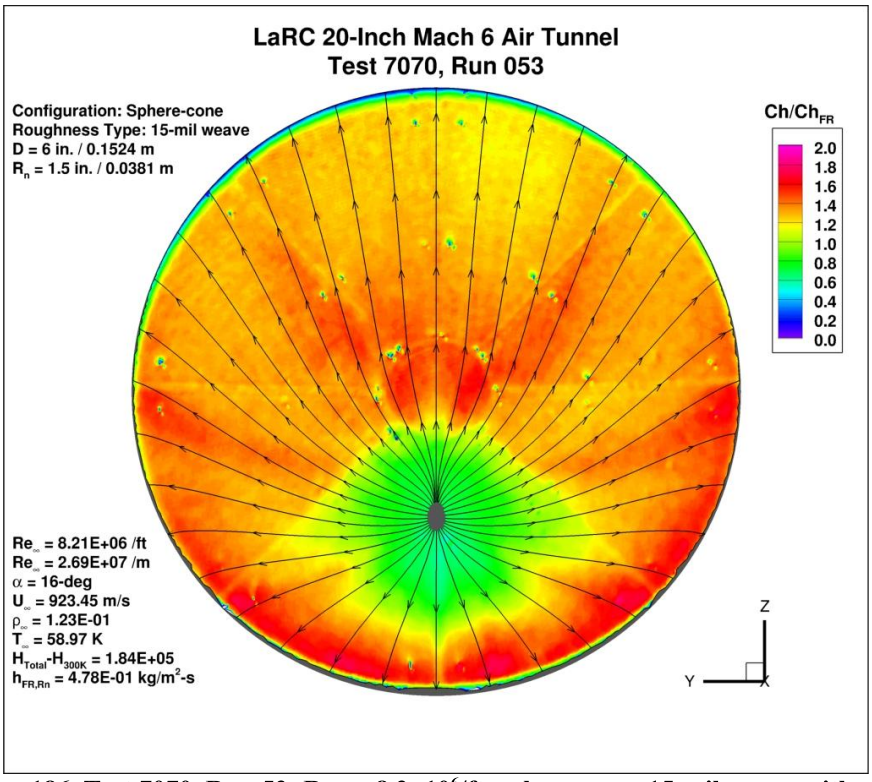


Figure 186. Test 7070, Run 53: $Re_\infty = 8.2\times10^6$/ft, sphere-cone, 15-mil weave with seam.

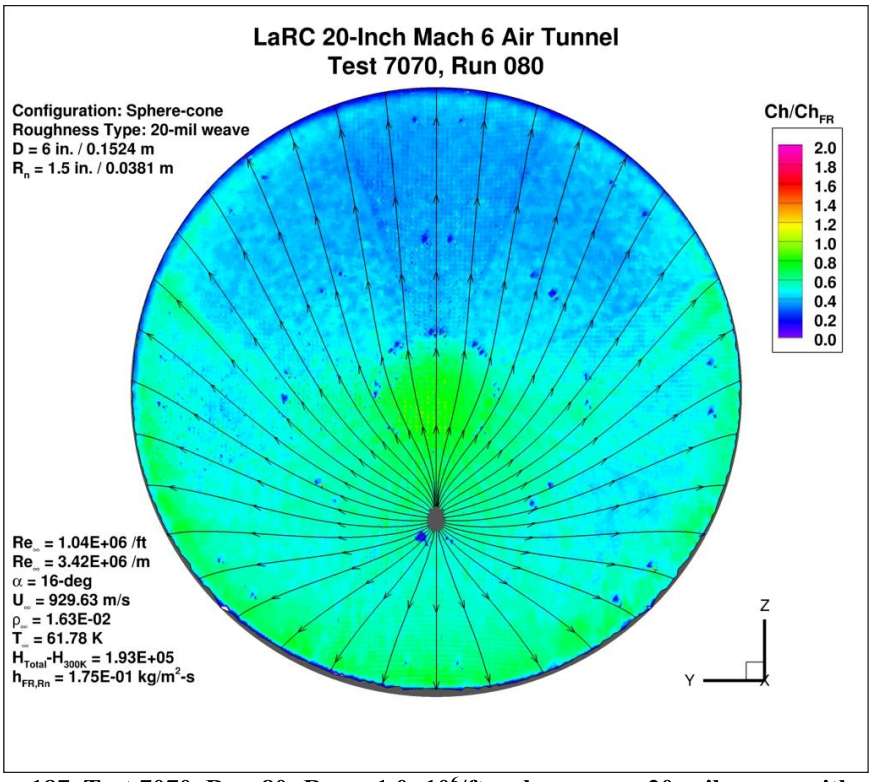


Figure 187. Test 7070, Run 80: $Re_\infty = 1.0\times10^6$/ft, sphere-cone, 20-mil weave with seam.

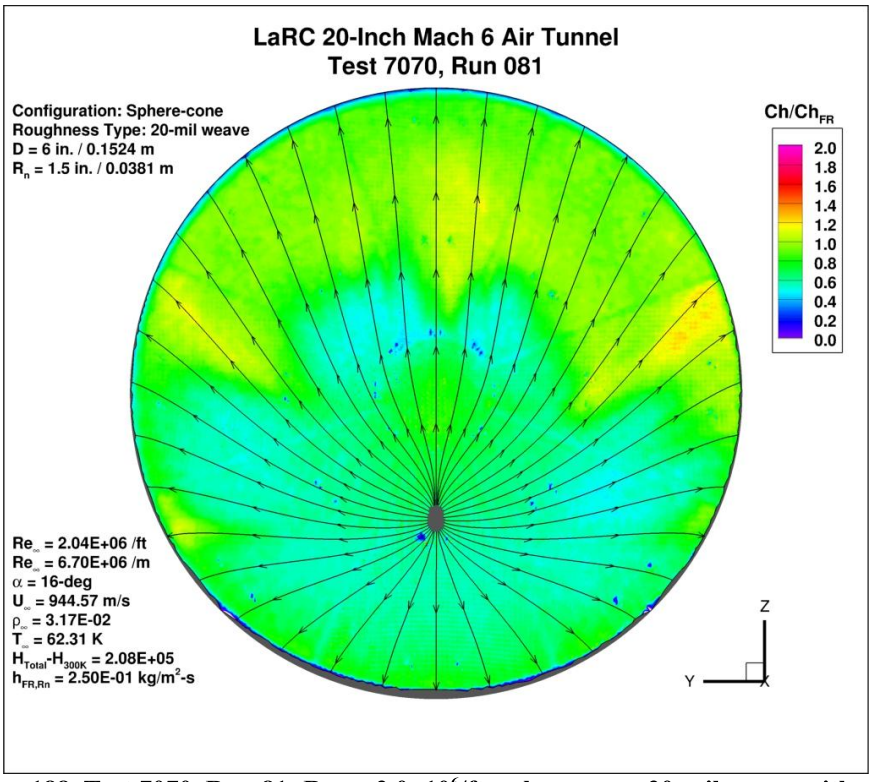


Figure 188. Test 7070, Run 81: $Re_\infty = 2.0\times10^6$/ft, sphere-cone, 20-mil weave with seam.

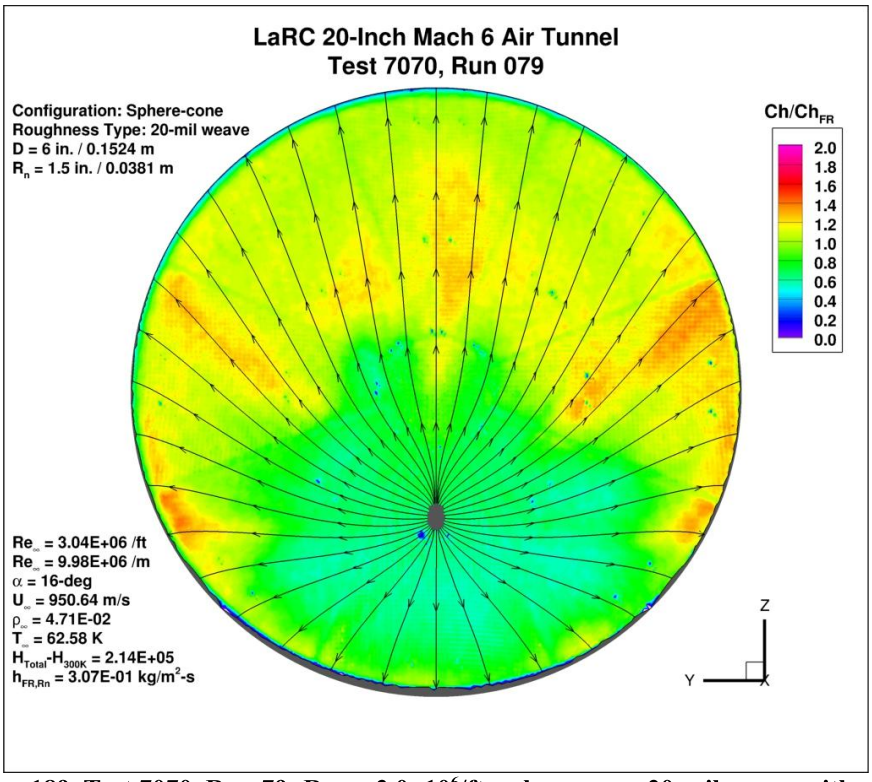


Figure 189. Test 7070, Run 79: $Re_\infty = 3.0\times10^6$/ft, sphere-cone, 20-mil weave with seam.

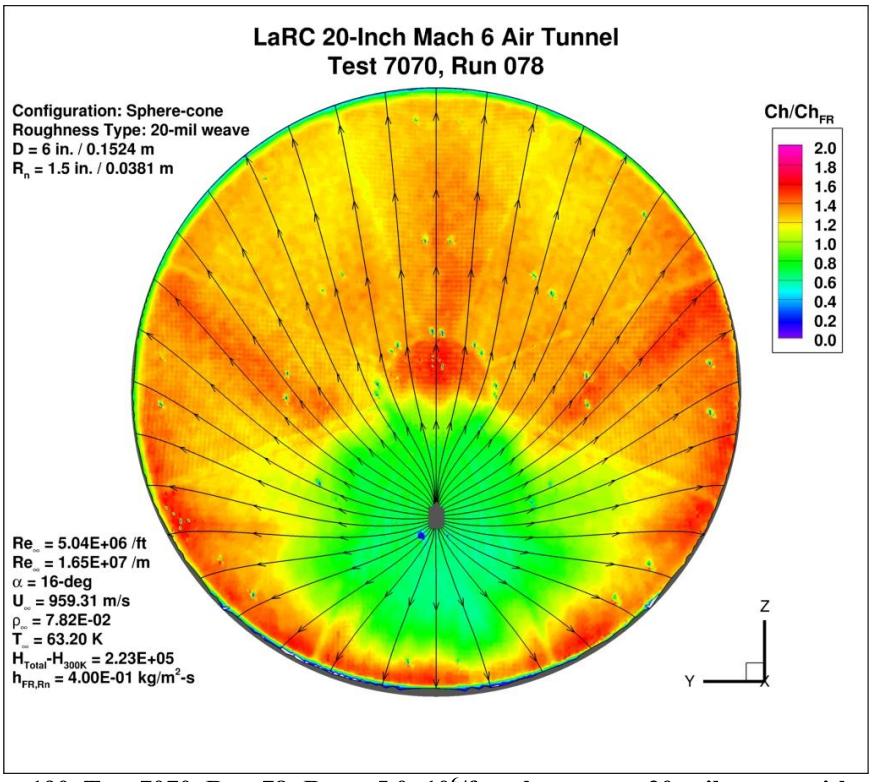
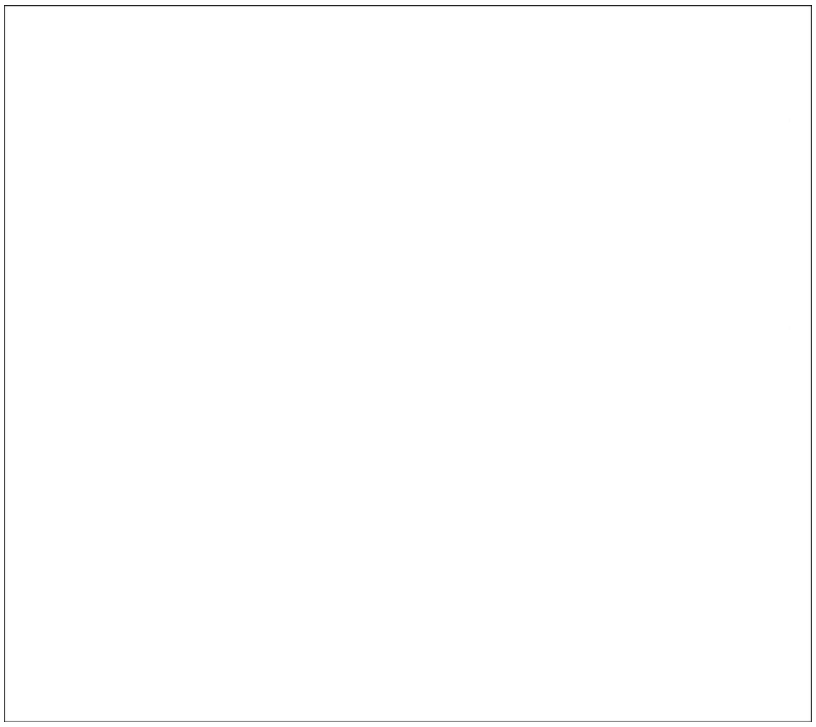
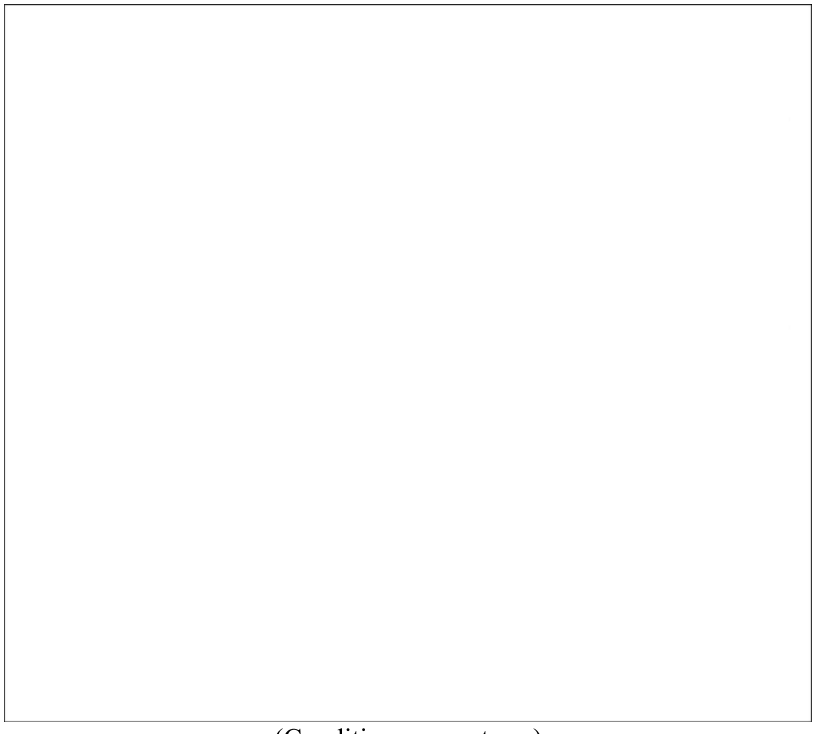


Figure 190. Test 7070, Run 78: $Re_\infty = 5.0\times10^6$/ft, sphere-cone, 20-mil weave with seam.



(Condition was not run)

Figure 191. Test 7070, Run XX: $Re_\infty = 5.3\times10^6$/ft, sphere-cone, 20-mil weave with seam.



(Condition was not run)

Figure 192. Test 7070, Run XX: $Re_\infty = 6.5\times10^6$/ft, sphere-cone, 20-mil weave with seam.

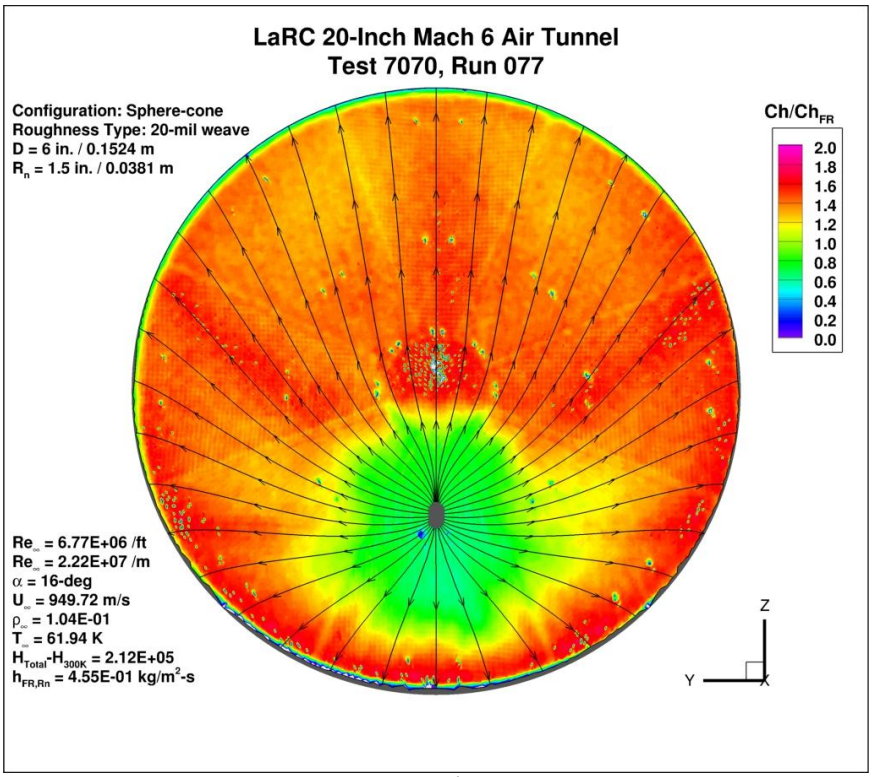


Figure 193. Test 7070, Run 77: $Re_\infty = 6.8\times10^6$/ft, sphere-cone, 20-mil weave with seam.

(Condition was not run)

Figure 194. Test 7070, Run XX: $Re_\infty = 7.3\times10^6$/ft, sphere-cone, 20-mil weave with seam.

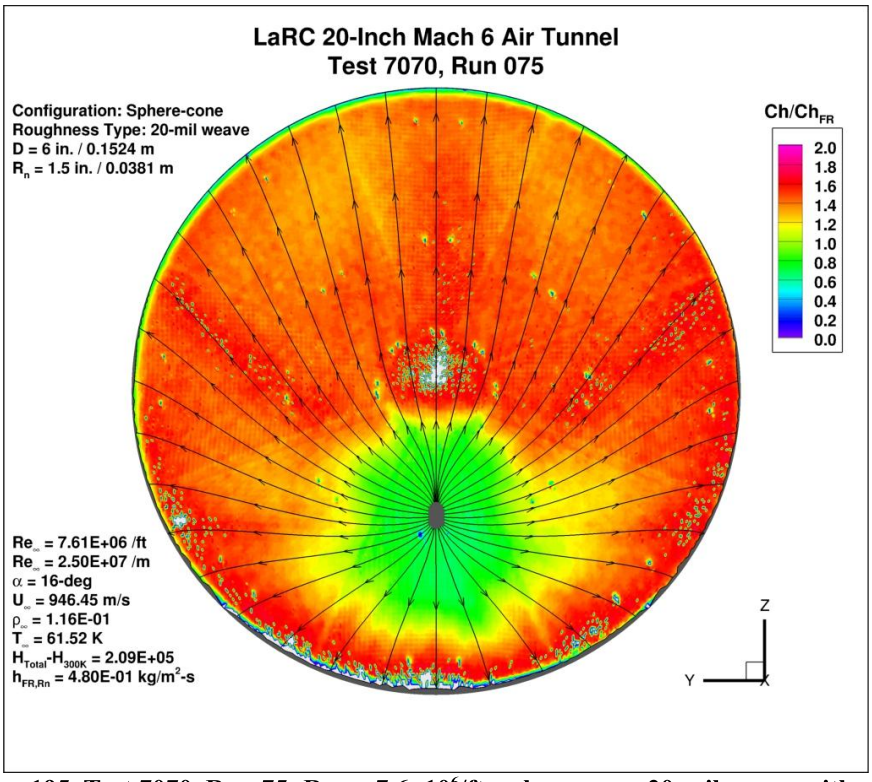


Figure 195. Test 7070, Run 75: $Re_\infty = 7.6\times10^6$/ft, sphere-cone, 20-mil weave with seam.

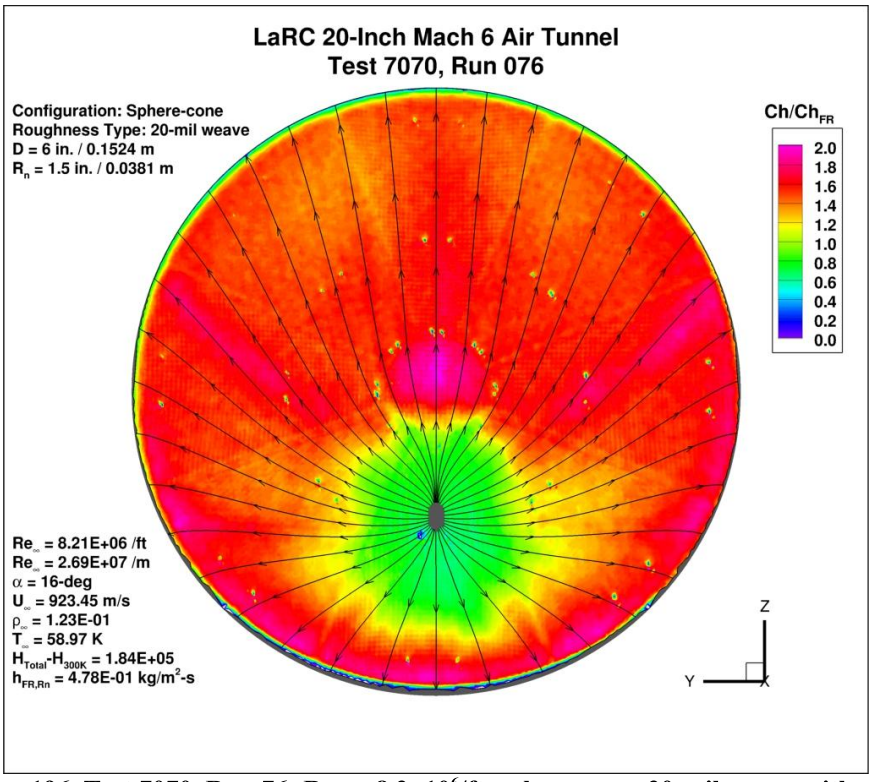


Figure 196. Test 7070, Run 76: $Re_\infty = 8.2\times10^6$/ft, sphere-cone, 20-mil weave with seam.

Appendix B. Spherical-Cap Geometry Global Heating Images

Global heating images for the spherical-cap geometry from Test 7070 and 7074 in the LAL 20-Inch Mach 6 Air Tunnel are presented in this Appendix. Smooth OML data are shown in Figure 197 through Figure 206. Woven TPS surface data without seams between the panels are show in Figure 207 through Figure 246. Woven TPS surface data with seams between the panels are show in Figure 247 through Figure 286.

At higher Reynolds numbers and/or larger roughness heights, white patches on the images indicate areas where the measured surface temperatures exceed the calibrated range of the phosphor thermography system and thus no valid data were obtained. Boundary-layer edge streamlines determined from laminar, smooth-surface LAURA simulations have been superimposed on the images to illustrate the nature of the flow field.

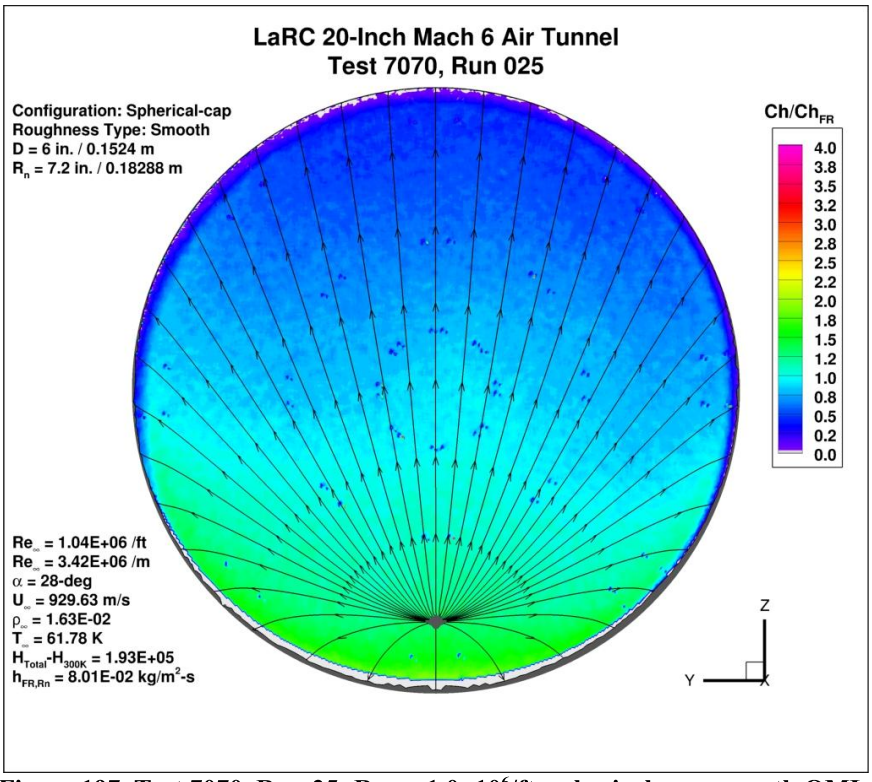


Figure 197. Test 7070, Run 25: $Re_\infty = 1.0\times10^6$/ft, spherical-cap, smooth OML.

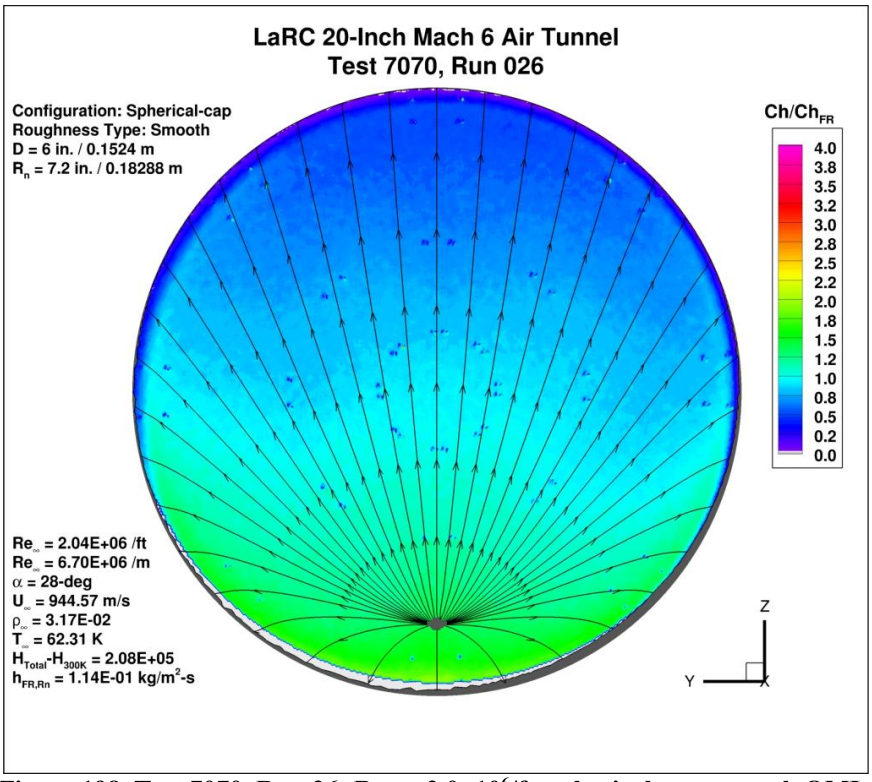


Figure 198. Test 7070, Run 26: $Re_\infty = 2.0\times10^6$/ft, spherical-cap, smooth OML.

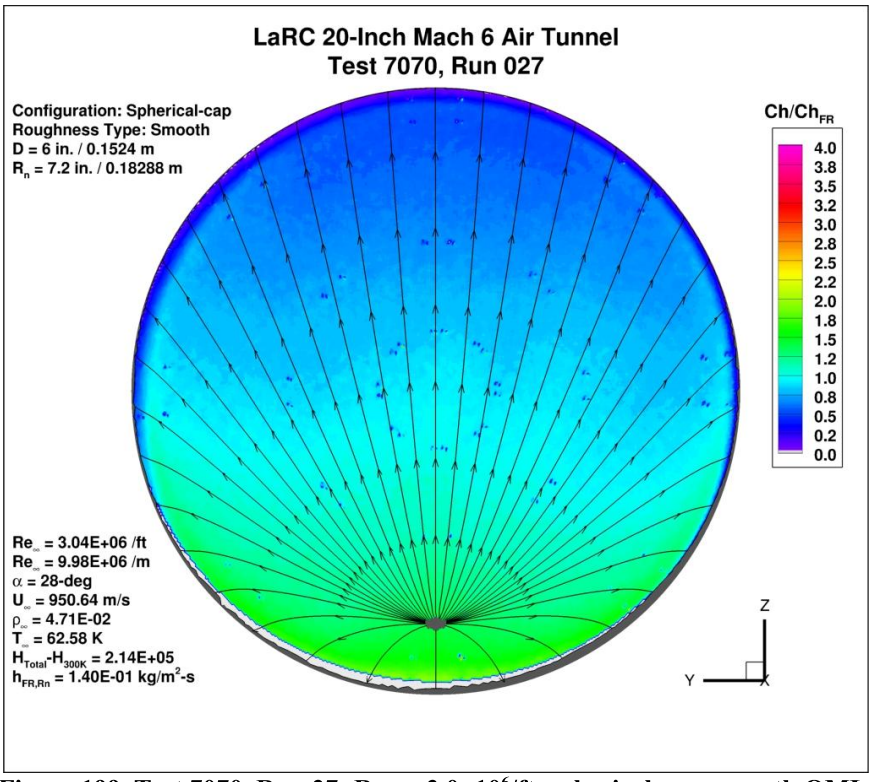


Figure 199. Test 7070, Run 27: $Re_\infty = 3.0\times10^6$/ft, spherical-cap, smooth OML.

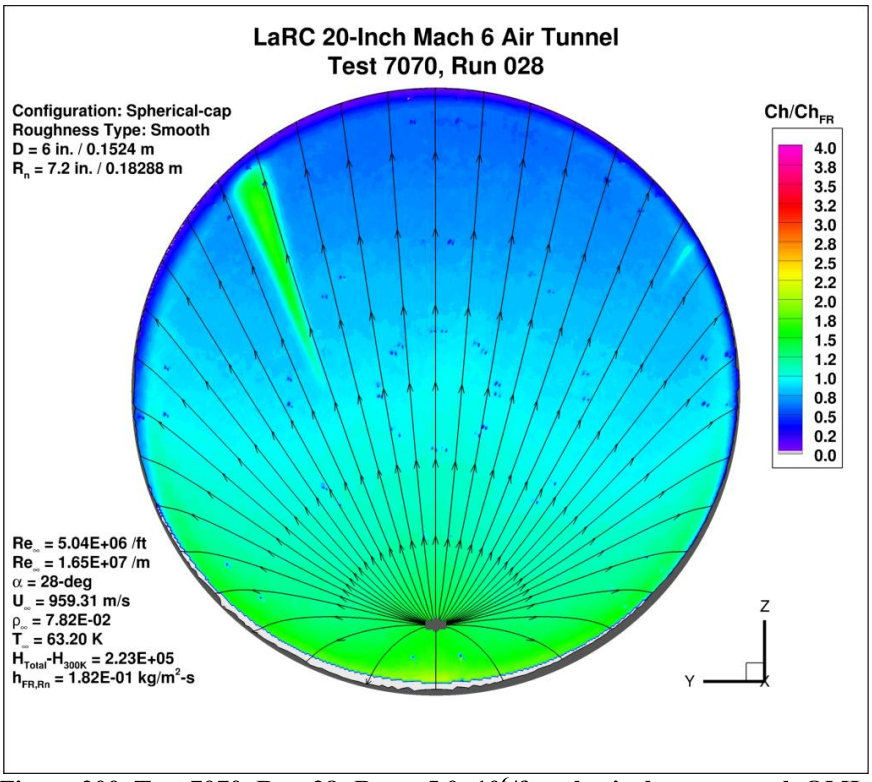


Figure 200. Test 7070, Run 28: $Re_\infty = 5.0\times10^6$/ft, spherical-cap, smooth OML.

(Condition was not run)

Figure 201. Test 7070, Run XX: $Re_\infty = 5.3\times10^6$/ft, spherical-cap, smooth OML.

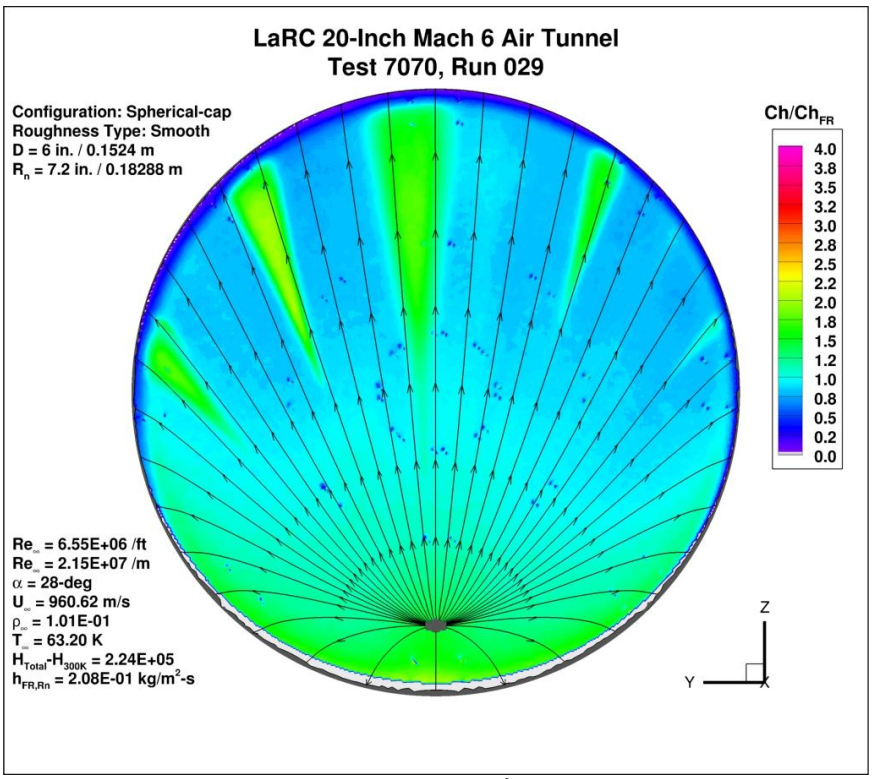


Figure 202. Test 7070, Run 29: $Re_\infty = 6.5\times10^6$/ft, spherical-cap, smooth OML.

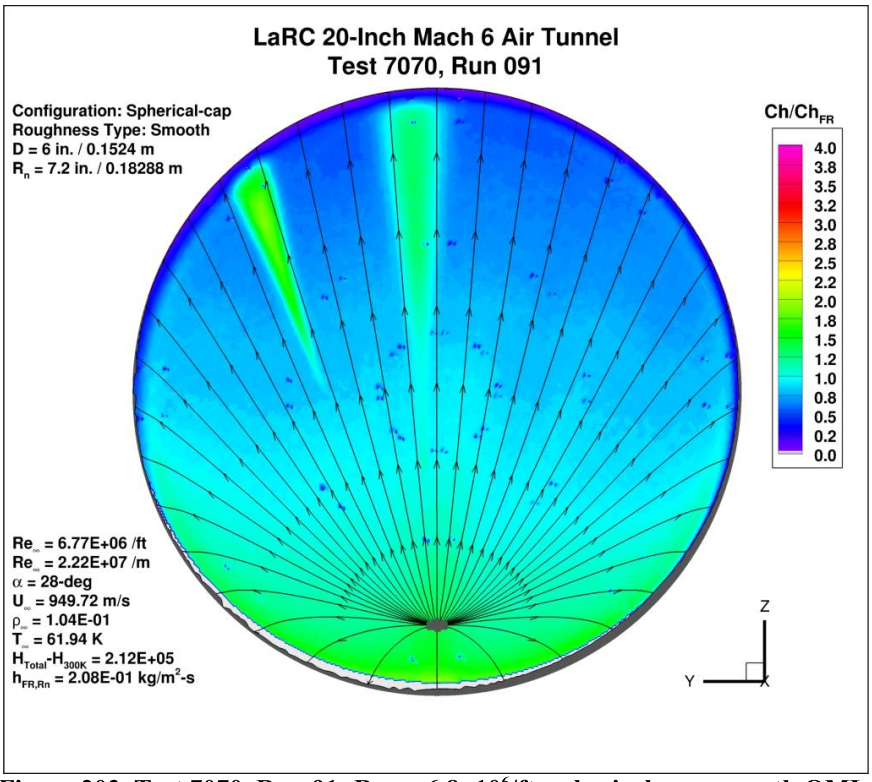


Figure 203. Test 7070, Run 91: $Re_\infty = 6.8\times10^6$/ft, spherical-cap, smooth OML.

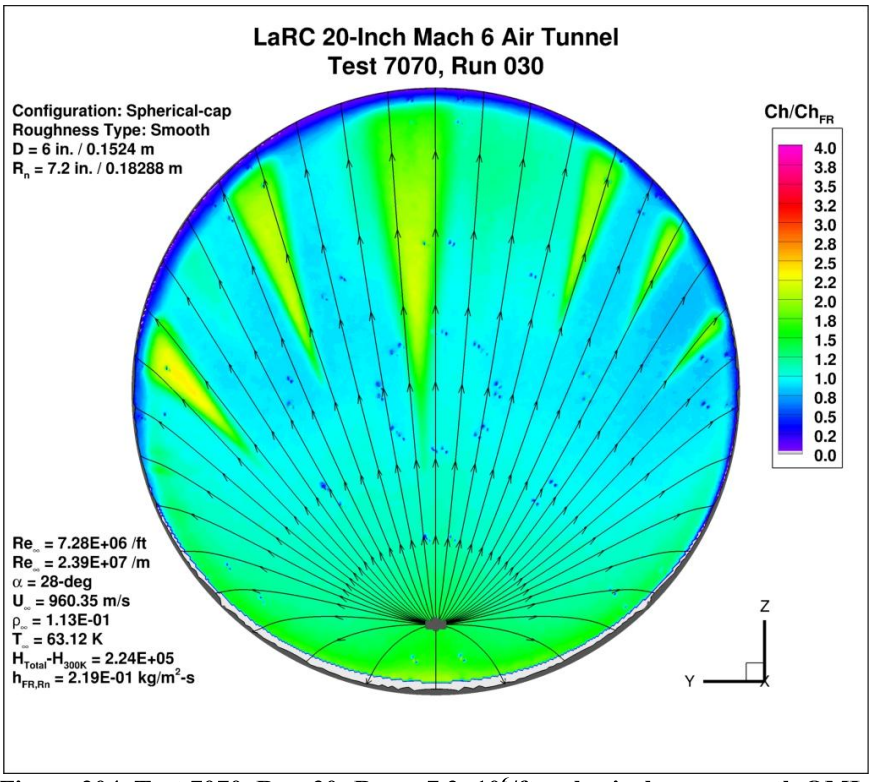


Figure 204. Test 7070, Run 30: $Re_\infty = 7.3\times10^6$/ft, spherical-cap, smooth OML.

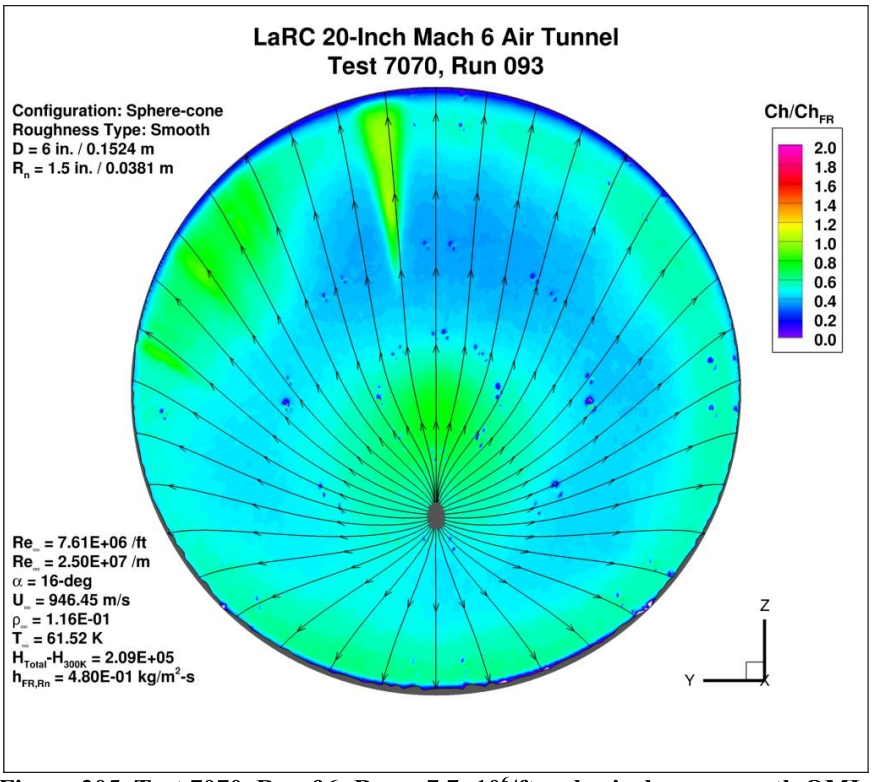


Figure 205. Test 7070, Run 96: $Re_\infty = 7.7\times10^6$/ft, spherical-cap, smooth OML.

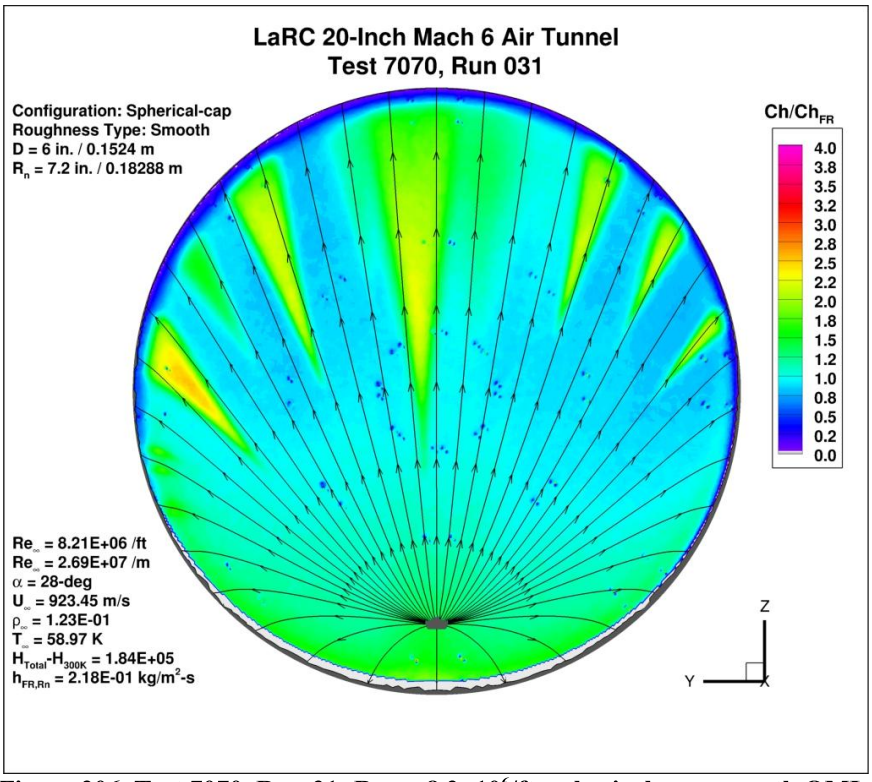


Figure 206. Test 7070, Run 31: $Re_\infty = 8.2\times10^6$/ft, spherical-cap, smooth OML.

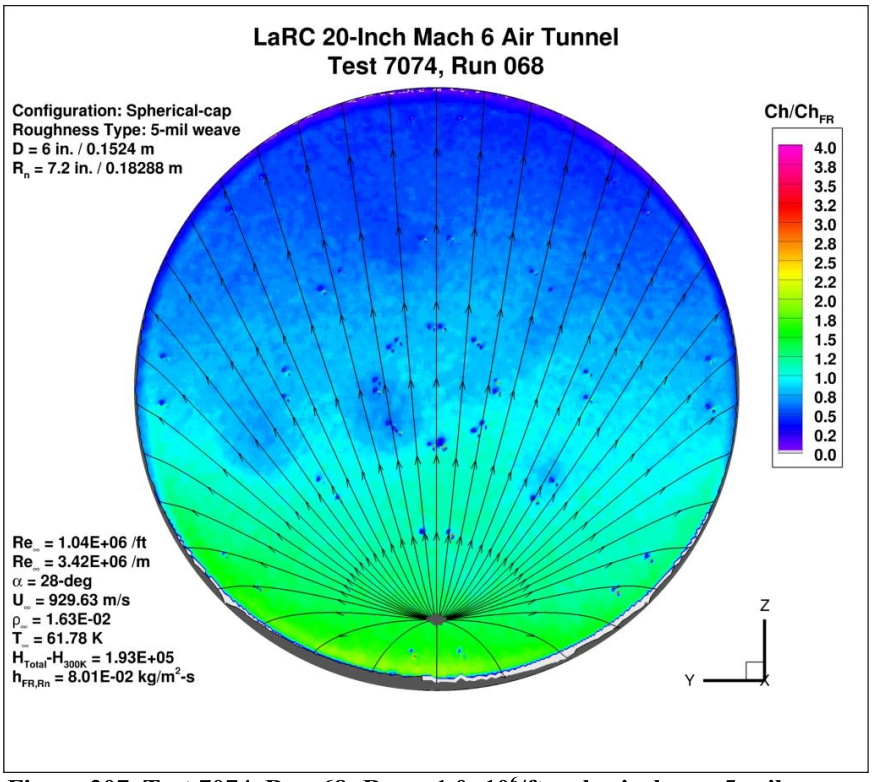


Figure 207. Test 7074, Run 68: $Re_\infty = 1.0\times10^6$/ft, spherical-cap, 5-mil weave.

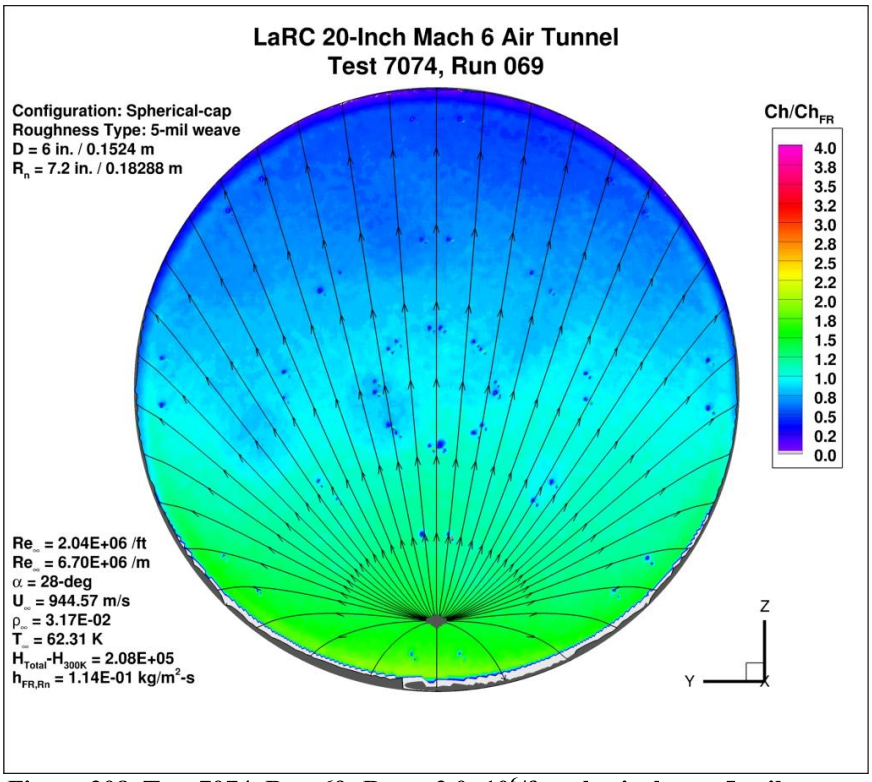


Figure 208. Test 7074, Run 69: $Re_\infty = 2.0\times10^6$/ft, spherical-cap, 5-mil weave.

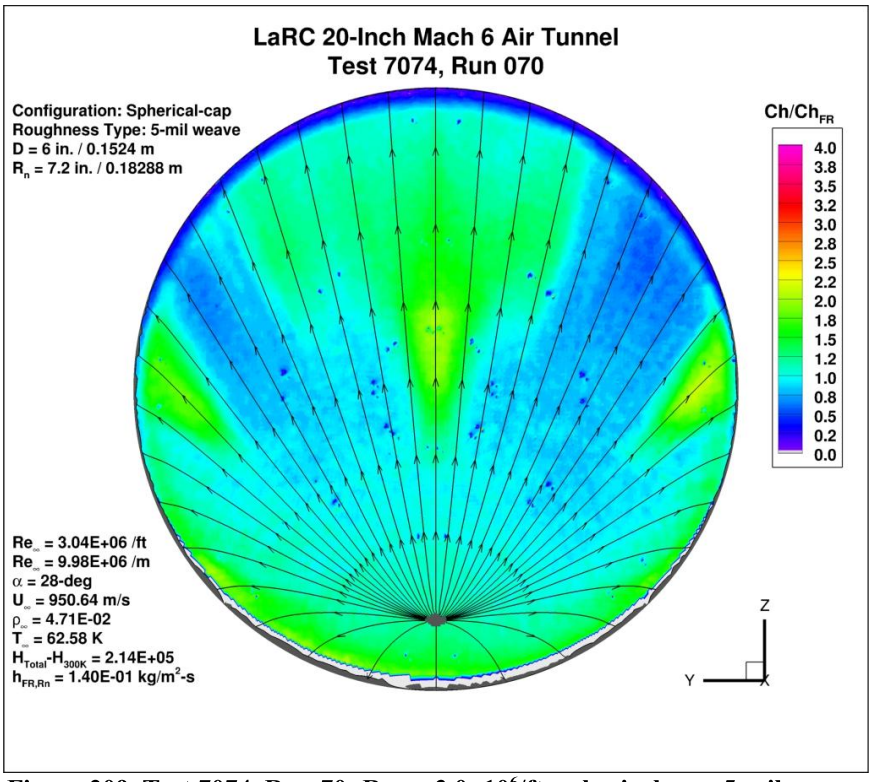


Figure 209. Test 7074, Run 70: $Re_\infty = 3.0\times10^6$/ft, spherical-cap, 5-mil weave.

(Condition was not run)

Figure 210. Test 7074, Run XX: $Re_\infty = 5.0\times10^6$/ft, spherical-cap, 5-mil weave.

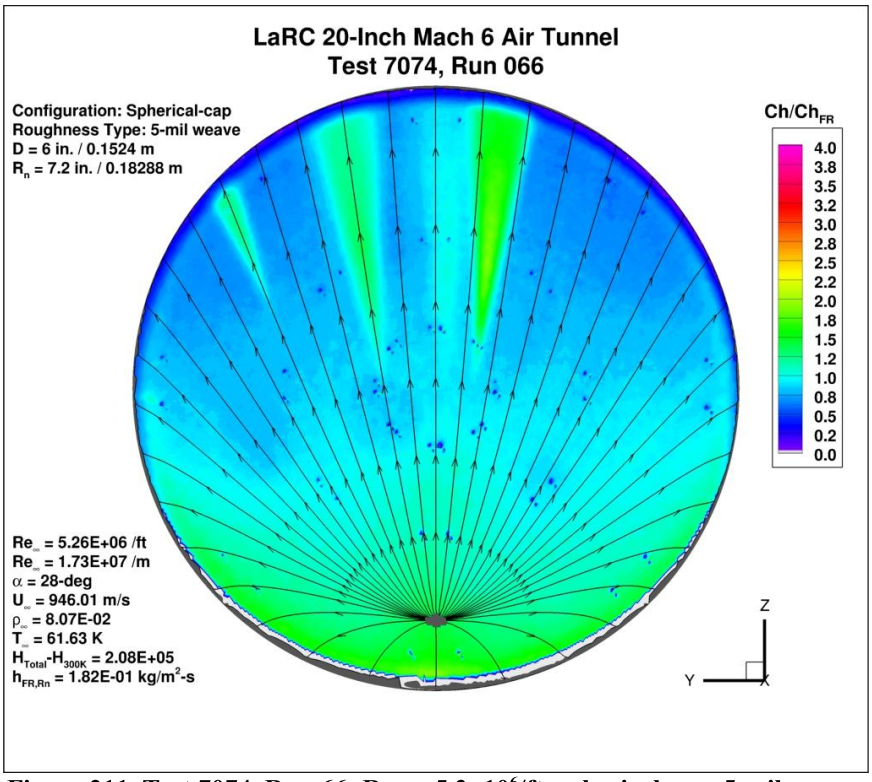


Figure 211. Test 7074, Run 66: $Re_\infty = 5.3\times10^6$/ft, spherical-cap, 5-mil weave.

(Condition was not run)

Figure 212. Test 7074, Run XX: $Re_\infty = 6.5\times10^6$/ft, spherical-cap, 5-mil weave.

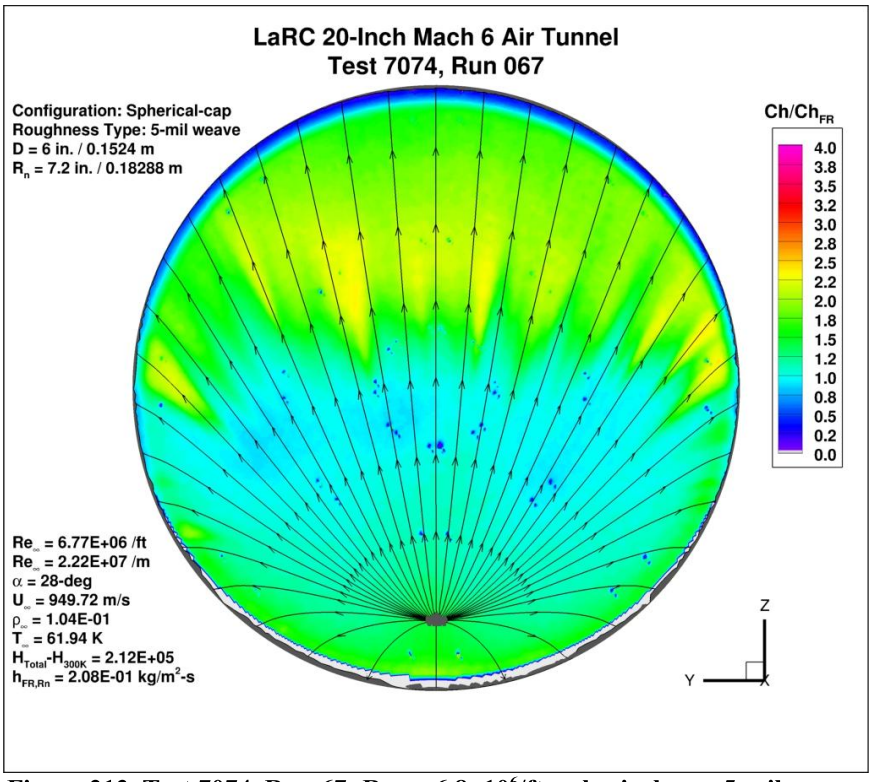


Figure 213. Test 7074, Run 67: $Re_\infty = 6.8\times10^6$/ft, spherical-cap, 5-mil weave.

(Condition was not run)

Figure 214. Test 7074, Run XX: $Re_\infty = 7.2\times10^6$/ft, spherical-cap, 5-mil weave.

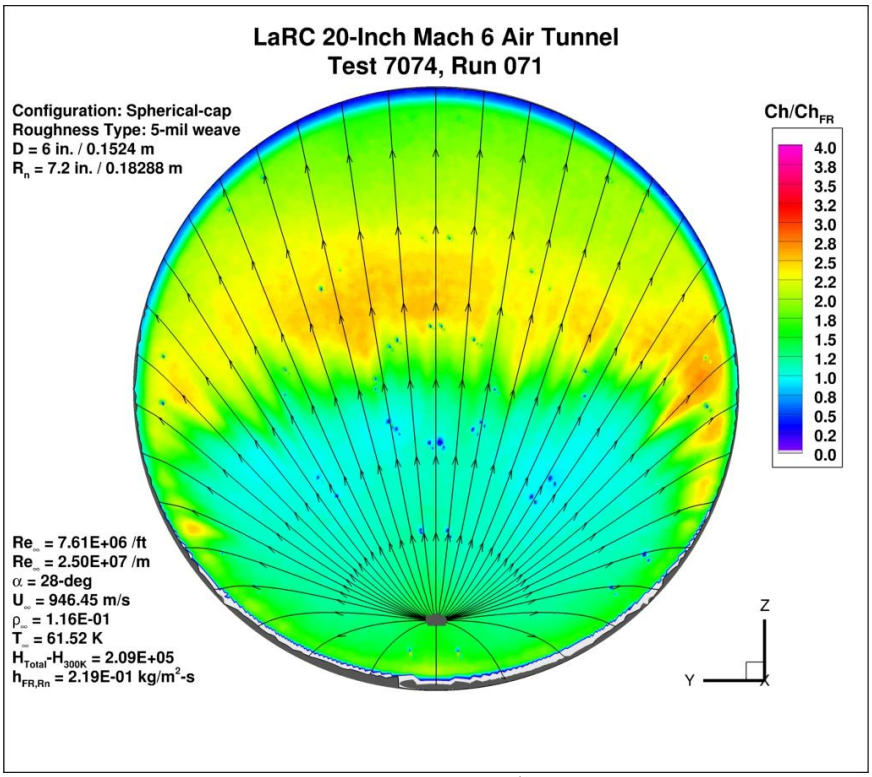


Figure 215. Test 7074, Run 71: $Re_\infty = 7.7 \times 10^6$/ft, spherical-cap, 5-mil weave.

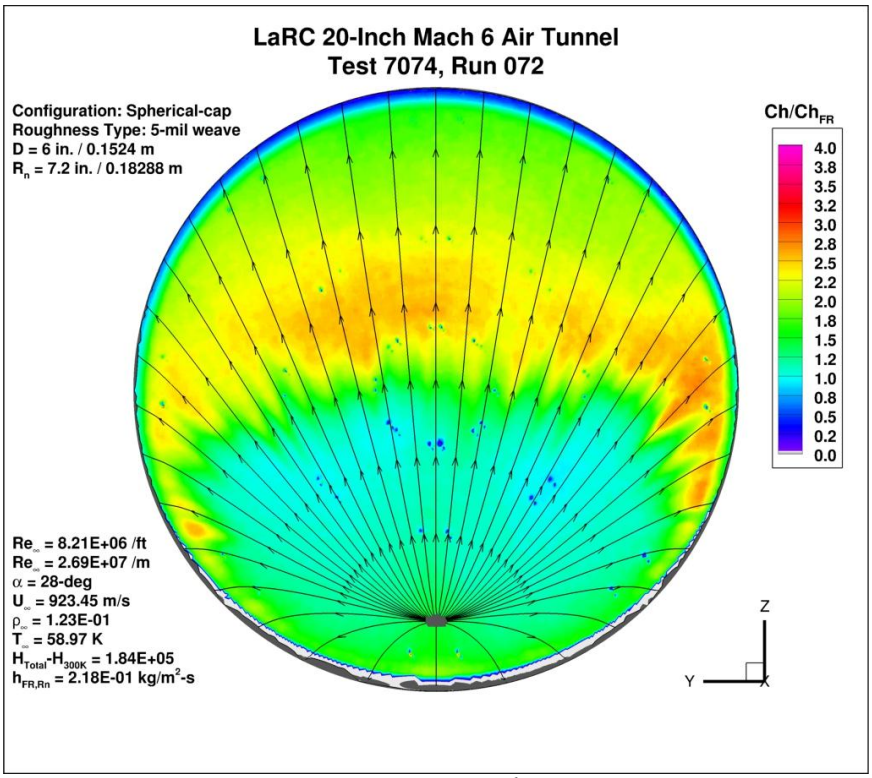


Figure 216. Test 7074, Run 72: $Re_\infty = 8.2 \times 10^6$/ft, spherical-cap, 5-mil weave.

(Condition was not run)

Figure 217. Test 7074, Run XX: $Re_\infty = 1.0\times10^6$/ft, spherical-cap, 10-mil weave.

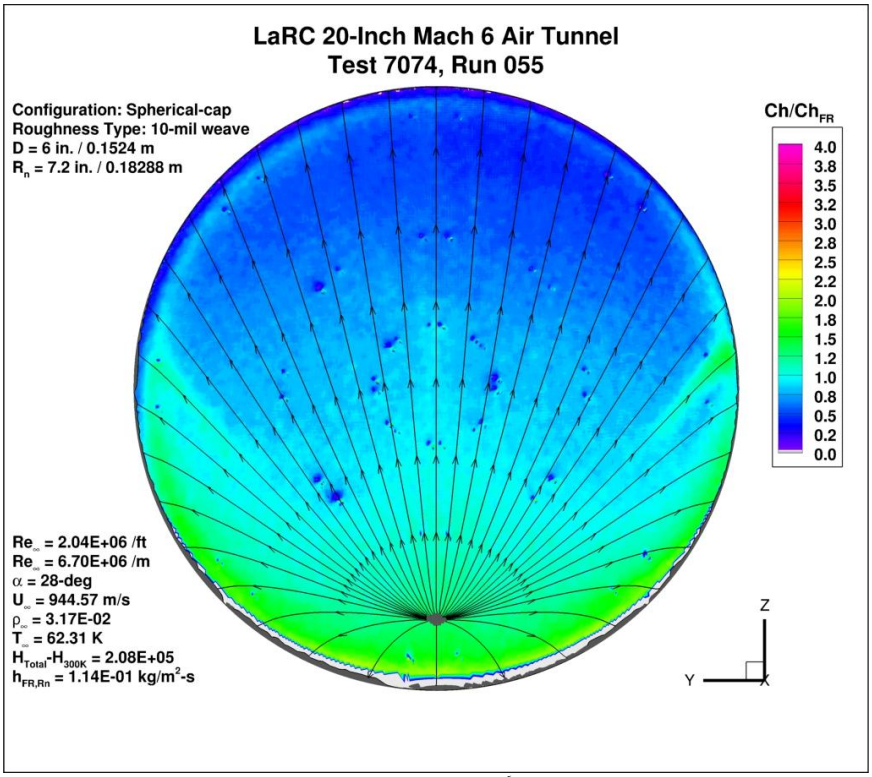


Figure 218. Test 7074, Run 55: $Re_\infty = 2.0\times10^6$/ft, spherical-cap, 10-mil weave.

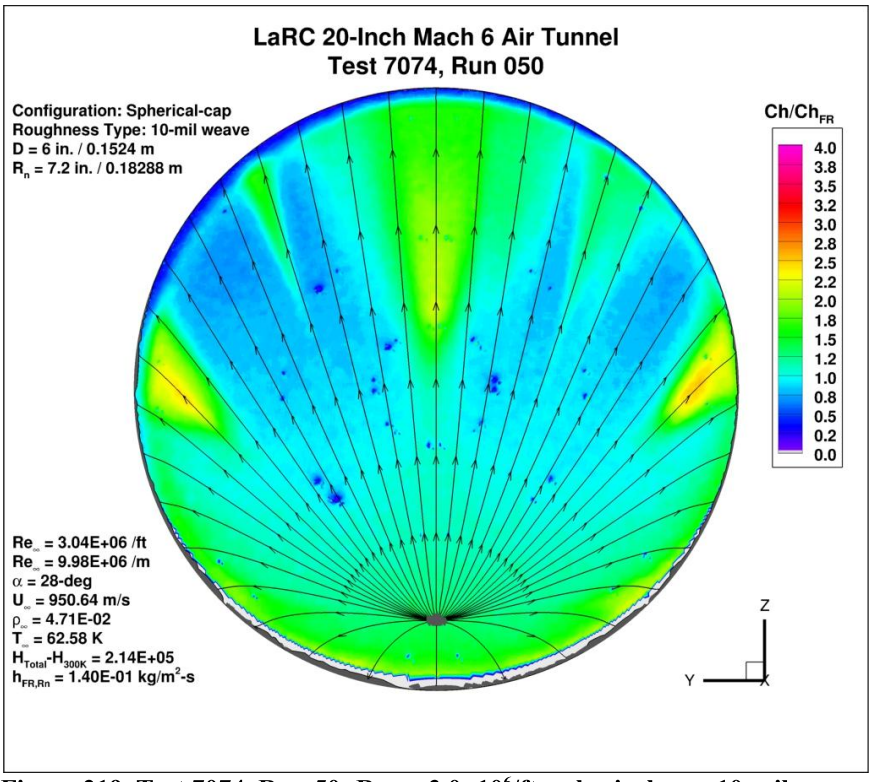


Figure 219. Test 7074, Run 50: $Re_\infty = 3.0\times10^6$/ft, spherical-cap, 10-mil weave.

(Condition was not run)

Figure 220. Test 7074, Run XX: $Re_\infty = 5.0\times10^6$/ft, spherical-cap, 10-mil weave.

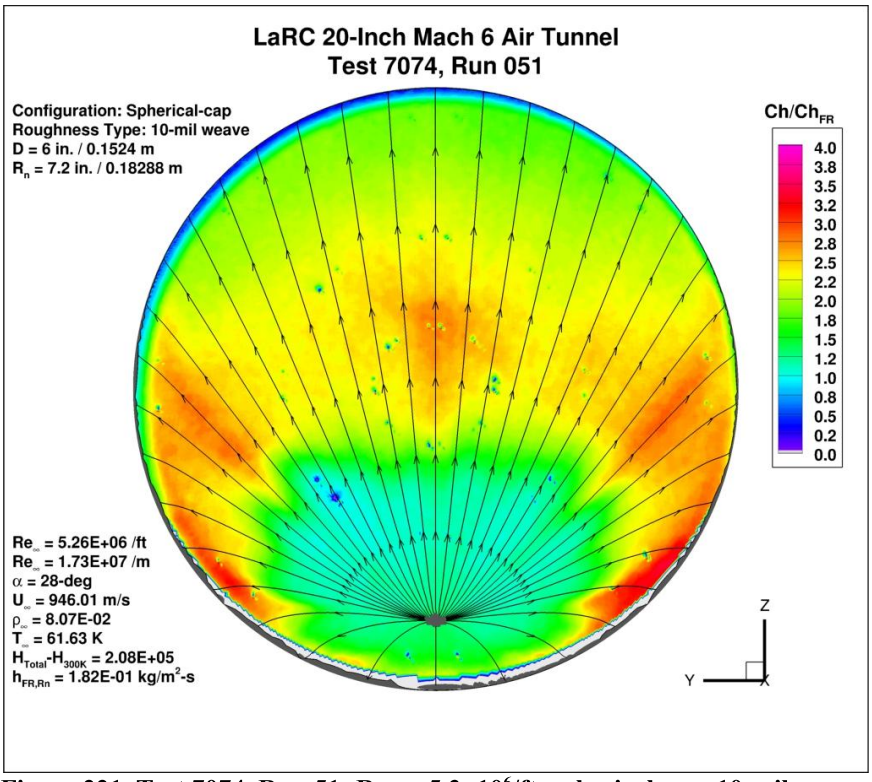


Figure 221. Test 7074, Run 51: $Re_\infty = 5.3\times10^6$/ft, spherical-cap, 10-mil weave.

(Condition was not run)

Figure 222. Test 7074, Run XX: $Re_\infty = 6.5\times10^6$/ft, spherical-cap, 10-mil weave.

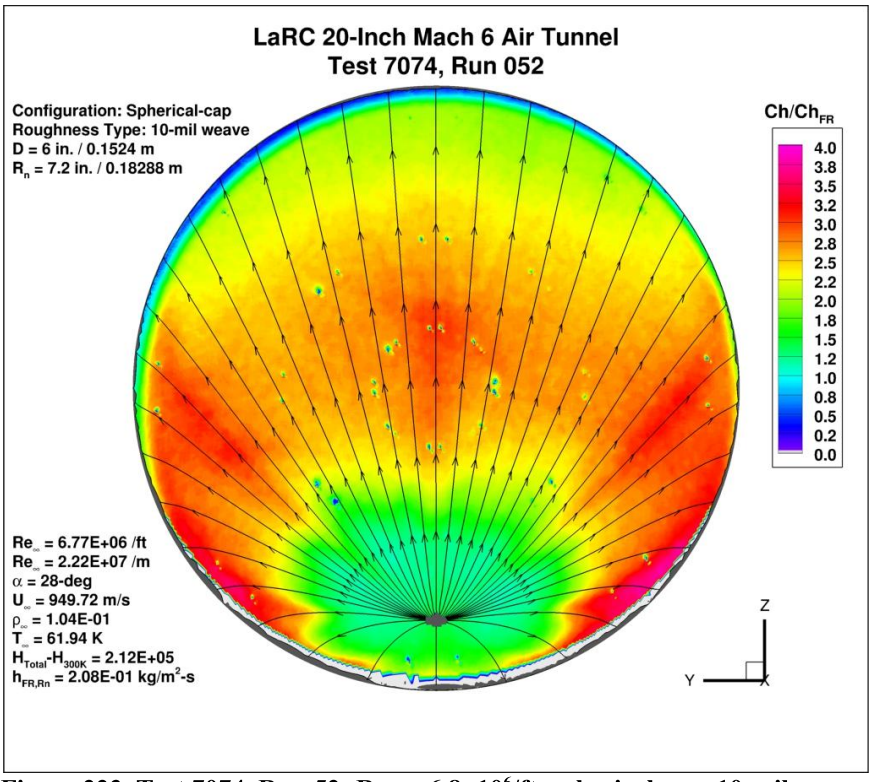


Figure 223. Test 7074, Run 52: $Re_\infty = 6.8\times10^6$/ft, spherical-cap, 10-mil weave.

(Condition was not run)

Figure 224. Test 7074, Run XX: $Re_\infty = 7.3\times10^6$/ft, spherical-cap, 10-mil weave.

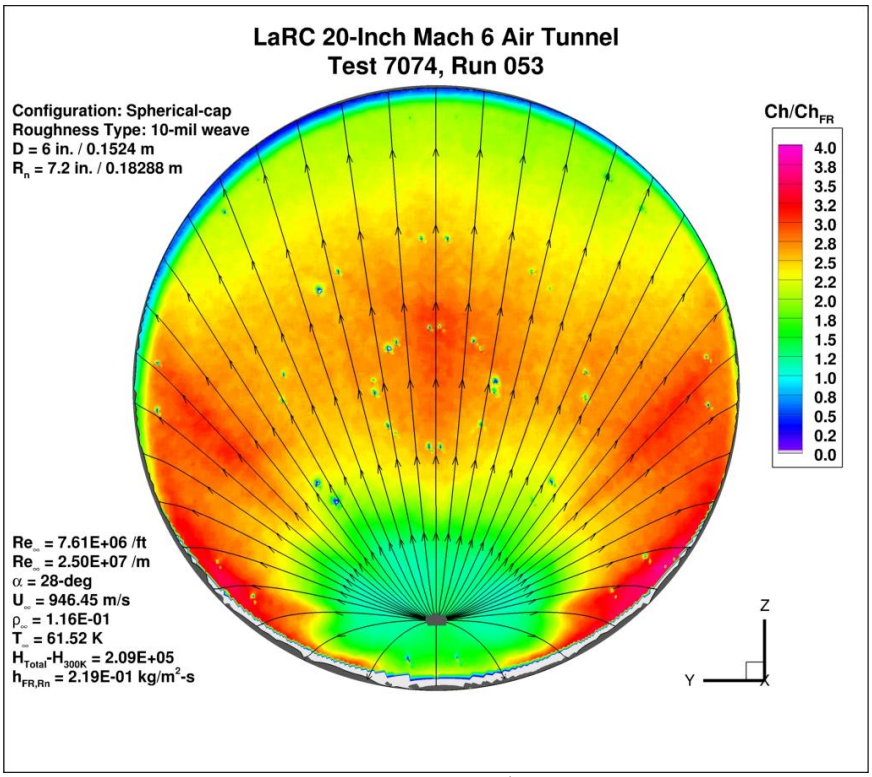


Figure 225. Test 7074, Run 53: $Re_\infty = 7.8\times10^6$/ft, spherical-cap, 10-mil weave.

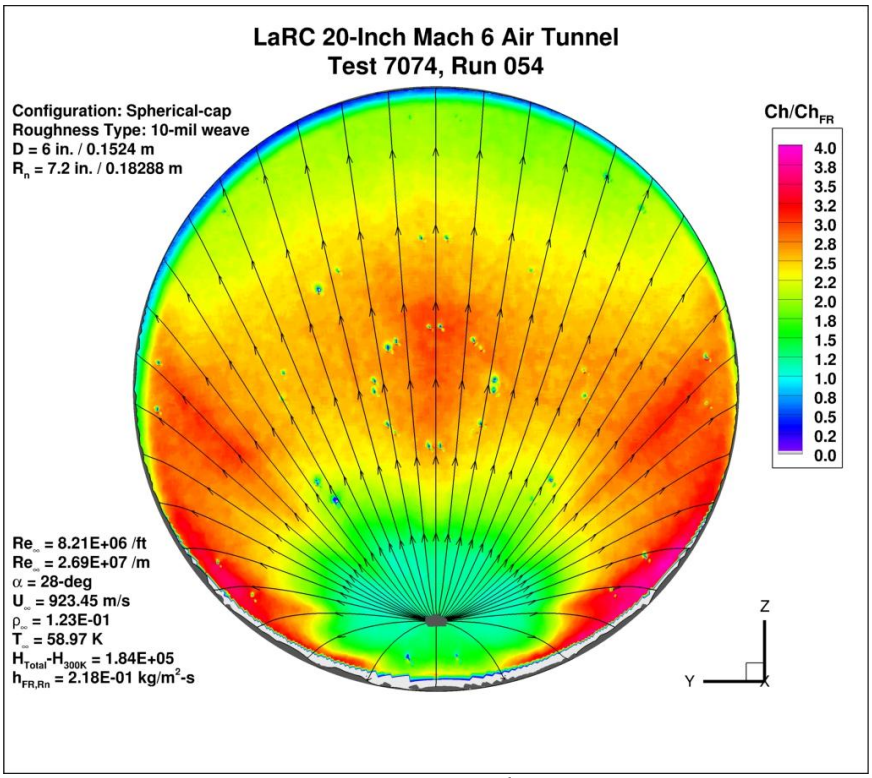


Figure 226. Test 7074, Run 54: $Re_\infty = 8.2\times10^6$/ft, spherical-cap, 10-mil weave.

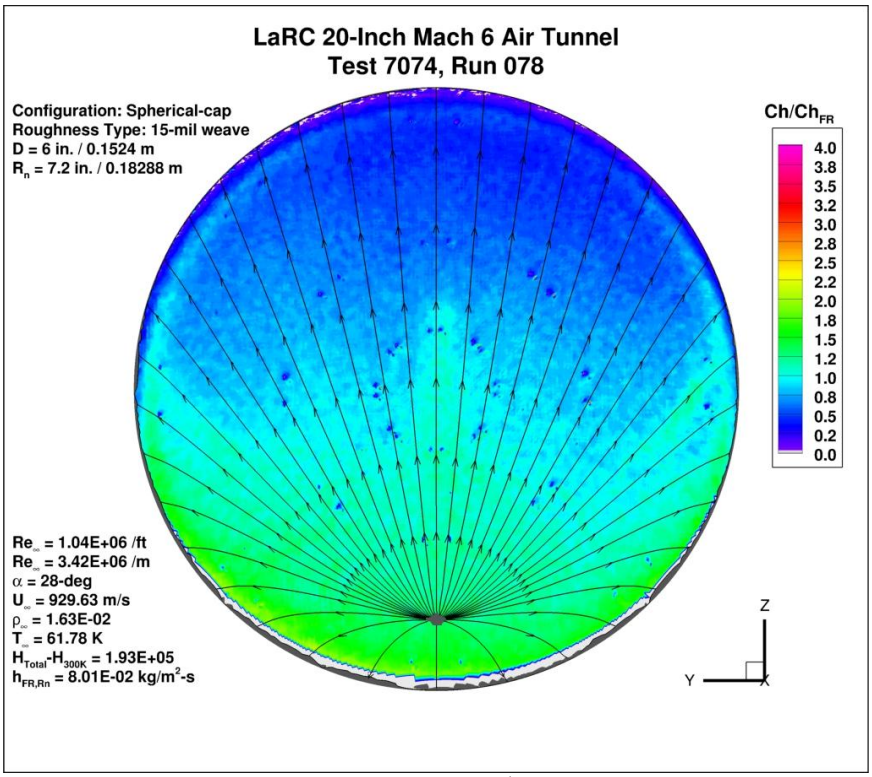


Figure 227. Test 7074, Run 78: $Re_\infty = 1.0\times10^6$/ft, spherical-cap, 15-mil weave.

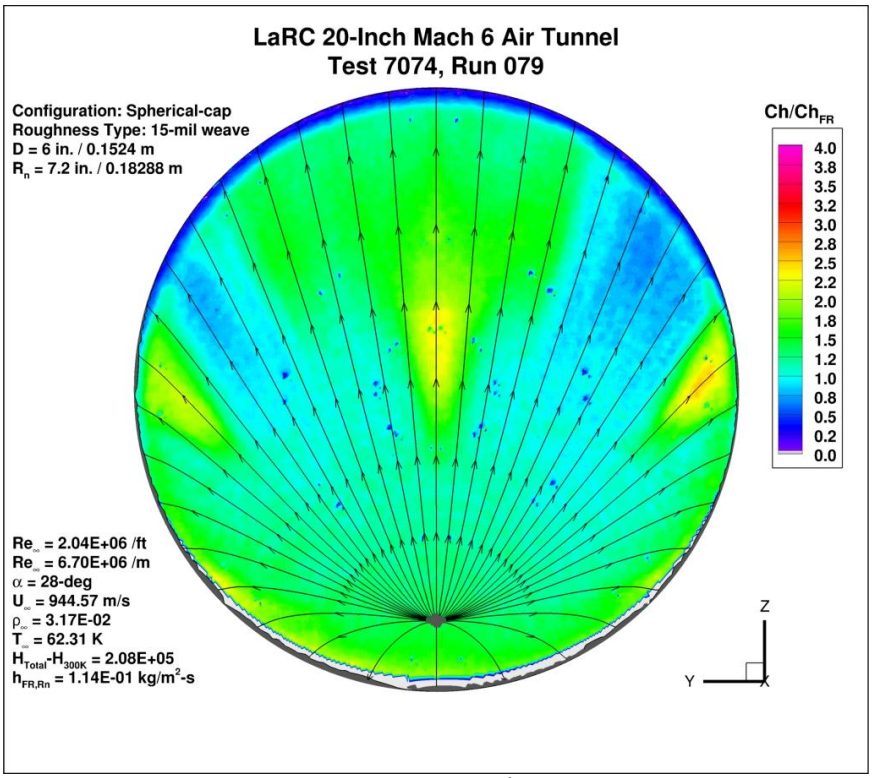


Figure 228. Test 7074, Run 79: $Re_\infty = 2.0\times10^6$/ft, spherical-cap, 15-mil weave.

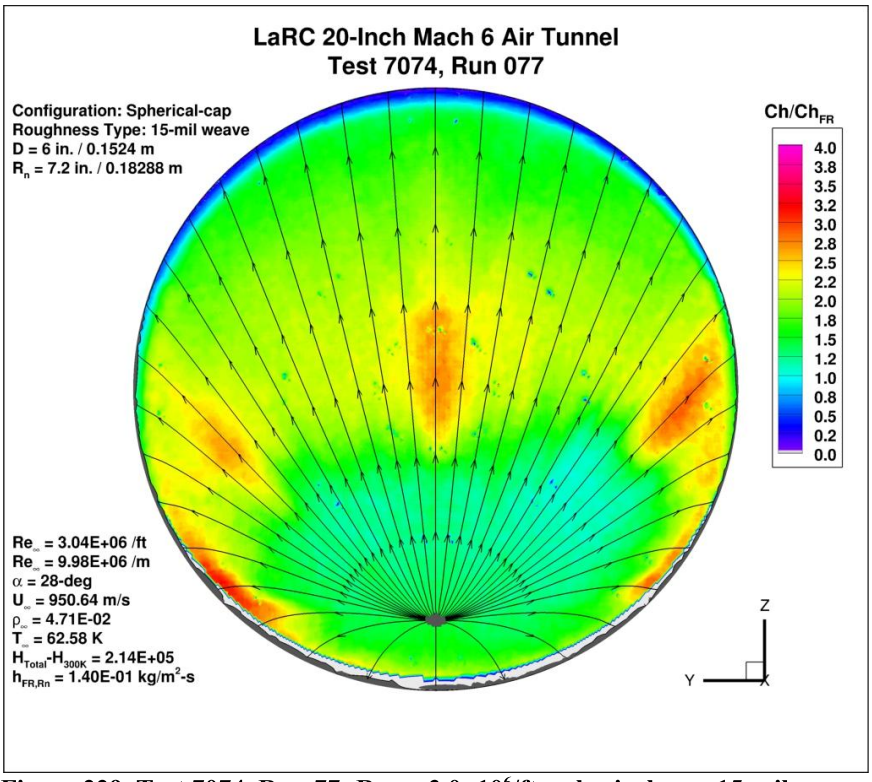


Figure 229. Test 7074, Run 77: $Re_\infty = 3.0\times10^6$/ft, spherical-cap, 15-mil weave.

(Condition was not run)

Figure 230. Test 7074, Run XX: $Re_\infty = 5.0\times10^6$/ft, spherical-cap, 15-mil weave.

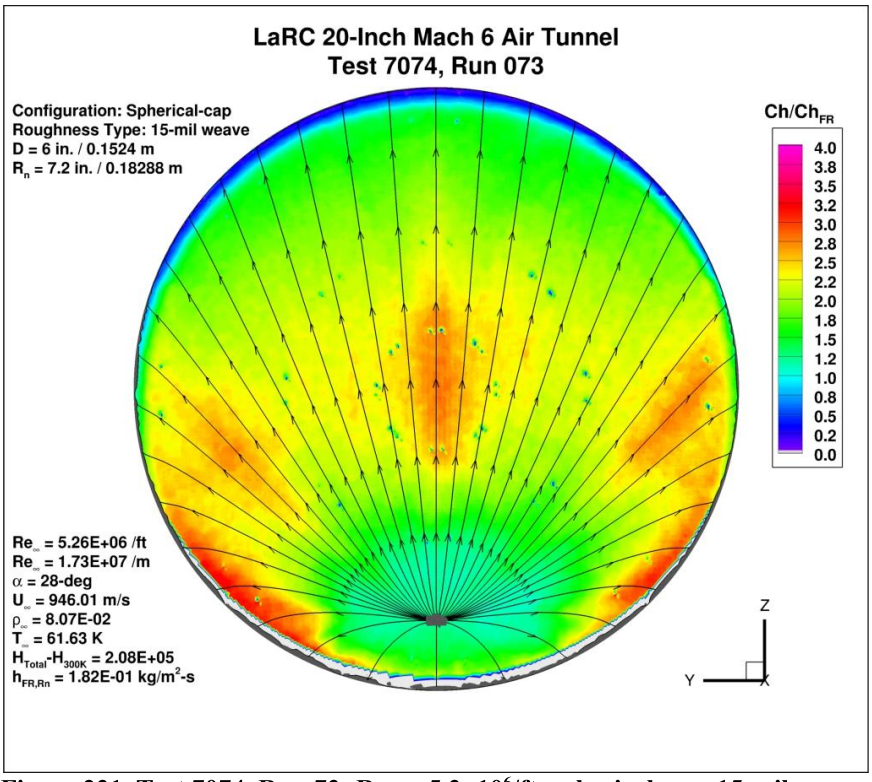


Figure 231. Test 7074, Run 73: $Re_\infty = 5.3\times10^6$/ft, spherical-cap, 15-mil weave.

(Condition was not run)

Figure 232. Test 7074, Run XX: $Re_\infty = 6.5\times10^6$/ft, spherical-cap, 15-mil weave.

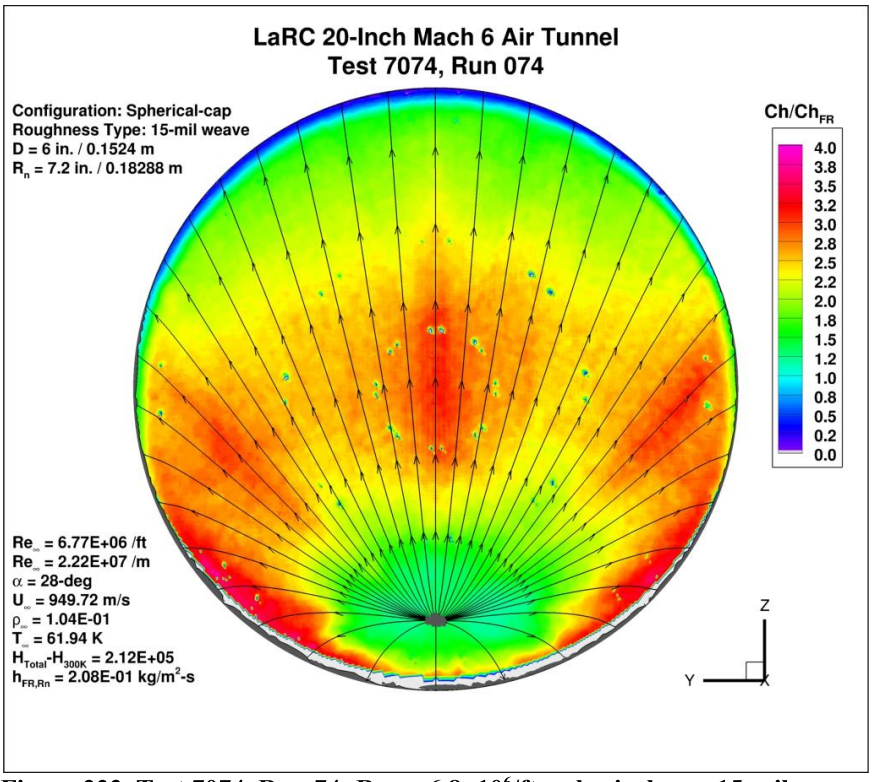


Figure 233. Test 7074, Run 74: $Re_\infty = 6.8\times10^6$/ft, spherical-cap, 15-mil weave.

(Condition was not run)

Figure 234. Test 7074, Run XX: $Re_\infty = 7.3\times10^6$/ft, spherical-cap, 15-mil weave.

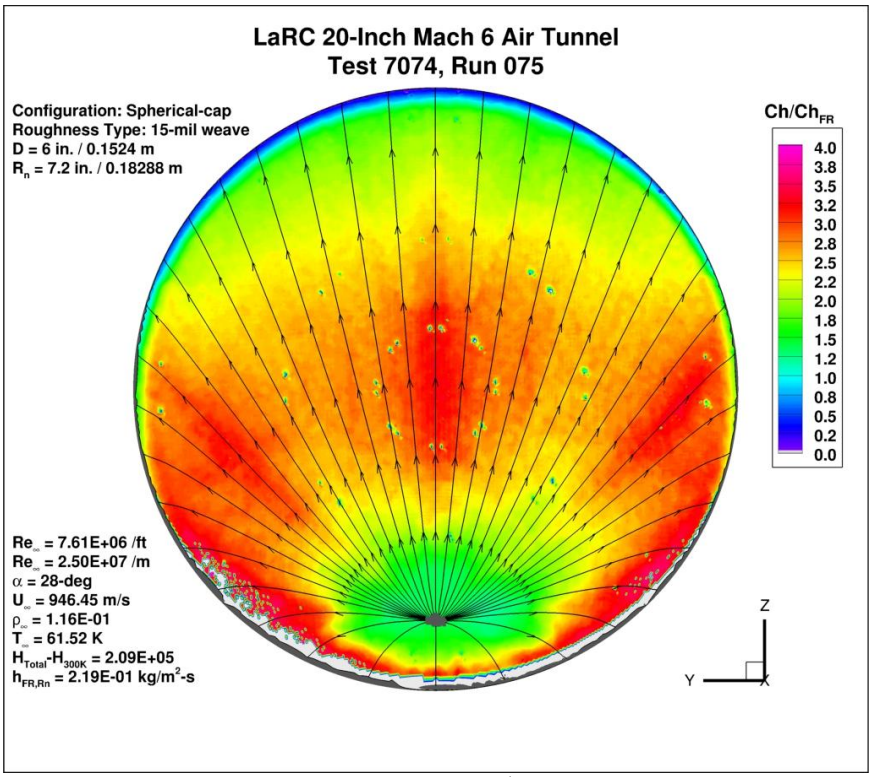


Figure 235. Test 7074, Run 75: $Re_\infty = 7.7\times10^6$/ft, spherical-cap, 15-mil weave.

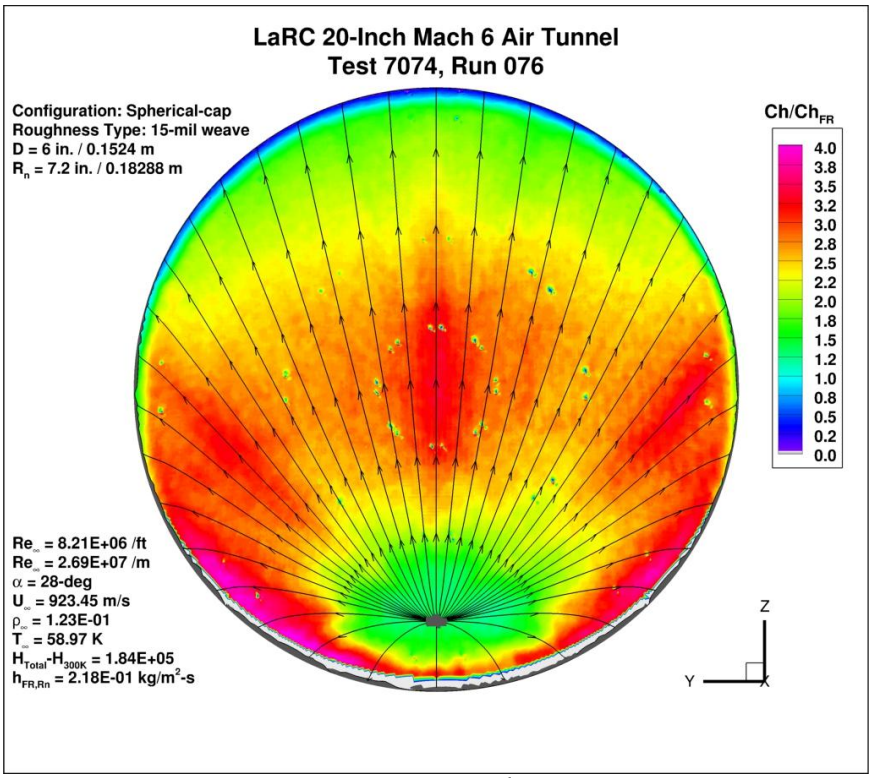


Figure 236. Test 7074, Run 76: $Re_\infty = 8.2\times10^6$/ft, spherical-cap, 15-mil weave.

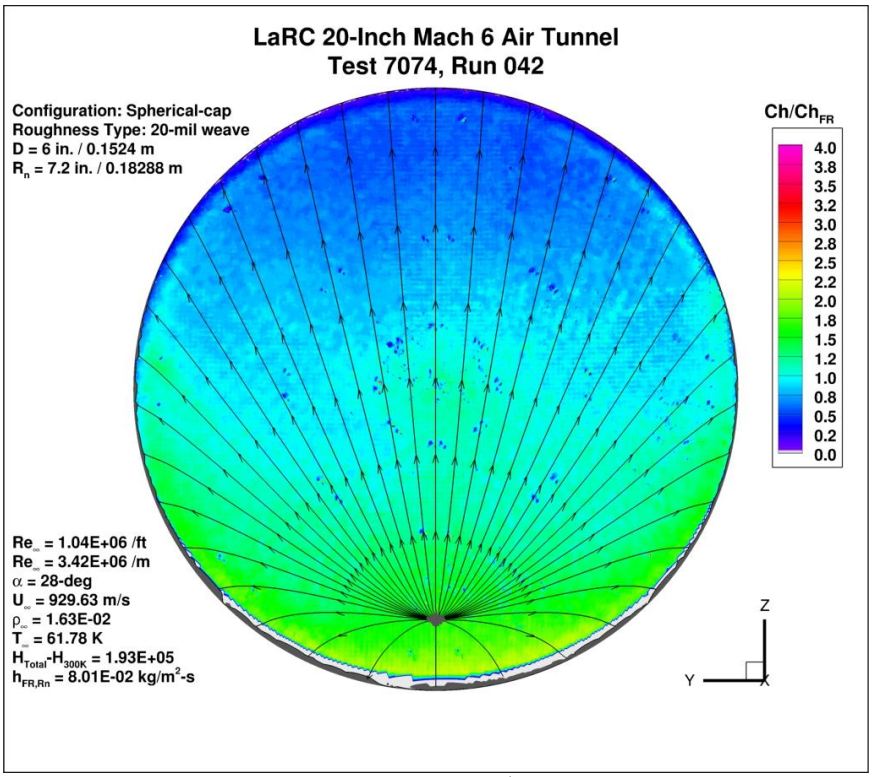


Figure 237. Test 7074, Run 42: $Re_\infty = 1.0\times10^6$/ft, spherical-cap, 20-mil weave.

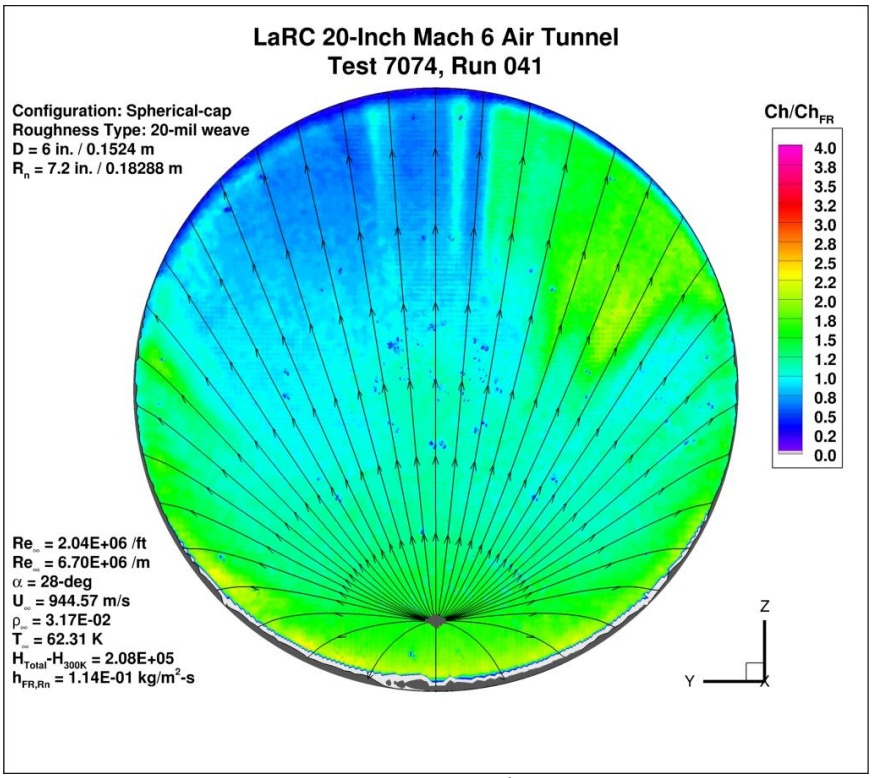


Figure 238. Test 7074, Run 41: $Re_\infty = 2.0\times10^6$/ft, spherical-cap, 20-mil weave.

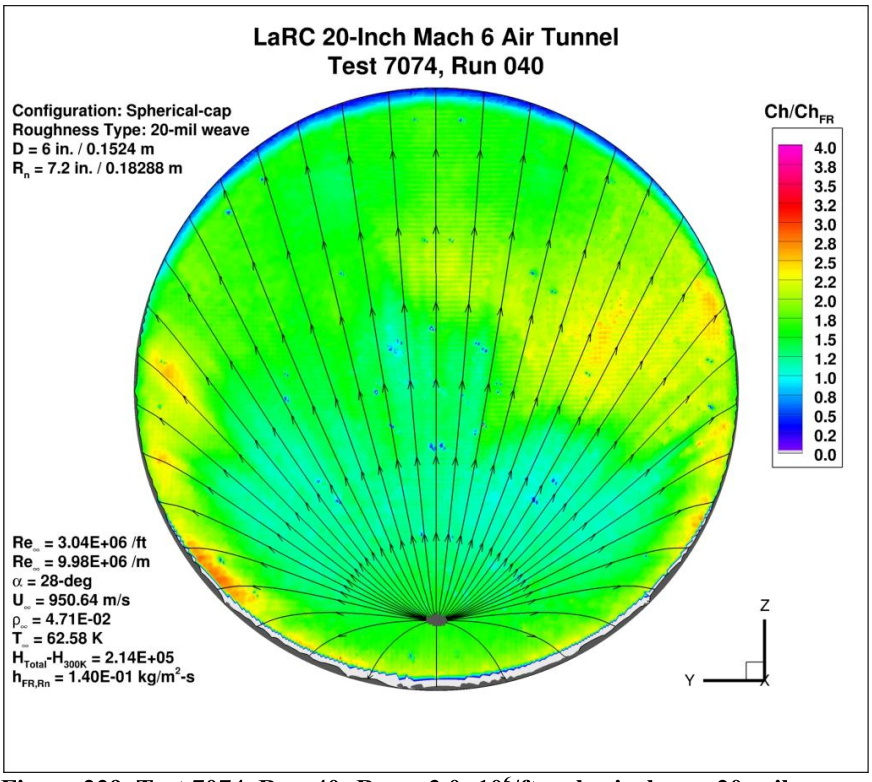


Figure 239. Test 7074, Run 40: $Re_\infty = 3.0\times10^6$/ft, spherical-cap, 20-mil weave.

(Condition was not run)

Figure 240. Test 7074, Run XX: $Re_\infty = 5.0\times10^6$/ft, spherical-cap, 20-mil weave.

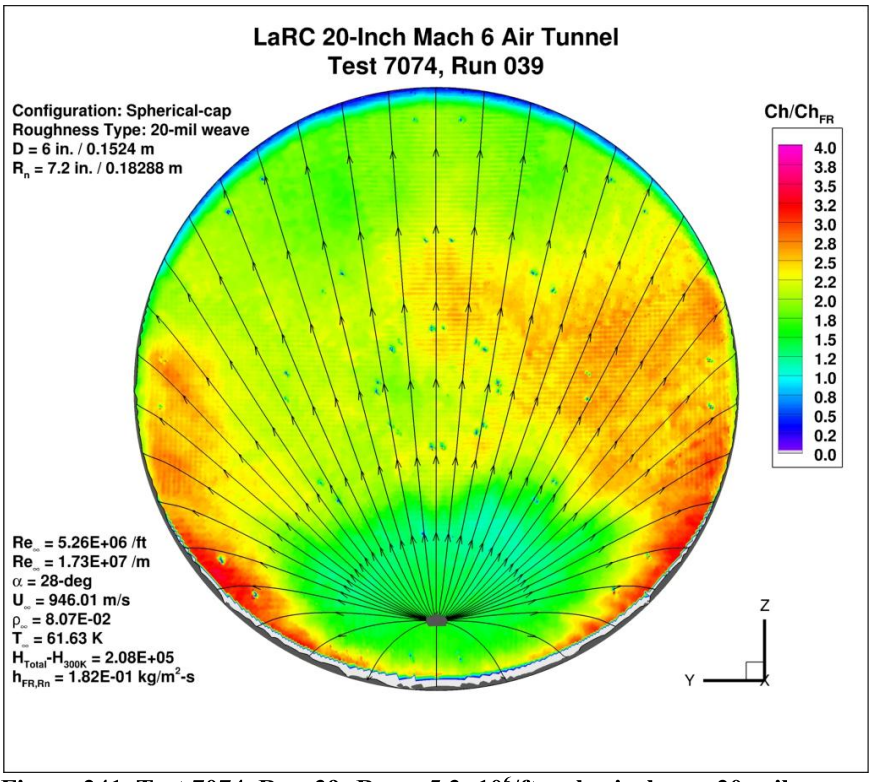


Figure 241. Test 7074, Run 39: $Re_\infty = 5.3\times10^6$/ft, spherical-cap, 20-mil weave.

(Condition was not run)

Figure 242. Test 7074, Run XX: $Re_\infty = 6.5\times10^6$/ft, spherical-cap, 20-mil weave.

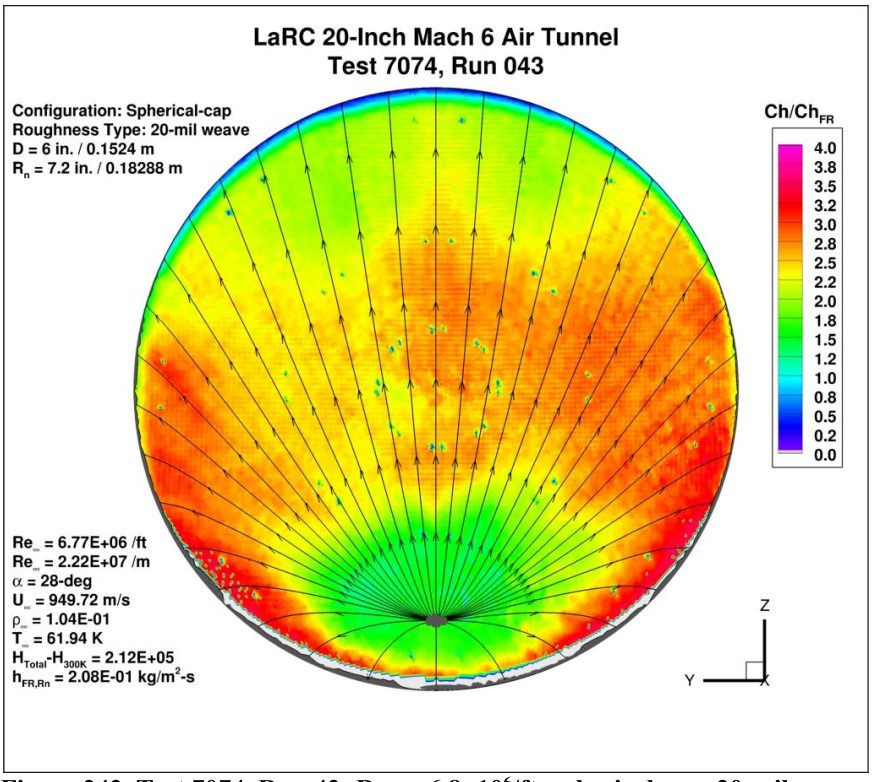


Figure 243. Test 7074, Run 43: $Re_\infty = 6.8\times10^6$/ft, spherical-cap, 20-mil weave.

(Condition was not run)

Figure 244. Test 7074, Run XX: $Re_\infty = 7.3\times10^6$/ft, spherical-cap, 20-mil weave.

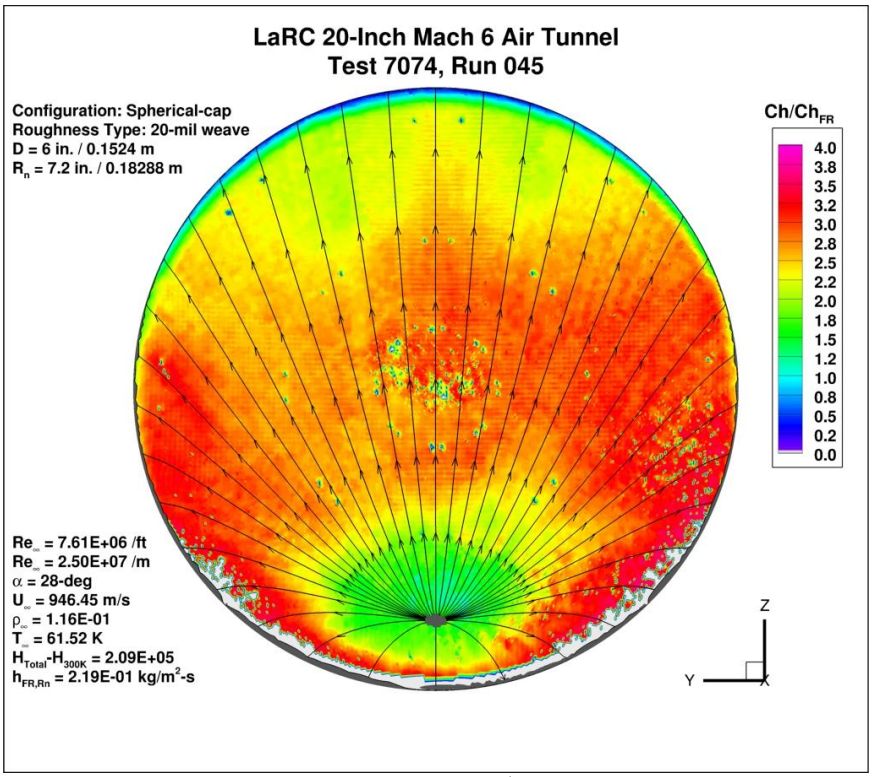


Figure 245. Test 7074, Run 45: $Re_\infty = 7.6\times10^6$/ft, spherical-cap, 20-mil weave.

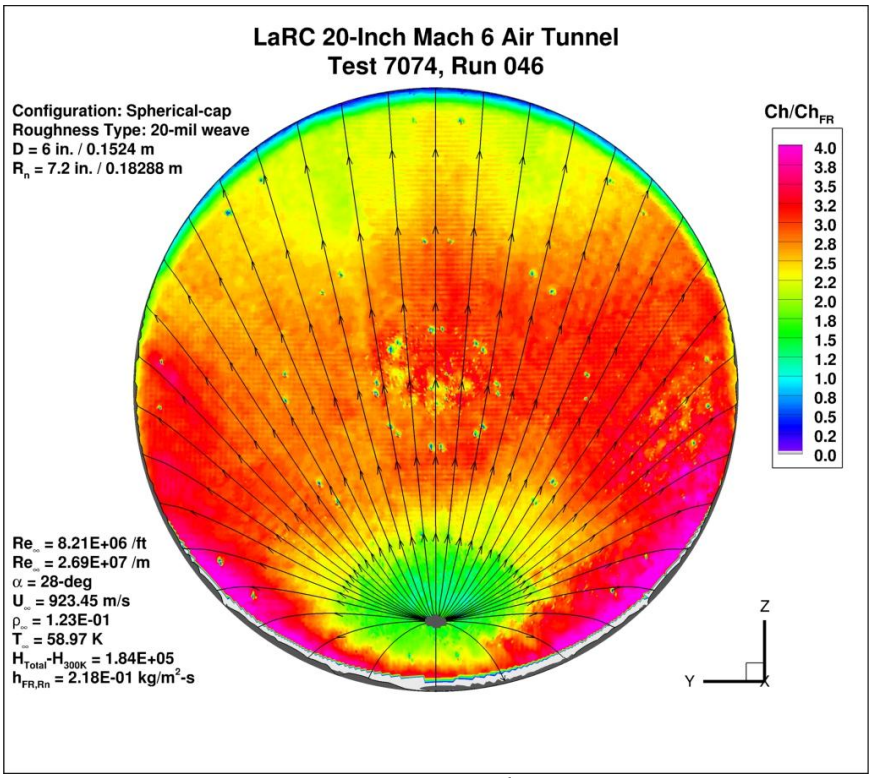


Figure 246. Test 7074, Run 46: $Re_\infty = 8.2\times10^6$/ft, spherical-cap, 20-mil weave.

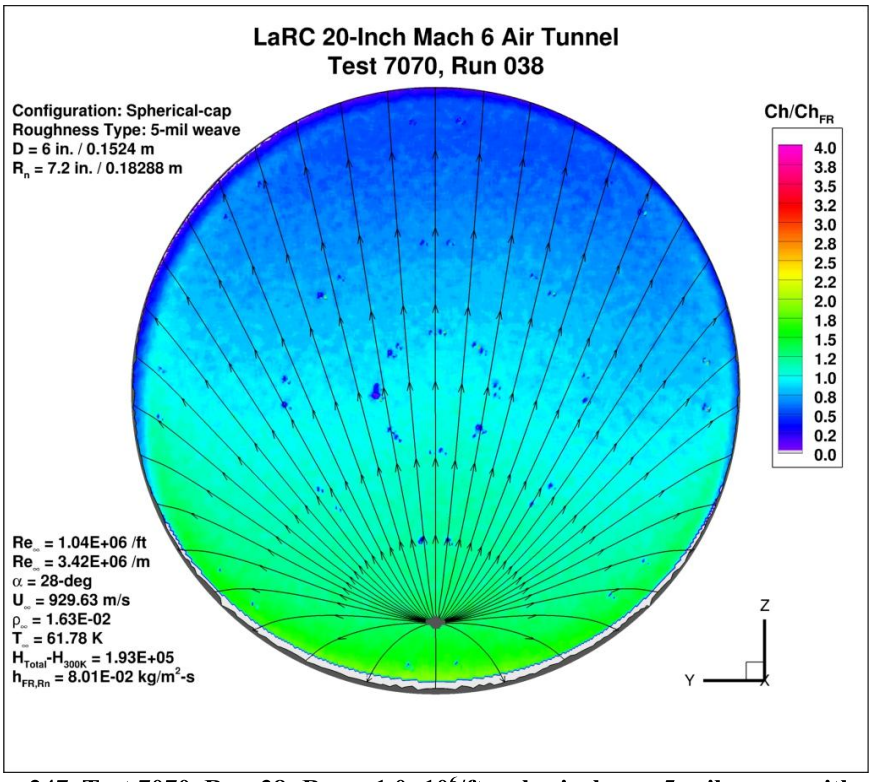


Figure 247. Test 7070, Run 38: $Re_\infty = 1.0\times10^6$/ft, spherical-cap, 5-mil weave with seam.

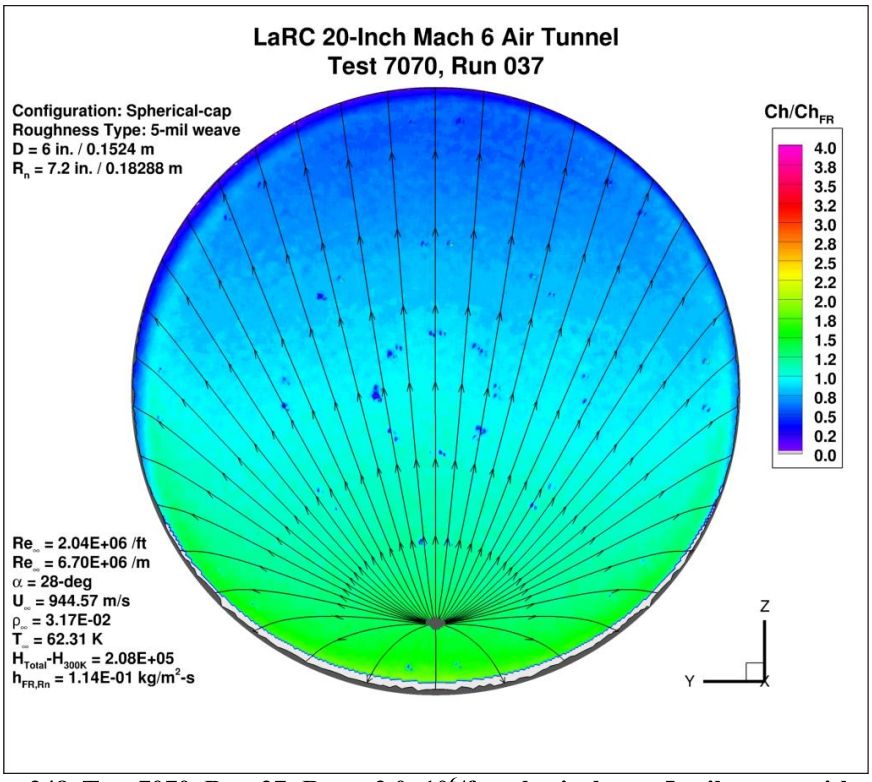


Figure 248. Test 7070, Run 37: $Re_\infty = 2.0\times10^6$/ft, spherical-cap, 5-mil weave with seam.

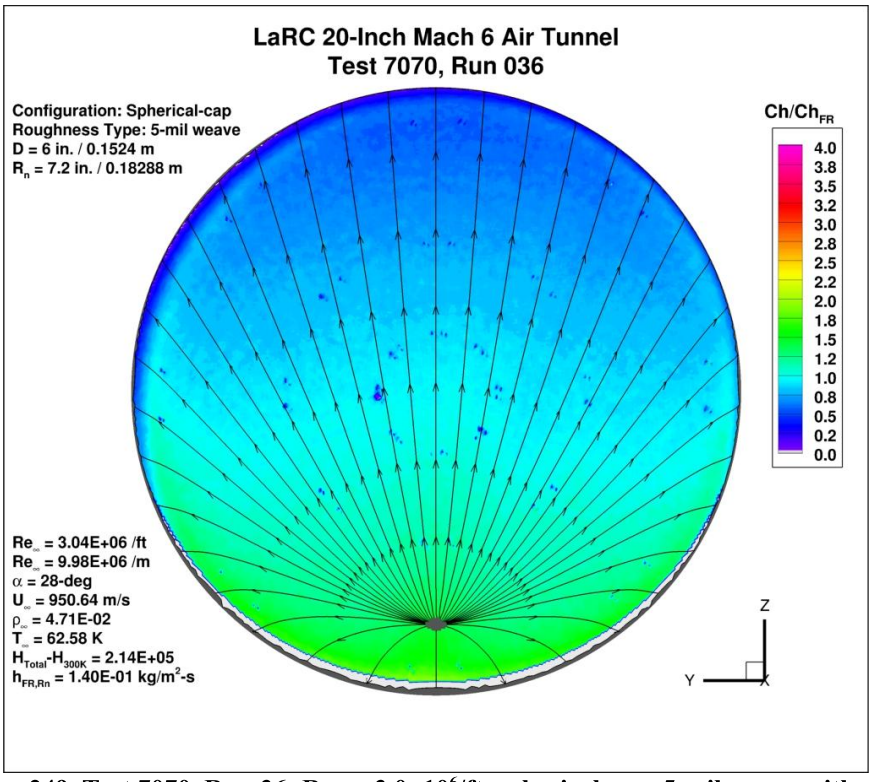


Figure 249. Test 7070, Run 36: $Re_\infty = 3.0\times10^6$/ft, spherical-cap, 5-mil weave with seam.

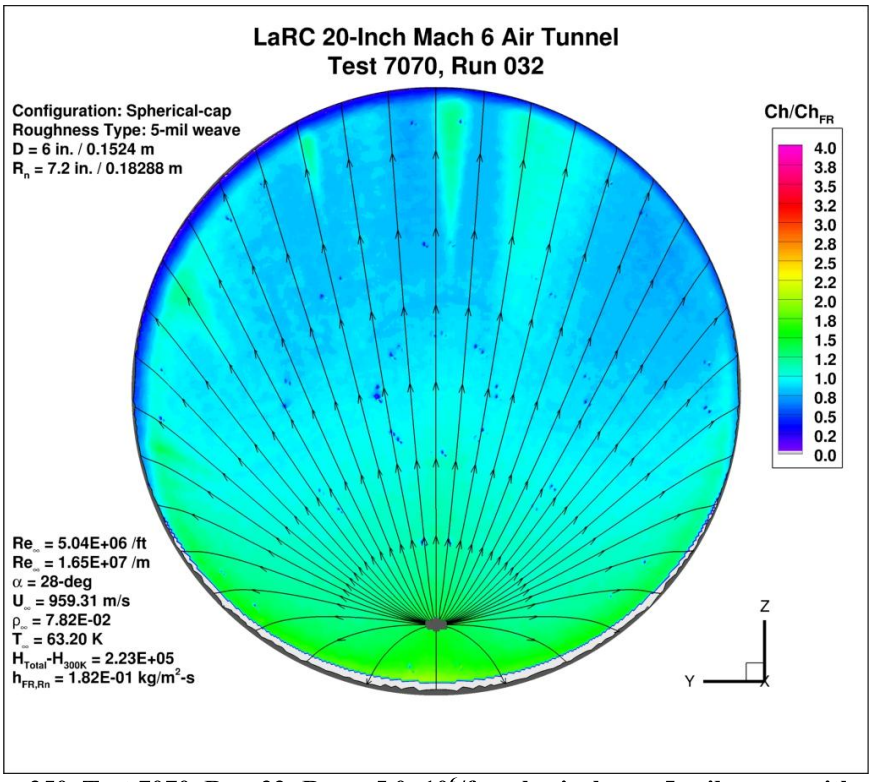
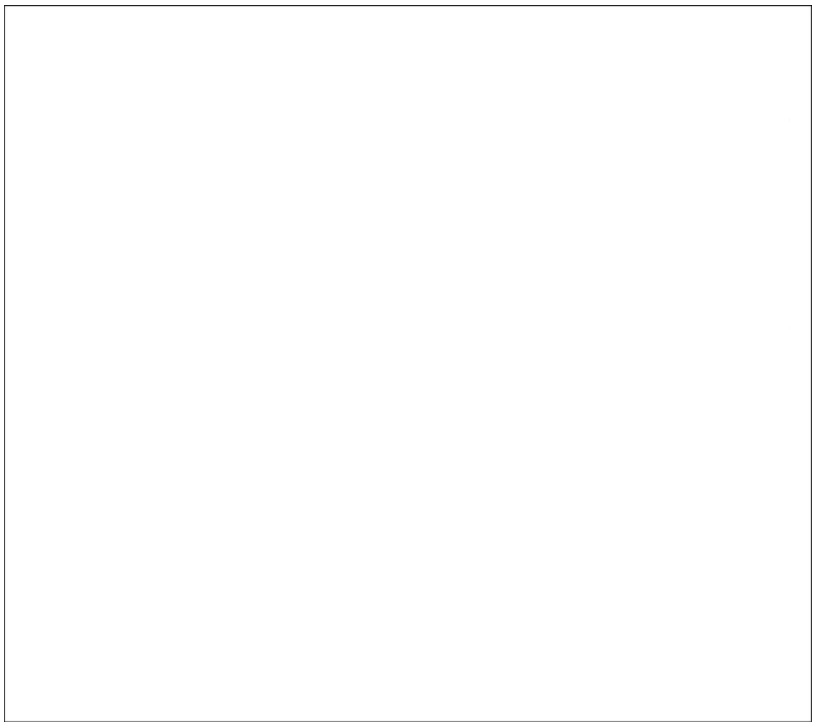


Figure 250. Test 7070, Run 32: $Re_\infty = 5.0\times10^6$/ft, spherical-cap, 5-mil weave with seam.



(Condition was not run)

Figure 251. Test 7070, Run XX: Re_∞ = 5.3×10^6/ft, spherical-cap, 5-mil weave with seam.

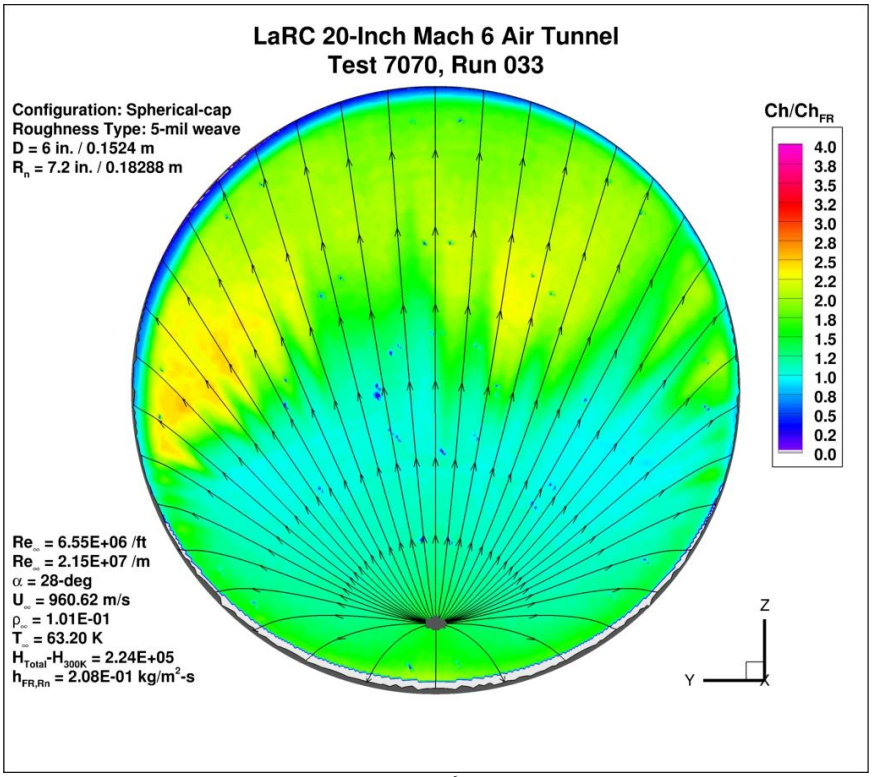


Figure 252. Test 7070, Run 33: Re_∞ = 6.5×10^6/ft, spherical-cap, 5-mil weave with seam.

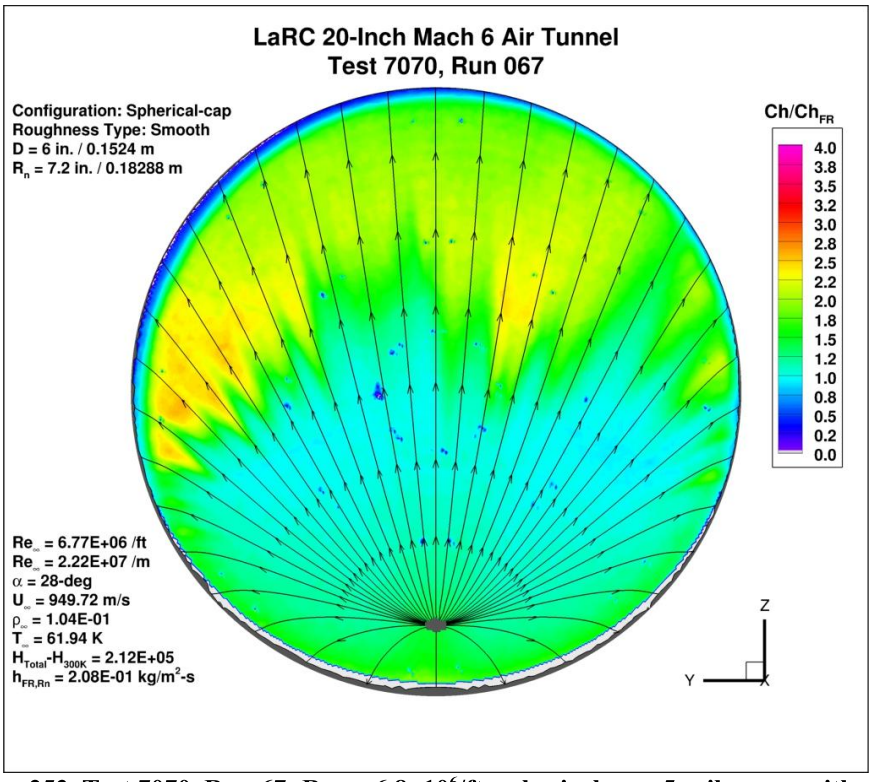


Figure 253. Test 7070, Run 67: $Re_\infty = 6.8\times10^6$/ft, spherical-cap, 5-mil weave with seam.

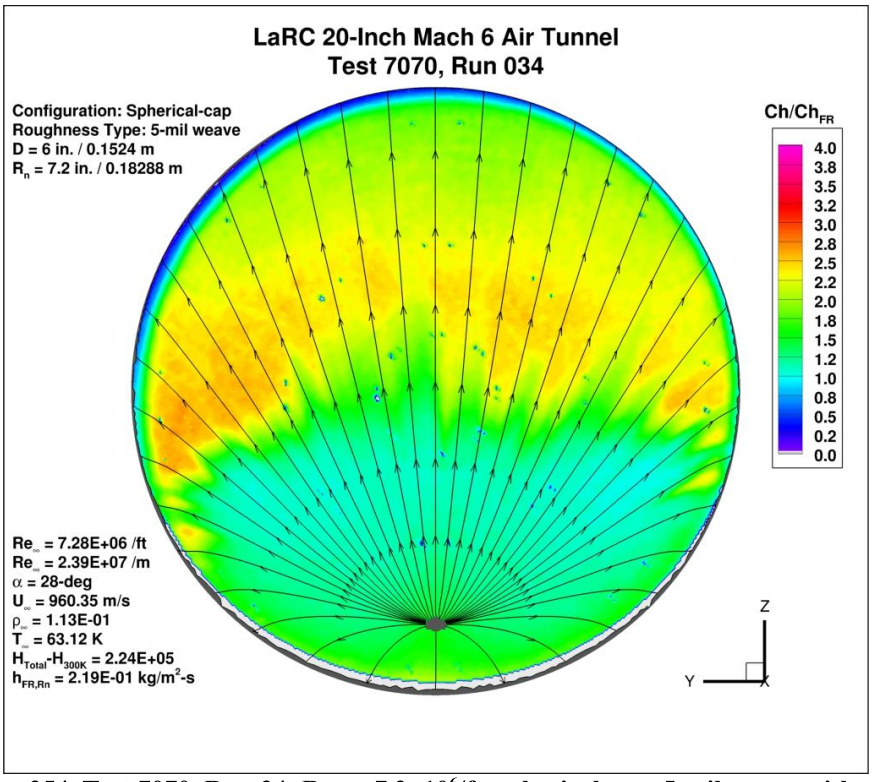


Figure 254. Test 7070, Run 34: $Re_\infty = 7.2\times10^6$/ft, spherical-cap, 5-mil weave with seam.

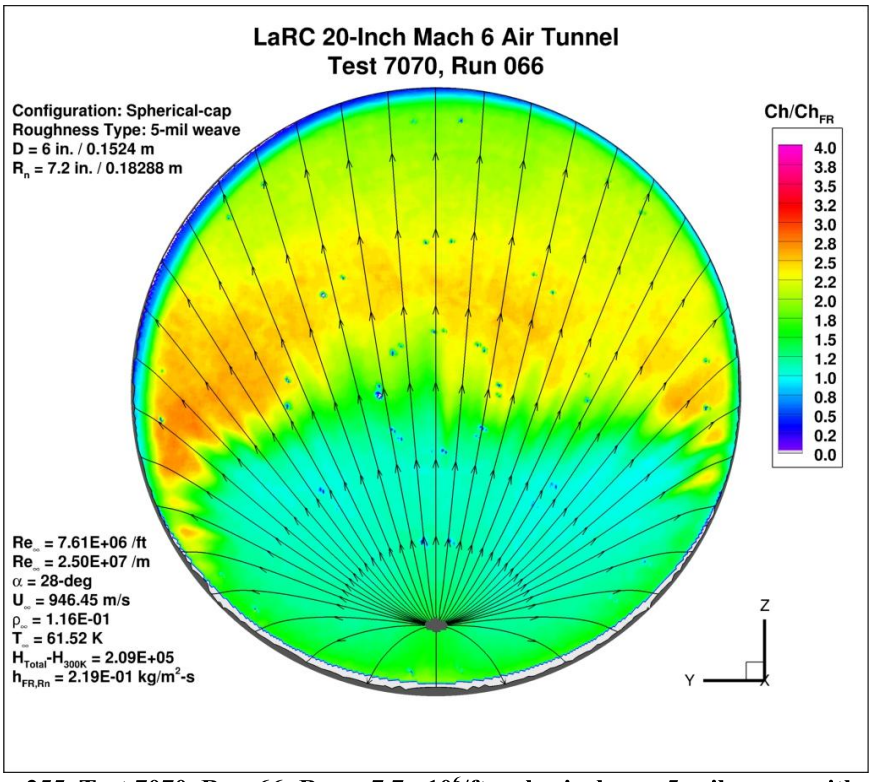


Figure 255. Test 7070, Run 66: Re_∞ = 7.7 ×10^6/ft, spherical-cap, 5-mil weave with seam.

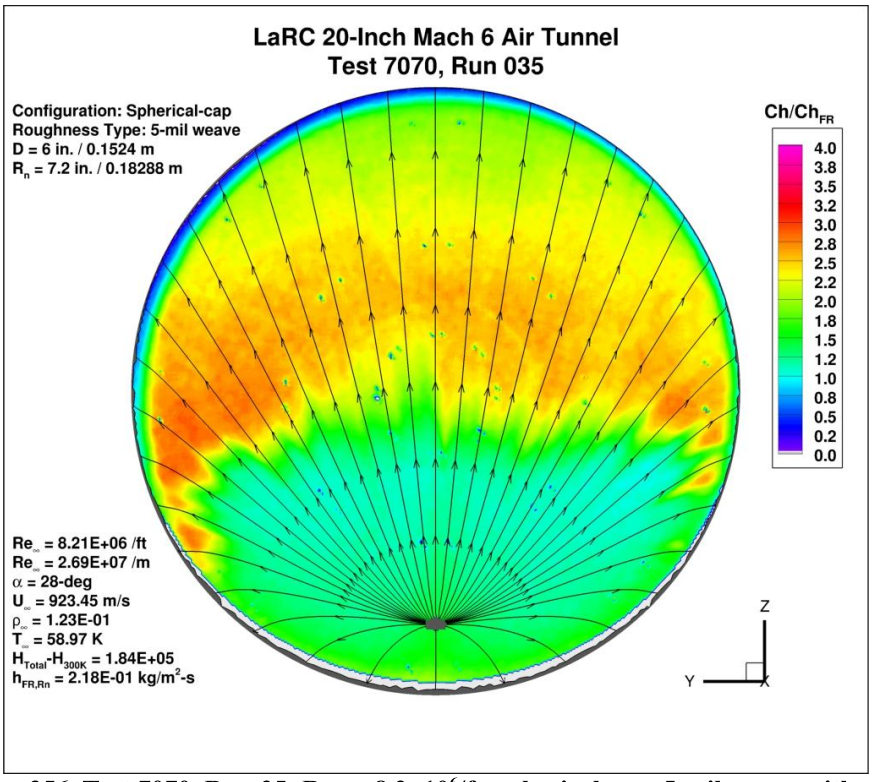
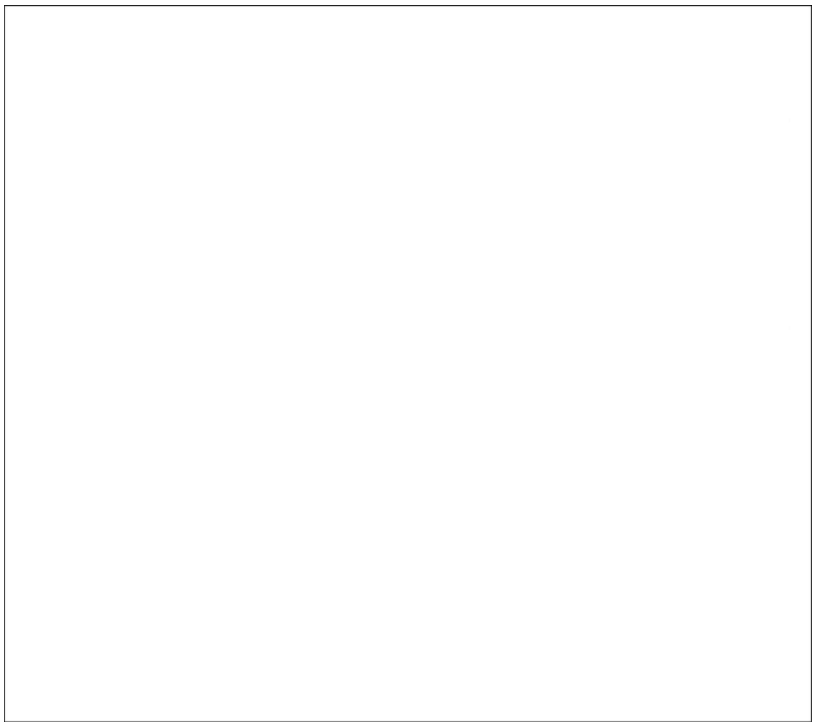
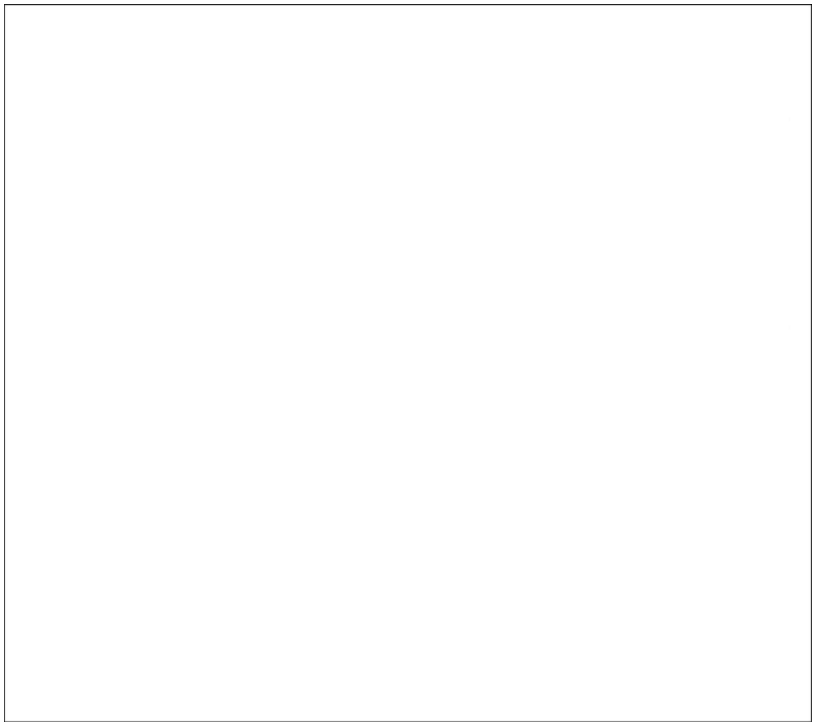


Figure 256. Test 7070, Run 35: Re_∞ = 8.2×10^6/ft, spherical-cap, 5-mil weave with seam.



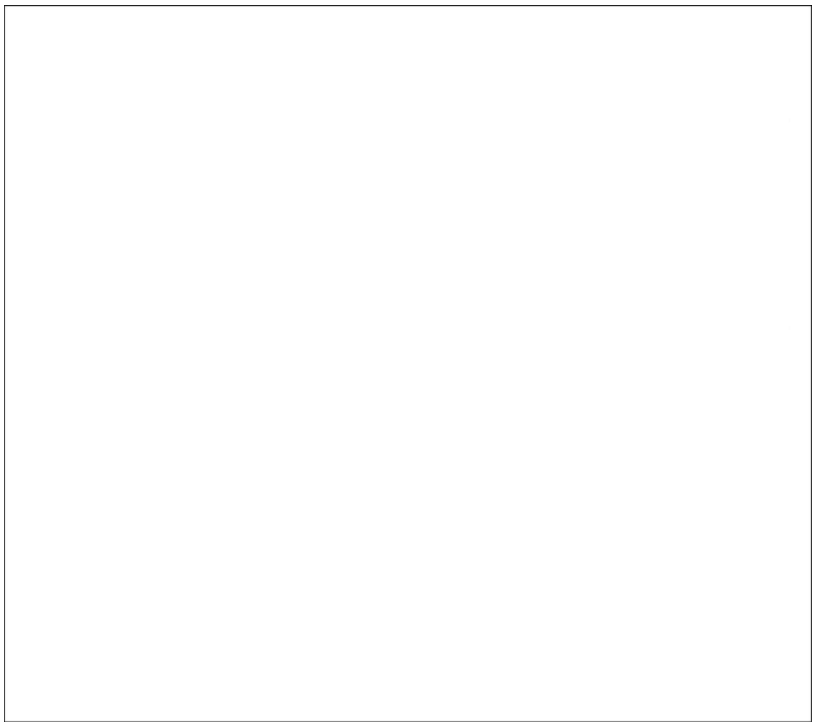
(Condition was not run)

Figure 257. Test 7070, Run XX: $Re_\infty = 1.0\times10^6$/ft, spherical-cap, 10-mil weave with seam.



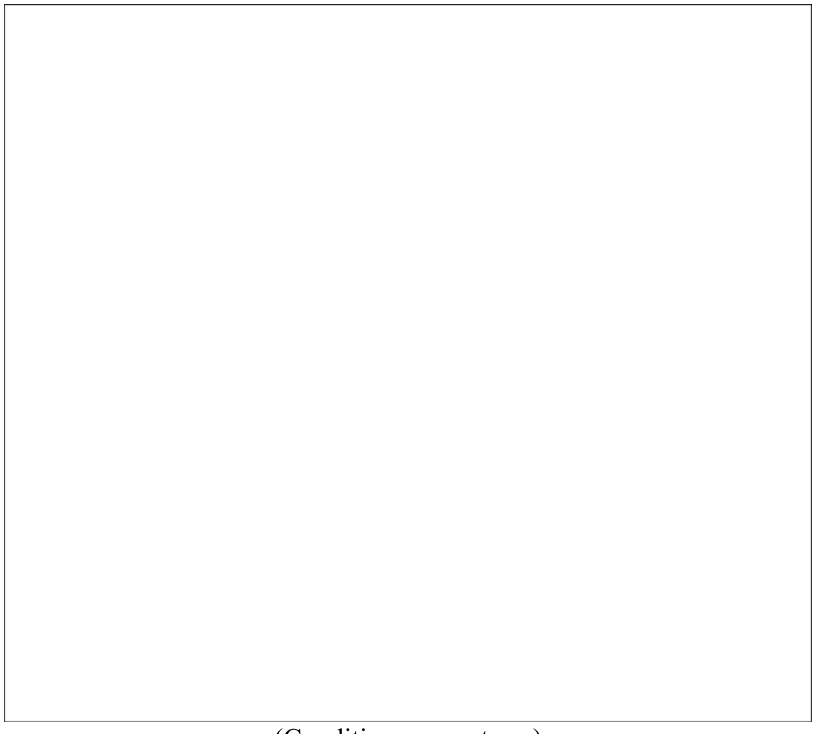
(Condition was not run)

Figure 258. Test 7070, Run XX: $Re_\infty = 2.0\times10^6$/ft, spherical-cap, 10-mil weave with seam.



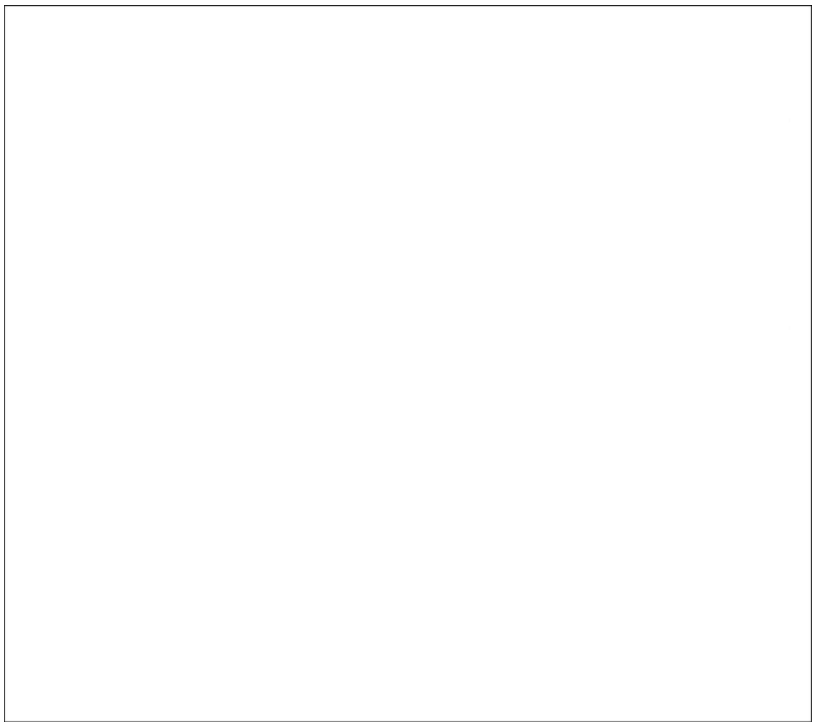
(Condition was not run)

Figure 259. Test 7070, Run XX: $Re_\infty = 3.0\times10^6$/ft, spherical-cap, 10-mil weave with seam.



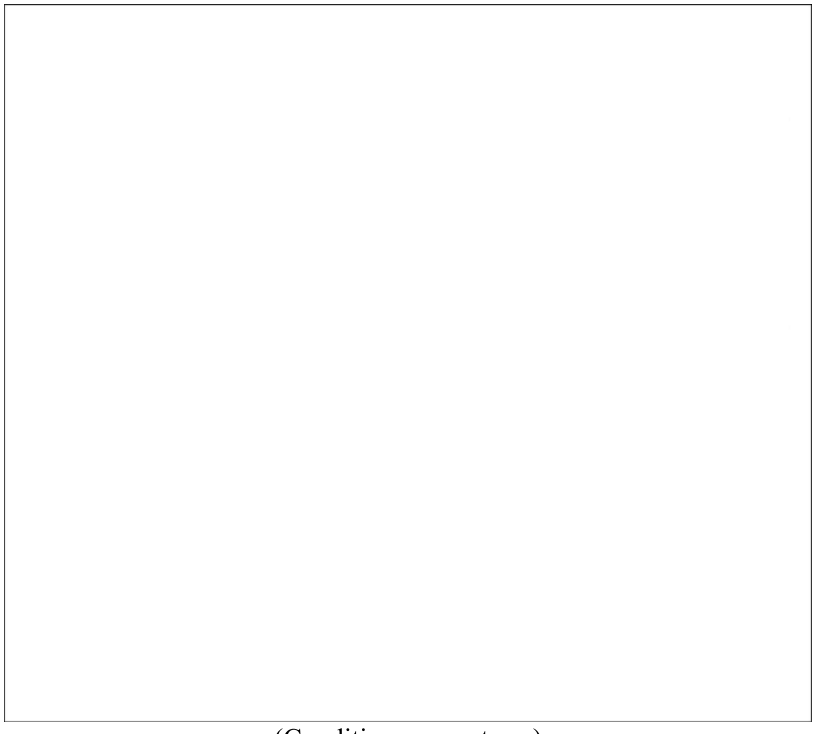
(Condition was not run)

Figure 260. Test 7070, Run XX: $Re_\infty = 5.0\times10^6$/ft, spherical-cap, 10-mil weave with seam.



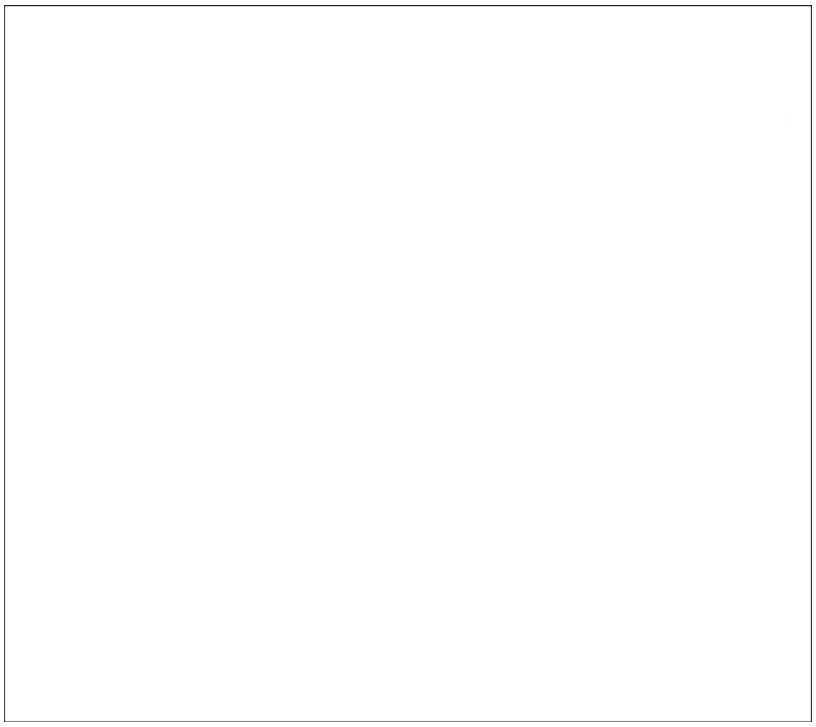
(Condition was not run)

Figure 261. Test 7070, Run XX: $Re_\infty = 5.3\times10^6$/ft, spherical-cap, 10-mil weave with seam.



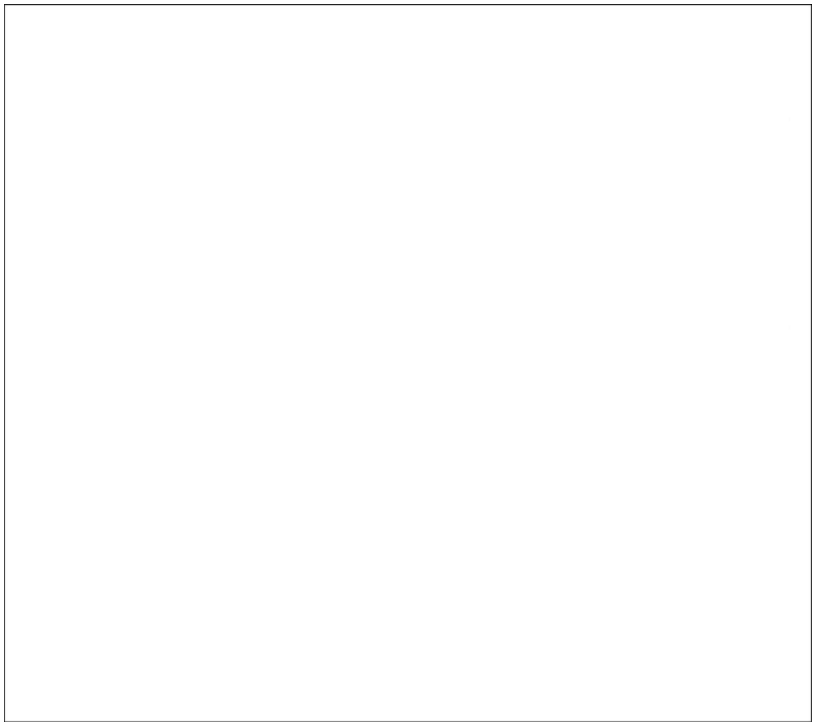
(Condition was not run)

Figure 262. Test 7070, Run XX: $Re_\infty = 6.5\times10^6$/ft, spherical-cap, 10-mil weave with seam.



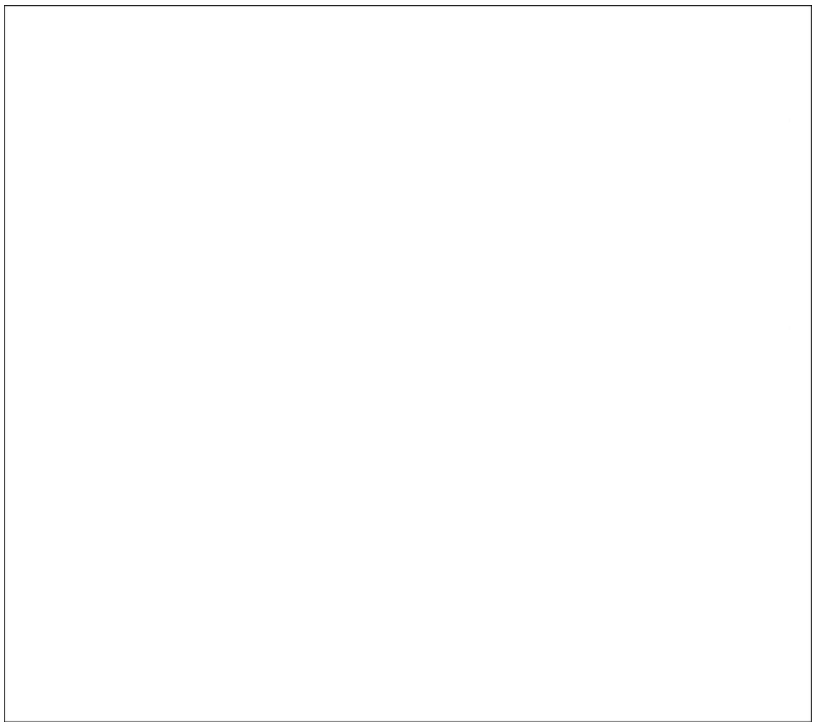
(Condition was not run)

Figure 263. Test 7070, Run XX: $Re_\infty = 6.8\times10^6$/ft, spherical-cap, 10-mil weave with seam.



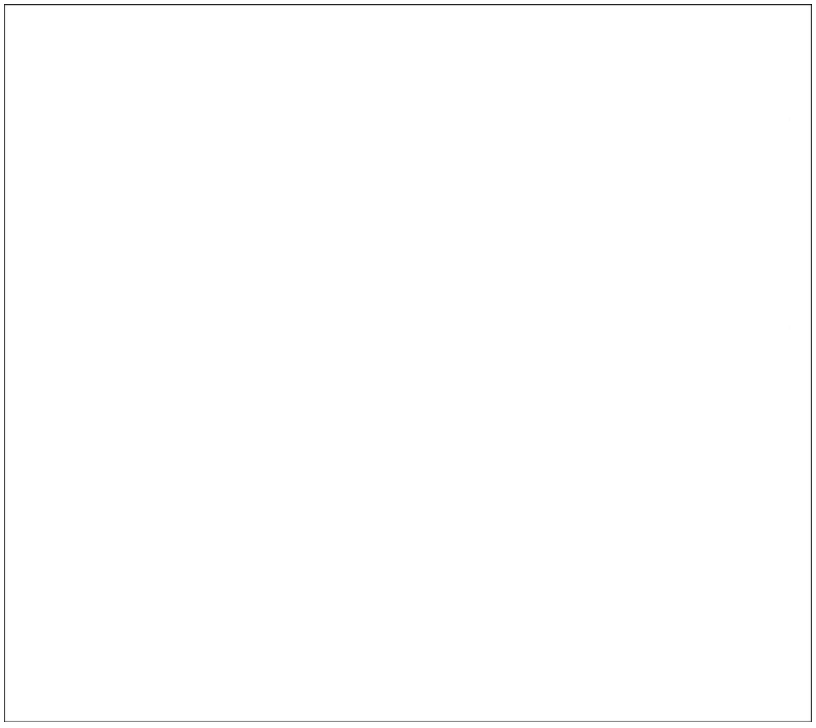
(Condition was not run)

Figure 264. Test 7070, Run XX: $Re_\infty = 7.3\times10^6$/ft, spherical-cap, 10-mil weave with seam.



(Condition was not run)

Figure 265. Test 7070, Run XX: $Re_\infty = 7.8\times10^6$/ft, spherical-cap, 10-mil weave with seam.



(Condition was not run)

Figure 266. Test 7070, Run XX: $Re_\infty = 8.2\times10^6$/ft, spherical-cap, 10-mil weave with seam.

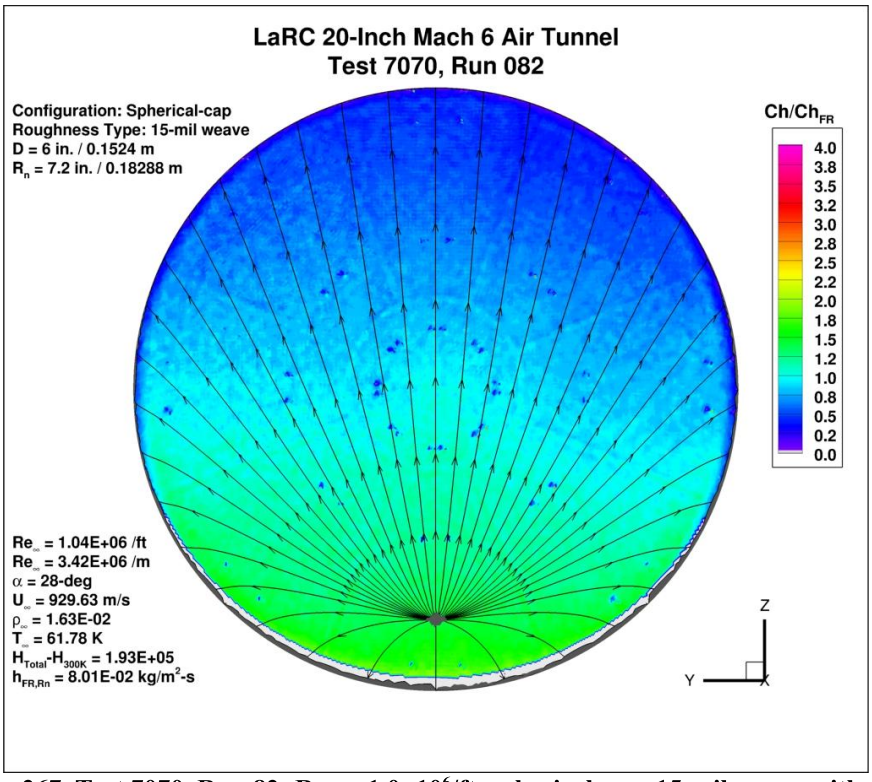


Figure 267. Test 7070, Run 82: $Re_\infty = 1.0\times10^6$/ft, spherical-cap, 15-mil weave with seam.

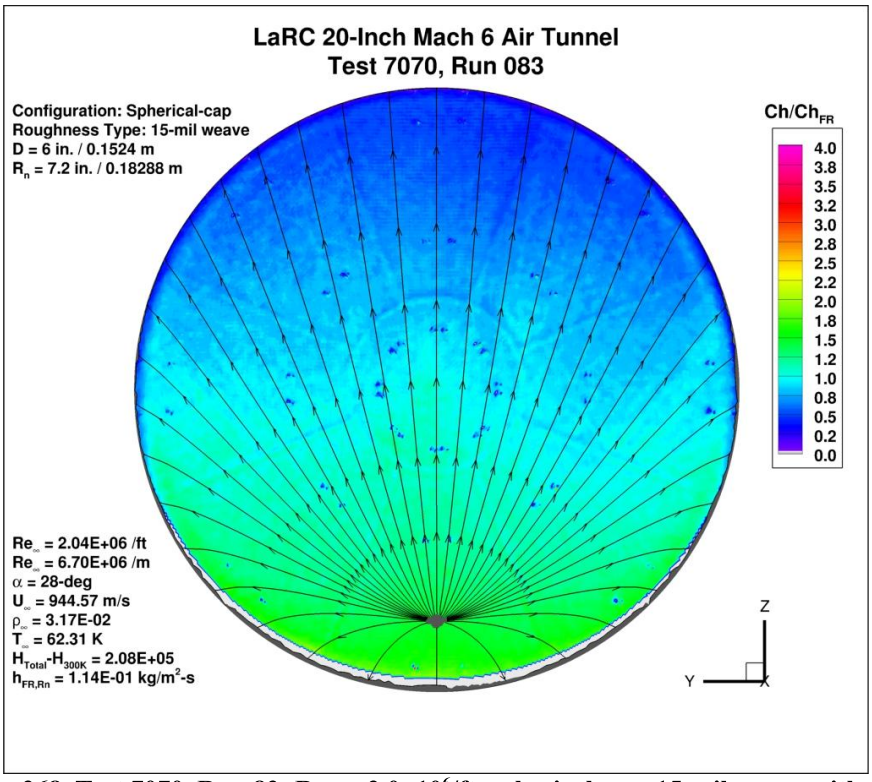


Figure 268. Test 7070, Run 83: $Re_\infty = 2.0\times10^6$/ft, spherical-cap, 15-mil weave with seam.

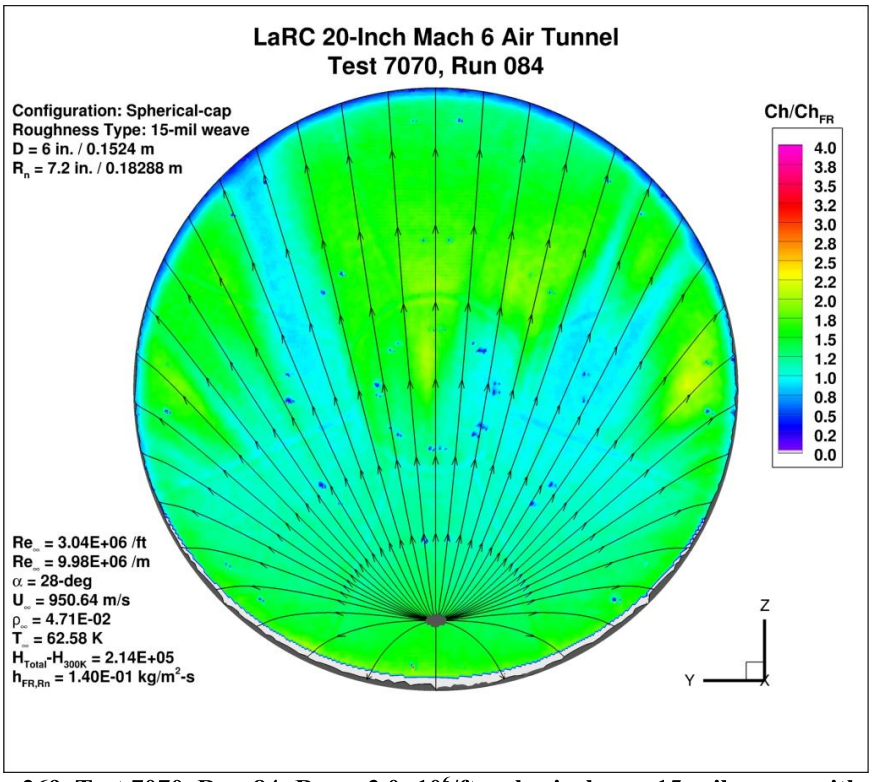


Figure 269. Test 7070, Run 84: $Re_\infty = 3.0\times10^6$/ft, spherical-cap, 15-mil weave with seam.

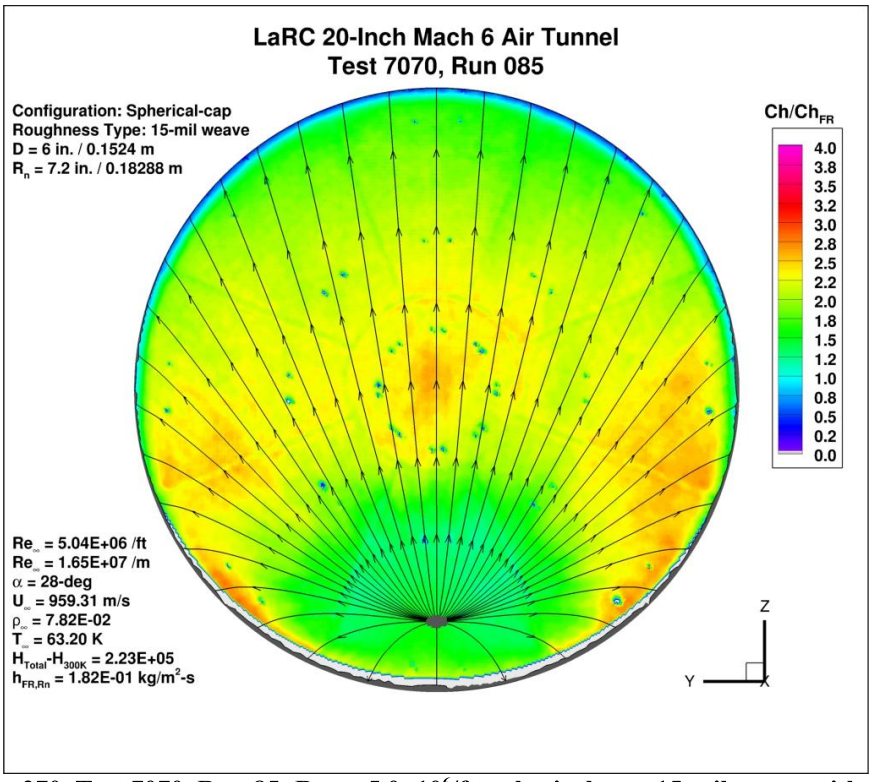
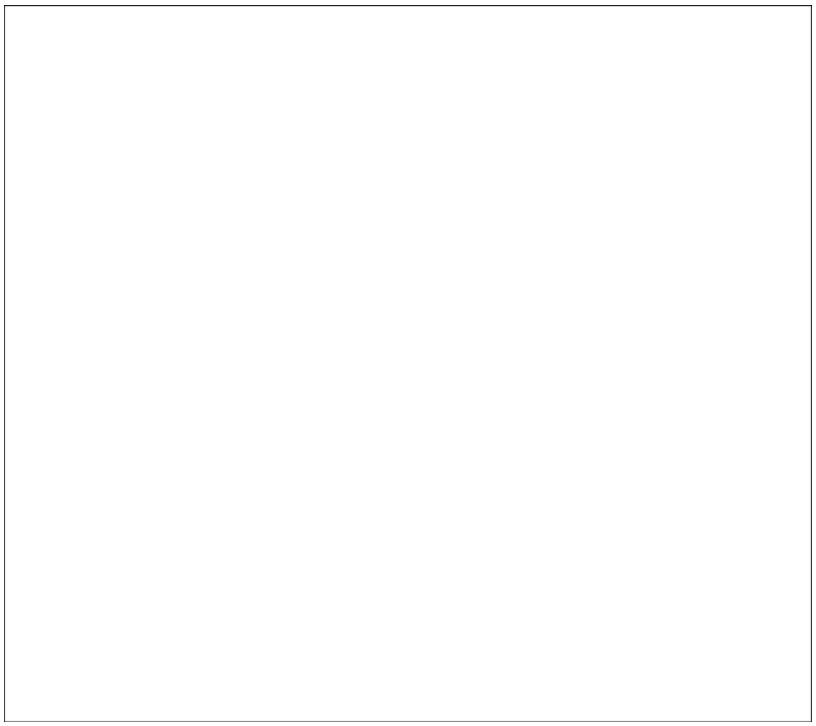
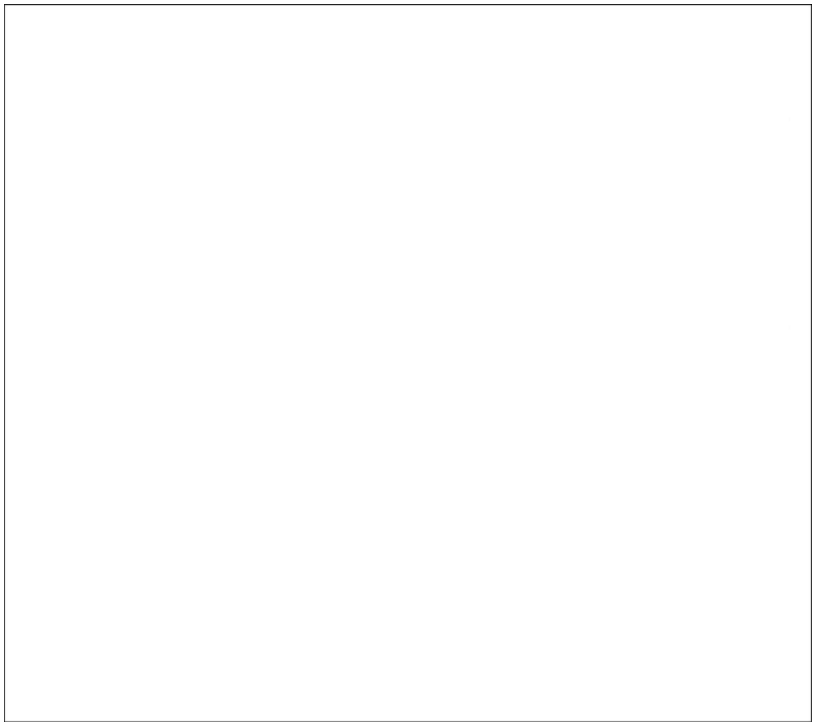


Figure 270. Test 7070, Run 85: $Re_\infty = 5.0\times10^6$/ft, spherical-cap, 15-mil weave with seam.



(Condition was not run)

Figure 271. Test 7070, Run XX: $Re_\infty = 5.3\times10^6$/ft, spherical-cap, 15-mil weave with seam.



(Condition was not run)

Figure 272. Test 7070, Run XX: $Re_\infty = 6.5\times10^6$/ft, spherical-cap, 15-mil weave with seam.

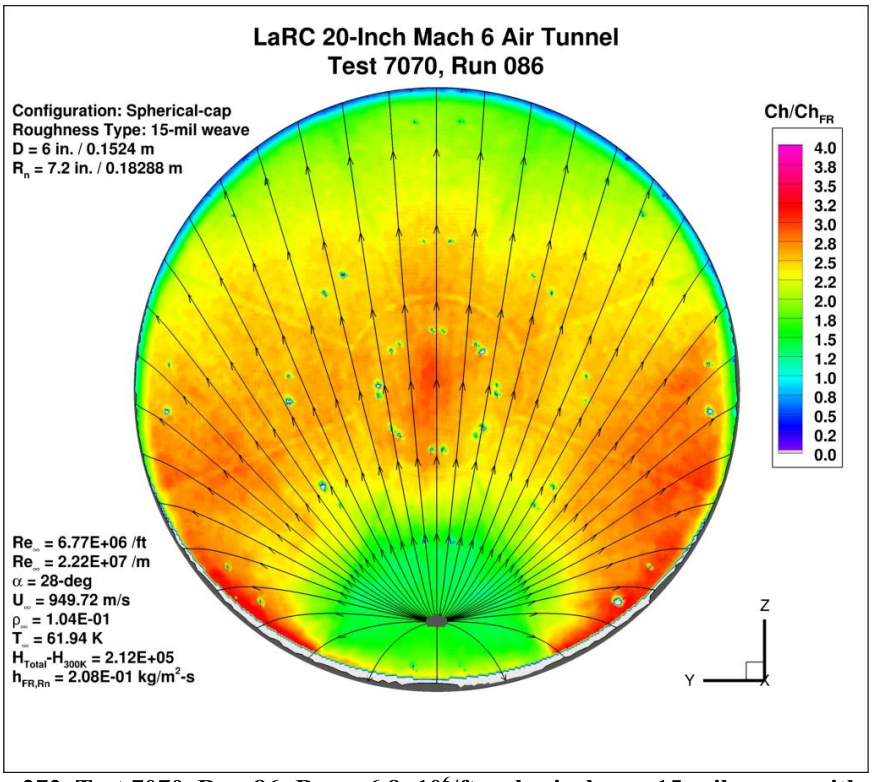


Figure 273. Test 7070, Run 86: $Re_\infty = 6.8\times10^6$/ft, spherical-cap, 15-mil weave with seam.

(Condition was not run)

Figure 274. Test 7070, Run XX: $Re_\infty = 7.3\times10^6$/ft, spherical-cap, 15-mil weave with seam.

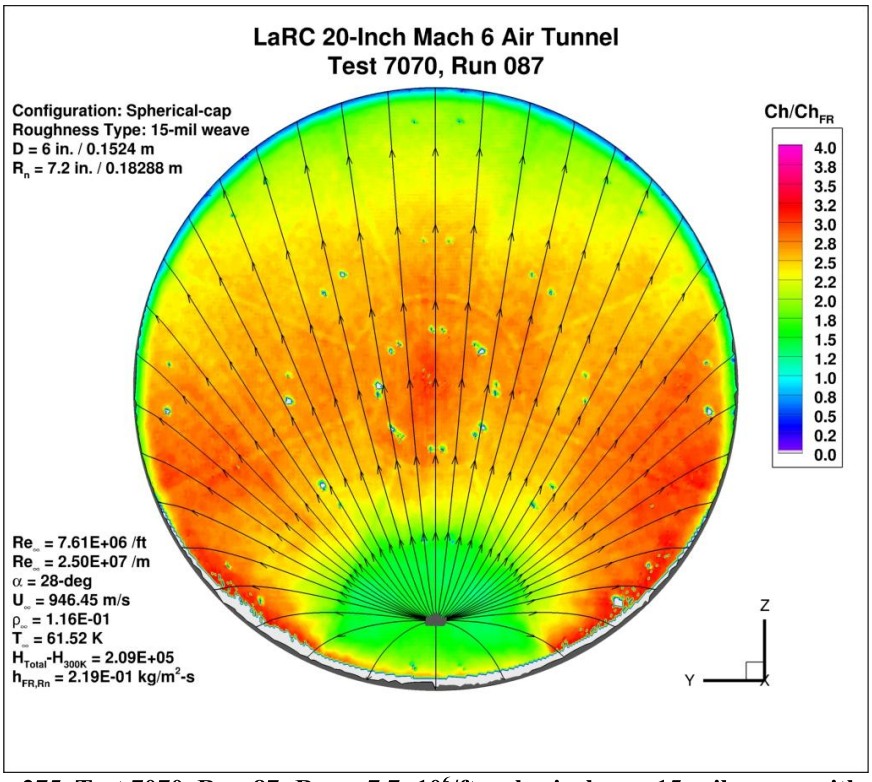


Figure 275. Test 7070, Run 87: $Re_\infty = 7.7\times10^6$/ft, spherical-cap, 15-mil weave with seam.

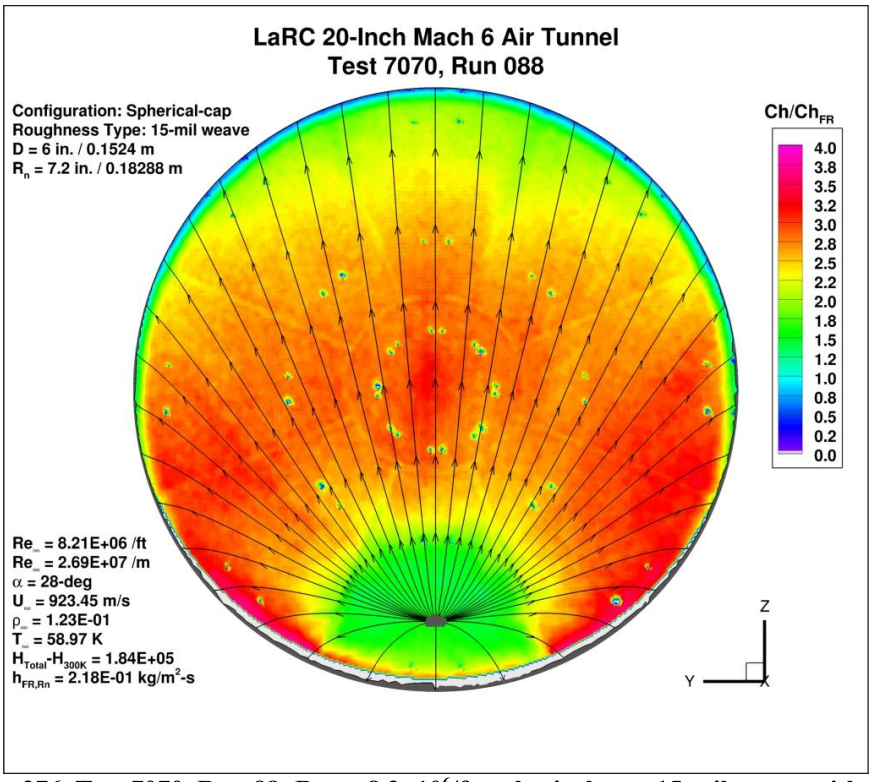


Figure 276. Test 7070, Run 88: $Re_\infty = 8.2\times10^6$/ft, spherical-cap, 15-mil weave with seam.

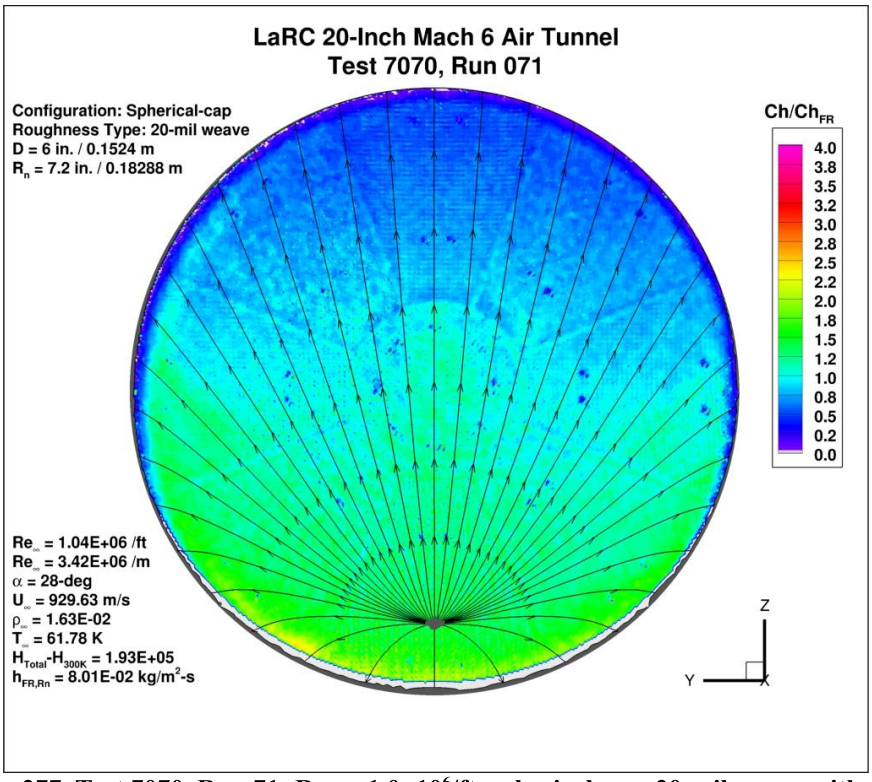


Figure 277. Test 7070, Run 71: $Re_\infty = 1.0\times10^6$/ft, spherical-cap, 20-mil weave with seam.

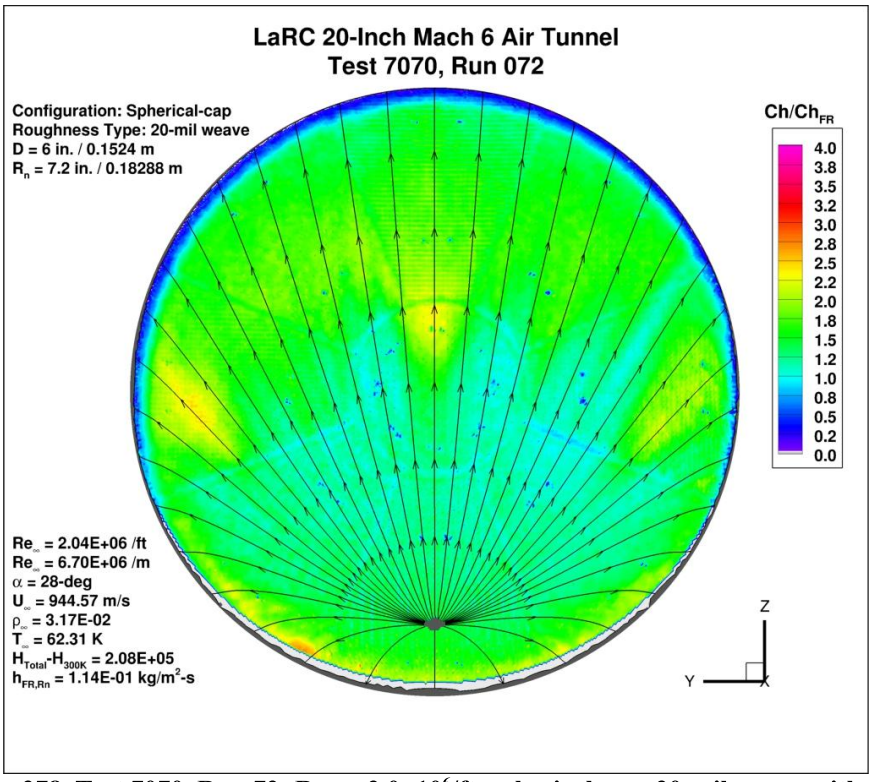


Figure 278. Test 7070, Run 72: $Re_\infty = 2.0\times10^6$/ft, spherical-cap, 20-mil weave with seam.

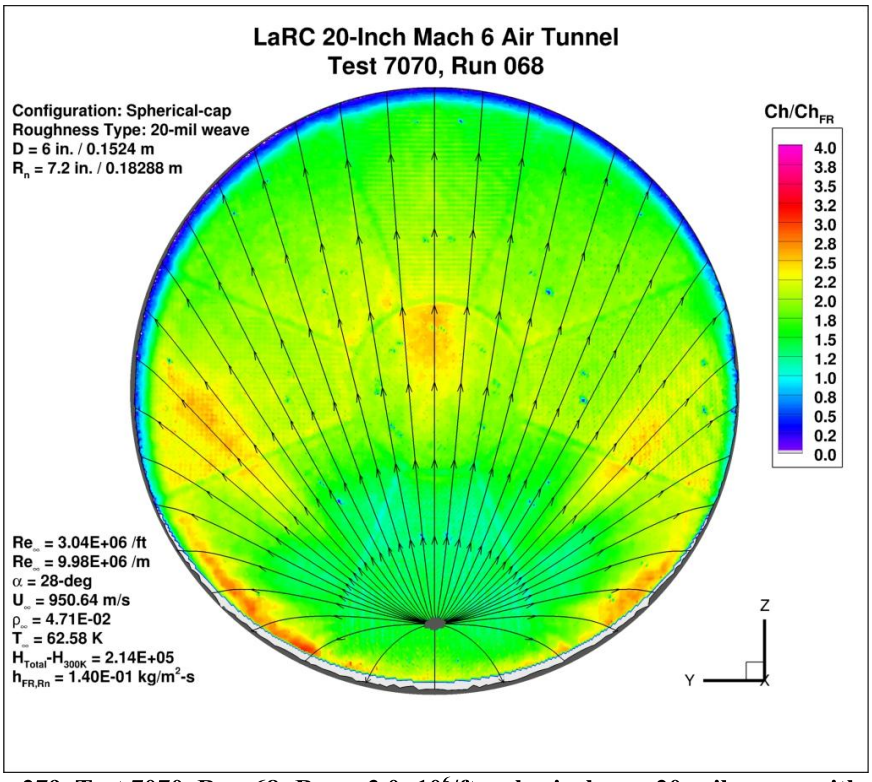


Figure 279. Test 7070, Run 68: $Re_\infty = 3.0\times10^6$/ft, spherical-cap, 20-mil weave with seam.

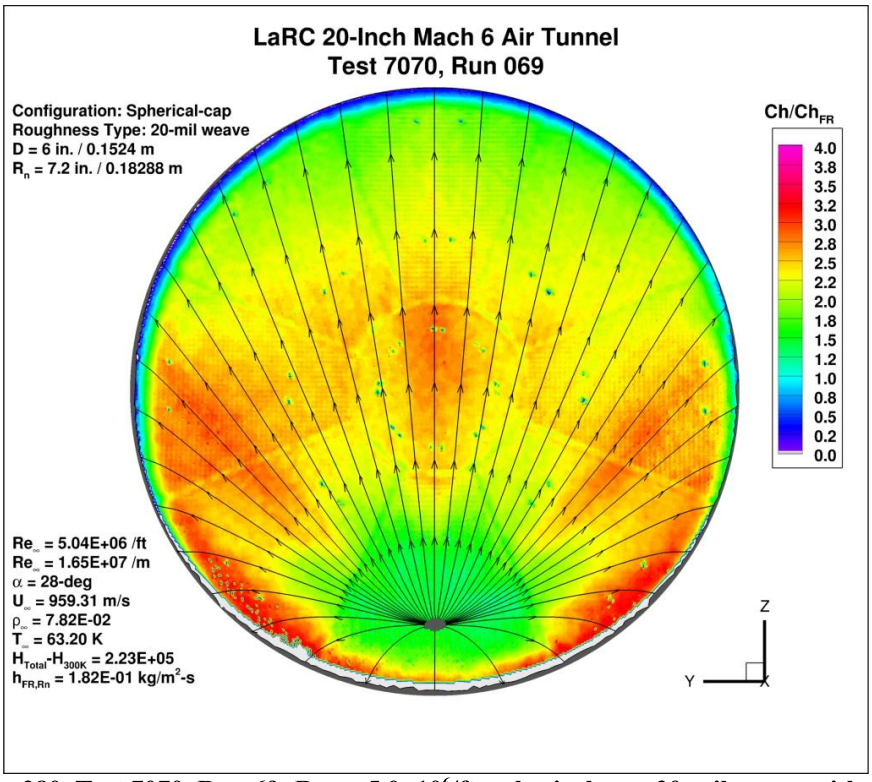
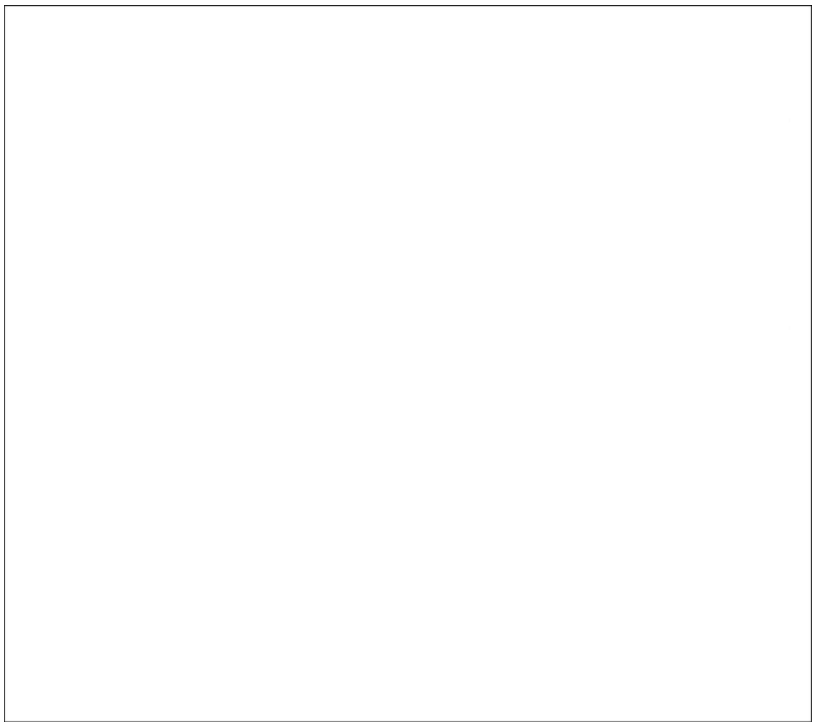
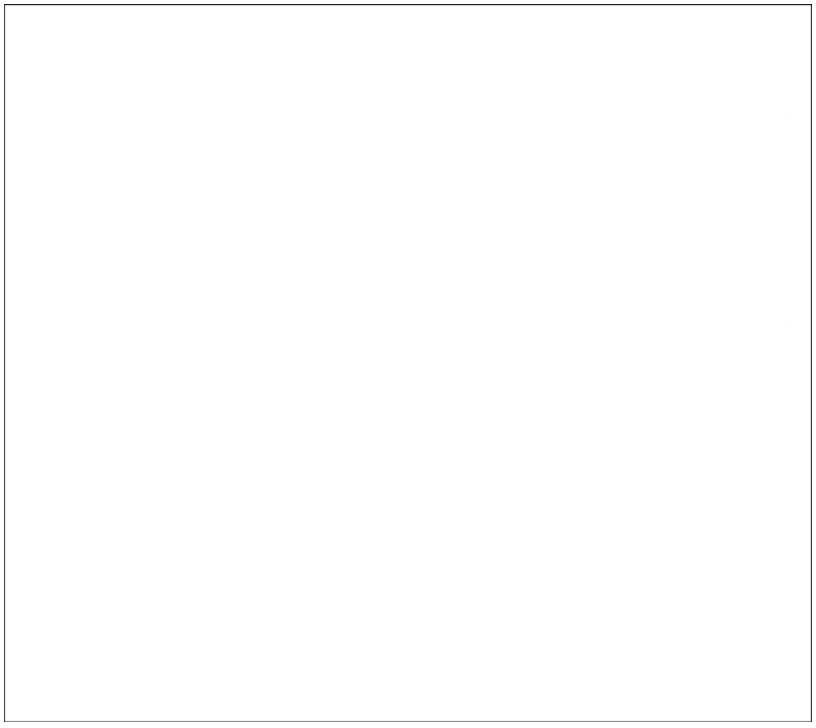


Figure 280. Test 7070, Run 69: $Re_\infty = 5.0\times10^6$/ft, spherical-cap, 20-mil weave with seam.



(Condition was not run)

Figure 281. Test 7070, Run XX: $Re_\infty = 5.3\times10^6$/ft, spherical-cap, 20-mil weave with seam.



(Condition was not run)

Figure 282. Test 7070, Run XX: $Re_\infty = 6.5\times10^6$/ft, spherical-cap, 20-mil weave with seam.

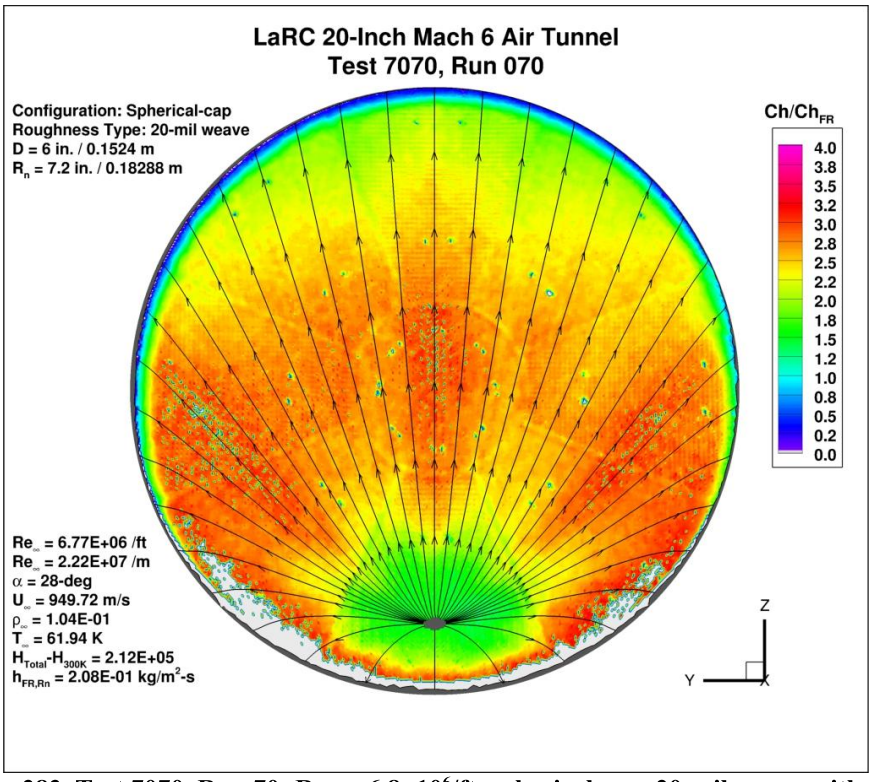


Figure 283. Test 7070, Run 70: $Re_\infty = 6.8\times10^6$/ft, spherical-cap, 20-mil weave with seam.

(Condition was not run)

Figure 284. Test 7070, Run XX: $Re_\infty = 7.3\times10^6$/ft, spherical-cap, 20-mil weave with seam.

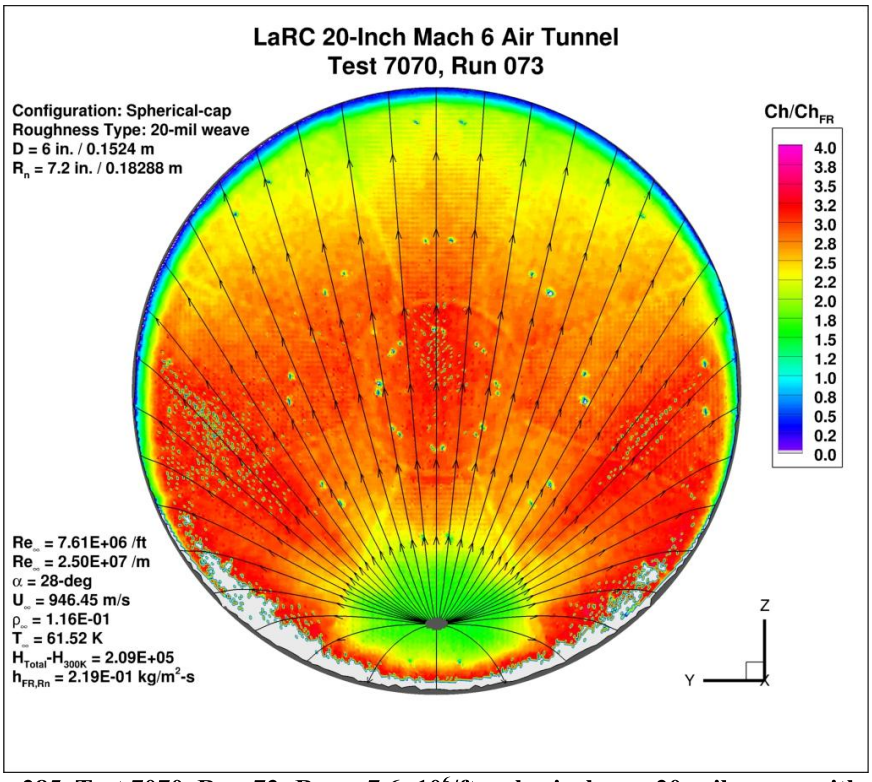


Figure 285. Test 7070, Run 73: $Re_\infty = 7.6\times10^6$/ft, spherical-cap, 20-mil weave with seam.

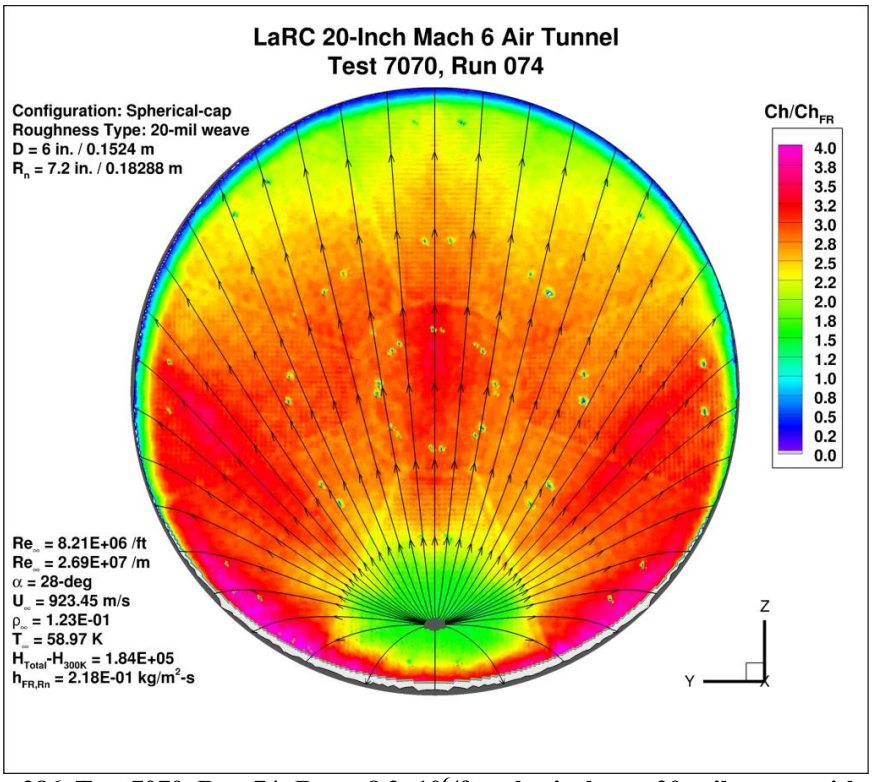


Figure 286. Test 7070, Run 74: $Re_\infty = 8.2\times10^6$/ft, spherical-cap, 20-mil weave with seam.